

# **Regulation and roles of nutrient-dependent mitochondrial Fusion**

**A thesis presented by  
Mahmud Abdullah**

**In fulfilment of the requirement for the degree of**

**Doctor of Philosophy**

**2019**

**Strathclyde Institute of Pharmacy and Biomedical Sciences**

**University of Strathclyde**

## **Declaration**

This thesis is the result of the author's original research. It has been composed by the author and has not been previously submitted for examination which has led to the award of a degree. The copyright of this thesis belongs to the author under the terms of the United Kingdom Copyright Acts as qualified by University of Strathclyde Regulation 3.49.

Due acknowledgement must always be made of the use of any material contained in, or derived from, this thesis.

Signed: Mahmud Abdullah

Date: 30/11/2019

## **Acknowledgements**

I give glory to Allah, the Exalted for giving me the opportunity to get to this stage of my studies. I would like to thank my supervisor Dr Edmond Chan for his mentorship, guidance and support all through the course of my studies. Due to his patience, discussions, criticisms and questions, he immensely brought out the best in me and he has made my research and studies at Strathclyde an enjoyable one.

I would also like to thank Dr Benjamin Pickard for his supervision, guidance and always being there during my studies. I would like to thank Dr David Watson for his time and discussions on metabolomics experiment. Also, I would like to thank all the staff at SIPBS who have engaged me at departmental meetings and also made my studying and research memorable. I would like to thank Graeme MacKenzie at the center for biophotonics for his guide and training on the microscopes. I would also use this opportunity to acknowledge the support of Dr Naser Al-Tannak, Mohammad Al-Rofaidi and also thank all past and present members of Chan's Lab for ensuring a good environment to discuss and practice science.

I would like to give special thanks to my wife Gbemisola, my daughters Niimah & Nadra, my mum and dad, my brothers and my inlaws. Their advice, support, prayers, patience and companionships made my studies memorable, as they all ensured I maintained a good balance between my studies and family life. I will forever cherish their concerns and motivation during my studies.

Finally, I would like to thank the former governor of Lagos State, Babatunde Raji Fashola (Senior Advocate of Nigeria) and the Lagos State Scholarship Board for providing part Scholarships for my studies. I also deeply appreciate Chan's Lab and the Faculty of Science in Strathclyde for providing funding support during my studies.

## Publication and Key Presentations

**Mahmud O. Abdullah**, Laura E. Gallagher, Edmond Y.W. Chan. June 2018. Regulatory amino acids glutamine, leucine and arginine stimulate mitochondrial hyperfusion via the Ulk1/2 signalling complex. Cell symposia, 'Multifaceted mitochondria', San-Diego. **[Poster communication]**

Gallagher, L. E., Radhi, O. A., **Abdullah, M. O.**, McCluskey, A. G., Boyd, M. & Chan, E. Y. W Lysosomotropism depends on glucose: a chloroquine resistance mechanism. 19 Jul 2017 in: Cell Death and Disease. 40 p **[Paper communication]**

**Mahmud O. Abdullah**, Laura E. Gallagher, Edmond Y.W. Chan. May, 2017. Amino acid-dependent mitochondrial remodelling. Strathclyde Institute of Pharmacy and Biomedical Sciences Cell Biology Meeting **[Verbal Talk]**

**Mahmud O. Abdullah** and Edmond Y.W. Chan. Nov, 2016. Identifying new regulators of mitophagy. Strathclyde Institute of Pharmacy and Biomedical Sciences Research Day Conference. **[Verbal Talk]**

# Table of Contents

Declaration .....	ii
Acknowledgements.....	iii
Publication and Key Presentations .....	iv
Table of Contents .....	v
List of Tables .....	x
List of Figures .....	xi
List of Abbreviations .....	xvii
Abstract .....	xix
Chapter 1.....	2
1.1 Introduction to Autophagy .....	2
1.1.1 Non-selective and selective autophagy .....	2
1.1.2 Historical contexts of autophagy.....	5
1.1.3 The autophagy genes and proteins .....	5
1.2 Molecular mechanisms of autophagy.....	9
1.2.1 Autophagy initiation .....	9
1.2.1.1 The signalling pathways that control the initiation of autophagy during nutrient stress.....	9
1.2.1.2 MTOR is the master regulator of autophagy initiation via its nutrient sensing mechanisms .....	10
1.2.1.3 The Unc-51-like autophagy activating kinase 1 (Ulk1) complex and the regulation of autophagy initiation .....	28
1.2.1.4 5'-AMP-activated protein kinase (AMPK) and the regulation of autophagy initiation.....	30
1.2.1.5 The crosstalk between MTORC1, AMPK and Ulk1 during autophagy initiation .....	36
1.2.2 Vesicle nucleation and autophagy progression.....	40
1.2.3 Vesicle expansion and maturation .....	43
1.2.4 Vesicle completion and fusion with lysosomes .....	46
1.3 Autophagy of mitochondria: role for mitochondrial remodelling .....	49
1.3.1 Biological significance of mitochondrial remodelling .....	52
1.3.1.1 Role of mitochondrial dynamics in ageing .....	53
1.3.1.2 Role of mitochondrial dynamics in <i>Charcot Marie Tooth type2A</i> disease (CMT2A).....	54
1.3.1.3 Role of mitochondrial dynamics in Optic atrophy.....	55
1.3.1.4 Role of mitochondrial dynamics in cancer .....	55

1.3.2 Mitochondrial pro-fusion initiators and their regulators.....	56
1.3.2.1 Mitofusin 1/2 (Mfn1/2) mediates outer mitochondrial fusion.....	57
1.3.2.2 Optic atrophy 1(Opa1) mediates inner mitochondrial fusion.....	59
1.3.2.3 Post-translational regulation of pro-fusion initiators.....	61
1.3.3 Mitochondrial pro-fission initiators and their regulators.....	62
1.3.3.1 Dynamin-related protein-1 severs mitochondria.....	62
1.3.3.2 Mitochondrial fission protein 1 (Fis1).....	64
1.3.3.3 Mff and other Drp1 receptors on mitochondria.....	66
1.3.3.4 Post-translational regulation of pro-fission initiators.....	68
1.4 Current model on mechanism linking nutrient availability and mitochondrial dynamics.....	75
1.5 Aims and objective.....	78
Chapter 2.....	79
2.0 Materials and Methods.....	80
2.1 Cells and Cell culture.....	80
2.2 SU9-GFP and GFP-OMP25 expression in cells.....	81
2.3 The stable knockdown of Drp1/Dnm1l.....	81
2.4 Amino acid and glucose starvation.....	83
2.5 Western blot analysis.....	83
2.6 Microscopy.....	86
2.6.1 Fixing and staining cells seeded on coverslips.....	86
2.6.2 Epifluorescence microscopy.....	87
2.6.3 Confocal microscopy.....	87
2.6.4 Transmission electron microscopy.....	88
2.6.5 Mitochondrial and autophagy quantification.....	88
2.7 Polymerase chain reaction (PCR) quantification of mRNA.....	89
2.8 Metabolomics.....	90
2.8.1 Sample preparation.....	90
2.8.2 Data processing.....	91
2.8.3 Metabolomics data analysis.....	93
2.9 Statistical analysis.....	94
Chapter 3.....	95
Mitochondrial response to changes in nutrient and amino acid pools.....	95
3.1 Introduction.....	96
3.2 Results.....	99
3.2.1 Mitochondrial response to nutrient availability.....	99

3.2.2 Mitochondrial remodelling in cells expressing GFP-tagged mitochondrial constructs.....	104
3.2.3 Amino acid-dependent mitochondrial fusion.....	106
3.2.4 Investigating the similarities between stress-induced mitochondrial hyperfusion and QLR-dependent mitochondrial hyperfusion .....	119
3.2.5 Investigating the role of mitochondrial division in QLR-dependent mitochondrial hyperfusion .....	125
3.3 Discussion .....	131
3.3.1 Mitochondrial fusion during starvation depends on the depleted nutrients	131
3.3.1.2 Mitochondria do not hyperfuse during serum starvation.....	131
3.3.1.3 Mitochondrial hyperfusion is not a response to changes in glycolysis ....	132
3.3.1.4 Mitochondria hyperfuse mainly during amino acid deprivation .....	134
3.3.1.5 Unique form of mitochondrial amino acid sensing.....	134
3.3.2 Is amino acid-dependent mitochondrial fusion an ER stress response .....	136
3.3.3 Conclusion .....	138
Chapter 4.....	139
4.1 Introduction.....	140
4.2 Result .....	147
4.2.1 Assessing the role of MTORC1 in amino acid-dependent mitochondrial hyperfusion .....	147
4.2.2 AMPK is a regulator of mitochondrial dynamics.....	153
4.2.3 The Ulk1-complex is a regulator of amino acid-dependent mitochondrial hyperfusion .....	155
4.2.3.1 Atg13 and FIP200 are required for amino acid-dependent mitochondrial hyperfusion.....	155
4.2.3.2 Ulk1 is required for QLR-dependent mitochondrial hyperfusion.....	162
4.2.4 Amino acid-dependent mitochondrial fusion is independent of autophagy. ....	170
4.2.5 Role of PKA-signalling in amino acid-dependent mitochondrial hyperfusion .....	173
4.3 Discussion .....	185
4.3.1 Regulatory roles of autophagy mediators in mitochondrial remodelling ....	185
4.3.1.1 Amino acid-dependent mitochondrial hyperfusion is MTORC1 independent.....	185
4.3.1.2 AMPK is a regulator of mitochondrial hyperfusion.....	186
4.3.1.3 Ulk1 is a regulator of mitochondrial dynamics .....	187
4.3.2 Amino acid-dependent mitochondrial hyperfusion is autophagy-independent .....	189
4.3.3 Roles of PKA and Drp1 phosphorylation in amino acid-dependent mitochondrial fusion .....	190

4.3.3.1 The phosphorylation role of Drp1 is context-specific .....	191
4.3.3.2 PKA signalling is compartmentalised .....	194
4.3.3.3 The role of phosphatases in amino acid-dependent mitochondrial hyperfusion .....	195
4.3.4 Conclusion .....	197
Chapter 5.....	198
5.1 Introduction.....	199
5.1.1 Mitochondria dynamics are regulators of cellular metabolism .....	199
5.1.2 Metabolic and physiologic significance of mitochondrial dynamics .....	200
5.1.2.1 OXPHOS-dependent regulation of mitochondrial hyperfusion .....	200
5.1.2.2 Amino acid regulates cell fate and cell survival .....	202
5.1.3 Metabolomics is a tool to study cellular metabolism .....	202
5.2 Results.....	204
5.2.1 Metabolic profile of cells undergoing amino acid-dependent mitochondrial hyperfusion .....	204
5.2.1.1 Confirmation of glucose starvation metabolic profile .....	211
5.2.1.2 QLR-addback increases amino acid metabolism.....	214
5.2.1.3 QLR-addback restores REDOX balance to reduce oxidative stress. ..	223
5.2.1.4 Cellular energetics is enhanced by QLR-addback.....	227
5.2.1.5 The effects of QLR-addback on nucleotide metabolic pathways. ....	231
5.2.2 The metabolic profile of cells treated to amino acid addback in the presence of glucose.....	235
5.2.2.1 QLR-addback restores amino acid catabolism in EBSS conditions ....	239
5.2.2.2 QLR-addback into EBSS increased cellular energy .....	246
5.2.2.3 Effects of QLR-addback into EBSS on nucleotide and lipid metabolism .....	249
5.2.2.4 Distinct cellular metabolism profiles following QLR or single amino acid addback.....	255
5.2.3 The Krebs cycle is required for QLR-dependent mitochondrial hyperfusion .....	259
5.2.4 The role of mitochondrial fusion in QLR-addback dependent metabolic re- programming.....	283
5.3 Discussion .....	298
5.31 Metabolomics as a high-resolution robust tool for studying cellular metabolism.....	298
5.32 Nucleotide metabolism is altered during amino acid-dependent mitochondrial hyperfusion. ....	298
5.33 Amino acid metabolism is altered during nutrient deprivation .....	300
5.3.3.1 The urea cycle and the Krebs cycle are regulated by amino acid- dependent mitochondrial hyperfusion .....	300

5.3.3.2 Truncation of the Krebs cycle and urea cycle lead to mitochondrial dysfunction .....	302
5.3.3.3 Wider effects of Fh deficiency on cellular metabolism .....	303
5.3.3.4 N (Asparagine) is a potential metabolic regulator of cell fate and mitochondrial dynamics .....	304
5.34 Mitochondrial hyperfusion prevents stress-induced oxidative stress.....	305
5.35 Cellular energetics do not require mitochondrial hyperfusion.....	306
5.36 Conclusion .....	307
Chapter 6.....	308
6.0 General Discussion.....	309
6.1 Amino acid-dependent mitochondrial hyperfusion is an amino acid-sensing response, not an mTORC1-inhibition response.....	310
6.2 Mitochondria have an intrinsic amino acid sensing mechanism that requires glutaminase.....	311
6.3 Ulk1/2 signalling, not PKA signalling regulate amino acid-dependent mitochondrial hyperfusion. ....	312
6.3.1 Amino acid-dependent mitochondrial hyperfusion does not require the cAMP-PKA-Drp1 signalling pathway .....	313
6.3.2 Ulk1/2 signalling regulates cellular metabolism.....	314
6.4 Mitochondria hyperfuse to meet metabolic demand during amino acid starvation-dependent stress .....	316
6.5 Future work .....	320

## List of Tables

Table 1.1: The nomenclatures of Autophagy-related genes (Atg).....	7
Table 1.2: AMPK-dependent regulation of cellular processes.....	31
Table 2.1: Sequences of Dnm1l shRNA.....	82
Table 2.2 Sigma molecular weight marker proteins.....	84
Table 2.3 List of antibodies used for western blot showing dilution factors and final concentration (where available).....	85
Table 2.4 List of antibodies used for immunofluorescence showing dilution factors and final concentration (where available).....	87
Table 2.5 List of PCR primers.....	90
Table 2.6: MZmine parameters used for data processing.....	92
Table 5.1: Detailed results of pathway analysis of relevant pathways (P < 0.05) following amino acid starvation with QLR supplementation relative to amino acid and glucose starvation in 4T1 cells.....	210
Table 5.2: Summary of key significant metabolic changes after QLR addback in no glucose media.....	234
Table 5.3: Detailed results of pathway analysis of relevant pathways after amino acid starvation with or without QLR supplementation.....	238
Table 5.4: Summary of key significant metabolic changes after QLR and Q addback in EBSS .....	257
Table 5.5: Detailed results of pathway analysis of relevant pathways after QLR supplementation into amino acid-starved Fh1 fl/fl cells relative to Fh1-/- clone1 cells.....	267
Table 5.6: Summary of key significant metabolic changes after QLR addback in Fh KO.....	280
Table 5.7: Detailed results of the pathway analysis of relevant pathways after QLR supplementation into amino acid-starved WT MEF relative to Mfn1 KO MEF.....	287
Table 5.8: Summary of key significant metabolic changes after QLR addback in Mfn1 KO.....	297

## List of Figures

Figure 1.1: The general autophagy process.....	4
Figure 1.2: MTOR and its binding partners.....	12
Figure 1.3: The regulation of MTORC1 by growth factors.....	16
Figure 1.4: Amino acids and the structure of L, Q and R.....	19
Figure 1.5: The regulation of MTORC1 at the lysosome by amino acids.....	22
Figure 1.6: The aldolase glucose-sensing model at the lysosome.....	34
Figure 1.7: The control of autophagy initiation by MTORC1 and the ULK1 complex.....	39
Figure 1.8: Vesicle nucleation and the recruitment of membranes during autophagy.....	42
Figure 1.9: The Ubiquitin-like conjugation complex drives cargo selection and autophagy progression.....	45
Figure 1.10: The formation of matured autophagosome and the fusion with lysosome.....	48
Figure 1.11: Mitochondrial remodelling during autophagy.....	51
Figure 1.12: The multiple sites of cAMP generation.....	74
Figure 3.1: The effects of nutrient starvation stress on mitochondrial dynamics....	100
Figure 3.2: Mitochondria remodel towards fusion during amino acid starvation stress.....	103
Figure 3.3: SU9-GFP and GFP-OMP25 localized to mitochondria.....	105
Figure 3.4: Glutamine, Leucine and Arginine (Q, L, R) induce mitochondrial hyperfusion in 4T1 cells during starvation stress.....	108
Figure 3.5: Mitochondrial hyperfusion in response to QLR is independent of glucose.....	109
Figure 3.6: Time-dependent amino acid-induced mitochondrial hyperfusion.....	111
Figure 3.7: Glutamine, Leucine and Arginine (Q, L, R) induce mitochondrial hyperfusion in U2OS cells.....	112

Figure 3.8: Mitochondrial hyperfusion requires combined addition of QLR in 4T1-SU9 GFP cells.....	115
Figure 3.9: Mitochondrial hyperfusion requires combined addition of QLR in U2OS-SU9 GFP cells.....	116
Figure 3.10: Mitochondrial hyperfusion is maximal upon supplementation with QLR.....	117
Figure 3.11: Transmission electron microscopy confirms glutamine, leucine and arginine induce mitochondrial hyperfusion in 4T1 cells.....	118
Figure 3.12: QLR-dependent mitochondrial hyperfusion resembles ER-Stress-related hyperfusion.....	121
Figure 3.13: OPA1 is required for amino acid-dependent mitochondrial hyperfusion.....	122
Figure 3.14: Mfn1 is required for amino acid-dependent mitochondrial hyperfusion.....	123
Figure 3.15: Mfn1 is required for amino acid-dependent mitochondrial hyperfusion.....	124
Figure 3.16: The effect of Drp1 inhibition on mitochondrial fusion.....	127
Figure 3.17: Knockdown of Dnm1L (also known as Drp1).....	128
Figure 3.18: Effect of Drp1 knock down on mitochondrial dynamics.....	129
Figure 3.19: Effect of Drp1 knockdown on amino acid-dependent mitochondrial fusion.....	130
Figure 4.1: Interaction map of the molecular regulators involved in amino acid sensing and mitochondrial dynamics.....	141
Figure 4.2: The regulation of MTORC1 by amino acids and growth factors.....	143
Figure 4.3: The regulation of MTORC1 signalling by amino acid availability.....	149
Figure 4.4: Mitochondrial dynamics in the presence of MTORC1 inhibition.....	150
Figure 4.5: Serum-dependent activation of MTORC1 signalling.....	151
Figure 4.6: Minimal effect of serum on amino acid-dependent mitochondrial hyperfusion.....	152
Figure 4.7: Role of AMPK in amino acid-dependent mitochondrial hyperfusion....	154

Figure 4.8: p62/SQSTM1 puncta formation is inhibited in Atg13 CRISPR 4T1 cells.....	157
Figure 4.9: LC3B puncta formation is inhibited in Atg13 CRISPR 4T1 cells.....	158
Figure 4.10: Mitochondrial hyperfusion is inhibited in Atg13 CRISPR 4T1 cells....	159
Figure 4.11: Mitochondrial hyperfusion is inhibited in FIP200 knockout MEF.....	161
Figure 4.12: The effect of CRISPR ULK1 targeting on amino acid-dependent mitochondrial hyperfusion.....	165
Figure 4.13: Pharmacological inhibition of ULK1 blocks mitochondrial hyperfusion.....	166
Figure 4.14: ULK1/2 is required for LC3-positive autophagosome formation.....	167
Figure 4.15: ULK1/2 is a regulator of amino acid-dependent mitochondrial hyperfusion.....	168
Figure 4.16: ULK1 reconstitution rescues QLR-induced mitochondrial hyperfusion.....	169
Figure 4.17: Autophagy deficiency in Atg5 KO MEF.....	171
Figure 4.18: QLR-induced mitochondrial hyperfusion is independent of autophagy.....	172
Figure 4.19: Drp1 localization during amino acid-dependent mitochondrial fusion.....	179
Figure 4.20: PKA activation does not correlate with mitochondrial hyperfusion.....	180
Figure 4.21: Rapid PKA activation upon amino-acid starvation.....	181
Figure 4.22: Mitochondrial fusion is regulated by both PKA activation and inhibition.....	182
Figure 4.23: H89 inhibition of PKA inhibits QLR-dependent mitochondrial hyperfusion.....	183
Figure 4.24: Detection of phosphorylation of PKA substrate motif during amino acid starvation.....	184
Figure 4.25: Drp1 phosphorylation site conservation in different isoforms and summary model.....	193

Figure 5.1: Metabolomics LC-MS/MS analysis of 4T1 cells after amino acid and glucose starvation (-AA), amino acid and glucose starvation with QLR supplementation (QLR).....	208
Figure 5.2: Pathway analysis of metabolites with significant changes after amino acid and glucose starvation relative to amino acid and glucose starvation with QLR supplementation in 4T1 cells.....	209
Figure 5.3: Metabolic changes due to glucose starvation.....	213
Figure 5.4: Heat map showing the profile of metabolites involved in amino acid metabolism after glucose starvation, amino acid starvation with or without QLR supplementation.....	216
Figure 5.5: The Urea cycle.....	217
Figure 5.6: QLR supplementation drives Argininosuccinate flux.....	218
Figure 5.7: Glutamate metabolism.....	221
Figure 5.8: The supplementation of QLR maximizes glutamate metabolism.....	222
Figure 5.9: The effect of QLR supplementation on NADH synthesis.....	225
Figure 5.10: QLR supplementation reduces ROS production.....	226
Figure 5.11: The electron transport chain showing the shuttling of electrons.....	229
Figure 5.12: QLR supplementation maximises cellular energy production.....	230
Figure 5.13: The effect of the supplementation of QLR on nucleotide metabolism.....	233
Figure 5.14: Metabolomics LC-MS/MS analysis of 4T1 cells starved of amino acid (-AA) with or without QLR supplementation.....	236
Figure 5.15: Pathway analysis of metabolites with significant changes after amino acid starvation with or without QLR supplementation in 4T1 cells.....	237
Figure 5.16: Heat map showing the profile of metabolites involved in amino acid metabolism after amino acid starvation with or without QLR supplementation.....	241
Figure 5.17: The supplementation of Glutamine (Q), Leucine (L) and Arginine (R) drives Argininosuccinate flux in 4T1 cells.....	242
Figure 5.18: The supplementation of Glutamine (Q), Leucine (L) and Arginine (R) drives Asparagine synthesis in 4T1 cells.....	243

Figure 5.19: QLR metabolism in Tricarboxylic Acid (TCA) cycle (also referred to as Krebs cycle).....	244
Figure 5.20: The supplementation of Glutamine (Q), Leucine (L) and Arginine (R) increased TCA cycle metabolites in 4T1 cells.....	245
Figure 5.21: QLR supplementation increased NADH synthesis.....	247
Figure 5.22: QLR supplementation into amino acid-starved cells restore cellular energy.....	248
Figure 5.23: QLR supplementation into amino acid-starved cells alter nucleotide metabolism.....	252
Figure 5.24: QLR supplementation into amino acid-starved cells alter lipid metabolism.....	253
Figure 5.25: Q, L, R-induced hyperfusion is independent of TSPO-mediated lipid transport.....	254
Figure 5.26: Metabolic variations between QLR and Q-addback.....	258
Figure 5.27: Q, L, R-induced hyperfusion requires an efficient Krebs cycle.....	261
Figure 5.28: Metabolomics LC-MS/MS analysis of Fumarate hydratase deficient cells.....	265
Figure 5.29: Pathway analysis of metabolites with significant changes after QLR supplementation into amino acid-starved Fh1 fl/fl relative to amino acid-starved Fh1-/- (clone1) cells.....	266
Figure 5.30: Heat map showing the profile of metabolites involved in amino acid metabolism in Fh deficient cells.....	268
Figure 5.31: Argininosuccinate flux is maximised in fumarate hydratase KO cells.....	269
Figure 5.32: QLR-induced glutamate metabolism flux is inhibited in fumarate hydratase KO cells.....	274
Figure 5.33: Effect of Fumarate Hydratase-1 (Fh1) KO on metabolites of the Krebs cycle during amino acid starvation with or without the supplementation of QLR.....	275
Figure 5.34: NADH levels are increased in Fumarate hydratase-1 (Fh1) KO.....	278
Figure 5.35: Cellular energy is reduced in Fumarate hydratase-1 (Fh1) KO.....	279

Figure 5.36: Q, L, R-induced hyperfusion requires the electron transfer process in complex I of the E.T.C.....	282
Figure 5.37: Metabolomics LC-MS/MS analysis of mitofusin-1 deficient cells.....	285
Figure 5.38: Pathway analysis of metabolites with significant changes after QLR supplementation into amino acid-starved WT MEF relative to Mfn1 KO MEF.....	286
Figure 5.39: Heat map showing the profile of metabolites involved in amino acid metabolism after Mfn1 KO.....	291
Figure 5.40: Argininosuccinate levels is increased in Mfn1 KO MEF.....	292
Figure 5.41: Effect of Mfn1 KO on glutamate metabolism after amino acid starvation with or without QLR supplementation.....	293
Figure 5.42: Effect of Mfn1 KO on metabolites of the Krebs cycle during amino acid starvation with or without QLR supplementation.....	294
Figure 5.43: Effect of Mfn1 KO on NADH level.....	295
Figure 5.44: Effect of Mfn1 KO on cellular energy during amino acid starvation with or without QLR supplementation.....	296
Figure 6.1: Proposed model for QLR-addback induced mitochondrial hyperfusion. .....	318
Figure 6.2: Summary model of amino acid-dependent mitochondrial dynamics....	319

## List of Abbreviations

AMBRA1	Autophagy and beclin-1 regulator 1
AMPK	AMP-activated protein kinase
Arf1	ADP ribosylation factor 1
Atg	Autophagy genes
Bcl-2	B-cell lymphoma 2
Bif-1	Bax interacting factor 1
cAMP	Cyclic adenosine monophosphate
Cas9	CRISPR-associated protein 9
CASTOR	Cellular Arginine Sensor for MTORC1
CRISPRs	Clustered Regularly Interspaced Short Palindromic Repeats
DMEM	Dulbecco's modified eagle's medium
DNA	Deoxyribonucleic acid
EBSS	Earle's balanced salt solution
E.T.C.	Electron transport chain
EPAC	Exchange protein activated by cAMP
EGFR	Epidermal growth factor receptor
ER	Endoplasmic reticulum
FBS	Fetal bovine serum
FIP200	FAK family interacting protein of 200 kD
GABARAP	Gamma-aminobutyric acid receptor associated proteins
GAP	GTPase-Activating Protein
GATOR	GTPase-activating protein (GAP) activity toward Rags
GDP	Guanosine-diphosphate
GEF	Guanine Nucleotide Exchange Factor
GFP	Green Fluorescent Protein
GLS	Glutaminase
GPCR	G-protein coupled receptors
GTP	Guanosine-triphosphate
MAM	Mitochondria-associated membranes
MEF	Mouse embryonic fibroblasts
mLST8	Mammalian lethal with SEC13 protein 8
MTOR	Mammalian target of rapamycin
MTORC1/2	Mammalian target of rapamycin complex 1/2
NAC	N-Acetyl-L-Cysteine
NADH	Nicotinamide adenine dinucleotide hydrogen
PAS	Pre-autophagosomal structure

PBS	Phosphate buffered saline
PI3K	Phosphoinositide 3-kinase
PI3P	Phosphatidylinositol 3-phosphate
PKA	Protein Kinase A
PP2A	Protein phosphatase 2A
PRAS40	Proline-rich Akt substrate, 40kDa
Rag	Ras-related GTPase
Raptor	Regulator-associated protein of MTOR
Rheb	Ras homolog enriched in brain
ROS	Reactive oxygen species
S6K1	Ribosomal protein S6 kinase beta-1
SLC38A9	Human member 9 of the solute carrier family 38
TCA	Tricarboxylic acid cycle
Tom20	Translocase of outer membrane 20
TSC	Tuberous sclerosis complex
Ulk	Unc-51 like autophagy activating kinase
UVRAG	UV radiation resistance-associated gene protein
v-ATPase	Vacuolar-type H <sup>+</sup> ATPase
VPS	Vacuolar protein sorting
WIPI	WD-repeat protein interacting with phosphoinositides
WT	Wild type

## Abstract

Mitochondria continuously alter their shape via fusion and fission and interestingly, this dynamic balance is critical for maintaining organelle function and cellular homeostasis. Studies have shown that mitochondria undergo fusion during amino acid starvation-induced autophagy. This mitochondrial response has been proposed to be regulated by MTORC1, a key regulator of nutrient-sensing signalling pathway. However, the mechanism linking MTORC1 and nutrient sensing to mitochondrial hyperfusion has not been fully elucidated.

This project aimed at studying mitochondrial remodelling during nutrient starvation. As a sensor of regulatory amino acids, the role of MTORC1 in the regulation of mitochondrial fusion was studied. In addition, this study also aimed to investigate the kinase-dependent regulation of mitochondrial fusion during amino acid starvation. This project studied the roles of the Ulk1, AMPK and PKA pathways in amino acid starvation-dependent mitochondrial fusion. Using a metabolomics approach, this project also studied changes in cellular metabolism during amino acid starvation-dependent mitochondrial fusion and how hyperfusion could crosstalk with these metabolic changes.

The results in this study indicated that mitochondria undergo remodelling towards a hyperfused state specifically in response to amino acid availability. Importantly, mitochondria surprisingly undergo extensive hyperfusion in response to elevated levels of glutamine (Q), leucine (L) and arginine (R). Contrary to predictions from the current model, mitochondria sensed Q, L and R levels independently of MTORC1. Interestingly, amino acid-dependent mitochondrial hyperfusion critically required the Ulk1/2 autophagy initiation complex. In addition, amino acid-dependent mitochondrial hyperfusion did not require AMPK and PKA-dependent phosphorylation of Drp1. However, amino acid-dependent mitochondrial fusion required the regulators, Optic atrophy 1 (Opa1) and Mitofusin 1 (Mfn1).

Metabolomic analysis revealed both QLR-dependent and fusion-dependent changes in levels of metabolites involved in the urea cycle, Krebs cycle and REDOX balance. Findings in this project suggest putative mechanisms linking amino acid metabolism, mitochondrial dynamics and mitochondrial function

# **Chapter 1**

## **Introduction**

# Chapter 1

## 1.1 Introduction to Autophagy

Autophagy is a vital catabolic process which recycles cellular contents such as proteins, macromolecules and organelles during starvation and stress (Kobayashi, 2015). During this process, a double membrane structure termed the phagophore firstly forms around the target content. Subsequently, the targeted content is sequestered in the autophagosome and finally the autophagosome fuses with the lysosome to form the autolysosome (Xie and Klionsky, 2007). The targeted contents are degraded in the autolysosome by the lysosomal hydrolases (**Overall scheme summarised in Fig 1.1**). Cells are highly dependent on autophagy for regular renewal of organelles and recycling of amino acids and other molecules. Autophagy plays important physiological roles in cellular immunity, apoptosis, cancer, neuronal functionality and aging (Nakagawa et al., 2004, Sanchez-Sanchez et al., 2015, Shibutani et al., 2015, Martinez-Lopez et al., 2015, Mizushima, 2009, Levine and Kroemer, 2019).

### 1.1.1 Non-selective and selective autophagy

Mammalian autophagy is classified into three categories depending on the type of cargos, and how the cargos are recruited to the lysosome. Cargoes can be delivered directly into lysosomes through the formations of tubular invaginations in a process called microautophagy (Ahlberg et al., 1982, Mortimore et al., 1988). In some cases, proteins are delivered directly into lysosomes through a protein translocation pathway in a process called chaperone-mediated autophagy (Chiang and Dice, 1988). The most characterized and well-defined process of autophagy and lysosomal delivery is through the formation of autophagosomes termed macroautophagy. In this project, macroautophagy is hereafter referred to as autophagy.

Autophagy is thought to be a non-selective bulk degradative process. However, it is now well established that cargo can be selectively targeted and sequestered into the autophagosome for degradation in the lysosome (Gatica et al., 2018). For example, invading microorganisms and pathogens have been shown to be degraded by autophagy in a distinct sub-category of autophagy called xenophagy. Other autophagy sub-categories are aggrephagy (turnover of misfolded proteins), pexophagy (clearance of peroxisomes), reticulophagy (Endoplasmic reticulum turnover), ribophagy (ribosome clearance), zymophagy (secretory granule removal)

and mitophagy (clearance of mitochondria) (Mizushima and Komatsu, 2011, Kim et al., 2007, Gatica et al., 2018).

Specific cargo are selected for autophagy via the activation of receptor proteins that can recruit light chain-3 (LC3), hence the autophagy machinery to its site (Kirkin et al., 2009, Sandoval et al., 2008). For example, sequestosome-1 (p62/SQSTM1) is suggested to serve as an adaptor protein by binding ubiquitinated mitochondrial proteins and LC3 during mitophagy (Katsuragi et al., 2015, Ding et al., 2010). Due to the important physiological functions of organelles sequestered through selective autophagy, understanding the specific mechanism of this process have been suggested to be relevant in preventing diseases such as neurodegeneration, ageing, immune-deficiencies and cancers (Boland et al., 2013, Stefano and Kream, 2015, Levine and Kroemer, 2019). Most importantly, the clearance of mitochondria through mitophagy has been linked to cancer (Chourasia et al., 2015), Parkinson's disease (Narendra et al., 2008), and there are many diseases suggested to have developed as a result of impaired mitochondrial clearance (Xu et al., 2019). As one main role, mitophagy has been proposed to maintain quality control by degrading damaged-mitochondria with mutated mtDNA and abnormal reactive oxygen species (ROS) production. Dysfunctional mitophagy will lead to the accumulation of damaged mitochondria thereby enhancing ROS production which can eventually induce cellular DNA mutation and cell damage or cell death. This basis for further cellular damage can also contribute to development of disease (Um and Yun, 2017). Initially, this project started by studying the mitophagy-autophagy process during mitochondrial damage. However, the focus shifted towards understanding how mitochondria respond to nutrient-dependent autophagy.

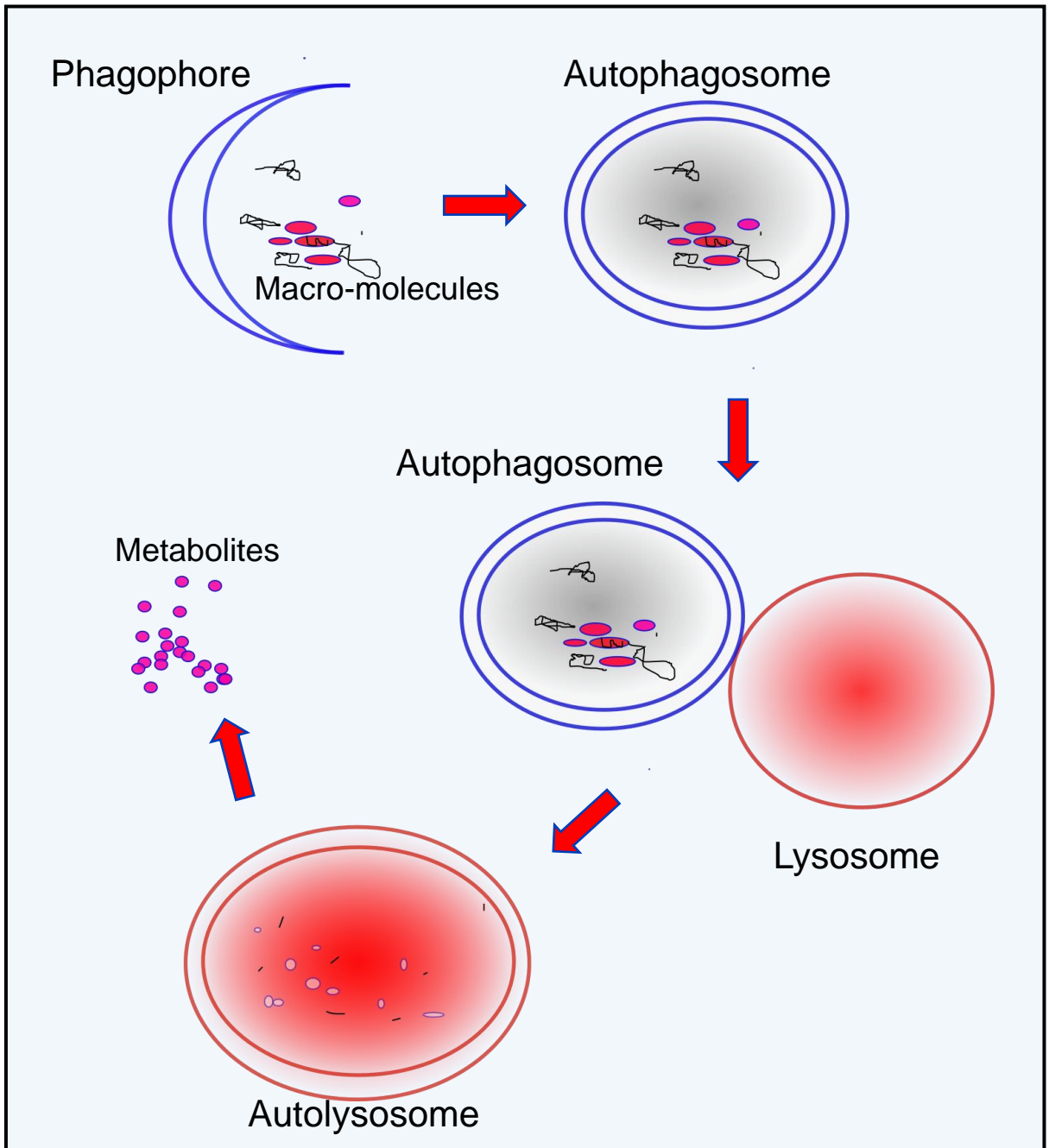


**Figure 1.1: The general autophagy process.** During autophagy, a phagophore is formed around macromolecules such as proteins and damaged organelles. Subsequently, the target cargo is enclosed in a double membrane termed the autophagosome which fuses with the lysosome to form an autolysosome. The macromolecules are degraded and recycled as metabolites such as amino acids and lipids.

### **1.1.2 Historical contexts of autophagy**

The term “Autophagy” meaning “self-eating” was first used in 1963 (De Duve, 1963). Autophagy became better understood for its molecular mechanisms in the early 1990s, following yeast studies of autophagy proteins (Dunn, 1990b, Dunn, 1990a, Lawrence and Brown, 1992, Tsukada and Ohsumi, 1993). Prior to this, protein degradation had been established and argued to occur either through a lysosomal-dependent process or a lysosomal independent process using the ubiquitin/proteasome pathway (Schworer et al., 1981, Mortimore and Poso, 1986, Mortimore et al., 1989).

Glucagon was discovered to regulate autophagy in rat liver (Deter et al., 1967). It was reported that an autophagosome, a double membrane bound structure lacking hydrolytic enzymes, is formed first before fusion with the lysosomes to form the autophagolysosome (Arstila and Trump, 1968). Subsequently, the physiological roles were studied, showing that autophagy is highly regulated by the availability of nutrients (Pfeifer and Warmuth-Metz, 1983). Similarly, Mortimore and Ward (1976) observed that autophagy is highly dependent on the availability of amino acids, after their studies on hepatocytes showed that protein degradation occurs rapidly when amino acids are in shortage, and then degradation was suspended when amino acids were present. Their findings were confirmed by Seglen et al. (1980). The race to understand the regulation of autophagy continued over the years and some autophagy inhibitors were discovered such as 3-methyladenine, which acts by blocking the autophagic/lysosomal protein degradation pathway by inhibiting the class III phosphoinositide 3-kinase (PI3K) complex (Seglen and Gordon, 1982, Holen et al., 1993).

In 1992, work by Ohsumi and colleagues opened the molecular era by isolating 15 autophagy-defective mutants (Takeshige et al., 1992, Tsukada and Ohsumi, 1993). By the late 1990s, the characterization and identification of the autophagy-related genes began and in 2004 a unified nomenclature for autophagy-related genes in yeast was accepted (Klionsky et al., 2003). Interestingly, Ohsumi’s work on the mechanisms of autophagy has been rewarded with a Nobel Prize in Physiology or Medicine in 2016 (Levine and Klionsky, 2017).

### **1.1.3 The autophagy genes and proteins**

Genetic studies have presently classified 41 genes that have important roles in autophagy (Klionsky et al., 2011, Klionsky et al., 2016). These genes, many of which were initially identified in yeast, are now termed Autophagy-Related Genes “*Atg*”. Some of the genes were identified using a microscopy-based screen to isolate autophagy-defective mutants (Tsukada and Ohsumi, 1993). In addition, cytoplasmic-to-vacuole targeting (*CVT*) genes, glucose-mediated autophagy (*GSA*) genes, peroxisome degradation-deficient genes (*PDD*), peroxisome degradation autophagy (*PGA*) genes and autophagocytosis defective mutants *AUT* genes were identified by independent studies (Harding et al., 1995, Thumm et al., 1994). The *AUT* and *CVT* genes were later discovered to correspond to *Atg* genes after studies showed that cells with *AUT* mutants had defective processing of targets from the cytoplasm to the vacuole. After years of accumulation of experimental studies and confusion due to gene terminology, a comprehensive nomenclature was adopted for all *Atg* genes in 2003 with a further update in 2010 (Klionsky et al., 2011, Klionsky et al., 2003). Interestingly, the *Atg* genes identified in yeast have structural and functional homologues in vertebrates, plants and humans. The *Atg* genes are highly conserved between yeast and humans (**Table 1.1**). For example, in mammals, the bcl2-binding protein Beclin1 is a structural homologue of *Atg6* in yeast (Liang et al., 1999). Similarly, LC3, a microtubule-associated protein 1 light chain-3, is a homologue of *Atg8* in yeast (Kabeya et al., 2000). The corresponding proteins of the genes are called the Autophagy-related proteins, and they are the drivers of non-selective and selective autophagy.

**Table 1.1: The nomenclature of Autophagy-Related genes (Atg).** List of autophagy genes in yeast and human showing the autophagy (APG), autophagocytosis defective mutants (AUT), cytoplasmic-to-vacuole targeting (CVT), glucose-mediated autophagy (GSA), peroxisome degradation-deficient genes (PDD) and pexophagy zeocin-resistant (PAZ) nomenclature.

Yeast Atg	Human	APG	AUT	CVT	GSA	PDD	PAZ
1	<i>Ulk1/2</i>	1	3	10	10	7	1
2	<i>Atg 2A/B</i>	2	8		11		7
3	<i>Atg3</i>	3	1		20		
4	<i>Atg4A/B/C/D</i>	4	2				8
5	<i>Atg5</i>	5					
6	<i>Beclin1</i>	6					
7	<i>Atg7</i>	7		2	7		12
8	<i>LC3, GABARAP</i>	8	7	5			2
9	<i>Atg9A/B</i>	9	9	7	14		9
10	<i>Atg10</i>	10					
11				9	9	18	6
12	<i>Atg12</i>	12					
13	<i>Atg13</i>	13					
14	<i>Atg14</i>	14		12			
15			5	17			
16	<i>Atg16L1/2</i>	16		11			3
17	<i>FIP200</i>	17					

**Table 1.1: The nomenclature of Autophagy-Related genes (Atg) Continuation.** List of autophagy genes in yeast and human showing the autophagy (APG), autophagocytosis defective mutants (AUT), cytoplasmic-to-vacuole targeting (CVT), glucose-mediated autophagy (GSA), peroxisome degradation-deficient genes (PDD) and pexophagy zeocin-resistant (PAZ) nomenclature.

Yeast ATG	Human	APG	AUT	CVT	GSA	PDD	PAZ
18	<i>WIPI1</i>		10	18	12		
19				19			
20				20			
21	<i>WIPI2</i>			21			
22			4				
23				23			
24	<i>SNX30/4</i>			13			16
25						4	
26							4
27				24			
28 - 31							
32	<i>BCL2L13</i>						
33 - 36							
37	<i>ACBD5</i>						
38 - 41							
	<i>Atg101</i>						

## 1.2 Molecular mechanisms of autophagy

### 1.2.1 Autophagy initiation

The hallmark of autophagy is the formation of autophagosomes, which at the end fuse with the lysosomes for degradation of their contents by hydrolases. Specific core protein complexes are responsible for the initiation and maturation of autophagosomes. The process of autophagosome formation is highly conserved between yeast and mammals. However, certain unique properties have been described for the phagophore membrane structure in mammals. Axe et al. (2008) observed a unique protrusion of the endoplasmic reticulum (ER) during the initiation of autophagy in mammalian cells which was termed an omegasome. The omegasome structure is now thought to be associated with (or serve as a marker for) a cradle-scaffold to support the formation of autophagosomes during autophagy initiation (Mercer et al., 2018, Karanasios et al., 2016). In yeast, autophagosomes are suggested to form from a single peri-vacuolar structure called phagophore assembly site (PAS), which act as the recruitment site for Atg proteins (Yang and Klionsky, 2009, Mari and Reggiori, 2010, Mari et al., 2010). However, in mammalian cells, multiple sites equivalent to PAS are observed (Tooze and Yoshimori, 2010). The molecular mechanisms leading to the activation of autophagy are complex and involve multiple protein complexes that converge at multiple nodes as described below.

#### 1.2.1.1 The signalling pathways that control the initiation of autophagy during nutrient stress

The first phase is the initiation of autophagy which involves three main kinases in yeast/mammalian cells which are Atg1/Ulk1, TOR/MTOR and SNF1/AMPK (Orlova et al., 2006) (Mizushima, 2010, Yang and Klionsky, 2009). Note: Protein kinase-A PKA also functions as a negative regulator of autophagy induction in yeast and mammals (Budovskaya et al., 2004, Mavrakis et al., 2006). The yeast autophagy induction machinery, which is first described below, entails a distinct pathway from mammalian autophagy initiation.

In yeast, Atg1 recruits other autophagy proteins such as Atg13, Atg17, Atg29 and Atg31 to successfully initiate autophagy. In nutrient rich conditions, a nutrient-sensitive TOR signalling complex is activated. TOR, a serine-threonine kinase,

normally hyper-phosphorylates Atg13. In the hyper-phosphorylated state, Atg13 loses its binding ability to the Atg1-Atg17-Atg31-Atg29 complex, inhibiting autophagy (Kamada et al., 2010). TOR is deactivated during starvation or stress while Atg13 is dephosphorylated, thereby recruiting Atg1, Atg17, Atg31 and Atg29 to induce autophagy (Kabeye et al., 2005). Atg13 recruitment of Atg17 activates Atg1 by autophosphorylation at Thr266 residue (Yeh et al., 2010). Although there is much similarity in the molecular machinery of autophagy in yeast and mammalian cells, Atg17 recruitment of Atg13 at the PAS is an aspect of the mechanism that is specific to yeast (Suzuki et al., 2007). There is also no Atg101 (mammalian) homologue in the yeast autophagy machinery. In yeast, Atg29 and Atg31 may provide homologous function to mammalian Atg101 (Noda and Fujioka, 2015). This project will focus on autophagy in mammalian cells, which is generally regulated by core pathways homologous to these yeast systems.

### 1.2.1.2 MTOR is the master regulator of autophagy initiation via its nutrient sensing mechanisms

MTOR is a serine/threonine protein kinase known as the mechanistic target of rapamycin. MTOR is made up of five domains: 1) The Huntington, Elongation factor 3, A subunit of protein phosphatase 2A (PP2A) and TOR1 (HEAT) repeat; 2) FRAP-ATM-TTRAP (FAT) domain; 3) FKBP12-Rapamycin binding (FRB) domain; 4) a catalytic kinase domain; and 5) a FAT domain at C terminus (FATC) domain. MTOR is linked to the discovery of rapamycin as an antifungal, anti-tumour and immunosuppressant agent (Vezina et al., 1975, Martel et al., 1977, Eng et al., 1984). Subsequently, MTOR was identified as the mammalian/yeast target of rapamycin after it was reported that rapamycin inhibits cell proliferation and cell growth by forming a complex with FKBP12 to negatively regulate MTOR (Chung et al., 1992, Brown et al., 1994, Sabatini et al., 1994, Sabers et al., 1995, Heitman et al., 1991). MTOR belongs to the PI3K-related kinase (PIKK) family of protein kinases and can form two structurally distinct complexes with other proteins as either MTOR-complex-1 (MTORC1) or complex-2 (MTORC2). In addition to their structural differences, MTORC1 and MTORC2 also have distinct overall functions. For example, MTORC1 controls protein synthesis, growth, cellular metabolism and autophagy while MTORC2 primarily regulates cell proliferation and cell survival (Saxton and Sabatini, 2017).

MTORC1 is made up of regulatory associated protein (Raptor) (Hara et al., 2002), DEP domain-containing MTOR-interacting protein (DEPTOR) (Peterson et al., 2009),

mammalian lethal with SEC13 protein 8 (mLST8) (Kim et al., 2002), proline-rich AKT substrate of 40kDa (PRAS40) (Sancak et al., 2007), tel2 and Tti1 (Kaizuka et al., 2010) (**Fig 1.2A**). In addition, Ras homologue enriched in brain (Rheb) also binds MTORC1 and this interaction is also required for MTORC1 localization and function (Long et al., 2005). MTOR, Raptor, DEPTOR and mLST8 represent the core members of the MTORC1, and each member has a distinct role in the regulation of MTORC1 activity. For example, Raptor stabilizes and recruits MTORC1 substrates by binding to their TOR signalling motif while DEPTOR negatively regulates MTORC1 by binding directly to MTOR at the C-terminal sequence upstream of the MTOR kinase domain (Aylett et al., 2016, Peterson et al., 2009, Nojima et al., 2003). mLST8 is a positive regulator of MTORC1 where it binds to the catalytic unit and stabilizes the kinase activation loop (Yang et al., 2013a). PRAS40 binds indirectly to MTOR via Raptor leading to the inhibition of MTOR kinase activity (Wang et al., 2007). In this way, PRAS40 coordinates the presence of growth factors to MTORC1 by negatively regulating the complex (Vander Haar et al., 2007). This inhibitory role on MTORC1 is blocked via the direct phosphorylation of PRAS40 at Thr246 by Akt in the presence of growth factors, thereby, activating MTORC1 (Vander Haar et al., 2007, Kovacina et al., 2003).

MTORC2 also includes core binding members DEPTOR and mLST8 (**Fig 1.2B**). However, the core complex also binds distinct proteins such as mammalian stress-activated protein kinase-interacting protein (mSin1) (Yang et al., 2006), Raptor-independent companion of MTOR (RICTOR) (Sarbasov et al., 2004) and Protein observed with Rictor-1/2 (Protor1/2) (Pearce et al., 2007). In contrast to MTORC1 which is responsive to rapamycin inhibition through FKBP12, MTORC2 only responds to longer time-point rapamycin treatment (Sarbasov et al., 2006, Lamming et al., 2012). This project will focus on MTORC1 due to its roles in the regulation of autophagy and nutrient sensing.

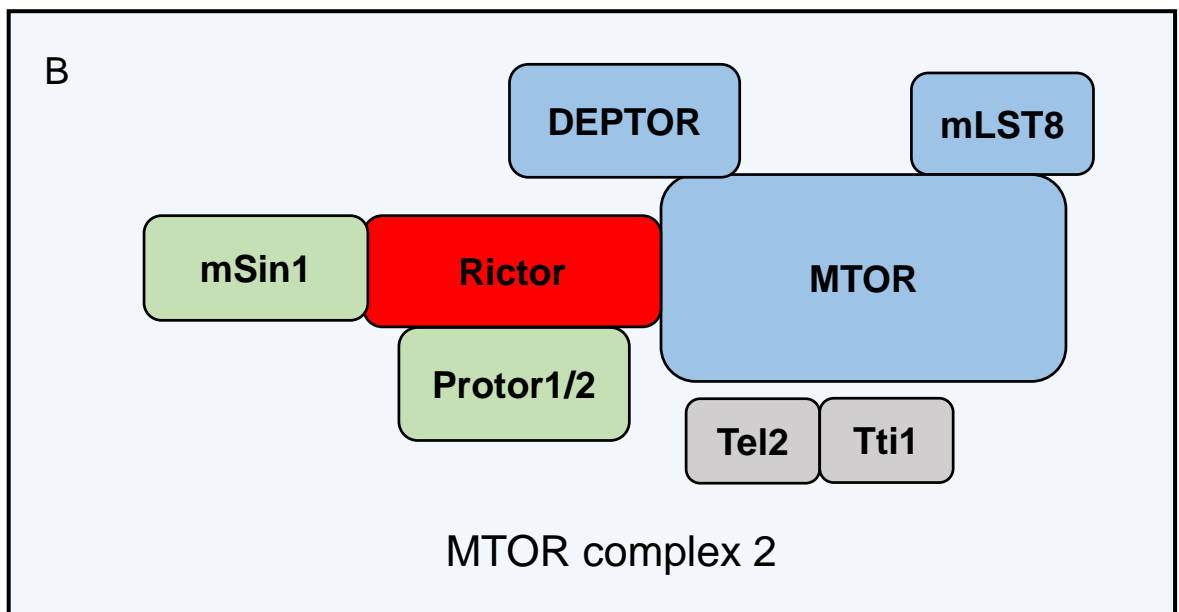
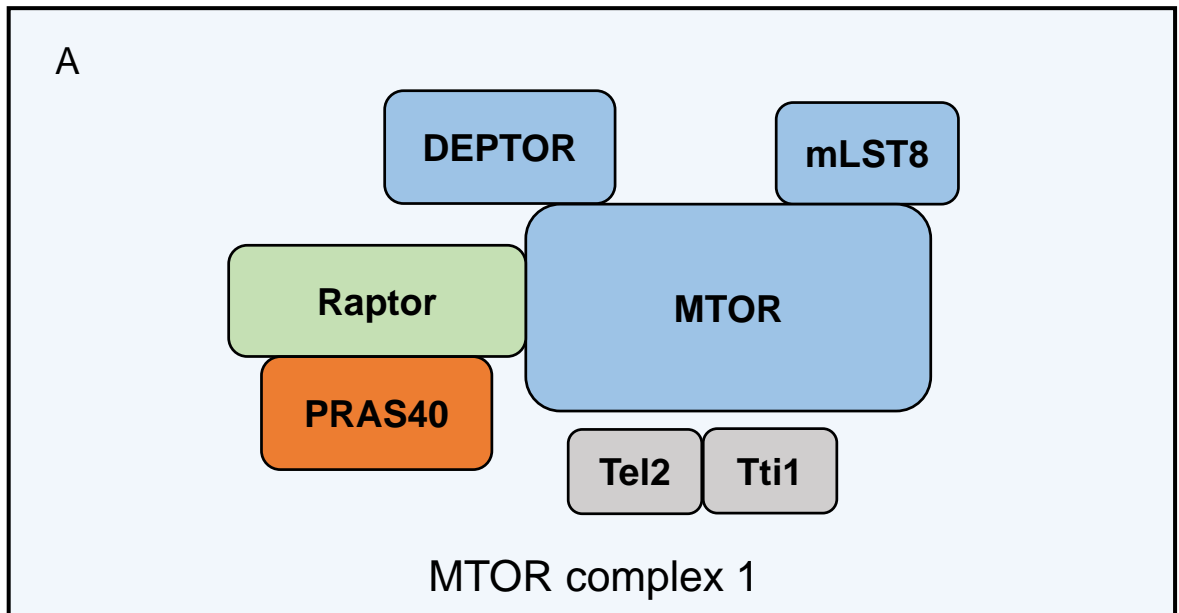


**Figure 1.2: MTOR and its binding partners.** The core MTOR complex members are MTOR, mLST8 and DEPTOR. The other binding members of complex 1 are A) Raptor, PRAS40, Tel2 and Tti1. DEPTOR and PRAS40 serve as a negative regulator of MTOR. DEPTOR binds directly to MTOR at the C-terminal sequence upstream of MTOR kinase domain. PRAS40 binds indirectly to MTOR via Raptor leading to the inhibition of MTOR kinase activity. Other members of complex 2 are B) Rictor, mSin1, Protor1/2 and also Tel2 and Tti1.

### 1.2.1.2A MTORC1 senses growth factors via multiple mechanisms

Cells coordinate a network of inter-dependent mechanisms for the intake of extracellular nutrients and subsequent sensing to control proliferation and cellular metabolism. Specific receptors are embedded in the plasma membrane to detect nutrients such as growth factors, hormones, neurotransmitters, and amino acids, (Mortimore and Poso, 1986). These receptors relay extracellular conditions to the cell by activating multiple downstream signal transduction such as the PI3K signalling cascade and the Ras-signalling cascade. These mechanisms indirectly converge on MTORC1 which in turn coordinates cellular processes such as autophagy and cell growth (Laplante and Sabatini, 2012, Saxton and Sabatini, 2017, Kim and Guan, 2019, Jia and Bonifacino, 2019).

MTORC1 senses the availability of insulin via the tumour suppressor protein Tuberous Sclerosis complex (TSC), which is a heterodimer complex consisting of TSC1, TSC2 and TBC1D7 (Dibble et al., 2012) (**Fig 1.3A**). Mechanistically, TSC1 acts as the scaffold maintaining the stability of the complex while TSC2 functions as the main GTPase binding and activating protein (GAP). Mutations in TSC2 have been implicated in the pathogenesis of tuberous sclerosis (Cheadle et al., 2000). TSC serves as an intermediate linking PI3K and PDK1/Akt pathway to Rheb and MTORC1 activity (Manning et al., 2002, Inoki et al., 2002, Garami et al., 2003, Menon et al., 2014, Potter et al., 2002).

At the lysosome, TSC negatively regulates Rheb-MTORC1 by binding to Rheb loaded with GTP. This binding induces hydrolysis of GTP and a resulting conformational change on Rheb. Thereby TSC primarily controls the GDP/GTP loading status of Rheb. Rheb-GTP (active form) interacts with MTORC1 and this binding promotes the full activation of MTORC1 at the lysosome (Long et al., 2005). A more recent cryo-electron microscopy study demonstrated that Rheb induces a conformational change in MTORC1 which leads to repositioning in the active site, thereby enhancing catalysis (Yang et al., 2017).

TSC also can regulate MTORC1 via additional mechanisms (**Fig 1.3A**). For example, Wnt inhibits glycogen synthase kinase 3 (GSK3) $\beta$ -dependent activation of TSC2. In this way, Wnt can inhibit TSC2 leading to the activation of Rheb-MTORC1 (Inoki et al., 2006). Similarly, TNF $\alpha$  activates IKK $\beta$ -dependent inhibition of TSC1, thereby, enhancing Rheb-MTORC1 activation (Lee et al., 2007). The epidermal growth factor receptor (EGFR) (Ras-dependent) signalling pathway activates MTORC1-Rheb through mitogen-activated protein kinase (MEK/MAP2K). MEK activates extracellular

signal-regulated kinase (ERK)-dependent inhibition of TSC2 or 90kDa ribosomal protein S6K (RSK)-dependent inhibition of TSC2 (Ma et al., 2005, Roux et al., 2004). These two MEK-dependent regulations lead to the activation of MTORC1.

Akt remains one of the better-characterised mechanisms upstream of MTORC1. In the presence of insulin or growth factors, Akt phosphorylates TSC2 at multiple sites such as S939 or T1462 (Menon et al., 2014, Inoki et al., 2002, Manning et al., 2002, Potter et al., 2002). The phosphorylation of TSC2 disrupts its lysosomal localization leading to the inhibition and dissociation from Rheb, hence enhancing MTORC1-Rheb activity (Menon et al., 2014) (**Fig 1.3B**). Similarly, Akt also directly regulates MTORC1 activity independently of the TSC-Rheb mechanism. In insulin-rich conditions, Akt phosphorylates PRAS40 at T246 and inhibits PRAS40-dependent inhibition of MTORC1, leading to MTORC1 activation (Sancak et al., 2007, Vander Haar et al., 2007, Kovacina et al., 2003). Interestingly, PRAS40 is also a substrate of MTORC1 where it is phosphorylated at S183 and S221 (Wang et al., 2008, Oshiro et al., 2007). PRAS40 phosphorylation weakens its interaction with MTORC1 while promoting binding to 14-3-3 chaperone proteins (Dubois et al., 2009, Sancak et al., 2007). The regulation of TSC2 and PRAS40 by Akt together provides parallel signalling routes linking growth factor signal to MTORC1.

In low growth factor conditions, Rheb and MTORC1 remain inactive, therefore promoting autophagy (**Fig 1.3C**). In addition to the PI3K-Akt mechanism that links growth factors to autophagy via PRAS40 and TSC2 (described above), there are other parallel Akt-independent pathways controlling autophagy. Growth factor deprivation has been shown to induce autophagy via the activation of GSK3 (Lum et al., 2005, Lin et al., 2012). While GSK3 $\beta$  activation can lead to MTORC1 inhibition and autophagy via activation of TSC2, GSK3 can also phosphorylate acetyltransferase HIV-1 Tat interactive protein, 60 kD (TIP60) on S86 (Lin et al., 2012). It was shown that phosphorylated-TIP60 had a strong binding affinity with Ulk1 which leads to the acetylation and activation of Ulk1. The activation of Ulk1 (Atg1 homologue) generally promotes the induction of autophagy as described in section 1.2.1.3 below.

The inhibition of Akt also mediates the synthesis of core autophagy proteins to further enhance autophagy during growth factor deprivation. The inhibition of Akt terminates the phosphorylation and inhibition of forkhead box O3 transcription factor (FOXO3) (Brunet et al., 1999). Upon activation, FOXO3 also promotes the expression of LC3B which functions in the biogenesis of autophagosomes downstream of MTORC1 inhibition. However, FOXO3-dependent autophagy can also occur independently of

MTORC1 (Mammucari et al., 2007, Sengupta et al., 2009). Interestingly, the growth factor-dependent regulation of MTORC1 is distinct from the amino acid-sensing mechanism, however, both contribute (Demetriades et al., 2014). For example, it was recently reported that the presence of arginine enhances MTORC1 ability to respond to growth factors (Carroll et al., 2016a). Arginine represses the localization of TSC to the lysosomal membrane, thereby, reducing Rheb-TSC2 interaction, further activating MTORC1. The regulation of MTORC1 by the above mechanisms coordinates the progression of autophagy during limited growth factors.

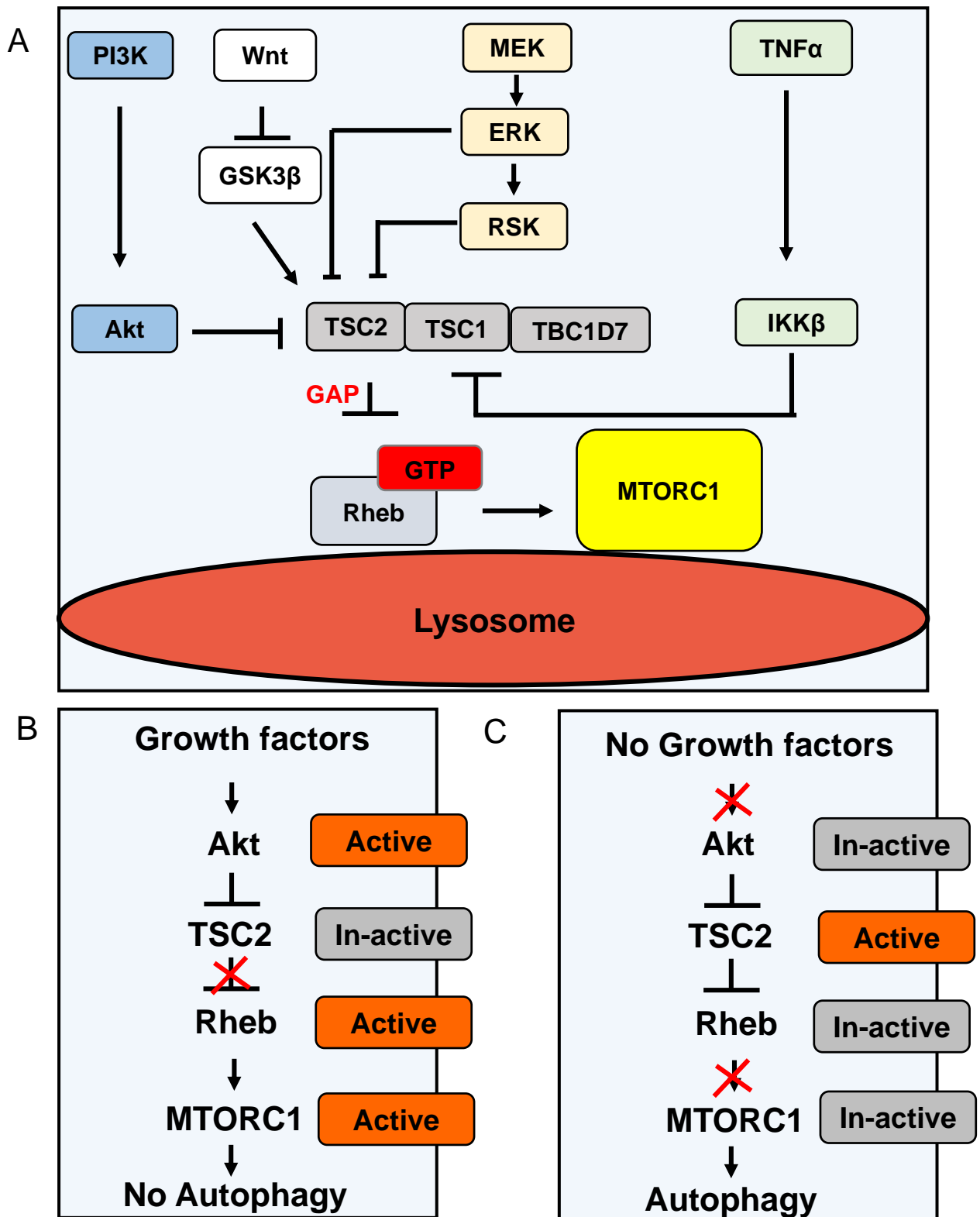


**Figure 1.3: The regulation of MTORC1 by growth factors.** A) The multiple signalling pathways that converge on MTORC1 via the regulation of the TSC2 complex. PI3K activates Akt which leads to the inhibition of TSC2. This abrogates TSC2 inhibition of Rheb at the lysosome thus allowing MTORC1 recruitment and activation. Wnt can also inhibit GSK3 $\beta$  activation of TSC2. MEK and TNF $\alpha$  also indirectly activate MTORC1 by activating ERK and IKK $\alpha$  respectively which both serve as repressors of the TSC complex. B) shows the regulatory state of Akt, TSC2, Rheb and MTORC1 when growth factors are available and autophagy is blocked. C) shows their regulatory status when growth factors are not available and autophagy is activated.

### 1.2.1.2B MTORC1 senses amino acid through Rag-dependent and Rag-independent mechanisms

A balanced mixture of amino acids is a key prerequisite for protein synthesis, and as such, it is important for a cell to readily sense their availability (van Venrooij et al., 1972). There are currently 22 known naturally proteinogenic amino acids (although only 20 commonly used in eukaryotic cells), characterized into two main groups: essential amino acids and non-essential amino acids (**Fig 1.4**). Essential amino acids, by definition, must be supplied exogenously primarily through nutrients from food because mammalian cells cannot synthesize them. In contrast, non-essential amino acids are readily synthesized in cells in sufficient amounts from metabolic precursors. Amino acids are also characterised based on their structure, charge and organic content. For example, leucine is an essential amino acid, characterized by its hydrophobic branched-chain R-group (side-chain). On the other hand, glutamine is a polar, neutral charged, non-essential amino acid. Arginine, a non-essential amino acid and in neutral pH, is positively charged. Apart from their biochemical roles in protein synthesis, leucine, glutamine and arginine have also gained attention due to their function during nutrient-sensing signalling.

Recent studies have begun to unravel the mechanisms linking amino acid sensing to key cellular processes such as autophagy. In mammalian cells, leucine, glutamine and arginine are sensed by parallel pathways in a MTORC1-dependent manner involving either Rag-dependent or independent mechanisms (Zhang et al., 2002, Abraham, 2015, Shimobayashi and Hall, 2016). This project will focus on how MTORC1 senses the availability of amino acids and the effects on autophagy and mitochondrial processes.

To begin, the extracellular pool of amino acids is transported into the cell by an array of amino acid transporters embedded in the plasma membrane (Porcelli et al., 2014, Palmieri, 2013, Taylor, 2014, Hyde et al., 2003). These mechanisms are driven by the solute-linked carrier (SLC) family of transporters that generally serve to shuttle small molecules such as vitamins, metabolites, inorganic/metal ions and neurotransmitters into cells and organelles. There are over 430 SLC members characterized by the HUGO gene nomenclature committee encoded by 400 genes in humans (César-Razquin et al., 2015, Perland and Fredriksson, 2017). In parallel with the transport of amino acids into cells, amino acids are sensed in the cytosol and from within the lysosome via an inside-out mechanism (as further discussed, below) (Zoncu et al., 2011). This project focuses majorly on: leucine, glutamine and arginine, which are the

3 regulatory amino acids potently sensed upstream of MTORC1 (Chantranupong et al., 2016, Saxton et al., 2016a, Wolfson et al., 2016). In addition, a sensor for methionine upstream of MTORC1 was recently identified (Gu et al., 2017).

Essential AA	Non-essential AA
Leucine (L)	Arginine (R)
Methionine (M)	Glutamine (Q)
Isoleucine (I)	Tyrosine (Y)
Lysine (K)	Glutamate (E)
Phenylalanine (F)	Serine (S)
Threonine (T)	Proline (P)
Valine (V)	Asparagine (N)
Tryptophan (W)	Histidine (H)
--	Glycine (G)
--	Aspartate (D)
--	Alanine (A)
--	Cysteine (C)
--	Selenocysteine (U)
--	Pyrrolysine (O)

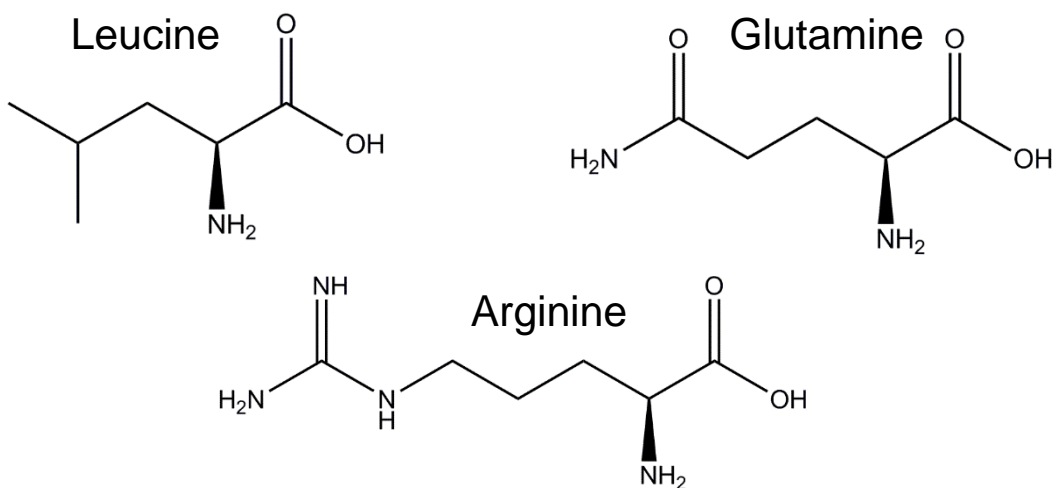


**Figure 1.4: Amino acids and the structure of L, Q and R.** The list of 22 amino acids grouped into essential and non essential amino acids. In red, are the amino acids that are specifically sensed by MTORC1. Subset shows the biochemical structure of Leucine, Glutamine and Arginine.

### 1.2.1.2B.1 Regulation of Rag-dependent MTOR signalling

Amino acids such as arginine and leucine regulate MTORC1 via a Rag-complex that includes Rag GTPases, Ragulator, KICSTOR, lysosomal H<sup>+</sup>-ATPase (v-ATPase) and SLC38A9 at the lysosome (**Fig 1.5A**). Each of these proteins has a distinct mechanistic role in the activation of MTORC1 by amino acid.

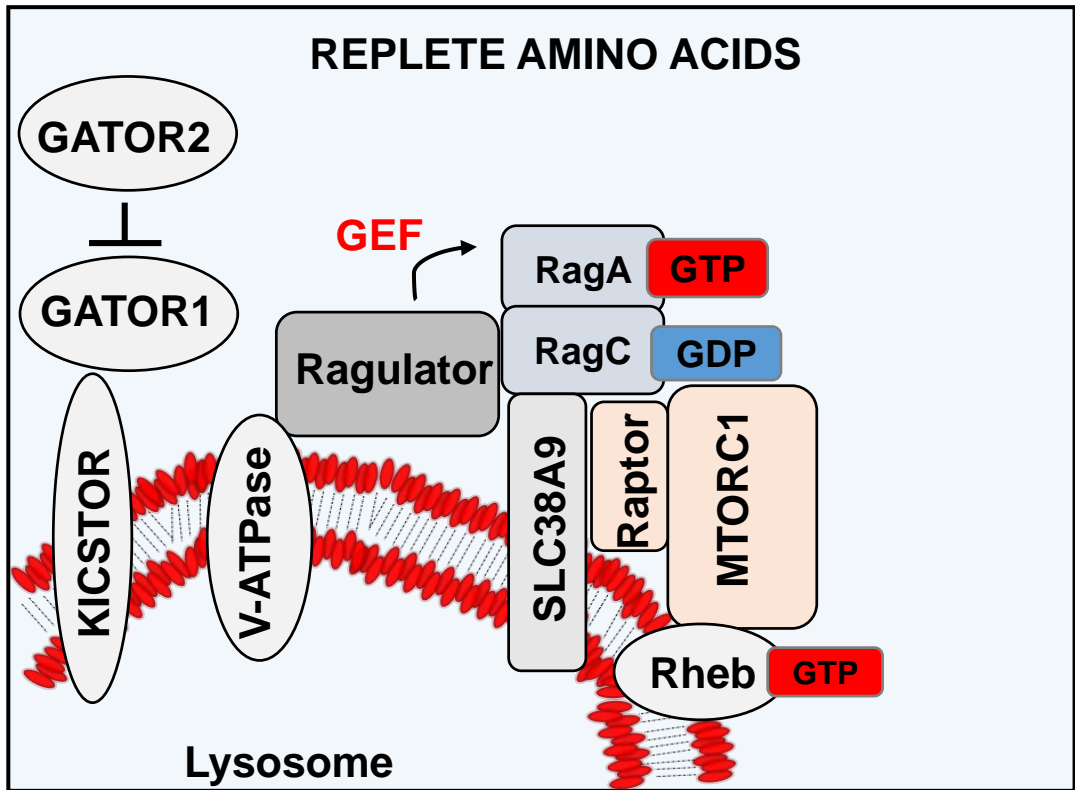
The Rag GTPases are comprised of members Rag A, B, C and D, and these form heterodimers in which Rag A (or RagB) binds RagC (or RagD). In the active state, RagA/B is GTP loaded while RagC/D is GDP bound, and this conformation is required for MTORC1 localization and activation. The activated RagA/B binds MTORC1 via Raptor, recruiting the complex to the lysosome membrane (Kim et al., 2008, Sancak et al., 2008, Gong et al., 2011). Furthermore, the Rag heterodimer maintains lysosomal anchorage by interacting with the Ragulator complex (a pentameric protein consisting of p18, p14, MP1, c7orf59, and HBXIP also termed LAMTOR 1, 2, 3, 4 and 5 respectively), in a vATPase dependent manner (Sancak et al., 2010, Zoncu et al., 2011, Bar-Peled et al., 2012, Rasheed et al., 2019). Initially, studies suggested that Ragulator functions as the guanine exchange factor (GEF) towards RagA/B by promoting a RagA/B GTP-activated state that stimulates MTORC1 localization and activity (Bar-Peled et al., 2013, Bar-Peled et al., 2012). However, recent findings that GTP readily dissociates from RagC due to Ragulator-dependent opening of RagC nucleotide-binding pocket suggest that the Ragulator also has a non-canonical GEF function on RagC (Shen and Sabatini, 2018).

Moreover, KICSTOR recruits GATOR1, a member of the GATOR complex and a negative regulator MTORC1 (Wolfson et al., 2017, Peng et al., 2017). The GATOR complex is composed of GATOR 1 (DEPDC5, NPRL2 and NPRL3) and GATOR 2 (MIOS, WDR24, WDR59, SEH1L and SEC13) (Bar-Peled et al., 2013). GATOR1 inhibits RagA/B-dependent recruitment and activation of MTORC1 by serving as a GAP towards RagA/B (promoting the inactive RagA/B GDP state), and this is mediated via the Arg-78 residue of GATOR1 subunit (Neinast et al., 2019, Shen et al., 2019, Shen et al., 2018). In contrast, GATOR2 serves as the negative regulator of GATOR1 and therefore, a positive regulator of MTORC1. GATOR1 and GATOR2 both connect amino acid sensors to the control of Rag and MTORC1 activation.

Overall, the presence of amino acid promotes GATOR2 inhibition of GATOR1, suppressing GATOR1 function for MTORC1-inhibition. In the presence of amino acids, RagA/B is in an active state due to the binding of GTP. This active state promotes the recruitment of MTORC1 to the lysosome and then its activation (**Fig**

**1.5A).** Upon amino acid starvation, this conformation changes to RagA/B-GDP due to the inhibition of GATOR2 and the activation of GATOR1. The activation of GATOR1 promotes its GAP activity towards RagA/B, thereby, leading to MTORC1 dislodgement from the lysosome and its inhibition (**Fig 1.5B**). Further details are discussed below on how sensing of specific amino acid feeds into the Rag-MTORC1 mechanism.

A



B

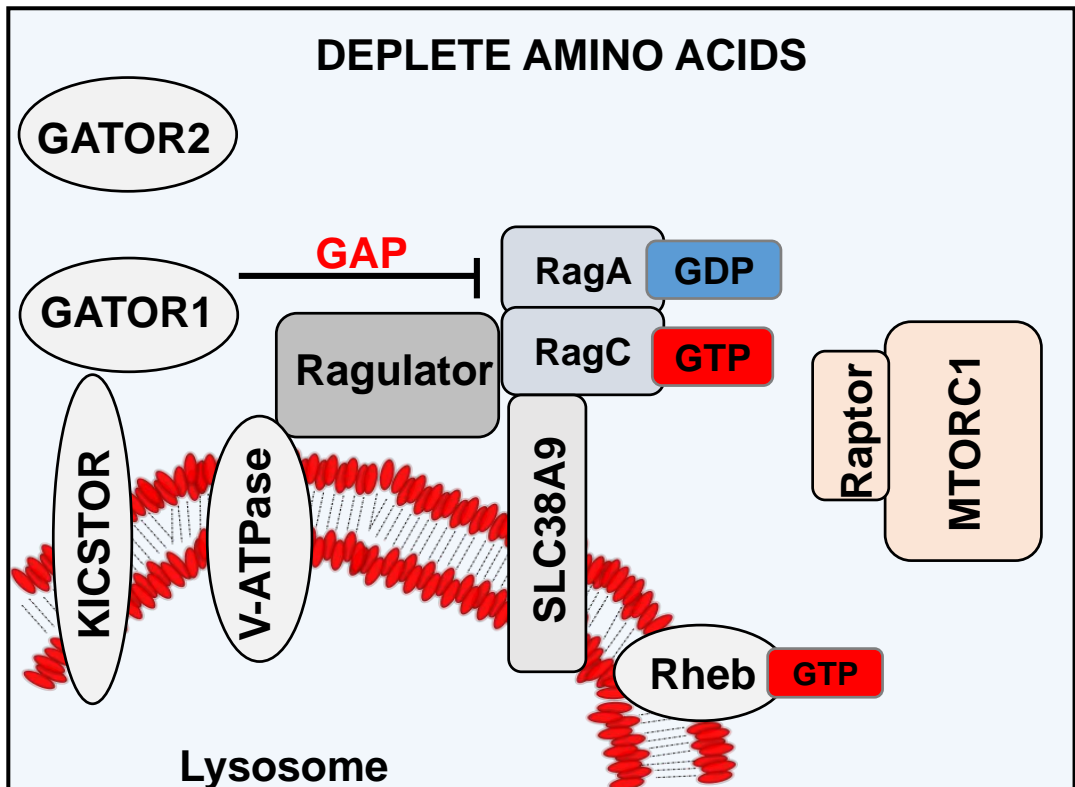


**Figure 1.5: The regulation of MTORC1 at the lysosome by amino acids.** Multiple protein complexes are localised at the lysosome where they play important roles in amino acid sensing A) In the presence of amino acids, GATOR2 is active and GATOR1 is inhibited. This allows Ragulator to serve as GEF for RagA. The RagA-GTP state promotes MTORC1 activity and its recruitment to the lysosome. KICSTOR stabilizes GATOR1 while vATPase, SLC38A9 and Rheb are embedded in the lysosome and are required for MTORC1 activation. B) In the absence of amino acids, GATOR2 is inactive while GATOR1 is active. GATOR1 serve as the GAP for RagA conversion to a GDP state. This leads to the inhibition of MTORC1 and its delocalization from the lysosome.

### 1.2.1.2B.2 Arginine transport and sensing

Extracellular arginine is shuttled into cells by the SLC7 family which are generally cationic transporters (CAT) and include SLC7A1 (CAT-A), SLC7A2A (CAT-2A), SLC7A2B (CAT-2B) and SLC7A3 (CAT-3) (Closs et al., 2006). 4F2hc/y+LAT2 heterodimer also serves as another arginine uptake mechanism into cells (Broer et al., 2000). Once inside, arginine is sensed by two mechanisms within the cell.

SLC38A9 senses arginine from within the lysosomal lumen, therefore, bypassing the GATOR2 and GATOR1 pathway (Rebsamen et al., 2015, Wang et al., 2015). The SLC38A9 protein was identified by mass spectrophotometry after it precipitated with the Ragulator, RagA and RagC protein complex. Structural studies showed that SLC38A9 is embedded in the lysosomal membrane in a manner where the N-terminus is facing the cytosol and its C-terminus protrudes into the lysosomal lumen (Lei et al., 2018). SLC38A9 binds the Rag-Ragulator complex with its N-terminal domain and its overexpression sufficiently activates MTORC1 independently of amino acids (Rebsamen et al., 2015, Wang et al., 2015). At the lysosome, SLC38A9 functions as an amino acid transporter for the efflux of essential amino acids and also an arginine sensor (Wyant et al., 2017, Jung et al., 2015, Scalise et al., 2019).

The role of SLC38A9 in arginine sensing and MTORC1 regulation was shown in SLC38A9-depleted HEK-293T cells after it was observed that MTORC1 did not phosphorylate its downstream substrates when amino acids were present (Wang et al., 2015). SLC38A9 was also shown to have a high preference for arginine binding (Jung et al., 2015). It is suggested that the binding of arginine to SLC38A9 leads to a conformational change that promotes the interaction of SLC38A9 with Rag-GTPases (Shen and Sabatini, 2018). Furthermore, SLC38A9 binds strongly with RagA/B loaded with GDP and its ability to activate MTORC1 was suggested to depend on Ragulator-GEF activity on RagGTPases. Affinity and kinetic studies revealed that both Ragulator and SLC38A9 have distinct but parallel GEF roles in activating Rag-GTPases in response to arginine binding (Shen and Sabatini, 2018). Shen and Sabatini (2018) showed that SLC38A9 promoted the release of GDP from RagA in the presence of arginine, thereby, stimulating the binding of GTP to RagA. In contrast, Ragulator stimulates the release of GTP from RagC, thereby, both SLC38A9 and Ragulator promote the activated-Rag conformations required for MTORC1 activation thus serving as a mechanism for sensing arginine levels within the lysosome.

Alternatively, arginine is also sensed at the cytosol by cellular arginine sensor for MTORC1 protein 1 (CASTOR1) (Chantranupong et al., 2016, Saxton et al., 2016a). CASTOR1/2 was identified in a protein-protein interaction screen which was pulled down with GATOR2. Although CASTOR1 has a 63% sequence similarity with CASTOR2 and are both able to bind three subunits of GATOR2, only CASTOR1 exclusively binds arginine. CASTOR1 has four tandem ACT domains (ACT1, ACT2, ACT3, ACT4) and it binds arginine via a narrow pocket at the interphase of ACT2 and ACT4 (Saxton et al., 2016a). It has been proposed that the binding of arginine to CASTOR1 induces a conformational change leading to an intramolecular interaction of ACT2 and ACT4 domain. This conformational change rearranges the residues required for CASTOR1 and GATOR2 interaction therefore blocking their binding. The inability of CASTOR1 to bind GATOR2 activates GATOR2 inhibitory role on GATOR1 which leads to MTORC1 activation. Therefore, in the absence of arginine, CASTOR1/2 binds and inhibits GATOR2 upstream of MTORC1. However, in rich arginine conditions, arginine directly binds CASTOR1 (disrupts CASTOR1-GATOR2 binding) leading to the activation of GATOR2 hence activating MTORC1.

### **1.2.1.2B.3 Leucine transport and sensing**

Leucine is transported into the cells by a neutral amino acid carrier; L-type transporter belonging to the family (LAT1-4). This includes SLC7A5 (LAT1), SLC7A8 (LAT2), SLC43A1 (LAT3) and SLC43A2 (LAT4) (Wang and Holst, 2015). As one mechanism, it has been suggested that leucyl-tRNA synthetase (LRS) can sense intracellular levels of leucine via its interaction with Rag GTPase where it functions as a GAP for RagD (Han et al., 2012, Lee et al., 2018). In the presence of leucine, LRS activates MTORC1 by inducing the hydrolysis of RagC/D leading to its activation. LRS also induce leucylation (addition of leucine) of RagA on Lys142 which leads to the activation of MTORC1 (He et al., 2018). Interestingly, it was recently reported that leucine is sensed through its metabolic product acetyl-CoA (Son et al., 2019). In leucine-rich conditions, acetyl-CoA level increases leading to the acetylation of RAPTOR at K1097 by E1A-associated protein p300 acetyltransferase (EP300), therefore, activating MTORC1.

In addition, leucine can interact with Sestrin2 in the cytosol to signal into the GATOR1/2 pathway (Wolfson et al., 2016). Sestrins are conserved to the family of stress-inducible proteins and were originally shown to regulate cellular homeostasis during stress conditions (Chen et al., 2019a). Sestrins have three isoforms (Sestrin1, Sestrin2, Sestrin3), and structural studies have shown that Sestrin2 has two

functionally-distinct globular subdomains (The N-terminal and C-terminal domain) (Kim et al., 2015). Sestrins was identified as amino acid-sensing modulators after they precipitated with GATOR2 after studies initially reported that it inhibits MTORC1 (Chantranupong et al., 2014, Budanov and Karin, 2008, Parmigiani et al., 2014). Further studies on the roles of Sestrins in amino acid sensing revealed that during amino acid deprivation, Sestrin binds tightly to GATOR2, leading to the inhibition of GATOR2 (Chantranupong et al., 2014, Wolfson et al., 2016). The Sestrin-dependent inhibition of GATOR2 was also shown to occur upstream of MTORC1 after it was observed that the knockdown of Sestrin rescued the activation of MTORC1 during amino acid starvation. In contrast, the overexpression of Sestrin2 was shown to prevent MTORC1 localization to the lysosome, thereby, leading to MTORC1 inhibition.

Further studies confirmed Sestrin2-negative regulation of MTORC1, and its specificity for leucine-binding was identified. It was reported that cells expressing mutated-Sestrin2 that were unable to bind leucine did not sense the availability of leucine, thereby leading to the inhibition of MTORC1 by GATOR1 (Wolfson et al., 2016). Wolfson et al, (2016) also observed that Sestrin2 binds to leucine with an affinity of approximately 20 $\mu$ M which resulted in the destabilization of Sestrin2-GATOR2 binding thus promoting GATOR2 activation. Although it is suggested that Sestrin2 binds leucine via a single pocket at the intersections of helices C2, C3 and C7 in the C-terminal domain which leads to a thermal shift that increases its melting point, it is not clear whether this binding induces a conformational change on Sestrin2 that leads to a reduced interaction with GATOR2 (Saxton et al., 2016b, Wolfson et al., 2016). However, the current model stipulates that in the presence of leucine, Sestrin2 detaches from GATOR2, thus allowing GATOR2 to block GATOR1-dependent inhibition of MTORC1 (Saxton et al., 2016b, Chantranupong et al., 2014, Parmigiani et al., 2014). The inhibition of GATOR1 promotes the activation of RagA/B, further enhancing MTORC1 activity.

#### **1.2.1.2B.4 Glutamine transport and sensing**

Glutamine import into cells occur via multiple mechanisms but it is primarily transported in by a group of symporters and antiporters from families SLC1, SLC6, SLC7 and SLC38. They include SLC1A5 (ASCT2), SLC6A19 (BOAT1), SLC6A14 (ATBO), SLC7A5 (LAT1) and SLC38A1, 2 (SNAT1, 2) and SLC38A3, 5, 7 (SNAT3, 5, 7) (Scalise et al., 2017, Bhutia and Ganapathy, 2016). The antiporters SLC1A5 and SLC7A5 transport glutamine via a bi-directional amino acid exchange mechanism.

For example, the efflux of glutamine for leucine import at the plasma membrane by heterodimer SLC7A5/SLC3A2 is required for MTORC1 activation (Nicklin et al., 2009). Although it is not totally clear how these mechanisms are coordinated, the MTORC1-dependent sensing of cytosolic glutamine has been shown to occur in a Rag-independent manner, in contrast to leucine and arginine (Jewell et al., 2015).

Glutamine is sensed at the cytosol independently of RagA-dependent MTORC1 activation. For example, glutamine still led to the activation and localization of MTORC1 to lysosomal membranes in RagA/B double knockout MEF, while arginine and leucine-dependent MTORC1 activation were abrogated (Jewell et al., 2015). However, glutamine-dependent activation of MTORC1 requires v-ATPase and the Golgi-localized ADP ribosylation factor 1 (Arf1) GTPase. Arf1 was first linked to the regulation of MTORC1 in *Drosophila* studies after RNAi screens for GTPases that regulates MTORC1 identified Arf1 as a putative regulator of MTORC1. It was observed that the depletion and inhibition of Arf1 led to the inhibition of MTORC1 (Li et al., 2010). Li et al, (2010) also showed that the knockdown of Arf1 sufficiently induced autophagy. Similarly, it was observed that inhibition or siRNA-mediated knockdown of Arf1 in RagA/B KO cells blocked glutamine-dependent activation of MTORC1 (Jewell et al., 2015). Arf1 was shown to promote the localization of MTORC1 to the lysosomes. However, upon forced-lysosomal localization of MTORC1, Arf1 did not have any effect. This observation led to the conclusion that Arf1 signals glutamine availability to MTORC1 which leads to the translocation of MTORC1 to the lysosome, where it is activated.

MTORC1 is also suggested to be regulated by metabolites synthesised during glutaminolysis (Duran et al., 2012). During glutaminolysis, glutamine is metabolized to glutamate. Leucine binds and activates glutamate dehydrogenase (GDH) which further converts glutamate to alpha-ketoglutarate by deamination (Carobbio et al., 2009). It was observed that the inhibition of glutaminolysis in the presence of glutamine and leucine blocked RagB GTP-activated state which prevented the recruitment of MTORC1 to the lysosomes (Duran et al., 2012). Interestingly, it was also observed that supplementation of alpha-ketoglutarate stimulated MTORC1 lysosomal localization and activation. Due to the roles of mitochondria in the metabolism of glutamine and leucine (Wang et al., 2019a) (where they utilise glutaminase (GLS) and GDH to produce glutamate and alpha-ketoglutarate, respectively), a possible mitochondrial role in amino acid sensing is suggested.

### **1.2.1.2B.5 Methionine transport and sensing**

Similar to leucine intracellular import, methionine is imported by L-type amino acid transporter 1 SLC7A5 (LAT1) (Kanai et al., 1998, Christensen, 1990). The sensor of intracellular methionine was recently identified as a previously-uncharacterised protein termed SAMTOR by Gu et al (2017). SAMTOR was originally identified as an interacting protein of KICSTOR or GATOR1 as it co-immunoprecipitated with components of GATOR1 and KICSTOR. However, SAMTOR interaction with GATOR1 is dependent on the co-expression of KICSTOR. SAMTOR bypasses GATOR2 by directly activating GATOR1 in the absence of S-adenosylmethionine (SAM), a direct metabolite synthesised from methionine.

The sequence analysis of SAMTOR revealed that it contains domains that have a high binding affinity for SAM. Interestingly, binding assays also showed that SAMTOR binds the de-methylated form of SAM, S-adenosylhomocysteine. In the presence of methionine, SAM binds to SAMTOR leading to the destabilization of SAMTOR-GATOR1-KICSTOR interaction in both in vitro and in vivo models. This blocks GATOR1-dependent inhibition of MTORC1 thereby activating MTORC1. Interestingly, SAM serves as a major donor for methyl groups during the methylation of nucleic acids and proteins. Although the enzyme driving SAM metabolism is mainly cytosolic, mitochondria are reservoirs of SAM where it is metabolised to S-adenosylhomocysteine (Farooqui et al., 1983, Horne et al., 1997). This suggests that mitochondrial metabolism of methionine to SAM may be a prerequisite for MTORC1 activation at the lysosome.

### **1.2.1.2B.6 Other amino acid sensing mechanisms**

Multiple modes of transport and sensing mechanisms for amino acid converge onto the regulation of MTORC1, thus highlighting the complexity of amino acid sensing in the regulation of cellular homeostasis. While the above amino acid sensing mechanisms seem to occur simultaneously in the cytosol and the lysosome, yet other MTORC1-dependent general amino acid sensing mechanisms have also been defined. Amino acids are sensed by Folliculin (FLCN) and Folliculin interacting proteins (FNIP) at the lysosomes by communicating amino acid availability to MTORC1 (Tsun et al., 2013). Mechanistically, FLCN-FNIP act as a GAP which regulates the GDP status of RagC/D GTPases. During amino acid starvation, it is suggested that FLCN-FNIP localised to the lysosomes where it binds RagA/B GDP and exhibits its GAP activity on RagC/D GDP leading to MTORC1 inhibition (Meng and Ferguson, 2018, Shen et al., 2017).

Another study reported that amino acids are sensed via a Rab1A GTPase mechanism at the Golgi (Thomas et al., 2014). In this model, amino acid stimulation induces GTP loading on Rab1 which subsequently forms a complex with MTORC1-Rheb on the Golgi apparatus. This interaction activates MTORC1, though, independently of Rag. Upon amino acid starvation, Rab1A is maintained in a GDP state leading to MTORC1 inhibition. Interestingly, Rab1 also plays important roles in the membrane transport between the Golgi, ER, mitochondrial-associated membrane and mitochondria (Barr, 2013, Chae et al., 2018). Overall, these studies highlight a possible multi-organelle mechanism of amino acid sensing that includes the lysosomes, Golgi, ER and mitochondria. Although the lysosome seems to play a well-established role in amino acid sensing, how these organelles coordinate changes in amino acids whether dependently or independently remain unclear. For example, how does the ER, which is highly dependent on changes in amino acids due to protein synthesis, sense amino acids? Also, how do mitochondria sense amino acids that are required as substrates for mitochondrial metabolites?

Nevertheless, it is established that the presence of any regulatory amino acid (glutamine, leucine and arginine) at least in part, sufficiently activates MTORC1 and blocks autophagy (Nwadike et al., 2018, Jewell et al., 2015, Carroll et al., 2016a). Upon amino acid starvation, there is a shortfall in amino acid sensing, hence MTORC1-inhibition. This subsequently leads to the induction of autophagy via the downstream activation of MTORC1 substrates such as Ulk1.

### 1.2.1.3 The Unc-51-like autophagy activating kinase 1 (Ulk1) complex and the regulation of autophagy initiation

Ulk1 (Unc-51-like autophagy activating kinase 1) represents the best characterised mammalian homologue of the yeast Atg1 serine-threonine autophagy protein kinase. Ulk1 has a closely related family member Ulk2 with nearly identical kinase domain at about 78% (Chan and Tooze, 2009). However, three other Ulk homologues have been characterised as Ulk3, Ulk4, and STK36 in mammals, but with less clear functional conservation. Ulk1 appears to play predominant roles in autophagy relative to the other homologues (Chan et al., 2007, Lee and Tournier, 2011), since functional defects have been described in many cell contexts in multiple laboratories due to genetic targeting of Ulk1 alone.

Ulk1 contains an N-terminal kinase domain, a serine and proline-rich spacer domain (S/P spacer) and a C-terminal domain (Tomoda et al., 1999, Kuroyanagi et al., 1998).

The C-terminal domain encodes sequences for Atg13 binding (Chan et al., 2009). It was observed that Ulk1 forms a complex with Atg13, Focal adhesion kinase interacting protein of 200kD (FIP200) and Atg101 (Hara et al., 2008, Chan, 2009, Hosokawa et al., 2009b, Mercer et al., 2009). Subsequently, further details on specific interactions within the complex were revealed. Ulk1 binds Atg13 directly while Atg101 interacts indirectly with Ulk1 through Atg13. Moreover, FIP200 can directly or indirectly (through Atg13) bind to Ulk1. The interaction of Atg13 and FIP200 with Ulk1 is required for the activity and stability of Ulk1 and ultimately critical for autophagy (Ganley et al., 2009, Jung et al., 2009, Hosokawa et al., 2009a). Ulk1 phosphorylates multiple members of the complex; Atg13 (at S318), FIP200 (at S943, S986 and S1323), and Atg101 (at S11 and S203) (Egan et al., 2015, Joo et al., 2011, Jung et al., 2009). Although the role of Ulk1 phosphorylation of Atg13 is associated with the degradation of mitochondria. Furthermore, Atg13 and FIP200 also have distinct Ulk1-independent roles in mitophagy (Zachari et al., 2019). Atg101 phosphorylation sites have not yet been defined.

Ulk1 was identified as a critical regulator of autophagy in mammalian cells in a siRNA screen (Chan et al., 2007). However, initial genetic studies identified its homologue uncoordinated-51 first in *C. elegans* and subsequently the role of Atg1 in autophagy in *Saccharomyces cerevisiae* (Matsuura et al., 1997, Ogura et al., 1994). The structural characterization of Ulk1 has helped develop specific kinase targeting inhibitors (Lazarus et al., 2015, Egan et al., 2015, Petherick et al., 2015). Ulk1 has been shown to have other autophagy-independent roles in ER-to-Golgi trafficking and in axon guidance during mammalian forebrain development (Wang et al., 2018, Joo et al., 2016). However, attention on Ulk1 mechanistic function has generally focussed on roles for early initiation and (more recently) late stages of autophagy (Konno et al., 2013, Ganley et al., 2009).

During autophagy initiation, the Ulk1 complex translocates to autophagy initiating sites at the ER where it phosphorylates and recruits VPS34, Beclin1, Atg14L and VPS15 which all serve as the initial template for early autophagosome formation and are members of the class III phosphatidylinositol 3-kinase PI3K-complex (Karanasios et al., 2016, Russell et al., 2013, Wold et al., 2016, Egan et al., 2015). Upon amino acid starvation, activated Ulk1 phosphorylates Beclin1 at Ser14 leading to the activation of Atg14L-VPS34 complex (Russell et al., 2013). Recently, another Ulk1-phosphorylating site on Beclin1 was identified as Ser30 for which is required for the formation of autophagosomes and effective autophagy flux (Park et al., 2018). Meanwhile, Ulk1 phosphorylates Atg14L at Ser29 to potentiate autophagy induction

during amino acid starvation (Park et al., 2016, Wold et al., 2016). Ulk1 forms puncta at the ER which sometimes are in close proximity to mitochondria (Karanasios et al., 2013, Karanasios et al., 2016, Nishimura et al., 2017). However, the cellular localization of Ulk1 in normal basal conditions is not yet known.

Ulk1 also plays important roles in the termination of autophagy after the protein autophosphorylates and becomes ubiquitinated by KLHL20 leading to the degradation of Ulk1, Atg13, Atg14 and Beclin1 (Liu et al., 2016a). Interestingly, a factor identified as UPS20 deubiquitinates Ulk1 which is essential for the stability of Ulk1 during autophagy induction (Kim et al., 2018). To induce autophagy, Ulk1 receives signals in the form of multiple regulatory phosphorylation events from the upstream nutrient sensors, MTORC1 and AMPK.

#### 1.2.1.4 5'-AMP-activated protein kinase (AMPK) and the regulation of autophagy initiation

The regulatory function of AMPK was initially identified after it was observed that acetyl-CoA carboxylase was phosphorylated and inhibited in an ATP-dependent manner (Carlson and Kim, 1973). Subsequently, AMPK was characterized and identified as a master regulator of glucose metabolism (Munday et al., 1988, Grahame Hardie et al., 1989, Carling et al., 1994). AMPK exist as a heterotrimeric protein complex consisting of a catalytic  $\alpha$  subunit and regulatory  $\beta$  and  $\gamma$  units (Lin and Hardie, 2018). PRKAA1 and PRKAA2 encode the two catalytic alpha subunits  $\alpha$ 1 and  $\alpha$ 2 subunits. PRKAB1 and PRKAB2 encode  $\beta$ 1 and  $\beta$ 2 while PRKAG1, PRKAG2 and PRKAG3 code for the  $\gamma$ 1,  $\gamma$ 2 and  $\gamma$ 3 subunits of AMPK in mammals (Thornton et al., 1998, Cheung et al., 2000). AMPK is a master energy sensor that is activated during energy stress such as glucose starvation with the main aim to maintain metabolic homeostasis that rejuvenates ATP (Hardie, 2007, Hardie and Carling, 1997, Hardie et al., 1998). For example, AMPK coordinates gluconeogenesis, mitochondrial biogenesis, mitochondrial dynamics, lipid metabolism and autophagy by differentially regulating an array of downstream substrate proteins (**Table 1.2**) (Herzig and Shaw, 2018).

**Table 1.2: AMPK-dependent regulation of cellular processes.** AMPK regulates a variety of substrates such as Forkhead box protein O (FOXO) and cAMP response element-binding protein (CREB) during gluconeogenesis, Peroxisome proliferator-activated receptor- $\gamma$  co-activator 1 $\alpha$  (PGC1 $\alpha$ ) during mitochondrial biogenesis, Mitochondrial fission factor (MFF) during mitochondrial dynamics, Acetyl-CoA carboxylase 1/2 (ACC1/2) during lipid metabolism and regulators of autophagy as indicated.

<b>AMPK Substrates</b>	<b>Cellular Process</b>
FOXO, CREB	Gluconeogenesis
PGC1 $\alpha$	Mitochondrial biogenesis
MFF	Mitochondrial dynamics
ACC1/2	Lipid metabolism
Ulk1, Raptor, TSC2, Atg9, Beclin1, VPS34	Autophagy

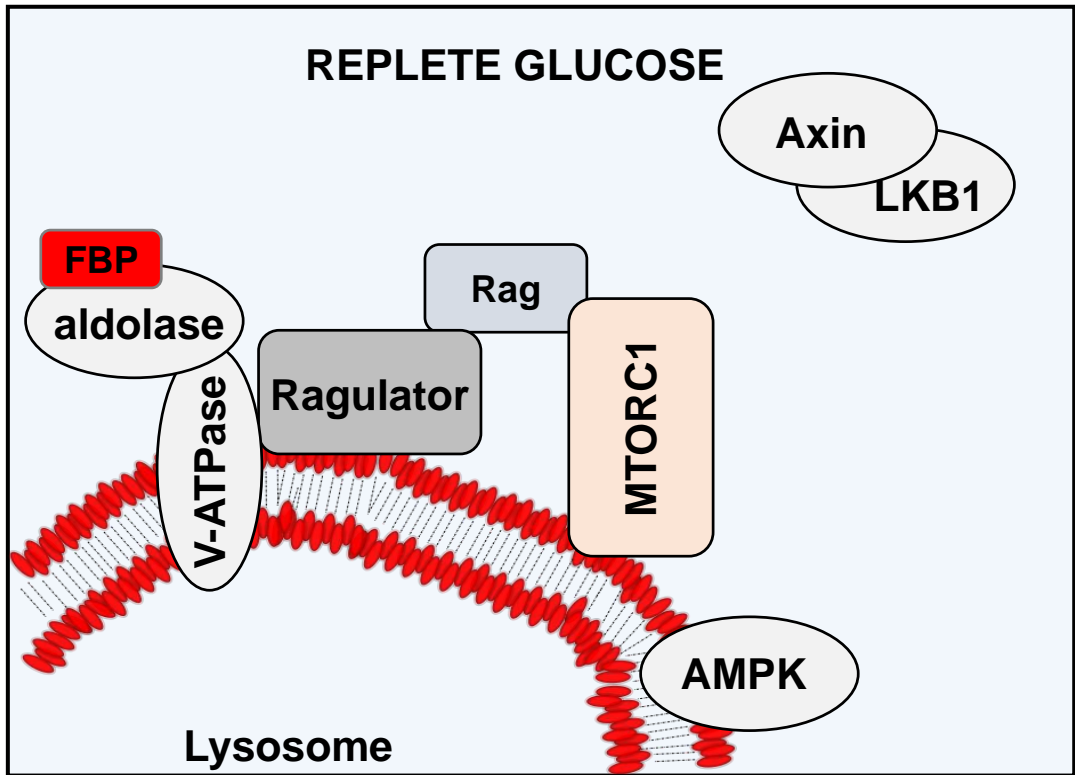
The activation of AMPK is dependent on its upstream activators such as CaMKK $\beta$ , TAK1 and LKB1 (Hawley et al., 2005, Hawley et al., 2003, Woods et al., 2005, Woods et al., 2003, Hurley et al., 2005, Momcilovic et al., 2006). As a prerequisite for its activity during energy stress, LKB1 must phosphorylate AMPK at the conserved threonine site (T172) mapped to the activation loop of its catalytic  $\alpha$ -subunit (Woods et al., 2003, Hawley et al., 2003). AMPK senses low energy levels by detecting changes in ADP, AMP and ATP levels mainly through AMP/ATP ratios. ADP is used in the synthesis of ATP with a reverse process catalysed by AMP. A high AMP/ATP ratio conforms to a low energy state (a low AMP/ATP ratio represents a high energy state). During high glucose conditions, the AMP/ATP ratio is reduced leading to the inactivation of AMPK.

It has been suggested that AMP binds allosterically (Sanders et al., 2007) to the regulatory  $\gamma$ -subunit of AMPK leading to activation and phosphorylation of AMPK at Thr172 (Oakhill et al., 2011, Xiao et al., 2007). Conversely, it is also suggested that ADP albeit at higher concentration binds to the regulatory unit of AMPK inhibiting the dephosphorylation of AMPK at Thr172 (Xiao et al., 2011). These models suggest that AMPK can readily sense ADP and AMP. Interestingly, in contrast, independent studies have also shown that the phosphorylation of AMPK at Thr172 is independent of AMP levels (Woods et al., 2003, Oakhill et al., 2010, Ross et al., 2016). More recent findings suggest that AMPK is activated via other AMP/ADP-independent mechanisms by directly sensing the shortage of fructose-1,6-bisphosphate (FBP), a metabolite synthesized from glucose via glycolysis (Zhang et al., 2017a).

In addition, an alternative recently proposed model involves differential binding of AXIN, LKB1, FBP aldolase, vATPase, Ragulator, AMPK and MTORC1 at the lysosome (Lin and Hardie, 2018, Zhang et al., 2017a) (**Fig 1.6**). Initial studies revealed that the v-ATPase-Ragulator complex and the AXIN-LKB complex are required for AMPK activation (Zhang et al., 2013, Zhang et al., 2014a). Subsequently, it was observed that aldolase enhanced the binding of these complexes and promoted AMPK activation during acute glucose starvation when AMP/ATP or ADP/ATP ratios were mostly unaltered. Aldolase was further proposed as the glucose sensor at the lysosomes linking AMPK to glucose availability (Zhang et al., 2017a). In high glucose conditions, FBP forms a complex with aldolase, v-ATPase, regulator, Rag and MTORC1 at the lysosome (**Fig 1.6A**). AMPK remains localised to the lysosome, however, remains inactive and unable to bind AXIN/LKB1 complex. In depleted glucose conditions, FBP level is reduced and it is not available to bind aldolase (**Fig 1.6B**). This leads to a conformational change in the complex which dislodges

MTORC1 from the lysosome due to the inhibition of Rag. This allows AXIN/LKB1 to form a complex with aldolase, vATPase, Ragulator, and AMPK. These interactions bring AXIN/LKB1 to close proximity with AMPK leading to its phosphorylation and activation.

A



B

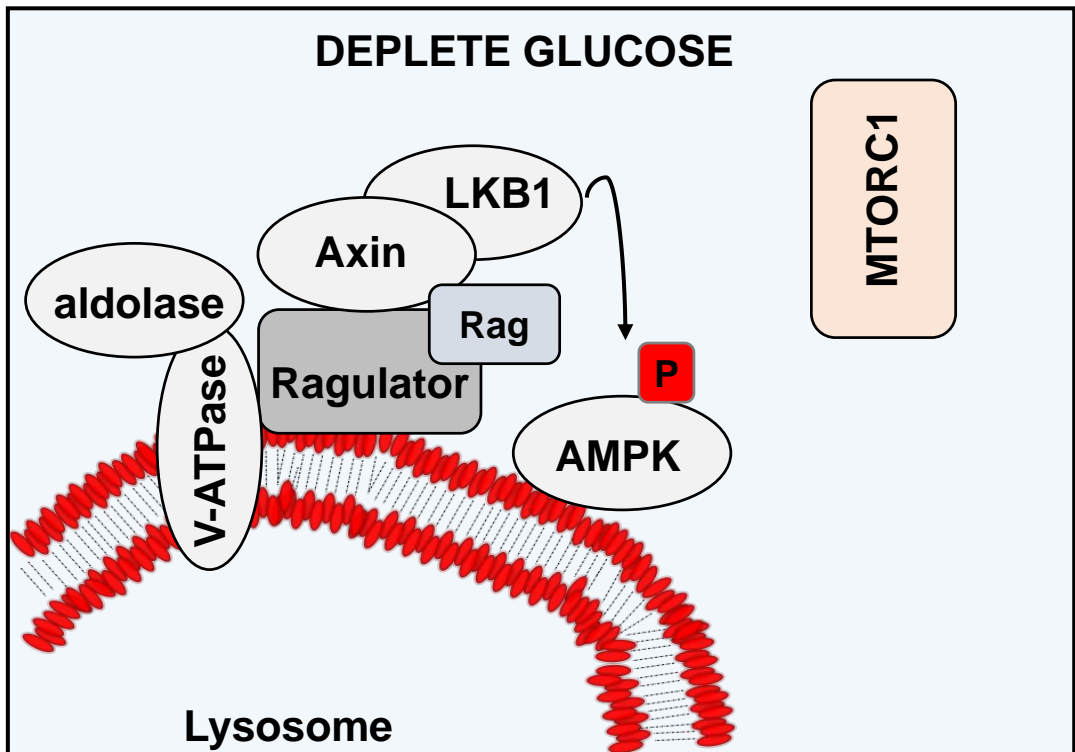


**Figure 1.6: The aldolase glucose-sensing model at the lysosome.** A) In this model, Fructose-1,6-bisphosphate (FBP) accumulates in the presence of glucose. FBP is sensed by aldolase which is in a complex with v-ATPase, Ragulator and MTORC1 at the lysosome. Axin and LKB1 are recruited away from the lysosome therefore leading to the inhibition of AMPK. B) In low glucose, FBP is depleted. This leads to a conformational change in the aldolase complex. This displaces MTORC1 from the lysosome while Axin and LKB1 translocate to the lysosome where they bind the Ragulator complex. This places LKB1 at close proximity to AMPK leading to AMPK phosphorylation at Thr172 hence AMPK activation.

AMPK also has other mechanisms which enable MTORC1 regulation by glucose levels. For example, upon glucose starvation, AMPK phosphorylates TSC2 at S1345, enhancing the GAP activity (Inoki et al., 2006, Inoki et al., 2003). This has the downstream effect of inhibiting Rheb and MTORC1 due to the termination of TSC-dependent inhibition. Moreover, the observation that TSC2-deficient cells were able to respond to energy stress led to the identification of a direct mechanism where AMPK inhibits MTORC1 by phosphorylating Raptor at two sites (S722 and S792) (Gwinn et al., 2008). While it was initially thought that AMPK signals glucose availability to MTORC1, recent evidence suggests that MTORC1-dependent glucose sensing can also occur via AMPK-independent mechanisms. For example, it was reported that glucose starvation inhibited MTORC1 in TSC2-KO MEF and AMPK KO MEF (Efeyan et al., 2013, Zhang et al., 2014a, Kalender et al., 2010). These studies show that in TSC2-KO and AMPK KO cells, MTORC1 dissociates from the lysosome during glucose starvation. These findings further highlight the multiple routes leading to MTORC1 in nutrient sensing.

While some studies have shown that glucose starvation leads to the induction of autophagy (Kim et al., 2011b, Chang et al., 2015, Roberts et al., 2014), other studies (including one from our laboratory) have shown the opposite: inhibition of autophagy upon glucose starvation (Ramirez-Peinado et al., 2013, Moruno-Manchon et al., 2013, Nwadike et al., 2018). Although this remains a controversial area, a recently proposed model from our laboratory is that during glucose starvation, upstream initiation and downstream autophagy flux are both inhibited (Nwadike et al., 2018). In this study, we reported that glucose starvation was not able to induce bulk autophagy responses such as the early autophagy signal of Ulk1 translocation to assembly sites, the initiation of autophagosomes formation and lysosomal acidification. In addition, it was concluded that AMPK activation could inhibit autophagy via novel mechanisms involving Ulk1-dependent autophagosome initiation and Ulk1-independent lysosomal activity (Nwadike et al., 2018). However, AMPK has a wide range of substrates (presently suggested to be at least 60) that are regulated during changes in energy levels (Hardie et al., 2016). For example, proteomic studies revealed that AMPK binds Ulk1 leading to at least seven phosphorylation events on Ulk1 (Kim et al., 2011b, Egan et al., 2011, Shang et al., 2011, Puente et al., 2016). Overall, the control of autophagy by MTORC1 and the Ulk1 complex seems tightly coordinated by AMPK, potentially by multiple positive and negative acting mechanisms

### 1.2.1.5 The crosstalk between MTORC1, AMPK and Ulk1 during autophagy initiation

The autophagy initiation process involves a complex signalling pathway which keeps expanding by the identification of new regulators. For example, Src was recently identified as a regulator of MTORC1 and autophagy, where Src bypasses amino acid regulation of MTORC1 to disrupt GATOR1-Rag interaction and recruit MTORC1 to lysosomes (Pal et al., 2018). This Src-MTORC1 pathway presumably functions independently of Src targeting as an autophagy substrate (Sandilands et al., 2011). For context purposes, emphasis is made in this project on how MTORC1, AMPK and Ulk1 are interconnected during autophagy initiation.

AMPK regulates autophagy initiation through multiple stress-dependent phosphorylations of its substrates. The functional roles of these AMPK-dependent phosphorylations are not fully known especially regarding nutrient-stress response. For example, the roles of AMPK in the initiation of autophagy could be context specific to a selective form of autophagy where mitochondria are specifically targeted for degradation during energy stress (Egan et al., 2011). This AMPK mechanism seems to occur through its regulation of Ulk1 at multiple phosphorylation sites. Consistent with this model, initial knockout studies have shown that Ulk1 <sup>-/-</sup> cells are unable to degrade mitochondria during erythroid maturation leading to the accumulation of damaged mitochondria (Kundu et al., 2008). It is suggested that AMPK phosphorylates Ulk1 at S467, S555, T574 and S637 leading to the induction of Ulk1-dependent autophagy of mitochondria (Egan et al., 2011). Consistent findings were reported by Tian et al. (2015) where it was reported that active AMPK phosphorylates Ulk1 at S555 during hypoxia leading to Ulk1 translocation to damaged mitochondria hence degradation. This is consistent with observations on Ulk1 phosphorylation of the substrate FUNDC1 during hypoxia stress to induce mitochondrial degradation (Wu et al., 2014). In addition, Ulk1 has also been shown to mediate Atg13 translocation to damaged mitochondria by phosphorylating Atg13 at S318, leading to mitochondrial degradation (Joo et al., 2011). All these support a model in which AMPK and Ulk1 regulate mitochondrial homeostasis with the overall trend that AMPK function activates Ulk1 and autophagy/mitophagy.

AMPK regulation of Ulk1 is dependent on MTORC1 (Kim et al., 2011b). In full nutrients when MTORC1 is active, it inhibits Ulk1 thereby preventing AMPK and Ulk1 from interacting. This MTORC1-dependent regulation of the AMPK-Ulk1 interaction inhibits AMPK-dependent activation of Ulk1 thus blocking autophagy. Kim (2011b) also

suggested that upon prolonged glucose starvation, AMPK inhibits MTORC1, therefore promoting AMPK and Ulk1 interaction. This interaction allows AMPK phosphorylation of Ulk1 at S317 and S777 to drive autophagy (Kim et al., 2011b).

In contrast to the model by Kim et al. (2011b), Shang et al. (2011) suggested that in full nutrients, all three subunits of AMPK binds Ulk1 thereby preventing Ulk1 association with its downstream substrates leading to autophagy inhibition. Upon amino acid starvation, MTORC1 inhibition promotes the dissociation of AMPK from the Ulk1 complex leading to the activation of Ulk1 and autophagy. The interaction of Ulk1 with AMPK in this context was independent of AMPK activity but dependent on MTORC1 phosphorylation of Ulk1 at S757 as the mutation of the site or reduced phosphorylation hampers AMPK-Ulk1 interaction.

Moreover, our laboratory recently reported that AMPK inhibits Ulk1 function by phosphorylation at the S555 site during glucose starvation (Nwadike et al., 2018). In addition, a double starvation signal (from glucose and amino acid starvation) was inhibitory over a single amino acid (autophagy activating) signal. This AMPK-dependent inhibition blocked Ulk1 localization and autophagy, in contrast to a pro-autophagy role for AMPK in Kim et al. (2011b) model. Therefore, the multiple AMPK-dependent phosphorylation events on Ulk1 appear to be able to have positive or negative regulatory roles, perhaps depending on the context. In contrast, there is much more consistent agreement on how MTORC1 and Ulk1 are regulated during amino acid starvation-induced autophagy.

The current MTORC1-Ulk1 model (**Fig 1.7A**) postulates that in mammalian cells with sufficient nutrients, autophagy is blocked. Mechanistically, MTORC1 phosphorylates Ulk1/2 on at least two possible sites S757 and S637 (mouse annotation) (Kim et al., 2011b, Shang et al., 2011, Wong et al., 2015, Hosokawa et al., 2009a). MTORC1 also phosphorylates Atg13 at S258 (Chan, 2009, Puente et al., 2016, Hosokawa et al., 2009a, Ganley et al., 2009, Jung et al., 2009). These phosphorylation events ultimately block the Ulk1 complex from initiating autophagy, although underlying structural/biochemical mechanisms remain elusive at this time.

Upon amino acid starvation, MTORC1 is inactivated and MTORC1-dependent phosphorylation of Ulk1 is inhibited (Shang et al., 2011). Starvation also induces the activation of protein phosphatase 2 (PP2A) which dephosphorylates MTORC1 phosphorylation of S637 on Ulk1 (Wong et al., 2015). The de-phosphorylation at S637 responds rapidly to amino acid starvation and it is critical for autophagosome formation (Shang et al., 2011, Wong et al., 2015). Together, MTORC1 inhibition and

PP2A-dependent de-phosphorylation together lead to the activation of the Ulk1 complex and its translocation to autophagosome initiation site (**Fig 1.7B**). Upon localization at the initiation sites, the Ulk1 complex regulates phagophore formation and activates downstream autophagy proteins in the PI3K complex. These events are the early regulatory mechanisms that mark the initiation of autophagy during amino acid starvation.

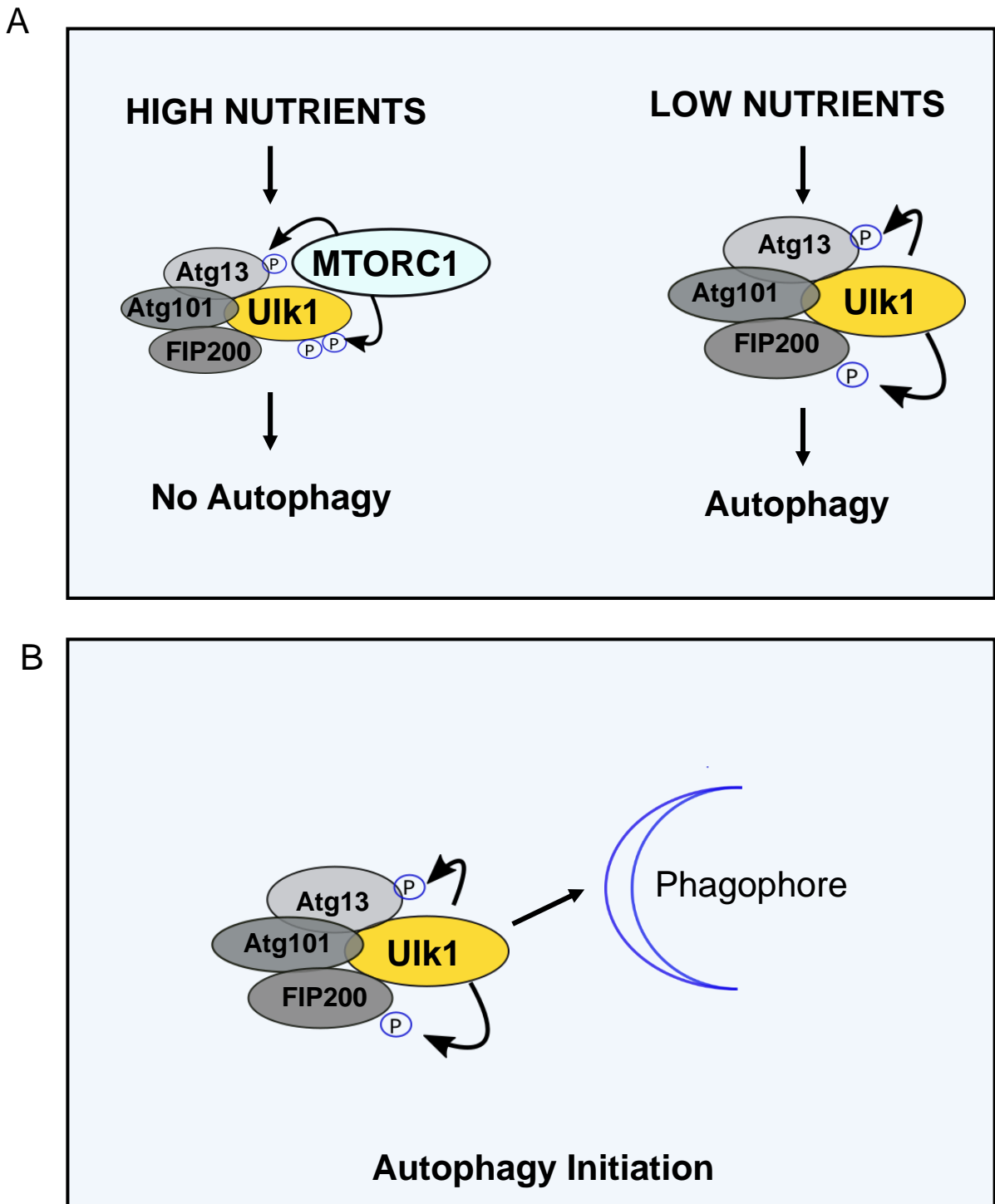


**Figure 1.7: The control of autophagy initiation by MTORC1 and the Ulk1 complex.**  
 A) In high nutrients, MTORC1 inhibits autophagy by phosphorylating and repressing the Ulk1 complex. Upon starvation, MTORC1 is inactivated and it dissociates from the Ulk1 complex. This leads to the activation of Ulk1 and B) its translocation to autophagosome initiation site where it phosphorylates its downstream substrates.

## 1.2.2 Vesicle nucleation and autophagy progression

A primary mechanism for autophagy initiation is thought to be Ulk1-mediated phosphorylation of Beclin1. The initiation of the autophagosomal membrane by the PI3K complex is directed by Beclin1 in a mechanism involving the differential binding of proteins Atg14/Atg14L/Barkor, UVRAG, Rubicon and VPS15/p150 (Takahashi et al., 2007, Matsunaga et al., 2009, Zhong et al., 2009, Sun et al., 2008). Beclin1 serves as the nexus point for the formation of distinct complexes that regulate autophagy differentially. Beclin1 can also bind Ambra1, Bcl2 and Bif1 during the initiation of autophagy (Takahashi et al., 2007, Fimia et al., 2007). Ambra1 is an activating binding molecule of Beclin1 and also a substrate of Ulk1. The interaction of Ambra1 promotes the binding of Beclin1 with Vps34 and it is required for autophagy initiation (Di Bartolomeo et al., 2010). In contrast, Bcl2 binding inactivates Beclin1, by competing for Ambra1, therefore blocking autophagy (Strappazzon et al., 2011). Bif1 regulates the biogenesis of autophagosomes by modulating the generation of membrane curvature, for example at sites marked by the omegasome (Takahashi et al., 2007, Takahashi et al., 2009). Overall, the type of PI3K complex formed is dependent on the Beclin1-associated protein which directs the distinct stage of autophagy the complex will be regulating.

The PI3K complex (complex type-I) consists of Atg14L, Beclin1, VPS34 and VPS15 which is recruited to the nascent autophagosomal membrane (Zhong et al., 2009, Sun et al., 2008) (**Fig 1.8A**). This leads to the generation of phosphatidylinositol-3-phosphate (PI3P) at the membrane which enhances Ulk1 translocation to omegasomes and the induction of autophagy (Karanasios et al., 2013). The second possible PI3K complex (Complex type-II) includes VPS34, UVRAG, VPS15, and Beclin1, and is required for the fusion of lysosomes with autophagosome at the final stages of autophagy (Bento et al., 2016). As autophagosome generation progresses and finally leads to closure of the phagophore, Beclin1 recruits UVRAG leading to the activation of VPS34 activity in a VPS15 dependent manner. This interaction displaces Atg14L from the initial PI3K complex (Matsunaga et al., 2009, Itakura et al., 2008). Beclin1 can also be in another complex (Complex type-III) consisting of UVRAG, Rubicon, VP34 and Vps15. It was observed that the overexpression of Rubicon led to the accumulation of immature autophagosomes which suggests that the Rubicon containing complex inhibits autophagosome maturation (Matsunaga et al., 2009, Zhong et al., 2009). This observation also correlated with a decrease in VPS34 activity mediated by Rubicon. Overall, these Beclin1-dependent signalling pathways together dynamically help drive the progression of autophagy.

The molecular responses above-mentioned are required for the recruitment of vesicles to the autophagy membrane assembly sites as described below. The main complexes involved in membrane vesicle nucleation are the Ulk1 complex and (PI3K) complex I (**Fig 1.8A**). Upon activation and translocation of the Ulk1 complex to sites where autophagosomes are formed, Ulk1 phosphorylates substrates in the PI3K-complex which lead to the formation of PI3P phospholipid at the nascent autophagosomal membrane (Russell et al., 2013).

Subsequently, Atg9A, a transmembrane protein, recruits membrane vesicles for autophagosome generation although Atg9A itself is not embedded in autophagosome (**Fig 1.8B**). Interestingly, Ulk1 phosphorylates Atg9A at S14 which is required for the recruitment of Atg9A from the plasma membrane to autophagy initiation site (Zhou et al., 2017). Atg9A translocation to autophagosomes also requires phosphorylation by AMPK at S761 which triggers a conformational change and increases the interaction between 14-3-3 $\zeta$  and Atg9A (Weerasekara et al., 2014). Mechanistically, this AMPK-dependent phosphorylation is dependent on Ulk1 under normal cellular states. However, in hypoxic conditions which induces autophagy, AMPK directly mediates Atg9A phosphorylation. Therefore both AMPK and Ulk1 induces autophagy via distinct mechanisms. Although the ER is reported to be the major site for autophagosome initiation (where it forms a cradle by membrane protrusion (Ktistakis, 2019)), Atg9A is suggested to recruit lipids and membranes from the Golgi, ER, endosomes, plasma membrane and mitochondria (Orsi et al., 2012, Ravikumar et al., 2010, Hailey et al., 2010, Hayashi-Nishino et al., 2009). In the process of recruiting membranes, Atg9A recruits other important autophagy proteins such as PI4KIII $\beta$ , Atg2 and WIPI1/2 that are required for autophagy progression (Velikkakath et al., 2012, Gómez-Sánchez et al., 2018, Judith et al., 2019, Valverde et al., 2019). Therefore, the overall consensus is that autophagosome formation may utilize different membrane sources, perhaps depending on the type of autophagy, cargo or stimulation context. The formation of phagophore marks the end of autophagy nucleation.

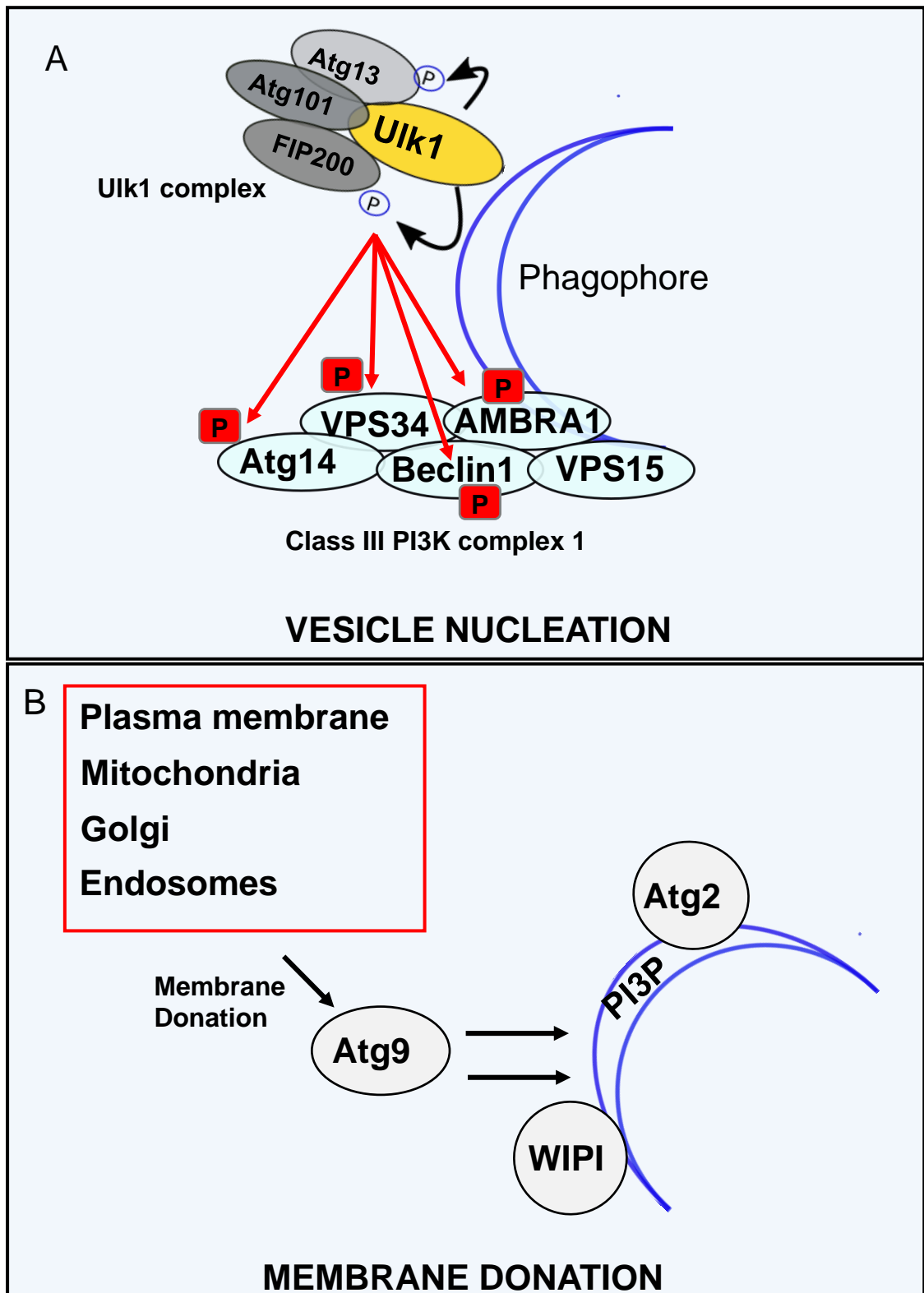


**Figure 1.8: Vesicle nucleation and the recruitment of membranes during autophagy.**  
 A) Uik1 phosphorylates members of the class III phosphatidylinositol 3-kinase (PI3K) complex Vps34 (S249), Beclin1 (S14, S30) and Atg14 (S29). This nucleates the phagophore and allows B) Atg9 to recruit membranes from the plasma membrane, mitochondria, Golgi and endosomes to the phagophore.

### 1.2.3 Vesicle expansion and maturation

Subsequently, after membrane nucleation, the phagophore is expanded to engulf contents needed to be degraded or recycled through autophagy. The PI3P phospholipid recruits members of the Ubiquitin-Like Conjugation (UBL) complex UBL complex to autophagosomes by interacting with WIPI1/2 (Dooley et al., 2014, Polson et al., 2010). Similar to ubiquitination, (addition of ubiquitin to substrates for the proteasome), the UBL complex tags substrates with LC3 to drive autophagy through the lysosome.

LC3 and  $\gamma$ -aminobutyric acid (GABA)-receptor-associated protein (GABARAP) are mammalian homologues of yeast Atg8. The LC3 and GABARAP subfamilies comprise of a group of seven proteins (LC3A, LC3B, LC3B2, LC3C, GABARAP, GABARAPL1, GABARAPL2). The LC3 and GABARAP proteins are well conserved (have 2 N-terminal  $\alpha$ -helices and a C-terminal ubiquitin domain) with high sequence similarity (Sugawara et al., 2004). However, studies have shown that some of the LC3 proteins have distinct functions in autophagy. For example, LC3B has been shown to be critical in the early stages of autophagy during the formation and elongation of autophagosomes while GABARAPL2 promotes autophagosome maturation and closure (Weidberg et al., 2010).

GABARAP and GABARAPL1 have a higher affinity for binding and recruiting Ulk1 to phagophore nucleation site (Alemu et al., 2012, Grunwald et al., 2019). Grunwald et al. (2019) suggested that LC3B and LC3C inhibit Ulk1 while GABARAP subfamilies promote Ulk1 activity during phagophore formation. Although the genetic ablation of both LC3 and GABARAP proteins have been shown to impair the formation of autophagosomes, LC3B is widely used as a biomarker for autophagy (Weidberg et al., 2010).

The UBL complexes are made of Atg3, Atg4, Atg5, Atg7, Atg8/LC3, Atg10, Atg12 and Atg16/Atg16L1. Each of these protein plays specific roles in the elongation of the vesicle, and the concerted function of these complexes is absolutely essential for canonical autophagy (**Fig 1.9**). Atg7 activates Atg12, which is followed by the recruitment of Atg10. Atg12 is subsequently conjugated covalently with Atg5 which then forms a complex with Atg16/Atg16L1 (Mizushima et al., 1999). The Atg12-Atg5-Atg16/Atg16L1 complex is attached to phagophore where it catalyses the covalent conjugation of phosphatidylethanolamine to Atg8/LC3 at the carboxyl-terminal glycine. Prior to this, Atg7 also activates Atg8/LC3, allowing its transfer to Atg3. LC3-I is converted to LC3-II, a phosphatidylethanolamine conjugated lipidated form. LC3-

II subsequently binds to autophagy adaptor proteins that possess a LC3-interacting regions (LIR), which form a molecular bridge to autophagy target for specific degradation (Birgisdottir et al., 2013). This unique step also makes LC3-II an excellent marker of autophagosome formation and autophagy in laboratory experiments (Kabeya et al., 2000).

The LIR on autophagy adaptor proteins is a well conserved short linear motif containing canonical aromatic residue of either W/F/Y, followed by either of hydrophobic residue L/I/V, however, separated by any two amino acids [W/Y/F]xx[L/I/V]. The LIR motif was first characterised in p62/SQSTM1 where it was shown that p62/SQSTM1 binds both mono and poly-ubiquitinated targets with its ubiquitin associated domain (UBA) and interacts with LC3 via its LIR motif (Pankiv et al., 2007, Vadlamudi et al., 1996).

Importantly, the presence of LIR motifs is suggested to be a prerequisite for selective autophagy such as mitophagy. However, the role of p62/SQSTM1 in mitophagy has been controversial. p62/SQSTM1 was shown to interact with poly-ubiquitinated damaged mitochondria while cells transfected with p62/SQSTM1 siRNA lost the ability to clear dysfunctional mitochondria. This observation suggested that p62/SQSTM1 functions as an adaptor protein for mitophagy (Geisler et al., 2010). In contrast, Narendra et al. (2010) showed that p62/SQSTM1 is not required for the clearance of dysfunctional mitochondria after it was observed that MEF and HeLa cells lacking p62/SQSTM1 cleared dysfunctional mitochondria within 24-hours. Nevertheless, p62/SQSTM1 was shown to be required for the concentrating and clustering of damaged mitochondria for subsequent degradation (Narendra et al., 2010, Okatsu et al., 2010). Interestingly, another study confirmed that p62/SQSTM1 is indispensable for mitophagy and it is suggested that the primary mitophagic adaptor proteins that bind to ubiquitinated mitochondria are Optineurin (OPTN) and NDP52 (Lazarou et al., 2015). However, other mitophagy adaptors have been identified and the prominent ones include NIX/BNIP3, FUNDC1, AMBRA1 and Bcl2L13 (Strappazzon et al., 2015, Novak et al., 2010, Hanna et al., 2012, Liu et al., 2012, Murakawa et al., 2019, Murakawa et al., 2015). These adaptors were shown to have LIR and are able to bind LC3, thereby, recruiting damaged mitochondria to nascent phagophore where they are encapsulated as autophagosome closes up.

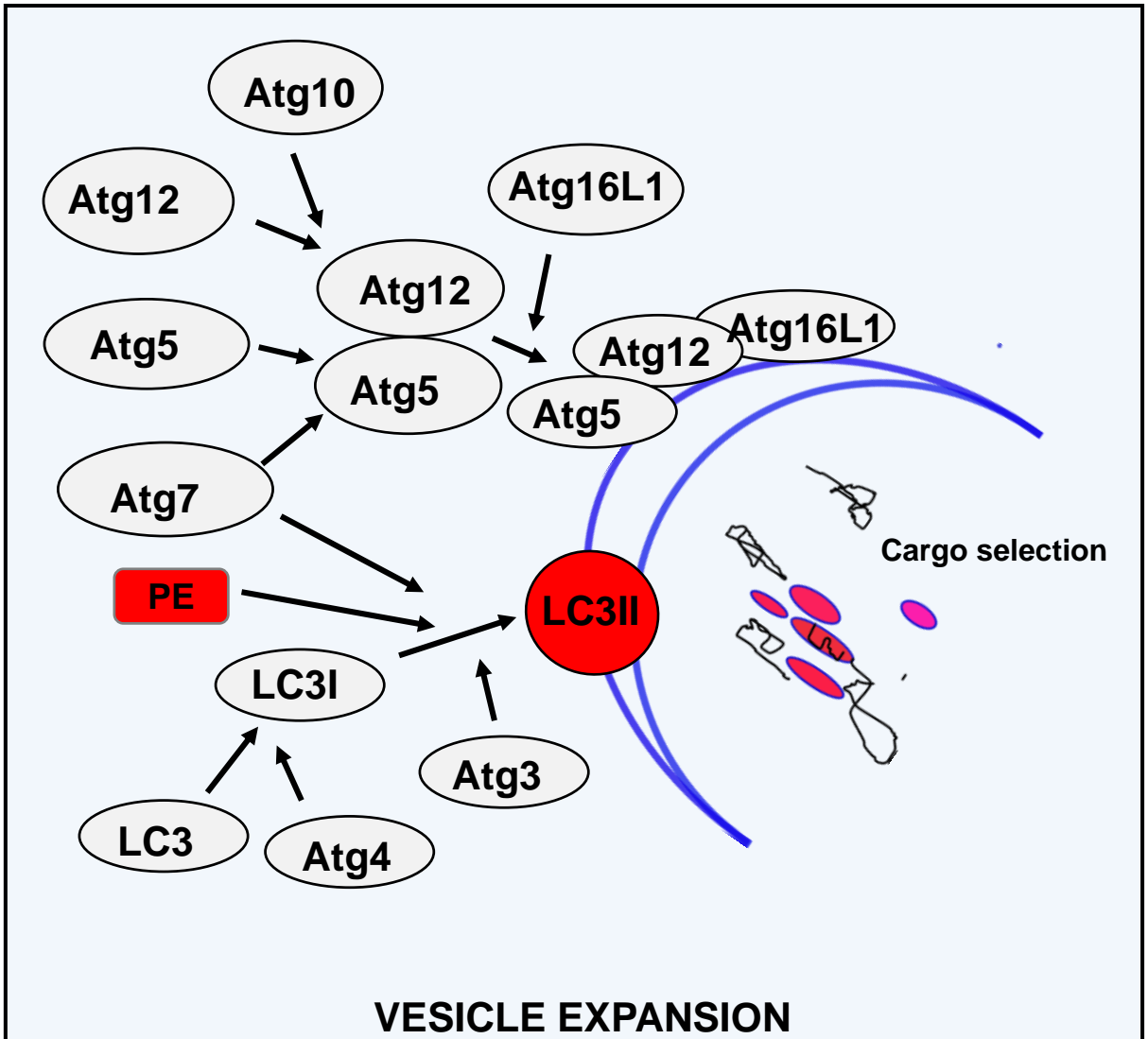


**Figure 1.9: The Ubiquitin-like conjugation complex drives cargo selection and autophagy progression.** LC3 is cleaved to form LC3I which is subsequently conjugated with PE to form LC3II in a process catalysed by Atg3 and Atg7. Atg7 and Atg10 are also required for the formation of Atg5-Atg12-Atg16L1 complex at the phagophore. The formation of the Atg5 complex and LC3II are critical for autophagy progression.

## 1.2.4 Vesicle completion and fusion with lysosomes

The final phase of autophagosome formation is closure to generate a fully matured double bilayer membrane sac which eventually undergoes fusion with lysosomes (**Fig 1.10**). The closing of autophagosomes is mediated by Atg3, Atg5 and Atg7 (Tsuboyama et al., 2016). Interestingly, only fully enclosed autophagosomes are able to progress with lysosomal fusion (Tsuboyama et al., 2016). At this stage, the autophagosome may contain varying contents such as misfolded proteins, mitochondria, peroxisomes and other cytoplasmic contents depending on the cues inducing the autophagy.

Autophagosomes are transported to the lysosomes via actin filaments after interaction with Tom1 and Myosin VI motor proteins (Tumbarello et al., 2012). Similarly, microtubule-associated movement is mostly reported and well characterised. In this transport system, Rab7, a small GTPase is recruited to mature autophagosomes where it tethers autophagosomes to microtubule motor proteins such as Kinesin and dynein to mediate both retrograde or anterograde movement of autophagosomes (Gutierrez et al., 2004, Pankiv et al., 2010, Jordens et al., 2001, Wijdeven et al., 2016). The anterograde movement directs mature autophagosomes to the perinuclear sites in the cytosol. Live-imaging studies provided insights into autophagosomal transport where it was shown that mature autophagosomes are transported towards lysosomal-rich perinuclear regions on the microtubule involving dynein-dynactin motor proteins (Kimura et al., 2008). In vivo studies also confirmed that the deregulation of the autophagosomal transport system reduces autophagy and it is one of the pathogenesis of age-induced autophagy defects (Bejarano et al., 2018). Interestingly, the perinuclear concentration of lysosomes is also required for autophagy flux as it was reported that enhancing lysosomal localization at these sites by depleting kinesin motor protein enhances autophagosomal fusion (Bejarano et al., 2018). This also correlated with the overexpression of kinesins reducing perinuclear lysosomal concentration and reducing autophagy (Korolchuk et al., 2011). These studies show that every step of the canonical autophagy process is critical for an effective autophagy flux

At the perinuclear region, the autophagosome fuses with the lysosome which is enriched with acidic hydrolases. These hydrolytic enzymes are grouped into different classes such as lipases (digest lipids), glycosidases (digest glycosides), nucleases (digest nucleic acids) and proteases (digest proteins). For example, cathepsins promote proteolytic degradation within the lysosome (McGlinchey and Lee, 2015).

The digestive hydrolases digest both the autophagosome and its contents to generate simple molecules such as amino acids. These simple molecules can then be recycled for other purposes such as protein synthesis or amino acid metabolism.

Importantly, lysosomal fusion with the autophagosome is mediated by membrane-tethering complexes, SNAREs (soluble N-ethylmaleimide-sensitive factor attachment protein receptor) complexes and Rab GTPases. Rab7 localises to late endosomes and lysosomes where it recruits effector proteins such as Pleckstrin homology domain-containing family M member 1 (PLEKHM1) and Rab-interacting lysosomal protein (RILP), and also tethering membranes HOPS subunits (Homotypic fusion and vacuole protein sorting) (Jiang et al., 2014, Wijdeven et al., 2016). SNARE protein syntaxin-17 mediates the physical interaction and fusion of the lipid bilayers after binding HOPS tethering complexes which also include VPS33A, VPS16, VPS18 VPS11, VPS39 and VPS41 (Jiang et al., 2014). In addition, Atg14L binds and stabilizes Syntaxin17-SNAP29 complex where it potentiates the interaction with VAMP8, allowing autophagosome–endolysosomal fusion (Diao et al., 2015).

Recent studies have also shown that specific members of the LC3 protein family, GABARAPs, are required for autophagosomal fusion with lysosomes (Nguyen et al., 2016). Upon lysosomal fusion, the acidic content of the lysosome mediates the degradation. The consistent pH range of the lysosome is maintained mainly by vATPase an ATP-dependent proton pump that also mediates the efflux of non-essential amino acid from the lysosomes (Abu-Remaileh et al., 2017). This mechanism is used as a drug-able target to study autophagosomal delivery into lysosomes. For example, Bafilomycin A1 is commonly used to block vATPase activity which in turn inhibits autolysosomes degradation and autophagosome fusion with lysosomes (Zoncu et al., 2011, Yoshimori et al., 1991, Yamamoto et al., 1998). The fusion and degradation of the autophagosome signify the end of the dynamic autophagy process. This can be a general process to restore amino acids following amino acid starvation or a quality control mechanism to remove damaged proteins and organelles such as mitochondria.

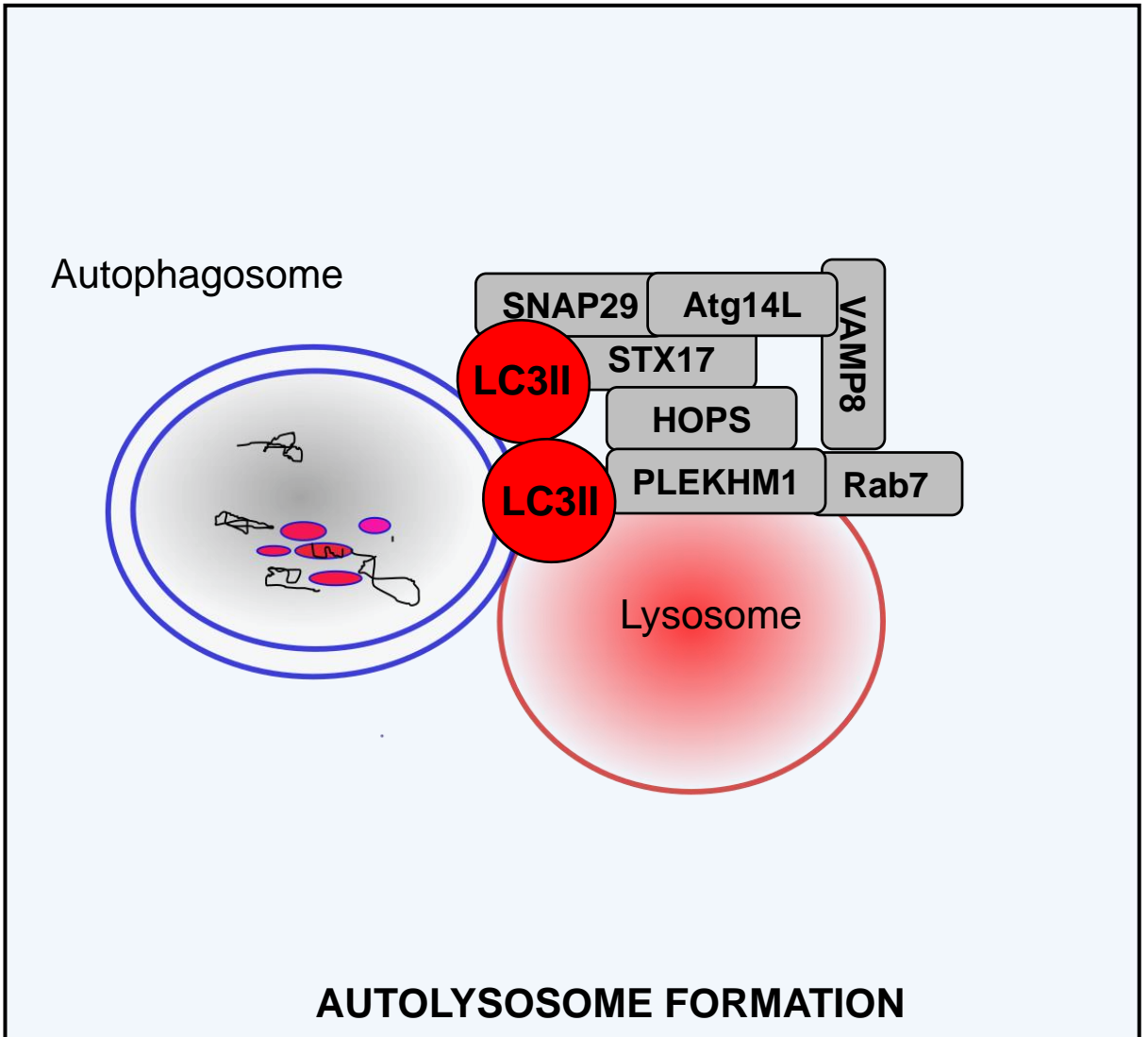


**Figure 1.10: The formation of matured autophagosome and the fusion with lysosome.** Upon autophagosome formation, it fuses with the lysosome. This process is coordinated by LC3II, STX17, SNAP29, PLEKHM1, Atg14L, VAMP8, HOPS and Rab7. Rab7 tethers autophagosomes to microtubules for transport to perinuclear sites enriched with lysosomes. Also, Rab7 and VAMP8 are recruited to late endolysosome or lysosomes where they promote autophagosome fusion by binding LC3II via the PLEKHM1, HOPS, ATG14L, STX17 and SNAP29 complex.

### 1.3 Autophagy of mitochondria: role for mitochondrial remodelling

Mitochondria are symbiotic organelles that have successfully colonized mammalian cells in an event historically predated to a million years (Dyall et al., 2004, Schwartz, 2007, Katz, 2012, Roger et al., 2017). Mitochondria are now stably inherited and play essential roles for their host as evidenced in their numerous numbers in mammalian cells where they can divide, be degraded and be synthesized (Youle, 2019). While they have retained some portions of their own genome (mtDNA), they have also adapted many key cellular events for their own maintenance and housekeeping. These include cellular protein synthesis, nutrient uptake and energy synergisms. Although mitochondria have been extensively studied over the years, they have been poorly exploited for medical and health benefits, especially regarding how they respond to nutrients and amino acid availability.

Mitochondria are double membrane organelles with a diameter of approximately 0.5 – 1µm. Mitochondria are generally numerous in cells and their numbers are dependent on different physiological conditions (Albert et al., 2002). For example, mature red blood cells have no mitochondria while paternal mitochondria are degraded during fertilization (Mortensen et al., 2010, Sato and Sato, 2011, Dumollard et al., 2007). Mitochondria synthesize ATP via the electron transport chain (E.T.C.) and oxidative phosphorylation (OXPHOS). It has been suggested earlier that mitochondria can transition in morphology between highly fused, fragmented or rounded, depending on the cells metabolic conditions (Amchenkova et al., 1988). Due to their highly specific roles in ATP generation and metabolic homeostasis, mitochondria have their own mtDNA of 15 -20kb with 37 genes. The mtDNA is circular and codes for several important subunits (13 out of 90 protein subunits) needed by mitochondria for ATP generation through the E.T.C. (Saccone et al., 2000, Anderson et al., 1981, Youle, 2019, Gammage and Frezza, 2019). However, the relationships between mitochondrial function, metabolism and remodelling of mitochondria are still an expanding area.

During the complex events of autophagy and mitophagy, an interesting coordinated response involving mitochondrial fusion has been suggested (**Fig 1.11**). In this pathway, mitochondria undergo both inner and outer membrane fusion during amino acid starvation, which may represent a means for mitochondria to avoid degradation and sustain cell energy (Gomes et al., 2011a, Rambold et al., 2011). Mitochondrial dynamics is defined as the balance of processes that alter mitochondrial shapes,

length and size under both normal and stress response conditions (Westermann, 2010). The key molecular regulators of mitochondrial dynamics are well characterised. These include Mitofusin-1 (Mfn-1) (and Mfn-2) regulating outer membrane fusion (Santel and Fuller, 2001) and optic atrophy 1 (Opa1) regulating inner membrane fusion (Cipolat et al., 2004). On the other hand, dynamin-related protein 1 (Drp1) GTPase and adaptor proteins such as mitochondrial fission 1 (Fis1) and Mff direct mitochondrial fission (Smirnova et al., 2001, James et al., 2003, Otera et al., 2010). These regulators are each discussed in further detail later in this Introduction.

Mitochondrial dynamics are normally required in the maintenance of a healthy mitochondrial pool. During mitochondrial damage, it has been suggested that mitochondrial division occurs prior to mitochondrial degradation. On the other hand, it has been proposed that mitochondrial fusion occurs to prevent untargeted mitochondrial degradation during autophagy (Gomes et al., 2011a). This is based on the observation that hyperfused mitochondria are not rapidly degraded while fragmented mitochondria are suggested to be recycled more efficiently (Parone et al., 2008, Twig et al., 2008). In contrast, other findings also suggest that mitochondria can be readily degraded when in a fused state. For example, it was reported that mitophagy occurred during amino acid starvation (where mitochondria are generally fused) at similar levels to when mitochondria were damaged with proton ionophore (Allen et al., 2013). This finding suggests that the mitochondrial fusion during amino acid starvation does not occur to prevent mitochondrial degradation.

Interestingly, it has been shown that mitochondria form contact sites with lysosomes without being degraded (Wong et al., 2018). In Wong et al. (2018), it was observed that mitochondrial fission occurred at sites marked with lysosomal-associated membrane protein 1 (LAMP1), a lysosomal marker. The observation that mitochondrial-lysosomal contact marked sites of mitochondrial fission suggest that there is a direct lysosomal role in the regulation of mitochondrial dynamics. Since mitochondrial fusion only responds to changes in amino acids rather than overall nutrient starvation (Rambold et al., 2011), fusion may be more a direct mitochondrial response to amino acids rather than a mechanism to avoid degradation. This concept will be relevant as we discuss experimental results in this thesis.

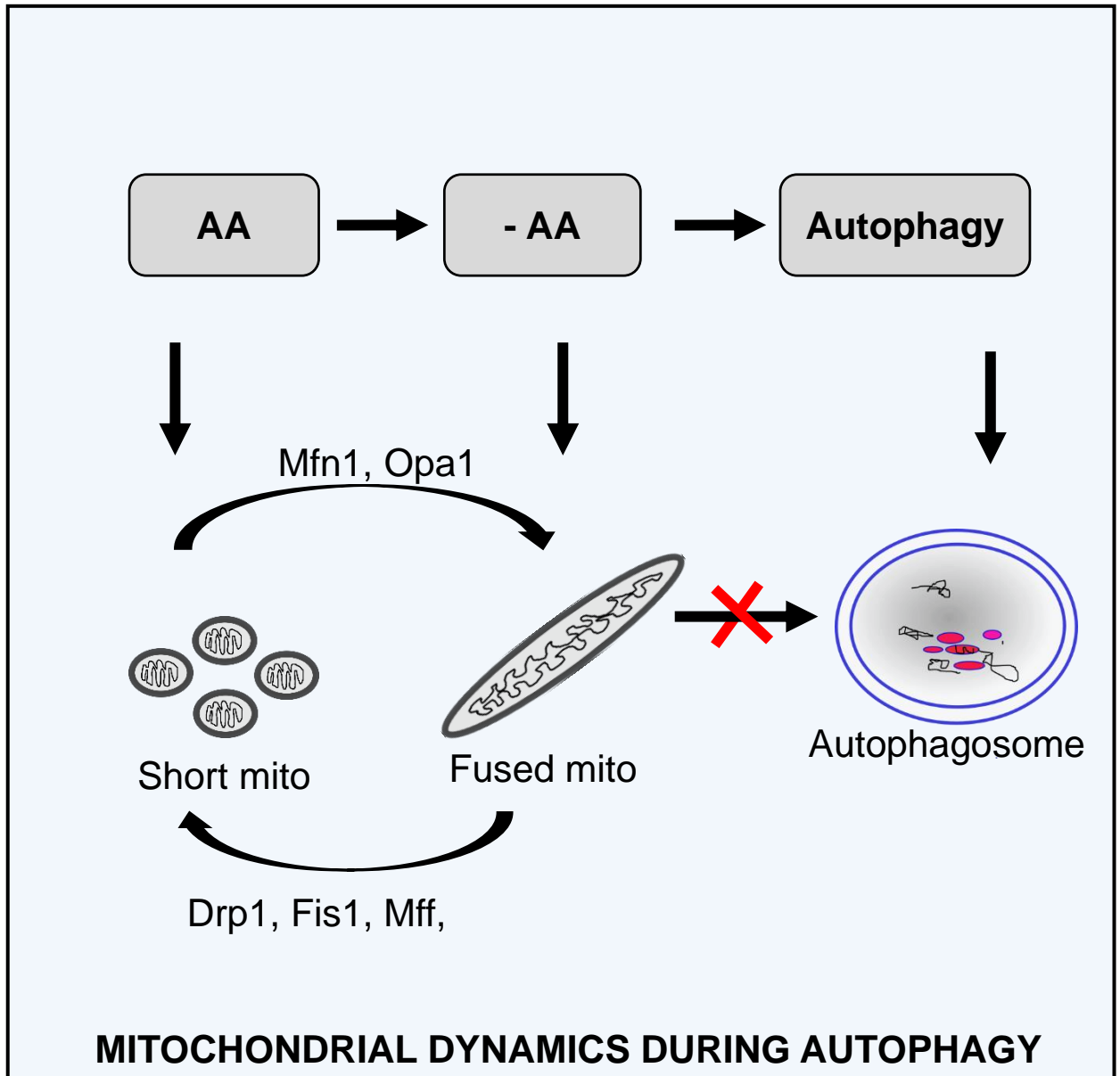


**Figure 1.11: Mitochondrial remodelling during autophagy.** During amino acid (AA) starvation, mitochondria fuse to form tubulated forms that are supposedly protected from degradation during autophagy. Mitochondrial remodelling is achieved via Mfn1 and Opa1 which mediate the outer and inner mitochondrial fusion respectively. In contrast, Drp1 is recruited to mitochondria by its receptors Fis1 and Mff to mediate mitochondrial division.

### 1.3.1 Biological significance of mitochondrial remodelling

The study of mitochondrial dynamics can be traced back to 1914 when it was first observed that mitochondria divide and fuse (Lewis and Lewis, 1914). Citing more recent findings, mitochondrial dynamics have been shown to play a central causative role in the modulation of overall cellular fate (Song et al., 2015). Alteration of mitochondrial dynamics is critical for cellular division (Mitra et al., 2009) and apoptosis (Pyakurel et al., 2015). For example, mitochondria have been shown to form punctate and short structures during cytochrome c release in apoptotic events, while individual cristae fuse and cristae junction narrow (Martinou et al., 1999, Frank et al., 2001, Scorrano et al., 2002). Also, during quality maintenance of the cellular mitochondrial population through mitophagy, mitochondria dynamics are altered toward short fragmented forms to favour mitochondrial enclosure by autophagosomes (Wu et al., 2016b, Wu et al., 2016a, Yamashita et al., 2016). Conversely, it has been shown that mitochondrial shape is modified towards a fused state in response to OXPHOS-dependent generation of ATP (Rossignol et al., 2004, Mishra et al., 2014). These studies propose that the mitochondrial response to OXPHOS activity ensures that mitochondrial structure and function correlates with energy production in different nutrient conditions (Mishra et al., 2014).

Furthermore, mitochondrial dynamics are associated with the generation of reactive oxygen species (ROS), with increased ROS levels being linked to mitochondrial fragmentation (Willems et al., 2015). This is consistent with the observation that cells with aberrant mitochondrial fragmentation due to Mfn1/2 depletion have increased ROS (Munoz et al., 2013). Similarly, treatment of cells with hydrogen peroxide (H<sub>2</sub>O<sub>2</sub>) (to increase cellular ROS) stimulated mitochondrial fragmentation (Rakovic et al., 2011). In contrast, an increase in ROS has also been linked to mitochondrial fusion after it was shown that L-buthionine-S, R-sulfoximine (BSO), an inhibitor of glutathione (GSH) promotes the accumulation of ROS stimulated mitochondrial fusion (Shutt et al., 2012). Clearly, these roles of mitochondrial remodelling are in response to cellular stress and it is proposed to be a requirement for attaining cellular homeostasis (Eisner et al., 2018).

The disruption of mitochondrial remodelling can be detrimental to cellular health. For example, mitochondria have been implicated in the pathogenesis of many diseases ranging from ageing-related to metabolic dysfunction. This correlates with the observation that the genetic loss of key factors of mitochondria remodelling cause life-threatening diseases (Bach et al., 2003, Zuchner et al., 2006, Zuchner et al., 2004).

Unfortunately, epidemiological data seems to indicate these mitochondria-deregulated associated diseases are still a major burden (Gorman et al., 2015). Below, we further summarise key examples of biological significance characterised for mitochondrial remodelling.

### 1.3.1.1 Role of mitochondrial dynamics in ageing

Ageing includes the gradual decline in multiple physiological functions that enhance mortality or loss of normal biological function. Many mitochondrial processes such as ROS generation, mitophagy, mitochondrial apoptotic events, ATP generation and mutated mtDNA have been associated with ageing at the cellular level (Jendrach et al., 2005, Korwitz et al., 2016). Hence, it is not surprising that mitochondrial dynamics have been intimately associated with ageing (Rana et al., 2017, Chaudhari and Kipreos, 2017). Mitochondrial fusion and fission mechanisms have been noted to evolve as ageing progresses (Jendrach et al., 2005). It is not yet totally clear which mitochondrial phenotype is more prominent in aged animals, fragmented or fused.

Recent evidence suggests that mitochondrial fusion may be overall beneficial in ameliorating age-related defects. For example, mitochondrial elongation suppresses ageing-induced neurodegeneration in mouse neurons as a result of metalloendopeptidase (OMA1) inhibition thereby increasing lifespan (Korwitz et al., 2016). Interestingly, expression of fission initiator Drp1 is suppressed in aged muscles, suggesting that overall mitochondrial fusion increases with age (Crane et al., 2010). Increased mitochondrial size has also been reported in aged cells, and this has been associated with decreased mitophagy and the pile-up of damaged mitochondria (Murakoshi et al., 1985). Interestingly, enhancing Drp1-dependent mitochondrial fission and mitophagy has been reported to reverse ageing and increase life span in midlife fruit flies (Rana et al., 2017). In contrast, enhanced mitochondrial fusion increased longevity in aged *C. elegans* (Chaudhari and Kipreos, 2017).

These studies all highlight the multi-functional roles of mitochondrial dynamics during ageing. More in vivo studies are still needed to clarify fusion and fission roles, which still are controversial. This is because mitochondria are highly ubiquitous organelles and their roles are tissue and cell-specific. Therefore, conclusion made from a particular tissue or cell may not be directly translatable to others, thus creating challenges in defining mitochondrial shapes during ageing that can be generalised. Despite this limitation, it is suggested that fusion may be the main altered mitochondrial phenotype in ageing because mitochondria fission has been shown to

be involved in the pathology of many age-related disorders such as Alzheimer's disease (Cho et al., 2009).

### 1.3.1.2 Role of mitochondrial dynamics in *Charcot Marie Tooth type2A* disease (CMT2A)

Deregulation of key mitochondrial dynamic genes underlies developmental disorders such as Charcot Marie Tooth type2A disease (CMT2A) and optic dystrophy. CMT2A is an inherited peripheral neuropathy subtype of CMTD. Importantly, this disorder is caused by an autosomal dominantly inherited mutations in Mitofusin-2 (*Mfn2*) (Zuchner et al., 2006). Although rare recessive forms of *Mfn2* mutation have been reported, it is not yet clear how either dominant or recessive *Mfn2* mutations cause neuropathy (Polke et al., 2011, El Fissi et al., 2018). However, CMT2A mutations in *Mfn2* has been mapped to the coiled-coil and GTPase domain which is required for *Mfn2*-dependent mitochondrial transport and fusion (Zuchner et al., 2004, Misko et al., 2010).

Phenotypically, CMT2A patients have dysfunctional motor neurons leading to stork-leg deformity and abnormal gait. At the cellular level, mitochondrial transport and mitochondrial-dependent energetics are greatly impaired. Intriguingly, by modifying *Mfn2* to structurally favour a pro-fusion conformation ameliorates mitochondrial dysfunction in mutant neurons and fibroblast that carry CMT2A mutations (Franco et al., 2016, Rocha et al., 2018). This is based on a previous study which showed that the heptad-repeat region 2 (HR2) of *Mfn2* promotes mitochondrial fusion through intermolecular HR2-HR2 binding on opposite mitochondria (Koshiba et al., 2004). However, HR2 intermolecular binding is only efficient when the HR2-domain extend towards the cytosol, a conformation that is normally less prominent due to HR1-HR2 intramolecular interaction that folds up the HR2-domain. Interestingly, Franco et al designed a cell-permeable *Mfn2*-HR1 mini peptide that disrupts HR1-HR2 intramolecular binding, thereby, promoting HR2 extension towards the cytosol. The introduction of this engineered fusion-permissive peptide into wildtype and *Mfn2* knockout MEF was shown to promote HR2 intermolecular interaction and mitochondrial fusion. Similarly, this peptide-construct was also shown to restore mitochondrial fusion in neurons from CMT2A mouse models with *Mfn2* T105M (Detmer et al., 2008, Franco et al., 2016). These studies, therefore, suggest that therapeutic approaches that promote mitochondrial fusion may be useful in the treatment of CMT2A and other diseases where fusion is disrupted.

### 1.3.1.3 Role of mitochondrial dynamics in Optic atrophy

Mutations in *Opa1* represent the most frequent (60% - 80%) molecular lesions of optic atrophy, which is an autosomal dominantly inherited defect affecting 1 in 25,000 people in the United Kingdom (Delettre et al., 2000, Yu-Wai-Man and Chinnery, 2013). Note, mutations in *Mfn2* have also been associated with the development of optical atrophy (Zuchner et al., 2006). Most heterozygous mutations in *Opa1* causes either dominant-negative effect or haploinsufficiency and the majority of the mutations have been mapped to its GTPase domain (Alexander et al., 2000, Yu-Wai-Man et al., 2011). It has been shown that *Opa1* mRNA transcripts from patients carrying mutated-*Opa1* are mostly truncated, unstable and are degraded leading to a reduction in *Opa1* protein levels (Pesch et al., 2001, Schimpf et al., 2006). The pathogenesis of these mutations in *Opa1* has been shown to involve dysfunctional mitochondrial dynamics such as aberrant mitochondrial fragmentation, disorganised and swollen cristae in patient fibroblasts (Amati-Bonneau et al., 2008, Olichon et al., 2007, Chevrollier et al., 2008). Similarly, mitochondrial function in optic atrophy patients has been shown to be affected, and it is majorly characterised by increased apoptosis, reduced ATP synthesis, depolarised mitochondria and reduced OXPHOS capacity in patient's fibroblasts (Carelli et al., 2004, Zanna et al., 2008, Olichon et al., 2007). The clinical manifestation of optic atrophy patient includes a gradual and progressive loss of sight, which occasionally leads to blindness. This also agrees with the recent observation that mice lacking YME1L, an enzyme required for *Opa1* processing developed ocular dysfunctions, cataracts and degradative spinal cord axons (Sprenger et al., 2019). Interestingly, YME1L-deficient mice developed reduced mitochondrial respiration, swollen mitochondrial cristae and aberrant mitochondrial fragmentation in their spinal cord. This further highlights the strong deleterious effects of altered mitochondrial fusion on mitochondrial metabolism, cellular homeostasis and apoptosis.

### 1.3.1.4 Role of mitochondrial dynamics in cancer

The deregulation of mitochondrial dynamics has been implicated in the progression of cancer and cell transformation. For example, it was reported that mitochondrial fission mediated by the phosphorylation of Drp1 at S616 was required for Ras-dependent transformation of mouse embryonic fibroblasts (Serasinghe et al., 2015). Serasinghe et al, 2015 expressed oncogenic Ras G12V which drives proliferative cellular hallmarks of cancer. This led to extensive mitochondria fragmentation, which

they could show was an integral requirement of cell transformation. Interestingly, genetic ablation of Drp1 ameliorates Ras-G12V-induced cancer progression thereby suggesting that mitochondrial fission can be potentially be exploited as a direct or sensitising therapeutic in tumours where the Ras/MAPK pathway is deregulated. This agrees with more recent suggestions that mitochondrial dynamics are promising candidates for the development of new drugs for cancer treatment (Anderson et al., 2018). Pro-fission activation via Drp1 phosphorylation at S616 as a result of MAPK activation was also reported to drive tumorigenesis in pancreatic cancer (Kashatus et al., 2015). Interestingly, in pancreatic cancer tumours, phosphorylation of Drp1 and abnormal mitochondrial fragmentation was commonly observed, and shRNA targeting Drp1 in the BxPC3 pancreatic cancer model led to reduced tumour size and growth.

Similarly, hyperactivation of Drp1 was reported in lung cancer cells, thereby leading to increased mitochondrial fission and apoptotic resistance. Interestingly, by blocking Drp1 activation, apoptosis increased while cellular proliferation decreased (Rehman et al., 2012). While, these findings indicate that mitochondrial fusion may inhibit the transformation of cancer cells, and further suggest that it may be exploited in cancer therapeutics, contradictory observations have been made. It has also been reported that defective Drp1-dependent fission (leading to mitochondrial fusion) promotes apoptotic resistance and survival in lung cancer cells A549. Similarly, mitochondrial fusion induced by the inhibition of Drp1 promoted tumour survival in hepatocellular carcinoma cells (Li et al., 2017). These contradictory observations may reflect in part cancers heterogeneity and plasticity. Therefore, both mitochondrial fusion or fission could be deregulated in cancer (depending on context), and exploitation of either end of mitochondrial dynamics would depend on the particular patient molecular lesion as recently proposed (Anderson et al., 2018). These findings further highlight the importance of maintaining the overall proper balance between mitochondrial fission and fusion for crucial cellular homeostasis. To achieve this, cells have adapted multiple signalling mechanisms to regulate pro-fusion and pro-fission mediators.

### 1.3.2 Mitochondrial pro-fusion initiators and their regulators

At a steady state, mitochondria continuously cycle between the fused state and a fragmented state (Lewis and Lewis, 1914). However, a particular mitochondrial morphology can be favoured to facilitate the needs of a cell such as high energy demand, response to stress-conditions or ROS. These cellular events directly regulate at least one member of the proteins responsible for mitochondrial dynamics.

Below, we further summarise how proteins involved in mitochondrial dynamics mediate mitochondrial fusion or fragmentation.

### 1.3.2.1 Mitofusin 1/2 (Mfn1/2) mediates outer mitochondrial fusion

Mfn1/2 were originally identified as mammalian homologs of *Drosophila* fuzzy onions protein Fzo (Santel and Fuller, 2001). Mfn1/2 have at least 60% identity with each other, and have at least 32% identity with Fzo. Structurally, Mfn1/2 contains an N-terminal GTPase domain and a C-terminal transmembrane domain (TM). Importantly, Mfn1/2 contains two heptad repeats (HR); HR1 is situated after the N-terminal GTPase domain, and HR2 is located in the C-terminal domain after the TM. The N-terminal domain and C-terminus extrudes to the cytosol. Despite Mfn1/2 strong sequence similarity, they are not totally functionally redundant (Eura et al., 2003).

Mfn1/2 can coordinate mitochondrial fusion together by forming both homotypic and heterotypic complexes in a cell type-dependent manner (Chen et al., 2003a). It is not surprising that the combined loss of Mfn1 and Mfn2 can lead to drastic mitochondrial fission and reduced cellular health (Chen et al., 2005). However, Mfn1 KO cells have severely more fragmented mitochondria than Mfn2 KO cells, indicating that Mfn1 homotypic binding may be prioritised during fusion. Therefore, distinct roles have been suggested for Mfn1 vs Mfn2 (Ishihara et al., 2004). It has been proposed that Mfn1 mediates a higher GTPase activity and is the main inducer of GTPase-dependent mitochondrial fusion. This finding suggested that Mfn1 may be the main player in mitochondrial fusion and Mfn2 may have other mitochondrial fusion-independent roles.

Further studies subsequently suggested that Mfn2 is not required for mitochondrial fusion, but is actually essential for tethering mitochondria to the ER (de Brito and Scorrano, 2008). The loss of Mfn2 in these experiments drastically led to the disruption of mitochondria-ER contact sites thereby reducing mitochondrial Ca<sup>2+</sup> uptake. Interestingly, this was independently confirmed in different cell types by other groups (Chen et al., 2012, Schneeberger et al., 2013, Sebastian et al., 2012). In addition, Mfn2 also regulates mitochondria-ER contacts by also recruiting mitochondrial ubiquitin ligase (MITOL) to induce ubiquitination of mitochondria-bounded Mfn2 (Sugiura et al., 2013). Intriguingly, while ubiquitinated proteins are expected to be proteasomally degraded, MITOL-dependent ubiquitinated Mfn2 is not degraded but rather activated via enhanced GTP-dependent oligomerization.

One of the suggested roles of Mfn2 at the ER site was to regulate mitochondria cristae and ER contacts by regulating Opa1 cleavage, as shown *in vivo* (Sood et al., 2014). These authors suggested that during postprandial physiological homeostasis after 12-hours of fasting in mice, MTORC1 signalling is downregulated and mitochondria-ER contact site increases in number and length in mouse liver lysates. Furthermore, mitochondria were fragmented with a decrease in cristae density and respiration rate. Interestingly, these mitochondrial remodelling events and the metabolic shift were mediated by an increase in Opa1 cleavage and surprisingly these changes involved Mfn2, but not Mfn1. However, to note, further contradicting results have been documented. For example, some results suggest an Mfn2-independent ER-mitochondria juxtaposition, and that rather than a reduction of ER-mitochondria contact sites, contact sites were increased upon Mfn2 loss (Cosson et al., 2012, Filadi et al., 2015). Naon et al. (2016) have also used electron microscopy to confirm that ER-mitochondria juxtaposition was reduced following Mfn2 loss. While the exact role of Mfn2 in mitochondria-ER contact sites is not yet totally clear, the importance of this functional link seems consistent amongst all the studies. Novel functions of Mfn2 in the maintenance of mitochondrial level of Coenzyme Q was recently reported, thereby linking Mfn2 to energy metabolism (Mourier et al., 2015).

The mechanism and model of Mfn1 during fusion has been proposed after intriguingly exploring Mfn1 structure. The original functional model was that Mfn1 mediates fusion via HR2 binding and tethering of two adjacent mitochondrial membranes (Ishihara et al., 2004, Koshiba et al., 2004). Recent evidence suggests mitochondrial tethering can occur at the GTPase domain in contrast to HR2-C-terminal mediated tethering (Qi et al., 2016, Yan et al., 2018, Daumke and Roux, 2017). Qi et al (2016) generated a crystal structure using a short form of Mfn1 containing the GTPase domain and a distal part of HR2 in the C-terminal tail (that is similar to bacterial dynamin-like protein). Upon purification and *in vitro* study, they observed that the GTPase domain can dimerize shortly after GTP binding. The new revised model proposes that a conformational change occurs upon GTP hydrolysis. This conformational change drives the interaction of helix bundles, and then the dimerization of the GTPase domain, thereby bridging opposing mitochondria to close proximity for outer mitochondrial membrane tethering to occur. Interestingly, this model has been independently supported (Cao et al., 2017). This subsequent study also reported that upon GTP hydrolysis, GTPase domain mediates conformational change to enhance GTPase domain dimerization.

It is possible that Mfn1 domains may mediate a step by step tethering process that first involves GTPase-domain mediated dimerization and subsequently HR2-mediated tethering. In agreement with this model, further studies have now shown that the HR and GTPase domains have distinct roles in the induction of mitochondrial fusion (Daste et al., 2018). These studies clearly highlight the complexities in outer mitochondrial fusion which may explain why Opa-mediated inner membrane fusion is highly dependent on Mfn1-mediated outer membrane fusion (Cipolat et al., 2004).

### 1.3.2.2 Optic atrophy 1 (Opa1) mediates inner mitochondrial fusion

Opa1 was identified as the molecular lesion in dominant optic atrophy and as a homologue of *mgm1p* and *ms1p* in yeast (Delettre et al., 2000). Opa1 includes multiple isoforms formed from 30 exons that can be alternatively spliced at exon 4, 4b and 5b to generate eight mRNA species. Opa1 structural characteristics were revealed to entail a GTPase domain, middle domain and a GTPase effector domain (GED), placing the protein as a member of the dynamin protein family. In addition, Opa1 may carry between one and three coiled-coil domains (CC0-CC2), and between one and three transmembrane helices (TM1-TM3) depending on the splice variant. CC1 and CC2 complexes have been suggested to drive the formation of homotypic dimers between Opa1 proteins while CC0 and CC1 have been linked with the formation of heterotypic dimers (Akepati et al., 2008, Belenguer and Pellegrini, 2013). Recent studies have further suggested that during fusion, Opa1 interacts with the lipid cardiolipin to induce heterotypic inner membrane space (IMS) fusion in a GTPase independent manner (Ban et al., 2017).

Opa1 protein is translated in the cytoplasm but these proteins contain a mitochondrial import sequence that is cleaved by mitochondrial processing peptidase (MPP) protease during mitochondrial import to form initially a long L-Opa1 isoform. L-Opa1 is anchored into the inner membrane where it is functionally regulated via a series of protease-dependent cleavages events that shifts its protein length from the long isoform to a soluble short isoform, s-Opa1. The s-Opa1 is released from the transmembrane regions as a result of the cleavage.

There are at least two cleavage sites on L-Opa1 that are recognized by inner membrane peptidases Yme1L and OMA1. The cleavage sites have been mapped as S1 and S2 on exon 5 and exon 5b respectively (Duvezin-Caubet et al., 2006, Ishihara et al., 2006). Yme1L is an i-AAA ATP-dependent metalloprotease which consists of AAA-domain and a metallopeptidase domain carrying a zinc binding site (Truscott et al., 2010). Yme1L cleaves Opa1 at site 2 (S2) (Song et al., 2007, Mishra et al., 2014).

On the other hand, OMA1 is a membrane potential-dependent protease that cleaves Opa1 at exon 5 on site 1 (S1) during stress to s-Opa1 (Head et al., 2009, Ehses et al., 2009).

Opa1-induced fusion is achieved by the alteration in relative levels of s-Opa1 and L-Opa1. During normal basal conditions, levels of s-Opa1 and L-Opa1 are balanced and the presence of both is critical for basal levels of mitochondrial fusion (Song et al., 2007). However, the relative accumulation of L-Opa1 has been suggested to be sufficient to induce mitochondrial fusion (Ishihara et al., 2006, Anand et al., 2014, Tondera et al., 2009). This conclusion is based on the observation that cristae and fusion integrity is maintained in OMA1/Yme1L double knockouts that only expressed L-Opa1 forms. In contrast, the continuous cleavage of L-Opa1 by OMA1 has been shown to accumulate s-Opa1 forms resulting in mitochondrial fragmentation (Head et al., 2009, Ehses et al., 2009, MacVicar and Lane, 2014). The homeostasis of both L-Opa1 and s-Opa1 is therefore critical for the continuous remodelling of mitochondria and this could affect cellular metabolism.

Interestingly, the biological significance of OMA1 and Yme1L-dependent cleavage of Opa1 suggest that they can be differentially activated during distinct cellular processes. For example, it has been shown that OMA1-dependent cleavage of Opa1 is increased during stress-induced mitochondrial dysfunction (Head et al., 2009, Ehses et al., 2009, Baker et al., 2014). This correlates with the observation that OMA1 has a positively-charged amino acid sequence in the N-terminal region that is required for stress-induced mitochondrial fragmentation but dispensable for OMA1-dependent Opa1 cleavage (Baker et al., 2014). This sequence is therefore proposed to be a stress-sensor on OMA1. On the other hand, Yme1L-dependent cleavage of Opa1 has been shown to induce mitochondrial fusion (Mishra et al., 2014). Interestingly, it was shown that the stimulation of OXPHOS led to mitochondrial inner-membrane fusion via Yme1L-dependent cleavage of Opa1. These studies suggest that Yme1L and OMA1-dependent cleavage of Opa1 may have different functional outcomes.

Furthermore, Opa1 is also suggested to be processed by other proteases. It has been shown that Presenilin-associated Rhomboid-like protein (PARL) is required for effective Opa1 processing (Cipolat et al., 2006). PARL is a resident of the inner mitochondrial domain where it functions as an anti-apoptotic protein. Cipolat et al. (2006) observed small variants of soluble Opa1 at the IMS, which was inhibited in PARL knock out model. However, independent studies indicated that loss of PARL did not alter Opa1 processing (Duvezin-Caubet et al., 2007). It is possible that there

are unidentified proteases that are involved in the proteolytic processing of Opa1 to mediate mitochondrial fusion, and this may be dependent on the type of mitochondrial stress. Overall, these studies suggest that the proteolytic processing of Opa1 is required for maintaining the balance between L-Opa1 and s-Opa1. Hence, proteases play a key regulatory role in Opa1-dependent mitochondrial fusion.

Opa1-induced inner mitochondrial membrane fusion is critical for energy metabolism, as Opa1 KO cells are extensively fragmented with fewer cristae and OXPHOS capacity (Chen et al., 2005). Recently, Lee et al. (2017) reported that in L-Opa1 deficient cells, s-Opa1 mediates mitochondrial energy production and cristae structure while mitochondria remained fragmented. Interestingly, L-Opa1 deficient cells were generated by expressing Opa1-variant 5 containing exon 4, 4b and cleavage S1 but not S2 in Opa1 KO cells (Song et al., 2007). Therefore, the protein product of Opa1-variant 5 is completely cleaved at S1 after mitochondrial targeting, resulting in the production of only s-Opa1 in the Opa1 KO cells. It was shown that cells expressing only s-Opa1 had similar cristae widths relative to wildtype cells. Similarly, s-Opa1-expressing cells were viable at similar levels to wildtype when forced to utilize mitochondrial-generated energy (Lee et al., 2017). In addition, a similar oxygen consumption rate was also observed in cells expressing only s-Opa1 vs. wildtype, thus suggesting that cells expressing only s-Opa1 are competent in synthesizing energy via OXPHOS. As mitochondrial fusion is coordinated by Mfn1 and Opa1 to maintain cellular homeostasis, the process can also be regulated by post-translational modifications, which we further clarify below.

### 1.3.2.3 Post-translational regulation of pro-fusion initiators

While it is well-established that mitochondrial fusion is critical for embryonic development, mitochondrial fitness and metabolic efficiency, it is surprising that only few post-translational regulations of profusion proteins have so far been established (as reviewed (Tilokani et al., 2018, Escobar-Henriques and Joaquim, 2019)). Recent studies have shown that Mfn1 is regulated by phosphorylation, ubiquitination and acetylation. For example, ERK1/2 phosphorylates Mfn1 at Thr-562 or T564 which inhibits fusion during conditions such as oxidative stress, oxygen limitation and glucose starvation. This phosphorylation promotes cytochrome release, BAK oligomerization and apoptosis (Pyakurel et al., 2015). ERK immunoprecipitated with Flag-Mfn1 but not Flag-Mfn2 indicating an Mfn1-specific modification. Similar to ERK canonical phosphorylation site, the sequence on the sites was ASTPTAP, suggesting that the Mfn1 phosphorylation site is well conserved. Interestingly, the activation of

ERK using pharmaco-activators and genetic overexpression also amplifies Mfn1-T562 phosphorylation, confirming this site is directly phosphorylated by ERK.

Phosphorylation of fusion mediators may also serve as a priming upstream signal for other regulation such as ubiquitination. For example, c-jun N-terminal kinase (JNK) phosphorylates Mfn2 at Ser-27 during doxorubicin-induced-stress, which is a prerequisite for its ubiquitination by E3-ARF-BP1 to mediate mitochondrial fragmentation and cell death (Leboucher et al., 2012). Similarly, Pink1 initially phosphorylates Mfn1 and Mfn2, followed by Parkin-ubiquitination during early mitophagy event to promote Mfn1/2 proteasomal degradation and mitochondrial fragmentation (Gegg et al., 2010, Chen and Dorn, 2013). Furthermore, the stability of Mfn1 is regulated by MARCH5, which ubiquitinates acetylated Mfn1 forms leading to their degradation by proteasomes (Park et al., 2014). Park et al. (2014) reported that during mitochondrial stress induced by a low dosage of antimycin A (which inhibits complex III of the E.T.C), mitochondrial hyperfusion first occurs, preceding later acute mitochondrial fragmentation to aid cell survival. Interestingly, it is also suggested that HDAC6 deacetylates Mfn1 to induce mitochondrial fusion during glucose starvation which protects cells from oxidative stress (Lee et al., 2014). These all further suggest that modulation of mitochondrial fusion may have specific roles in maintaining metabolic homeostasis and cell survival under stress conditions.

### 1.3.3 Mitochondrial pro-fission initiators and their regulators

As the contrast to mitochondrial fusion, mitochondria can be severed into smaller, shorter or rounded organelles via the action of pro-fission initiators. These include pro-fission proteins: Drp1 in conjunction with receptor proteins mitochondrial fission factor (Mff), mitochondrial fission protein 1 (Fis1) and mitochondrial dynamics protein (MiD49 and MiD51) (that are resident in the outer mitochondrial membrane). Together, these factors coordinate to help promote mitochondrial division. This section summarises how currently known fission initiators together alter mitochondrial shape by receiving signals from upstream regulators.

#### 1.3.3.1 Dynamin-related protein-1 severs mitochondria

Drp1 belongs to the large dynamin protein family of GTPases. A key characteristic of the dynamin protein family is their ability to assemble inter multimeric ring-shaped structures via GTP hydrolysis. Drp1 is 80kDA cytosolic protein and its structural contains N-terminal GTPase domain, a middle and variable domain, and a C-terminal GTPase effector domain (GED) (Smirnova et al., 2001). The GTPase domain drives

GTP binding for hydrolysis (Chappie et al., 2010). The middle domain is critical for assembling and oligomerization of Drp1. The molecular function of the variable domain has not been fully characterized but the GED promotes Drp1 intramolecular interaction. In addition, the variable domain and GED carry important phosphorylation sites S616 and S637 (human Drp1 isoform-1) respectively that mediates Drp1 function in response to specific cellular stimuli. For example, phosphorylation of Drp1 at S616 promotes recruitment to the outer mitochondrial membrane to initiate mitochondrial constriction and division during cell growth (Taguchi et al., 2007).

Drp1 was identified as a key player of mitochondrial fission after it was discovered that mutations of Drp1 led to increased and unopposed mitochondrial fusion (Smirnova et al., 2001). The role of Drp1 in mitochondrial remodelling was then shown to be critical for development, cell cycle, mitochondrial-dependent apoptosis, cristae remodelling and mitophagy (Otera et al., 2016, Qian et al., 2012). This led to interests in identifying the mechanism in which Drp1 drives mitochondrial fission. It was revealed that upon mitochondrial division, cytosolic oligomers of Drp1 assemble on the mitochondrial membrane to form large oligomers dependent on the activation of GTPase hydrolysis (Ingerman et al., 2005, Mears et al., 2011).

Advancement was also made by the identification of Drp1 inhibitors and specific receptors on mitochondria. Mitochondrial division inhibitor (Mdivi-1) was initially proposed to selectively block Dnm1-dependent GTPase activity (in yeast), as identified via a chemical library screen (Cassidy-Stone et al., 2008). Mdivi-1 induces mitochondrial fusion in mammalian cells independent of GTPase activity, and it has been widely used in different studies as a purported Drp1 inhibitor. However, this area has controversy as more recent evidence suggests that Mdivi-1 is more likely a E.T.C complex-I inhibitor (Bordt et al., 2017). Bordt et al. (2017) showed that Mdivi-1 inhibits oxygen consumption as a result of a collapse in the E.T.C, independent of Drp1. Mdivi-1 failed to induce mitochondrial fusion in neurons suggesting it may be a cell type-dependent response or its induction of fusion as previously reported is totally independent of Drp1 inhibition. Interestingly, another Drp1 inhibitor P110 has been identified (Qi et al., 2013). P110 is a peptide that disrupts the interaction of Drp1 with its mitochondrial receptors Fis1. The recruitment of Drp1 to mitochondria to form punctate oligomeric structures and its interaction with outer mitochondrial receptors has been shown in wide studies to be critical for mitochondrial division.

However, related protein Dynamin-2 (Dyn2) has also been shown to mediate mitochondrial fission in collaboration with Drp1. In this model, Drp1 initially initiates

mitochondrial constriction and Dyn2 further assembles and mediates the division (Lee et al., 2016). In Lee (2016), it was observed that knockdown of Dyn2 led to mitochondrial hyperfusion. Interestingly, live-cell imaging showed that Dyn2 was recruited to Drp1-marked constriction sites on mitochondria where it mediates the final mitochondrial division. This agreed with the observation that mitochondrial division was halted in Dyn2-depleted cells undergoing mitochondrial fission induced with BAPTA (a calcium chelator). Similarly, electron microscopy also showed stalled mitochondrial division in Dyn2-depleted cells. These findings clearly support a pro-fission role for Dyn2, where it functions downstream of Drp1 to complete mitochondrial division. Presently, four Drp1 receptors have been proposed to bridge Drp1 onto the outer mitochondrial membrane.

### 1.3.3.2 Mitochondrial fission protein 1 (Fis1)

Fis1 was first identified as a novel mitochondrial resident receptor of Dnm1 in yeast (Mozdy et al., 2000). A human conserved form (hFis) was later identified and characterised to recruit Drp1 to mitochondria (James et al., 2003). Fis1 is structurally made up of two tetratricopeptide repeats (TPR); the interaction domain and a carboxy-terminal mitochondrial membrane-bound domain. hFis1 anchors to outer mitochondria membrane via a transmembrane domain in the C-terminal tail. However, the role of hFis1 in the recruitment of Drp1 to mitochondria and mitochondrial division has been controversial.

Fis1 was proposed to be a Drp1-receptor after it was shown that the overexpression of Fis1 induces mitochondrial fragmentation and cytochrome-c dependent apoptosis (James et al., 2003). This was consistent with the observation that the expression of Drp1 mutant (K38A) blocks hFis-induced mitochondrial fragmentation. Further evidence supporting Drp1-Fis1 role in mitochondrial fission has been proposed as it was shown that this pathway mediates fission-dependent heart dysfunction and fission-dependent apoptosis (Zhang et al., 2016, Tian et al., 2017). Similarly, by using immunoprecipitation assay, another study also suggested that Drp1 interacts with Fis1 to induce mitochondrial dysfunction in neurons treated with Amyloid  $\beta$  (A $\beta$ ) (Joshi et al., 2017). However, these experiments did not directly show Drp1 recruitment to Fis1 on mitochondrial axis or monitor functional effects of Drp1-Fis1 interaction on mitochondrial fission. Using a MEF KO model, Fis1 was also suggested to promote mitochondrial fission mutually exclusive of mitochondrial fission factor (Mff) (another Drp1 receptor) (Loson et al., 2013). Fis1 KO MEF had moderately fused mitochondria,

and Drp1 recruitment was partially inhibited, thereby supporting only a partial contributing role for Fis1 mitochondrial fission.

On the other hand, recent studies have raised controversy and suggested that Fis1 may have a limited role as a Drp1 receptor. Otera et al. (2010) reported that the genetic deletion of Fis1 in human colorectal carcinoma HCT116 did not alter mitochondrial morphology. However, these authors suggested that Mff was primarily driving mitochondrial fission. Similarly, by using proximity-based labelling, it was shown that there is no interaction between Fis1 and Drp1 (Osellame et al., 2016). However, Drp1 strongly interacted with Mff and other Drp1 receptors on mitochondria. Interestingly, it was also observed that KO of Fis1 in MEF did not alter mitochondrial infrastructure. The observation that Drp1 does not readily interact with Fis1 suggests that P110 (used to block Fis1/Drp1 interactions) is likely mislabeled mechanistically. Another study also supports Fis1-independent Drp1 recruitment, as Fis1 did not bind Drp1 but binds TBC1D15 protein (a RAB7 GAP) in a stable complex (Onoue et al., 2013). Interestingly, it was recently shown that hFis1 can mediate mitochondrial fission independent of Drp1 and Dyn2 (Yu et al., 2019). This study reported that hFis1 binds and inhibits the GTPase activity of profusion proteins Mfn1, Mfn2 and Opa1 leading to reduced fusion, further differentiating it from a bona fide Drp1 receptor. The observations from these studies overall suggest that Fis1 is not an intrinsic Drp1 adaptor.

Nevertheless, recent studies have suggested that Fis1 may have other non-canonical functions in mitophagy. For example, the Fis1 KO was shown to block degradation of damaged mitochondria in *C. elegans* and mammalian cells (Shen et al., 2014). Similarly, Fis1 interaction with TBC1D15/17 was required for mitophagy (Yamano et al., 2014) and TBC1D15/17 was shown to anchor mitochondria to LC3 during mitophagy. This agrees with the observation that Fis1 KO cells were unable to recruit TBC1D15/17 to mitochondria, resulting in the build-up of abnormal LC3 aggregates, swollen lysosomes and increased mitochondrial-lysosomal contacts (Yamano et al., 2014, Wong et al., 2018). These roles of Fis1 in mitophagy suggest that it is a prerequisite for an effective mitochondrial clearance during mitochondrial damage.

Overall, these studies support a multiple Drp1 mitochondrial receptor localization mechanisms that may be dependent on the cell type or functional divergence between human and yeast. However, other evidence better supports that Mff serves a stronger role as a receptor for mitochondria fission because its overexpression led to excessive mitochondrial fragmentation (Loson et al., 2013).

### 1.3.3.3 Mff and other Drp1 receptors on mitochondria

The presence of multiple candidate receptors for Drp1 on mitochondria highlights the importance of mitochondrial division. Gandre-Babbe and van der Bliet (2008) identified mitochondrial fission factor (Mff) as a mitochondrial outer membrane resident protein functioning as a component of mitochondrial fission using a small interfering RNA screen. Mff was later confirmed to be a Drp1 receptor after studies revealed Mff co-localizes *in vitro* and *in vivo* with Drp1 on mitochondria (Otera et al., 2010). Furthermore, overexpression of Mff was shown to result in extensive mitochondrial fragmentation. The knockdown of Mff also reduced Drp1 recruitment to mitochondria resulting in mitochondrial fusion (Gandre-Babbe and van der Bliet, 2008, Otera et al., 2010). However, Mff KO had the strongest effect on inhibiting mitochondrial fission relative to other receptors, suggesting that Mff is the main Drp1 adaptor on mitochondria (Loson et al., 2013). A two-hybrid screen also suggested that Mff binds oligomerized Drp1, further strengthening the evidence of a direct link between Mff and Drp1-mediated mitochondrial fission (Liu and Chan, 2015). This is consistent with the observation that Mff, but not Fis1, rescued defective Drp1 recruitment to the mitochondria in cells where all proposed Drp1 receptors were simultaneously knocked out (Osellame et al., 2016). While it was surprising that Drp1 has multiple receptors resident on mitochondria, yet more novel receptors were further identified.

MiD49 and MiD51 also known as MIEF2 (Mitochondrial elongation factor) and MIEF1 (respectively), were identified as novel members of the mitochondrial fission signalosome (Palmer et al., 2011, Zhao et al., 2011). MiD49/MiD51 were previously identified as Smith-Magenis syndrome chromosome region candidate gene 7 (SMCR7 and SMCR7L) as 2 related proteins with 45% amino acid similarity (Simpson et al., 2000). Structural and functional analysis of MiD49 and MiD51 have been independently confirmed (Richter et al., 2014, Loson et al., 2015). These data collectively show that MiD51 contains a nucleotidyltransferase fold domain and can bind ADP and GDP. MiD51 mediates Drp1 recruitment to mitochondria via a domain within the nucleotidyltransferase fold. Similar to MiD51, MiD49 also carries a nucleotidyltransferase domain and external loop that binds Drp1. Despite their close structural similarity, MiD49 has been proposed to adopt a monomeric structure that cannot bind ADP. In contrast, MiD51 is thought to adopt a dimeric structure and these differences have been suggested to promote a differentially regulated mechanism (Loson et al., 2015).

The roles of MiD49 and MiD51 in Drp1-recruitment and mitochondrial fission have been studied by genetically targeting their expression in different cell models. MiD49 and MiD51 are classified as Drp1 receptors due to the observation that their knockdown together resulted to reduced Drp1 recruitment to mitochondria thereby promoting mitochondrial fusion (Palmer et al., 2011, Loson et al., 2013). However, it was also observed that the knockdown of either MiD49 or MiD51 did not alter mitochondrial shape (Palmer et al., 2011). In contrast, Zhao et al (2011) showed that the knockdown of MiD51 resulted in mitochondrial fission (Instead of fusion). This unexpected observation was later attributed to being a cell-dependent response and variability in the efficiency of shRNA (Dikov and Reichert, 2011). Further studies in MEF knock out cells model indicated that the deletion of either MiD49 or MiD51 is not sufficient to greatly alter mitochondrial morphology (Osellame et al., 2016). However, it was observed that the triple KO of Mff, MiD49 and MiD51 led to mitochondrial hyperfusion, and MiD49 and MiD51 sufficiently rescued Drp1 recruitment and mitochondrial fission. While these studies suggest that the presence of one receptor can sufficiently compensate for the loss of another, it was also suggested that functional consequences from loss of certain Drp1 receptors may be cell type-dependent.

Indeed, findings from overexpression studies suggest that MiD49 and MiD51-dependent regulation of fission via Drp1 recruitment is context-specific. The overexpression of either MiD49 or MiD51 increased the recruitment of Drp1 to mitochondria further identifying them as direct Drp1 receptors (Zhao et al., 2011). Paradoxically, recruitment of Drp1 to mitochondria upon MiD49 and MiD51 overexpression does not correlate with mitochondrial fission. While MiD49 and MiD51 overexpression led to increased Drp1 recruitment to mitochondria, extensive mitochondrial fusion was observed (Zhao et al., 2011, Palmer et al., 2011, Palmer et al., 2013, Liu et al., 2013). This finding seemed to suggest that MiD49 and MiD51 negatively regulate Drp1. Although this unexpected observation was later shown to occur as a result of inhibitory post-translational phosphorylation at Drp1 S637 when MiD51 is overexpressed (indicating that MiD49 and MiD51 recruits inactive Drp1). Other studies have shown that MiD51 can also directly inhibit Drp1-GTPase activity (Loson et al., 2013, Zhao et al., 2011).

While observations indicate that Drp1 have multiple receptors that can be functionally redundant, it has been proposed that MiD49, MiD51 and Mff together facilitate Drp1-mediated mitochondrial fission. It is suggested that MiD49 and MiD51 specifically promote the recruitment of Drp1 to mitochondria where it inhibits the GTPase activity

(Osellame et al., 2016). Mechanistically, since Mff has been shown to bind MiD49 and MiD51, it is suggested that MiD49/51-dependent recruitment of Drp1 enhances the amount of Drp1 located at the mitochondrial axis. This mitochondrial pool of Drp1 is subsequently used for the next round of fission that would be initiated by Mff-dependent activation of Drp1-GTPase.

Insights from crystal structural studies suggest full wildtype Drp1, truncated MiD49 and MiD51 can bind to four molecules of Drp1 to form linear inter-Drp1 organisation (Kalia et al., 2018). Interestingly, it was observed that this linear arrangement changes upon GTP-hydrolysis to a ring shape Drp1. It was shown that MiD49 is unable to bind to Drp1 in its ring state thereby suggesting that MiD49 detaches from Drp1 prior to mitochondrial constriction. This observation agrees to the proposed model that MiD49 and MiD51 recruit Drp1 to mitochondria after which Drp1 constricts mitochondria upon GTPase activity that occur independently of MiD49 or MiD51.

In addition, recent studies also show that the ER can also regulate Drp1 recruitment to mitochondrial constriction sites (Ji et al., 2017). Interestingly, it was shown that Mff and Fis1 are also ER-bound Drp1 receptors due to the observations of Mff and Fis1 subpopulations on ER independently of mitochondria and peroxisome populations. Ji et al (2017) proposed another mitochondrial fission model where ER donates ER-bound Drp1 to mitochondria to increase the rate of Drp1-mediated mitochondrial fission. Overall, these multiple pro-fission mechanisms may serve as a resilient set of coordinated mechanisms to keep mitochondrial fission in check. While there is still lack of clarity in how these pro-fission proteins mediate fission together, there is general consensus that Mff or MiD49 and MiD51 can each independently mediate some Drp1 recruitment to mitochondria. However, whether this Drp1-recruitment will lead to mitochondrial fission is also dependent on other post-translational regulatory signals dictated by cellular events.

#### 1.3.3.4 Post-translational regulation of pro-fission initiators

Mitochondrial fission is an important biological process that has been proposed to regulate key cellular events such as cell division, apoptosis and mitophagy. Since mitochondrial remodelling is continuous, cells would thus need to modulate this process in response to particular contexts. Key post-translational regulation of pro-fission initiators include phosphorylation, SUMOylation, ubiquitination, S-nitrosylation and acetylation. Regulatory sites on pro-fission initiators have now become better

characterised at the molecular level. This section summarises key regulatory pathways mapped for the pro-fission initiators.

#### **1.3.3.4A AMP-activated kinase (AMPK) regulates Drp1 receptors on mitochondria**

During a metabolic crisis such as ATP depletion, for example, caused by damage to subunits of the E.T.C., AMPK is phosphorylated at Thr127 leading to its activation. AMPK centrally enhances ATP-catabolic pathways while limiting ATP consuming processes. AMPK phosphorylates key members (eg Raptor) of the MTORC1 nutrient-sensing pathway to signal low energy status and inhibit cell growth and phosphorylates Ulk1 to promote autophagy (under certain contexts) (Egan et al., 2011, Kim et al., 2011b).

However, AMPK also is able to promote ATP generation by directly phosphorylating mitochondrial resident proteins. Proteomic studies in COS-1 cells firstly suggested Mff to be a downstream target of AMPK (Ducommun et al., 2015). Subsequently, Toyama et al. (2016) reported that during mitochondrial stress induced by E.T.C collapse, AMPK is activated, leading to the phosphorylation of Mff (and also Ulk1 and ACC) in U2OS cells. Phosphorylation of Mff enhanced Drp1 localization to mitochondria thereby promoting mitochondrial fragmentation. Mff-phosphorylation-induced fragmentation was associated with increased ROS and enhanced mitophagy. Therefore, increased mitophagy served as a survival mechanism by facilitating mitochondria turnover and biogenesis of new healthy mitochondria. Due to the role of AMPK as an energy sensor, phosphorylation of Mff, therefore, links energy sensing to mitochondrial remodelling. Further characterization indicated that AMPK phosphorylates Mff Ser155 and Ser172, which map between the Drp1 binding site and transmembrane domain. The identification of these sites indicated that Drp1 receptors such as Mff can be directly regulated by stress-sensing kinases, thus widening the scope of mechanisms converging onto mitochondrial regulation.

#### **1.3.3.4B Cyclin-dependent kinase 1 (Cdk1) regulates Drp1 to enhance mitochondrial fragmentation**

Cyclin-dependent kinase1 belongs to a large family kinases that includes Cdk1 through Cdk20. The Cdk superfamily is further divided into subfamilies based on their functional role. Cdk1 belongs to the cell cycle-dependent subgroup containing Cdk1, Cdk4 and Cdk5. Cdk1 is structurally made up of a catalytic and a regulatory subunit. Cdk1 mainly functions as a critical regulator of cell-cycle by binding cell cycle regulatory proteins termed cyclins (Santamaria et al., 2007). The binding of specific

cyclins to Cdk1 promotes its activation, followed by the phosphorylation of its target genes. During cell cycle which is made up of a long growth phase (G1), a DNA replicating phase (S), a short growth phase (G2), and cell division (mitosis, M) phase, cellular contents and organelles such as mitochondria must be divided into daughter cells.

Progression through the cell cycle clearly is only favoured under high energy conditions. Thus, this may explain why mitochondrial morphology has been described to be differentially altered continuously through various phases of the cell cycle. For example, mitochondria were detected in a hyper-fused state during the G1-S phase, a shift that was suggested to sustain ATP. On the other hand, mitochondria remodel to a fragmented state in the pre-mitotic phase, which was proposed to aid in the segregation of smaller mitochondria to daughter cells upon cytokinesis. As mitochondrial division has been proposed to be critical for proper progression of the cell cycle, it was further shown that Cdk1 regulates pro-fission proteins during mitochondria division (Mitra et al., 2009). Cdk1/CyclinB was shown to phosphorylate Drp1 at Ser565 (rat nomenclature similar to human Ser616) to initiate the translocation of Drp1 to fragment mitochondria during mitosis (Taguchi et al., 2007). The Ser616 site is located in the variable domain and its phosphorylation is suggested to enhance Drp1 binding to Fis1 (Han et al., 2008). Other kinases phosphorylate Drp1 at S616 such as Protein kinase C (Qi et al., 2011). Interestingly, this phosphorylation site was also associated with oncogenic induced Ras tumorigenesis. In this case, Drp1-S616 phosphorylation by ERK1 induces mitochondria fission for cell transformation (Serasinghe et al., 2015).

Surprisingly, the S616 site has also been linked to the NF- $\kappa$ B-inducing kinase (NIK) pathway (Jung et al., 2016). NIK enhanced mitochondrial fragmentation by binding Drp1 to form a complex that enhanced S616 phosphorylation while repressing a negative phosphorylation-S637 site. The phosphorylation of S616 is so far the only identified regulatory signal for Drp1 that enhances mitochondrial fission. However, the S637 site on Drp1 is phosphorylated by PKA to overall enhance mitochondrial fusion in response to elevated cAMP. Therefore, phosphorylation of Drp1 at different sites can have both positive and negative effects.

#### **1.3.3.4C cAMP signalling and the PKA regulation of mitochondrial dynamics**

cAMP (3'-5'-cyclic adenosine monophosphate) is a second messenger which is generated by soluble adenylyl cyclase (sACs) or transmembrane adenylyl cyclase

(tmACs). There are presently one sAC and nine tmACs isoforms identified in mammalian cells (Buck et al., 1999). sACs are localised to different cellular compartments such as the nucleus, centrioles and mitochondria. In contrast, tmACs are localised at the plasma membrane. However, no mitochondrial-localised tmACs have been identified. tmACs are coupled with G-protein coupled receptors (GPCRs) that transmit an extracellular signal to intracellular molecular factors by inducing the release of G-proteins subunits initiating downstream signalling (Hilger et al., 2018).

cAMP can be generated at multiple cellular locations (**Fig 1.12**). For example, cAMP is distinctly generated in the cytosol and this cannot cross mitochondrial membranes to reach IMM or matrix in yeast and mammalian cells (Acin-Perez et al., 2009, Di Benedetto et al., 2013, Lefkimmiatis et al., 2013, Hess et al., 2014, Zhang et al., 2015). These studies all suggested that cAMP functioning in the mitochondrial matrix would need to be generated within the matrix itself. cAMP is also generated at the plasma membrane following the binding of a ligand to a GPCR. This leads to a conformational change that releases the G- $\alpha$  subunit from the heterotrimeric guanosine-binding protein complex. Subsequently, G- $\alpha$  binds to ACs leading to its activation and cAMP is formed from ATP.

In contrast to G-protein regulation of tmACs, cAMP is formed from sACs independently of GPCR regulation. sACs are regulated by changes in calcium and bicarbonate levels (Chen et al., 2000). Interestingly, studies have shown that calcium activates sAC by increasing the affinity for ATP (Litvin et al., 2003). On the other hand, sACs senses bicarbonate generated during the diffusion and hydration of carbon dioxide (CO<sub>2</sub>). This hydration process is catalysed by carbonic anhydrase (CA) localised at different cellular compartments such as the cytoplasm and mitochondria (Dodgson et al., 1980, Acin-Perez et al., 2009). Mechanistically, bicarbonate binds and activates sAC by increasing the activation of the active site closure on sAC (Steebhorn et al., 2005, Kleinboelting et al., 2014). This is consistent with the observations that an increase in mitochondrial bicarbonate levels increase cAMP generation from sAC localised within the mitochondrial matrix (Zippin et al., 2003, Acin-Perez et al., 2009, Bitterman et al., 2013). Acin-Perez et al. (2009) suggested that the activation of sAC ensures that equilibrium is maintained between the supply of reducing equivalents and the generation of ATP within mitochondria. Interestingly, many pharmacological activators and inhibitors have been identified as tools for studying cAMP-dependent regulation and treatment of disease. Most prominent examples include  $\beta$ -adrenoceptor agonist isoproterenol and forskolin (Awad et al., 1983, Laurenza et al., 1989). While isoproterenol activates G $\alpha$ , forskolin activates

ACs to stimulate cAMP generation (Litvin et al., 2003). On the other hand, it has been shown that KH7 specifically inhibits sAC while 2,5-dideoxyadenosine blocks the activation of tmACs (Bitterman et al., 2013).

cAMP signalling is mediated by multiple effector proteins such as cyclic nucleotide-gated Ca(2+)-channel (CNG), exchange proteins activated by cAMP (EPAC) and Protein kinase-A (PKA). CNG is a cyclic nucleotide-gated ion channel that plays vital roles in sensory neurons (Matulef and Zagotta, 2003). EPAC (isoform 1 and isoform 2) is a guanine nucleotide exchange protein (for Rap1 and Rap2) activated by cAMP (Kawasaki et al., 1998, Enserink et al., 2002). PKA is a protein kinase that plays a multifunctional role in regulating a diverse downstream signalling network for the maintenance of cellular homeostasis in different contexts (Walsh et al., 1968). PKA is a tetrameric kinase with two catalytic subunits (I and II) and 2 regulatory unit (I and II) (Corbin et al., 1978). The regulatory subunits have four unique isoforms which are characterized as two classes RI and RII, each having the alpha or beta subunits (Lee et al., 1983, Jahnsen et al., 1986, Scott et al., 1987). PKA is activated by the binding of ubiquitous (cAMP) to its regulatory subunit which leads to the dissociation of the regulatory unit and the release of the catalytic units. The catalytic units further initiate the phosphorylation of target proteins such as CREB and Drp1.

Recent studies have shown that PKA can be regulated by distinctly localised cAMP levels at different cellular confinements (Lefkimmiatis and Zaccolo, 2014, Lefkimmiatis, 2014). The levels of cAMP are regulated by phosphodiesterases (PDEs) which are located at different cellular locations, with some isoforms distinctly localized to mitochondria (Acin-Perez et al., 2011b). At their localised sites, PDEs degrade cAMP which leads to termination of PKA activity thus serving as a molecular switch for PKA (Lomas and Zaccolo, 2014). Mechanistically, PDEs mediates cAMP degradation by removing the phosphate group in cAMP and cGMP, and this functional role is dependent on the family of PDE (Neves-Zaph, 2017). For example, studies have shown that PDEs families 1, 2, 3, 10 and 11 hydrolyse both cAMP and cGMP. In contrast, PDE families 4, 7 and 8 are specific for the hydrolysis of cAMP while families 5, 6 and 9 directly target cGMP. Interestingly, recent studies have also shown that the effects of cAMP signalling are indirectly modulated by phosphatases (Burdyga et al., 2018, Cribbs and Strack, 2007, Cereghetti et al., 2008). This is due to the observation that phosphatases such as protein phosphatase 2A (PP2A) target the substrates that are phosphorylated in response to cAMP generation. However, this process can be differentially activated at different cellular localization to further finetune the activity of cAMP-dependent signals.

cAMP regulation of mitochondrial pathways is regulated by specific members of the PKA anchorage protein (AKAP) family (Affaitati et al., 2003). In humans, AKAPs are encoded by 47 genes which encode multiple splice variants. AKAPs act as anchorage for PKA and stations the kinase at close proximity to cAMP generation sites. AKAPs are multifaceted adaptor proteins that can bind the regulatory subunit of PKA and also phosphatases and PDEs (Dodge et al., 2001, Tasken et al., 2001). Therefore, AKAPs direct PKA activity to different subcellular compartment upon cAMP generation. For example, it has been shown that AKAP79 is targeted and localised to the plasma membrane where it anchors PKA, protein kinase C (PKC) and calcineurin (Dell'Acqua et al., 1998). Importantly, a subgroup of AKAPs (AKAP1, AKAP84, AKAP121 and AKAP149), which are all splice variants of the *AKAP1* gene, are localised on outer mitochondrial membrane where they direct PKA mitochondrial recruitment (Chen et al., 1997, Ma and Taylor, 2002).

Overall, cAMP-signalling involves the dynamic interplay of multiple modulators including: 1) localization and type of ACs generating cAMP; 2) type of effector translating the signal; 3) anchoring proteins for the effector; 4) location of substrates; 5) phosphatases; and finally, 6) PDEs neutralizing the signal. While the role of PKA in mitochondrial dynamics has been established, the mechanisms of this complex interplay in the context of mitochondrial dynamics remain unclear. For example, the regulatory and catalytic subunits of PKA have been purified from different mitochondrial compartments but how cAMP and PKA are activated in response to amino acid starvation-induced stress is not clear (Papa et al., 1999). Since sAC is a sensor of ATP, and ATP also serves as the substrate for cAMP, it is still not clear how cAMP increases during amino acid starvation (since amino acid starvation should lead to a reduction in ATP levels). In addition there are over 60 substrates of PKA that have been proposed to signal to mitochondria and their regulation can alter apoptosis, oxidative phosphorylation, mitochondrial cristae and mitochondrial function (Grimsrud et al., 2012, Harada et al., 1999a, Darshi et al., 2011, Garcia-Bermudez et al., 2015, Acin-Perez et al., 2009).

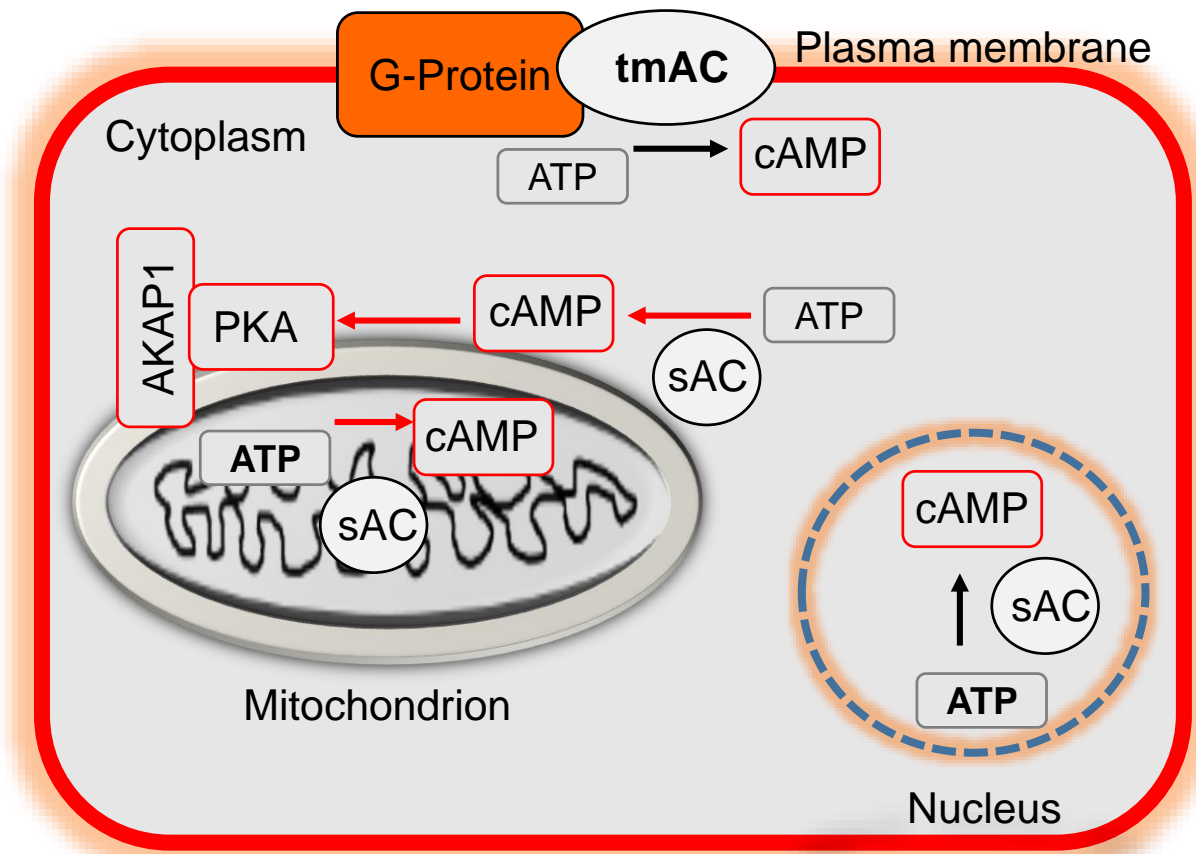


**Figure 1.12: The multiple sites of cAMP generation.** cAMP is generated within a cell by plasma membrane-coupled transmembrane adenylyl cyclase tmAC in response to G-Protein activation. cAMP is also generated in the cytosol, nucleus and mitochondria by soluble adenylyl cyclase (sAC) which converts ATP to cAMP. These multiple cAMP generation sites lead to the formation of microdomains with a distinct cAMP signalling at different cellular compartments. This enables the activation of cAMP effectors such as PKA at the mitochondrion where it is attached to its scaffold AKAP1.

#### **1.3.3.4D Protein kinase A (PKA) regulation of mitochondrial dynamics**

PKA was amongst the first set of signalling regulators identified upstream of Drp1. PKA phosphorylation of Drp1 on Ser637 (also Ser656 in alternative Drp1 splice variants), was first identified using two-dimensional tryptic phospho-peptide mapping (Chang and Blackstone, 2007). In this seminal study, HeLa cells expressing Myc-Drp1 were treated with Forskolin and IBMX (PKA activator and PDE inhibitor respectively) to induce PKA-dependent phosphorylation, leading to the identification of Drp1-S637. Phosphorylation of Drp1-S637 was confirmed with *in vitro* phosphorylation and mutagenesis to test effects of S637A substitution. The Ser637 phosphorylation site on Drp1 was mapped to the GTPase effector domain, and this domain is critical for Drp1 intramolecular and intermolecular interactions. Interestingly, by using phosphomimetic studies in the yeast two-hybrid system, Chang and colleagues showed that intramolecular interactions are inhibited during Drp1-S637 phosphorylation (due to reduced Drp1 GTPase activity).

An independent study confirmed PKA phosphorylation of Drp1 at S637 and importantly, calcineurin was identified as the specific phosphatase that dephosphorylates this site (Cribbs and Strack, 2007). Calcineurin de-phosphorylation of Drp1 could remodel mitochondria from a fused to a fragmented state. This promotion of fission was determined to be a result of the re-activation and translocation of Drp1 onto mitochondria (Cereghetti et al., 2008). Therefore, dephosphorylation of Drp1 at S637 positively regulated fission (which is indirectly opposite to Drp1-S616 phosphorylation by Cdk members, summarised earlier). The phosphorylation of Drp1 by PKA at S637 has been shown to enhance tumour survival by promoting mitochondria-generated ATP (Li et al., 2017). The phosphorylation of Drp1 at S637 is also shown during amino acid starvation that activates PKA (Gomes et al., 2011a). Interestingly, PKA has been shown to phosphorylate MTOR and Raptor at three plausible sites during cold dependent-adipose browning (Liu et al., 2016b).

### **1.4 Current model on mechanism linking nutrient availability and mitochondrial dynamics**

The relationship between MTORC1, mitochondrial dynamics and cellular metabolism remains not totally clear despite evidence supporting biological importance for this pathway. Amino acid starvation has been reported by 2 independent groups to induce mitochondrial fusion (Gomes et al., 2011a, Rambold et al., 2011). While amino acids could be sensed via changes in downstream metabolites (Duran et al., 2012, Gu et

al., 2017, Son et al., 2019), details of this dynamic metabolite sensing in response to amino acid starvation have not been studied. Since amino acid are shuttled into mitochondrial matrix where it is broken down into different metabolic precursors that are utilized for cell growth and survival, how mitochondria coordinate these metabolic changes to MTORC1, a master regulator of cell growth needs to be studied.

It has been suggested that the fusion of mitochondria observed during amino acid starvation serves to prevent non-selective autophagic degradation (mitophagy) hence rescuing healthy mitochondria to maintain a sufficient cellular population (Gomes et al., 2011a). However, there are still limitations and open questions in this model. Interestingly, mitochondrial fusion does not occur in other stress conditions that stimulate autophagy such as hypoxia and serum starvation (Bellot et al., 2009, Kim et al., 2011a, Lum et al., 2005). This suggests that a purpose of mitochondrial fusion is to promote ATP production via E.T.C. during limited energy and low ATP levels (Gomes and Scorrano, 2011, Gomes et al., 2011a). Although studies have assessed the relationship between specific amino acid levels and MTORC1 activation in the regulation of autophagy (Jewell et al., 2015, Nwadike et al., 2018), it is not known whether mitochondria specifically respond to distinct amino acids.

Since MTORC1 serves as the master sensor of amino acids, this mechanism was initially proposed as a key molecular controller of mitochondrial fusion during amino acid starvation (Gomes et al., 2011a). Some evidence suggests that MTORC1 inhibition via RNA interference is sufficient to induce mitochondrial fusion (Gomes et al., 2011a). In addition, the pharmacological inhibition of MTORC1 led to mitochondrial hyperfusion via the reduced expression of mitochondrial fission protein Mtfp1 (Morita et al., 2017). Despite these links between MTORC1 and mitochondrial dynamics, cellular signalling events involving MTORC1 regulation and mitochondrial dynamics during nutrient starvation remain unclear.

In addition to MTORC1, the current model of starvation-induced mitochondrial fusion also features involvement of PKA, but how these 2 kinase pathways may coordinate this process is not clear. For example, mitochondrial fusion during amino acid starvation was accompanied by PKA phosphorylation of Drp1 at S637 (to block Drp1 fission activity) (Gomes et al., 2011a, Rambold et al., 2011). It was proposed that during amino acid starvation, cAMP accumulates leading to PKA activation, but the mechanisms driving cAMP generation is not known. Interestingly, other studies showed that the addition of essential amino acids and glutamine into cell culture media did not induce mitochondrial fusion, but still led to the synthesis of cAMP

(Gomes et al., 2011b). This suggests that cAMP generation and amino acid starvation-induced fusion can be independent responses. Hypothetically, it is possible that mitochondria directly sense the presence of these essential amino acids and glutamine, hence inhibiting mitochondrial fusion. Is mitochondrial fusion in response to full amino starvation due to lack of specific amino acids? These questions are addressed in part by the experiments in this Ph.D. thesis project.

## 1.5 Aims and objective

There is a wide range of evidence indicating that quality of mitochondria within a cell affects cellular function. Mechanistic and clinical evidence has shown that mitochondria are deregulated in ageing, cancer and metabolic diseases. Therefore, maintaining the quality of mitochondria can be a beneficial strategy, as it could prevent the development of age-related disorders, reduce deleterious effects of ROS and ensure cellular metabolic fitness. Understanding how autophagy and mitochondrial dynamics directly control the fitness of mitochondria is therefore critical. The study of these processes can lead to the discovery of new drug targets that could be exploited to enhance mitochondrial fitness and treat diseases where mitochondria are dysfunctional.

Therefore, the overall objective of this PhD thesis project was to study the amino acid sensing signalling pathway that regulates mitochondrial dynamics during starvation stress and the effects of mitochondrial remodelling on cellular metabolism.

The overall aims are:

1. To study mitochondrial remodelling during nutrient availability and to investigate whether mitochondria respond to specific amino acids during starvation conditions.
2. To identify the main signalling pathway connecting nutrient availability to mitochondrial remodelling.
3. To explore the metabolic changes occurring during nutrient starvation and how these metabolic changes are affected by mitochondrial remodelling.

**Chapter 2**  
**Materials and Methods**

## 2.0 Materials and Methods

### 2.1 Cells and Cell culture

Mouse breast cancer cells (4T1) and human cervical cancer cells (HeLa) were obtained from American Type Culture Collection (ATCC). Human osteosarcoma cells (U2OS) were obtained from the Cancer Research UK London Research Institute Central cell bank. Human embryonic kidney cells (HEK-293FT and HEK-293A) were obtained from Invitrogen Life Technologies. Wildtype MEF and *Ulk1/2* DKO MEF were generated by Edmond Chan (McAlpine et al., 2013). Paired wildtype MEF and *Atg5* KO MEF were provided by Noboru Mizushima (Kuma et al., 2004). The generation of *Ulk1*-retrovirally reconstituted DKO cells were generated by Edmond Chan and was previously reported in (Nwadike et al., 2018). AMPK  $\alpha1/\alpha2$  DKO MEF were provided by Benoit Viollet and have been described previously in (Laderoute et al., 2006). Immortalized kidney cells from mice homozygous for a conditionally targeted Fumarate hydratase (*Fh1*) allele which contains *LoxP* sites flanking exons 3 and 4 expressing *Fh1* (*Fh1* fl/fl) and *Fh1* KO clones isolated from *Fh1* fl/fl cells infected with recombinant adenovirus expressing Cre recombinase were provided by Christian Frezza and Eyal Gottlieb (Zheng et al., 2015). *FIP200* KO MEF were provided by Guan Jun-Lin (Gan et al., 2006). The *Mfn1* KO, *Mfn2* KO, *Mfn1/2* DKO, *Opa1* KO MEF and their pairing wildtype MEF were generated previously from (Chen et al., 2003a, Koshiba et al., 2004, Song et al., 2007) but were provided by Luca Scorrano. The CRISPR *Atg13* and CRISPR *Ulk1* targeted 4T1 cell clones were generated in-house by Dr L. Gallagher (unpublished data, Chan laboratory). The Translocator Protein 18 kDa (TSPO) CRISPR and wild type ARPE19 cells were a gift from Dr Xinhua Shu (Biswas et al., 2017).

All cell types were maintained in regular culture medium DMEM (Lonza, Be12-614F) supplemented with 10% fetal bovine serum South American origin, sterile filtered (Labtech, 40811), 4mM L-glutamine (Lonza; Be17-605E) and 1% (100 units/mL) (penicillin-streptomycin) (Lonza, DE17602E) at 37°C with 5% CO<sub>2</sub> in standard cell culture coated plates bought from Griener. Cells were continuously maintained and kept healthy by subculturing at least twice a week by using a standard operating procedure of pre-wash with phosphate buffered saline (PBS; BE17-605E) and cell dissociation using Trypsin/EDTA (Lonza, BE17-161E). For experiments, cells were counted and diluted to attain a concentration of either 0.1 X 10<sup>6</sup> cells/ml or 0.05 X 10<sup>6</sup> cells/ml for 4T1 cells, or 0.075 X 10<sup>6</sup> cells/ml for U2OS and MEF. Cells at these concentrations were plated for experiments in 24 well plates (0.5ml), 12 well plates

(1.0ml), 6 well plates (2.0ml), 6 cm dishes (5ml) or 10 cm dishes (10 ml). Cells for experiments were plated in DMEM (Lonza; BE12-614F) on either, plastic well plates, glass coverslips or fibronectin (Sigma, #F1141) coated glass coverslips (typically 16 to 18 hours prior to treatments and starvation conditions on the following day).

## **2.2 SU9-GFP and GFP-OMP25 expression in cells**

The stable expression of subunit 9 of mitochondrial ATPase- green fluorescent protein (SU9-GFP) and GFP-mitochondrial outer membrane protein 25 (GFP-OMP25) in target cells was achieved by using retroviral vector expression systems. SU9-GFP and GFP-OMP25 plasmids were sourced from Addgene and their maps are published on Addgene website as (Plasmid #23214) and (Plasmid #38249) respectively. Retroviruses were made by transfecting plasmids constructs MXIP-SU9-GFP or MXIP-GFP-OMP25 (Yoshii et al., 2011) and pseudo-retrovirus packaging plasmids; pMDLG polymerase + pMD-VSV-G (Kind gifts from F. Randow, MRC Laboratory of Molecular Biology (LMB), Cambridge, UK) into HEK-293FT packaging cells using standard Calcium phosphate transfection. To achieve this, the packaging plasmids and GFP-plasmid were added into a 1.5ml microcentrifuge tube containing 0.4M  $\text{CaCl}_2$  in a final volume of 350 $\mu\text{l}$  with distilled water. This was mixed in another tube containing 350 $\mu\text{l}$  of 2X HBS (Hepes buffered saline) (280mM NaCl, 1.5mM  $\text{Na}_2\text{HPO}_4$  and 50mM HEPES pH 7.0). The mix was incubated at room temperature for 30 mins and subsequently added slowly to HEK293FT cells cultured in a 6cm tissue culture dish (in 4ml normal DMEM growth medium), followed by incubation for 4hours at 37°C, 5%  $\text{CO}_2$ . The mix was then replaced with 5ml fresh regular media and cells were further incubated for 48hours. Retroviruses were harvested by adding polybrene (2 $\mu\text{g}/\text{ml}$ ) and then passing through a syringe/filter of 0.22 $\mu\text{m}$ . Virus stocks were used fresh or stored at -80. Target cells plated in 6cm dishes were transduced with 1ml of the packaged virus (for 1hr) followed by the addition of 3ml regular media with further incubation for 48hr. Retrovirally transduced cells were selected in 2 $\mu\text{g}/\text{ml}$  puromycin for 72-hours (Sigma, P9620) followed by confirmation via fluorescence microscopy.

## **2.3 The stable knockdown of Drp1/Dnm1l**

Bacteria cultures of mouse Dnm1l pLKO lentiviral shRNA constructs (**Table 2.1**) were obtained from Dharmacon, Open Biosystems. The plasmids were amplified in LB-Amp broth (200ml) by following standard microbiological operating procedure and subsequently purified using a Qiagen Plasmid Maxi Kit (Qiagen, 12163). Pelleted bacteria were dissolved in Qiagen buffers and centrifuged (3279 x g for 15 minutes at

4°C). Supernatants were passed through a glass wool and allowed to drip through the plasmid binding column by gravity. Plasmids were collected on the column, washed and eluted. The eluted DNA was precipitated with 2-propanol and resuspended and washed twice with 70% ethanol and 95% ethanol by centrifugation (13672 x g for 1 minute). Pelleted DNA was air-dried overnight and resuspended in Tris-EDTA (TE) buffer. Plasmid DNA quantification were done using Thermo Scientific NanoDrop 2000c instrumentation.

**Table 2.1: Sequences of Drp1/Dnm1I shRNA**

pLKO shRNA Dnm1I plasmids	Sequence
RMM3981-201744182 - TRCN0000012604	GCCAACTGGATATTAACAATA
RMM3981-201744183 - TRCN0000012605	GCTTCAGATCAGAGAACTTAT
RMM3981-201744184 - TRCN0000012606	CGGTGGTGCTAGGATTTGTTA
RMM3981-201744185 - TRCN0000012607	CCTGCTTTATTTGTGCCTGAA

Lentiviruses were made by transfecting pLKO shRNA plasmids and Lentivirus packaging plasmids into HEK293FT cells using Lipofectamine 2000 (Life Technologies) and standard protocols. To achieve this, the transfection pre-mix was made up by adding 6.4µl of Lipofectamine 2000 to 320µl of OptiMEM (Life Technologies) into a 1.5ml microcentrifuge tube and left to incubate for five minutes at room temperature. This was added into another tube containing 400µl of optiMEM, 1µg of pLKO shRNA plasmids, 0.5µg of psPAX2 (Addgene 12260) and 0.25µg pCMV-VSVG. The mix was incubated at room temperature for 20 minutes to package plasmid into lipid vesicles. The plasmid/Lipofectamine mix was further diluted with optiMEM and added onto HEK293FT cells. After incubation for 4 hours at 37°C, 5% CO<sub>2</sub> the transfection mix was replaced with 5ml regular media. The cells were further incubated for 48 hours at 37°C, 5% CO<sub>2</sub>. Lentiviruses were harvested and transduced into target cells as described for retrovirus systems above.

## 2.4 Amino acid and glucose starvation

Cells were starved of all amino acids by replacing regular DMEM culture medium (containing 4.5g/l glucose, amino acid and vitamins as stated in Lonza DMEM, Be12-614F formulation) with PBS (0.5ml for 24 well plates and 1ml 12 well plates) to rinse the cells. Subsequently, PBS was aspirated with vacuum aspirator to ensure no residual PBS or culture medium, and then replaced with Earle Balanced Salt Solution (EBSS) (Sigma; E2888) containing 1g/l glucose but no amino acid. Where indicated, 4mM glutamine (Lonza, Be17-605E), 0.48mM arginine (Sigma; A8094), 0.78mM isoleucine (Sigma, 12752), 0.78mM leucine (Sigma; L8912), 0.78mM valine (Sigma; V0500) or 0.8mM lysine (Sigma L5501) were added back into EBSS for specific amino acid addback/starvation. Amino acid stocks (except glutamine) were made from powder in distilled water and sterile-filtered (Millex GP, SLGPO33RS).

All amino acid addback starvation experiments were done in the presence of 10% dialyzed fetal bovine serum (Sigma; F0392) except where indicated for serum-starved cells with no added serum. For glucose starvation, glucose-free DMEM media containing 4mM L-glutamine with no sodium pyruvate (Gibco, #11966-025) was used. For amino acid and glucose double starvation, we used PBS (containing Ca/Mg) (Lonza; BE17-513F) lacking sodium pyruvate but supplemented with phenol red and 0.22% sodium bicarbonate (Sigma; S8761). As a pairing media control, PBS with 1g/l glucose and sodium pyruvate (Lonza 04-479Q, containing Ca/Mg) supplemented with phenol red and 0.22% sodium bicarbonate was also used as amino acid starvation media where indicated. For starvation media with drug treatments, we used starvation media as above in the presence or absence of the following drugs; Ulk1 inhibitor MRT68921 (Petherick et al., 2015), MTOR inhibitor Torin1 (TOCRIS, 4247) and cycloheximide (Sigma, C7698).

## 2.5 Western blot analysis

Lysates were harvested by cell scraping (on ice) into 30µl lysis buffer (per well of 12 well dish) (TNTE buffer or TNTE-FB buffer). The TNTE buffer consist of (150mM NaCl, 20mM Tris pH7.5, 5mM EDTA, 0.3% TX100), supplemented with EDTA free protease inhibitor cocktail (Roche Diagnostics, #5892791001). 10mM sodium fluoride (NAF) and 40mM Beta-glycerol phosphate phosphatase inhibitors were added to TNTE to make TNTE-FB lysis buffer. Cell lysates were processed after scraping by centrifugation at (15294 x g, 5mins at 4°C). The protein sample was mixed with 1.5x concentrated Laemmli sample buffer (94mM Tris pH 6.8, 30% glycerol, 3% SDS, supplemented with 5% β-mercaptoethanol (Sigma, M318)) in a ratio of 1 volume

(1.5xLSB) : 2 volume (protein sample). The protein sample was heated at 95°C for 5 mins and then centrifuged for 13672 x g for 1min.

The heated sample was loaded on hand poured 1.5mm Bis-Tris gels made up of 10% acrylamide lower stack (separating gel) with 0.33M Bis-Tris (Sigma, #B9754) and 5% acrylamide upper stack (with 0.33M Bistris) from (30% (w/v) Acrylamide stock [National Diagnostics, EC-890]). Hand poured gels were polymerized by addition of 10% ammonium Persulphate (APS) (Sigma, #T9281) + tetramethylethylenediamine (TEMED) (45µl APS + 15µl TEMED into 9ml lower gel mix and 60µl + APS 20µl TEMED into 6ml upper gel mix).

Pre-stained molecular weight maker (Sigma #SDS7B2) (26kDa to 180kDa) was used as a standard weight guide (**Table 2.2**).

**Table 2.2 Sigma molecular weight marker proteins**

Pre-stained	protein Weight (Da)
α2-macroglobulin from human blood plasma	180,000
β-galactosidase from <i>E.coli</i>	116,000
Lactoferrin from human milk	90,000
Pyruvate kinase from rabbit muscle	58,000
Fumarase from porcine heart	48,500
Lactic dehydrogenase from rabbit muscle	36,500
Triosephosphate isomerase from rabbit muscle	26,600

Gels were typically run for 1-hour at 150V using MES-SDS running buffer (NOVEX life technologies, #NP0002) and then transferred to Immobilon-FL PVDF membrane (Millipore, U.K) with Towbin transfer buffer (250mM Tris, 2mM Glycine, 20% (v/v) methanol) using a submerged wet-transfer apparatus (Idea Scientific Company, Minneapolis U.S.A). The transfers were performed for 35 minutes at 20V and membranes were stained with Ponceau S solution (Sigma, #170729) to confirm the efficiency of transfer.

After membranes were trimmed and excised, membranes were blocked in 5% (w/v) skimmed milk powder in TBS (150mM NaCl, 25mM Tris-base pH 7.4). After blocking, membranes were washed in TBS 3x (1minute each wash). The membranes were probed for corresponding proteins overnight for primary antibody (**Table 2.3**) incubation (RT, Dark) and 1hour secondary incubation with interval washes with 0.05% Tween-20/TBS (TTBS). Images were analyzed and acquired by Licor Odyssey infrared imager (Image studio v2.0).

**Table 2.3 List of antibodies used for western blot showing dilution factors and final concentration (where available)**

<b>Protein</b>	<b>Weight (kDa)</b>	<b>Primary antibody</b>	<b>Secondary antibody</b>
<b>Actin</b>	48	Monoclonal anti-actin mouse, 0.25µg/ml (BD Bioscience: #612657)	Alexa fluor 680 goat anti-mouse IgG. Final conc. : 0.4µg/ml (Thermo scientific, #A21057)
<b>pS6 (S240/244)</b>	32	Polyclonal rabbit (Cell signaling, #2215) (1:1000)	Dylight 800 conjugated goat anti rabbit IgG (Thermo scientific) (1:4000)
<b>Total S6</b>	32	Monoclonal mouse antibody (Cell signaling, 2317) (1:1000)	Alexa fluor 680 goat anti-mouse IgG. Final conc. : 0.4µg/ml (Thermo scientific, #A21057)
<b>Phospho-Ulk1 757</b>	120	Polyclonal rabbit (Cell signaling, #6888) (1:1000)	Dylight 800 conjugated goat anti-rabbit IgG (Thermo scientific)
<b>Ulk1</b>	120	monoclonal rabbit (Cell signaling, 8054) (1:1000)	Dylight 800 conjugated goat anti-rabbit IgG (Thermo scientific)
<b>Atg13</b>	72	monoclonal Rabbit D4P1K (Cell signaling, #13273) (1:1000)	Dylight 800 conjugated goat anti-rabbit IgG, (Thermo scientific)
<b>Mfn2</b>		monoclonal Rabbit D2D10 (Cell signaling, #9482) (1:1000)	Dylight 800 conjugated goat anti-rabbit IgG, (Thermo scientific)
<b>Opa1</b>	80 - 100	Mouse IgG1 (BD anti-transduction, #612606) (1:1000)	Alexa fluor 680 goat anti-mouse IgG. Final conc. : 0.4µg/ml (Thermo scientific, #A21057)
<b>Phospho-Drp1 S637 (1)</b>	78 - 82	Polyclonal rabbit (Cell signaling, #4867) (1:1000)	Dylight 800 conjugated goat anti rabbit IgG (Thermo scientific)
<b>Phospho-Drp1 S637 (2)</b>	78 - 82	monoclonal rabbit (Cell signaling, #6319) (1:1000)	Dylight 800 conjugated goat anti rabbit IgG (Thermo scientific)
<b>Phospho-Drp1 S616</b>	78 - 82	monoclonal rabbit (Cell signaling, #4494) (1:1000)	Dylight 800 conjugated goat anti-rabbit IgG (Thermo scientific)
<b>Drp1</b>	78 - 82	monoclonal Mouse (BD Bioscience, #611113) (1:1000)	Alexa fluor 680 goat anti-mouse IgG. Final conc. : 0.4µg/ml (Thermo scientific, #A21057)
<b>Phospho-PKA substrates (RRXS*/T*)</b>		monoclonal Rabbit 100G7E (Cell-signaling, #9624) (1:1000)	Dylight 800 conjugated goat anti-rabbit IgG, (Thermo scientific)

<b>Phospho-CREB S133</b>	43	monoclonal Rabbit (Cell-signaling, #9198) (1:1000)	Dylight 800 conjugated goat anti rabbit igG, (Thermo scientific)
<b>CREB</b>	43	monoclonal Mouse (Cell-signaling, #9104) (1:1000)	Alexa fluor 680 goat anti-mouse IgG. Final conc. : 0.4µg/ml (Thermo scientific, #A21057)
<b>Fumarase</b>	49	monoclonal Rabbit D9C5 (Cell signaling, #4567) (1:1000)	Dylight 800 conjugated goat anti-rabbit IgG, (Thermo scientific)

## 2.6 Microscopy

### 2.6.1 Fixing and staining cells seeded on coverslips

Cells were seeded on to fibronectin-coated (for 4T1 cells) or uncoated (all other cell types) glass coverslips in 24-well tissue culture plates. After stress/starvation treatments, cells were rinsed with PBS once and then fixed with 3.2% paraformaldehyde/PBS (Agar Scientific, #R1026) for 15 minutes. The coverslips were washed twice with PBS followed by permeabilisation with 0.2% TritonX100 (Sigma #T-9284) for 5 minutes and then rinsed with PBS twice. Methanol was used for permeabilisation for 5 minutes specifically for LC3B staining. Blocking of fixed cells was achieved with incubation in 0.2% (v/v) porcine gelatin/PBS solution (Sigma, #G6144) for 20 minutes. Coverslips were incubated for 20 minutes on parafilm onto drops of primary or secondary antibodies (**Table 2.4**) diluted in gelatin/PBS. After antibody incubation, coverslips were washed with 3-times PBS incubation. Coverslips were rinsed in PBS 3x and finally mounted on 8µl 4mM Mowiol (Sigma #81381) on glass slides.

**Table 2.4 List of antibodies used for immunofluorescence showing dilution factors and final concentration (where available)**

Protein	Primary antibody	Secondary antibody
<b>p62/SQSTM1</b>	Polyclonal guinea pig (PROGEN, #GP62-C) (1:500)	Alexa 555 anti guinea pig (Invitrogen, #A21435)
<b>LC3B</b>	Polyclonal rabbit (Cell signaling, #2775) (1/200)	Alexa 555 anti-rabbit, (Invitrogen, #1037302)
<b>TOM20</b>	Rabbit polyclonal (Santa cruz, FI-145) (1:400) (0.5µg/ml)	Anti-rabbit Alexa Fluor-555 (Invitrogen, 1037302) (1:400) (5µg/ml).
<b>Drp1</b>	monoclonal Mouse (BD Bioscience, #611113) (1:400)	Alexa 555 anti-mouse, (Invitrogen, A21422)

## 2.6.2 Epifluorescence microscopy

Mitochondria were visualized by epifluorescence upright microscopy (Nikon Eclipse E600 using a 60X 1.40 NA objective using MetaMorph software (MDS Analytical Technologies) or WinFluor software (Strathclyde University). 5 – 10 images of different fields were acquired at random from each coverslip. The mitochondrial length was quantified as pixels in at least 50 cells per treatment in epifluorescence microscopy-generated images as detailed below.

Live cell imaging was achieved by epifluorescence inverted microscopy (Nikon Eclipse TE300) coupled with Solent Scientific Incubator and LAMBDA Sc smart shutter controller (Sutter Instrument). Cells were plated on glass-bottom coverslip embedded 35mm plates (Invitro Scientific) overnight in an incubator 5% CO<sub>2</sub> 37°C. The growth medium was replaced with PBS/glucose supplemented with 10% dFBS, 50mM HEPES, 4mM glutamine, 0.78mM leucine, 0.48mM arginine as addback/amino acid starvation media. Microscope environmental chamber temperature was maintained at 37°C. Time-lapse Images were acquired with a 63 x 1.40 NA oil immersion lens at one image per minute for one hour by using the Metamorph software.

## 2.6.3 Confocal microscopy

Micrograph images were acquired using confocal microscopy (Leica, SP5) equipped with a HCX PL APO CS-63x objective- 1.40 NA and HyD detector system. Sequential excitation was provided by Argon (480nm wavelength) and Helium-Neon (HeNe)

(543nm wavelength) gas lasers. The following settings were used; scanspeed (200Hz), line average (4), frame average (1) and lasers: Dapi (PMT1), YFP (HYD), Alexa 555 (HYD). Images were processed using Leica application suites (Advanced fluorescence Lite, version 2.6.0) and exported as TIFF. 3 – 5 images were acquired per coverslip and mitochondrial length was quantified in at least 40 cells per treatment (as detailed below). Images were adjusted for brightness/contrast as required using ImageJ software (Rueden et al., 2017).

## **2.6.4 Transmission electron microscopy**

Transmission electron microscopy (TEM) images of mitochondria were acquired in collaboration with Professor Eeva-Liisa Eskelinen, University of Helsinki, Finland. 4T1 cells treated with amino acid starvation media as stated above were fixed in 2% glutaraldehyde (diluted from 25% stock Sigma G5882) in 0.2 M Hepes pH 7.5 (diluted from 1M stock Invitrogen Life Sci/ Gibco 15630-049) for 2 hours at room temperature and stored in 0.2 M Hepes without fixative at 4°C. Sample coverslips were delivered to collaborator stored in 0.2 M Hepes on cool wet ice packs. Image acquisition were done as previously described in (Anwar et al., 2019). Images were acquired using a JEM-1400 (Jeol, Tokyo, Japan) transmission electron microscope (primary magnification of 5000X). At least two images at different scales (1µm and 500nm) per region were acquired and between 10 and 18 mitochondrial regions were acquired per treatment group.

## **2.6.5 Mitochondrial and autophagy quantification**

Mitochondrial length was quantified in images opened using Image-J software (Rueden et al., 2017). For measurements, free-hand line was traced on mitochondria. Each line was measured by using the analyse/measure function of Image-J. This generated values directly related to the longest estimated mitochondria length. In each cell, ten mitochondrial lengths were quantified and then averaged to calculate a mean mitochondrial length per cell. The number of cells quantified per experiment is stated in each figure legend (typically 40 - 50, per coverslip sample). Experiments were repeated to typically represent 3 - 4 coverslips representing at minimum 2 independent days. Each treatment group in all mitochondrial length graphs were indicated for their mean  $\pm$ SEM. Quantified mitochondria were chosen by random among mitochondria distributed within the cytosol. Collapsed mitochondria that could not be classified as a distinct structure or shape were avoided (e.g collapsed mitochondria close to the nucleus). To limit bias, some experiments were blinded

before quantification or observed blinded by another member of the Lab to corroborate results. Notable, QLR-hyperfusion response were blindly-confirmed on multiple occasions and representative of results in Figure 3.5 and Figure 4.13 were quantified blinded.

To measure Drp1 colocalization with mitochondria, colocalization score was generated by using Image-J as follows. Images were converted to 8 bit formats and split into two channels. By using the colocalization plugin, the colocalization was highlighted and the colocalisation channel was split to identify colocalization alone. The threshold was adjusted to filter out background noise signal, and the threshold values of the first quantified image was noted and used in the quantification of subsequent images to ensure threshold were kept the same. The number of white pixels (indicating colocalization) was counted using analyze particle tab and normalized to the total mitochondrial area in each image multiplied by 100 to calculate the percentage of colocalization. Mitochondrial area was measure using Mitochondrial Network Analysis (MiNA) image-J plugin.

LC3B and p62 puncta were counted manually on the microscope and representative images were acquired. Mean puncta and standard error of mean (SEM) were generated and graphed on Prism.

## **2.7 Polymerase chain reaction (PCR) quantification of mRNA**

Wildtype MEF, *Mfn1*, *Mfn2* and *Mfn1/2* knock out MEF in 6 well plates were lysed and total RNA was extracted using 350 $\mu$ l RNA lysis buffer + 1%  $\beta$ -mercaptoethanol (RLY) following standard operating procedures of Isolate II RNA kit (Bioline). The procedure involved filtering the lysate at 11,000 x g and conditions were adjusted with 70% ethanol. RNA was collected on silica membrane followed by desalting and digestion of DNA with DNase. The silica membrane was washed, dried and total RNA was eluted with RNase-free water. The nucleic acid concentration was determined by using the nano-spectrophotometer (Thermo Scientific NanoDrop 2000c).

First strand cDNA was synthesized from 1 $\mu$ g of total RNA by using 0.4  $\mu$ g oligo-dT primer according to standard protocols. The first annealing reaction in a final volume of 12 $\mu$ l with water was heated in the PCR cycler for 70°C/5mins. For the second step, cDNA extension reaction, 8 $\mu$ l reaction mix containing 0.5 $\mu$ l M-MuLV reverse transcriptase (New England Biolabs #M0253S) was added to make a final volume of 20 $\mu$ l and further incubated at 42°C/1-hour. This reaction mix contained, 2 $\mu$ l of 10X

PCR buffer (New England Biolabs #B90142) and 2.5mM dNTPs (dATP, dCTP, dGTP and dTTP) (Promega #U1511). In the final enzyme deactivation step, volume was made up to 100ul with water and heated at 70°C/5mins.

For semi-quantitative PCR of *Mfn1* and  $\beta$ -actin, the following primers (**Table 2.5**) were used. Primers were designed on RefSeq (Ye et al., 2012) and ordered from Life technologies Invitrogen. The PCR reaction mixes contained 200nM (each) forward and reverse primers, 5 $\mu$ l of cDNA (from 100 $\mu$ l reactions prepared above from equal amounts of total RNA), 2.5mM of dNTPs (Promega #U1511), 5 $\mu$ l of 10X buffer (New England Biolabs) and 0.25 $\mu$ l Taq DNA polymerase (New England Biolabs #M0273S) to make a volume of 50 $\mu$ l. The PCR program was denaturation step at 94°C/2 mins, denaturation at 94°C/30 seconds (40X), annealing at 55°C/30 seconds and extension at 68°C/1 min (Calculated at 1min/kb).

**Table 2.5 List of PCR primers**

Primer Name	Forward sequence	Reverse sequence
<i>Mfn1</i>	GAAAGCTGGCTGTCTTGTGC	GTTTTCCAAATCACGCCCCC
<i>Mfn1</i>	GTTGTTGGGGGCGTGATTTG	TCAAAGCTTCCAGTGGGGAC
<i>Mfn1</i>	TGGTCACACAACCAACTGCT	CTAGGGACCTGAAAGAtgGCG
$\beta$ -actin	GCCTTC CTT CTT GGGTAT	GCACTGTGTTGGCAT GAGG
	GG	

The 100 $\mu$ l PCR product was purified and eluted with 30 $\mu$ l Milli-Q nuclease-free water using standard QiaQUICK microcentrifuge spin columns kit (Qiagen). To visualize the DNA sample, equivalent fractions of sample was mixed with 6X loading dye (0.5M EDTA pH 8, 1M Tris pH 7.5, 100% (v/v) glycerol, bromophenol, xylene cyanol). The PCR products were separated on 1% (w/v) agarose gels using 1X TAE (40mM Tris-Acetate and 1mM EDTA) stained with SYBR safe (Invitrogen #1942037). The DNA bands were visualized using a UV transilluminator (GeneFlash, Syngene) equipped with a PULNIX TM-300 CCD camera as a means to estimate levels of *Mfn1* mRNA in original cell samples. The molecular sizes were estimated by using the 2-log DNA ladder (New England Biolabs, #3200S) as a reference.

## 2.8 Metabolomics

### 2.8.1 Sample preparation

For metabolite analysis experiments, 960000 cells were seeded in 100mm x 20mm (10ml) tissue culture dishes (Greiner) 16 hours before the experiment. After treatments, cells were placed on ice and the media aspirated and replaced with pre-

cooled PBS. The PBS was aspirated and replaced with 1 ml pre-cooled 80/20% HPLC-grade (methanol/water) and cells were scraped and transferred to 1.5 ml microcentrifuge tubes. The cell lysates were rocked for 5 minutes in the cold room and then centrifuged (15294 x g, 5 mins at 4°C). 900 µl of the supernatant was transferred into glass, screw top, autosampler vials (Fisher Scientific #12765058). Also, 100 µl from each sample was pooled together to generate an internal control samples to allow confirmation of no mass spectrometer instrument drift. Extracted metabolites were stored at -80 °C until analysis.

## 2.8.2 Data processing

The extracted metabolites were analysed on a Thermo Scientific Orbitrap Exactive liquid chromatography/mass spectrometer (LC/MS/MS) at Strathclyde Institute of Pharmacy and Biomedical Sciences in collaboration with Dr David Watson, Dr Naser Al-Tannak and Mohammad Al-Rofaidi. pHILIC column was used with a gradient mobile phase solvents system consisting of 20 mM ammonium carbonate in water at pH 9.2 (A) and acetonitrile (B) with flow rate of 300 µl/min (Watson et al., 2013). For downstream data processing, the LC/MS raw data files were separated into positive or negative ionisation mode signals (negmzxmlfiles and posmzxmlfiles) using a windows command batch script written in-house to customise the msconvert tool from ProteoWizard (Chambers et al., 2012).

Next, the negative data was imported first into MZmine 2.10 program for data processing followed by the positive data using the parameters below (**Table 2.6**) and peak lists were generated. For the identification of metabolites, the generated peak list (negative and positive) were screened via an Excel macro library database containing metabolites mass data from the human metabolome, Kyoto Encyclopedia of Genes and Genomes (KEGG), Lipidmaps, MetaCyc and Metlin databases (Creek et al., 2012). Peak quality and retention time was also crosschecked with standards run on pHILIC column.

**Table 2.6: MZmine parameters used for data processing**

<b>Step</b>	<b>Parameters</b>
<b>PEAK and mass detection</b>	Noise level: 1000
<b>Chromatogram building</b>	0.3 min, minimum height of 104, m/z, tolerance range from 0.001 to 10 ppm
<b>For chromatogram deconvolution</b>	Algorithm: local minimum search chromatographic threshold of 1%, search minimum in RT range of 0.3 min, a minimum relative height of 5%, a minimum absolute height of 104, minimum ratio of peak and top edge of 5 and peak duration range from 0.1 to 10 min
<b>Isotope detection</b>	m/z tolerance from 0.001 to 5 ppm, relative retention time tolerance of 5%, a maximum charge equal to 1, and the most intensive isotope was selected
<b>Alignment</b>	Aligned using join aligner m/z tolerance: 0.001 – 10 ppm weight for m/z: 15, retention time tolerance: 5% relative Weight for RT (15)
<b>Filtering</b>	Minimum peaks in a row: 1, Minimum peak in an isotope pattern = 0, M/Z=auto range, retention time: Autorange min = 2, max = 30, peak duration (0.00 – 3.00). For duplicating peak filler m/z tolerance = 0.001m/z or 5.0ppm, RT tolerance = 0.3 absolute min
<b>Gap filling</b>	m/z tolerance 0.001m/z or 5.0ppm
<b>Peak identification</b>	Ionization (M-H)- for negative value (M+H)+ for pos value. Retention tolerance = 0.3, 0.001 (m/z) or 5.0ppm, max complex peak height 50.0%.
<b>Data exportation</b>	Positive and negative peak lists were exported as CSV showing the export row ID, M/Z, retention time, name, peak area, Export Identify

### 2.8.3 Metabolomics data analysis

Data analysis on the metabolite levels were done on the MetaboAnalyst-4.0 online resource (Chong et al., 2018). The peak intensities of each metabolite were uploaded to metaboAnalyst (without data normalization). Metaboanalyst was used to generate the principal component analysis (PCA) which showed the unsupervised multivariate analysis of the variance of data by scoring the data and estimating the separation between the groups within a set of data.

Metaboanalyst also generated the partial least square discriminant analysis (PLS-DA) as a supervised data analysis by using linear regression to optimise the separation found in the PCA. The PLS-DA calculated the Q squared and R squared ratio as a means to measure the quality of the data. For example, when  $R^2/Q^2$  is greater than 0.7, the data is categorized as sufficiently robust.

Pathway enrichment analysis was done on MetaboAnalyst to estimate the biological significance of changes in a set of metabolites in the biological setting by comparing how enriched the metabolites are (based on the number of hits they return) when cross-analysed with a database of metabolic pathways listed in KEGG (Kanehisa et al., 2018). Hypergeometric test was selected for overrepresentation analysis. Metabolites selected for upload into the enrichment analysis were first filtered to be significant at  $p < 0.05$  based on t-test analysis between two groups (as indicated in the figure legends).

Pathway analysis was performed on MetaboAnalyst to enhance the metabolite set enrichment analysis using relative-betweenness centrality. This analysis used an algorithm to measure centrality and connectivity between metabolites relative to biological pathway libraries in the small molecule pathway database (SMPDB) (Frolkis et al., 2010). This analysis ranked the pathways by impact based on the centrality of metabolites. Pathway impact analysis uses the log fold change of metabolites, the statistical significance of the pathways and the topology of the signalling pathway. Overall, high- $-\log P$ /impact values correlate with increased significance of alterations (bigger graphical circles signify more metabolites involved in the data set statistically).

After the integrative set of analyses outlined above which identified pathways that are altered between two treatment groups, further data mining was done in Microsoft Excel to identify specific changes in metabolites of interest such as the metabolites of

the Krebs cycle, nucleotide synthesis and energy synthesis. This was achieved by filtering metabolites based on their pathways as indicated in the Excel macro library database (Creek et al., 2012).

Graphs of peak intensities were plotted using GraphPad Prism-4 (GraphPad Software, La Jolla California USA) and heatmaps were generated to show significant changes in metabolite peak intensities by using online resource Heatmapper (Babicki et al., 2016).

## **2.9 Statistical analysis**

Statistical analysis was performed with either unpaired t-test or 1-way ANOVA with Bonferroni post-test using GraphPad Prism-4. For mitochondrial length analysis, one way ANOVA with Bonferroni post-test was typically done. Altered metabolites were highlighted between two groups for example (glutamine, leucine and arginine addback into amino acid starvation media versus full amino acid starvation cells). Therefore unpaired t-test was used to analyse metabolomics experiments based on existing statistical protocol in Dave Watson lab (Alamri et al., 2019, Alonezi et al., 2017). Significance was denoted as  $P < 0.05$ , \*\*  $P < 0.01$ , \*\*\*  $P < 0.001$ .

## **Chapter 3**

# **Mitochondrial response to changes in nutrient and amino acid pools**

### 3.1 Introduction

Mitochondrial fusion occurs in response to different cellular processes such as ER stress, increased OXPHOS, nutrient-dependent stress and autophagy. Mitochondrial hyperfusion occurs as a physiological response to stress (Tondera et al., 2009, Lebeau et al., 2018). This unique stress-induced mitochondrial hyperfusion (SIMH) is activated during ER-stress, and the mechanism linking ER-stress to fusion and fission initiators has been studied. It has been shown that during ER-stress, the protein kinase RNA-like ER kinase (PERK) arm of unfolded protein response (UPR) is activated (Rainbolt et al., 2014, Teske et al., 2011, Lebeau et al., 2018). The activation of PERK-UPR signalling protects mitochondria from extensive mitochondrial fragmentation and metabolic collapse by enhancing fusion and mitochondrial metabolic fitness. This is due to the observation that SIMH requires the mitochondrial scaffolding protein SLP2 which maintains the stabilization of L-Opa1 for the induction of mitochondrial fusion (Tondera et al., 2009, Wai et al., 2016). This is consistent with the observation that *SLP2* knockout MEFs are more sensitive to ER-stress relative to wildtype MEF as it was shown that SLP knockout MEF have reduced mitochondrial respiratory chain capacity. The findings from these studies show that mitochondria have intrinsic mechanisms in response to stress, and these responses can affect mitochondrial metabolism.

Interestingly, studies have shown that there is a correlation between mitochondrial metabolism, ATP production and mitochondrial hyperfusion (Rossignol et al., 2004, Mishra et al., 2014). These studies observed that mitochondria hyperfuse to accommodate increases in OXPHOS when glutamine is used as a sole substrate for energy production. While it was shown that the increase in OXPHOS promotes Opa1 cleavage by Yme1L, leading to inner membrane fusion, it is not totally clear how bioenergetics and glutamine metabolism regulates mitochondrial hyperfusion (Mishra et al., 2014). For example, the role of the regulators of outer membrane fusion during OXPHOS-induced hyperfusion is not yet known.

The essential roles of mitochondria as central hubs for the generation of cellular energy further highlights the need to understand the link between fusion, metabolism and energy production. For example, energy in the form of ATP is generated via transformation of the proton gradient formed from the electron transport chain, and the overall rate for this process is directly linked to nutrient availability such as glucose and amino acid (Johnson et al., 2014, Mishra et al., 2014). Glucose is metabolised to pyruvate by glycolysis in the cytoplasm. Pyruvate is then transported into

mitochondria and converted to acetyl CoA that then enters the Krebs cycle, where NADH and FADH substrates are produced to drive OXPHOS. On the other hand, branched-chain amino acids (BCAAs; leucine, Isoleucine and valine) are converted into acetyl-CoA or succinyl-CoA, which serve as substrates for the Krebs cycle. In addition, amino acids such as glutamine and arginine can be metabolized to glutamate to produce alpha-ketoglutarate, thus providing another channel to feed the Krebs cycle. However, the conversion of glutamate to alpha-ketoglutarate is dependent on leucine, which serves as an allosteric activator of glutamate hydrogenase (GDH) (Carobbio et al., 2009). Since all these metabolites serve as a precursor of mitochondrial-generated energy, mitochondria may have devised means to sense the nutrient required for metabolism.

Nutrients are required to fuel energy and it is a metabolic requirement for cell growth and cell replication. Changes in nutrient availability in many cellular contexts are rapidly sensed and cells have evolved multiple survival mechanisms to function during nutrient shortages (Gomes and Scorrano, 2011). The availability of regulatory amino acids is detected at the lysosome by a number of specific specialized sensor proteins to regulate the formation of protein complexes for the activation of MTORC1 (Palmieri, 2013, Bar-Peled et al., 2012). MTORC1 activation at the lysosome also interconnects with nutrient-dependent cellular signalling pathways involving GSK3 and AMPK that respond to changes in growth factors and glucose levels respectively (Lin et al., 2012). While cells sense amino acids by activating MTORC1 to inhibit autophagy, it is not yet clear whether mitochondria sense the availability of amino acids or overall nutrients. Although it has been shown that the knockdown or pharmacological inhibition of MTORC1 leads to mitochondrial fusion, how MTORC1 regulates mitochondrial fusion and fission initiators is not also clear (Gomes et al., 2011a, Morita et al., 2017). For example, it is observed that the supplementation of essential amino acids and glutamine alongside amino acid starvation blocked mitochondrial fusion (Gomes et al., 2011b). Since regulatory amino acids are sufficient to activate MTORC1, more evidence is therefore needed to fully understand the role of MTORC1 and its amino acid signalling pathway in the regulation of mitochondrial fusion during amino acid starvation.

Amino acid deprivation leads to the activation of the autophagy process, which has been shown to be a cellular survival mechanism (Vera-Ramirez et al., 2018). Interestingly, this catabolic process is accompanied by increased mitochondrial fusion (Gomes et al., 2011a). The autophagy and fusion processes have been closely linked due to the observations that mitochondrial fusion prevents mitophagy during amino

acids starvation-induced autophagy (Rambold et al., 2011a, Gomes et al., 2011a, Gomes and Scorrano, 2013). However, recent evidence suggests that they are two independent processes. For example, it has been shown that mitochondrial fusion occurs in Atg5 knockout MEF that are unable to undergo autophagy (Rambold et al., 2011). In addition, it is also observed that mitochondrial fusion does not occur in other stress conditions that stimulate autophagy such as hypoxia and serum starvation (Bellot et al., 2009, Kim et al., 2011a, Lum et al., 2005). These studies, therefore, suggest that mitochondrial fusion during amino acid starvation may be a direct response to amino acid shortages.

### **Chapter 3 Aims**

The aim of this chapter is to characterize the mitochondrial response to nutrient availability and further understand the roles of amino acids in the regulation of mitochondrial dynamics. Mitochondrial response to nutrients will be characterized in U2OS, RPE1, HeLa, MEF, and 4T1 cells, encompassing varieties of transformed cells and non-transformed cell lines that are established cellular models for studying mitochondrial dynamics (Toyama et al., 2016, MacVicar and Lane, 2014, Darshi et al., 2011, Mishra et al., 2014, Zhang et al., 2017b). The objectives of this chapter are:

1. Investigate the mitochondrial remodelling responses to glucose, amino acids and serum starvation.
2. Establish a robust model for studying mitochondrial remodelling.
3. Decipher the mitochondrial remodelling response to distinct regulatory amino acids glutamine, leucine and arginine, since they are the main activators of MTORC1.
4. Investigate the role of fusion and fission mediators in amino acid-dependent mitochondrial remodelling.

## 3.2 Results

### 3.2.1 Mitochondrial response to nutrient availability.

It has been suggested that mitochondria respond to nutrient scarcity (to aid survival, escape apoptosis or enhance mitochondrial function) by undergoing fusion to form an interconnected network (Rambold et al., 2011, Gomes et al., 2011a). Recent studies have also suggested that mitochondria increase their overall metabolic activity and that this was specific to amino acid starvation rather than overall nutrient changes or energy demand (Johnson et al., 2014). To understand how mitochondria undergo morphology remodelling, responses to various forms of nutrient starvation were first examined. For this survey, we used a range of cell types.

We studied mitochondrial remodelling in mouse breast cancer 4T1 cells (Zhang et al., 2017b), human U2OS osteosarcoma cells (Toyama et al., 2016), human retinal pigment epithelial RPE1 cells (MacVicar and Lane, 2014) and human cervical cancer HeLa cells (Rossignol et al., 2004). Mitochondrial remodelling was studied in these cells because they are established models for the study of mitochondrial responses to nutrient changes (Toyama et al., 2016, MacVicar and Lane, 2014, Darshi et al., 2011, Mishra et al., 2014, Zhang et al., 2017).

4T1, U2OS, RPE1 and HeLa cells were starved of nutrients; glucose or all amino acids. In addition, we also tested serum starvation, either alone or in combination (i.e. serum + amino acid starvation, or serum + glucose starvation). After starvation for 4-hours, cells were fixed and stained for outer mitochondrial membrane protein translocase of outer membrane-20 (TOM20). Cell images were taken and the mitochondrial length was measured using an ImageJ based quantification approach.

It was observed that mitochondrial morphologies in untreated 4T1 cells cultured in full nutrient media were short and generally fragmented (**Fig 3.1**). A similar observation was seen in serum-starved cells with mitochondria having a punctate and fragmented morphology. In contrast, it was observed that mitochondria remodel their shape to a fused, long and tubular state during amino acid starvation. Similarly, the withdrawal of both serum and amino acids by using EBSS led to mitochondrial fusion. It was observed that glucose starvation led to a mild increase in mitochondrial fusion relative to untreated cells. This mild fusion effect was inhibited upon serum and glucose double starvation cues as mitochondria were observed as greatly fragmented.

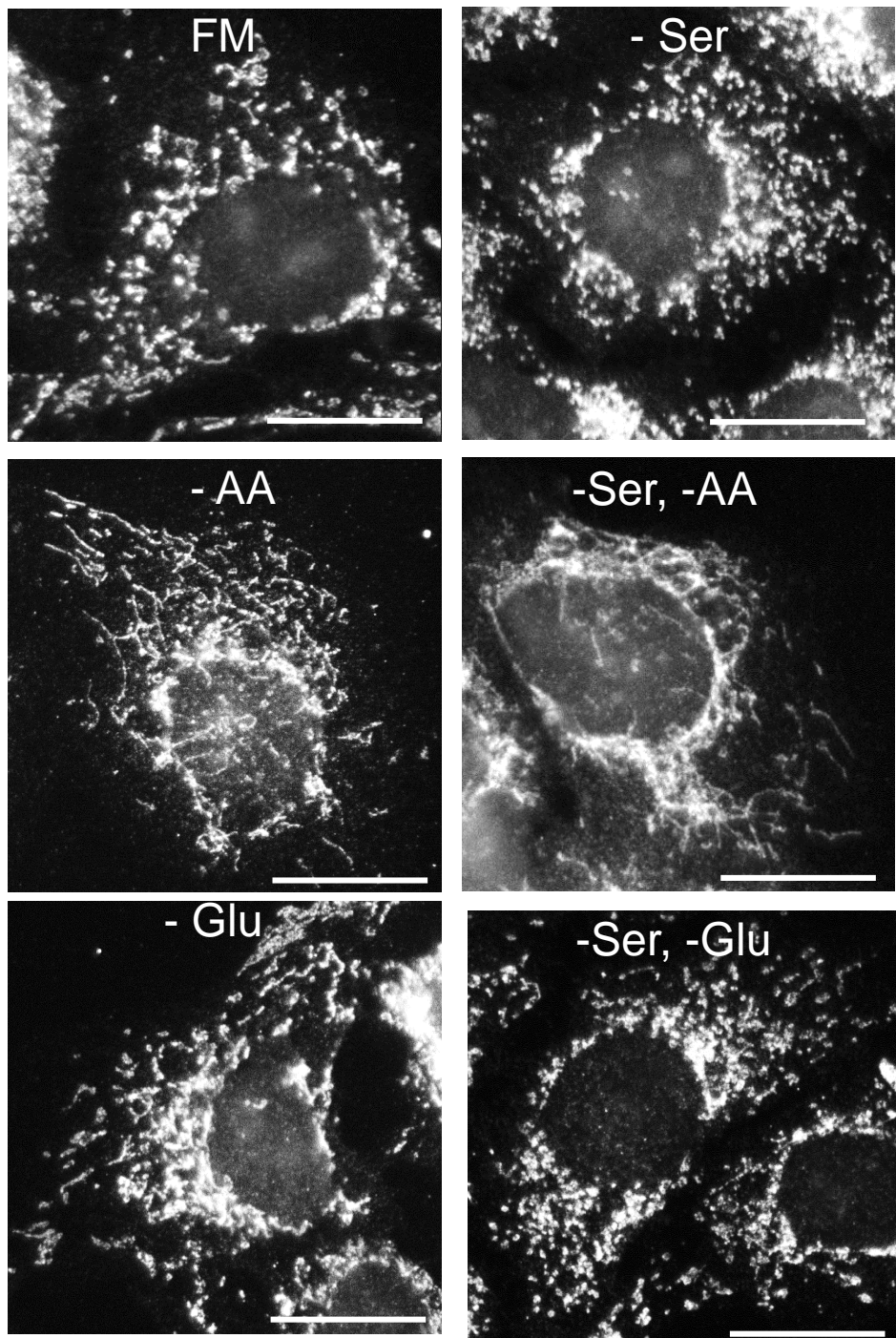


**Figure 3.1: The effects of nutrient starvation stress on mitochondrial dynamics.** Epi-fluorescence microscope representative images of mouse breast cancer 4T1 cells starved of different nutrients; None (Full Media), Glucose (-Glu), Serum (-Ser) and Amino acid (-AA) for 4 hours. Cells were stained for TOM20 outer mitochondrial membrane protein. Scale bars: 17μm

To better understand nutrient-dependent fusion and responses across the cell population, mitochondria sizes were quantified in 150 cells per condition in 4T1, U2OS, RPE1 and HeLa cells

Consistent with imaging shown in Fig 3.1, 4T1 in the basal full nutrient state (plot: green dots) contained predominantly mitochondria in a small-sized (fragmented) morphology. Interestingly, quantification detected that serum starvation caused mitochondria to further shift (not significant) toward smaller sizes (plot: red dots) (**Fig 3.2A**). Importantly, starvation of amino acids (and serum) (using EBSS) led to high levels of mitochondrial elongation (plot: blue dots).

In contrast, glucose and serum starvation did not stimulate mitochondrial fusion (**Fig 3.2A**). Interestingly, similar trends were observed when dialysed fetal bovine serum was supplemented to allow only amino acid starvation. In fact, re-addition of serum significantly promoted fusion after amino acid starvation. The supplementation of dialysed serum to glucose starved cells also led to a mild but significant increase in mitochondrial length relative to untreated 4T1 cells.

Similar results were observed when the same starvation conditions were tested in U2OS cells (**Fig 3.2B**). Amino acid starvation led to a robust 5-fold increase in mitochondrial length relative to the basal full nutrient controls. Glucose starvation did not stimulate mitochondrial fusion. The presence or absence of dialysed serum did not have large effect, in comparison with amino acid starvations signals. In RPE1 cells, we also detected similar responses. Amino acid starvation led to at least 3-fold increase in mitochondrial length relative to controls (**Fig 3.2C**).

In contrast to the observation that amino acid starvation led to mitochondrial fusion (by 4-hours) in 4T1, U2OS and RPE1 cells, there was no amino acid-starvation effect on mitochondrial morphologies at 4-hours in HeLa cells (Data not shown). To investigate whether HeLa cells required more time to respond to amino acid starvation, the nutrient starvation time was extended to 24-hours.

Consistent with observations in 4T1, U2OS and RPE1 cells (where amino acid starvation led to mitochondrial fusion at 4-hours), at 24-hours amino acid starvation (plus or minus dialysed serum) led to mitochondrial fusion in HeLa cells (**Fig 3.2D**). Taken together, it was observed that amino acid starvation alone induced a higher mitochondrial length relative to cells starved of both amino acid and serum-starved cell. This suggests that serum removal might have an inhibitory role in mitochondrial fusion. Overall, these findings show that mitochondria respond to amino acid

starvation specifically, rather than to general nutrient insufficiency, by remodelling their shape from short, fragmented forms, to long and fused forms.

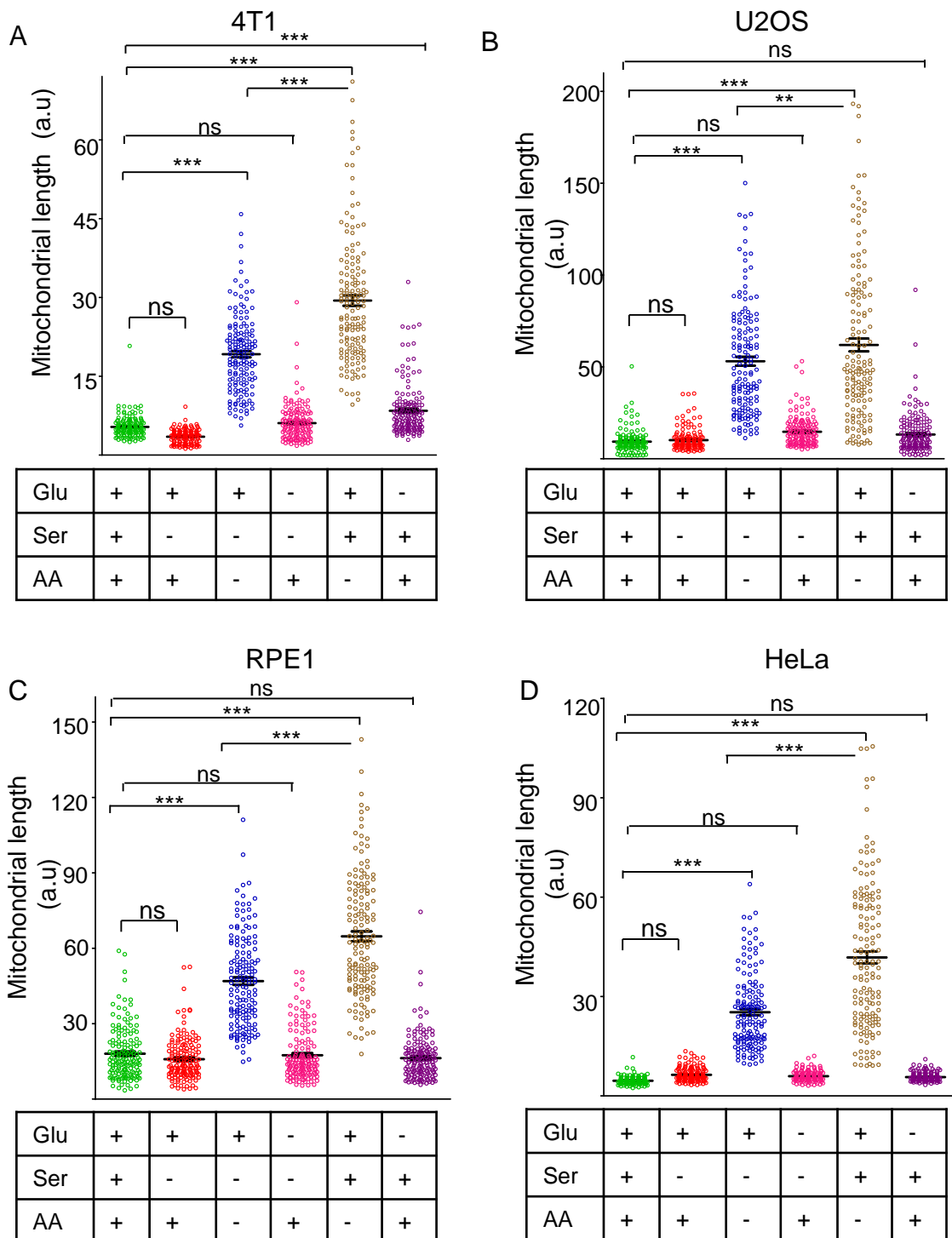


**Figure 3.2: Mitochondria remodel towards fusion during amino acid starvation stress.** Cells were starved of different nutrients; Glucose (Glu), Serum (Ser) and Amino acid (AA) in

(A) Mouse breast cancer 4T1 cells for 4h

(B) Human Osteosarcoma bone cancer U2OS cells for 4h

(C) Retinal pigmented epithelial RPE1 cells for 4h

(D) Cervical cancer HeLa cells for 24h.

Each dot represents the mean length of 10 mitochondria within a cell. Each treatment shows 150 cells quantified from 3 independent experiments. \*\*\* indicate  $P < 0.001$ , ns (not significant) analysed with one way ANOVA with Bonferroni post test.

### **3.2.2 Mitochondrial remodelling in cells expressing GFP-tagged mitochondrial constructs.**

To study and visualize mitochondria shapes independently of staining mitochondrial membranes with antibodies, plasmids of GFP-tagged outer mitochondrial protein OMP25 (GFP-OMP25) or inner mitochondrial ATPase subunit protein SU9 (SU9-GFP) constructs were expressed in 4T1, U2OS and HeLa cells. To confirm mitochondrial localization of GFP-OMP25 and SU9-GFP, cells were stained with antibodies against TOM20. We next examined whether expression of GFP-tagged proteins altered mitochondrial fusion phenotypes following amino acid starvation.

It was observed that the TOM20 signal co-localised with the GFP green signal, indicating that both GFP-OMP25 and SU9-GFP were correctly localized to mitochondria (**Fig 3.3A**). Both 4T1 and HeLa cells expressing either SU9-GFP or GFP-OMP25 responded to amino starvation by inducing mitochondrial fusion after 4-hours and 24-hours respectively (**Fig 3.3B/C**). Following amino acid starvation, 100% of 4T1 cells expressing SU9-GFP or GFP-OMP25 had fused mitochondria above the basal length in cells with full nutrients (**Fig 3.3B**). Similar results were observed in HeLa cells, where at least 70% of the cells starved of amino acid have fused mitochondria relative to control cells with short mitochondria (**Fig 3.3C**). These findings indicate that cells expressing SU9-GFP or GFP-OMP25 are able to alter mitochondrial shapes in response to amino acid starvation as previously shown in wildtype cells.

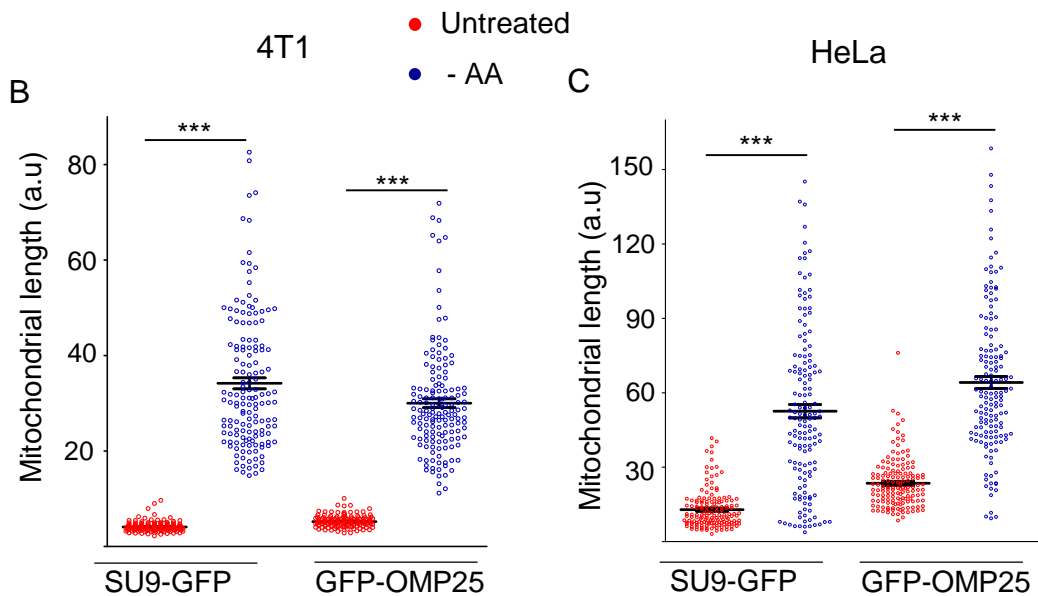
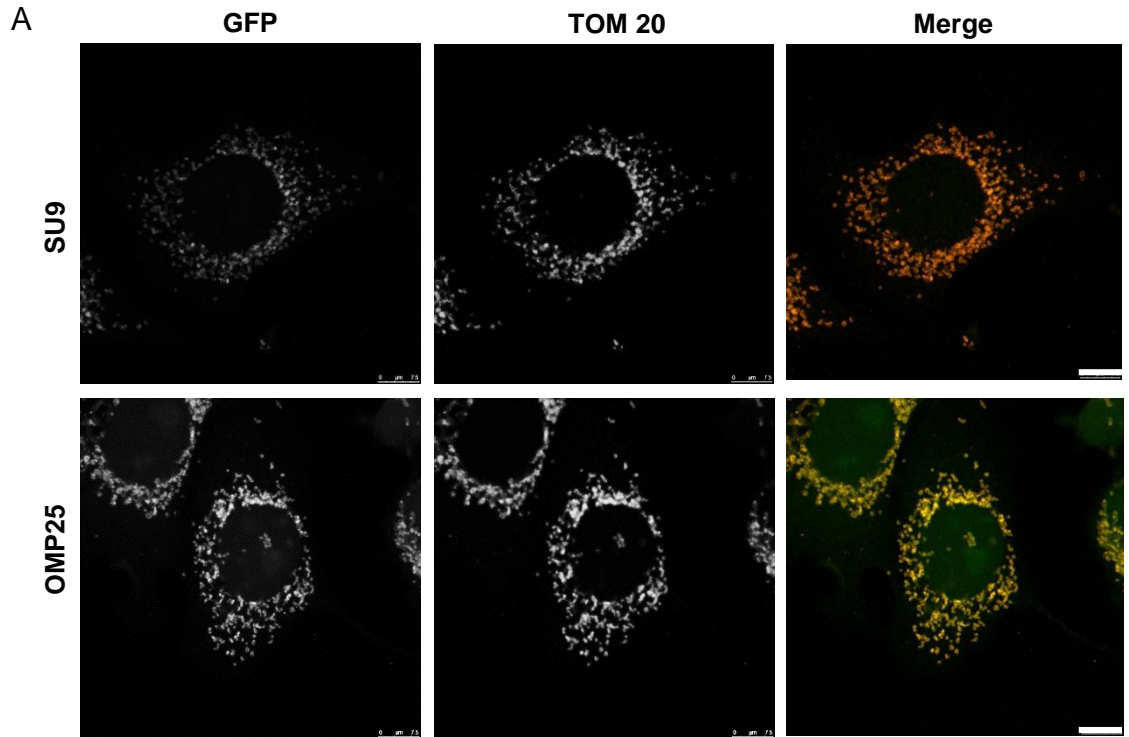


**Figure 3.3: SU9-GFP and GFP-OMP25 localized to mitochondria.**

(A) Representative images of 4T1 cells stably expressing either SU9-GFP or GFP-OMP25 in full media, stained with antibody against outer mitochondria protein TOM20. Bee-swam plot indicating normal mitochondrial fusion in cells expressing SU9-GFP or GFP-OMP25 during amino acid starvation in (B) 4T1 cells at 4hrs and (C) HeLa cells at 24h. Starvation media conditions also contained 10% dialysed FBS. Each dot represent the mean length of 10 mitochondria within a cell. Each treatment shows 150 cells quantified from 3 independent experiment. \*\*\* indicate  $P < 0.001$  analysed with one way ANOVA with Bonferroni post test. Scale bars:  $7.5\mu\text{m}$

### 3.2.3 Amino acid-dependent mitochondrial fusion.

Previous studies have shown that cells have multiple mechanisms to sense regulatory amino acids (glutamine, leucine and arginine) to control lysosome-based MTORC1 signalling (Rebsamen et al., 2015, Chantranupong et al., 2016). Interestingly, as demonstrated in different cell contexts, any single amino acid of these 3 is sufficient to activate MTORC1 signalling (Jewell et al., 2015, Carroll et al., 2016a) but our laboratory has documented that a greater response is observed in the presence of addition of all three (Nwadike et al., 2018). It has been suggested that MTORC1 inhibition has the ability to drive mitochondrial fusion (Gomes et al., 2011a, Morita et al., 2017). This would be overall consistent with a mechanism where starvation of glutamine (Q), leucine (L) and arginine (R) would lead to MTORC1 inactivation, and then downstream mitochondrial fusion. Based on this model, re-supplementation of Q, L and R should re-activate MTORC1 and then rescue/reverse mitochondrial fragmentation. To date, there was no reported evidence linking the availability of these amino acids to both MTORC1 activity and mitochondrial dynamics. Therefore, firstly, we investigated whether supplementation of Q, L and R would inhibit mitochondrial fusion.

We starved 4T1-SU9 GFP cells of either all amino acids (No amino acid) or starved of amino acid but supplemented with Q, L and R (only Q + L + R present) for 4h. Cells were fixed and mitochondrial fusion was quantified. Surprisingly, the supplementation of Q + L + R to the amino acid starvation medium led to dramatic and extensive hyperfused mitochondria relative to amino acid-starved cells (**Fig 3.4A**). Upon quantification, Q, L and R-supplementation treatment of 4T1-SU9 GFP cells led to increased mitochondrial length (up to three fold longer relative to cells that were starved of all amino acids) (**Fig 3.4B**). In contrast, supplementation with either Q, L or R (each singly) did not induce any hyperfusion above that observed in cells starved of all amino acids. This suggests that supplementation of QLR together might synergistically induce mitochondrial hyperfusion. Overall, the addback of QLR to starvation media led to mitochondrial hyperfusion, which was exactly the opposite of what was predicted based on the model in the literature. Therefore, we performed further studies to investigate the mechanism and role for this response.

In the above experiment, Q, L and R were supplemented fresh into Earle Balanced Salt Solution (EBSS), the buffer serving as the amino acid deprivation medium. QLR was supplemented to the same concentrations (4mM, 0.79mM and 0.48mM respectively) as listed in the DMEM (Dulbecco's Modified Eagle Medium) formulation.

To test whether the QLR-induced hyperfusion observed in starved cells requires the starvation of other amino acids present in DMEM, QLR was supplemented at a final 2X concentration (8mM, 1.58mM and 0.96mM respectively) into DMEM and EBSS. Next, 4T1-SU9 GFP cells were treated with these media for 4-hours and their effects on mitochondrial length were quantified.

It was observed that supplementation of QLR into DMEM (to make 2XQLR) did not alter mitochondrial length relative to untreated cells (**Fig 3.4C**). In contrast, supplementation of QLR into EBSS at 1X concentration led to mitochondrial hyperfusion. The supplementation of QLR into EBSS at 2X concentration did not block or enhance QLR-induced mitochondrial hyperfusion. These findings suggest that QLR-induced mitochondrial hyperfusion requires the starvation of other amino acids and that it is not occurring as a result of increased concentrations of Q, L and R.

We found earlier that glucose withdrawal led to an increase in mitochondrial length in a small fraction of 4T1 cells (Fig 3.2A). To clarify the role of glucose in QLR-dependent mitochondrial hyperfusion, we studied QLR-induced hyperfusion in Dulbecco's Phosphate-Buffered Saline (dPBS) (+ or – glucose). As an alternative to EBSS, dPBS was supplemented with sodium bicarbonate and phenol red pH indicator. Next, QLR was supplemented into dPBS in the presence or absence of glucose.

As controls, glucose starvation alone (using DMEM without glucose) led to the increase in mitochondrial length in some cells relative to untreated cells in full media (**Fig 3.5**), consistent with the observation in (Fig 3.2A). As expected, starvation of all amino acids in EBSS resulted in mitochondrial fusion while starvation of amino acid with supplementation of QLR led to extensive mitochondrial hyperfusion. Interestingly, in dPBS containing glucose, QLR supplementation led to an increase in mitochondrial length by approximately 2-fold relative to amino acid starved cells (**Fig 3.5**). Similarly, in dPBS without glucose, QLR supplementation also led to mitochondrial hyperfusion relative to amino acid starved cells (but did not reach significance). This indicated that QLR-dependent mitochondrial hyperfusion occurs independently of glucose usage / glycolysis.

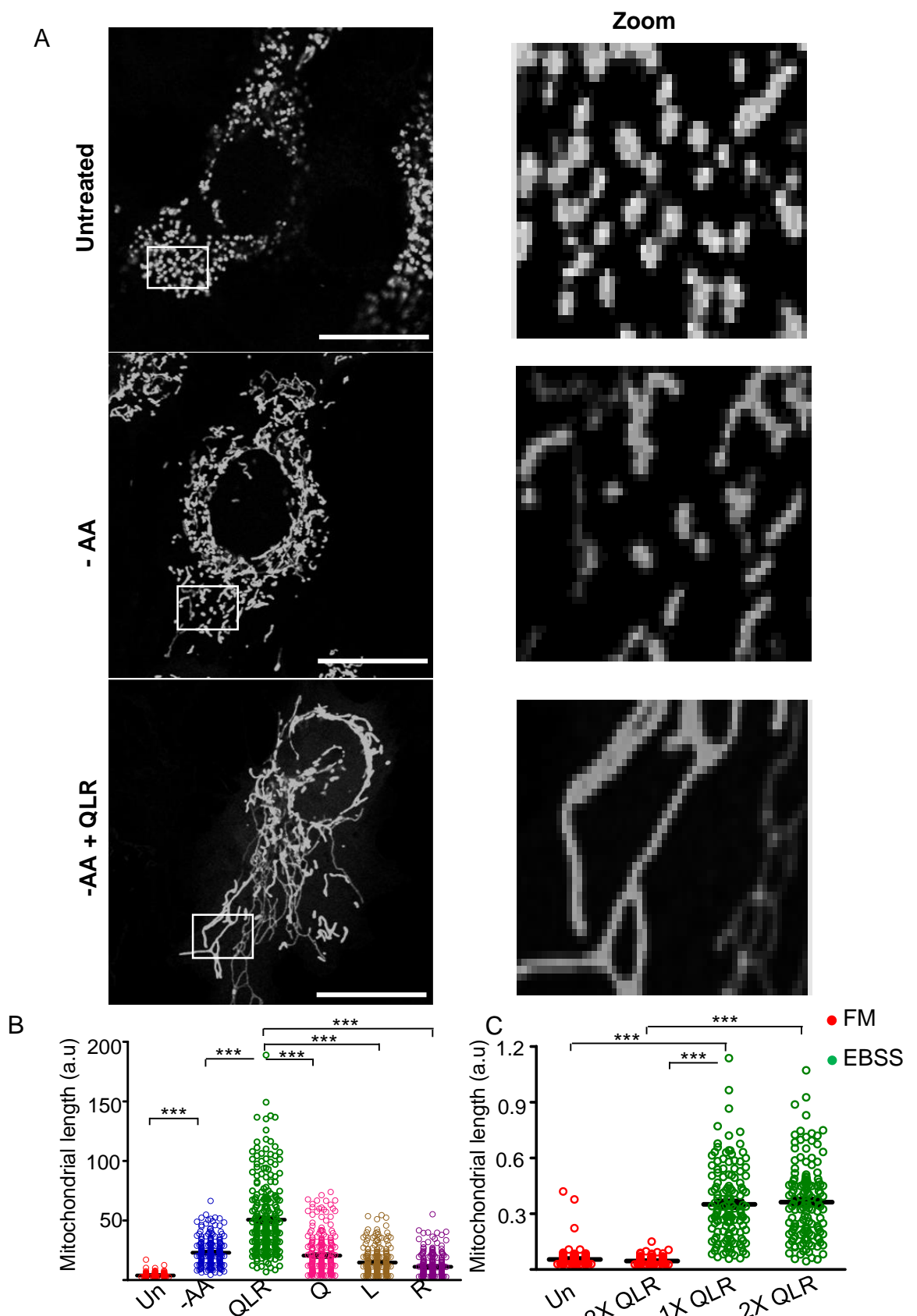


**Figure 3.4: Glutamine, Leucine and Arginine (Q, L, R) induce mitochondrial hyperfusion in 4T1 cells during starvation stress.**

(A) Representative images of 4T1-SU9 GFP cultured in full media (FM), starved of either all amino acids (-AA) or starved of amino acid but supplemented with QLR for 4h. Starvation media conditions also contained 10% dialysed FBS. (B) Bee-swarm indicating that only QLR induced mitochondrial hyperfusion, 250 cells quantified from five independent experiments.

(C) QLR did not induce hyperfusion when added to full media, QLR was added to full nutrient media (FM) (to yield 2X final concentration) or to EBSS at 1X concentration or 2X concentration. Concentrations of 1X based on DMEM were defined as Q= 4mM, 1X L= 0.79mM, 1X R= 0.48mM. N=3 independent experiment. \*\*\* indicate  $P < 0.001$  analysed with one way ANOVA with Bonferroni post test. Scale bars: 25µm

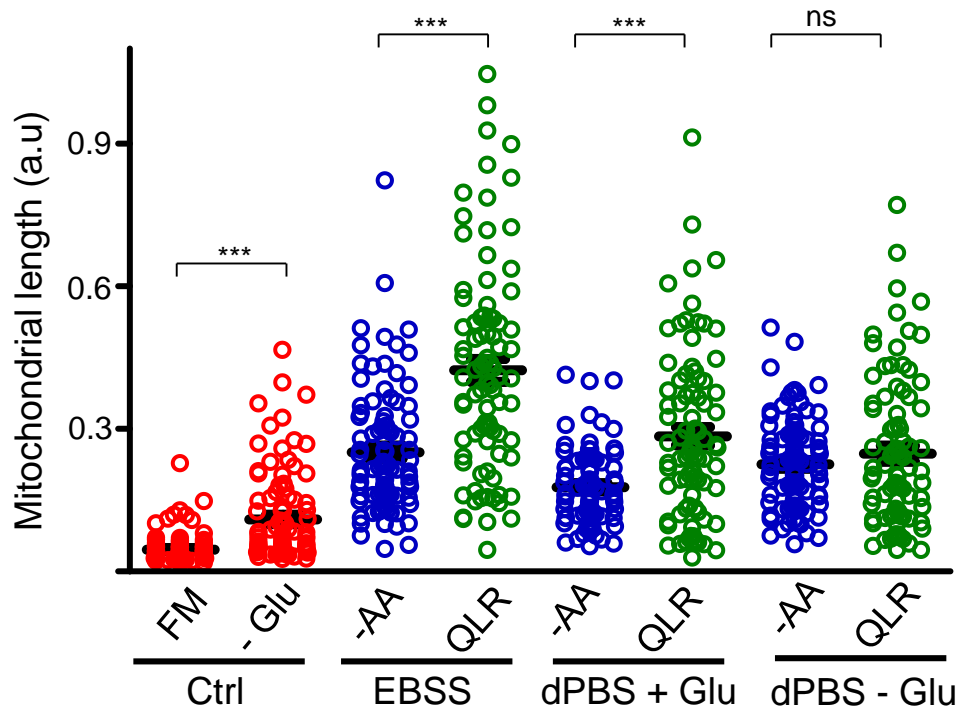


**Figure 3.5: Mitochondrial hyperfusion in response to QLR is independent of glucose.** 4T1-SU9 GFP were cultured in full media (Un) or starved of glucose (-glu). QLR was supplemented into EBSS (contains glucose) or PBS +/- glucose for 4h. Starvation media conditions also contained 10% dialysed FBS. Bee-swam plot indicating Q, L and R induce mitochondrial hyperfusion in the presence or absence of glucose. Each dot represents the mean length of 10 mitochondria within a cell. Each treatment shows 100 cells quantified from three independent experiments. \*\*\* indicate  $P < 0.001$ , ns (non significant) analysed with two-tailed T test.

Cells respond within 30-minutes to nutrient availability by regulating key signals to drive processes such as autophagy. This rapid cellular response controls cellular fate in the early and late stages of cellular stress (Jewell et al., 2015, Efeyan et al., 2013, Shen et al., 2017). Next, we wanted to know whether mitochondria respond to amino acid rapidly and if this response is maintained after 4-hours. The time-dependent response of Q, L and R-dependent mitochondrial hyperfusion was investigated. Firstly, cells incubated in dPBS but supplemented with QLR were observed by live-cell inverted epi-fluorescent microscope. Images were acquired every minute for 1-hour. Time-lapse images of a section of 4T1-SU9 GFP cell showed the dynamics of mitochondria during QLR-supplementation (in starvation media) (**Fig 3.6A**). It was observed that mitochondria responded to the presence of Q, L and R by inducing hyperfusion within 1-hour of incubation. Interestingly, mitochondrial fusion was not obvious before the 1-hour timepoint.

Further time course studies of mitochondrial hyperfusion from 1-hour to 8-hours (using conventional fixed cell methodology) confirmed that mitochondrial fusion occurs rapidly by 1-hour in response to both amino acid starvation alone or the presence of QLR (**Fig 3.6B**). By 4-hours of incubation, amino acid-dependent mitochondrial fusion increased by 2-fold relative to the 1-hour timepoint. As expected, at the 4-hours timepoint, QLR stimulated mitochondrial hyperfusion by 3-fold. At the 8-hours timepoint, the level of hyperfusion in QLR-supplemented cells was similar to 4-hours. These findings indicate that mitochondria respond to changes in amino acids rapidly which appears to peak approximately by 4-hours of incubation, but that this maximal hyperfused state can persist for up to 8-hours. However, it was observed that by 24-hours, either starved or starved but QLR-supplemented 4T1 cells undergo cell death (Data not shown).

Next, it was investigated whether QLR-induced mitochondrial hyperfusion could be observed in another cell type. QLR supplementation was tested on U2OS cells expressing SU9-GFP. Similar to 4T1-SU9 GFP, supplementation of Q, L and R into amino acid starvation media resulted in hyperfused mitochondria in U2OS-SU9 GFP (**Fig 3.7A**). Q, L, and R supplemented cells showed extensive hyperfusion with mitochondria length approximately 3-fold higher than mitochondrial length during full amino acid starvation (**Fig 3.7B**). Therefore, our results suggest that Q, L and R induced mitochondrial hyperfusion is conserved across multiple cell types.

QLR

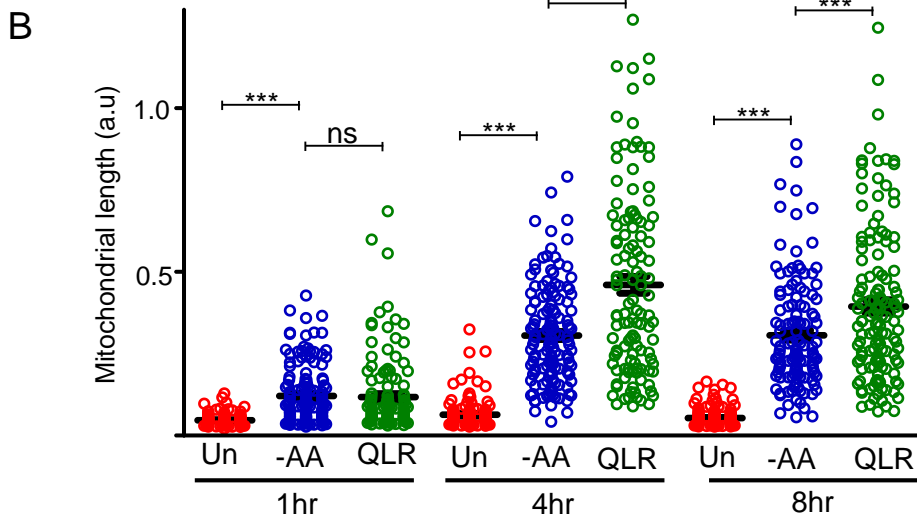
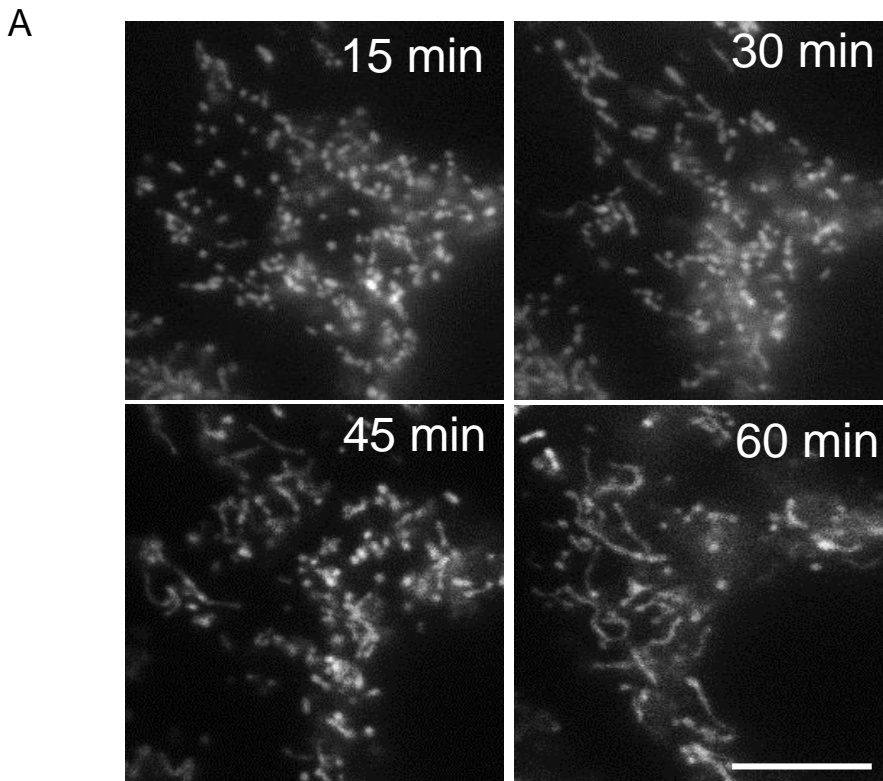


**Figure 3.6: Time-dependent amino acid-induced mitochondrial hyperfusion.**

(A) Time-lapse live-cell imaging indicates that Q, L and R-induced mitochondrial hyperfusion is rapid. 4T1-SU9 GFP cells were treated with PBS supplemented with Q, L and R. Starvation media conditions also contained 10% dialysed FBS. Live cell images were taken every minute for 1hr. Shown are representative times from the same field of cells. Scale bars: 17 $\mu$ m

(B) 4T1-SU9 GFP cultured in full media (Un), starved of either all amino acids (-AA) or starved of amino acid but supplemented with QLR for 1 hour, 4 hours and 8 hours. Starvation media conditions also contained 10% dialysed FBS. Each dot represents the mean length of 10 mitochondria within a cell. Each treatment show 120-150 cells quantified from three independent experiment. \*\*\* indicate  $P < 0.001$  analysed with one way ANOVA with Bonferroni post test.

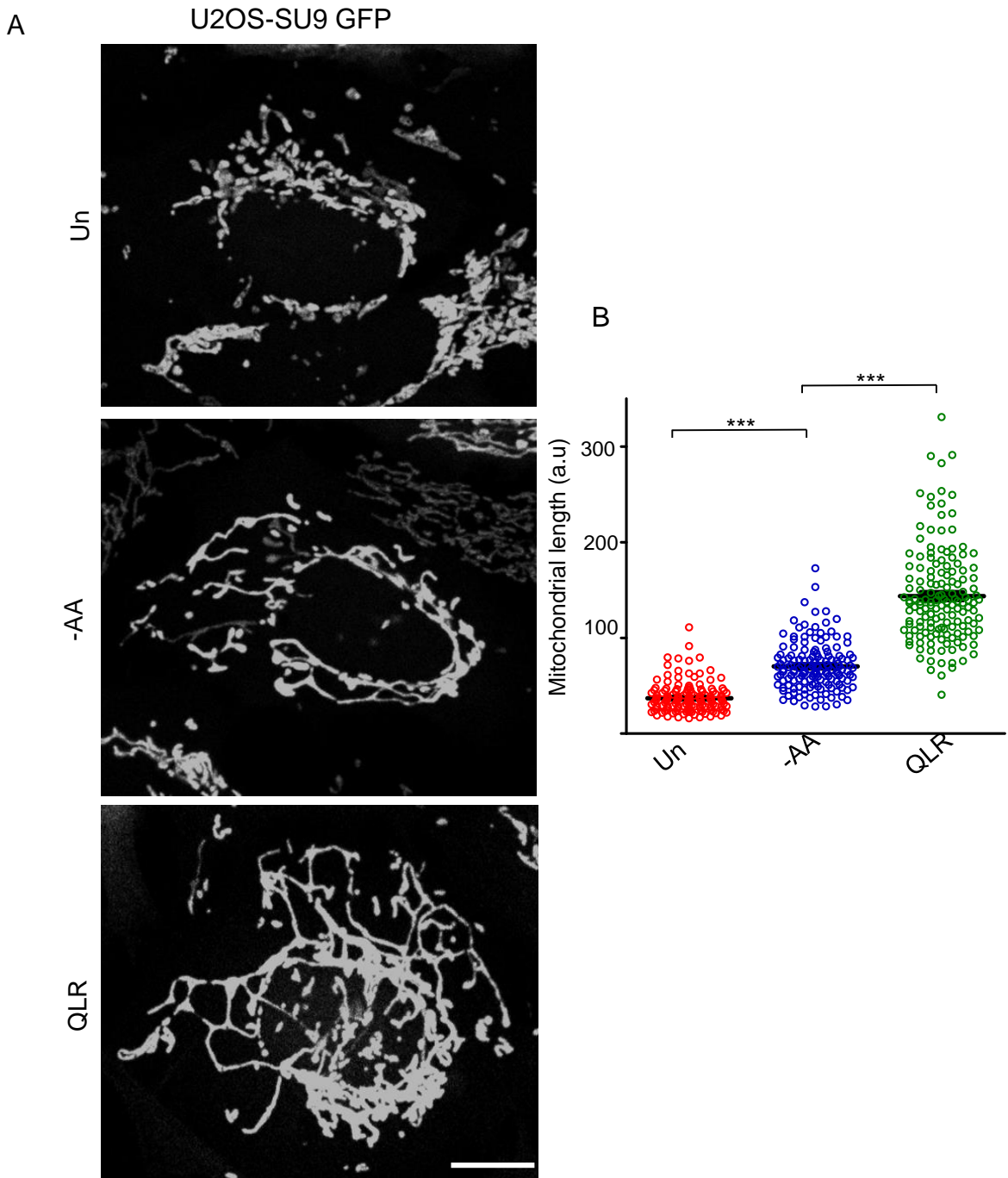


**Figure 3.7: Glutamine, Leucine and Arginine (Q, L, R) induce mitochondrial hyperfusion in U2OS cells.**

(A) Representative images of U2OS-SU9 GFP cultured in full media (Un), starved of either all amino acids (-AA) or starved of amino acid but supplemented with QLR for 4h. Starvation media conditions also contained 10% dialysed FBS.

(B) Bee-swarm plot indicating Q, L and R together induced mitochondrial hyperfusion. Each dot represents the mean length of 10 mitochondria within a cell. Each treatment shows 200 cells quantified from 4 independent experiments. \*\*\* indicate  $P < 0.001$  analysed with one way ANOVA with Bonferroni post test. Scale bars: 10 $\mu$ m

It was next investigated whether Q, L and R are all required for inducing QLR-dependent mitochondrial hyperfusion. Mitochondrial hyperfusion was assessed by comparing effects from supplementation with QLR together, or with only two of the regulatory amino acids: either QL, QR or LR. It was confirmed as control that, while full amino acid starvation induces moderate mitochondrial fusion, supplementation with Q + L + R induced extensive mitochondrial hyperfusion in 4T1-SU9 GFP cells (**Fig 3.8A**). In contrast, supplementation of any two of Q, L and R induced only moderate mitochondrial fusion but not as strongly as Q, L and R-induced hyperfusion (**Fig 3.8B**). Similar results were observed in U2OS-SU9 GFP, where only QLR combined addback exclusively led to robust mitochondrial hyperfusion (**Fig 3.9A/3.9B**). This suggests that the simultaneous addition of all three of Q, L or R are required for the stimulation of mitochondrial hyperfusion. Curiously, removal of any one amino acid from the QLR addback mixture reduced the signal that was driving hyperfusion.

Since a withdrawal effect was observed in the QLR-addback mixture, we next wanted to investigate whether substituting QLR with other amino acids will have similar hyperfusion effects. Leucine is one of three branched-chain amino acids (BCAA) (with valine (V) and isoleucine (I) representing the other 2). Importantly, all BCAA have been proposed to play similar metabolic roles as ketogenic amino acids (Green et al., 2016, Neinast et al., 2019). Amino acids R and lysine (K) have a positively charged side chain (at neutral pH) similar to histidine (H) which can be found in a protonated state at neutral pH (Betts and Robert, 2003).

To study whether BCAA has similar responses in the stimulation of QLR-dependent mitochondrial hyperfusion, we substituted L for V or I. In addition, we also investigated whether R substitution for K in the QLR addback mixture will have similar mitochondrial hyperfusion.

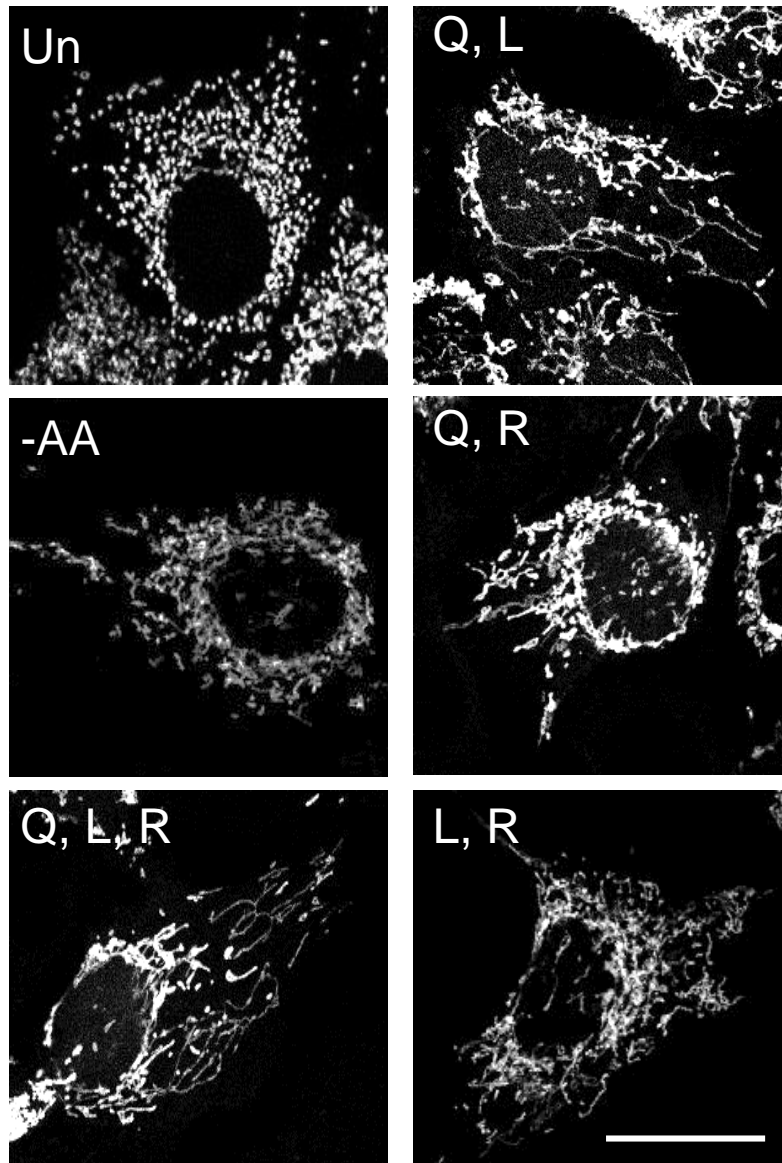
As shown earlier, QLR supplementation into amino acid starvation media led to mitochondrial hyperfusion by approximately 3-fold relative to cells starved of all amino acid (**Fig 3.10**). It was observed that the supplementation of Q + I + R into amino acid starvation media led to a reduction in hyperfusion relative to cells starved of amino acid but supplemented with QLR. Similarly, the supplementation of Q + V + R into amino acid starvation media led to a reduction in hyperfusion relative to cells starved of amino acid but supplemented with QLR. Interestingly, the supplementation with either Q + I + R or Q + V + R into amino acid starvation media did not induce any hyperfusion above that observed in cells starved of all amino acids but supplemented

with Q + R alone. Similarly, it was observed that the supplementation of Q + L into amino acid starvation media did not induce any hyperfusion above that observed in cells starved of all amino acids but supplemented with Q + L + K.

These findings suggest that L or R has a specific role in hyperfusion induced by the QLR addback mixture. Overall, results indicate that effects from L or R are lost when either amino acid is removed or replaced with another BCAA or K respectively. Therefore, indicating that Q, L and R exclusively stimulate mitochondrial hyperfusion in a synergistic manner in starved cells.

Since mitochondrial hyperfusion involves the fusion of outer mitochondrial membrane and inner membrane fusion mediated by Mfn1/2 and Opa1 respectively, we wanted to understand if these mechanisms were involved. Mitochondria are made up of the outer membranes, inner membranes, the intermembrane space, the cristae and the matrix. However, mitochondrial images acquired and studied on confocal microscope cannot distinguish between these compartments. To further understand the changes in mitochondrial morphology, transmission electron microscope (TEM) was utilized to observe mitochondrial membrane ultrastructure during QLR-dependent mitochondrial hyperfusion. TEM corroborated QLR-dependent mitochondrial hyperfusion. As observed in confocal images, untreated cells have rounded mitochondria but with clear matrix and continuous cristae structure (**Fig 3.11**). In contrast, amino acid-starved cells often showed condensed mitochondrial matrix compartments with no apparent cristae formation. Mitochondrial ultrastructure in amino starved cells often varied between averagely sized tubule forms and rounded forms with no obvious mitochondrial hyper-branching. In contrast, the supplementation of QLR into amino acid starvation media led to mitochondrial hyper-branching and hyperfused mitochondria relative to amino acid-starved cells. Similarly to amino acid starved cells, QLR supplementation led to the formation of condensed mitochondrial matrix, however, with often clear cristae structures within mitochondria. This finding confirms that QLR supplementation into amino acid starvation media stimulates mitochondrial hyperfusion and hyper-branching. Together, findings in this section reveal a previously undocumented and rapid mitochondrial hyperfusion response following addback of Q, L and R.

A



B

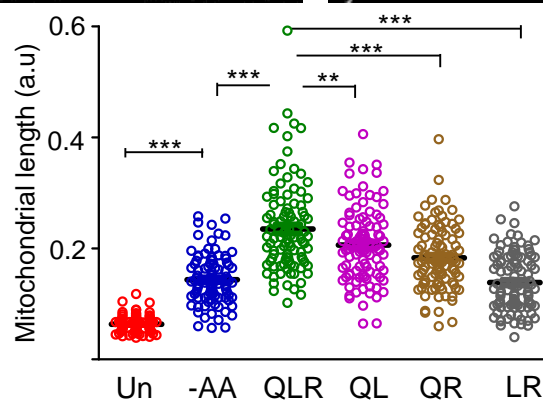
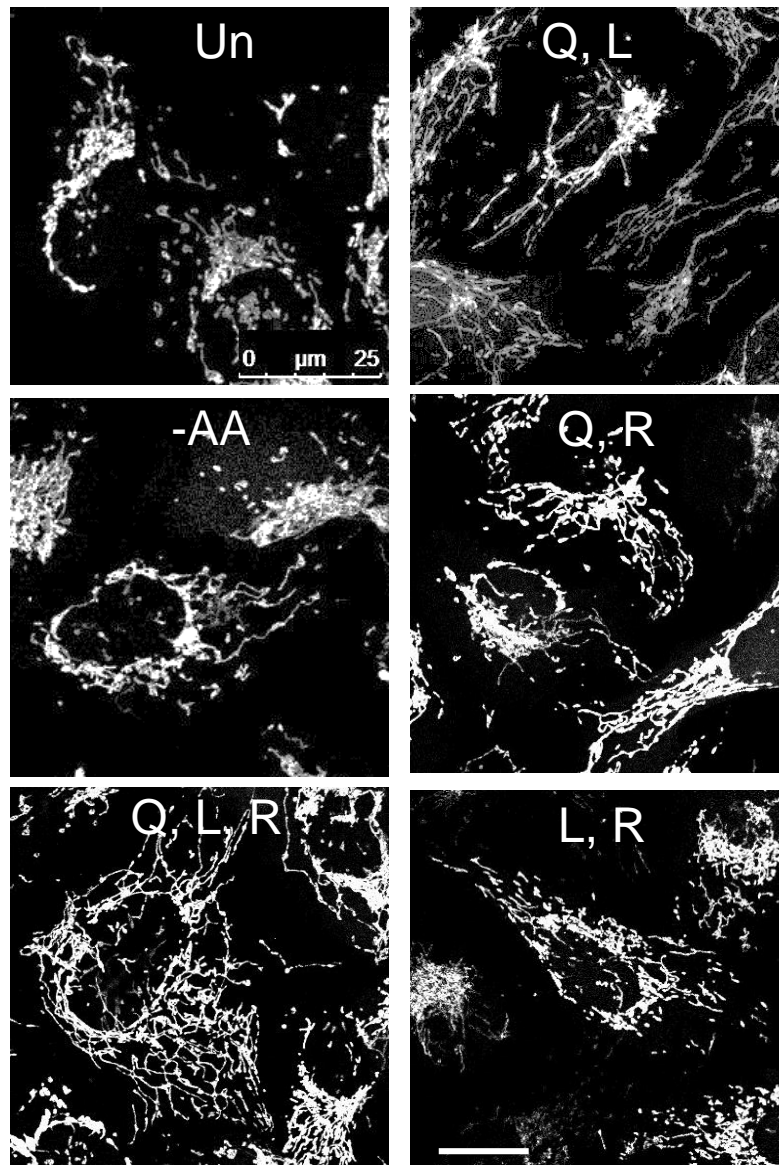


**Figure 3.8: Mitochondrial hyperfusion requires combined addition of QLR in 4T1-SU9 GFP cells** (A) Confocal representative images of 4T1-SU9 GFP cultured in full media (Un), starved of either all amino acids (-AA) or starved of amino acid but supplemented with either three or two of these amino acid; Q (Glutamine), L (Leucine) and R (Arginine) for 4h. Starvation media conditions also contained 10% dialysed FBS. (B) Bee-swarm plot indicating Q, L and R supplemented altogether induced mitochondrial hyperfusion higher than combination of any two. Each dot represents the mean length of 10 mitochondria within a cell. Each treatment shows 100 cells quantified from representatives of four independent experiments. \*\*\* indicate  $P < 0.001$ , \*\*  $P < 0.01$  analysed with one way ANOVA with Bonferroni post test. Scale bars: 25 $\mu$ m

A



B

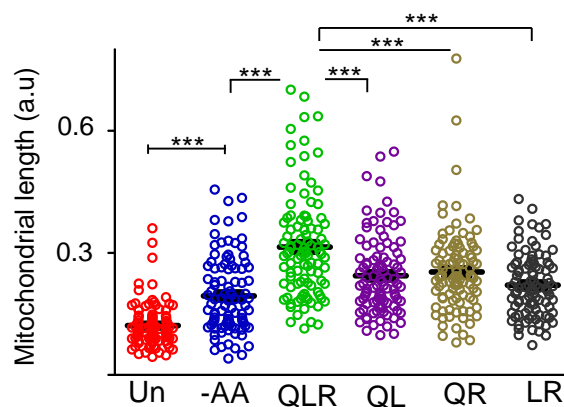


**Figure 3.9: Mitochondrial hyperfusion requires combined addition of QLR in U2OS-SU9 GFP cells** (A) Confocal representative images of U2OS-SU9 GFP cultured in full media (Un), starved of either all amino acids (-AA) or starved of amino acid but supplemented with either three or two of these amino acid; Q (Glutamine), L (Leucine) and R (Arginine) for 4h. Starvation media conditions also contained 10% dialysed FBS. (B) Bee-swarm plot indicating Q, L and R supplemented altogether induced mitochondrial hyperfusion higher than combination of any two. Each dot represents the mean length of 10 mitochondria within a cell. Each treatment shows 100 cells quantified from representatives of four independent experiments. \*\*\* indicate  $P < 0.001$ , \*\*  $P < 0.01$  analysed with one way ANOVA with Bonferroni post test. Scale bars:  $25\mu\text{m}$

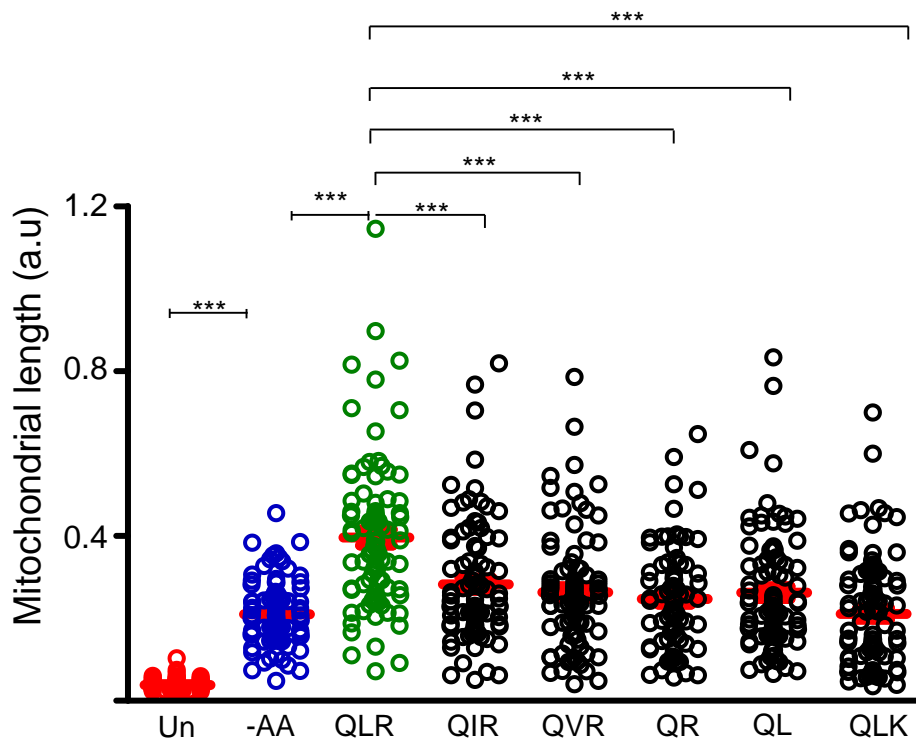


**Figure 3.10: Mitochondrial hyperfusion is maximal upon supplementation with QLR.** 4T1-SU9 GFP were cultured in full media (Un), starved of either all amino acids (-AA) or starved of amino acid but supplemented with different amino acid combinations (QLR, QIR, QVR, QR, QL or QLK) for 4h. Starvation media conditions also contained 10% dialysed FBS. Bee-swarm plot indicating Q, L and R altogether induced mitochondrial hyperfusion higher than any other combination. Each dot represents the mean length of 10 mitochondria within a cell. Each treatment shows 100 cells quantified from representatives of 3 independent experiments. \*\*\* indicate  $P < 0.001$ , analysed with one way ANOVA with Bonferroni post test.

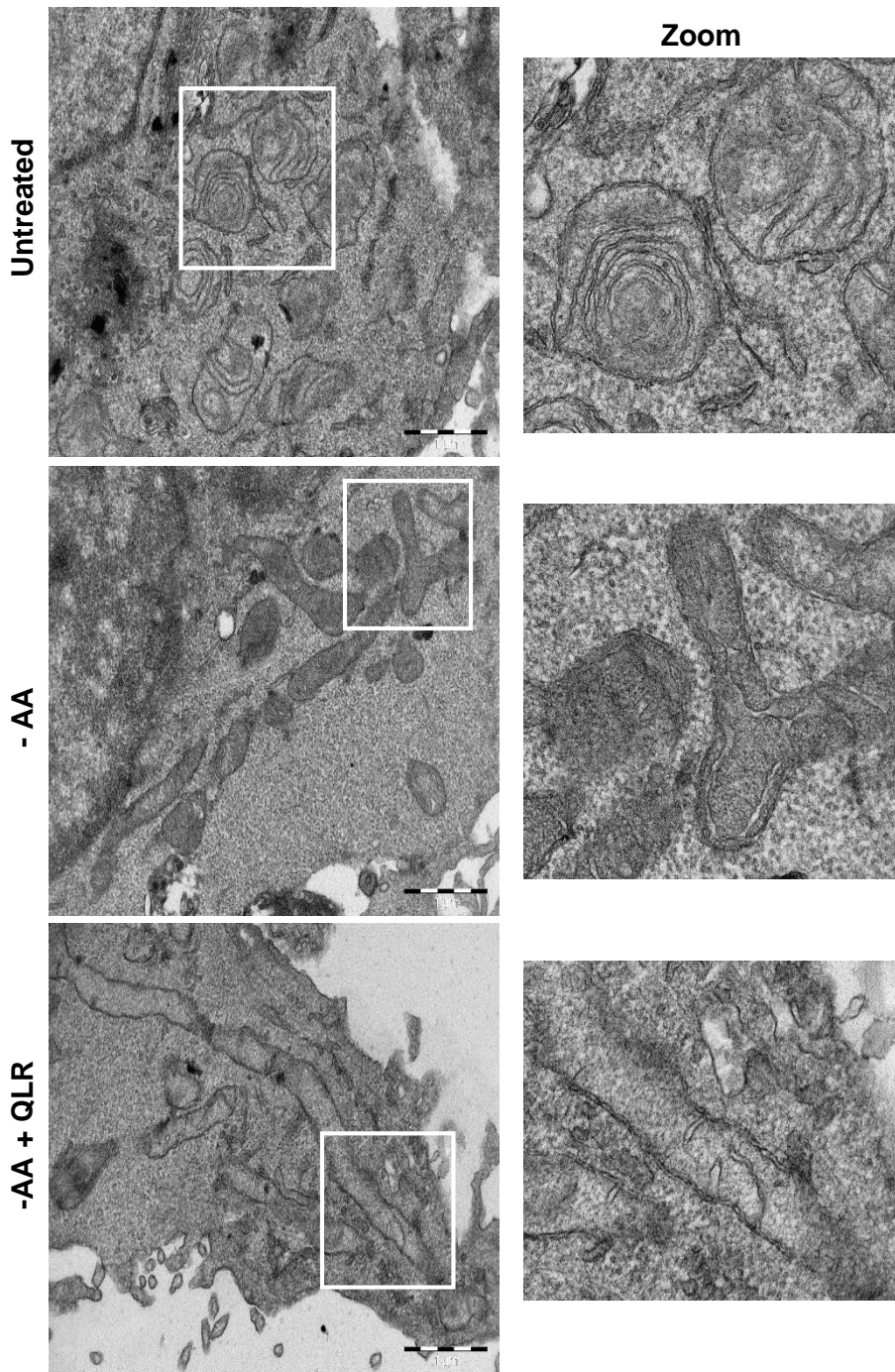


**Figure 3.11: Transmission electron microscopy confirms glutamine, leucine and arginine induce mitochondrial hyperfusion in 4T1 cells.** (A) T.E.M representative images of 4T1-SU9 GFP cultured in full media (FM), starved of either all amino acids (EBSS) or starved of amino acids but supplemented with QLR for 4h. Starvation media conditions also contained 10% dialysed FBS. Scale bars: 1μm

### 3.2.4 Investigating the similarities between stress-induced mitochondrial hyperfusion and QLR-dependent mitochondrial hyperfusion

Previous studies have reported a stress-induced mitochondrial hyperfusion response (SIMH) following protein synthesis inhibition or induction of endoplasmic reticulum (ER) stress (Tondera et al., 2009, Lebeau et al., 2018). In these studies, cells were tested under other stress stimuli conditions such as UV irradiation, thapsigargin (Tg) (an ER stressor) and cycloheximide (CHX) (a ribosomal inhibitor) which all led to rapid mitochondrial hyper-branching and hyperfusion. Our studies of amino acid starvation and addback identified an apparently novel mitochondrial hyperfusion response. Therefore, we aimed to explore how QLR-addback dependent hyperfusion may be related to the previously described SIMH response. To test this, CHX was used to induce SIMH in combination with amino acid-starvation and QLR-supplementation.

Mitochondrial hyperfusion was observed in CHX-treated cells, for example, when added under full-nutrient conditions, recapitulating the reported SIMH response (**Fig 3.12A**). Upon quantification, there was a 3-fold increase in mitochondrial length in CHX-treated cells relative to untreated cells (**Fig 3.12B**). Interestingly, CHX further increased mitochondrial length in amino acid-starved cells by approximately 2-fold. Lastly, while QLR supplementation into amino acid starvation media led to clear mitochondrial hyperfusion, addition of CHX in this condition had a yet small further stimulatory effect on mitochondrial length.

Since the induction of hyperfusion by CHX alone generally resembled QLR-induced hyperfusion, either may represent near-maximal levels of mitochondrial remodelling. Amino acid starvation alone leads to only mild sub-maximal levels of fusion. The findings also suggest that QLR-dependent hyperfusion may occur via a similar mechanism as SIMH.

The SIMH response (eg following CHX) was dependent on the function of Opa1, Mfn1 (but not Mfn2) (Tondera et al., 2009). Opa1 and Mfn1 drive inner and outer mitochondrial fusion, respectively, while Mfn2 is now better understood to primarily maintain ER-mitochondrial tethering. To investigate whether QLR-dependent mitochondrial hyperfusion also requires Mfn1/2 and Opa1 like SIMH, amino acid-dependent mitochondrial hyperfusion was next studied in Opa1 KO (Song et al., 2007), Mfn1 KO, Mfn2 KO (Chen et al., 2003a) and Mfn1/2 KO MEF (Koshiba et al., 2004).

Amino acid (QLR)-dependent mitochondrial hyperfusion was first confirmed in wildtype MEF (with functional Opa1) (**Fig 3.13A**). Untreated wildtype MEF have a more mixed mitochondria population (short and medium-sized) relative to untreated 4T1 (**Fig 3.12A**) with uniformly fragmented mitochondria. In contrast to wildtype MEF, amino acid starvation-induced mitochondrial fusion and QLR-induced mitochondrial hyperfusion were both completely blocked in Opa1 KO cells: mitochondrial length remained short and unchanged after amino acid starvation or QLR-supplementation in Opa1 KO cells (**Fig 3.13B**). Western blot analysis confirmed Opa1 KO status (**Fig 3.13C**). These findings show that Opa1 is required for both basal mitochondrial fusion and QLR-dependent mitochondrial hyperfusion

We next confirmed the expression levels of Mfn1 and Mfn2 in Mfn1 KO, Mfn2 KO and Mfn1/2 KO cells. We tested two commercially available Mfn1 and Mfn2 antibodies to detect Mfn1 and Mfn2 expression levels respectively. Unfortunately, Mfn1 antibodies failed to detect the expression levels of Mfn1 in MEF. Next, semi-quantitative reverse transcription polymerase chain reaction (PCR) was set up to detect mRNA levels of Mfn1. The PCR products of amplified Mfn1-sequence from Mfn1 KO, Mfn2 KO and Mfn1/2 KO cells were detected by agarose gel electrophoresis. Upon visualization, it was confirmed that Mfn1 is present in wildtype and Mfn2 KO while Mfn1 was undetected in Mfn1 KO and Mfn1/2 KO (**Fig 3.14A**). Similarly, using antibodies against Mfn2, western blot analysis confirmed that Mfn2 is expressed in wildtype and Mfn1 KO MEF while Mfn2 expression is undetectable in Mfn2 KO and Mfn1/2 KO cells.

Again, it was confirmed that amino acid starvation promoted mitochondrial fusion while QLR supplementation led to further mitochondrial hyperfusion in the control wildtype MEF (isolated in parallel with the Mfn KO lines) (**Fig 3.14B**). As in the Opa1 KO experiment, wildtype MEF displayed mixed mitochondrial sizes but overall average distributions increased upon amino acid starvation and QLR-addback. Interestingly, amino acid-dependent mitochondrial fusion was blocked in Mfn1 KO cells and Mfn1/2 KO cells but not in Mfn2 KO cells. Confocal images showed that Mfn1 KO and Mfn1/2 KO cells have punctate small-sized mitochondria regardless of the status of amino acids while wildtype and Mfn2 KO cells were able to form mitochondrial tubulation after amino acid starvation or QLR supplementation (**Fig 3.15**). Taken together, these findings indicate that QLR-dependent mitochondrial hyperfusion requires Opa1 and Mfn1, but not Mfn2. The data also suggest that amino acid dependent-mitochondrial hyperfusion is occurring as a result of an increase in mitochondrial fusion.

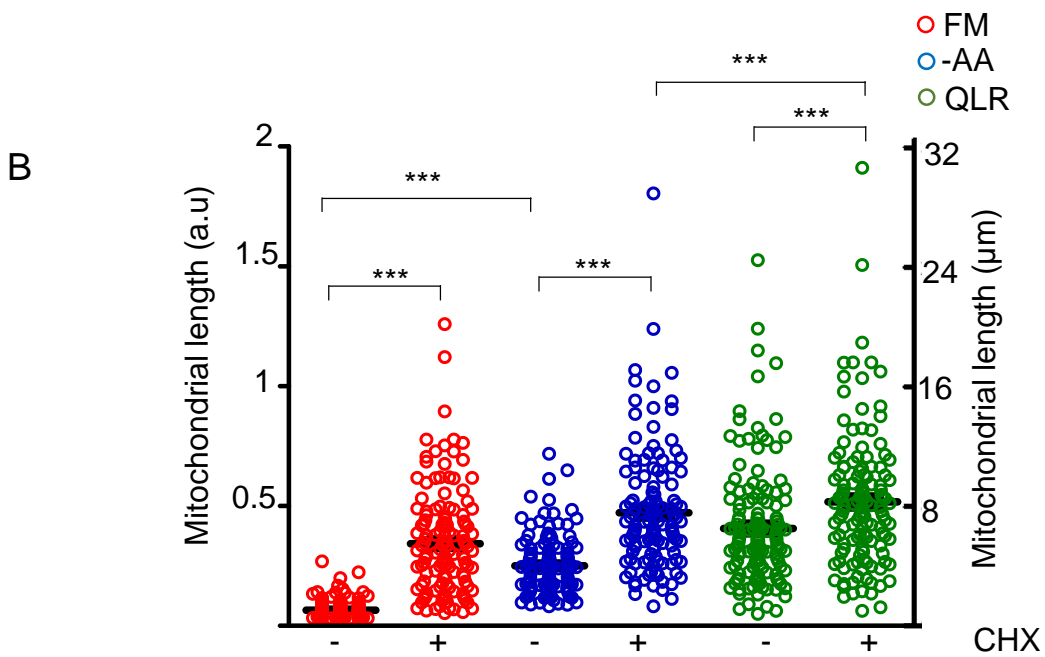
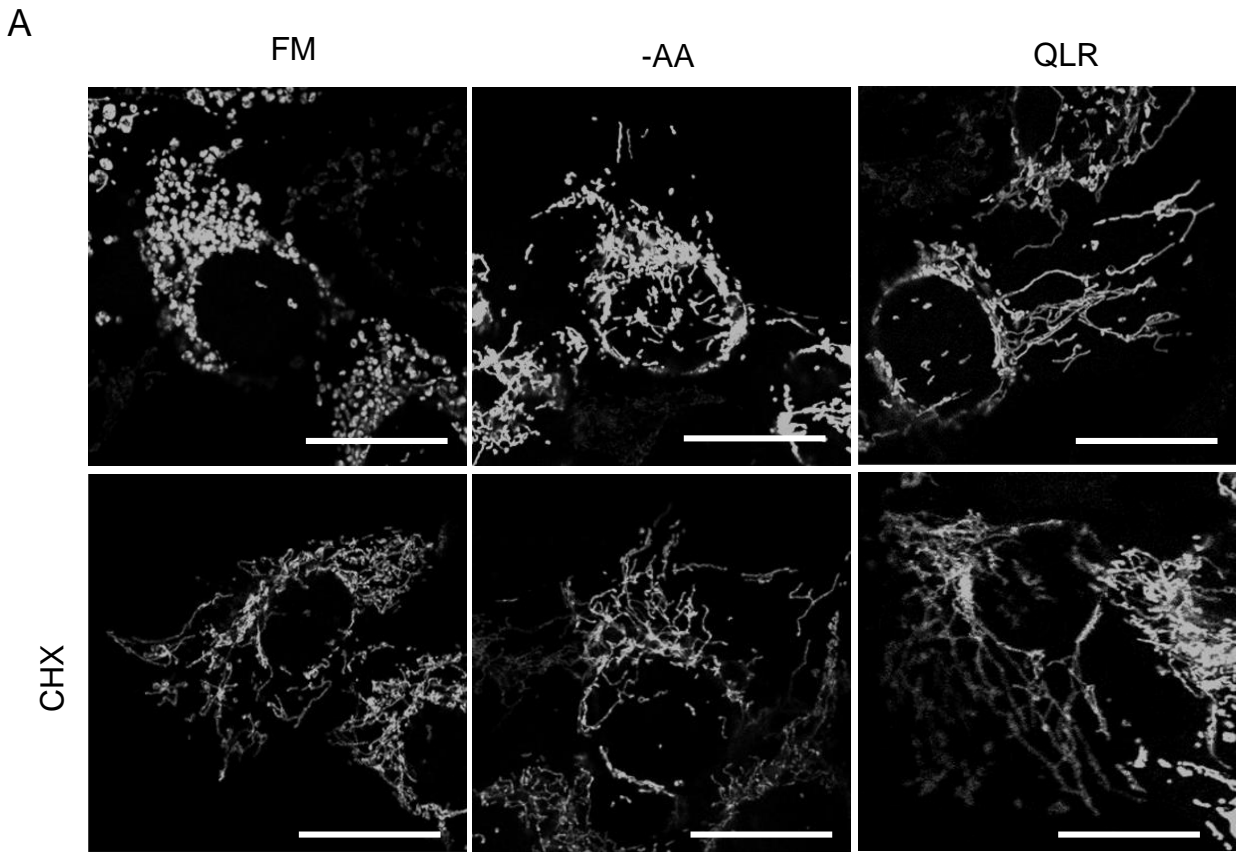


**Figure 3.12: QLR-dependent mitochondrial hyperfusion resembles ER-Stress-related hyperfusion**

(A) Representative images of 4T1-SU9 cells in full media (FM), starved of either all amino acids (-AA) or starved of amino acid but supplemented with QLR, +/- Cycloheximide (CHX) (10 $\mu\text{M}$ ) for 4h. Starvation media conditions also contained 10% dialysed FBS. B) Bees-warm plot of mitochondrial length. Each dot represents the mean length of 10 mitochondria within a cell. Each treatment shows 100-150 cells quantified from three independent experiments. \*\* p, 0.01, \*\*\* indicate  $P < 0.001$  analysed with one way ANOVA with Bonferroni post test. Scale: 25 $\mu\text{m}$

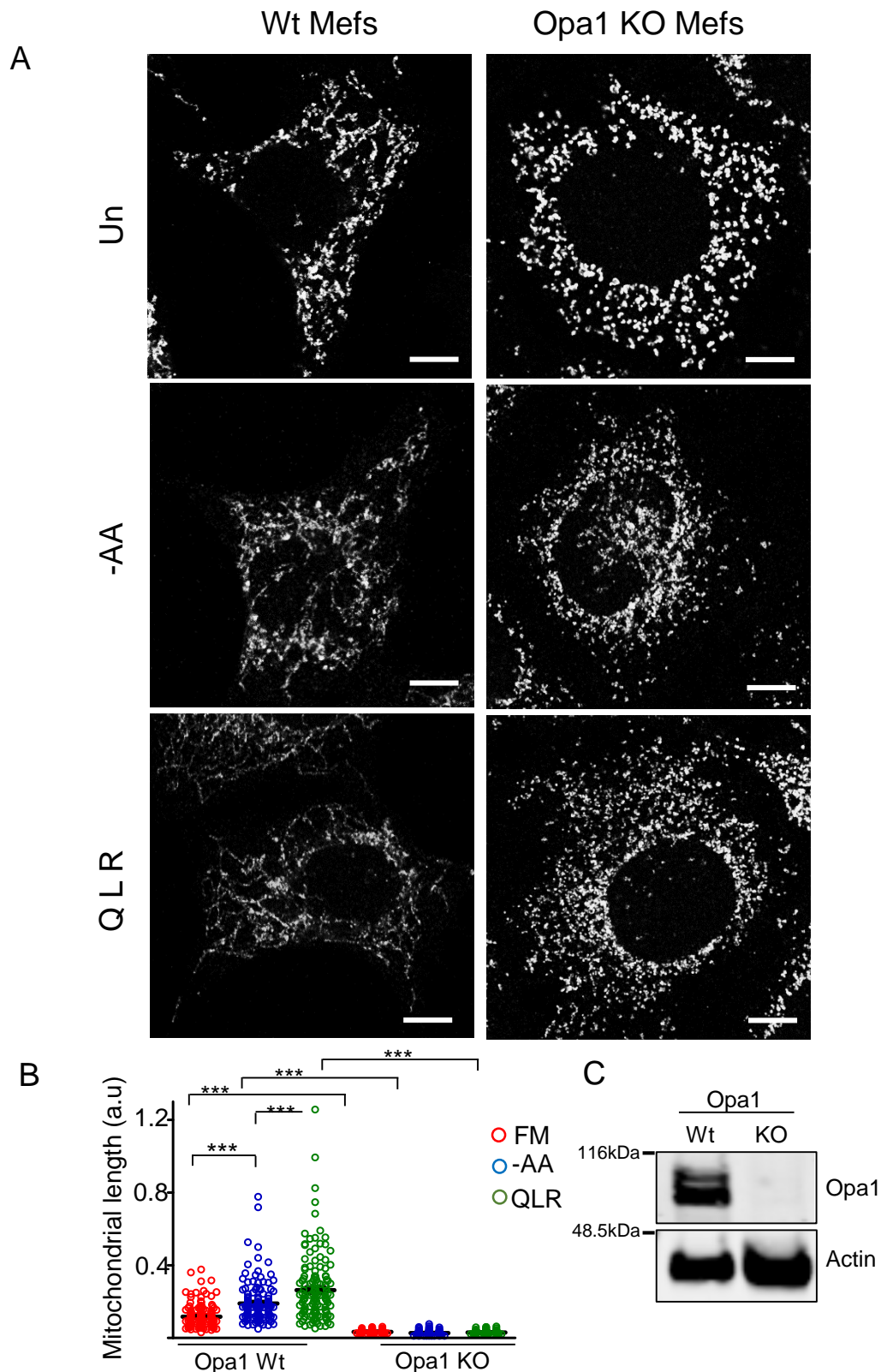


**Figure 3.13: Opa1 is required for amino acid-dependent mitochondrial hyperfusion.** A) Confocal representative images of wildtype MEF and Opa1 KO cells cultured in full media (Un), starved of either all amino acids (-AA) or starved of amino acid but supplemented with QLR for 4h. Starvation media conditions also contained 10% dialysed FBS.

(B) Bee-swarm plot indicating mitochondrial fusion is blocked in Opa1 KO cells. Each treatment shows 150 cells quantified from three independent experiments.

(C) Western blot showing the absence of Opa1. \*\*\* indicate  $P < 0.001$ , \*\*  $P < 0.01$  analysed with one way ANOVA with Bonferroni post test. Scale:  $10\mu\text{m}$

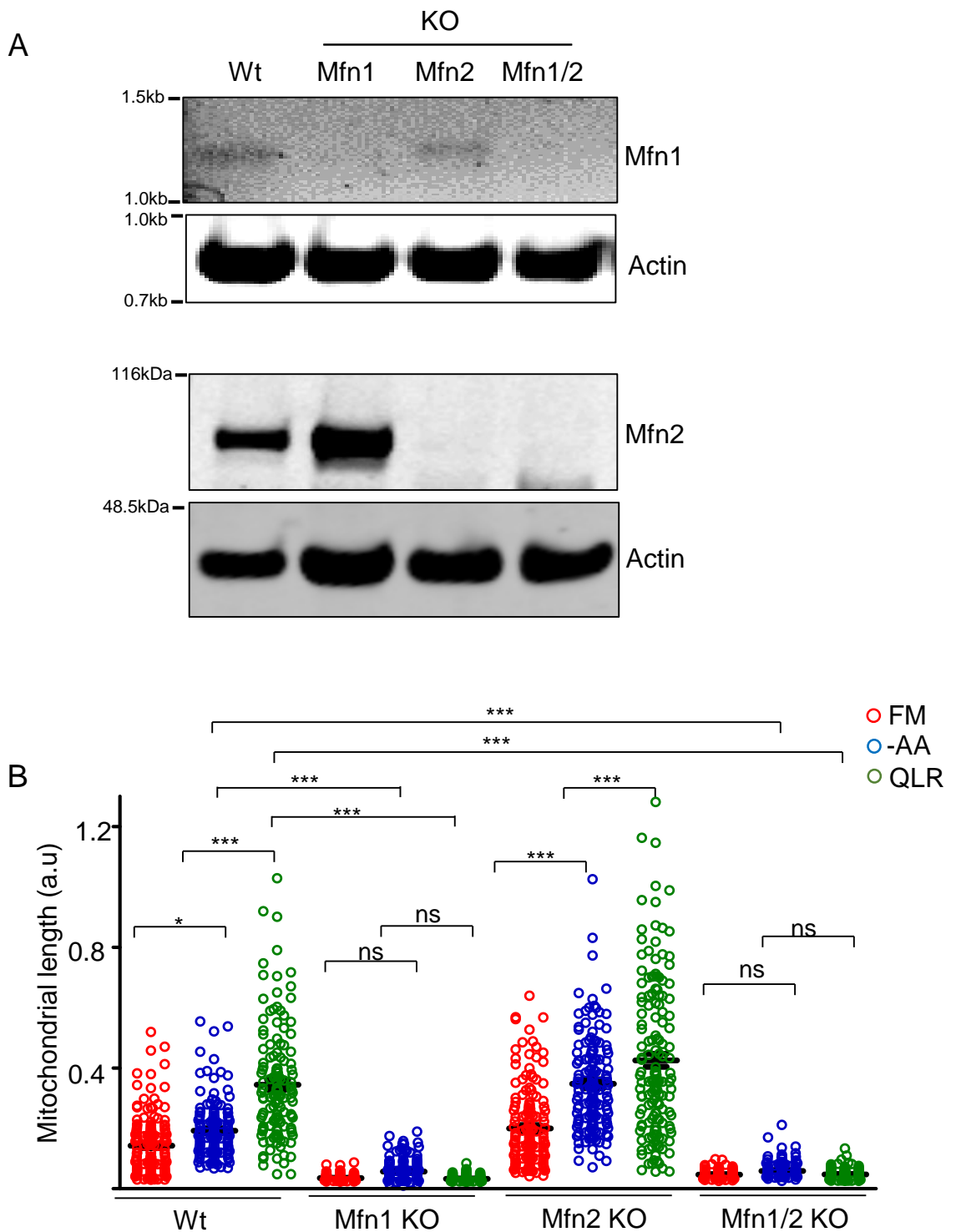


**Figure 3.14: Mfn1 is required for amino acid-dependent mitochondrial hyperfusion.**

(A) Wildtype, Mfn1 KO, Mfn2KO and Mfn1/2 KO cells were lysed for RNA and protein lysates. Semi-quantitative polymerase chain (PCR) was performed for Mfn1 on the RNA lysates and the product was analysed on agarose gel. Mfn2 protein levels was assessed in the protein lysate via western blot analysis. Actin was used as a loading control. Images show the absence of Mfn1 and Mfn2

(B) Wildtype, Mfn1 KO, Mfn2 KO and Mfn1/2 KO MEF cultured in full media (Un), starved of either all amino acids (-AA) or starved of amino acid but supplemented with QLR for 4hr. Starvation media conditions also contained 10% dialysed FBS. Bee-swarm plot indicating mitochondrial fusion is blocked in Mfn1 KO and Mfn1/2 KO cells. Each treatment shows 150 cells quantified from three independent experiments. \*\*\* indicate  $P < 0.001$ , \* $P < 0.05$  analysed with one way ANOVA with Bonferroni post test.

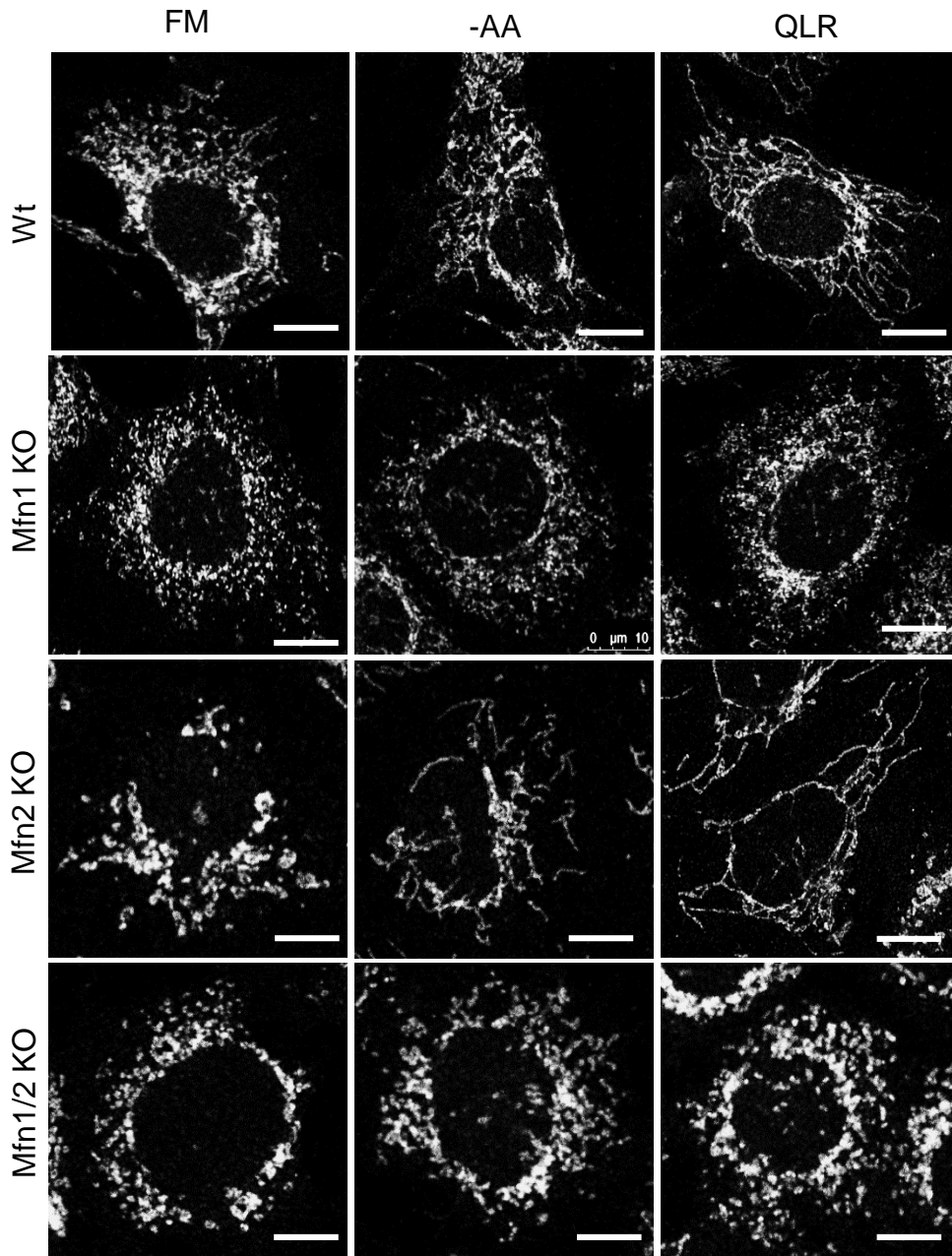


**Figure 3.15: Mfn1 is required for amino acid-dependent mitochondrial hyperfusion.** Confocal representative images of wildtype, Mfn1 KO, Mfn2 KO and Mfn1/2 KO MEF cultured in full media (Un), starved of either all amino acids (-AA) or starved of amino acid but supplemented with QLR for 4hr h. Starvation media conditions also contained 10% dialysed FBS. Scale: 10 $\mu$ m

### 3.2.5 Investigating the role of mitochondrial division in QLR-dependent mitochondrial hyperfusion

Mitochondrial dynamics is a continuous process involving a balance of mitochondrial division and mitochondrial fusion. An increase in net mitochondrial size may be a result of inhibited mitochondrial division or increased fusion. During mitochondrial division, Drp1 is recruited to mitochondria where it constricts and divides mitochondria into small forms (Smirnova et al., 2001). To determine whether mitochondrial fusion is enhanced or whether mitochondrial division is reduced during QLR-supplementation, we first tested the effects of the compound Mdivi-1 (Mitochondrial division inhibitor-1). Mdivi-1 has been shown to inhibit mitochondrial fission in mammalian cells where it promotes mitochondrial fusion (Cassidy-Stone et al., 2008). Mechanistically, it was initially suggested that Mdivi-1 selectively inhibits Drp1-GTPase activity and Drp1-polymerization. Here, as a simple pharmacological test, Mdivi-1 was included to induce mitochondrial fusion in combination with amino acid-starvation and QLR-supplementation.

Surprisingly, it was observed that Mdivi-1 did not stimulate strong mitochondrial fusion in 4T1-SU9 GFP and U2OS-SU9 GFP cells at 10 $\mu$ M (**Fig 3.16 A and B**). Mdivi-1 led to a mild (but insignificant) increase in mitochondrial length in Mdivi-1-treated cells relative to untreated cells. While amino acid starvation and QLR supplementation both led to expected increases in mitochondrial length, further Mdivi-1 treatment in either context did not alter mitochondrial phenotypes in both 4T1-SU9 GFP and U2OS-SU9 GFP cells. As these experiments were being performed, it was reported that Mdivi-1 may in fact not function as an effective Drp1 inhibitor (Bordt et al., 2017). These authors reported that Mdivi-1 did not alter mitochondrial dynamics nor inhibit Drp1-GTPase activity but rather served to inhibit complex-1 of the E.T.C in a distinct mechanism.

To overcome these issues, Drp1 was silenced in wildtype MEF and 4T1 cells using different shRNA Dnm1l constructs packaged into lentivirus (**Fig 3.17A**). It was observed that all shRNA-sequences tested targeted Drp1 which led to a stable reduction in the total Drp1 protein in MEF, with sh\_Dnm1l (F3) having the most efficient knockdown (**Fig 3.17B**). Interestingly, shRNA\_Dnm1l (F3) also effectively silenced Drp1 in 4T1 cells (**Fig 3.17C**).

Amino acid-dependent mitochondrial fusion was next tested in shDrp1 (F3 sequence) MEF and shDrp1 4T1 cells. Confocal images revealed that knockdown of Drp1 led to

increased mitochondrial fusion regardless of the status of amino acid starvation, for example in **(Fig 3.18)**. Upon quantification, we observed that mitochondrial length increased by approximately 2-fold in untreated shDrp1 MEF cells relative to wildtype cells **(Fig 3.19A)**. This increase in mitochondrial size would be expected based on lack of fission in combination with basal levels of fusion. Amino acid starvation led to mild mitochondrial fusion in wildtype cells (as expected) but levels of overall fusion were higher when this starvation condition was tested in shDrp1 MEF. This suggests that amino acid starvation increases levels of fusion, which are more pronounced since fission is inhibited upon loss of Drp1. Similarly, QLR-supplementation increased mitochondrial length in wildtype MEF which was further increased when Drp1 was knockdown. Therefore, QLR-supplementation appears to also increase rates of fusion. In wildtype MEF, QLR-supplementation may be stimulating maximal levels of fusion, but basal levels of fission are still operational.

Similar results were observed in 4T1 cells. The knockdown of Drp1 led to an increase in mitochondrial length by approximately 2-fold in untreated shDrp1 4T1 cells relative to wildtype cells **(Fig 3.19B)**. The knockdown of Drp1 further increased mitochondrial length in amino acid-starved cells by approximately 2-fold. In contrast to MEF, the level of increase in QLR-dependent hyperfusion in wildtype relative to shDrp1 4T1 cells was mild, although the shift in distribution is still seen and significant by ANOVA. These results suggest that QLR-dependent mitochondrial fusion occurs as a result of increased rates of mitochondrial fusion pathways (rather than the inhibition of mitochondrial fission). Collectively, findings in this chapter indicate that mitochondria specifically respond to the presence of QLR addition by inducing a mitochondrial hyperfusion mechanism similar to SIMH. This increase in mitochondrial fusion is dependent upon the activities of Mfn1 on the outer mitochondrial membrane and Opa1 for fusion of inner mitochondrial membranes.

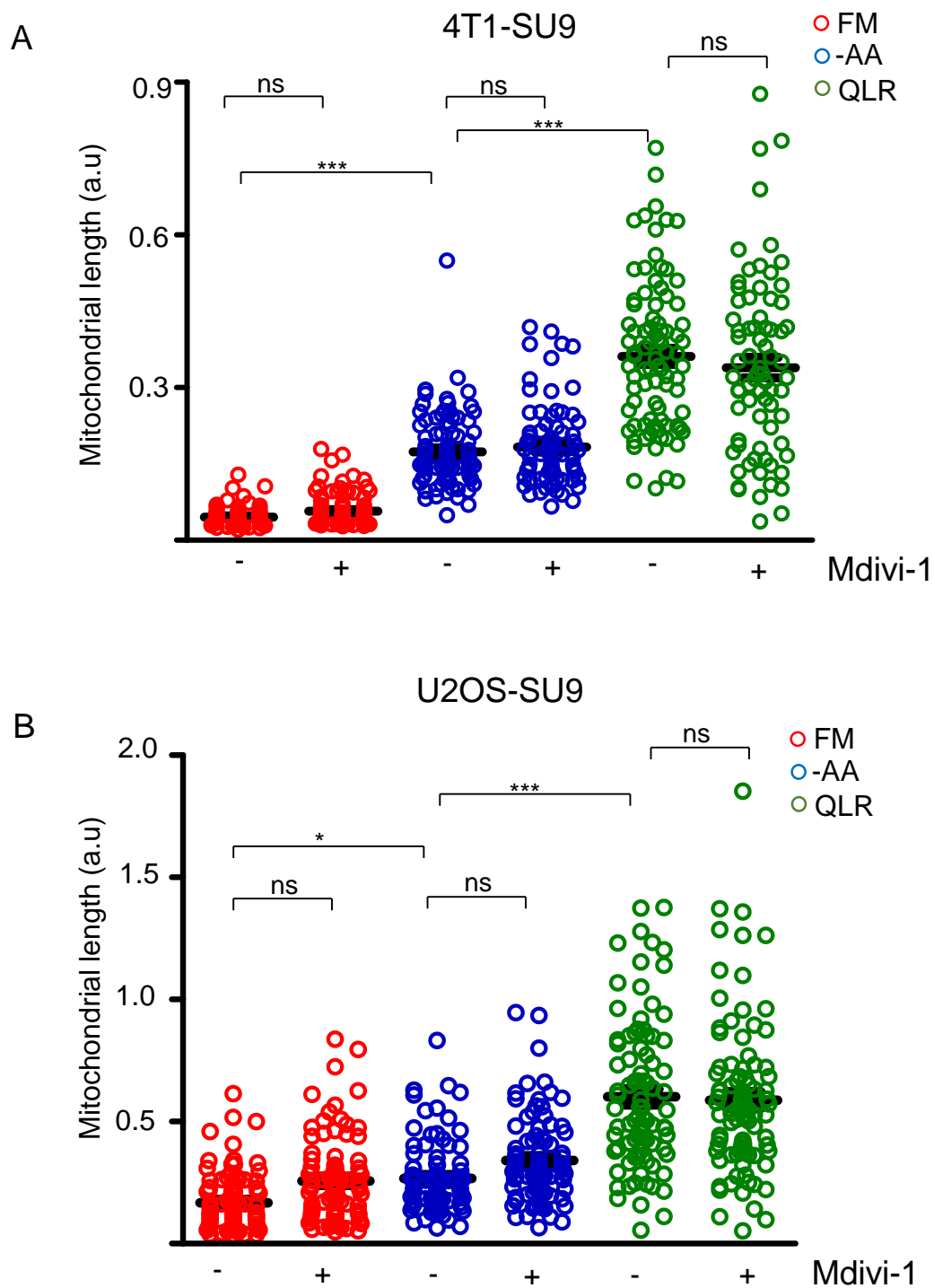


**Figure 3.16: The effect of Drp1 inhibition on mitochondrial fusion.** Cells were starved of either all amino acids (-AA) or starved of amino acid but supplemented with QLR, +/- Drp1 inhibitor (mdivi-1) (10 $\mu$ M) for 4h in (A) 4T1-SU9 B) U2OS-SU9. Starvation media conditions also contained 10% dialysed FBS. Each treatment shows 100 cells quantified from two independent experiments. n.s: non significant. Analysed with one way ANOVA, with Bonferroni post test.

A

pLKO shRNA Dnm1l plasmids	Code	Sequence
RMM3981-201744182 - TRCN0000012604	F2	GCCAACTGGATATTAACAATA
RMM3981-201744183 - TRCN0000012605	F3	GCTTCAGATCAGAGAACTTAT
RMM3981-201744184 - TRCN0000012606	F4	CGGTGGTGCTAGGATTTGTTA
RMM3981-201744185 - TRCN0000012607	F5	CCTGCTTTATTTGTGCCTGAA

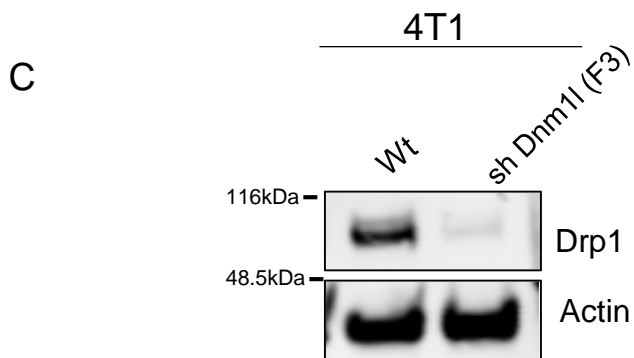
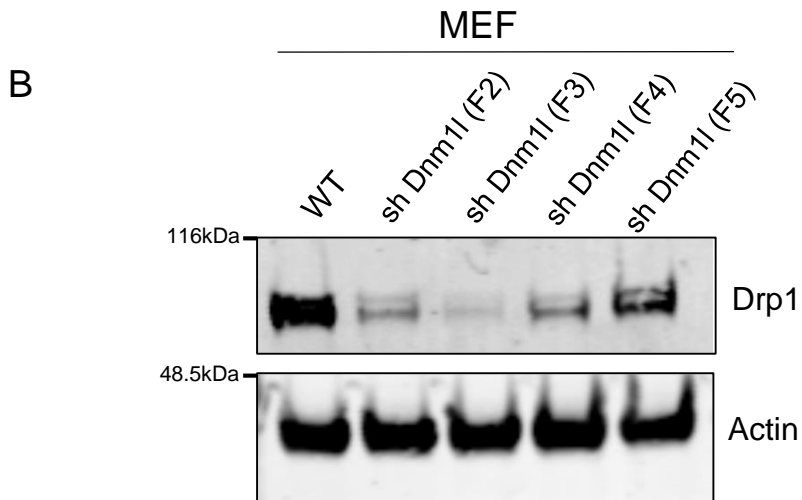


**Figure 3.17: Knockdown of Dnm1L (also known as Drp1).**

(A) pLKO shRNA sequences targeting Drp1

(B) Western blot showing the stable knockdown efficiency of Drp1 shRNA in MEF.

(C) Effective knockdown of Drp1 in 4T1 cells.

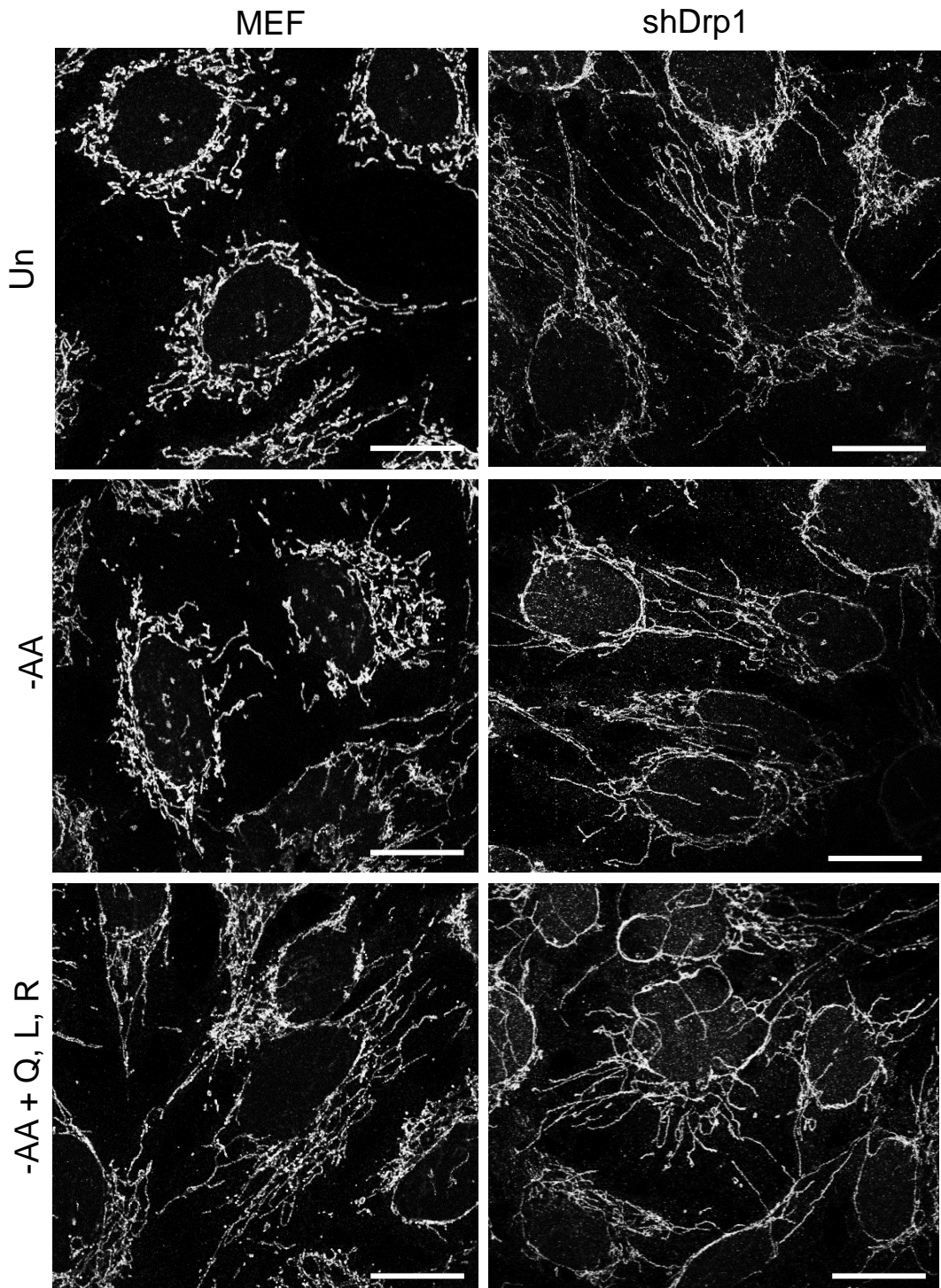


**Figure 3.18: Effect of Drp1 knock down on mitochondrial dynamics.** A) Confocal representative images of wildtype MEF and ShDrp1/MEF cultured in full media (Un), starved of either all amino acids (-AA) or starved amino acid but supplemented with QLR for 4h. Starvation media conditions also contained 10% dialysed FBS. Cells were stained with anti-Tom20. Scale: 25 $\mu$ m

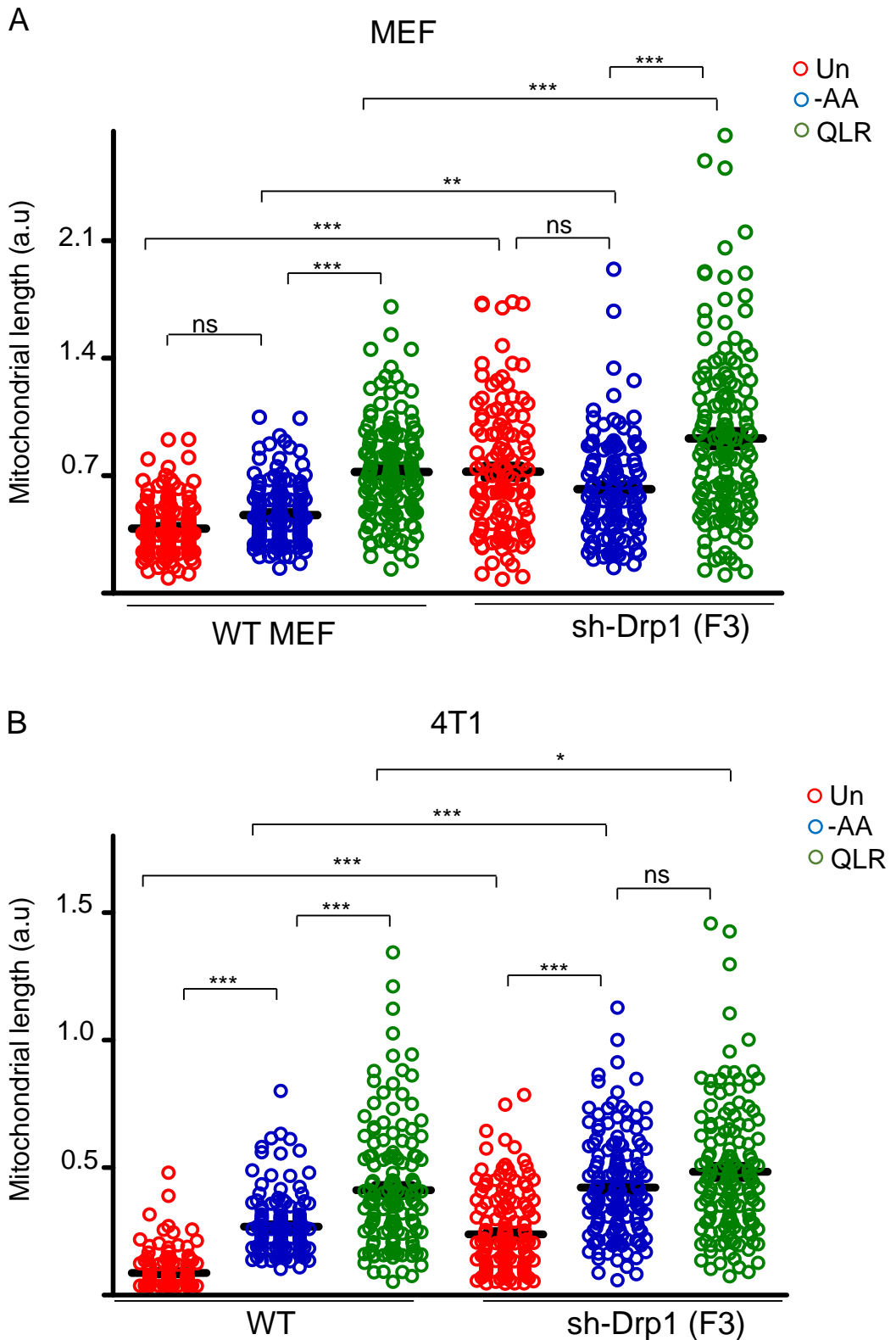


**Figure 3.19: Effect of Drp1 knockdown on amino acid-dependent mitochondrial fusion.** Wildtype cells ShDrp1 cells were cultured in full media (Un), starved of either all amino acids (-AA) or starved of amino acid but supplemented with QLR for 4h. Starvation media conditions also contained 10% dialysed FBS.

Bee-swarm plot showing increase in mitochondrial length following Drp1 knockdown in (A) MEF (B) 4T1 cells. Each treatment shows 150 cells quantified from three independent experiments. \*\*\* indicate  $P < 0.001$ , \*\*  $P < 0.01$ , \*  $P < 0.05$ , ns (not significant) analysed with one way ANOVA, with Bonferroni post test.

## **3.3 Discussion**

### **3.3.1 Mitochondrial fusion during starvation depends on the depleted nutrients**

Several studies have linked mitochondrial dynamics to nutrient availability. In the literature, it has been suggested that mitochondria may alter their shape and size as a stress response, for example, to maintain energy homeostasis, prevent mitophagy and ameliorate apoptosis (Gomes et al., 2011a, Rambold et al., 2011, Li et al., 2017, Molina et al., 2009). Recent studies have now suggested that cellular responses to stress are specific and it is dependent on the depleted nutrient or the type of stress. For example, while amino acid or serum starvation have been shown to induce autophagy, glucose starvation has been shown by our laboratory and others to inhibit autophagy (Nwadike et al., 2018, Lum et al., 2005). This suggests that autophagy is not a response to general nutrient starvation. Furthermore, the molecular pathway of mitophagy during mitochondrial damage with CCCP is Parkin-dependent while E.T.C. damage induced by chelating iron is Parkin-independent (Allen et al., 2013). This also suggests that there is a specialized mitochondrial response to stress. To better understand the mitochondrial responses to different nutrient deprivation-induced stress, we studied mitochondrial remodelling during serum, glucose and amino acid starvation in this chapter. We show here that mitochondria remodel to a fused state only during specific nutrient starvation stress.

#### **3.3.1.2 Mitochondria do not hyperfuse during serum starvation**

An important “nutrient” that is needed for cellular division and growth is serum, which provides stimulatory signals (Antoniades and Owen, 1982). The key pathway that is activated in response to growth factors (or insulin) is the PI3K-AKT pathway (Lin et al., 2012). Although the PI3K pathway has been reported to be involved in mitochondrial trafficking in cancer (Caino et al., 2015), interrelationships between PI3K-AKT signalling and mitochondria dynamics remain elusive. Interestingly, we observed that serum starvation does not stimulate mitochondrial hyperfusion. This suggests that members of the serum sensing pathways do not activate signals that promote mitochondrial fusion during serum starvation.

Our observation that mitochondria do not fuse during serum starvation in HeLa, 4T1, RPE1 and U2OS is in line with previous studies (Rambold et al., 2011). Rambold et al. (2011) showed in MEF that mitochondria undergo fission during serum starvation

despite the induction of autophagy. This is also consistent with recent studies which reported in other cell types that serum starvation in 3T3-L1 and HCT116 cells led to extensive mitochondrial fragmentation (Yao et al., 2019, Cesarini et al., 2018). These findings in multiple cell types indicate that the observation here that serum starvation does not induce fusion is conserved.

The inability of mitochondria to hyperfuse during serum starvation confirms that mitochondria fusion is a nutrient-specific effect. Mitochondria might hyperfuse in response to specific changes in mitochondrial function, which is caused by the effects of specifically-starved nutrients. Interestingly, serum depletion has been shown to have an adverse effect on mitochondrial processes such as the increase in ROS, cytochrome-c release and apoptosis (Lee et al., 2010, Cesarini et al., 2018). These mitochondria-dependent processes have been shown to correlate with enhanced mitochondrial fission which is suggested to occur via the increase in Drp1 recruitment to mitochondria (Cesarini et al., 2018, Germain et al., 2005). Hence, the fragmented mitochondria observed during serum-starvation is likely to contribute to cytochrome-c and sensitize towards apoptosis.

### **3.3.1.3 Mitochondrial hyperfusion is not a response to changes in glycolysis**

Acetyl-CoA is a major product of glucose metabolism and is further metabolised in mitochondria via the TCA cycle to generate NADH and FADH. As a result, mitochondria have been proposed to possibly sense changes in glucose levels since it is an important precursor of acetyl-CoA required for mitochondrial-generated energy. At the cellular level, AMPK activation serves as a major signal of glucose insufficiency (Lin and Hardie, 2018). As one mechanism for mitochondria, increases in fragmentation occur as a result of AMPK phosphorylation of Mff that brings Drp1 to localise on mitochondria (Toyama et al., 2016).

We found that mitochondria retain their normal (basal) small punctate forms during glucose starvation in RPE1, U2OS and HeLa. In contrast, glucose starvation mildly led to mitochondrial fusion in 4T1. This suggests that glucose-dependent regulation of mitochondrial dynamics may be context and cell type-dependent. Additional contradicting observations have been reported to indicate that glucose starvation did not induce mitochondrial fusion in MEF (Rambold et al., 2011, Mishra et al., 2014). Furthermore, the inhibition of glucose metabolism with 2-Deoxy-D-glucose (2-DG) or overall glucose deprivation has been shown to promote mitochondrial fusion in yet

other reports (Li et al., 2017, Lee et al., 2014). This cell type-dependent mitochondrial fusion response during glucose starvation may be associated with changes in bioenergetic capacities of the cell.

Interestingly, forcing cells to depend on mitochondrial ATP (by switching energy source from glucose to galactose or acetoacetate) led to mitochondrial fusion (Mishra et al., 2014). This carbon switch blocks ATP generation from glycolysis and it has been suggested that mitochondria thereby induce fusion to sustain energy demands. This suggests that the stimulation of mitochondrial fusion during glucose starvation is dependent on the switch from glycolytic to OXPHOS as a source of energy, an effect which varies in cells. For example, Q-driven OXPHOS has been reported to be the major source of energy for HeLa cells even in the presence of glucose (Reitzer et al., 1979) and it has been shown that HeLa cells mitochondria hyperfuse specifically in response to increases in glutaminolysis (Rossignol et al., 2004). It has also been shown that glucose deprivation led to a transient increase in mitochondrial ATP pool by five minutes in HeLa cells. However, this effect was followed by a great reduction in mitochondrial ATP pool by seven minutes (Depaoli et al., 2018). These studies suggest that glucose starvation does not necessarily increase in OXPHOS activity in HeLa cells. This may explain why glucose starvation did not have any major effect on mitochondrial fusion in HeLa cells.

In contrast to HeLa cells, it has been shown that RPE1 cells mainly generate energy via glycolysis (MacVicar and Lane, 2014). Similarly, bioenergetics studies suggest that U2OS are also highly dependent on glycolysis (Issaq et al., 2014). It is possible that these cells do not readily switch to OXPHOS upon glucose starvation, and thereby do not undergo mitochondrial fusion. Glucose starvation also led to fusion in 4T1 cells. In line with this, 4T1 cells have been shown to have high dependency on both glycolysis and glutaminolysis, and these cells readily switch to OXPHOS upon energy stress (Simões et al., 2015). Based on reports that mitochondrial fusion correlates with bioenergetic efficiency (Mishra and Chan, 2016), our data would be consistent with a model in which mitochondria only undergo fusion to enhance ATP production via glutaminolysis under glucose insufficiency. Therefore, our findings suggest that mitochondrial response in glucose starvation is dependent on the overall bioenergetic needs of the cell.

#### **3.3.1.4 Mitochondria hyperfuse mainly during amino acid deprivation**

It has been previously reported that cells respond to the starvation of amino acids by increasing mitochondrial fusion to enhance cellular viability via OXPHOS-dependent ATP production (Gomes et al., 2011a). Similar to these studies, we observed that mitochondria remodel towards a fused state during amino acid starvation in cancer cell models and non-cancer RPE1 and MEF cell types. Surprisingly, in several MEF cell models, we observed that amino acid starvation led to only mild mitochondria fusion, as compared to responses in 4T1, U2OS and HeLa cells. Others had previously reported mitochondrial fusion following amino acid starvation of MEF (Rambold et al., 2011, Gomes et al., 2011a). This apparent difference could be explained in part by varying methods of assessing mitochondrial fusion. MEF generally have a high level of intermediate variable mitochondria (mixed population of fused and fragmented) in the untreated basal condition. For example, 80% of untreated MEF in Rambold et al were categorised by manual scoring as having intermediate mitochondrial shape Rambold et al. (2011). Therefore, we propose that the mitochondrial fusion reported in the Gomes et al. (2011a) and Rambold et al. (2011) studies likely represent highly variable basal levels. This granularity may be normalised somewhat by their quantification method based on categorising percentages of cells having overall fusion phenotypes. In contrast, our ImageJ-based approach measures mitochondrial size cell-by-cell to assess levels of fusion in the population. Therefore, discrepancies between our data and previous reports could be explained if mild size increases that we measure are scored as positive-for-fusion via categorisation. Despite these method differences, altogether, the data are consistent with a mitochondrial fusion response following amino acid starvation and our data highlight that the extent of this response in MEF is not as robust relative to other cell types.

#### **3.3.1.5 Unique form of mitochondrial amino acid sensing**

Here, we aimed at reversing amino acid starvation-induced mitochondrial fusion by adding back three regulatory amino acids sensed by MTORC1 (Shen et al., 2019, Chantranupong et al., 2016, Wolfson et al., 2016, Wang et al., 2015, Jewell et al., 2015). It was expected that the addback of Q, L and R into amino acid starvation media would block amino acid starvation-induced mitochondrial fusion due to the reactivation of MTORC1. Surprisingly, in contrast to this model, we identified a distinct

mitochondrial hyperfusion response: supplementation of Q+L+R into amino acid starvation media led to further mitochondrial hyperfusion and hyper branching. Interestingly, this unique mitochondrial hyperfusion is exclusive to the addback of Q+L+R to starvation media. It was observed here that either the substitution of L with other BCAA or R for K stimulate lesser levels of mitochondrial fusion relative to QLR-dependent hyperfusion. In addition, the absence of one amino acid from the QLR-addback set greatly reduces mitochondrial hyperfusion. However, R seems to be the less important amino acid among the three for the stimulation of mitochondrial hyperfusion. Reflecting on the mitochondrial function of amino acid, our data suggest that mitochondria may directly sense these three amino acids by three separate pathways, as they are sensed at the cellular level. However, it is also possible that mitochondria sense Q, L and R through the same pathway. Nevertheless, all three signals are required for a maximal effect as consistently shown in U2OS and 4T1 cells.

We propose that mitochondrial fusion could be a direct cellular response to nutrient availability. Consistent with a direct effect, it has been established that mitochondria can respond differently to energy stress conditions depending on the deficient nutrient (Rambold et al., 2011). For example, amino acid starvation has been reported to induce ATP synthase dimerization and enhance mitochondrial ATP generation but not during glucose starvation (Gomes et al., 2011a). Here, we also found in our experiments that mitochondrial hyperfusion does not strongly occur under glucose starvation conditions, supporting the idea that mitochondria are more sensitive sensors of amino acids.

This notion is supported by the recent findings that demonstrate mitochondria can respond directly to specific amino acids such as serine (Gao et al., 2018). These authors showed that serine starvation led to extensive mitochondrial fragmentation. It is suggested that mitochondrial fragmentation occurs due to the reduction in mitochondrial-dependent lipid metabolism such as reduced mitochondrial ceramides. Interestingly, the serine mitochondrial transporter sideroflexin-1 (SFXN1), which is required for one-carbon metabolism, was also recently identified in an independent study (Kory et al., 2018). This study also showed that the knockout of all homologues of SFXN1 (SFXN2 and SFXN3) led to a reduction in mitochondrial length. Although serine effects were not studied in this chapter, findings from these studies support a model where mitochondrial-dependent metabolic processing of amino acids directly modulates mitochondrial dynamics.

Amino acid levels are sensed in the lysosomal lumen through both cytosolic and inside out mechanisms which require the lysosomal localization of MTORC1 (Lawrence and Zoncu, 2019, Lawrence et al., 2018, Yang et al., 2017). Interestingly, recent evidence in yeast has better defined a signalling mechanism interaction between mitochondria and lysosomes, involving the exchange of lipids and potentially direct sensing of amino acids (Todkar et al., 2017, Elbaz-Alon et al., 2014, Gonzalez Montoro et al., 2018). In these studies, mitochondrial contact sites with vacuoles were identified and shown to be enriched with amino acid transporters. Similar observations have been reported in HeLa cells where it was revealed that mitochondrial-lysosomal contact sites also function as a locus for mitochondrial fragmentation (Wong et al., 2018). These contact sites are also important for cellular metabolism where they enhance metabolites transfer (Honscher et al., 2014) thus driving the TCA cycle which is the main pathway for Q, L and R catabolism. These studies further support a possible direct mitochondrial amino acid sensing mechanism that may involve mitochondrial-lysosomal contacts.

In addition, mitochondrial solute carriers directly regulate mitochondrial dynamics by enhancing Opa1-oligomerization and cristae tightening also linking metabolic sensing to mitochondrial dynamics (Patten et al., 2014). Patten et al. (2014) suggested that mitochondrial solute carriers may also function as mitochondrial metabolite sensors in addition to their solute-carrying function. This is consistent with the observation that Opa1 oligomerize in response to the depletion of E.T.C substrates while the addition of E or malate reduces the formation of Opa1 oligomers. Furthermore, it was shown that mitochondrial carrier proteins (SLC25A) such as SLC25A11 and SLC25A12 which shuttles malate and E respectively into mitochondria interact with Opa1, and they are required for Opa1 oligomerization during depleted energy substrates. Together with the findings here, mitochondria seem to sense regulatory amino acids directly independent of the overall cellular nutrients status.

### **3.3.2 Is amino acid-dependent mitochondrial fusion an ER stress response**

Our data contradict Gomes et al. (2011b) where it was reported that the supplementation of essential amino acids (Leucine, Methionine, Isoleucine, Lysine, Phenylalanine, Threonine, Valine, Tryptophan) and glutamine blocked mitochondrial fusion. In our experiments, QLR was supplemented as we were originally studying MTORC1-reactivation and mitochondrial dynamics. In this way, we found that QLR-supplementation led to a high degree of mitochondrial hyperfusion. Interestingly, the

hyperfusion observed here is very similar to SIMH which occur as a result of different types of cell stress including abrogated protein synthesis (Tondera et al., 2009). Speculatively, this suggests that QLR-induced hyperfusion may be associated with the inhibition of protein synthesis. It is possible that addition of QLR (in an otherwise amino acid-deficient state) was not sufficient to continue protein synthesis, hence stalling translation and inducing a stress-induced mitochondrial fusion. In relation to the observations by (Gomes et al., 2011b), the presence of EAA and Q might be sufficient to continue translation hence blocking stress-induced hyperfusion. It would be interesting to investigate the role of SLP-2 and PERK in amino acid starvation-induced fusion and QLR-induced hyperfusion since they are required for SIMH (Tondera et al., 2009).

In addition to SLP-2 and PERK, SIMH was also reported to require fusion mediators Mfn1 and Opa1 as a result of increased fusion (Tondera et al., 2009, Lebeau et al., 2018). Interestingly, QLR-dependent hyperfusion also required Mfn1, Opa1 but not Mfn2. Therefore, both these forms of mitochondrial hyperfusion require Mfn1 and Opa1, which are well established critical fusion factors (Cipolat et al., 2004). However, mitochondrial hyperfusion occurs due to increased fusion or reduced fission. Similar to SIMH which occur due to enhanced fusion rather than the inhibition of fission, our QLR-dependent hyperfusion increased in shDrp1 cells that have less fission machinery. This finding indicates that an enhanced mitochondrial fusion is the main mechanism driving QLR-dependent hyperfusion.

Fusion is driven via coordinated steps mediated by Mfn1 and Opa1. Mfn1 forms homotypic dimers leading to the tethering of outer mitochondrial membrane and this function is independent of Mfn2, which plays another role as a regulator of ER-mitochondria contact site stabilization (Chen et al., 2003a, de Brito and Scorrano, 2008). ER-mitochondria contact sites serve as loci for mitochondrial constriction independent of Drp1 (Chakrabarti et al., 2018, Friedman et al., 2011, Korobova et al., 2013). In line with our findings, depletion of total Drp1 has been shown to be one of the diverse mechanism that can be activated for the stimulation of mitochondrial hyperfusion (Sabouny et al., 2017). Although QLR-induced hyperfusion increased in shDrp1 cells, post-translational regulation of Drp1 by PKA and other regulators cannot be totally ruled out (Gomes et al., 2011a). Similarly, post-translation regulation of Mfn1 and Opa1 during QLR-dependent mitochondrial hyperfusion are possible. For example, during glucose starvation-induced mitochondrial fusion, Mfn1 is deacetylated due to its interaction with protein deacetylase HDAC6 (Lee et al., 2014). Opa1 is also cleaved by Yme1L at the site (S2) during increased OXPHOS activity

thereby leading to mitochondrial fusion (Mishra et al., 2014). Despite the critical requirements of Mfn1 and Opa1 in amino acid-dependent mitochondrial fusion, their specific post-translational regulatory changes remain elusive.

### **3.3.3 Conclusion**

In this chapter, we first confirmed that amino acid starvation stimulates mitochondrial fusion, consistent with literature. Unexpectedly, we discovered a novel mitochondrial hyperfusion response stimulated by the supplementation of Q, L and R. This amino acid driven fusion suggests the potential involvement of a MTORC1-dependent sensing since these 3 amino acids have been directly linked to this nutrient sensor mechanism. This unique mitochondrial response requires both Mfn1 and Opa1 which drives the outer and inner mitochondrial membrane fusion. Therefore, QLR amino acid levels appear to promote proper canonical mitochondrial membrane fusion. The extent of QLR hyperfusion was similar to previously reported stress-sensing mitochondrial remodelling responses. In the following chapters, we investigate potential regulatory mechanisms and roles of QLR-dependent fusion.

## **Chapter 4**

# **Investigating roles for nutrient sensing kinase pathways during amino acid-dependent mitochondrial hyperfusion**

## 4.1 Introduction

The molecular definition of intracellular amino acid sensing pathways has substantially expanded in the last decade (Shimobayashi and Hall, 2016, Bar-Peled et al., 2012, Zoncu et al., 2011, Sancak et al., 2010). Overall, a network of multiple molecular sensors detect increases or decreases (ie starvation) in amino acid levels to coordinate protein translation, cell growth and catabolism via autophagy. This central control of cell expansion vs cell recycling thereby influences many downstream cellular processes such as apoptosis, cell division, cellular immunity and cellular metabolism (Gallagher et al., 2016, Villar et al., 2017, Wang and Proud, 2009, Shibutani et al., 2015, Galluzzi et al., 2014, Herzig and Shaw, 2018, Laplante and Sabatini, 2012). In Chapter 3, we described a unique pathway of mitochondrial dynamics that we discovered involving the stimulation of mitochondrial hyperfusion by Q, L and R. In this chapter, we further investigate kinase signalling pathways that may underlie the hyperfusion response.

Q, L and R are 3 main activating signals for MTORC1, the central cellular amino acid sensing pathway that further coordinates with AMPK and Ulk1 (Jewell et al., 2015, Carroll et al., 2016a, Chan, 2009, Kundu, 2011, Kim et al., 2011b). In addition, amino acid starvation has been suggested to increase cAMP levels and downstream activation of PKA, a proposed key regulator of mitochondrial dynamics (Gomes et al., 2011b, Gomes et al., 2011a). Interestingly, MTOR, AMPK, Ulk1/2 and PKA all have been shown by a range of biochemical and functional studies to form an interaction network that can serve to maintain cellular homeostasis by coordinating catabolic processes, energy balance, autophagy and mitochondrial processes (as shown upon our searches of interaction databases, **Fig 4.1**) (Lin and Hardie, 2018, Shin et al., 2015, Stephan et al., 2009, Tian et al., 2015, Xie et al., 2011). Recent studies have revealed the multiple roles of MTORC1 and AMPK, especially in the regulation of mitochondrial dynamics independent of their canonical role in autophagy (Morita et al., 2017, Toyama et al., 2016).

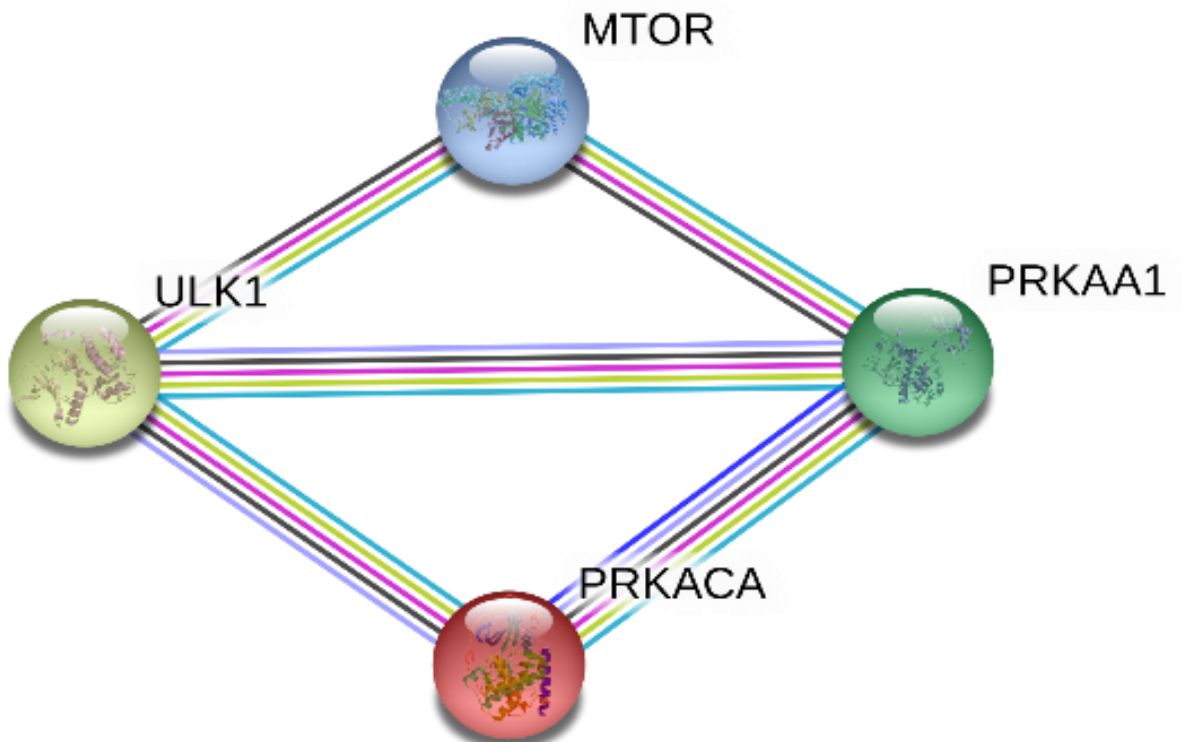


**Figure 4.1: Interaction map of the molecular regulators involved in amino acid sensing and mitochondrial dynamics.** The map generated from the STRING database show the interaction between MTOR (mechanistic target of Rapamycin), Ulk1 (Unc51-like autophagy activating kinase 1), PRKAA1 (5' AMP-activated protein kinase catalytic subunit alpha-1) and PRKACA (Protein kinase cAMP-activated catalytic subunit alpha).

MTOR is a drug target for the treatment of cancer and metabolic disorders (Bendell et al., 2015, Basu et al., 2015). In view of that, multiple potent MTOR inhibitors have been developed, some of which have been exploited in the study of mitochondrial dynamics (Thoreen et al., 2009, Morita et al., 2017, Sehgal, 2003). Rapamycin was first identified as an allosteric inhibitor of MTORC1 and it was initially used as an immunosuppressive and anti-proliferative agent. However, due to its poor solubility and pharmacokinetics, other soluble analogues such as temsirolimus and everolimus were developed for cancer treatment. Rapamycin and analogues inhibit MTOR by binding FKBP12 but rapamycin has been shown to poorly inhibit other MTOR functions such as protein synthesis and phosphorylation of 4E-BP1 (Thoreen et al., 2009, Thoreen and Sabatini, 2009).

More recently, new MTOR inhibitors with better efficacy have been developed (Rodrik-Outmezguine et al., 2016, Thoreen et al., 2009). Torin1, a competitive ATP agent was developed as a specific and potent MTOR inhibitor with an IC<sub>50</sub> of between 2 – 10nM (Thoreen et al., 2009). Mitochondrial studies have shown that rapamycin has a very weak effect on mitochondrial dynamics relative to the new class of ATP-competitive inhibitors. For example, pharmacological inhibition of MTOR for 24-hours using active-site inhibitors such as Ink1341 and Torin1 resulted in hyperfusion in 20% of mitochondria (relative to rapamycin-treated cells with fusion in 6% of mitochondria) (Morita et al., 2017). In one proposed mechanism, MTOR enhances translation of MTFP1 (Mitochondrial fission process-1) which has been shown to enhance recruitment of Drp1 to mitochondria to induce fragmentation (Morita et al., 2017, Morita et al., 2013). MTFP1 is an integral protein of the inner mitochondrial membrane which when overexpressed colocalises with Drp1 to promote mitochondrial fragmentation (Ehse et al., 2009, Tondera et al., 2005, Tondera et al., 2004). Upon MTOR inhibition, MTFP1 translation is inhibited, leading to the abrogation of mitochondrial fission, hence unopposed fusion.

Interestingly, MTORC1 has also been reported to regulate mitochondrial function by enhancing the translation of nucleus-encoded mRNA for the expression of factors required for OXPHOS and coupling of the E.T.C complexes (Morita et al., 2013). In addition, previous studies have shown that knockdown of MTOR could induce mitochondrial fusion (Gomes et al., 2011a). Since QLR activates MTORC1, our observations of mitochondrial hyperfusion suggest that MTORC1 may engage multiple mechanisms during amino acid-dependent remodelling of mitochondria. The sensing of amino acids and growth factors is integrated into MTORC1 activity levels via the function of the PI3K/Akt pathway (**Fig 4.2**).

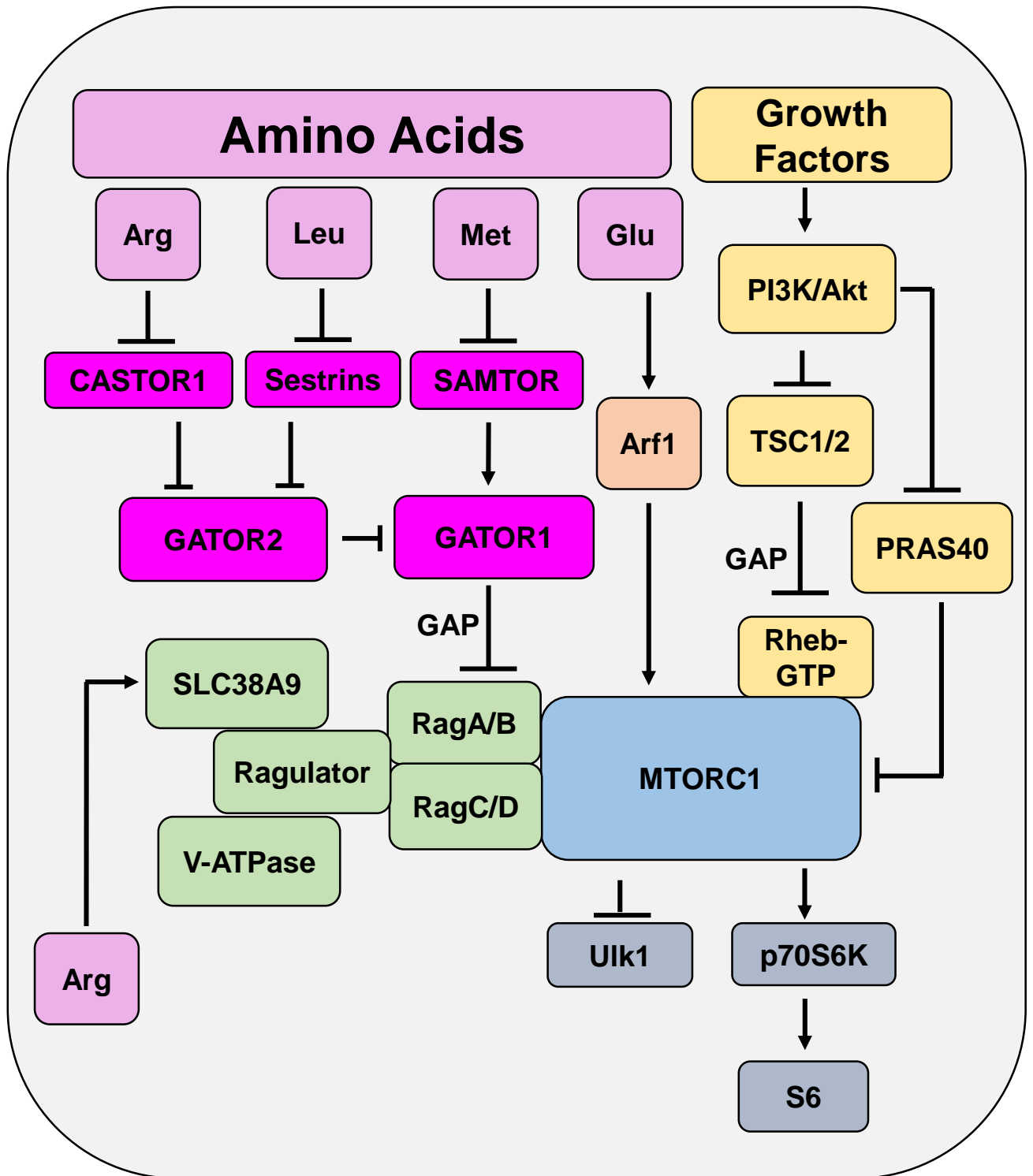


**Figure 4.2: The regulation of MTORC1 by amino acids and growth factors.** The signalling pathway shows how amino acids and growth factor are sensed by MTORC1. CASTOR1 and Sestrins sense Arginine (Arg) and Leucine (Leu) respectively in the cytosol which activates GATOR2 to block GATOR1 inhibition of MTORC1, thereby activating MTORC1. Arginine is also sensed at the lysosomes through SLC2889, leading to MTORC1 activation. The presence of Methionine (Met) is sensed as S-adenosylmethionine by SAMTOR, a positive regulator of GATOR1, thereby blocking GATOR1 inhibitory effect on MTORC1, activating it. Glutamine directly feed into MTORC1 via Arf1 independent of GATOR. The presence of growth factors amplify MTORC1 activity by enhancing Rheb/MTORC1 interaction and localization through the inhibition of TSC1/2 or PRAS40. An active MTORC1 phosphorylates and inhibit Ulk1, and also indirectly lead to the phosphorylation of S6 via p70S6K. Pathway modified from (Kim and Guan, 2019)

As introduced in Chapter 1, Akt phosphorylates and inhibits TSC2 and PRAS40, both of which are negative upstream regulators of MTORC1 (Sancak et al., 2007, Vander Haar et al., 2007). TSC2, in complex with subunit TSC1, inhibits Rheb, a GTP-binding protein that is required for MTORC1-lysosomal localization and activation. Therefore, in the presence of serum, Akt relieves Rheb from TSC1/2 inhibition, thereby promoting MTORC1 activation. MTORC1 phosphorylates downstream targets such as Ulk1 at Serine757 to mediate autophagy repression (Kim et al., 2011b). This phosphorylation event has been proposed to disrupt Ulk1 interaction with AMPK, thereby blocking autophagy (Kim et al., 2011b). Recent work from our laboratory has shown that upon supplementation of Q, L or R (or combination thereof), MTORC1 is activated and downstream targets such as Ulk1 are phosphorylated (Nwadike et al., 2018). In this chapter, the role of MTORC1 activation in amino acid-dependent mitochondrial dynamics will be investigated.

The activity of MTORC1 is also regulated by AMPK via multiple mechanisms (Lin and Hardie, 2018). AMPK activates TSC2 via phosphorylation at multiple sites leading to the inhibition of Rheb and MTORC1 (Inoki et al., 2003). Similarly, AMPK phosphorylates MTORC1 via Raptor (Gwinn et al., 2008). In addition, AMPK phosphorylates Ulk1 at Ser 317 and Ser 777, priming Ulk1 for the induction of autophagy (Kim et al., 2011b). AMPK also regulates Ulk1 via other phosphorylation events to connect cellular energy and nutrients stress to mitophagy (Tian et al., 2015, Egan et al., 2011). For example, in hypoxic conditions, AMPK phosphorylates Ulk1 at Ser555 thereby allowing Ulk1 to translocate to mitochondria during mitophagy (Tian et al., 2015). AMPK can also coordinate hypoxia-induced mitophagy by reducing mitochondrial potential in cardiomyocytes (Zhang et al., 2018). On the other hand, mitochondria can fine-tune AMPK regulation during the increased generation of reactive oxygen species (Hinchy et al., 2018, Rabinovitch et al., 2017). Lastly, AMPK directly phosphorylates fission mediator Mff, the mitochondrial receptor for Drp1 recruitment, under conditions that target mitochondrial-generated ATP (Toyama et al., 2016, Ducommun et al., 2015). This mechanism has been proposed to drive fission and thereby mitochondrial homeostasis during conditions of stress. Despite these direct roles of AMPK in mitochondrial dynamics, its potential role in mitochondrial remodelling during amino acid starvation was unclear, leading to our investigations in this chapter.

The upstream autophagy kinase Ulk1 has also been shown to play important roles in the cellular stress response involving mitochondria (Wu et al., 2014, Tian et al., 2015, Kundu et al., 2008, Joo et al., 2011). Multiple Ulk1 inhibitors have been developed in

view of exploiting autophagy inhibition as a drug target in cancer (Egan et al., 2015, Petherick et al., 2015). Ulk1 function is activated during amino acid starvation, as an early regulatory event in the induction of autophagy (Chan et al., 2007, Gallagher et al., 2016). Although Ulk1 has not been specifically linked to mitochondrial dynamics, previous studies have shown that Ulk1 can indirectly regulate mitochondrial fission via FUN14 domain-containing 1 (FUNDC1) protein during mitophagy (Wu et al., 2014, Wu et al., 2016b). During hypoxia, Ulk1 phosphorylates FUNDC1 at Ser-17 on the mitochondria. Interestingly, FUNDC1 knockdown was sufficient to stimulate mitochondrial fusion (Chen et al., 2016a). Additional studies have clarified that FUNDC1 stimulates recruitment of Drp1 to the mitochondrial-associated membrane thereby inducing fragmentation (Wu et al., 2016b). To note, FUNDC1 also interacts with Opa1, which is abrogated during stress. Although interaction with Drp1 and Opa1 is dependent on FUNDC1 phosphorylation by other kinases such as CK2 and SRC, the role of Ulk1 in regulation of FUNDC1 interactions is not fully understood (Chen et al., 2016a, Chen et al., 2014). Ulk1 has also been suggested to regulate mitochondrial processes via mitophagy. For example, a recent study reported that the Ulk1 complex also binds Bcl2-L-13 at the mitochondrial outer membrane to enhance mitophagy (Murakawa et al., 2019). It was shown that Ulk1 binds LC3B via its LC3-interaction region (LIR) and forms a complex with Bcl2-L-13. Interestingly, the Ulk1, LC3B and Bcl2-L-13 complex requires Ulk1 kinase activity, thereby suggesting that Bcl2-L-13 is also a Ulk1 substrate. The current evidence for Ulk1 in the regulation of mitophagy and mitochondrial dynamics led us to explore potential roles in mitochondrial fusion during amino acid starvation.

The molecular mechanism behind mitochondrial elongation during amino acid starvation has been previously shown to involve PKA regulation of Drp1 (Gomes et al., 2011a, Rambold et al., 2011). In Chapter 1, we summarised how PKA serves as effector of the second messenger cyclic-AMP (cAMP) (Lefkimiatis et al., 2013, Lefkimiatis and Zaccolo, 2014, Monterisi and Zaccolo, 2017, Valsecchi et al., 2013). Importantly, the interaction of PKA with downstream substrates can involve multiple mechanisms functioning at different subcellular locations. More specifically, mitochondria respond to cytosol-generated cAMP, therefore leading to the activation PKA and mitochondrial fusion (Di Benedetto et al., 2017). The current model suggests that PKA phosphorylates Drp1 at Ser637 at the cytosol to inhibit Drp1 translocation to mitochondria, thereby inducing unopposed mitochondrial fusion (Flippo and Strack, 2017, Lefkimiatis, 2014, Di Benedetto et al., 2017, Chang and Blackstone, 2007, Cribbs and Strack, 2007).

Apart from its role in mitochondrial fission, PKA intriguingly also has been reported to coordinate mitophagy, amino acid sensing and apoptosis (Akabane et al., 2016). cAMP accumulation activated via forskolin also can inhibit both MTORC1 and MTORC2 in a PKA dependent manner (Xie et al., 2011). PKA has been reported to phosphorylate Atg1 (Ulk1) and Atg13 in yeast (Stephan et al., 2009). Interestingly, another independent study suggested that PKA phosphorylates Ulk2 at Ser1027 in mammalian cells (Shin et al., 2015). The effects of these phosphorylation events on mitochondrial dynamics are not yet known.

Collectively, MTORC1, Ulk1, AMPK and PKA signalling pathways have been shown by a range of studies to converge on mitochondria through potentially cross-talking mechanisms. However, details on how they might regulate mitochondrial dynamics during nutrient shortages remain unclear. The aim of this chapter was to dissect the kinase-dependent molecular processes during amino acid-dependent mitochondrial remodelling.

The objectives are to:

1. Investigate whether amino acid-dependent mitochondrial hyperfusion is dependent on MTORC1.
2. Investigate whether energy-sensing regulator AMPK is required for amino acid-dependent mitochondrial fusion.
3. Utilize Ulk1 inhibitors, CRISPR-Cas9 and knockout models to study Ulk1 and its binding targets (Atg13 and FIP200) in the regulation of amino-acid-dependent mitochondrial fusion.
4. Assess the role of autophagy during amino acid-dependent mitochondrial fusion.
5. Investigate the role of PKA during amino acid-dependent mitochondrial hyperfusion.

## 4.2 Result

### 4.2.1 Assessing the role of MTORC1 in amino acid-dependent mitochondrial hyperfusion

The inhibition of MTOR via siRNA knockdown or long term pharmacological inhibition has been reported to induce mitochondrial hyperfusion (Gomes et al., 2011a, Morita et al., 2017). In the previous chapter, we demonstrated that addback of amino acids Q+L+R led to a dramatic and unexpected augmented mitochondrial hyperfusion. Since Q, L and R are critical regulatory amino acids that activate MTORC1 (Chantranupong et al., 2016, Wolfson et al., 2016, Jewell et al., 2015), this raised questions as to whether mitochondrial hyperfusion was caused by MTORC1 activation or inactivation. To first investigate MTORC1 in QLR-dependent mitochondrial hyperfusion, a pharmacological approach was used.

Torin1 is an ATP competitive potent MTOR inhibitor which actively targets both MTORC1 and MTORC2 (Thoreen et al., 2009). Here, 4T1 and U2OS cells were fully starved of all amino acids or supplemented with QLR in the presence or absence of Torin1 (0.25 $\mu$ M). Immunoblotting was first performed to assess MTORC1 activation status via phosphorylation of substrate Ulk1 at serine 757 and MTORC1-dependent phosphorylation of ribosomal protein S6 at Serine 240/244.

As expected, Torin1 effectively inhibited MTORC1, blocking both phosphorylation of Ulk1 and S6 in U2OS cells in full-nutrient untreated condition (Lanes 1 vs 2, **Fig 4.3A**). Similarly, MTORC1 was inhibited upon amino acid-starvation which was further inhibited in the presence of Torin1 (Lanes 3 and 4). As expected, QLR addback fully restored MTORC1-dependent phosphorylation of Ulk1 and S6, while Torin1 blocked this activation (Lanes 5 and 6). Similar results were observed in 4T1 cells treated with Torin1, amino acid starvation and QLR addback (**Fig 4.3B**). These findings indicated that Torin1 is a potent inhibitor of MTORC1 and that QLR are potent activators of MTORC1.

To investigate whether MTOR inhibition by Torin1 would stimulate mitochondrial hyperfusion, mitochondrial length was assessed in cells under basal full nutrient conditions in the presence and absence of Torin1. Surprisingly, Torin1 alone did not induce mitochondrial fusion (mitochondrial length did not increase relative to untreated cells) (**Fig 4.4A and 4.4B**). In contrast, amino acid-starvation induced moderate mitochondrial fusion, but further inhibition of MTOR with Torin1 did not

increase mitochondrial length further (rather a significant reduction in length) (**Fig 4.4B**). As established in Chapter 3, supplementation of Q, L and R induced extensive mitochondrial hyperfusion. However, QLR-dependent increases in mitochondrial length were significantly reduced by the presence of Torin1. These findings suggest that: 1) MTOR inhibition is not sufficient to induce mitochondrial fusion and 2) QLR-addback can still promote hyperfusion even with inhibited MTORC1. Overall, the results suggest that amino acid-dependent mitochondrial hyperfusion can be dissociated from MTOR activity.

Another approach was used to investigate the role of MTORC1 in QLR-induced mitochondrial hyperfusion. MTORC1 activation by amino acids is dependent on interaction with Rheb at the lysosome (Sancak et al., 2010, Sancak et al., 2007). The presence of serum (growth factors) is required for Rheb interaction on the lysosome. In the absence of growth factors, the TSC complex (TSC1, TBC1D7 and TSC2) inhibits Rheb, blocking its interaction with MTORC1. Upon serum availability, the TSC dependent-inhibition of Rheb is released, hence allowing Rheb interaction with MTORC1 at the lysosome and MTORC1 activation. As such, it was confirmed whether QLR-activation of MTORC1 requires serum in our cell system. As expected, withdrawal of serum fully blocked MTORC1-dependent phosphorylation of S6 in QLR supplemented cells (**Fig 4.5**).

To further investigate QLR-induced mitochondrial hyperfusion and the roles of MTORC1 activation, mitochondrial length was assessed in starved/QLR supplemented cells but in the presence or absence of serum. In 4T1-SU9 GFP cells, it was observed that mitochondria remained short and fragmented upon serum withdrawal alone (**Fig 4.6A, B**). Therefore, mild MTORC1 inhibition (serum starvation) did not promote mitochondrial fusion. Mitochondrial hyperfusion was strongly induced by amino acid starvation + QLR-addback and levels of hyperfusion were strong regardless of serum availability. However, we noted that mitochondrial elongation was significantly reduced in starved/QLR-supplemented 4T1-SU9 GFP cells where serum is depleted (**Fig 4.6B**).

Similar trends were observed in U2OS-SU9 GFP cells. QLR-addback stimulated strong mitochondrial hyperfusion in U2OS-SU9 GFP regardless of serum availability (**Fig 4.6C**) and mitochondrial length remained the same (+/-) serum in QLR-supplemented cells (**Fig 4.6D**). Taken together, these data suggest that the signalling mechanism that induces amino acid-dependent mitochondrial fusion is independent of MTORC1 activity.

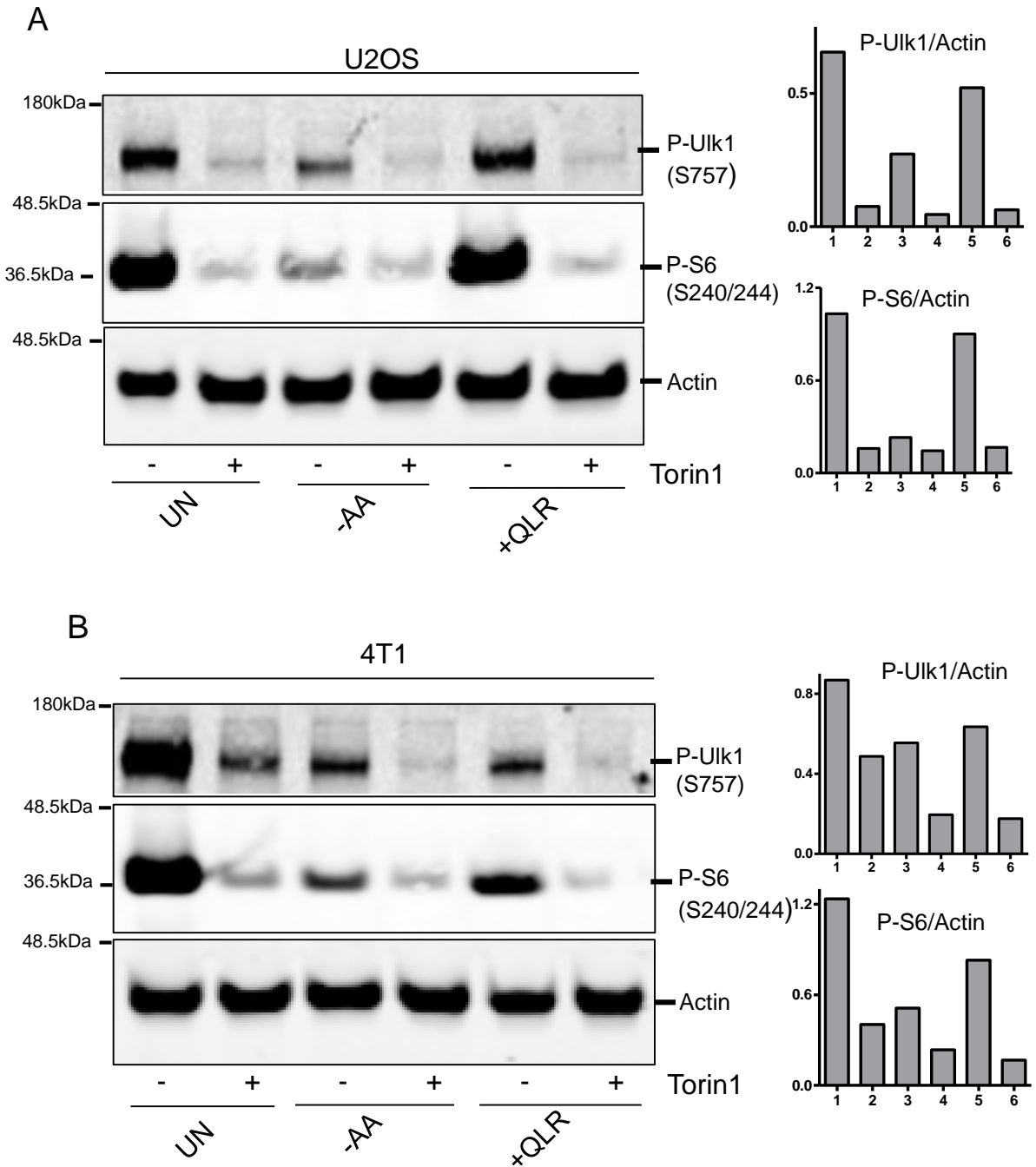


**Figure 4.3: The regulation of MTORC1 signalling by amino acid availability.**

Cells were maintained in full media (UN) or either fully starved of amino acid (-AA) or starved of amino acid but supplemented with Q, L and R (QLR) +/- MTOR inhibitor (Torin1: 0.25 $\mu$ M) for 4 hours in (A) 4T1-SU9 GFP and (B) U2OS-SU9 GFP. Starvation media conditions also contained 10% dialysed FBS. Representative of two independent experiments. Graphs show average of band density of n = 2 blots, each bar (1-6) represent each band from left to right

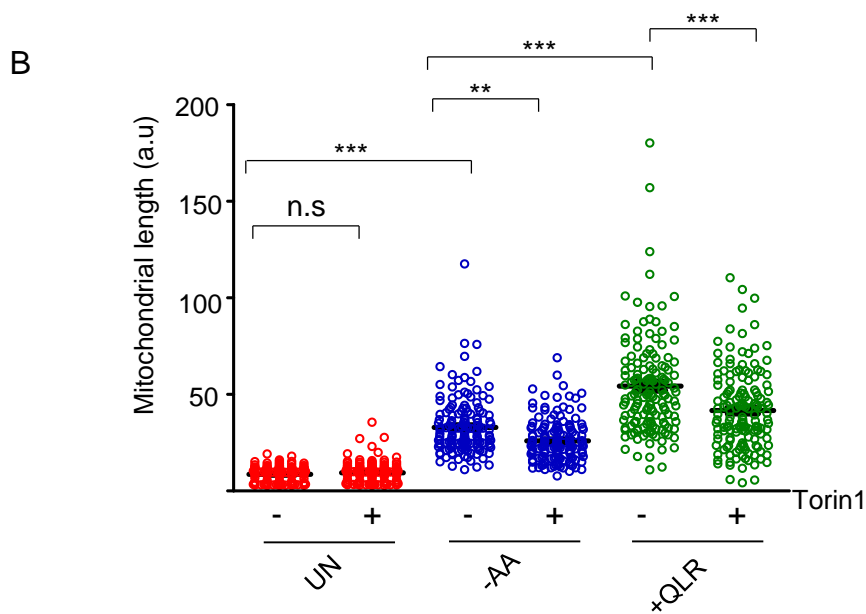
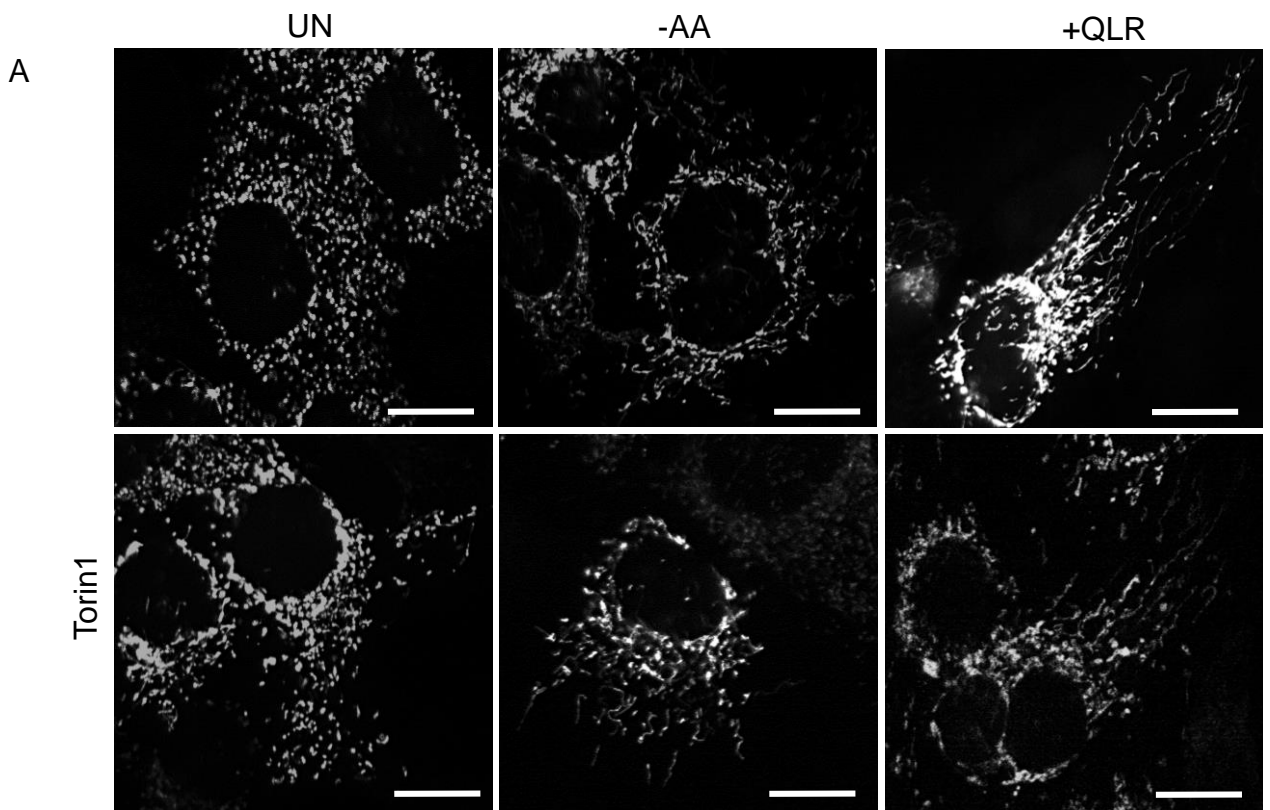


**Figure 4.4: Mitochondrial dynamics in the presence of MTORC1 inhibition.**

(A) Representative epifluorescent-microscope images of 4T1-SU9 GFP cells maintained in full media (UN) or either fully starved of amino acid (-AA) or starved of amino acid but supplemented with Q, L and R (QLR) +/- Torin1 (0.25 $\mu$ M) for 4 hours. Starvation media conditions also contained 10% dialysed FBS.

(B) Each dot represents the mean length of 10 mitochondria within a cell. Each treatment shows 150 cells quantified from 3 independent experiments. \*\*\* indicate  $P < 0.001$ , \*\*  $p < 0.01$ , n.s: non-significant, analysed with one way ANOVA with Bonferroni post test. Scale: 17 $\mu$ M

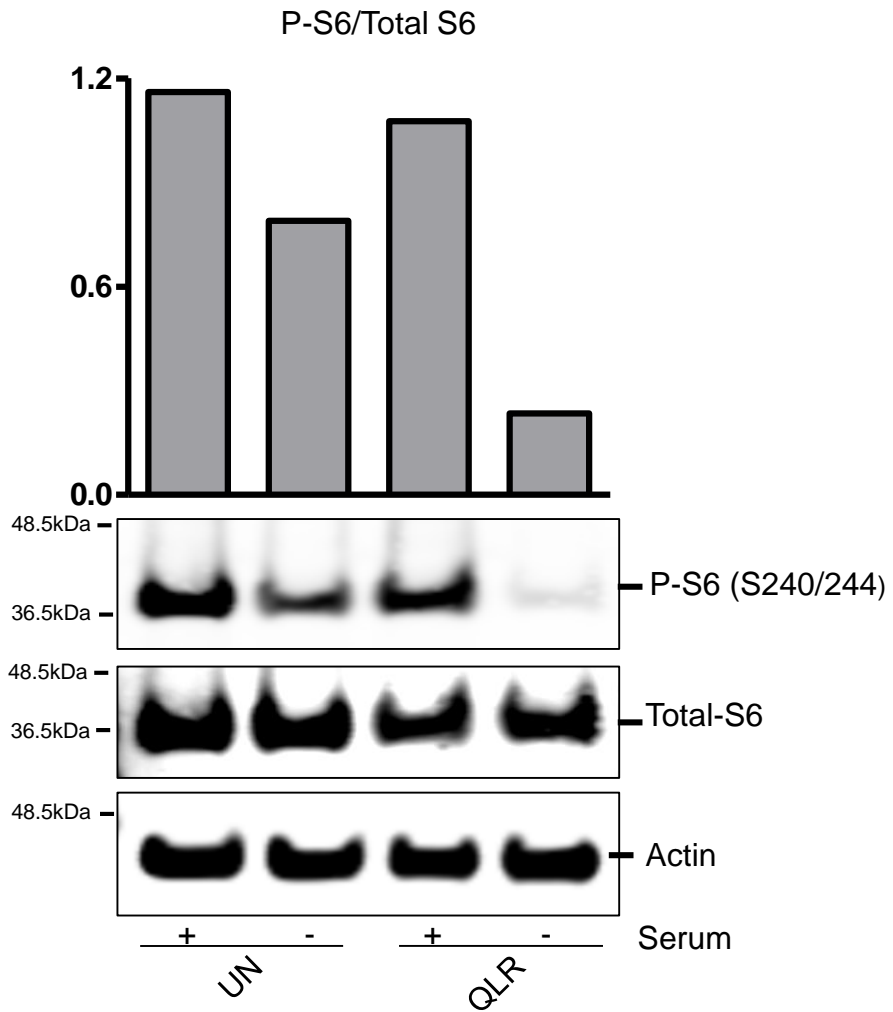


**Figure 4.5: Serum-dependent activation of MTORC1 signalling.** 4T1-SU9 GFP cells were maintained in full media (UN) or amino acid starvation media supplemented with Q, L and R (QLR) +/- dialysed FBS for 4 hours. Immunoblot representative of two independent experiments showing serum-dependent phosphorylation of S6, with actin as a loading control. Graphs show average of band density of n = 2 blots.

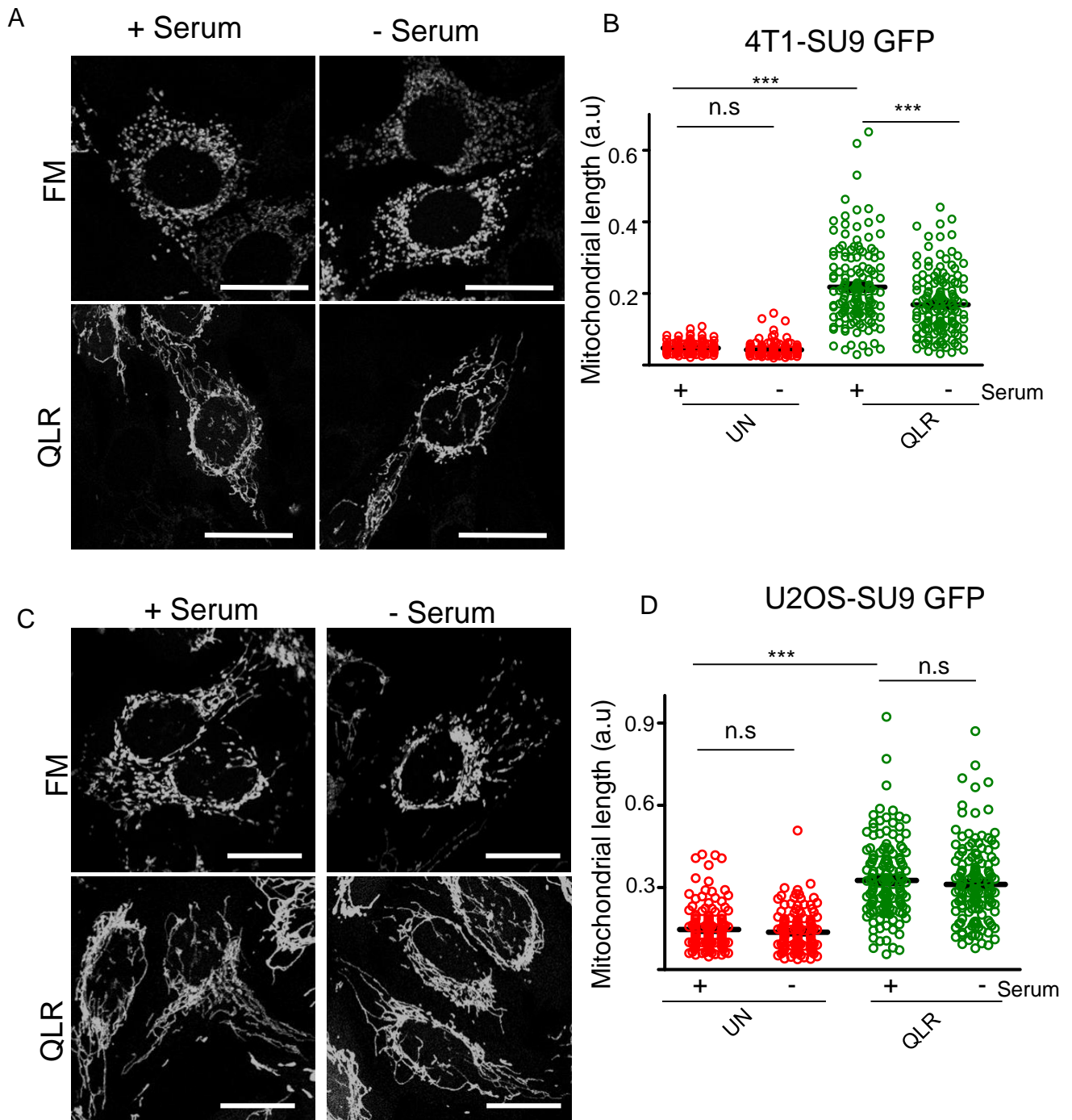


**Figure 4.6: Minimal effect of serum on amino acid-dependent mitochondrial hyperfusion.** (A) Representative images of 4T1-SU9 GFP cells treated with full media (FM), or amino acid starvation media supplemented with Q, L and R (QLR) +/- dialysed FBS. Mitochondrial length was measured in (B) 4T1-SU9 GFP, each dot represents the mean length of 10 mitochondria within a cell. (C) Representative images of U2OS-SU9 as treated in A. (D) U2OS-SU9 GFP, each dot represents the mean length of 10 Mitochondria within a cell. Each treatment shows 150 cells quantified from 3 independent experiment. \*\*\* indicate  $P < 0.001$ , n.s (non-significant), analysed with one way ANOVA with Bonferroni post test. Scale: 25 $\mu$ M

## 4.2.2 AMPK is a regulator of mitochondrial dynamics

AMPK is a master signalling sensor of cellular energy and it is also activated during mitochondrial damage (Kahn et al., 2005). AMPK phosphorylates Ulk1, which has been shown to be critical for the progression of mitophagy following mitochondrial damage (Egan et al., 2011, Kim et al., 2011b). During mitochondrial metabolic stress, AMPK also regulates mitochondrial dynamics by phosphorylating mitochondrial fission factor (Mff) at S155 and S172 leading to the recruitment of Drp1 to mitochondrial surface to induce fragmentation (Toyama et al., 2016).

Due to the emerging roles of AMPK in mitochondrial remodelling, it was investigated whether AMPK is required for amino acid-dependent mitochondrial hyperfusion. Matched wildtype and AMPK  $\alpha 1/\alpha 2$  double knockout (DKO) MEF (Laderoute et al., 2006) were starved of amino acids or supplemented with QLR. Cells were fixed and stained for TOM20. Subsequently, mitochondrial length was quantified. It was observed that amino acid starvation did not significantly increase mitochondrial length in both wildtype and AMPK DKO relative to untreated cells (**Fig 4.7A, B**). However, the level of mitochondrial fusion observed in untreated and amino acid starved AMPK DKO cells were significantly lower relative to corresponding wildtype. While QLR supplementation into amino acid starvation media led to strong mitochondrial hyperfusion in wildtype cells and AMPK DKO cells, this response was significantly impaired in AMPK DKO MEF (**Fig 4.7B**). Western blot confirmed that AMPK $\alpha$  forms were deleted in AMPK  $\alpha 1/\alpha 2$  DKO MEF (**Fig 4.7C**). Therefore, data suggest that AMPK plays a role in the regulation of mitochondrial dynamics. Mitochondria are overall more fragmented in the absence of AMPK signalling. However, the QLR-induced hyperfusion response remains partially active in the absence of AMPK function.

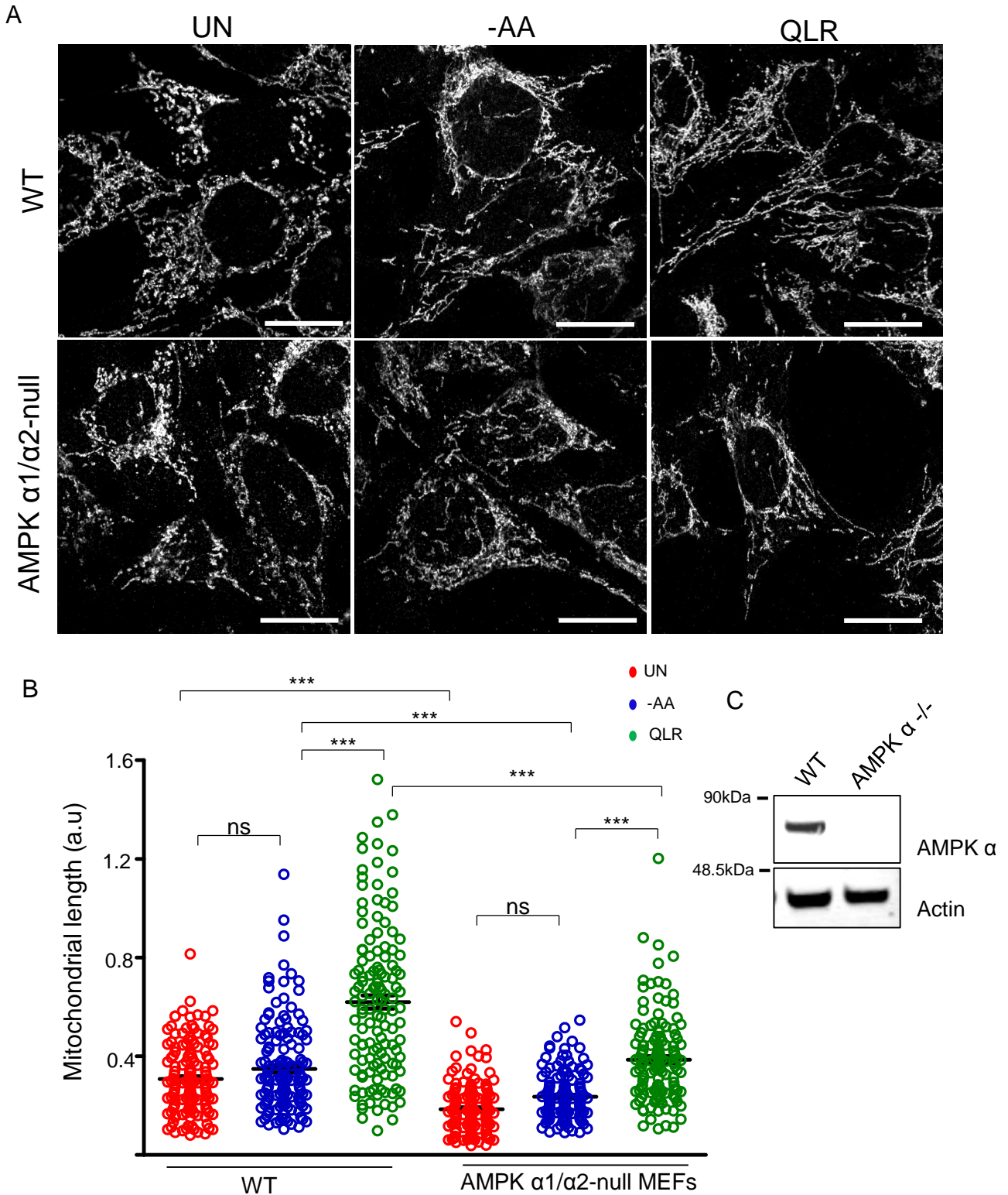


**Figure 4.7: Role of AMPK in amino acid-dependent mitochondrial hyperfusion.**

(A) Representative images of wildtype MEF and AMPK  $\alpha 1/\alpha 2$  null MEF maintained in full media (Un), or either fully starved of amino acid (-AA) or starved of amino acid but supplemented with Q, L and R (QLR) for 4h. Starvation media conditions also contained 10% dialysed FBS.

(B) Mitochondrial length was measured in wildtype and AMPK  $\alpha 1/\alpha 2$  null MEF, each dot represents the mean length of 10 mitochondria within a cell. Each treatment shows between 130-150 cells quantified from 3 independent experiment. \*\*\* indicate  $P < 0.001$ , \*\*  $P < 0.01$ , ns (non significant) analysed with one way ANOVA with Bonferroni post test

(C) Western blot confirming the absence of AMPK $\alpha$  in AMPK  $\alpha 1/\alpha 2$  null MEFs by using anti AMPK $\alpha$ . Scale: 25 $\mu$ M

### 4.2.3 The Ulk1-complex is a regulator of amino acid-dependent mitochondrial hyperfusion

The Ulk1 complex, which forms along with subunits Atg13, FIP200 and Atg101, has been shown to regulate mitochondrial remodelling during hypoxia (Wu et al., 2014, Wu et al., 2016b). Ulk1 has been more extensively demonstrated to serve critical roles in the activation of downstream autophagy-related proteins via direct phosphorylation of Atg13 and Beclin1 (Russell et al., 2013). Atg13 and FIP200 are important for Ulk1 localization to early autophagosomes during autophagy (Ganley et al., 2009, Jung et al., 2009, Hosokawa et al., 2009a, Hara et al., 2008). This translocation event is followed by p62/SQSTM1 accumulation, which forms a bridge between ubiquitinated protein targets and LC3B on the autophagosome membrane (Pankiv et al., 2007, Bjorkoy et al., 2005). During this autophagosome formation process, p62/SQSTM1 and LC3B form punctate structures which can be quantified to assess the extent of autophagy activation (Yoshii and Mizushima, 2017). While Ulk1 and Atg13 have been previously shown to regulate mitochondria biology, their role in mitochondrial hyperfusion during amino acid starvation remained unclear.

#### 4.2.3.1 Atg13 and FIP200 are required for amino acid-dependent mitochondrial hyperfusion

It was next tested whether the Ulk1 complex is required for amino acid-dependent mitochondrial hyperfusion. To study the Ulk1 complex, we first targeted essential subunits of the complex (e.g. Atg13). Firstly, amino acid-dependent mitochondrial fusion was studied in 4T1 clones (13.2.1 and 13.1.1b) in which Atg13 has been targeted with the CRISPR-Cas9 system. These Atg13 CRISPR cells were tested for autophagy by assessing p62 and LC3B puncta to confirm that they were unable to undergo autophagy during amino acid starvation.

A basal level of p62 puncta was observed in untreated wildtype 4T1 cells (**Fig 4.8A**). Upon amino acid starvation for 2-hours, p62 puncta accumulated in 4T1 wildtype which was blocked in the presence of Q, L and R. It was observed that the amino acid-dependent increase in p62 puncta was inhibited in CRISPR Atg13 cells although basal p62 puncta were maintained. Upon quantification, p62 spots accumulated in amino acid-starved 4T1 wildtype cells by at least 3-fold relative to untreated cells but this response was abrogated upon QLR-addback (**Fig 4.8B**). Interestingly, amino acid starvation did not stimulate an increase in p62 puncta in CRISPR Atg13 cells relative

to amino acid starved wildtype cells. In fact, there were no differences in the levels of p62 puncta between untreated, amino acid starved, and QLR supplemented CRISPR Atg13 cells. Also, western blot confirmed that Atg13 was targeted in the CRISPR Atg13 4T1 cells (**Fig 4.8C**).

Similar to the p62 puncta formation results, LC3B-positive puncta accumulated following amino acid starvation in 4T1 wildtype cells, which was suppressed when Q, L and R were supplemented into the amino acid starvation medium (**Fig 4.9A**). After amino acid starvation, LC3B spots accumulated in 4T1 wildtype cells by approximately 3-fold relative to untreated cells (**Fig 4.9B**). In contrast, LC3B puncta accumulation is inhibited following amino acid starvation in CRISPR Atg13 cells. These data confirm that CRISPR Atg13 cells were unable to undergo autophagy following amino acid starvation. In addition, the addback of Q, L and R is sufficient to reverse the normal amino acid starvation-induced autophagy response.

Mitochondrial hyperfusion following Q, L and R addback in autophagy-deficient CRISPR Atg13 cells was next examined. Cells were starved or supplemented with QLR for 4-hours, and stained for outer mitochondrial membrane protein TOM20.

In 4T1 wildtype cells, amino acid starvation led to a moderate mitochondrial fusion (as compared with untreated controls), while supplementation with Q, L and R stimulated mitochondrial hyperfusion, as observed previously (**Fig 4.10A**). In contrast, mitochondrial fusion was totally blocked in CRISPR Atg13 cells, both following amino acid starvation and QLR supplementation conditions. In quantitation, with 4T1 wildtype cells, addback of Q, L and R led to an increase in mitochondrial length by at least 2-fold relative to full amino starved cells, consistent with other experiments (**Fig 4.10B**). In contrast, Q, L and R addback did not induce any increase in mitochondria length in CRISPR Atg13 4T1 cells. Mitochondrial fusion was blocked by at least 4-fold in Q, L and R supplemented Atg13 CRISPR cells relative to Q, L and R supplemented wildtype cells. This suggests that Atg13 function is required for Q, L and R-induced mitochondrial hyperfusion.

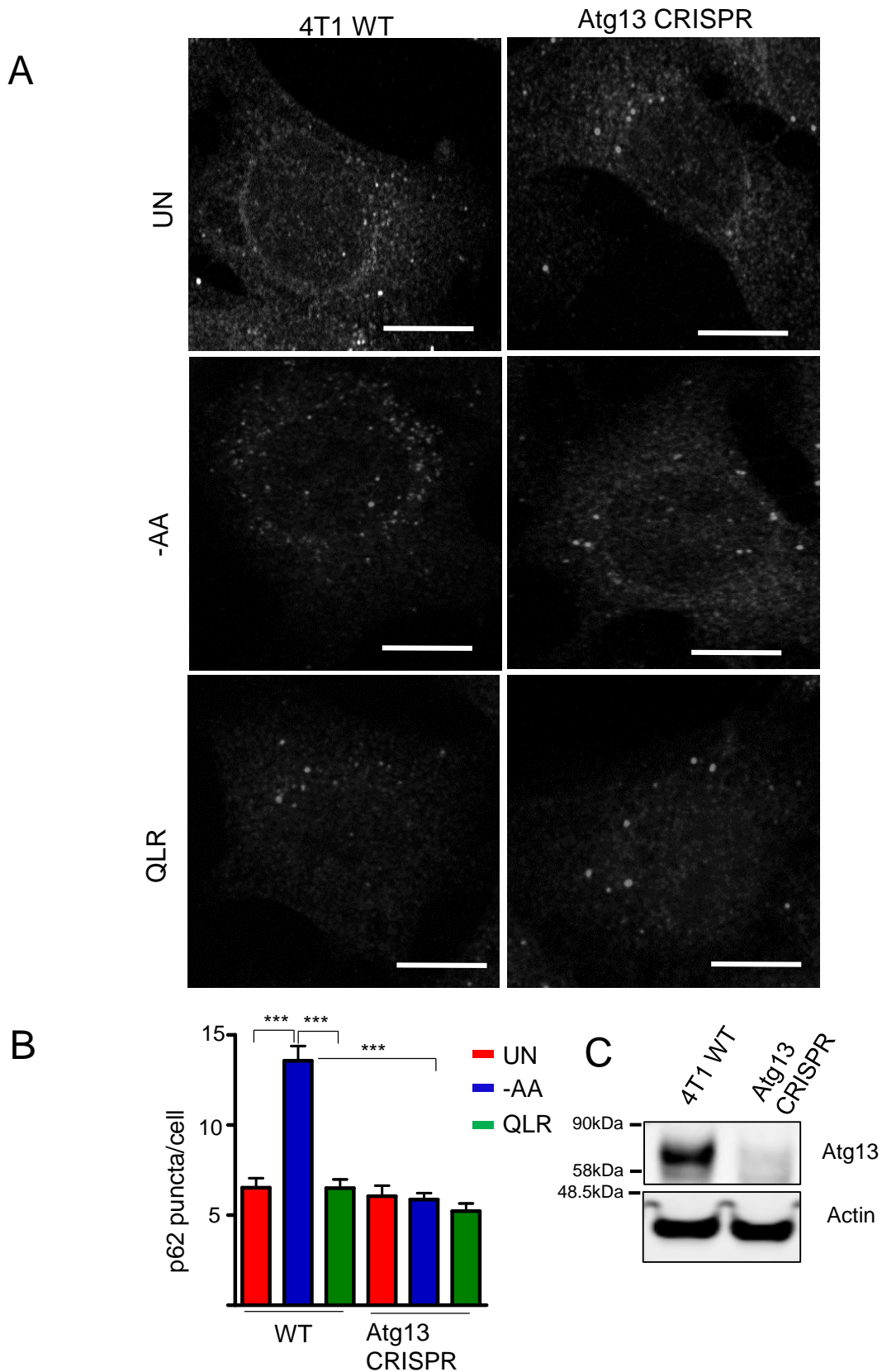


**Figure 4.8: p62/SQSTM1 puncta formation is inhibited in Atg13 CRISPR 4T1 cells.**

(A) Representative images of 4T1 WT and CRISPR Atg13 (13.1.1b) cells maintained in full media (UN), starved of either all amino acids (-AA) or starved of amino acids but supplemented with QLR for 2h. Starvation media conditions also contained 10% dialysed FBS. Cells were fixed and stained for p62. Starvation media conditions also contained 10% dialysed FBS.

(B) Each bar represents the mean p62 puncta/cell for N=90 cells from 3 independent experiment (30 cells per experiment). \*\*\* indicate  $P < 0.001$  analysed with one way ANOVA with Bonferroni post test.

(C) Western blot confirming targeting in CRISPR Atg13 4T1 cells. Scale: 10µm

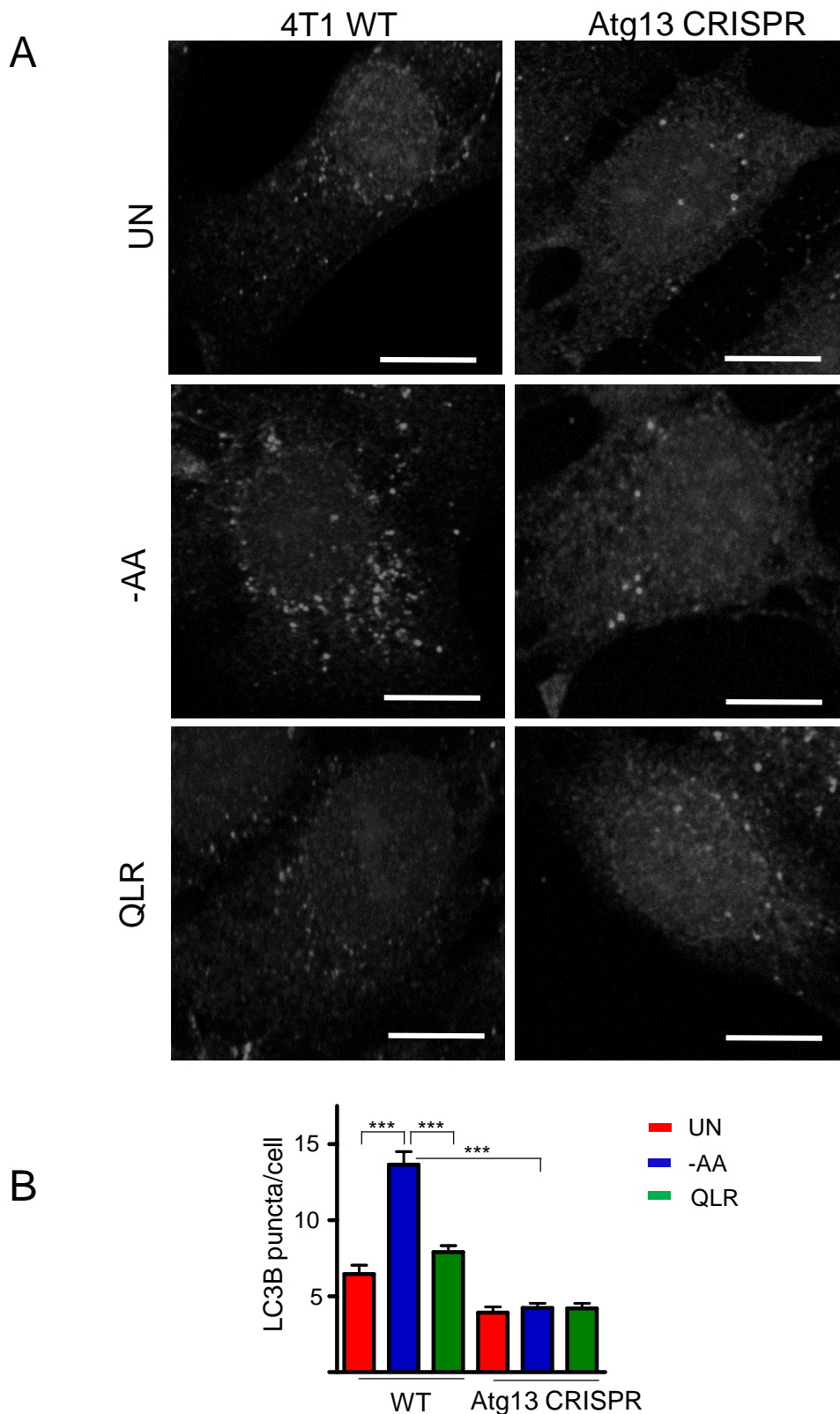


**Figure 4.9: LC3B puncta formation is inhibited in Atg13 CRISPR 4T1 cells.**

(A) Representative images of 4T1 WT and CRISPR Atg13 cells maintained in full media (UN), starved of either all amino acids (-AA) or starved of amino acids but supplemented with QLR for 2h. Starvation media conditions also contained 10% dialysed FBS. Cells were fixed and stained for LC3B.

(B) Each bar represent mean quantification of LC3B puncta/cell from 90 cells from 3 independent experiment (30 cells per experiment). \*\*\* indicate  $P < 0.001$  analysed with one way ANOVA with Bonferroni post test. Scale: 10 $\mu$ m

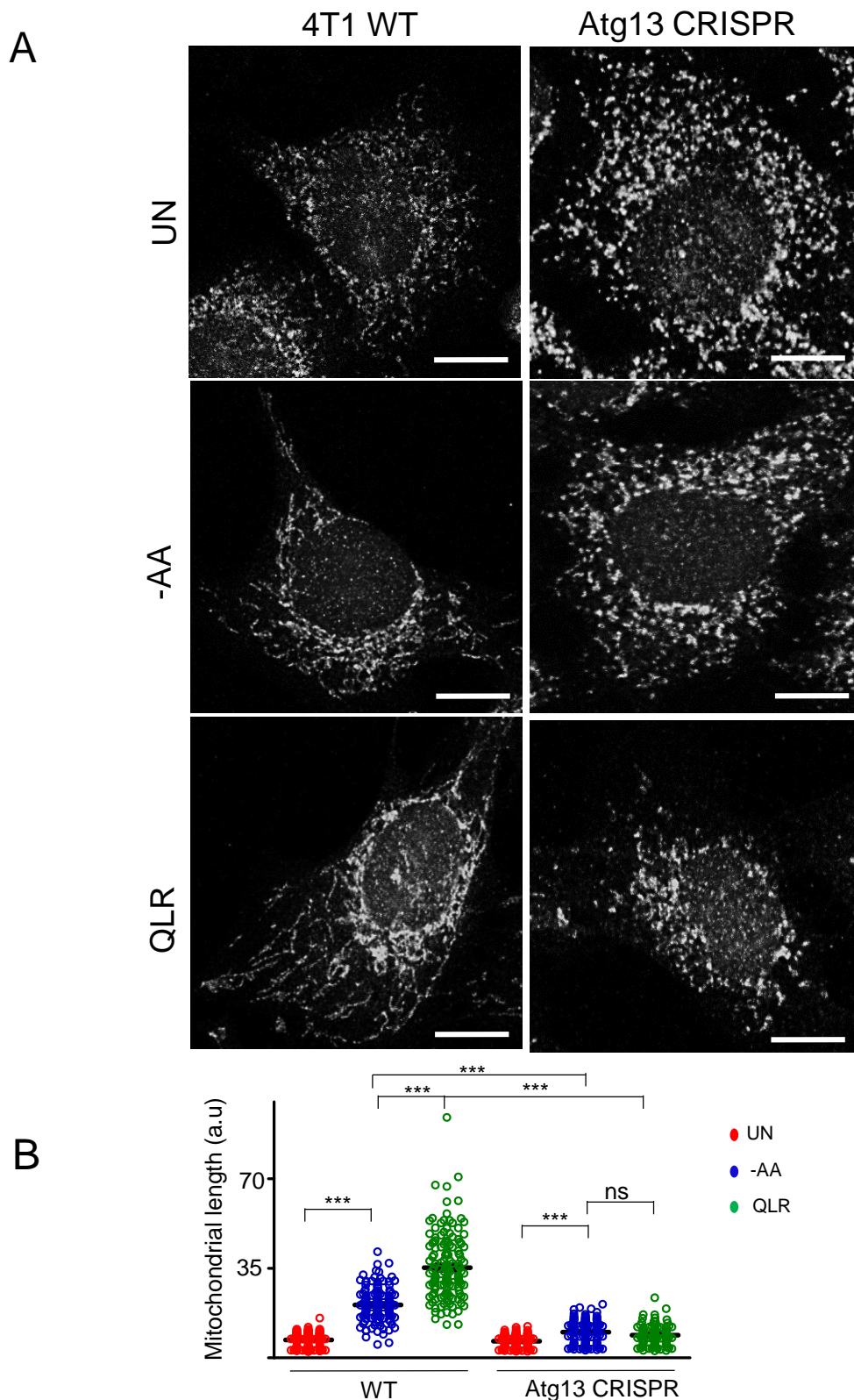


**Figure 4.10: Mitochondrial hyperfusion is inhibited in Atg13 CRISPR 4T1 cells.**

(A) Representative images of 4T1 WT and CRISPR Atg13 cells maintained in full media (UN), starved of either all amino acids (-AA) or starved of amino acid but supplemented with QLR for 4h. Starvation media conditions also contained 10% dialysed FBS. Cells were fixed and stained for outer mitochondrial outer membrane TOM20. (B) Each dot represent the mean length of 10 mitochondria within a cell. Each treatment shows 150 cells quantified from 3 independent experiment. \*\*\* indicate  $P < 0.001$ , \*\*  $P < 0.01$ , analysed with one way ANOVA with Bonferroni post test. Scale:  $10\mu\text{m}$

FIP200 is another essential functional component of the Ulk1/2 complex. It has been reported that disruption of members of the complex, including FIP200, affects the overall stability and functionality of the Ulk1 complex (Ganley et al., 2009, Hara et al., 2008). By exploring KO MEF, it was investigated whether FIP200 is required for amino acid-dependent mitochondrial fusion.

In wildtype MEF, amino acid starvation did not greatly induce mitochondrial fusion relative to untreated controls, while supplementation with Q, L and R stimulated mitochondrial hyperfusion, as shown previously (**Fig 4.11A**). In contrast, mitochondrial fusion was not observed after both amino acid starvation and QLR supplementation conditions in FIP200 KO MEF. Upon quantification, mitochondrial length in amino acid starved wildtype cells were similar to untreated wildtype cells (**Fig 4.11B**). In contrast, Q, L and R addback stimulated mitochondrial hyperfusion by at least 3-fold in wildtype MEF relative to cells maintained in full media or starved of all amino acid. However, Q, L and R addback did not induce any significant increase in mitochondria length in FIP200 KO cells. Mitochondria length is overall significantly reduced in FIP200 KO cells.

Taken together, loss of function in either Atg13 or FIP200 showed striking inhibition of QLR-dependent mitochondrial hyperfusion thereby suggesting that the Ulk1 complex is required for this amino acid sensing mechanism.

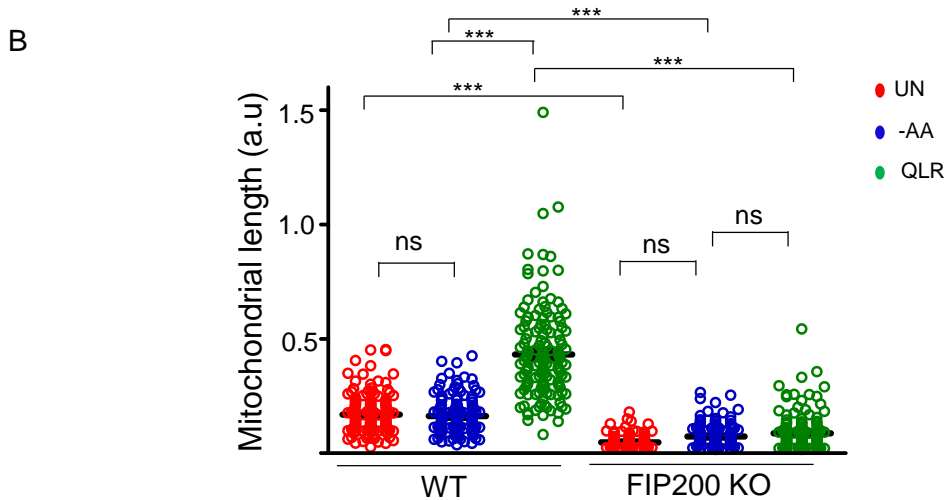
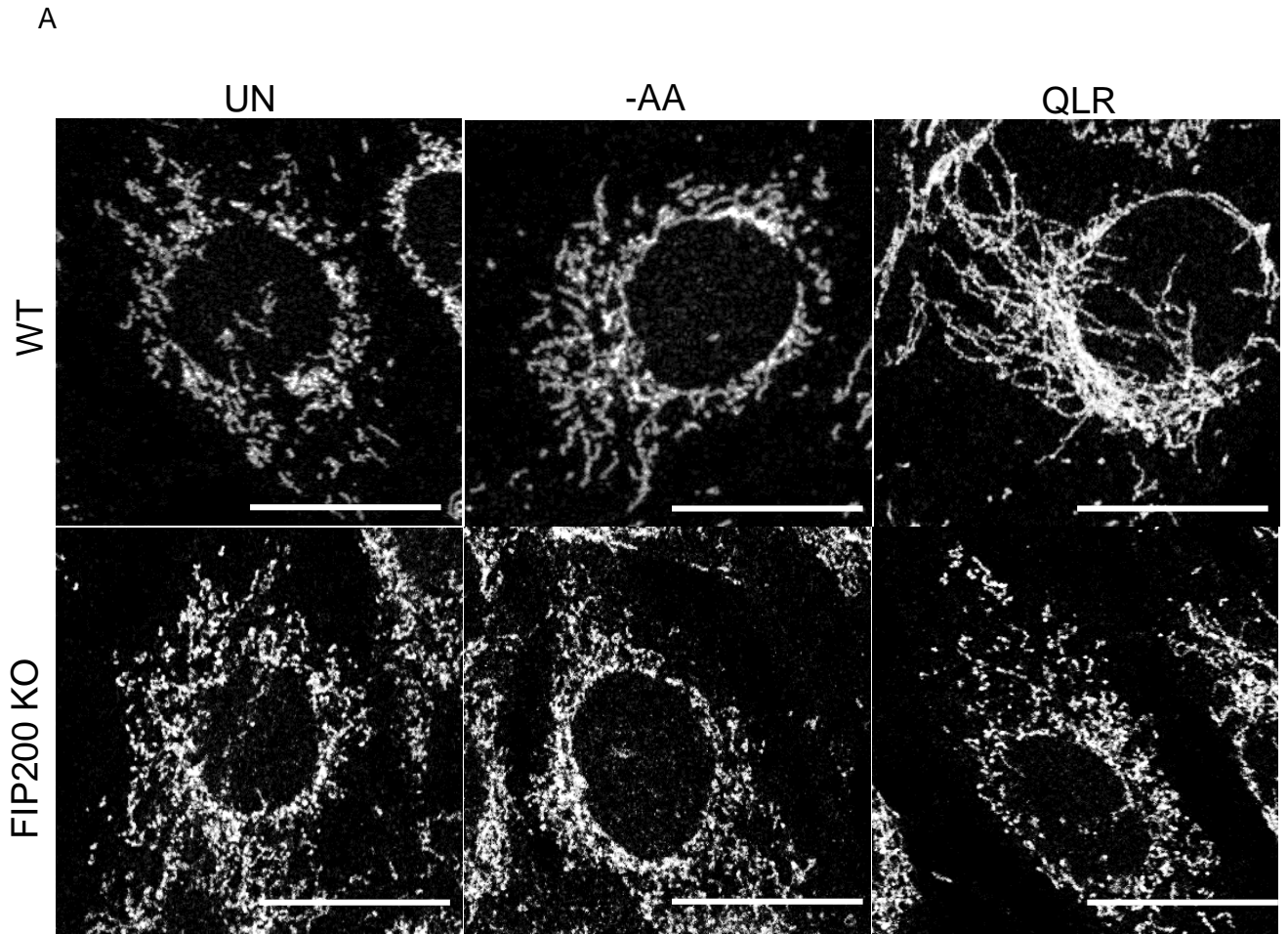


**Figure 4.11: Mitochondrial hyperfusion is inhibited in FIP200 knockout MEF.**

(A) Representative images of WT and FIP200 KO MEF maintained in full media (FM) or starved of either all amino acids (-AA) or starved of amino acid but supplemented with QLR for 4h. Starvation media conditions also contained 10% dialysed FBS. Cells were fixed and stained for outer mitochondria membrane (TOM20).

(B) Each dot represents mean length of 10 mitochondria within a cell. Each treatment shows 150 cells quantified from 3 independent experiments. \*\*\*  $P < 0.001$  analysed with one way ANOVA with Bonferroni post test. Scale: 25 $\mu$ m

### 4.2.3.2 Ulk1 is required for QLR-dependent mitochondrial hyperfusion

To further study the Ulk1 complex, amino acid-dependent mitochondrial fusion was investigated in 4T1 CRISPR Ulk1 cells. 4T1 CRISPR Ulk1 were previously generated in the lab by using CRISPR-Cas9 guide constructs targeting Ulk1. Multiple puromycin-resistant 4T1 clones were isolated (1.1.2, 1.4.1, 1.3.4 and 1.1.4). Western blot indicated that 4T1 CRISPR Ulk1 clone 1.3.4 had the most efficient targeting, hence further experiment was carried out using these (**Fig 4.12A**). To confirm that CRISPR Ulk1 4T1 cells had blocked autophagy due to loss of Ulk1, cells were starved of amino acids and p62 and LC3B puncta were assessed. Similar to CRISPR Atg13 cells, p62 and LC3B puncta accumulation was inhibited in starved CRISPR Ulk1 cells relative to starved wildtype cells (**Fig 4.12B, C**). Levels of autophagy inhibition due to Ulk1 targeting were significant, although some response was still observed in CRISPR Ulk1 cells, possibly due to residual Ulk1 (or Ulk2 function). As expected, QLR addback also blocked autophagy as observed via suppression of p62 and LC3B puncta accumulation (**Fig 4.12B, C**).

Following this confirmation, 4T1 CRISPR Ulk1 cells were next starved of amino acids or tested with QLR supplementation, and mitochondrial length was assessed. Interestingly, full amino acid starvation-dependent mitochondrial fusion was overall observed in both 4T1 wildtype cells and 4T1 CRISPR Ulk1 cells (**Fig 4.12D**).

In CRISPR Ulk1 cells, amino acid-starved-induced mitochondrial fusion was observed, but levels were significantly inhibited relative to amino acid starved wildtype (**Fig 4.12D**). In CRISPR Ulk1 cells, QLR-addback led to mild (insignificant) increase in mitochondrial length relative to cells starved of all amino acids. However, mitochondrial hyperfusion observed from QLR-addback in CRISPR Ulk1 cells was significantly lower relative to wildtype cells treated with QLR-addback. These results further suggest that the Ulk1 complex is required for the maximal mitochondrial fusion responses to amino acid starvation or QLR-supplementation. However, the observation of partial amino acid-dependent mitochondrial fusion in Ulk1 CRISPR cells (in contrast to CRISPR Atg13 and FIP200 KO cells) suggested that the Ulk1 complex was still partially functional due to residual Ulk1 or functional Ulk2.

Following these observations suggesting roles of the Ulk1 complex, pharmacological inhibitors of Ulk1 were used. Here, we tested reported Ulk1 kinase inhibitors

(e.g. MRT68921 from Petherick et al. (2015), SBI-0206965 from Egan et al. (2015)) that had been successfully used in our laboratory (Nwadike et al., 2018, Radhi et al., 2019). In addition, we tested several other unpublished candidate Ulk1 inhibitors (MRT239016 and MRT238993) obtained via collaboration from Medical Research Council Technology/Life Arc. MRT239016 and MRT238993 analogues were made with objective of minimising off-target effects. These two analogues have been demonstrated in our lab to inhibit Ulk1/2 kinase catalytic activity by reducing the phosphorylation of Atg13 at Ser 318, albeit without blocking amino acid starvation-induced autophagy (Chan, Radhi and Nwadike unpublished data).

Here, MRT68921 effectively blocked QLR-addback dependent mitochondrial hyperfusion at 10 $\mu$ M (**Fig 4.13A**). Upon quantification, MRT68921 treatment led to a reduction in mitochondrial length in both amino acid starvation-induced fusion and QLR-stimulated hyperfusion (**Fig 4.13B**). To further explore this promising effect, we tested dose responses at 1 $\mu$ M, 5 $\mu$ M and 10 $\mu$ M in cells treated with QLR-supplemented amino acid starvation media. The inhibition of QLR-induced mitochondrial hyperfusion with MRT68921 was dose-dependent, with 10 $\mu$ M having a greater inhibitory effect relative to 5 $\mu$ M and 1 $\mu$ M (**Fig 4.13C**). However, MRT68921 at 1 $\mu$ M sufficiently inhibited mitochondrial fusion by about 2-fold relative to QLR-supplemented cells. As we tested different Ulk1 inhibitors, surprisingly, only MRT68921 and MRT239016 inhibited QLR-induced mitochondrial hyperfusion while MRT238993 and SBI-0206965 did not have any effect. Although SBI-0206965 has been shown to block autophagy, inhibition of autophagy was weaker relative to MRT68921 (Radhi et al., 2019). Taken together, these findings suggest that MRT238993 and SBI-0206965 have a lower in vitro potency relative to MRT239016 and MRT68921.

To address this discrepancy, Ulk1/2 DKO MEF (McAlpine et al., 2013) were used to further clarify. Firstly, it was confirmed that Ulk1/ DKO MEF were unable to induce autophagy after amino acid starvation. Wildtype and Ulk1/2 DKO MEF were starved of amino acids for 1.5-hours and stained for LC3B puncta. It was observed that LC3B spots accumulated following amino acid starvation in wildtype MEF (**Fig 4.14A**). In contrast, in Ulk1/2 DKO, LC3B accumulation was inhibited following starvation. In wildtype MEF, LC3B spots increased by 3-fold upon amino acid starvation relative to cells maintained in full media but this response was inhibited 3-fold in starved Ulk1/2 DKO MEF (**Fig 4.14B**). This result confirms that Ulk1/2 DKO MEF are robustly targeted for autophagy.

Subsequently, mitochondrial hyperfusion following Q, L and R addback was assessed in wildtype MEF and two different lines of Ulk1/2 DKO MEF (4SVN and 5SVN, isolated from independent embryos) (McAlpine et al., 2013). It was observed that wildtype cells maintained in either full media or starved of amino acid have a mixture of short and intermediate mitochondria length (**Fig 4.15A, B**). However, as expected, the addback of Q+L+R (to starvation medium) stimulated extended mitochondrial hyperfusion in wildtype MEF. Surprisingly, Ulk1/2 DKO (5SVN) showed hyperfused mitochondria in full nutrient media relative to wildtype cells (**Fig 4.15B**). There was no further increase in mitochondrial length upon full amino acid starvation. Indeed, amino acid starvation tended to shift towards smaller mitochondrial sizes. Furthermore, Ulk1/2 DKO (5SVN) did not show similar patterns of hyperfusion upon QLR-addback.

Similar overall quantitation results were observed in the independent Ulk1/2 DKO cell line 4SVN (**Fig 4.15C**). In 4SVN, amino acid starvation or QLR supplementation did not lead to increases in mitochondrial length relative to untreated 4SVN cells. However, mitochondrial hyperfusion length was significantly reduced in QLR-supplemented Ulk1/2 DKO 4SVN cells relative to QLR-supplemented wildtype MEF. This data suggest that roles of Ulk1/2 in mitochondrial dynamics are complex since DKO of Ulk1/2 resulted in mitochondrial fusion, but led to amino acid starvation-induced mitochondrial fragmentation. However, these findings altogether suggest that Ulk1/2 are required for QLR-induced mitochondrial hyperfusion.

To clarify further the mitochondrial fusion patterns observed in **Fig 4.15C**, Ulk1 was reconstituted into Ulk1/2 DKO MEF (4SVN) and then investigated whether amino acid-dependent mitochondrial hyperfusion responses could be rescued. Interestingly, Ulk1 reconstitution blocked mitochondrial hyperfusion in untreated Ulk DKO cells (**Fig 4.16A, B**). Also, Ulk1 reconstitution blocked the significant amino acid starvation-induced mitochondrial fission observed in Ulk DKO cells. Ulk1 reconstitution did not stimulate mitochondrial hyperfusion upon amino acid starvation (this is consistent with previous result that wildtype MEF does not fuse in response to amino acid starvation). Indeed, Ulk1 reconstitution rescued QLR-addback dependent mitochondrial hyperfusion. Mitochondrial length increased by ~2-fold in QLR-supplemented (amino acid starvation) Ulk1 reconstituted cells (**Fig 4.16B**). Western blot confirmed that Ulk1 was successfully reconstituted into Ulk1/2 DKO (**Fig 4.16C**). Taken together, the findings from CRISPR Ulk1, Ulk1 inhibitors, and Ulk1/2 DKO rescue experiments suggest that the Ulk1 complex is required for QLR-induced mitochondrial hyperfusion.

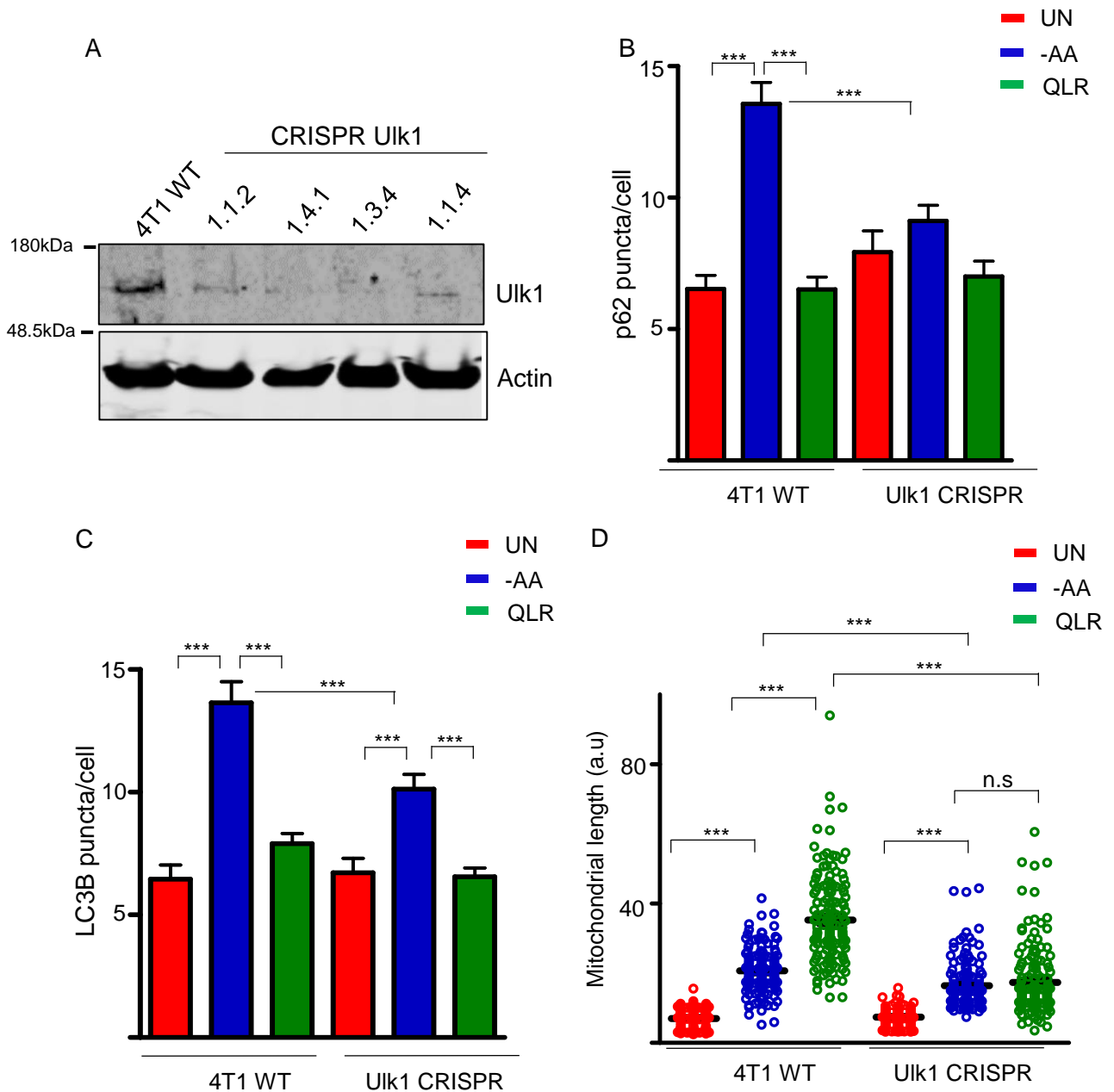


**Figure 4.12: The effect of CRISPR Uik1 targeting on amino acid-dependent mitochondrial hyperfusion.** (A) Western blot confirming levels of targeting in 4T1 Uik1-CRISPR clones. Clone 1.3.4 was selected and tested for autophagy.

(B) 4T1 wildtype and 4T1 Uik1 CRISPR cells were maintained in full media (UN), starved of either all amino acids (-AA) or starved of amino acid but supplemented with QLR. Starvation media conditions also contained 10% dialysed FBS. Each bar represents the mean p62 puncta/cell for 90 cells from 3 independent experiment (30 cells per experiment) for 2h.

(C) Each bar represent the mean quantification of LC3B puncta/cell from 90 cells from 3 independent experiment (30 cells per experiment) as treated in B for 2h. Starvation media conditions also contained 10% dialysed FBS.

(D) Mitochondrial length was measured after staining for outer mitochondria membrane, TOM20 after treatment as B for 4hours. Each dot represent the mean length of 10 mitochondria within a cell. Each treatment shows 150 cells quantified from 3 independent experiment. \*\*\* indicate  $P < 0.001$ , \*\*  $P < 0.01$ , n.s non significant, analysed with one way ANOVA with Bonferroni post test. Note: 4.12 B, C and D WT treatments are the same for Fig 4.8B, Fig 4.9B and Fig 4.10B respectively as they are parallel experiments.

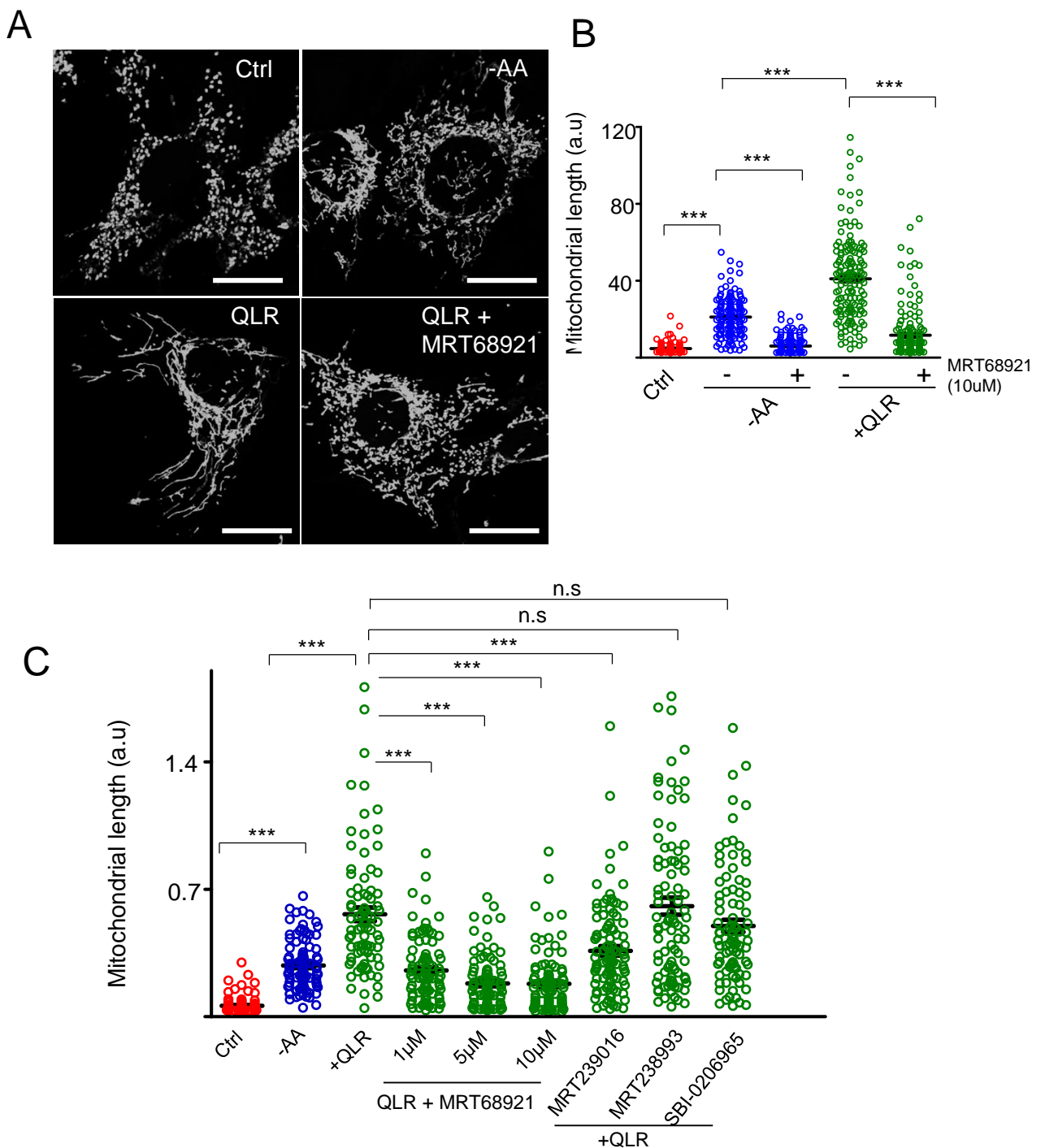


**Figure 4.13: Pharmacological inhibition of Ulk1 blocks mitochondrial hyperfusion.** (A) Representative images of 4T1-SU9 GFP maintained in full media (UN) or either fully starved of amino acids (-AA) or starved of amino acid but supplemented with QLR. Where indicated, starvation conditions were supplemented with Ulk1 inhibitor MRT68921 (10μM). Starvation media conditions also contained 10% dialysed FBS. (B) Mitochondrial hyperfusion was assessed after inhibiting Ulk1 with MRT68921 (10μM). Each dot represents the mean length of 10 mitochondria within a cell. Each treatment shows 150 cells quantified from 3 independent experiment (C) Mitochondrial hyperfusion was assessed after inhibiting Ulk1 with varying doses of MRT68921 and varying Ulk1 inhibitors (all at 10μM) (Each treatment shows 80-100 cells quantified from representative of 2-4 independent experiments.\*\*\* indicate  $P < 0.001$ , n.s (non-significant) with one way ANOVA with Bonferroni post test. Scale : 25μM

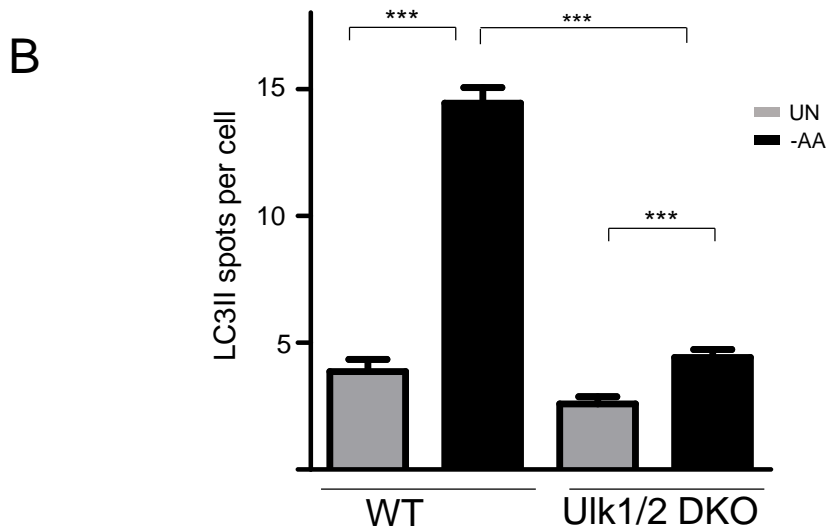
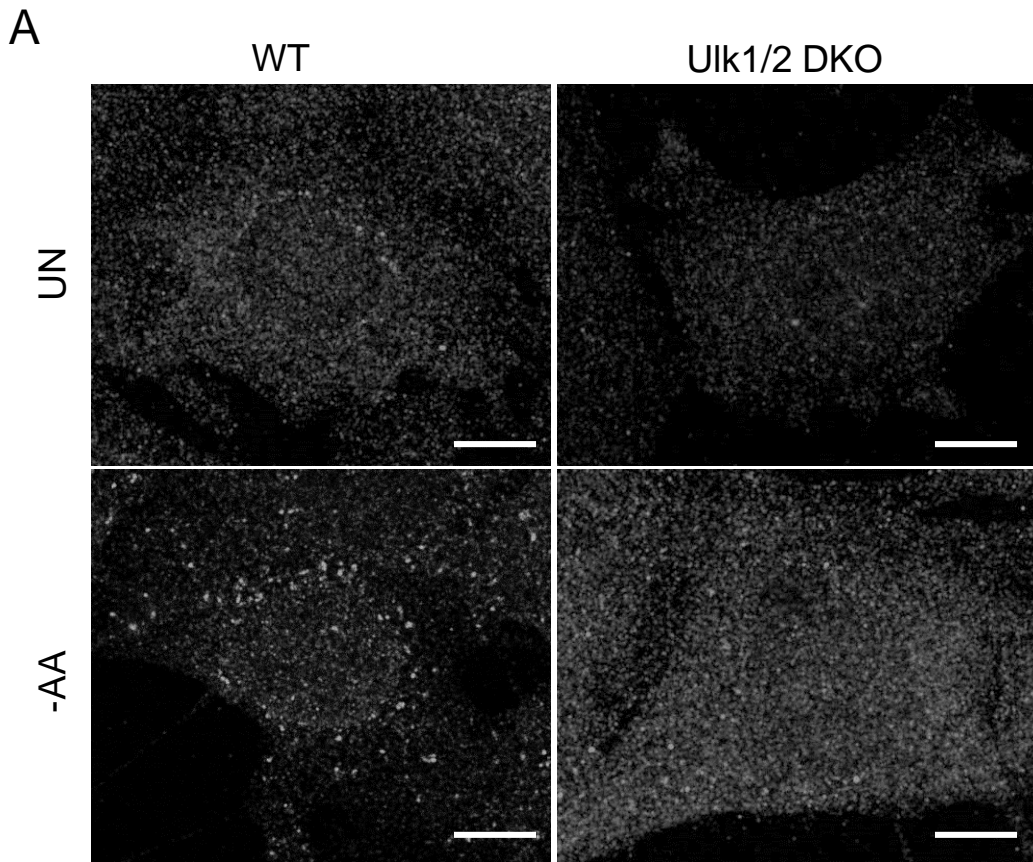


**Figure 4.14: Uik1/2 is required for LC3-positive autophagosome formation (A)** Representative images show LC3B puncta in WT MEF (clone 1SVN) and Uik1/2 DKO MEF (clone 4SVN). Cells were either maintained in full media (UN) or starved of all amino acids (-AA) for 1.50hr. Starvation media conditions does not contain 10% dialysed FBS. Cells were fixed and stained for LC3B. (B) Each bar is the mean of LC3B puncta/cell in 90 cells from three independent experiments. \*\*\* indicate  $P < 0.001$  unpaired t test. Scale: 10 $\mu$ m

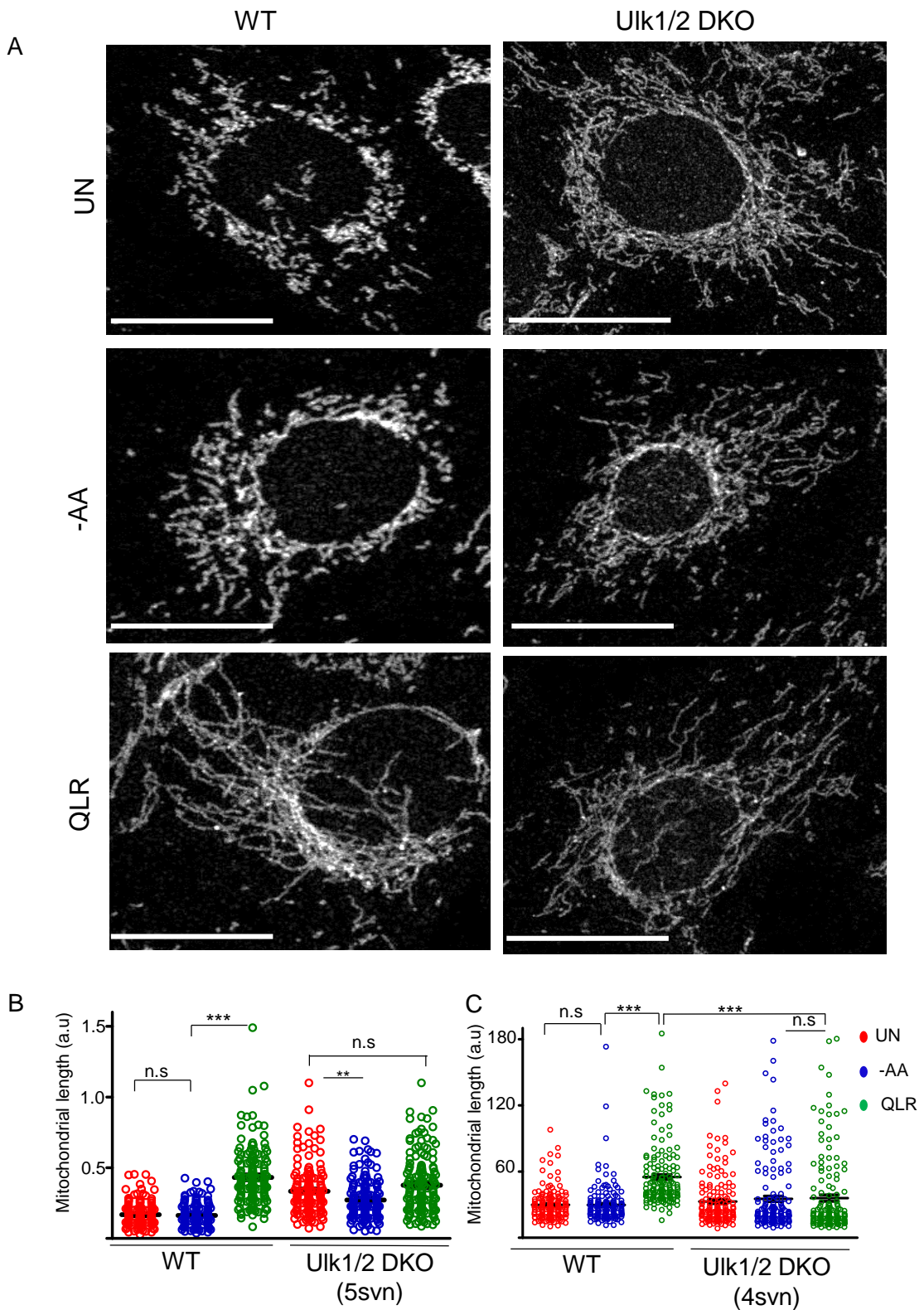


**Figure 4.15: Ulk1/2 is a regulator of amino acid-dependent mitochondrial hyperfusion.** (A) Representative images of WT MEF (clone: 1SVN) and Ulk1/2 DKO MEF (clone: 5SVN) cells maintained in full media (UN) or starved of either all amino acids (-AA) or starved of amino acid but supplemented with QLR for 4h. Starvation media conditions also contained 10% dialysed FBS. Cells were fixed and stained for outer mitochondrial membrane TOM20.

(B) Mitochondrial hyperfusion was measured in WT and Ulk1/2 DKO MEF (clones: 4SVN vs 5SVN). Note: 4.15B 1svn WT treatments are the same for Fig 4.11B as they are parallel experiments. Each dot represents the mean length of 10 mitochondria within a cell. Each treatment shows 150 cells quantified from 3 independent experiments. \*\*\* indicate  $P < 0.001$ , n.s (non-significant). Analysed with one way ANOVA with Bonferroni post test. Scale:  $25\mu\text{m}$



#### **4.2.4 Amino acid-dependent mitochondrial fusion is independent of autophagy.**

The Ulk1 complex is essential in the regulation of amino acid starvation-induced autophagy (McAlpine et al., 2013). Ulk1 phosphorylates Beclin1 to drive the activation of VPS34 PI3K and autophagy vesicle nucleation (Russell et al., 2013, Park et al., 2018). Mitochondrial fusion during starvation-induced autophagy has been suggested to be a mechanism for mitochondrial evasion possibly reflecting a balance between autophagy and excessive mitophagy (Rambold et al., 2011).

Since it was shown that loss of the Ulk1 complex would block autophagy, it was next investigated whether the block of mitochondrial hyperfusion was due to general inhibition of autophagy (or rather a more specific Ulk1 role). For this, Atg5 KO MEF that are unable to induce autophagosome formation were tested (Kuma et al., 2004, Gallagher et al., 2017). As done previously in Ulk1 and Atg13 KO cells, it was confirmed that Atg5 KO MEF were indeed unable to undergo autophagy during amino acid starvation.

It was observed that LC3B puncta accumulated as expected following amino acid starvation in wildtype MEF (derived in parallel with Atg5 KO) (**Fig 4.17A**). In contrast, in Atg5 KO MEF, LC3B puncta formation was completely inhibited following amino acid starvation. In wildtype MEF, LC3B spots increased by 4-fold upon amino acid starvation relative to cells maintained in full media. However, basal and starvation-induced accumulation of LC3B spots were totally inhibited in Atg5 KO MEF (**Fig 4.17B**). This finding is consistent with strong inhibition of autophagy in Atg5 KO cells.

In wildtype MEF, as observed in other cell systems, addback of Q, L and R induced extended mitochondrial hyperfusion (**Fig 4.18A**). In contrast, MEF maintained in either full nutrient media or fully starved of amino acid retained short mitochondrial length. Similar to wildtype MEF, Atg5 KO MEF produced hyperfused mitochondria in response to Q, L and R-addback, but not in amino acids-starved cells. Mitochondrial length increased by at least 3-fold in Q, L and R supplemented wildtype cells relative to amino acid-starved and untreated wildtype MEF (**Fig 4.18B**). In Atg5 KO MEF, supplementation of QLR increased mitochondria length by 2-fold relative to amino acid-starved and untreated cells. These findings indicate mitochondrial hyperfusion in response to Q, L and R addback can occur even in Atg5 KO autophagy-deficient cells.

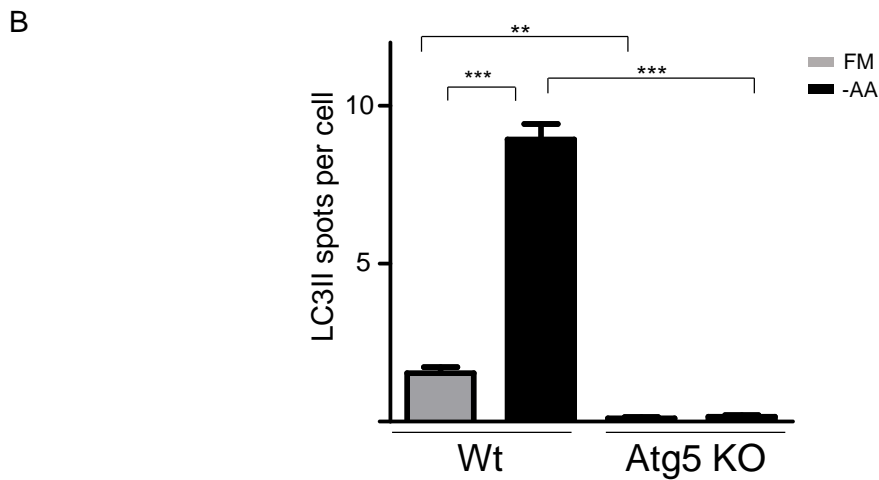
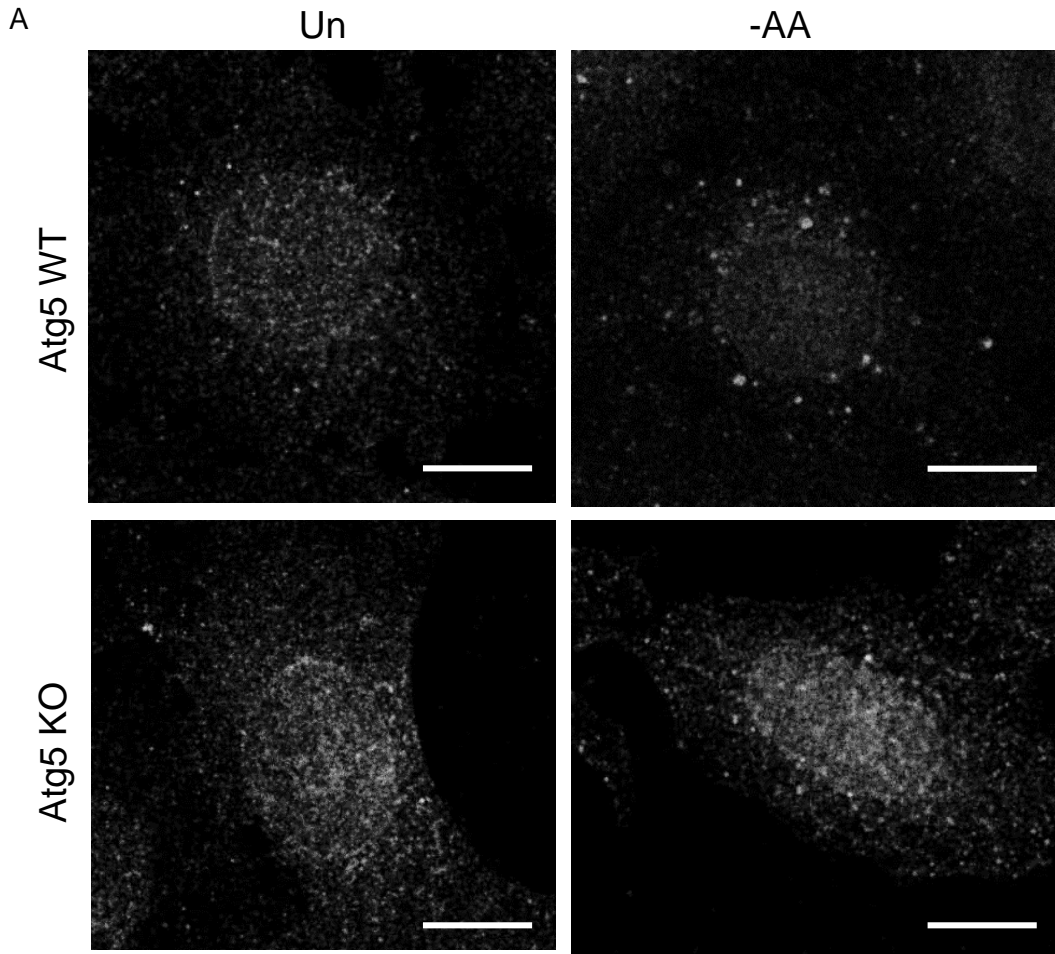


**Figure 4.17: Autophagy deficiency in Atg5 KO MEF.** (A) Representative images of WT and Atg5 KO MEF. Cells were either maintained in full media (UN) or starved of all amino acids (-AA) for 2hr. Starvation media conditions also contained 10% dialysed FBS. Cells were fixed and stained for LC3B and puncta quantified. (B) Each bar shows mean of LC3B puncta/cell in 120 cells from four independent experiments (30 cells quantified per experiment). \*\*\* indicate  $P < 0.0001$  analysed with one way ANOVA with Bonferroni post test. Scale: 10 $\mu$ m

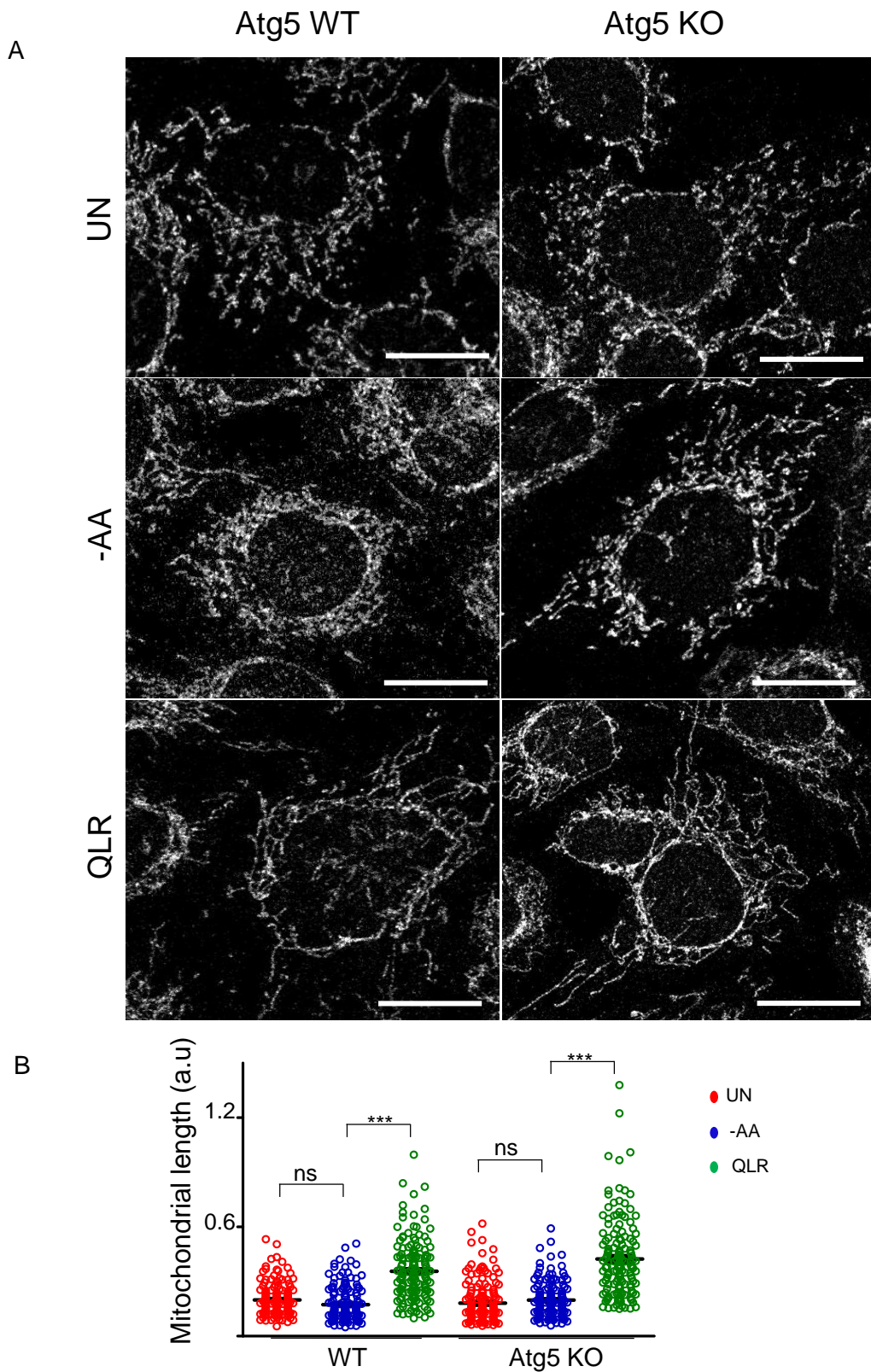


**Figure 4.18: QLR-induced mitochondrial hyperfusion is independent of autophagy (A)** Representative images of WT and Atg5 KO MEF. Cells were maintained in full media (UN) or starved of either all amino acids (-AA) or starved of amino acid but supplemented with QLR for 4h. Starvation media conditions also contained 10% dialysed FBS. Cells were fixed and stained for outer mitochondrial membrane TOM20. (B) Mitochondrial hyperfusion was measured in WT and Atg5 KO MEF. Each dot represents the mean length of 10 mitochondria within a cell. Each treatment shows 150 cells quantified from 3 independent experiments. \*\*\* indicate  $P < 0.001$ . Analysed with one way ANOVA with Bonferroni post test. Scale: 25 $\mu$ m

## 4.2.5 Role of PKA-signalling in amino acid-dependent mitochondrial hyperfusion

The stimulation of mitochondrial fusion during amino acid starvation has been reported to involve the activation of PKA which phosphorylates Drp1 at S637 (Gomes et al., 2011a). Phosphorylation of Drp1 at S637 has been shown to repress Drp1 recruitment to mitochondria, therefore favouring an unopposed mitochondrial fusion (Chang and Blackstone, 2007).

The localization of Drp1 during amino acid starvation and QLR-supplementation was thereby studied to determine if subcellular Drp1 distribution could explain hyperfusion results. 4T1-SU9 GFP cells fixed on glass coverslips were stained with antibody against Drp1. It was observed that Drp1 could be detected as punctate structures spread over the cytoplasm in untreated cells maintained in full nutrient conditions (**Fig 4.19A**). Interestingly, Drp1 localisation did not change upon amino acid starvation or QLR addback. Upon image analysis of Drp1 puncta co-localization, there was no significant difference in the number of Drp1 puncta localised on mitochondria (SU9-GFP) between untreated cells, starved cells or QLR-addback conditions (**Fig 4.19B**). This finding suggests that levels of Drp1 localized on mitochondria remained relatively constant in our experimental treatments. Therefore, amino-acid dependent hyperfusion could not be explained by Drp1 translocation away from mitochondria.

PKA is activated by accumulation of second messenger cAMP during low energy stress or pharmacological-activation by Forskolin (Frsk) (Gomes et al., 2011b, Gomes et al., 2011a, Chang and Blackstone, 2007). In contrast, PKA-activity can be inhibited using H89 dihydrochloride hydrate (Chijiwa et al., 1990). PKA phosphorylates multiple downstream targets such as CREB at S133 and pro-apoptotic protein BAD at S112 (Gonzalez and Montminy, 1989, Harada et al., 1999b). Phosphorylation of CREB at S133 is a well-established readout of PKA activation. To ascertain whether QLR-dependent mitochondrial hyperfusion is occurring as a result of PKA-activation and phosphorylation of Drp1 at pro-fusion site S637, western blot analysis was carried out. Here, we also investigated PKA-dependent phosphorylation following Frsk treatment as control.

It was observed that Frsk did not alter S6 phosphorylation, a reflection of MTORC1 activity (**Fig 4.20A**). On the other hand, amino acid starvation led the inhibition of the phosphorylation of S6, while QLR addback (in the presence of serum growth factors)

restored the phosphorylation of S6, consistent with the expected MTORC1 signalling pattern. Frsk led to increased phosphorylation of CREB relative to untreated cells. However, amino acid-starvation led to even stronger levels of CREB phosphorylation and these levels remained high even with QLR-supplementation (**Fig 4.20A**). Therefore, PKA appears activated in all three treatments but to differing extents. Surprisingly, while Frsk-dependent PKA activation led to phosphorylation of Drp1 at S637, amino acid starvation and QLR-supplementation did not induce this response (although PKA was activated according to P-CREB) (**Fig 4.20A**). As this was entirely unexpected, another commercially-available phospho Drp1-S637 antibody was also tested. This additional immune blot further confirms the result, indicating that Drp1 is not phosphorylated at S637 during amino acid starvation or further QLR-supplementation (**Fig 4.20A**).

Next, another Drp1-phosphorylation site was investigated. In contrast to the phosphorylation of Drp1-S637 which leads to overall mitochondrial fusion, multiple kinases Cdk1, PKC and Erk2 phosphorylate Drp1 at S616, leading to an increased Drp1 recruitment to mitochondria hence mitochondrial fission (Taguchi et al., 2007, Kashatus et al., 2015, Qi et al., 2011, Serasinghe et al., 2015). Less phosphorylation of Drp1 at S616 is associated with mitochondrial fusion. It was observed that phosphorylation of Drp1 at S616 did not greatly change under our different treatments. For example, relative to untreated cells, Drp1 phosphorylation at S616 did not decrease after Frsk treatment, even though mitochondrial fusion (and S637 phosphorylation) is promoted by this drug (**Fig 4.20B**). Amino acid starvation led to mild dephosphorylation of S616 but QLR-supplementation (hyperfusion) did not lead to further S616 dephosphorylation. Therefore, dephosphorylation of Drp1 S616 does not appear to be a driver of Frsk- or QLR-dependent mitochondrial hyperfusion.

Mitochondrial dynamics can also be altered via Opa1-proteolytic processing to form long (L) Opa1 or short (S) Opa1 oligomers. The accumulation of L-Opa1 favours fusion while the accumulation of S-Opa1 enhances mitochondrial fragmentation (Duvezin-Caubet et al., 2006, Ishihara et al., 2006, Head et al., 2009). Therefore, it was also investigated here whether Opa1 proteolysis occurs during Frsk treatment, amino acid starvation or QLR supplementation. Interestingly, it was observed that Opa1 was present in both L-Opa1 and S-Opa1 forms at generally unchanged ratios in all treatments (**Fig 4.20C**). There were no changes in the relative levels of L-Opa1 or S-Opa1 to correlate with mitochondrial hyperfusion during amino acid starvation

and QLR-supplementation. This finding also suggested that Opa1 remodelling cannot explain the regulation of amino acid-dependent mitochondrial hyperfusion.

To further explore the unexpected lack of phosphorylation on Drp1 at (pro-fusion) S637 after amino acid starvation and QLR supplementation, we considered that the phosphorylation might occur at earlier time points. To test this, PKA-dependent phosphorylation of Drp1 at S637 was re-examined. Furthermore, since it was shown in the previous chapter that amino acid-dependent mitochondrial fusion begins rapidly at 1-hour (peaking at 4-hours), it was investigated whether phosphorylation of Drp1 at S637 precedes mitochondrial fusion after amino acid starvation or QLR supplementation.

It was observed that PKA led to basal steady levels of phosphorylated CREB in untreated cells (collected as controls) at 1, 2 and 4-hours (**Fig 4.21**). In contrast, Frsk treatment led to phosphorylation of CREB at 1-hour, which reduced by 2 and 4-hours. However, amino acid starvation or starvation with QLR supplementation led to phosphorylation of CREB at a higher level relative to Frsk treated cells, with sustained activation between 1, 2 and 4-hours. As observed previously, only Frsk treated cells were able to phosphorylate Drp1 at S637. Frsk led to the phosphorylation of S637 at an early time point of 1-hour which was maintained at 2-hours and 4-hours despite only transient phosphorylation of CREB. This further confirms that amino acid starvation leads to PKA activation but QLR-addback dependent mitochondrial fusion occurs independently of Drp1-phosphorylation at S637.

Since PKA was shown to be activated during amino acid-dependent mitochondrial hyperfusion, the role of PKA-activation on mitochondrial dynamics was examined. 4T1-SU9 GFP cells were starved of amino acids or further supplemented with QLR. In addition, we further tested effects of activating PKA with Frsk or inhibiting PKA with H89. Mitochondrial length was assessed and western blot was performed to confirm changes in phosphorylation of CREB, Drp1 and S6 as a readout of PKA and MTORC1.

As expected, Frsk alone in untreated cells (under full nutrients) led to a moderate mitochondrial fusion relative to untreated cells (**Fig 4.22**). Unexpectedly, the inhibition of PKA alone with H89 (under full nutrients) also led to mitochondrial fusion relative to untreated cells. Interestingly, while amino acid starvation led to mitochondrial fusion, further PKA activation with Frsk increased mitochondrial length (column 4 vs 5). However, H89 did not alter amino acid starvation-induced mitochondrial fusion

(column 4 vs 6). Surprisingly, while QLR addback led to mitochondrial hyperfusion, further activation of PKA did not enhance mitochondrial length (column 7 vs 8). However, inhibition of PKA with H89 blocked QLR-dependent mitochondrial hyperfusion (column 7 vs 9).

Western blot analysis confirmed that PKA is activated in all Frsk treated cells via phosphorylation of Drp1 S637 (lanes 2, 5 and 8). Similarly, H89 effectively blocked PKA activity via its inhibition of the phosphorylation of CREB (lanes 3, 6 and 9). However, H89 was also observed to inhibit phosphorylation of S6 (lanes 3 and 9), thereby indicating a potential off-target effect (**Fig 4.22**). These findings suggest that there are multiple distinct PKA signalling mechanisms during Frsk treatment, amino acid starvation and QLR supplementation. The H89 data suggest that full amino acid starvation-induced mitochondrial fusion is independent of PKA, while QLR-dependent mitochondrial hyperfusion might be PKA-dependent.

Based on the potential off-target inhibition by H89, the role of PKA in QLR-dependent mitochondrial hyperfusion required further clarification. H89 has been reported to have multiple targets with IC<sub>50</sub> values of 80nM for S6K1 and 135nM for PKA (Davies et al., 2000). Since S6K1 phosphorylates S6, this interaction may explain why H89 decreased phospho S6 levels. Davies et al. (2000) reported that at 10 $\mu$ M concentration, H89 inhibits other kinases such as AMPK, CHK1, ROCKII and S6K, some of which have been reported to regulate mitochondrial dynamics. To limit this off-target interference in H89-inhibition of QLR-dependent mitochondrial hyperfusion, dose-dependent phosphorylation of CREB and S6 was examined by western blot.

As shown previously, PKA led to the phosphorylation of CREB in QLR-supplemented cells, with phosphorylation of S6 at relatively high levels, similar to untreated cells (**Fig 4.23A**). It was observed that H89 effectively blocked the phosphorylation of CREB (in the presence of QLR) at all concentrations tested from 5 $\mu$ M – 20 $\mu$ M. H89 at 20 $\mu$ M led to inhibition of PS6 but this was greatly reduced at 10 $\mu$ M and 5 $\mu$ M. This result indicated that lower concentrations of H89 can effectively inhibit PKA while having less effect on the phosphorylation of S6. Next, the effect of H89-inhibition of PKA on mitochondrial fusion was re-examined at 5 $\mu$ M concentration.

Similar to our previous experiment, H89 at 5 $\mu$ M led to mitochondrial fusion in untreated cells under full nutrients (**Fig 4.23B**). This lower concentration of H89 did not alter amino acid-starvation induced mitochondrial fusion. In contrast, H89 mildly (but significantly) reduced QLR-dependent mitochondrial hyperfusion. Although the

H89 effect at 5 $\mu$ M effect was less than what was observed with 20 $\mu$ M, the data are still consistent with some PKA-dependent regulation during QLR-induced mitochondrial hyperfusion. However, the level of mitochondrial fusion observed during Frsk treatment or QLR-dependent mitochondrial hyperfusion did not correlate with patterns of Drp1 phosphorylation at S637. This distinct pattern of PKA signalling involving CREB, but not Drp1 S637, was next examined.

PKA has been reported to have multiple spatially distinct phosphorylation pathways located in the cytoplasm, nucleus, outer mitochondrial membrane and inner mitochondrial membrane (Burdyga et al., 2018). At these subcellular localisations, PKA can drive unique phosphorylation events on specific target proteins, generally containing a PKA substrate consensus defined as RRx(S/T) (Zetterqvist et al., 1976, Kemp et al., 1977). Next, it was explored whether global PKA-signalling patterns are different in Frsk treated cells, amino acid-starved cells and QLR-supplemented cells.

PKA-phosphorylation of cellular target proteins was examined by western blot using a pan phospho-PKA consensus RRx(S/T) antibody. It was observed that Frsk distinctively increased the phosphorylation of multiple PKA substrates (corresponding to 180kDA, 116kDA and 60kDA protein size) relative to untreated cells (**Fig 4.24**). In contrast, amino acid starvation or QLR addback did not lead to the phosphorylation of these substrates (red arrows). Interestingly, relative to untreated and Frsk-treated cells, amino acid starvation or QLR addback led to the dephosphorylation of PKA substrate corresponding to 36kDA (blue arrow). Therefore, there were distinct PKA substrate phosphorylation patterns in amino acid-starved cells, QLR-addback and Frsk treated cells (marked by red and blue arrow). On the other hand, Frsk treatment, amino acid starvation or QLR addback increased the phosphorylation of PKA substrates relative to untreated cells (black arrows), thereby indicating that PKA is activated. Interestingly, QLR addback into amino acid starvation led to similar phosphorylation pattern as observed in amino acid starved cells. However, relative to amino acid starved cells, QLR addback increased the phosphorylation of the PKA substrate corresponding to 36kDA. These findings suggest that Frsk-dependent PKA signalling is different from amino acid starvation or QLR-addback dependent PKA activation.

Collectively, the data from this section suggest that PKA may have multiple roles in the regulation of mitochondrial dynamics. 1) Amino acid starvation leads to the activation of PKA as shown in the phosphorylation of CREB and other PKA-substrates. 2) Upon PKA activation during amino acid starvation, PKA does not

phosphorylate certain substrates as it would during Frsk treatment as shown in Drp1 phosphorylation at S637 and other substrates. 3) QLR addback into amino acid starvation led to a PKA-dependent phosphorylation that is absent during amino acid starvation. These all suggest that there is a distinct PKA mechanism during amino acid-dependent mitochondrial hyperfusion.

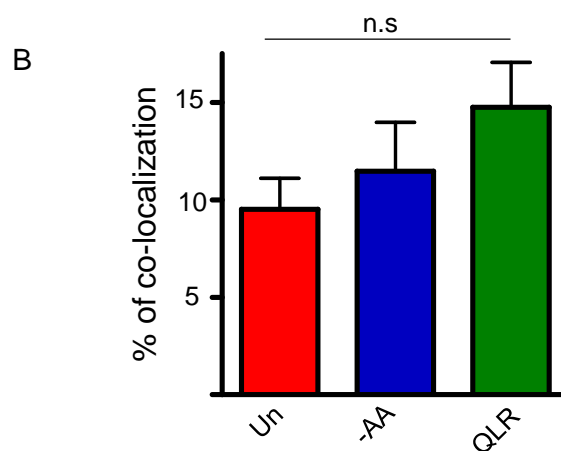
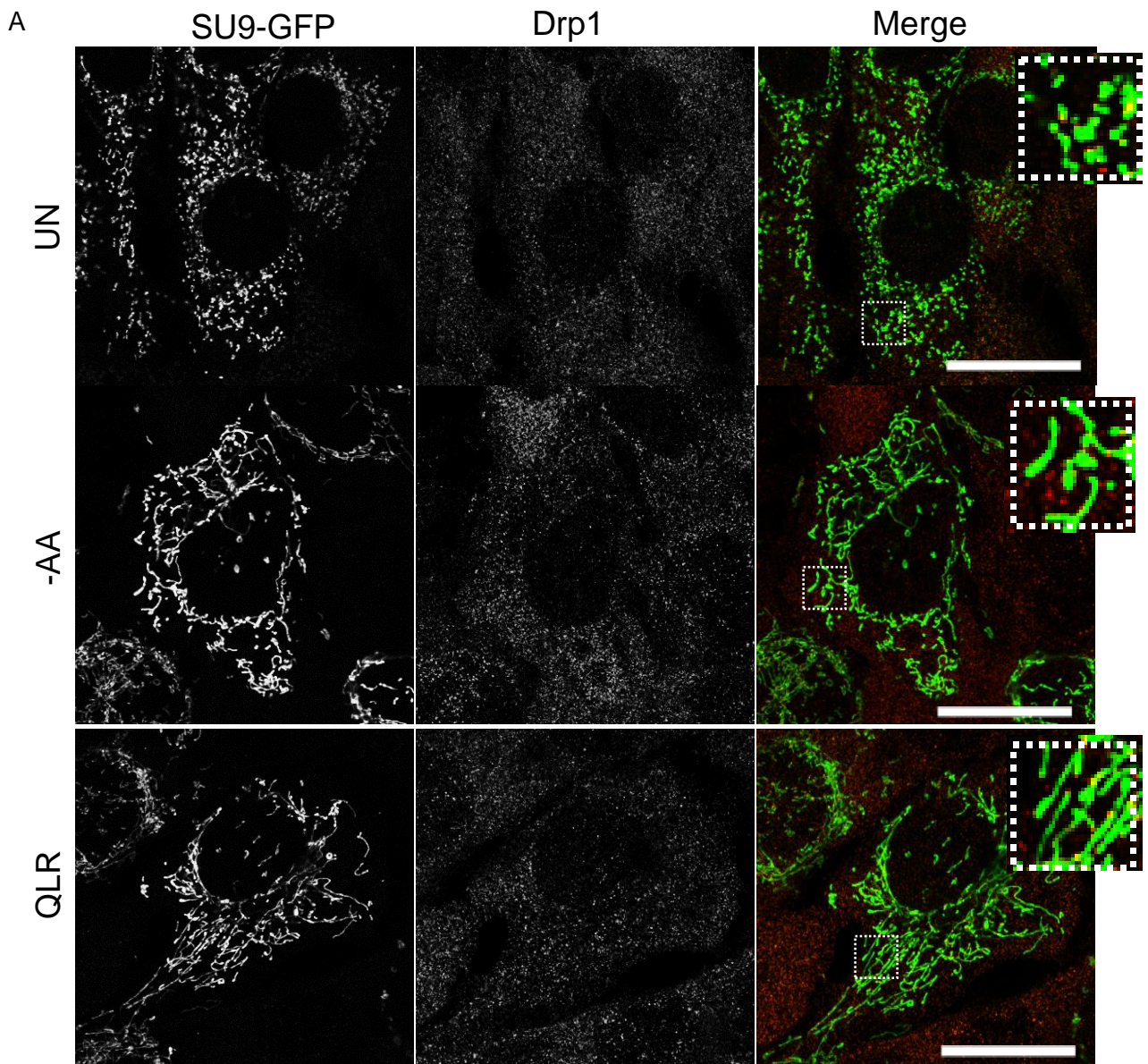


**Figure 4.19: Drp1 localization during amino acid-dependent mitochondrial fusion** (A) Representative images of 4T1-SU9 GFP cells stained with anti-Drp1 antibody after amino acid starvation and QLR supplementation for 4 hours. Starvation media conditions also contained 10% dialysed FBS. (B) Bar chart indicating the percentage of co-localization of Drp1 spots with mitochondria (quantification of co-localization normalised to total mitochondrial area). Merged confocal images of Drp1 and SU9-GFP were analysed on Image-J to identify co-localization. The highlighted co-localization was counted with analyse-particle after all the images were adjusted to the same threshold. Average of 11 cells per image, 9 images per treatment were analysed from 3 independent experiments. Analysed with one way ANOVA. n.s: No significance. Scale bar: 25µm

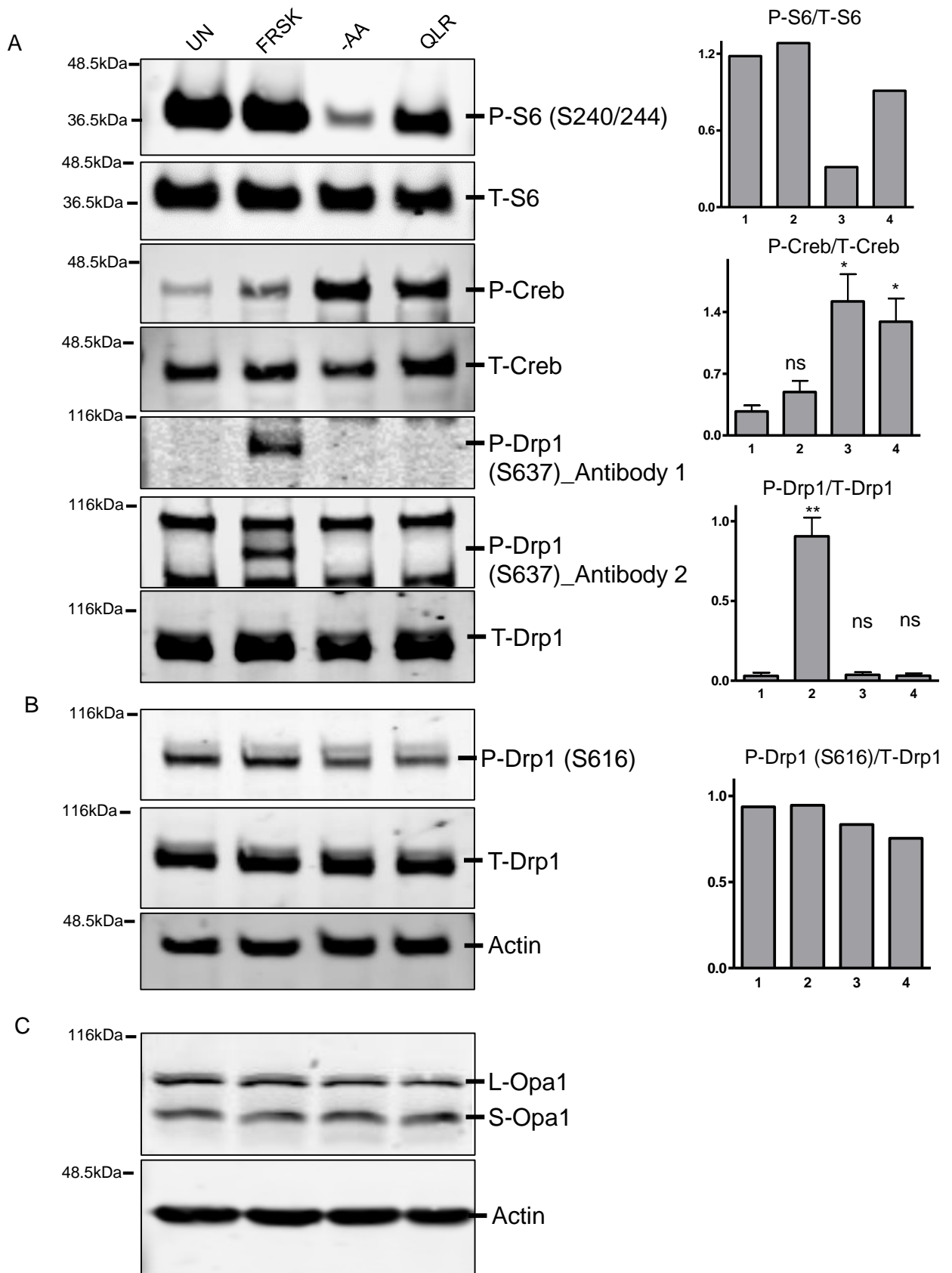


**Figure 4.20: PKA activation does not correlate with mitochondrial hyperfusion** (A) Western blot showing the PKA-dependent phosphorylation after treatment of 4T1 cells with Forskolol (20 $\mu$ M), amino acid starvation and amino acid starvation/QLR supplementation for 4 hours. Starvation media conditions also contained 10% dialysed FBS. Graphs show band densitometry, average of  $n=2$  for P-S6/T-S6, mean of  $n=3$  for P-Creb/T-Creb, mean of  $n=3$  for P-Drp1/T-Drp1 (B) Western blot showing phosphorylation of Drp1 at S616 after indicated treatments. Graph of average of  $n=2$  for P-Drp1 (S616)/T-Drp1 (C) Western blot showing Opa-1 processing after indicated treatments. Representing  $N=3$  independent experiments. \* ( $P < 0.05$ ), \*\* ( $P < 0.01$ ), ns (non significant), relative to untreated. Analysed with T-test unpaired.

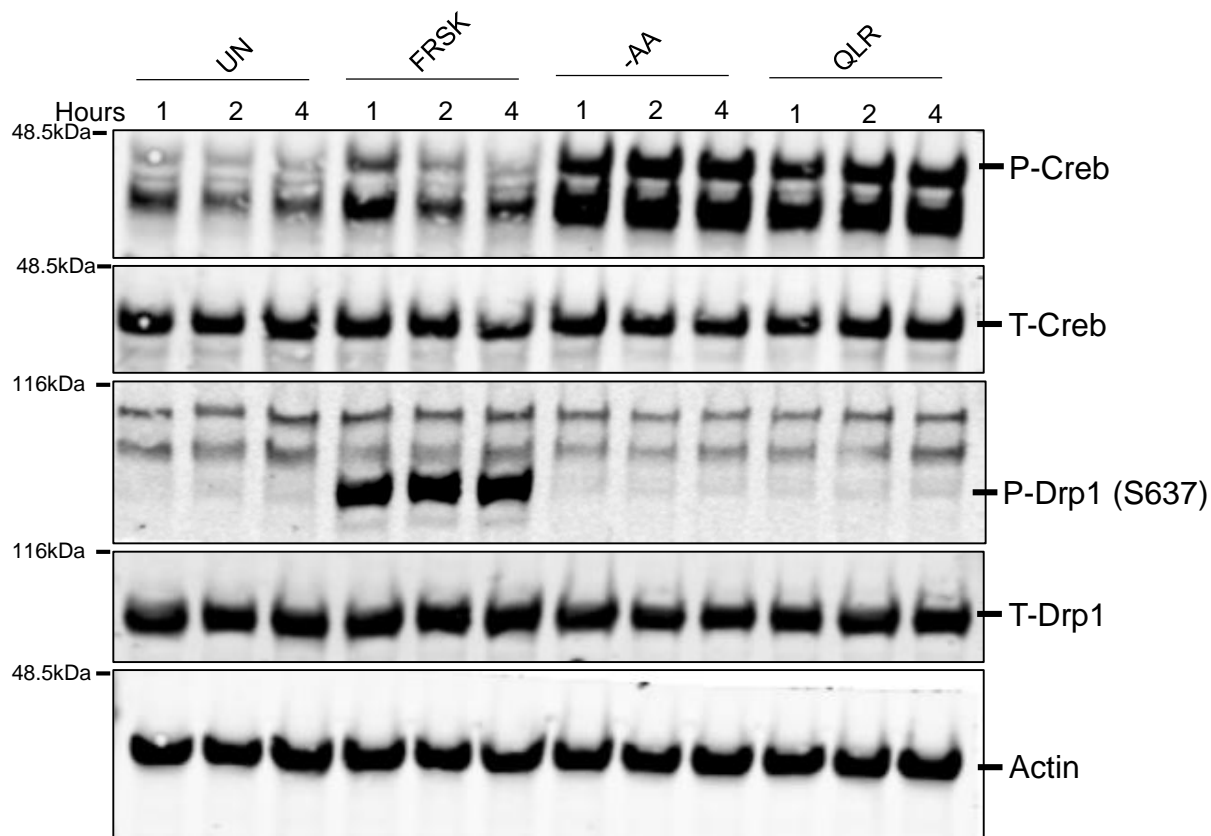


**Figure 4.21: Rapid PKA activation upon amino-acid starvation.** Western blot showing PKA-dependent phosphorylation events in 4T1 cells after treatment with Forskolin (20 $\mu$ M), amino acid starvation or amino acid starvation/QLR supplementation for 1 hour, 2 hours and 4 hours. Representing N=2 independent experiments. Starvation media conditions also contained 10% dialysed FBS.

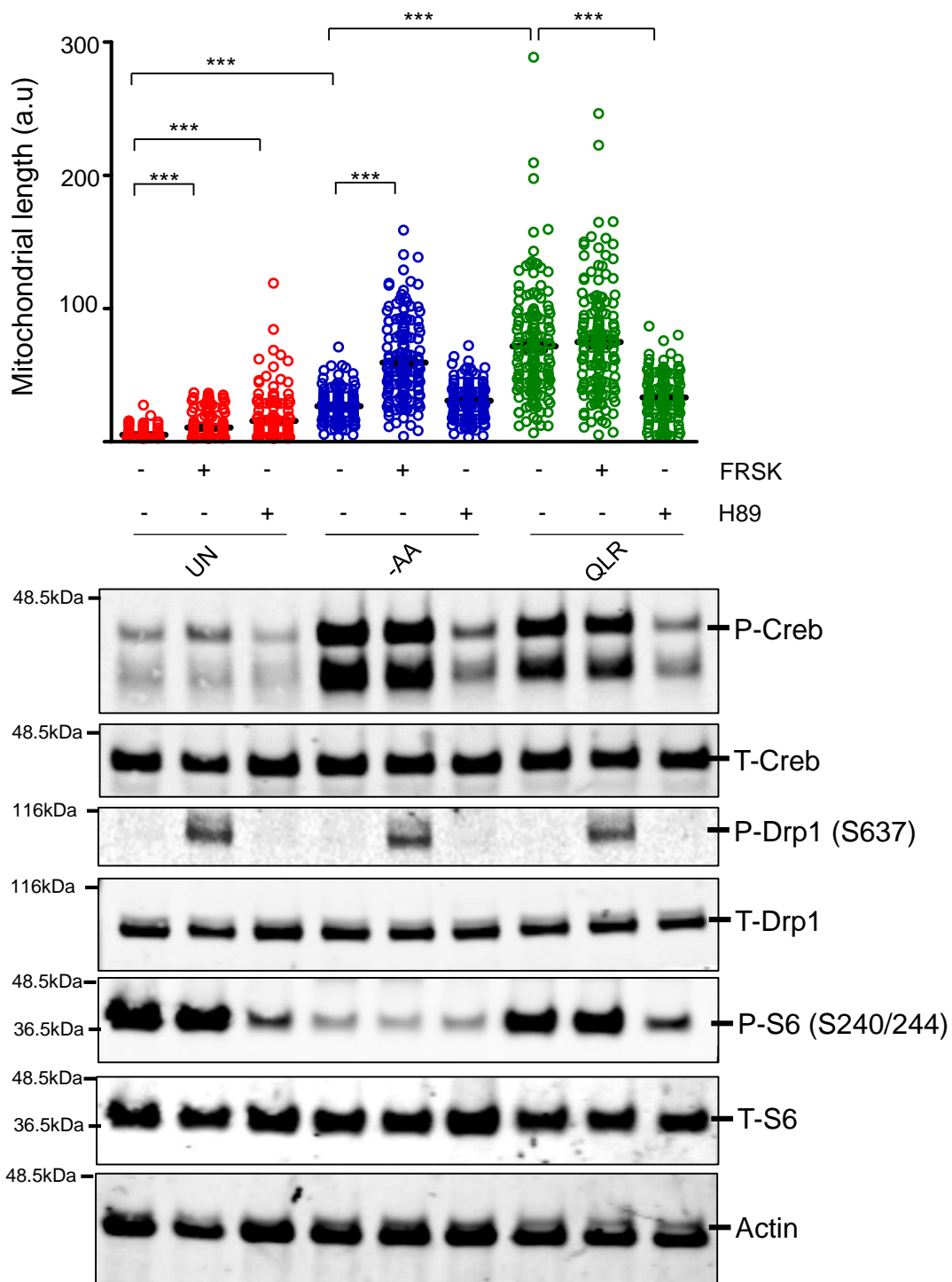


**Figure 4.22: Mitochondrial fusion is regulated by both PKA activation and inhibition.** 4T1-SU9 GFP cells were starved of either all amino acid or starved of amino acid but supplemented with Q, L and R plus/minus either: PKA activator (Forskolin 20 $\mu$ M), or PKA inhibitor (H89 20 $\mu$ M) for 4 hours. Starvation media conditions also contained 10% dialysed FBS. Each dot represents the mean length of 10 mitochondria within a cell. Each treatment shows 150 cells quantified from 3 independent experiments. \*\*\* indicate  $P < 0.001$ . Analysed with T.test unpaired. Western blot showing PKA and MTORC1 regulation of downstream targets. Representing N=3 independent experiments

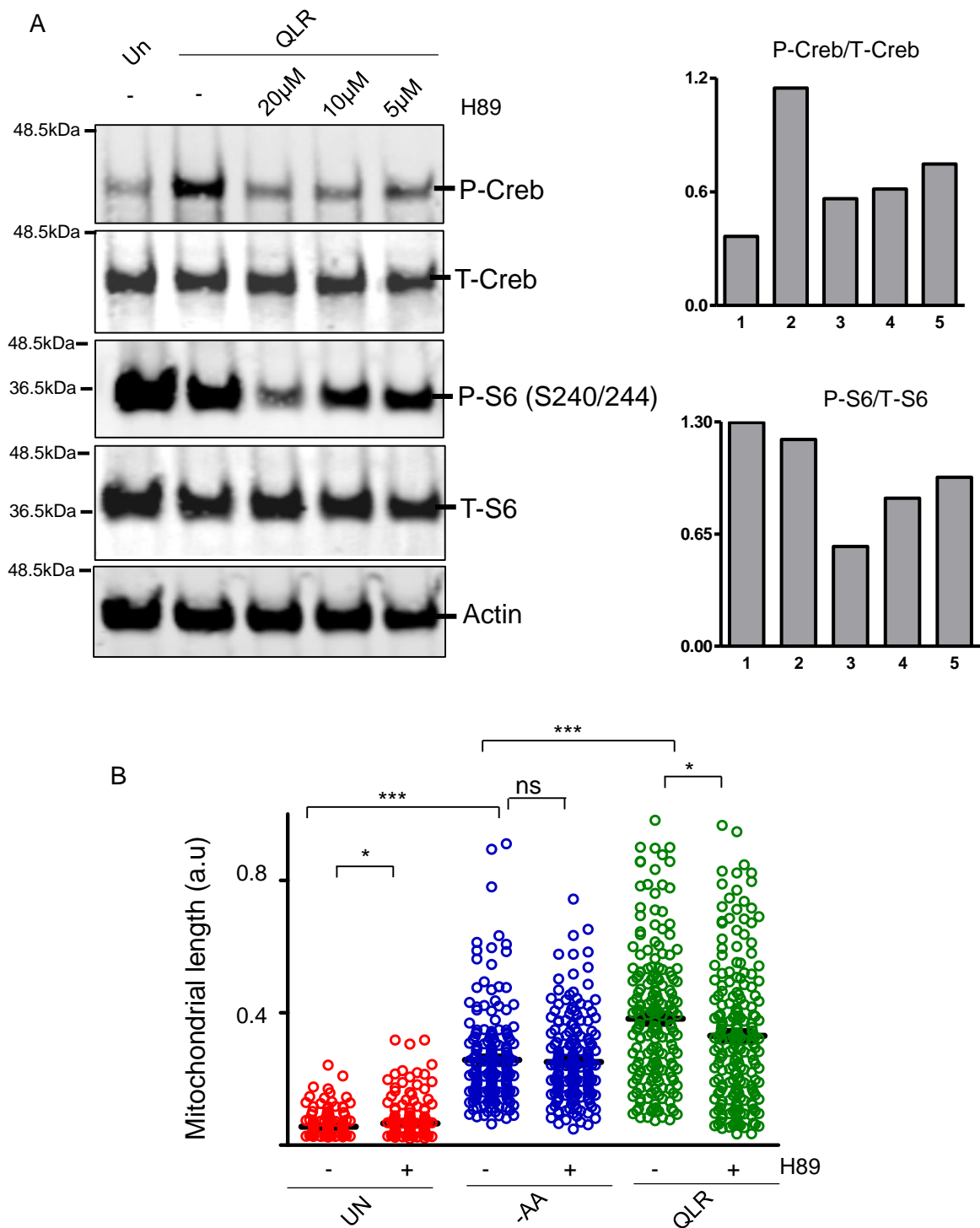


**Figure 4.23: H99 inhibition of PKA inhibits QLR-dependent mitochondrial hyperfusion.** (A)

Western blot showing H99 dose-dependent inhibition of PKA in 4T1-SU9 GFP cells treated to amino acid starvation/QLR supplementation for 4 hours. Starvation media conditions also contained 10% dialysed FBS. Representing N= 2 independent experiments. Graphs show average of band density of n = 2 blots, P-Creb/T-Creb, P-S6/T-S6, each bar (1-5) represent each band from left to right.

(B) Mitochondrial length of 4T1-SU9 cells starved of all amino acid or amino acid starved but supplemented with Q, L and R plus/minus PKA inhibitor (H99 5µM) for 4 hours. Starvation media conditions also contained 10% dialysed FBS. Each dot represents the mean length of 10 mitochondria within a cell. Each treatment shows 180 - 200 cells quantified from 4 independent experiments. \* indicate P < 0.05. Analysed with T-test unpaired.

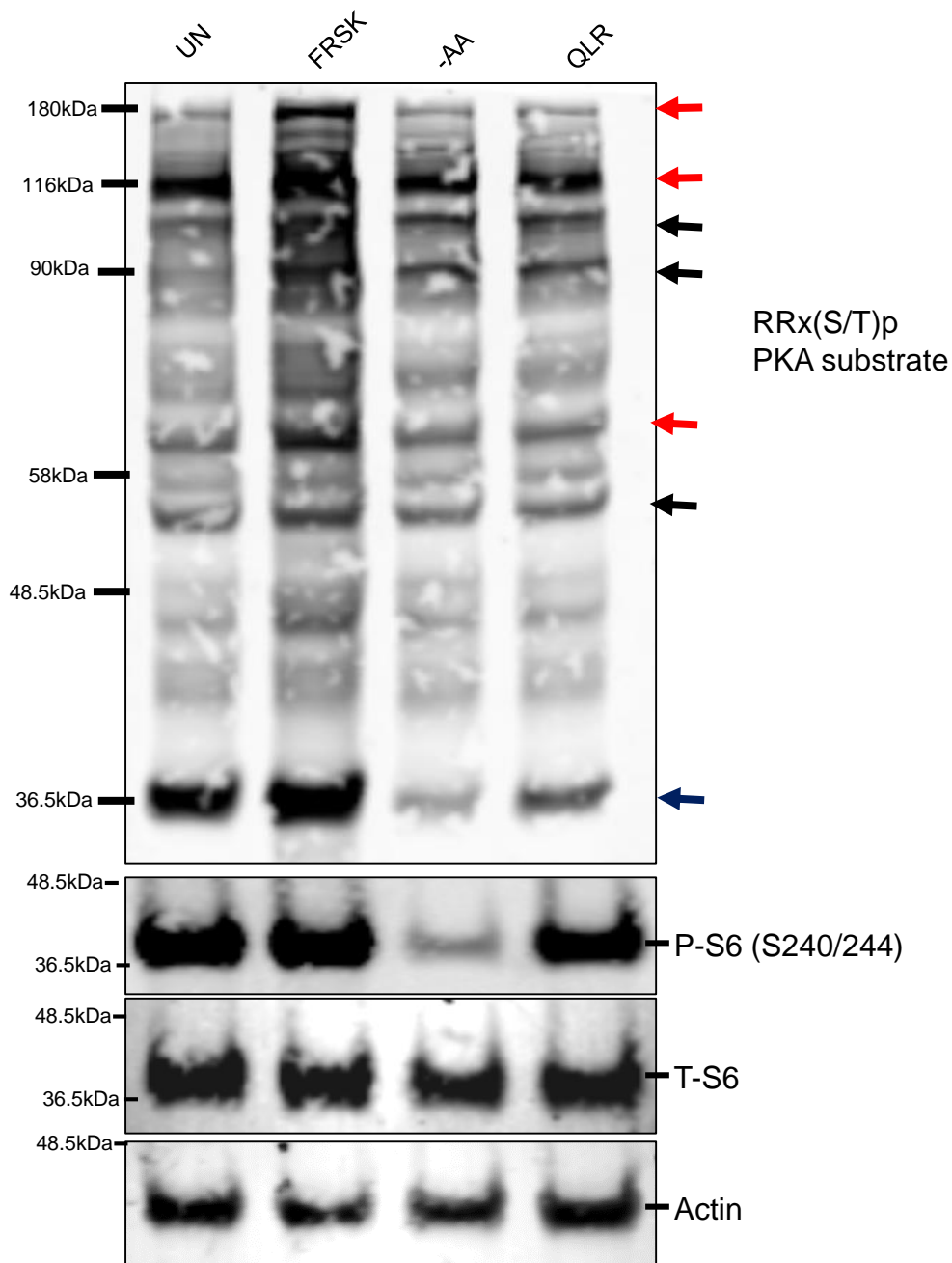


**Figure 4.24: Detection of phosphorylation of PKA substrate motif during amino acid starvation.** Western blot showing the phosphorylation of PKA substrates motif (detected with phospho-PKA substrate antibody RRx(S/T)<sup>p</sup>) after PKA activation with Forskolin (20 $\mu$ M), amino acid starvation, amino acid starvation with QLR supplementation for 4 hours. Starvation media conditions also contained 10% dialysed FBS. Representing N=4 independent experiments. (Red and blue arrows indicating differential phospho events in FRSK, -AA and QLR treated cells. Black arrow identifying similar phosphorylation pattern)

## **4.3 Discussion**

### **4.3.1 Regulatory roles of autophagy mediators in mitochondrial remodelling**

We proposed that mitochondrial hyperfusion in response to Q, L and R might be explained by the function of MTORC1, AMPK, and Ulk1 since these pathways are critical regulators of amino acid sensing. MTORC1, AMPK and Ulk1 also have been implicated as key regulators of mitochondrial biology (e.g. MTORC1 regulation of mitochondrial hyperfusion (Morita et al., 2017), AMPK-dependent induction of mitochondrial fragmentation (Toyama et al., 2016) and Ulk1-dependent regulation of mitochondrial degradation (Wu et al., 2014, Tian et al., 2015, Egan et al., 2011)). These studies highlighted the possible roles of MTORC1, AMPK and Ulk1 in amino acid-dependent mitochondrial hyperfusion. In this chapter, we discovered that some (but not all) of these nutrient-sensing kinase pathways are required for amino acid-dependent mitochondrial hyperfusion.

#### **4.3.1.1 Amino acid-dependent mitochondrial hyperfusion is MTORC1 independent**

Here, we showed that amino acid addback-dependent mitochondrial hyperfusion is independent of MTORC1. Interestingly, our results are in contrast to another study Gomes et al. (2011a) that linked MTORC1 inhibition to mitochondrial fusion. We found that MTOR inhibition with Torin1 in otherwise normal conditions clearly was not sufficient to induce mitochondrial fusion despite total inhibition of MTORC1-dependent phosphorylation of downstream substrates. Conversely, we observed only a minimal block in QLR-dependent mitochondrial fusion in response to Torin1 or serum withdrawal in 4T1 cells. These results do not fit with the MTOR inhibition-mitochondrial fusion model. Overall, a major MTORC1-dependent effect (for example, from addback of Q, L and R) was not found that correlates with QLR-dependent mitochondrial hyperfusion. Therefore, our data suggest that mitochondria have a distinct amino acid sensing mechanism independent of MTORC1.

Furthermore, it was reported that long term inhibition of MTORC1 stimulated mitochondrial hyperfusion as a result of a reduction in MTFP1 translation. In Morita et al. (2017) MTOR was inhibited for 24-hours while in our study MTOR was inhibited for 4-hours. The inhibition of MTOR for 4-hours corresponds to the optimal time for amino acid starvation–inhibition of MTORC1 which occur rapidly before 2-hours

(Nwadike et al., 2018). Similarly, the timing also correlates with the optimal response of mitochondria to amino acids shortages. Clearly, MTOR inhibition-induced fusion occurs in response to translational break down which can be ruled out at 4-hours. In addition, cellular response to starvation-induced stress is a short term survival mode, which over time if the stress continues, cell death will be inevitable (Sadasivan et al., 2006). These, therefore, lead us to conclude that amino acid-dependent mitochondrial fusion is a separate cellular response from long term MTOR-inhibition induced fusion.

#### **4.3.1.2 AMPK is a regulator of mitochondrial hyperfusion**

We show here that AMPK is partially required for amino acid-dependent mitochondrial hyperfusion. Amino acid addback of QLR still stimulated some fusion in AMPK KO MEF but the response was much reduced. Therefore, our data suggest that AMPK is required for maximal mitochondrial hyperfusion. Interestingly, AMPK has been shown to regulate mitochondria via multiple mechanisms such as transcriptional upregulation of PGC-1 $\alpha$  which is required for mitochondrial biogenesis (Baur et al., 2006, Marin et al., 2017). AMPK also regulates mitochondrial dynamics via the phosphorylation of Mff (Toyama et al., 2016). Yet, roles for AMPK in mitochondrial biology remain still not fully explored. Due to the roles of AMPK as a master regulator of energy, it was suggested that AMPK regulates yet to be identified substrates resident in mitochondria (Herzig and Shaw, 2018). The role of AMPK in the regulation of mitochondrial dynamics has mostly been associated with mitophagy and metabolic challenges via phosphorylation of Mff to enhance mitochondrial fragmentation (Egan et al., 2011, Toyama et al., 2016). Another recent study has identified ARMC10 as a novel substrate of AMPK via a phospho-proteomic analysis of CRISPR-targeted AMPK $\alpha$ 1 and AMPK $\alpha$ 2 HEK293A cells (Chen et al., 2019b). This study found that AMPK can phosphorylate ARMC10 at S45 to promote mitochondrial fragmentation by interacting with Drp1. In contrast to the above AMPK-pro-fission model, our data indicate that AMPK also as a pro-fusion role in basal states since mitochondria of AMPK DKO MEF tend to shift toward fragmentation.

Interestingly, AMPK deficiency is reported in many metabolic diseases such as obesity and it is currently a drug target for diseases where mitochondrial metabolism is altered (Peralta et al., 2016, Marcinko et al., 2015, Bujak et al., 2015). Mitochondrial generated ROS have been reported to activate AMPK by increasing its phosphorylation of Uik1, for the maintenance of metabolic homeostasis (Rabinovitch et al., 2017, Hinchy et al., 2018). Vice-versa, in AMPK DKO cells, mitochondrial ROS

is elevated (Rabinovitch et al., 2017). Since an increase in mitochondrial ROS has been reported to induce mitochondrial fragmentation, it is possible that the reduction in mitochondrial fusion in AMPK DKO cells is an effect of elevated ROS (Wu et al., 2011). Our findings also complement the observation that AMPK promotes longevity in *C.elegans* by maintaining the continuous interplay between mitochondrial fusion and fission (Weir et al., 2017). Therefore, our data highlight that detailed roles of AMPK in fission and fusion still lack full clarity.

#### **4.3.1.3 Ulk1 is a regulator of mitochondrial dynamics**

We show here by multiple approaches that members of the Ulk1 complex (Ulk1, Atg13 and FIP200) are critical for Q, L and R induced mitochondrial hyperfusion. How Ulk1 regulates nutrient-dependent mitochondrial dynamics remains unclear, but this interaction is particularly intriguing due to the laboratory's long-standing interest in the Ulk1 pathway. While we had effective targeting of Ulk1 using the CRISPR-Cas9 system, it is not entirely surprising that mitochondrial fusion in Q, L and R addback conditions was only partially blocked. With Ulk1 loss, Ulk2 has been reported to complement for Ulk1 functions in a cell type-dependent manner (Lee and Tournier, 2011). Pharmacological inhibition of Ulk1 greatly inhibited both full amino acid starvation and Q, L, R induced hyperfusion, consistent with the notion that Ulk1-dependent phosphorylation is critical for mitochondrial fusion.

It was surprising that Ulk1/2 DKO MEF showed a mixed phenotype with hyperfused mitochondria in basal untreated cells. However, consistent with our other results, Q, L and R addback did not induce further hyperfusion in Ulk1/2 deficient cells. The reconstitution of wildtype Ulk1 into Ulk1/2 DKO reduced mitochondrial fusion in basal untreated cells and rescued QLR-induced hyperfusion responses, thereby further supporting the idea that Ulk1 function is a critical regulator of mitochondrial dynamics.

Surprisingly, not all the Ulk1 inhibitors blocked mitochondrial hyperfusion to the same extent. MRT68921 and newer "2nd generation" MRT239016 both showed a similar strong effect (Petherick et al., 2015). MRT68921 inhibition of amino acid-dependent mitochondrial fusion is consistent with other results from our lab where MRT68921 strongly inhibited the Ulk1-dependent phosphorylation of Atg13-S318 and autophagy ((Radhi et al., 2019) (Nwadike et al., 2018) and Chan, Nwadike, Radhi, unpublished data). In these studies from our group, 2nd generation MRT238993 and reported compound SBI0206921 (Egan et al., 2015) also blocked autophagy and phospho Atg13-S318. However, unexpectedly, these compounds did not alter mitochondrial

fusion phenotypes here. In contrast to MRT68921 and MRT239016 (which blocked QLR-dependent mitochondrial fusion), MRT238993 and SBI0206921 did not inhibit this response. However, while MRT238993 and SBI0206921 did not have an effect on mitochondrial dynamics, the MRT68921 and MRT239016 inhibitory effect further suggests that Ulk1 is required for amino acid-dependent mitochondrial hyperfusion.

Complementing Ulk1 targeting results, Atg13 and FIP200 loss of function led to extensive mitochondrial fission, thereby further supporting a role of the Ulk1 complex in QLR-induced mitochondrial hyperfusion. Previous studies have reported that Atg13 is released from Ulk1 and then translocates to damaged mitochondria where it aids their degradation (Joo et al., 2011). Similarly, FIP200 has been recently associated with mitochondria dynamics (Yamashita et al., 2016). FIP200 is shown to be critical for mitochondrial fragmentation during mitophagy. Interestingly, studies have also shown that the absence of Atg13 or FIP200 destabilizes the Ulk1 complex and also inactivates Ulk1/2 (Akers et al., 2011, Hosokawa et al., 2009a, Hara et al., 2008, Hosokawa et al., 2009b). These findings are consistent with our observation that Atg13 CRISPR, FIP200 KO, Ulk1 targeting all mediate the same mechanism during amino acid-dependent mitochondrial hyperfusion.

Ulk1 has been previously shown to regulate mitochondrial fission (albeit indirectly) during hypoxia. Under hypoxia stress, Ulk1 was observed to translocate onto mitochondria where it phosphorylated a novel identified substrate, FUNDC1 (Wu et al., 2014). Subsequently, FUNDC1 initiates the recruitment and binding of Drp1 to mitochondria-ER contact sites to induce mitochondrial fission (Wu et al., 2016b). Under normal conditions, FUNDC1 interacts with both L-Opa1 and S-Opa1 forms, and this interaction is reduced during mitochondrial stress (Chen et al., 2016a). Interestingly, other studies have shown that Ulk1 is required for mitochondrial remodelling during skeletal muscle regeneration (Call et al., 2017). This study reported that muscular injury led to mitochondrial fragmentation but wildtype mice are able to recover by remodelling mitochondria to a striated state. In contrast, it was observed that conditional Ulk1 muscle-specific KO mice are unable to remodel the mitochondrial network following muscular injury. Therefore, this supports a direct role of Ulk1 in mitochondrial dynamics. Another independent study has shown that the Ulk1 complex was critical for Bcl2-L-13- dependent mitophagy (Murakawa et al., 2019). It was shown that Ulk1 forms a complex with LC3B via its LIR and this interaction is required for Ulk1 interaction with Bcl2-L-13. Interestingly, similar to our observation, all members of the Ulk1 complex are required for the Ulk1-Bcl2-L-13

interaction (Murakawa et al., 2019). Therefore, our findings highlight a novel role of the Ulk1 complex in the regulation of amino acid-dependent mitochondrial fusion but the direct mechanism remains an open question.

### **4.32 Amino acid-dependent mitochondrial hyperfusion is autophagy-independent**

Autophagy is a self-degradative process that non-specifically sequesters cellular compartments to the lysosomes or specifically identifies damaged proteins, damaged organelles or foreign organisms, priming them for degradation (Okamoto et al., 2009, Losier et al., 2019). Acute amino acid starvation initiates a non-specific autophagy process to aid cell survival and maintain cellular homeostasis by differentially regulating MTORC1, AMPK and Ulk1 (Bujak et al., 2015, Ho et al., 2017). As shown here, this autophagy response can be exclusively abrogated in the presence of Q, L and R and are therefore identified as the main regulatory amino acids sensed.

During amino acid starvation, a cascade of signalling events take place whereby MTORC1 is inhibited and Ulk1 is activated. Here, Q, L and R-addback were sufficient to switch off autophagy as a result of activation of MTORC1, inhibition of Ulk1. This agrees with previous studies where QLR addback activates MTORC1, blocks Ulk1 and Atg13 translocation to autophagosomes, and also inhibits LC3B accumulation (Nwadike et al., 2018). Similar results were also reported in Duran et al. (2012) as the addition of Q and L activated MTORC1 by increasing E catabolism and enhancing alpha-ketoglutarate production. These suggest that apart from amino acid-dependent regulation of MTORC1, mitochondrial-dependent metabolites are also regulators of MTORC1.

To our surprise, autophagy-specific regulatory signals do not correlate with mitochondrial fusion. It was observed here that Q, L and R extensively induced mitochondrial hyperfusion despite reducing accumulation of p62 and LC3B-positive autophagosomes. QLR-induced mitochondrial hyperfusion was also functional in Atg5 KO autophagy-deficient cells. Therefore, this supports a model that mitochondria directly respond to the presence of QLR during amino acid starvation independently of the autophagy status.

### **4.3.3 Roles of PKA and Drp1 phosphorylation in amino acid-dependent mitochondrial fusion**

The cAMP-PKA signalling pathway has been previously demonstrated to be a key regulator of mitochondrial dynamics during complete amino acid starvation (Gomes et al., 2011a). We show here contrasting results that amino acid-dependent mitochondrial fusion can be largely independent of increased phosphorylation of Drp1 at S637. We also observed that there were no significant changes in Drp1 localization on mitochondria despite increased activity of PKA (from CREB phosphorylation levels) in amino acid-starved and QLR-stimulated cells. This subcellular localisation is consistent with low phosphorylation of Drp1 at S637 since phosphorylation at S637 has been reported to promote Drp1 displacement from mitochondria (Chang and Blackstone, 2007, Morita et al., 2017). We also show that complete amino acid starvation-induced fusion occurs independently of PKA because kinase inhibitor H89 did not show any effect on this response. Our findings, therefore, challenge the current model where PKA is activated and subsequently, Drp1 is phosphorylated at S637 (pro-fusion site) upon amino acid starvation (Gomes et al., 2011a, Rambold et al., 2011, Li et al., 2017). Our data suggest that complete amino acid starvation can stimulate mitochondrial fusion rather than an indirect effect due to inhibition of Drp1-mediated fission.

Complementary to this, we indeed found that Frsk led to strong phosphorylation of Drp1 S637 and increased mitochondrial size, entirely consistent with the PKA-Drp1 translocation model previously established in other studies (Chang and Blackstone, 2007, Cribbs and Strack, 2007). Despite the rapid and strong phosphorylation of Drp1 after Frsk, the level of mitochondrial fusion was lower relative to QLR addback-dependent mitochondrial hyperfusion. This suggests that other molecular events are responsible for amino acid-dependent mitochondrial fusion since patterns of Drp1-S637 phosphorylation did not correlate with mitochondrial hyperfusion. This notion is supported by the observation that H89 did not have a major effect on mitochondrial fusion after amino acid starvation or QLR supplementation when tested at a low dose to minimize off-target effects. Interestingly, H89 as a specific PKA inhibitor has been controversial and H89 has been shown to block multiple kinases (Davies et al., 2000, Limbutara et al., 2019). Nevertheless, our data indicate that QLR-dependent mitochondrial hyperfusion occurs independently of the PKA-Drp1 phosphorylation model.

### 4.3.3.1 The phosphorylation role of Drp1 is context-specific

The Drp1 phosphorylation sites are overall well conserved between multiple species (**Fig 4.25**). The differences in amino acid numbering relate to the range of Drp1 isoforms. For example, phospho Drp1 S600 of mouse isoform-b, mapped to the GTPase effector domain (GED), corresponds to S637 in human Drp1 Isoform-1. Similarly, the pro-fission phosphorylation site S579 corresponds to S616 in human Drp1 isoform-1. Interestingly, multiple kinases such as CDK1, ERK1/2, PKC $\delta$  and CDK5 have been shown to phosphorylate Drp1 at S616 (**Fig 4.25**) (Taguchi et al., 2007, Kashatus et al., 2015, Qi et al., 2011, Serasinghe et al., 2015, Cho et al., 2014, Strack et al., 2013, Prieto et al., 2016, Zaja et al., 2014). Similarly, in addition to PKA, CAMK1 $\alpha$ , ROCK1 and PIM1 have been shown to phosphorylate Drp1 at S637 (Han et al., 2008, Wang et al., 2012b, Din et al., 2013). While these two phosphorylation sites (S616 and S637) have been characterised by multiple studies, some controversy (as summarised below) exists in their respective roles for fission or fusion.

Contradicting functional roles from phosphorylation of Drp1 at S600, (human S637 (initially understood as pro-fusion)) have been reported. It was observed here that Frsk led to the phosphorylation of Drp1 at S637 hence promoting mitochondrial fusion. This finding correlates with studies identifying phosphorylation of S637 site as a pro-fusion mediator (Chang and Blackstone, 2007, Kim et al., 2011a, Gomes et al., 2011a). In contrast, phosphorylation of Drp1 at S600 by PKA has been reported to promote mitochondrial fragmentation and increased mitochondrial function for heat production and energy consumption in brown adipocytes (Wikstrom et al., 2014). Similarly, a pro-fission role for phosphorylation of S637 by CAMK1 $\alpha$  and ROCK1 has been reported in HeLa cells and mouse kidney glomeruli, in which phospho-Drp1 S637 promoted Drp1 localization to mitochondria (Han et al., 2008, Wang et al., 2012b). This was further supported by an independent study (Jhun et al., 2018a, Jhun et al., 2018b) suggesting that opposing functional consequences of Drp1 S637 phosphorylation may reflect specific cell type or stimulus-dependent responses.

These apparently contradicting observations may reflect complex or multiple roles of the Drp1 pathway. It has been proposed that Drp1 is phosphorylated at the cytoplasm thereby preventing its translocation to mitochondria or alternatively that Drp1 phosphorylation at the outer mitochondrial mitochondria to enhances translocation off mitochondria (Di Benedetto et al., 2017) (Ould Amer and Hebert-Chatelain, 2018).

Conversely, it has been reported that PKA-phosphorylation of Drp1 also can reduce GTPase activity of Drp1, thereby reducing fission without necessarily altering mitochondrial localisation (Merrill et al., 2011). Nevertheless, amino acid-dependent mitochondrial fusion observations here appear to avoid these controversies since we found low Drp1-S637 phosphorylation levels during starvation and amino acid addback in a range of normal and cancer cell lines.

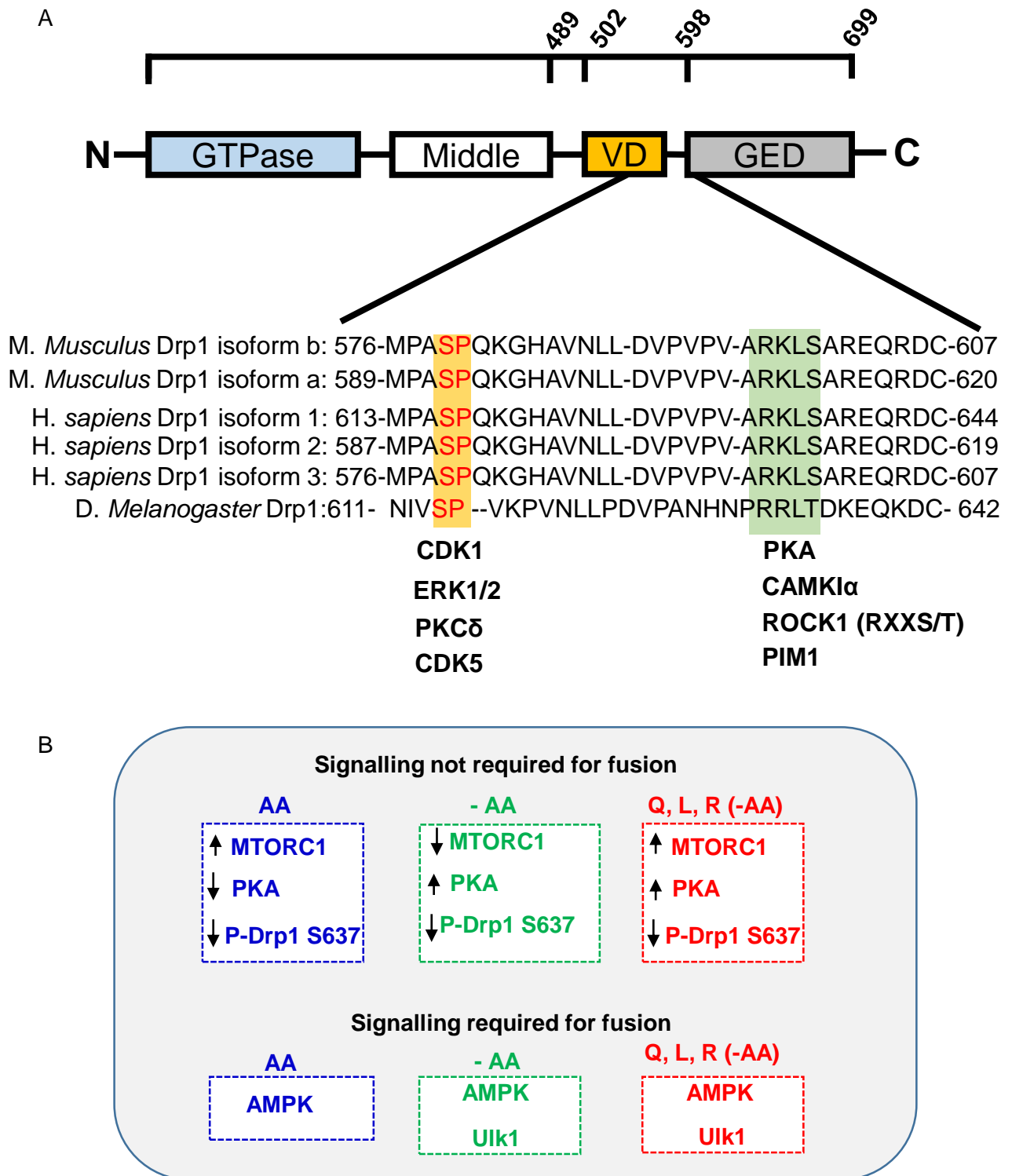


**Figure 4.25: Drp1 phosphorylation site conservation in different isoforms and summary model:** (A) Sequence alignment of the Drp1 isoforms due to splice variants of different species. Indicated are phosphorylation consensus sites of CDK1 (Annotated in red and shaded orange) and PKA consensus sequence (shaded green). Schematic shows the GTPase domain, middle domain, variable domain (VD) and GTPase effector domain (GED). (B) Chapter summary model of MTORC1, PKA and P-Drp1 S637, AMPK and Uik1 during amino acid-dependent mitochondrial fusion. The arrow indicates activity status (Increase or decrease)

### 4.3.3.2 PKA signalling is compartmentalised

PKA compartmentalisation may explain opposing PKA-dependent Drp1 phosphorylation roles during Frsk and amino acid-dependent mitochondrial fusion. Studies have shown that cAMP signalling is compartmentalised into multiple subcellular domains (Lefkimmiatis and Zaccolo, 2014, Torres-Quesada et al., 2017). This compartmentalization leads to differential regulation of cAMP-PKA-dependent substrates (Lefkimmiatis et al., 2013). Here, we observed that PKA can differentially phosphorylate CREB and Drp1 following amino acid starvation, QLR addback or Frsk. Speculatively, one possible explanation for this finding is that Frsk and amino acid starvation induce PKA activation at different cellular compartments. Differentially localised PKA can be directed via the action of phosphodiesterases (PDEs) which neutralise cAMP signals (Lomas and Zaccolo, 2014). Also, the localization of transmembrane ACs at the plasma membrane and outer mitochondrial membrane, in addition to soluble ACs at different sites (cytosol, nucleus and mitochondrial-matrix) can also direct differential cAMP-dependent pathways (Zippin et al., 2003, Acin-Perez et al., 2009).

Acin-Perez et al. (2009) reported that cAMP can be generated within mitochondria by sAC which leads to activation of PKA within mitochondria. Mitochondrial-generated cAMP was suggested to be a metabolic sensing mechanism that identifies changes in mitochondrial-generated ATP and ROS. Furthermore, fluorescence resonance energy transfer (FRET) reporter / cAMP studies revealed that Frsk induces cAMP at the outer mitochondrial membrane via transmembrane AC independent of GCPRs/AC route (Acin-Perez et al., 2011a, Burdyga et al., 2018). Burdyga et al. (2018) found that Frsk activates cAMP in the cytosol and outer mitochondrial membrane (OMM) but it has greater PKA-dependent phosphorylation at the OMM, including phosphorylation of Drp1. This suggests that Frsk activates PKA at the OMM leading to the phosphorylation of Drp1, but PKA does not appear to be activated at the OMM during amino acid starvation or QLR addback.

### **4.3.3.3 The role of phosphatases in amino acid-dependent mitochondrial hyperfusion**

Our phospho PKA substrate motif blot further indicates differential patterns in Frsk vs. amino acid-starved cells. This supports our hypothesis that Frsk and amino acid starvation have different downstream PKA signalling patterns. Apart from the possible roles of PDE and the sub-cellular localization of cAMP-PKA signalling, phosphatases can play a major role in differential PKA-regulation (Haj Slimane et al., 2014, Burdyga et al., 2018). Burdyga et al. (2018) reported that during physiological cAMP activation, cAMP levels in cytosol and OMM are mostly comparable but downstream PKA phosphorylation of target proteins greatly differ. It was proposed that this opposite observation in cAMP and PKA is as a result of local PP2A-dependent dephosphorylation (Burdyga et al., 2018). Frsk was reported to promote PKA activation at the outer mitochondrial membrane than in the cytosol. Cytosolic and OMM cAMP was measured by using soluble and OMM targeted- EPAC respectively. Similarly, PKA activity in the cytosol and at the OMM was measured using soluble and OMM-targeted FRET-based sensors respectively. This difference in PKA activation was concluded to be directed by reduced activity of PP2A at the outer mitochondrial membrane (Burdyga et al., 2018). Interestingly, inhibition of mitochondrial phosphatases increased the phosphorylation CREB by Frsk. This, therefore, suggests that mitochondrial phosphatases are activated during Frsk treatment, thereby, explaining the low phosphorylation of CREB by Frsk in our study.

Despite calcineurin being a direct phosphatase of Drp1-S637 (Cereghetti et al., 2008, Cribbs and Strack, 2007), inhibition of PP2A was proposed to be the major factor to enhance PKA-activity at the cytosol and outer mitochondrial membrane (Burdyga et al., 2018, Dickey and Strack, 2011). Therefore, PP2A is the proposed main phosphatase that drives lower PKA activity at the cytosol. Interestingly, amino acid starvation has been shown to lead to an increase in PP2A activity on Ulk1 (Wong et al., 2015). It is possible that this starvation-induced PP2A activity is responsible for the reduced PKA-dependent phosphorylation of Drp1-S637 we observed. Whether PP2A regulates the mitochondrial fusion via its activity on Ulk1 during amino acid-dependent mitochondrial fusion will need to be examined.

PGAM5 is another phosphatase that is strongly linked to the regulation of mitochondrial dynamics such as fusion, degradation and motility. PGAM5 dephosphorylates Drp1 at S637 during necrotic cell-death, leading to the activation of

Drp1 GTPase activity and mitochondrial fragmentation (Wang et al., 2012c). Interestingly, PGAM5 also dephosphorylates Ulk1-substrate FUNDC1 at Ser-13 to promote mitochondrial degradation during hypoxia (Chen et al., 2014, Liu et al., 2012, Sugo et al., 2018). In addition, PGAM5 enhances mitochondrial motility via Miro2 activity during stress induced by proteasome inhibition (O'Mealey et al., 2017). Interestingly, PGAM5 inhibition has been implicated in the pathogenesis of hereditary spastic paraplegia, a neurological disorder associated with (Receptor Expression-Enhancing Protein-1) REEP1 mutations (Beetz et al., 2008, Solowska and Baas, 2015, Züchner et al., 2006, Lavie et al., 2017). The inhibition of PGAM5 in hereditary spastic paraplegia is due to its reduced interaction with REEP1, which ultimately leads to hyperphosphorylation of Drp1-S637 (Lavie et al., 2017).

Localization of PGAM5 to mitochondria was dependent on Syntaxin-17 (Sugo et al., 2018), a protein that also regulates mitochondrial-ER contacts and mitochondrial remodelling (Arasaki et al., 2018, Arasaki et al., 2015, Arasaki et al., 2017). It was reported that the depletion of Syntaxin-17 disrupts PGAM5 localization to outer mitochondrial membrane thereby enhancing phospho-Drp1 S637 and mitochondrial fusion (Sugo et al., 2018). Syntaxin-17 also regulates autophagy and autophagosome maturation from the ER-mitochondrial contact site (Itakura et al., 2012, Arasaki et al., 2018, Hamasaki et al., 2013). Interestingly, amino acid starvation abrogates the interaction of Syntaxin-17 with Drp1 but increases its affinity with Atg14L (Arasaki et al., 2018). Although it is suggested that the dissociation of Syntaxin-17 from Drp1 during starvation induces the phosphorylation of Drp1 at S637, it is not clear whether it is involved in the reduced activity of PGAM5 or the enhanced activity of PKA. While this evidence strongly implicates PGAM5 in the regulation of mitochondrial dynamics, amino acid-dependent mitochondrial hyperfusion appears to occur independently of PGAM5/syntaxin 17 mechanism since changes in phospho Drp1-S637 were not observed. Therefore, this suggests multiple independent mechanisms.

Our findings clearly show that amino acid-dependent mitochondrial fusion occurs independently of phospho Drp1-S637. Taken together, it will be interesting to know whether amino acid starvation or QLR-addback will lead to the phosphorylation of Drp1 at S637 upon phosphatase inhibition. Also, whether cAMP regulates PKA activation in the cytosol or on OMM during amino acid-dependent mitochondrial-hyperfusion will need to be assessed.

#### 4.3.4 Conclusion

In summary (**Fig 4.25B**), we show here that amino acid-dependent mitochondrial hyperfusion occurs independent of MTORC1 but requires AMPK in part. Amino acid-dependent mitochondrial hyperfusion required the Ulk1 complex. We also show that QLR addback sufficiently block autophagy via its inhibition of LC3B and p62/SQSTM positive puncta accumulation but QLR-addback dependent hyperfusion occurred independently of autophagy. The inhibition of PKA during starvation did not block fusion but had a mild effect on QLR-dependent mitochondrial hyperfusion. Interestingly, we identified a differential regulation of PKA-targets which revealed that PKA-phosphorylation of Drp1 S637 is not the major cue driving amino acid-dependent mitochondrial hyperfusion. This also correlated with unaltered Drp1 co-localization with mitochondria indicating that mitochondria can hyperfuse even when Drp1 is mitochondrial-bounded. Our findings support an intrinsic amino acid sensing mechanism within mitochondria which connects mitochondrial dynamics to the presence of regulatory amino acids.

## **Chapter 5**

### **Roles of amino acid-dependent mitochondrial hyperfusion in regulating cellular metabolism**

## 5.1 Introduction

Mitochondria are central hubs for cellular metabolism, hosting a complex network of biochemical reactions involved in REDOX balance, cellular energetics, nucleotide synthesis, lipid metabolism and amino acid metabolism (Spinelli and Haigis, 2018). Relevant to this thesis here, mitochondria are specialised in the processing of carbon and nitrogen backbones of amino acids to metabolic intermediates required in the Krebs cycle (Wang et al., 2019b, Coloff et al., 2016, Lane and Fan, 2015, Hosios et al., 2016). Despite the intimate role of mitochondria in cellular metabolism, how mitochondrial dynamics regulate cellular metabolism is not yet clear.

### 5.1.1 Mitochondria dynamics are regulators of cellular metabolism

Mitochondria have distinct roles in regulating cellular metabolism. Within mitochondria, ROS is produced normally as a by-product of cellular metabolism. Due to the roles of ROS in the control of cell death, apoptosis and tumorigenesis, mitochondria thereby regulate levels of ROS to promote cellular homeostasis (Schieber and Chandel, 2014). One mechanism involves the synthesis of antioxidants such as Nicotinamide adenine dinucleotide-hydrogen (NADH) and glutathione (GSH) (which is synthesized from glutamate, cysteine and glycine) (Garcia et al., 2010, Korge et al., 2015). Therefore, the synthesis of these antioxidants requires sufficient levels of amino acids. On the other hand, another mechanism involves changes in mitochondrial fusion and fission to regulate ROS synthesis during nutrient-dependent stress. For example, it has been shown that high glucose availability increases ROS and oxidative stress as a result of enhanced mitochondrial fragmentation (Yu et al., 2006). Conversely, mitochondrial fusion has been shown to prevent oxidative stress by ameliorating metabolic-induced stress via the increase in Mfn1 deacetylation (Lee et al., 2014). These studies indicate that mechanisms of mitochondrial dynamics are able to mitigate oxidative stress and maintain metabolic homeostasis.

In the previous chapter, we observed that amino acid-dependent mitochondrial hyperfusion requires Ulk1 signalling. Interestingly, other studies have shown that the Ulk1 signalling pathway regulates mitochondrial processes such as mitophagy and mtDNA maintenance (Webster et al., 2014, Cogliati et al., 2016). The disruption of these processes promotes the accumulation of dysfunctional mitochondria which is implicated in the pathogenesis of metabolic disorders, age-related disorders and ageing (Srivastava, 2017). The mitochondria-ageing model suggests that there is a

correlation between mitochondrial fragmentation, reduced metabolic rate and poor ageing (Wai et al., 2015, Guo et al., 2013, Disatnik et al., 2013, Srivastava, 2017). Therefore, it has been suggested that cells undergoing mitochondrial hyperfusion have a greater metabolic rate. For example, it has been shown that mitochondrial fragmentation is prominent in aged rat (Latorre-Pellicer et al., 2016). These authors also reported that there is an age-dependent increase and reduction in the levels of Drp1 and Opa1 respectively. Similarly, Chaudhari and Kipreos (2017) suggested that mitochondrial fusion is critical in aiding the survival of aged animals which is associated with an increase in mitochondrial metabolism. Mitochondrial fusion also ameliorates ageing-induced neuropathy in Purkinje cells that have reduced E.T.C. activity due to the inability of mitochondria to fuse effectively (Chen et al., 2007). These studies, therefore, suggest that mitochondrial fusion can be targeted to ameliorate age-related depletion of cellular metabolism

Mitochondria are key regulators of amino acid catabolism and nucleotide metabolism (Liesa and Shirihai, 2013, Wai and Langer, 2016). Studies have demonstrated that amino acid starvation led to reduction in the synthesis of purine nucleotides (Boss, 1984). Interestingly, the cyclic nucleotide cAMP has been shown to increase upon amino acid starvation (Gomes et al., 2011b, Gomes et al., 2011a). It has also been proposed that fused mitochondria generate more ATP relative to fragmented mitochondria due to the increase in electron coupling and ATPase activity (Gomes et al., 2011a, Cogliati et al., 2013). While ATP and cAMP can be synthesized in the cytosol and mitochondria, how mitochondria generate these nucleotides when their precursors are limiting remain unclear.

## **5.1.2 Metabolic and physiologic significance of mitochondrial dynamics**

### **5.1.2.1 OXPHOS-dependent regulation of mitochondrial hyperfusion**

Mitochondrial dynamics have been shown to be interdependent on energy metabolism. For example, it has been demonstrated in mouse models that muscle fibres that are highly dependent on OXPHOS have increased mitochondrial fusion, in contrast to fibres dependent on glycolysis with fragmented mitochondria (Mishra et al., 2015). In this study, it was shown that glycolytic fast-twitch fibres such as extensor digitorum longus (EDL) normally have low OXPHOS activity with small and non-connected mitochondria. Interestingly, when EDL muscles were isolated and cultured in acetoacetate-containing media that force them to switch to OXPHOS, an increase

in oxygen consumption rate (OCR) was accompanied with mitochondrial fusion. Similarly, MEF cultured in galactose or acetoacetate-containing media also have high OCR with enhanced mitochondrial fusion relative to MEF maintained in glucose-containing media (Mishra et al., 2014). The significance of OXPHOS-dependent mitochondrial fusion has also been demonstrated in RPE1 cells expressing YFP-Parkin required for CCCP-induced mitophagy (MacVicar and Lane, 2014). It was shown that mitochondrial fusion is stimulated in YFP-Parkin RPE1 cells cultured in galactose media to escape CCCP-induced mitophagy. In this study, YFP-Parkin RPE1 cells cultured in galactose-containing media have higher OCR relative to those cultured in glucose-containing media. Mechanistically, CCCP treatment of YFP-Parkin RPE1 cells cultured in either glucose or galactose media led to the recruitment of Parkin, p62 and LC3 to mitochondria, but mitochondrial incorporation into autophagosome was impaired in galactose containing media. It was shown that mitophagy impairment in galactose media occurred due to the inability of CCCP-treated YFP-Parkin RPE1 cells to degrade 40-kDa OMA1 required for Opa1 processing and mitochondrial fission. These studies, therefore, indicate that mitochondrial fusion can be regulated by mitochondrial energy status.

Studies have also shown that mitochondrial hyperfusion regulates immune response specifically in memory T cells through metabolic reprogramming to favour OXPHOS (Buck et al., 2016). It was shown that memory T cells generated from naïve T cells after infection (with *Listeria monocytogenes* ovalbumin) have increased OCR accompanied with fused mitochondrial phenotype relative to effector T cells with low OCR and smaller mitochondria. In Buck et al. (2016), Opa1 was knocked down in T cells by crossing Opa1 floxed mice with OT-I CD4 Cre transgenic mice. It was demonstrated that upon infection, Opa1 deficient naïve T cells differentiated into effector T cells but memory T cells generation was impaired due to lack of mitochondrial fusion. Interestingly, it was shown that the activation of mitochondrial fusion with M1 and Mdivi-1 (fusion inducing drugs (Wang et al., 2012a, Cassidy-Stone et al., 2008)) or by virus-mediated Opa1 overexpression in IL-2 effector T cells increased OCR and OXPHOS. Upon mitochondrial fusion, IL-2 effector T cells have the same metabolic properties as IL-15 memory T cells. Importantly, it was also demonstrated that fusion-activated IL-2 effector T cells are more competent in preventing tumour growth. Overall, it was demonstrated in Buck et al. (2016) that cells undergoing mitochondrial fusion are metabolically more efficient and the increase in both fusion and metabolism is required for differentiation and cell-specific functions.

Furthermore, mitochondrial dynamics is also altered to favour OXPHOS and energy production during the exclusive utilization of amino acid Q as an energy source in HeLa cells (Rossignol et al., 2004). It has been demonstrated that mitochondrial hyperfusion tightens the cristae leading to closely associated E.T.C. complexes that are more efficient in OXPHOS (Patten et al., 2014). This promotes the rate of NADH production from the Krebs cycle and also enhance NADH utilization as electrons in complex I of the E.T.C. (Buck et al., 2016). Since amino acids are critical upstream of OXPHOS, these studies highlight the importance of amino acids and mitochondrial fusion in the maintenance of energy metabolism.

#### **5.1.2.2 Amino acid regulates cell fate and cell survival**

The distinct roles of amino acid in cellular metabolism serve as mechanisms that can be exploited in the pathogenesis of cancer. For example, it has been demonstrated that R withdrawal or blocking R metabolism can reduce tumour mass (Poillet-Perez et al., 2018). These authors demonstrated that the deletion of Atg5 or Atg7 in tumour cells blocked autophagy and reduced tumour growth. Interestingly, reduction of tumour growth was shown to occur due to the inability of autophagy-deficient tumour cells to restore serum R levels. Similarly, it has been shown that the dietary restriction of serine and glycine prevents glycolytic-ATP synthesis and tumour growth (Maddocks et al., 2017, Maddocks et al., 2016, Maddocks et al., 2013). In these studies, it was demonstrated that serine starvation promoted *de novo* serine synthesis which enhanced OXPHOS and promoted Krebs cycle flux. Interestingly, it was also reported that lymphoma tumour mouse models that were fed serine- and glycine-free chow survived longer than mouse fed control chow-diet with amino acids or protein source. These studies demonstrate that amino acid availability can dramatically alter cancer cell survival and tumour progression. Further studies are therefore justified in order to understand the potential role of mitochondrial dynamics in the context of amino acid-dependent metabolism (Wai and Langer, 2016).

#### **5.1.3 Metabolomics is a tool to study cellular metabolism**

Metabolomics has benefitted from improved instrument sensitivity over the last decade to increase reproducibility and become a more feasible tool to routinely study mitochondrial and cellular metabolism (Chen et al., 2016b, Chen et al., 2017). This involves the use of liquid chromatography and tandem mass spectrometry (LC/MS/MS) to identify metabolites involved in both cellular and mitochondrial metabolism based on their polarities, masses, retention times and charges. A spectral bin is generated and screened to known metabolite bins in a comprehensive database

to identify the metabolite pool. Importantly, the use of metabolomics to identify and quantify metabolites can involve two final data analysis approaches (Bowen and Northen, 2010). A targeted approach identifies and analyses metabolites in known specific metabolic pathways of interest. Untargeted approaches identify all metabolic changes in an unbiased manner occurring in a diseased state. Interestingly, metabolomics has been used to identify changes in the Krebs cycle, amino acid metabolism and urea cycle in bipolar disorder (Yoshimi et al., 2016). Metabolomics has also been used to study changes in stress conditions such as autophagy, therefore making it relevant for this project (Shen et al., 2016, Weckmann et al., 2018, Johnson et al., 2018a).

### **Chapter Aims**

Due to the prominent roles of mitochondrial dynamics in modulating cellular metabolism, cancer and ageing, the aim of this chapter was to explore cellular metabolic profiles following amino acid starvation and QLR-addback. Since mitochondrial hyperfusion has generally been associated with increased metabolism, we hypothesised that QLR-dependent hyperfusion increases mitochondrial energetic and biosynthetic activity. To investigate this hypothesis, we used LC/MS/MS to carry out the following:

1. Identify the metabolic profile of cells treated with amino acid starvation media plus/minus QLR addback
2. To study mitochondrial dynamics and cellular metabolism in fumarase deficient cells that have dysregulated Krebs cycle so as to identify the relationship between metabolism and amino acid-dependent mitochondrial hyperfusion
3. Identify the metabolic significance of amino acid-dependent mitochondrial hyperfusion by studying cellular metabolism in Mfn1 KO cells that are unable to undergo hyperfusion

## 5.2 Results

### 5.2.1 Metabolic profile of cells undergoing amino acid-dependent mitochondrial hyperfusion

Studies have suggested that mitochondrial dynamics and the rate of cellular metabolism are closely linked (Mishra and Chan, 2016, Schrepfer and Scorrano, 2016, Wai and Langer, 2016, Liesa and Shirihai, 2013). We established in the previous chapters that supplementation of Q, L and R into amino acid starvation conditions led to extensive mitochondrial hyperfusion in the treated cells. Interestingly, in addition to regulatory roles in the amino acid sensing pathway, Q, L and R also can be transformed into important intermediate metabolites of the Krebs cycle, urea cycle, ammonia synthesis, bio-energetics and nucleotide synthesis (Spinelli et al., 2017, Lane and Fan, 2015). Therefore, we were interested in studying if QLR-addback, mitochondrial hyperfusion and cell metabolism could be interconnected. We determined the metabolic profile of cells treated to QLR-addback using LC/MS/MS.

We showed earlier that QLR-dependent mitochondrial hyperfusion occurs regardless of glucose availability (Chapter-3, Fig 3.5). Since glucose metabolism is the more prevalent carbon and energy source in cultured mammalian cells, we reasoned that the flux through this pathway would mask our ability to detect patterns of amino acid metabolism (Szablewski, 2011). Therefore, we set up metabolomics experiment in the absence of glucose to limit contributions of glycolysis.

We tested 4 nutrient conditions on 4T1 cells: 1) Cells maintained in full-nutrients (containing glucose and amino acids) as controls; 2) Cells starved of glucose alone (with amino acids); 3) Cells incubated in a modified PBS buffer (with no glucose and amino acids) as double starvation media; and 4) QLR supplemented into PBS double starvation media. All four treatment groups were supplemented with 10% dialysed FBS. After 4-hours starvation, cells were lysed in 80/20% (methanol/water) to extract metabolites for analysis on LC/MS/MS.

Raw data from LC/MS/MS were converted into mzXML files and peak lists were generated for metabolite identification (refer to Methods for details). The list of named metabolites with their peak intensities was uploaded into Metaboanalyst (Chong et al., 2018) for multivariate analysis to assess the quality and experimental noise of the dataset. Principal component analysis (PCA) was used to estimate the clustering between replicates within each treatment and to explore data separation between

treatment groups (Ivosev et al., 2008, Kirwan et al., 2012). PCA specifically separate that data within each sample groups into two dimensions to show differences and similarities between samples within a group of data.

PCA demonstrated clear clustering between the three replicates of the controls (**Fig 5.1A**). Similar clustering between replicates was observed in cells subjected to glucose starvation, and QLR-supplemented double (glucose and amino acid) starvation media. However, replicates of cells treated with amino acid starvation (blue points) were the least well clustered. PCA also showed that metabolites across the four treatment groups were well separated. However, it was observed that cells treated with double (glucose and amino acid) starvation media versus QLR-supplemented double (glucose and amino acid) starvation media had overlapping PCA points. This analysis suggests that the overall metabolomics workflow is robust. Individual samples within treatment groups show reproducibility and different nutrient starvations (including QLR addback) produce clear shifts in metabolite profiles. In this set of data, the double starved cell samples showed relatively higher variability.

PCA does not supervise the classification between treatments groups (Kirwan et al., 2012). In contrast, partial least squares-discriminant analysis (PLS-DA) specifically classifies and analyses differences between the treatment groups. Therefore, PLS-DA detects differences between groups relative to differences within groups in a three-dimensional model. The combined use of PLS-DA is recommended when PCA illustrates a clustering pattern (Alamri et al., 2019). PLS-DA component scores were used to analyse the separation points between treatment groups observed in Fig 5.1A to assess the robustness of the data. PLS-DA corroborated PCA data separation as all the four treatment groups were individually well clustered and they have separate data points, further indicating that the dataset is sound (**Fig 5.1B**).

Metabolomic analyses generally generate large unbiased profiles of metabolites across all active cellular pathways (Lee et al., 2019). Due to the complex global view of these metabolites, strategized analytical approaches are required to robustly identify top and most significantly altered metabolites. To identify pathways containing the most significantly-altered metabolites between cells treated with double (glucose and amino acid) starvation versus QLR-supplementation, overrepresentation analysis (ORA) was used. ORA demonstrates whether a set of specific metabolites in a particular pathway are more represented within a list of random metabolites (Chagoyen and Pazos, 2013). A subset list of metabolites was first generated with significant differences ( $p < 0.05$  based on t-test) comparing QLR supplementation vs

double (glucose and amino acid) starved cells. This subset of significantly altered metabolites was then uploaded into Metaboanalyst for ORA (refer to Methods).

ORA indicated at least 20 pathways that were significantly enriched in the subset of metabolites affected by QLR supplementation (relative to double starved cells) (**Fig 5.2A**). More specifically, ORA analysis highlighted that metabolites of the urea cycle, ammonia recycling, R/P amino acid metabolism are the most significantly enriched between these 2 conditions.

Pathway analysis is also used to measure the importance of metabolites by analysing the degree of centrality and connection of metabolites within a pathway library (Xia and Wishart, 2011, Xia and Wishart, 2010). Pathway analysis on the subset of significant metabolites (used above for ORA) with the biological pathway library Small Molecule Pathway Database (SMPDB) confirmed that the urea cycle, ammonia cycle and R/P metabolism are the most significantly altered pathways between QLR-supplemented vs double starvation conditions (**Fig 5.2B**).

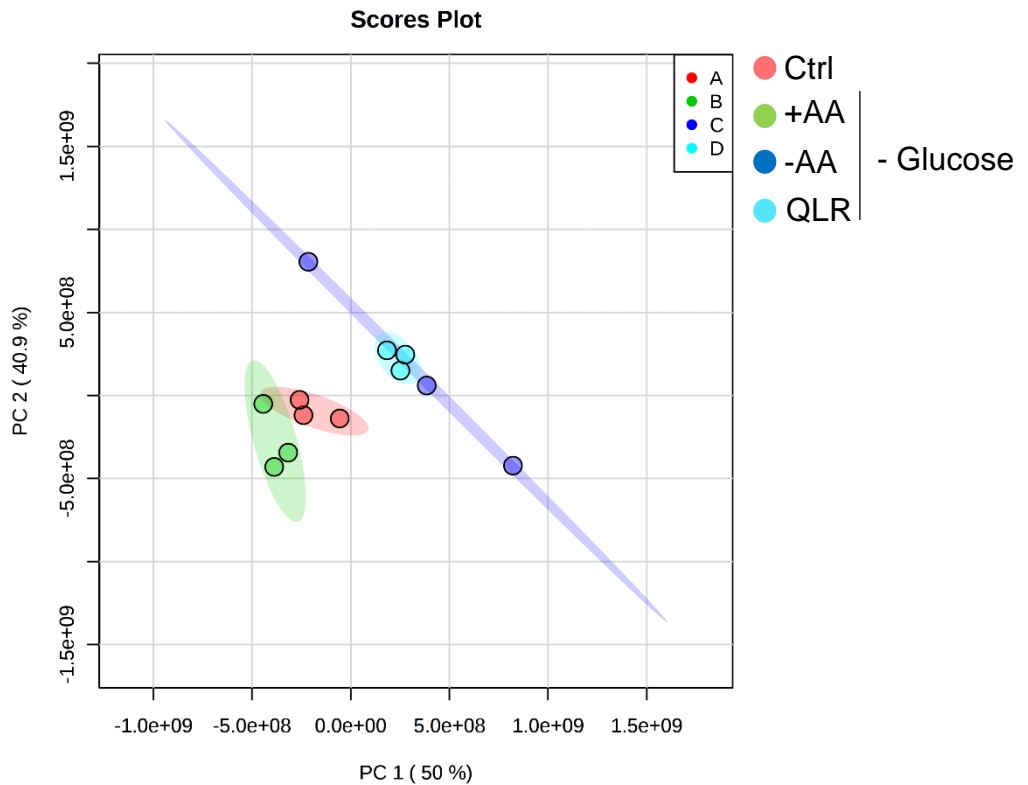
This identification of significantly altered pathways was associated with the following parameter readouts (**Table 5.1**): 1) total number of metabolites in the pathway (Total); 2) number of metabolites in the uploaded list that match metabolites in the pathway (Hits); 3) p-value of the enrichment analysis (Raw p); 4) p-value adjusted using the false discovery rate (FDR); and 5) Pathway impact value calculated from pathway topology analysis (as cumulative percentage from matched metabolite nodes - maximum of 1 (indicating 100% importance)). FDR is the recommended measure of significance because it ensures fewer false-positive pathways and significance is set at  $< 0.05$  (Benjamini and Hochberg, 1995, Drusian et al., 2018, Cheng et al., 2018).

The urea cycle, ammonia cycle and R/P metabolism presented the lowest FDR at 0.004 respectively as shown in **Table 5.1**. It was observed that 9 metabolites in the significant metabolite list were among the 25 metabolites involved in the urea cycle. The pathway impact of these 9 metabolites suggested that they have 49% importance in the urea cycle. Similarly, there were also 9 hits in the 27 metabolites of ammonia recycling pathway with importance of 38%. For R/P metabolism, there were 12 hits in the 47 metabolites and these hits had 30% importance.

Overall, this initial analysis establishes a robust workflow that has allowed us to demonstrate significant changes in the metabolic profiles of cells treated with different starvation conditions including QLR-addback. Satisfyingly, this analysis identified

amino acid-dependent pathways (ammonia cycle, urea and R metabolism) as the most prominent altered metabolites when QLR were supplemented back into double starvation media. Therefore, this suggests that QLR-addback was able to immediately re-enter several amino acid-dependent metabolic pathways and further highlight granular details on the most affected pathways.

A



B

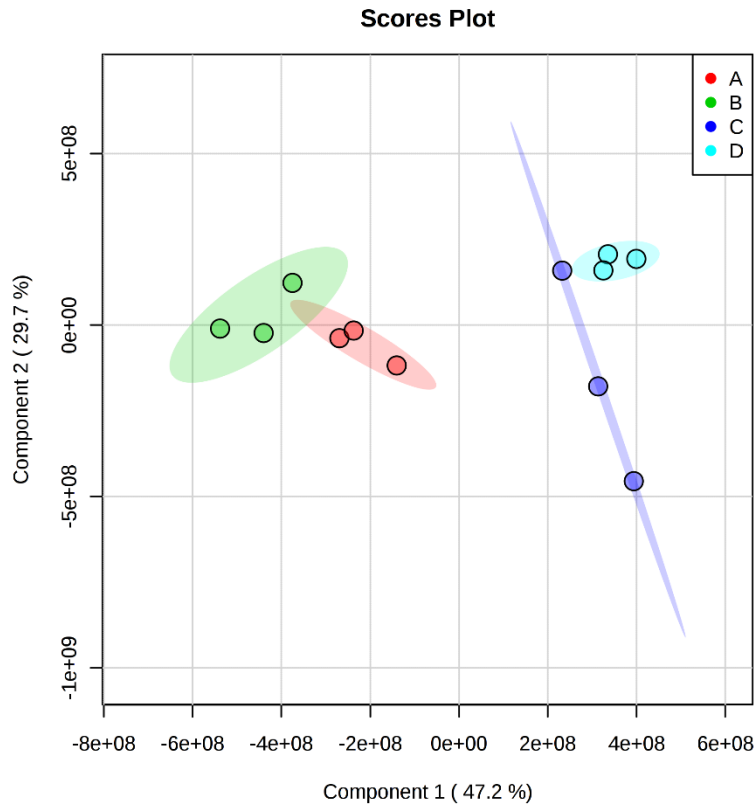
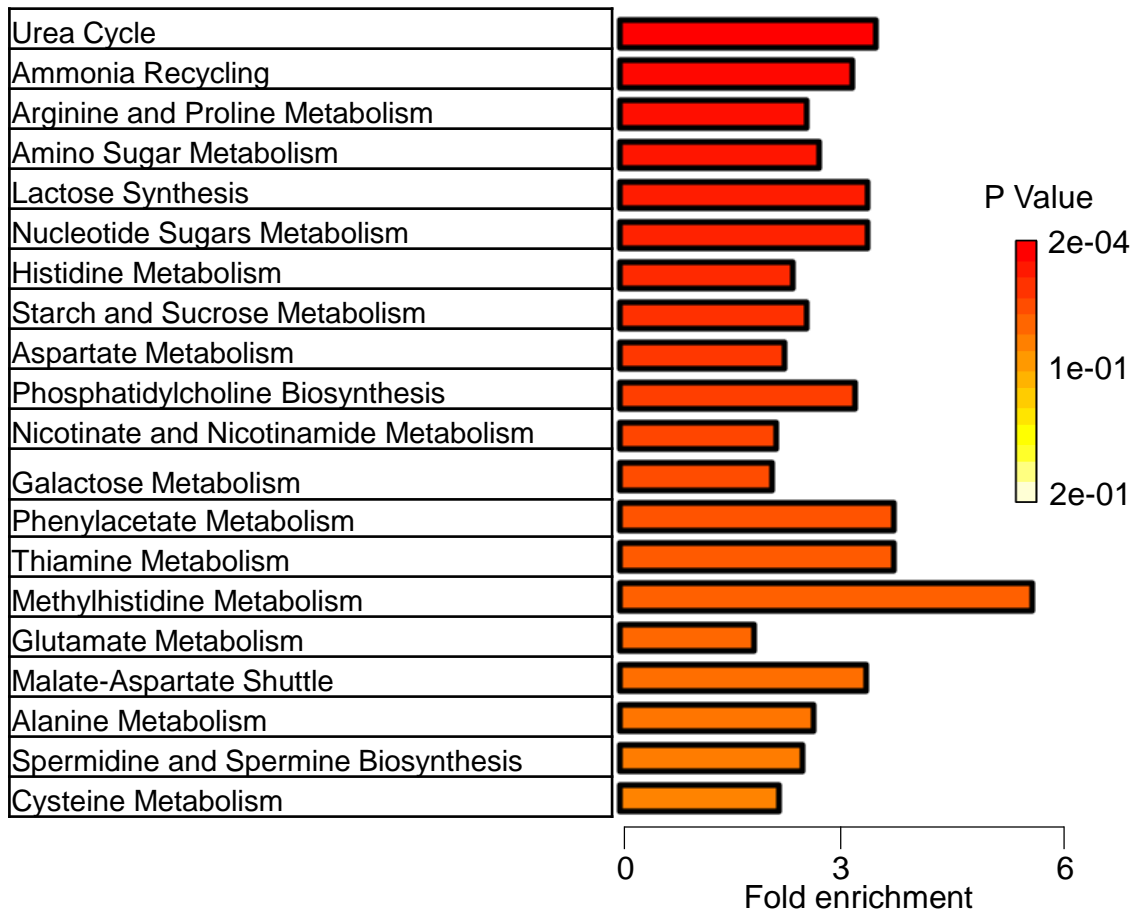


**Figure 5.1: Metabolomics LC-MS/MS analysis of 4T1 cells after amino acid and glucose starvation (-AA), amino acid and glucose starvation with QLR supplementation (QLR).** 4T1 cells were maintained in full media (Ctrl), starved of glucose alone (+AA, -glucose), starved of all amino acids and glucose (-AA, - glucose) or starved of amino acid and glucose but supplemented with QLR (QLR, - glucose) for 4h. Starvation media conditions also contained 10% dialysed FBS. A) Principal-Component Analysis (PCA) score plot showing the separation between treatment groups. B) Partial Least Squares- Discriminant Analysis (PLS-DA) showing the supervised classification of the treatment groups. N=3 independent biological replicates.

A



B

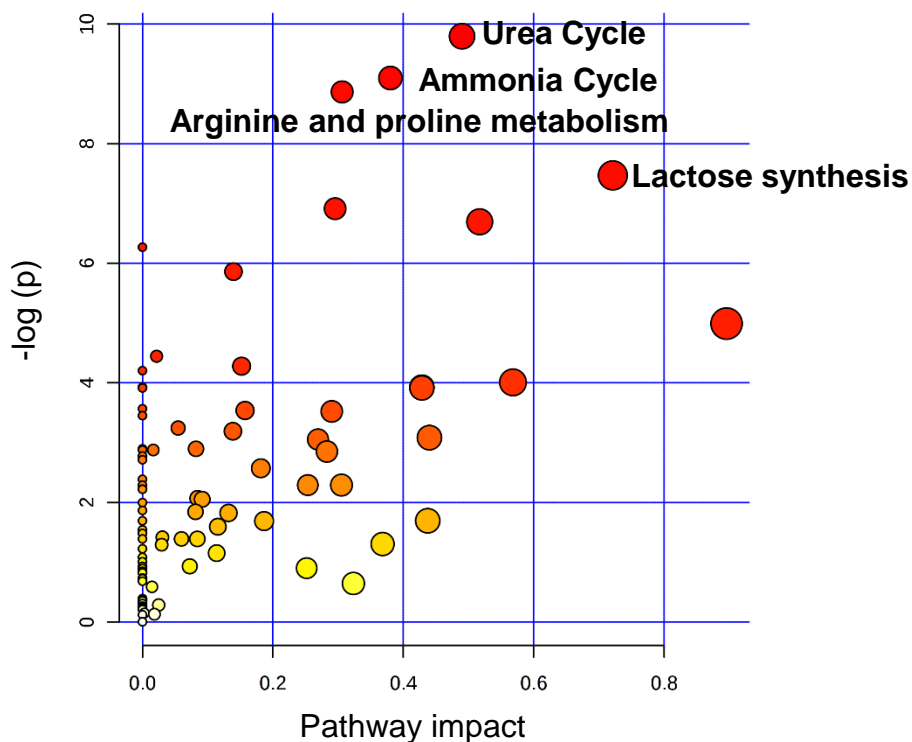


**Figure 5.2: Pathway analysis of metabolites with significant changes after amino acid and glucose starvation relative to amino acid and glucose starvation with QLR supplementation in 4T1 cells.** (A) Over-representation analysis (ORA) showing the top 20 enriched pathways based on significantly ( $p < 0.05$ ) altered metabolites after QLR supplementation relative to AA starvation. Ranked according to significant p values (Top  $\rightarrow$  Down, Darkest shade most significant) (B) Pathway analysis indicating the most relevant pathways. The p values (from pathway enrichment analysis) is plotted on the Y-axis against the impact values (from pathway topology analysis) on the X-axis. The darker the shade the greater the significance and the larger the circle, the more the metabolites involved in the pathway. Starvation media conditions also contained 10% dialysed FBS.

**Table 5.1: Detailed results of pathway analysis of relevant pathways (P < 0.05) following amino acid starvation with QLR supplementation relative to amino acid and glucose starvation in 4T1 cells.** Total: total number of metabolites in the pathway; the hits indicate the matched number from the analysed data; Raw p signifies the original P value calculated from the enrichment analysis; FDR is the adjusted p value using the false discovery rate; the impact represents the pathway impact value calculated from the topology analysis.

Pathway	Total	Hits	Raw p	FDR	Impact
Urea Cycle	25	9	5.57E-05	0.004658	0.49012
Ammonia Recycling	27	9	0.000112	0.004658	0.38031
Arginine and Proline Metabolism	47	12	0.000141	0.004658	0.30624
Lactose Synthesis	15	6	0.00057	0.014114	0.72143
Histidine Metabolism	35	9	0.000995	0.019701	0.29545
Nucleotide Sugars Metabolism	17	6	0.001239	0.020444	0.51724
Amino Sugar Metabolism	31	8	0.001895	0.026804	0
Starch and Sucrose Metabolism	26	7	0.002851	0.035277	0.13959
Aspartate Metabolism	30	7	0.0068	0.074796	0.89583
Galactose Metabolism	33	7	0.011742	0.11617	0.021739
Nicotinate and Nicotinamide Metabolism	34	7	0.013858	0.11617	0.15203
Alanine Metabolism	13	4	0.014947	0.11617	0
Glutamate Metabolism	44	8	0.01817	0.11617	0.56822
Phosphatidylcholine Biosynthesis	14	4	0.019687	0.11617	0
Spermidine and Spermine Biosynthesis	14	4	0.019687	0.11617	0.42857
Phenylacetate Metabolism	8	3	0.019949	0.11617	0
Malate-Aspartate Shuttle	8	3	0.019949	0.11617	0.42857
Thiamine Metabolism	9	3	0.02824	0.14617	0
Purine Metabolism	66	10	0.029084	0.14617	0.15733
Cysteine Metabolism	23	5	0.02953	0.14617	0.29032
Ethanol Degradation	16	4	0.031696	0.14942	0
Butyrate Metabolism	17	4	0.039012	0.16792	0.054688
Mitochondrial Beta-Oxidation of Long Chain Saturated Fatty Acids	25	5	0.041155	0.16977	0.1387
Pyrimidine Metabolism	52	8	0.045806	0.17979	0.44013
Mitochondrial Beta-Oxidation of Short Chain Saturated Fatty Acids	18	4	0.047218	0.17979	0.26923

### 5.2.1.1 Confirmation of glucose starvation metabolic profile

This initial metabolomics experiment was performed in starvation media lacking glucose (to allow us to detect metabolic re-fuelling via QLR-addback). To further confirm the robustness of our metabolic workflow, we first surveyed the effects of glucose starvation on metabolites of glycolysis.

Glycolysis begins with the conversion of glucose to glucose-6-phosphate and further biochemical intermediates leading to the formation of pyruvate (Chaudhry and Varacallo, 2018). It was observed that the deprivation of glucose alone reduced the peak intensity of glucose-6-phosphate by at least 70% relative to the control under full nutrients (**Fig 5.3A**). Similarly, double starvation of glucose and amino acids or QLR-supplementation into double starvation media led to 60% reduction in glucose-6-phosphate relative to the full nutrient control.

As expected, the downstream metabolite of glucose-6-phosphate (i.e. fructose-1,6-phosphate) was totally depleted in all 3 glucose-starvation conditions, regardless of amino acid or QLR-addback conditions (**Fig 5.3B**).

Studies have also shown that glucose-6-phosphate enters the pentose phosphate pathway (PPP) where it is oxidized to ribose-5-phosphate (Berg et al., 2002b). Ribose-5-phosphate is used for the synthesis of nucleotides in combination with Q which serves as the primary nitrogen donor (Tardito et al., 2015). Interestingly, it was observed that glucose starvation alone did not alter the levels of ribose-5-phosphate relative to control cells (**Fig 5.3C**). In contrast, double amino acid and glucose starvation led to a clear increase in ribose-5-phosphate (by 10-fold) relative to cells starved of glucose alone. This change suggests that cells lacking amino acids accumulate ribose-5-phosphate, possibly due to lack of Q. Consistent with this idea, QLR-addback into the starvation media reversed the accumulation of ribose-5-phosphate (by 20-fold relative to cells with double starvation). Therefore, QLR addback can lead to dramatic effects on intermediates in the PPP.

During glycolysis, the main net metabolic result is the conversion of glucose to pyruvate. Pyruvate is catabolised through oxidative decarboxylation by pyruvate dehydrogenase into acetyl-CoA, which serves as a substrate to generate citrate in the Krebs cycle (Lee et al., 2011). Therefore, acetyl-CoA levels should reduce upon glucose starvation. It was observed that glucose starvation alone led to a mild reduction (insignificant) in acetyl-CoA levels relative to the full nutrient condition control (**Fig 5.3D**). Double (glucose and amino acid) starvation led to a further

reduction in acetyl-CoA levels (resulting in 50% relative to the full nutrient control). In contrast, QLR supplementation into double starvation media restored acetyl-CoA levels to similar levels in cells treated with glucose starvation media (red bar) (approximately 2-fold increase relative to cells in double starvation (green vs. blue bars). These changes suggest that amino acids QLR are able to be metabolized to generate acetyl-CoA during other amino acid starvation conditions.

Overall, this experiment shows that upon glucose starvation, glycolysis is reduced to background levels (as expected) but acetyl-CoA levels are maintained due to amino acid metabolism. These data also show that amino acid metabolism remained generally functional despite reduction in glycolytic metabolism.

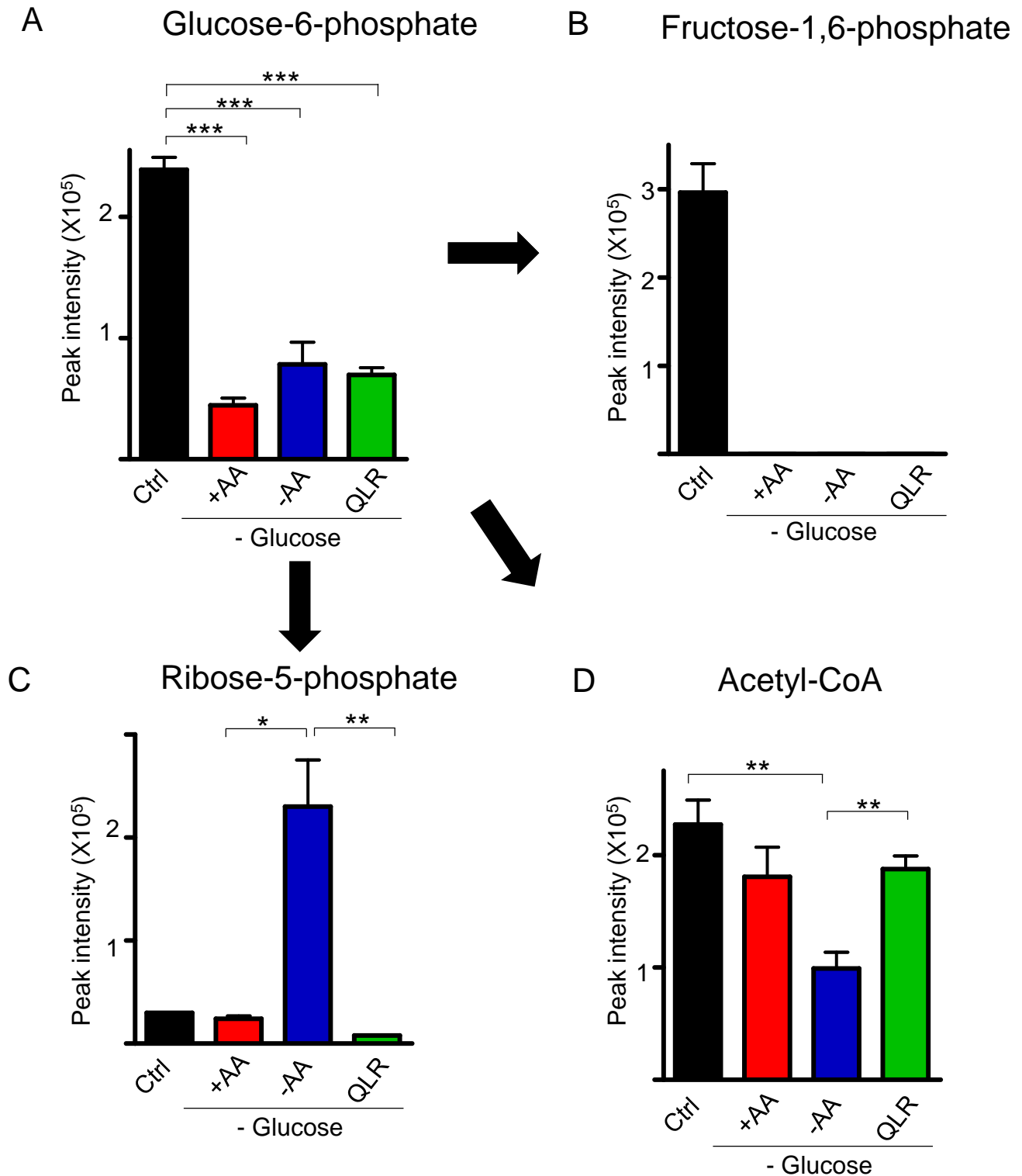


**Figure 5.3: Metabolic changes due to glucose starvation.** 4T1 cells were maintained in full media (Ctrl), starved of glucose alone (+AA, -glucose), starved of all amino acid and glucose (-AA, - glucose) or starved of amino acid and glucose but supplemented with QLR (QLR, - glucose) for 4h. Starvation media conditions also contained 10% dialysed FBS. Bar graphs show the mean peak intensity of (A) Glucose-6-phosphate (B) fructose-1,6-phosphate (C) Ribose-5-phosphate (D) Acetyl-CoA. N=3 independent biological replicates. \* represents  $p < 0.05$ , \*\* ( $p < 0.01$ ), \*\*\* ( $p < 0.001$ ).

### 5.2.1.2 QLR-addback increases amino acid metabolism.

ORA and pathway analysis in Fig 5.2 revealed that metabolites of the urea cycle, ammonia recycling, R and P metabolism were the most significantly altered following QLR supplementation into double starvation media. These indicate that QLR directly feed into these pathways through amino acid metabolism. Therefore, we further analysed the effects of QLR-supplementation into double starvation media by focussing on amino acid metabolism pathways.

Here, we identified metabolites using an Excel macro library database containing metabolite mass data from the human metabolome, KEGG, Lipidmaps, MetaCyc and Metlin databases (Creek et al., 2012) (see Methods for details). This Excel macro library also characterises metabolites based on their associated pathway (i.e. data can be filtered to view only metabolites involved in a particular pathway). We thus filtered for metabolites involved in amino acid metabolism. We further filtered data to focus on significant differences (by t-test) between QLR supplementation (relative to double starved cells). To filter out noisy metabolites (insignificant between double starvation and QLR-addback), we selected a cut-off of  $p < 0.2$ . The peak intensity values of these metabolites were normalised and fold change was calculated for each treatment. Fold change values were visualised via the online resource Heatmapper using average linkage as the clustering method (Babicki et al., 2016).

There were distinct clusters of metabolites from amino acid pathways that appear to be robustly altered in coordinated fashion when comparing the 3 different experimental nutrient conditions (**Fig 5.4**). Interestingly, each treatment specifically led to either an increase or reduction in amino acid-dependent metabolites. We next explored this dataset via a focussed approach.

Since the urea cycle was the most significantly altered pathway in cells treated with QLR-supplemented double starvation media, we further investigated metabolites associated with this pathway. The urea cycle involves the conversion of R to ornithine, ornithine to citrulline and citrulline to argininosuccinate (**Fig 5.5**), to thereby process amino groups into urea as bi-product (Krebs, 1982). We graphed the peak intensities of several key urea cycle metabolites that could be detected in our data set. It was observed that glucose starvation alone did not have any effect on R levels relative to controls (**Fig 5.6A**). In contrast, double starvation of amino acids and glucose led to the depletion of R by 95% (relative to cells starved of glucose alone). Interestingly, the supplementation of QLR into double starvation media restored R to

a greater level than control cells. This finding demonstrates the depletion of R in cells treated with double (glucose and amino acid) starvation and the expected strong replenishment upon QLR addback.

Glucose starvation alone led to a 70% reduction in ornithine levels despite the presence of all other amino acids (**Fig 5.6B**). Interestingly, double starvation of glucose and amino acids mildly increased ornithine levels relative to cells treated with glucose-starvation media alone. Surprisingly, supplementation of QLR into double starvation media restored the level of ornithine to the same level as control cells treated in full nutrients media. Ornithine levels in QLR-supplemented double starvation cells was 3-fold higher than cells starved of glucose alone or double starved cells. This suggests that QLR-addback maximised the generation (or accumulation) of ornithine in double (glucose and amino acid) starvation media.

Glucose starvation alone led to about 95% reduction in citrulline, which is generated from ornithine and carbamoyl phosphate (**Fig 5.6C**). A similar reduction was seen in cells treated with double starvation (citrulline levels reduced by at least 90% relative to control). Interestingly, QLR supplementation into double starvation media did not replenish citrulline levels. In fact, there was a mild reduction of citrulline upon QLR addback (relative to double starved cells). These data suggest that glucose is critically required for maximal citrulline synthesis in the urea cycle, regardless of the amino acid status.

In contrast, glucose starvation alone led to a mild (but significant) increase in argininosuccinate levels (**Fig 5.6D**). Interestingly, this glucose starvation dependent-increase in argininosuccinate is dependent on the presence of amino acids. Double (glucose and amino acid) starvation led to a 100% reduction in argininosuccinate levels. Surprisingly, QLR supplementation into double starvation media restored the level of argininosuccinate but to a higher level (3-fold more) relative to controls. Similarly, QLR addback into double starvation media increased argininosuccinate levels (e.g. 2-fold higher vs. cells starved of glucose alone or 15-fold higher vs. double starved cells). This finding suggests that QLR-supplemented double starved cells produce high levels of argininosuccinate.

Taken together, these findings suggest that the urea cycle may be enhanced in cells treated with QLR-addback due to apparent increases in R and ornithine levels and possibly the enhanced processing of citrulline to argininosuccinate (a process requiring aspartate and ATP).

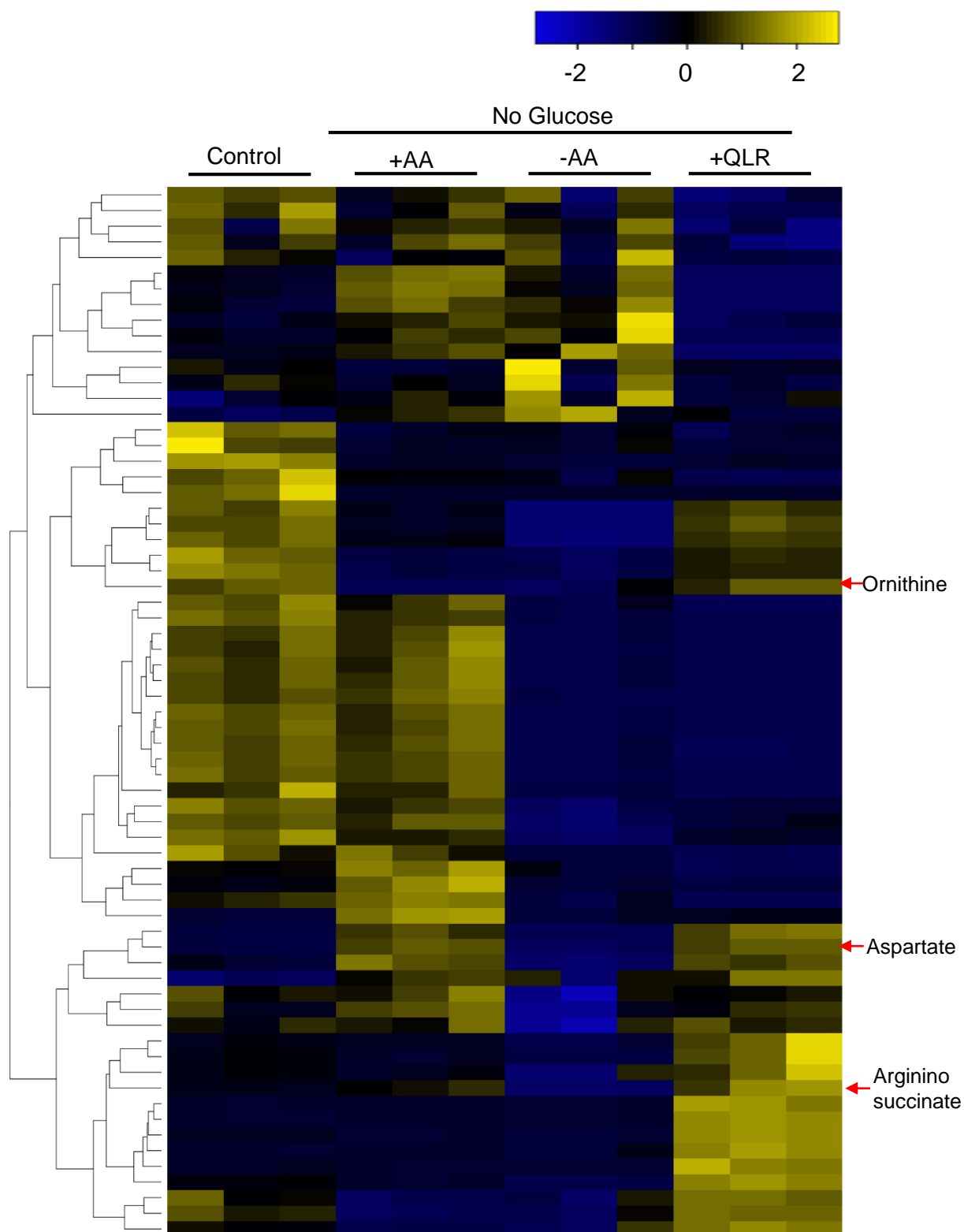


**Figure 5.4: Heatmap showing the profile of metabolites involved in amino acid metabolism after glucose starvation, amino acid starvation with or without QLR supplementation.** 4T1 cells were maintained in full media (Ctrl), starved of glucose alone (+AA, -glucose), starved of all amino acid and glucose (-AA, - glucose) or starved of amino acid and glucose but supplemented with QLR (QLR, -glucose) for 4h. Each treatment group has three independent biological replicates. Starvation media conditions also contained 10% dialysed FBS. Metabolites involved amino acid metabolism were highlighted on the excel macro library and those whose p-value is less than 0.2 based on t.test analysis between double starvation and QLR addback were processed into heatmap.

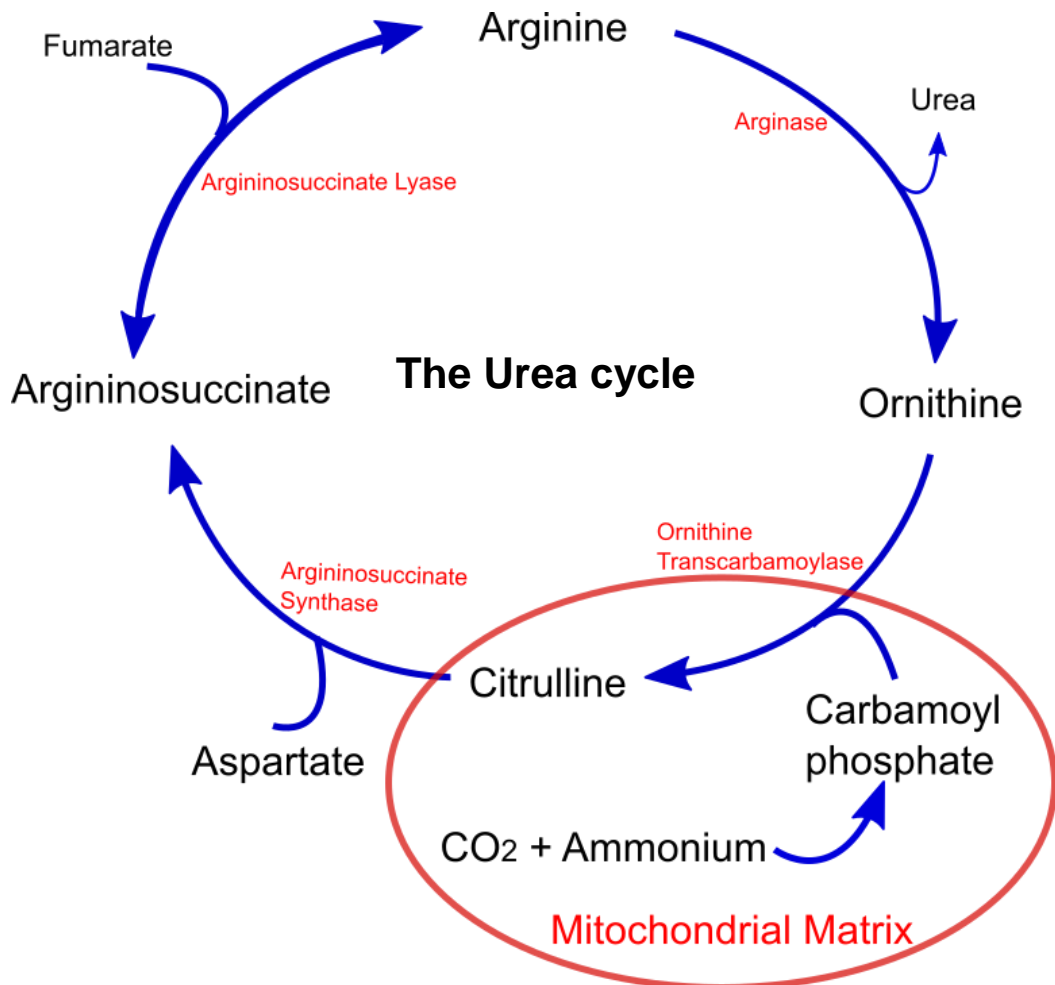


**Figure 5.5: The urea cycle.** The urea cycle showing the four metabolites that are recycled by their corresponding enzymes for the synthesis of urea as their bi-product. The urea cycle begins with the formation of carbamoyl phosphate from ammonium and  $\text{CO}_2$  in the mitochondrial matrix. Carbamoyl phosphate is used as a substrate for the conversion of ornithine to citrulline by ornithine transcarbamoylase. The urea cycle continues with the conversion of citrulline to argininosuccinate by argininosuccinate synthase and the donation of nitrogen by aspartate. Argininosuccinate is reversibly converted to arginine and fumarate by argininosuccinate lyase. Arginine is catabolised to ornithine by arginase to produce urea.

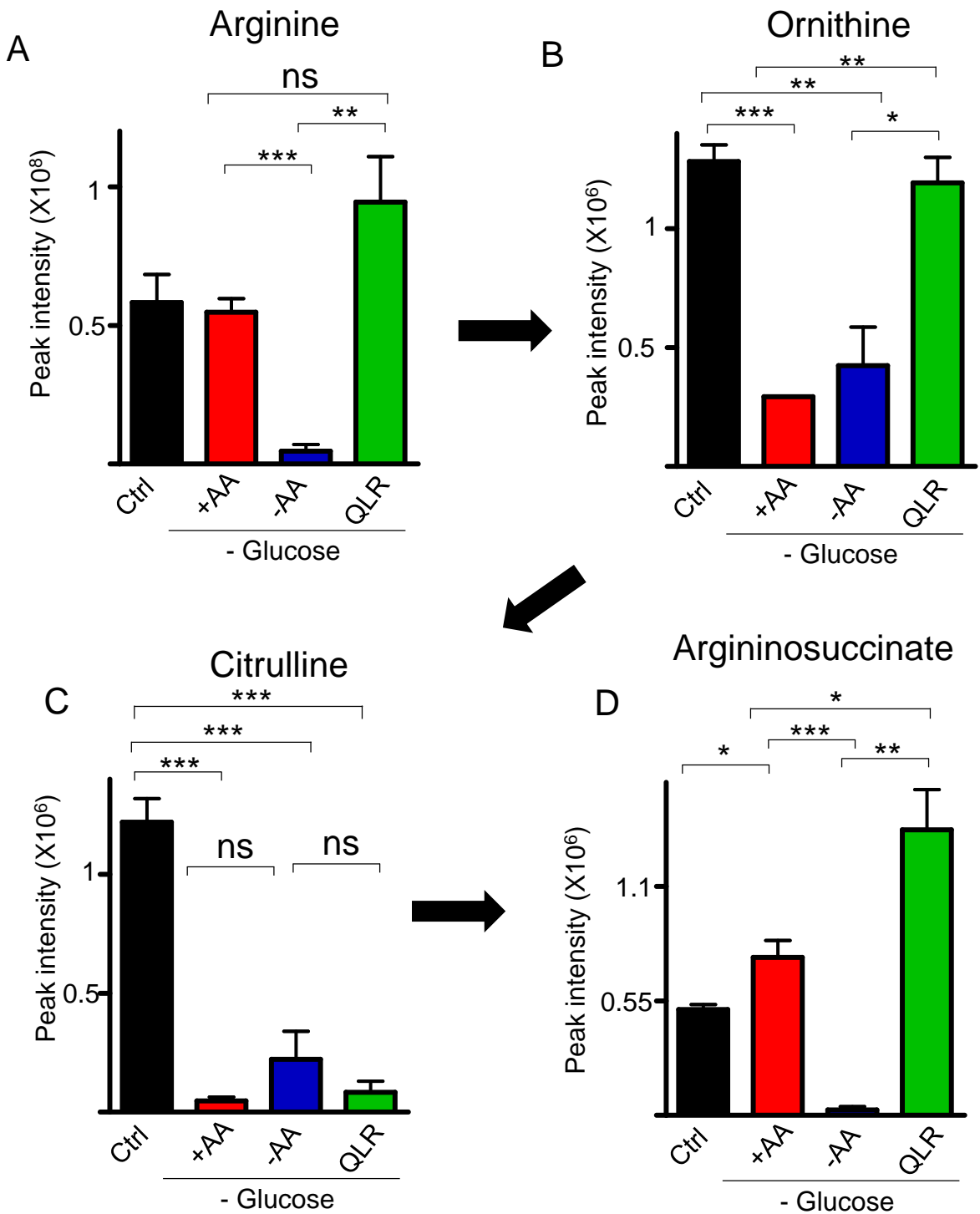


**Figure 5.6: QLR supplementation drives Argininosuccinate flux.** 4T1 cells were maintained in full media (Ctrl), starved of glucose alone (+AA, -glucose), starved of all amino acids and glucose (-AA, -glucose) or starved of amino acid and glucose but supplemented with QLR (+QLR, -glucose) for 4h. Starvation media conditions also contained 10% dialysed FBS. Bar graphs show the mean peak intensity of (A) Arginine (B) Ornithine (C) Citrulline (D) Argininosuccinate. N=3 independent biological replicates. \* represents  $p < 0.05$ , \*\* ( $p < 0.01$ ), \*\*\* ( $p < 0.001$ ).

The urea cycle is closely inter-connected with overall cellular nitrogen metabolism (Berg et al., 2002a). Glutamine (Q) serves as a central reservoir for nitrogen and metabolites formed from Q such as D and oxaloacetate are required in reactions of the urea cycle (Wise and Thompson, 2010). Amino acid Q is firstly converted by glutaminase to E (glutamate) to release ammonia. Amino acid E is used as the main substrate for the *de novo* synthesis of nonessential amino acids such as P, D and N (**Fig 5.7**). Due to the important roles and interconnection of the urea cycle and E metabolism, we studied the effects of QLR-supplementation into double (glucose and amino acid) starvation media on metabolites involved in glutamine metabolism.

It was observed that relative to controls, glucose starvation alone led to a 50% reduction in E levels and upon double starvation, E was totally depleted (**Fig 5.8A**). As expected, supplementation of QLR into double starvation media led to a 15-fold increase in E levels (relative to double starvation) and fully restored levels similar to full-nutrient control conditions. These findings indicate that E is efficiently produced (inter-converted) from QLR in the addback conditions.

Interestingly, relative to controls, glucose starvation alone led to a 2-fold increase in D levels while upon double starvation, D levels were almost depleted (**Fig 5.8B**). As expected, supplementation of QLR into double starvation media restored D levels to a similar high level observed in cells treated with glucose-starvation media (higher than normal basal levels). Downstream of D, there were no changes in N levels following glucose starvation alone or double starvation relative to the control (**Fig 5.8C**). Surprisingly, QLR supplementation greatly increased N levels by at least 10-fold relative to the other three treatment groups. This suggests that N is strongly synthesized via amino acid inter-conversion in QLR-supplemented cells.

In addition, P synthesis was clearly altered following starvation conditions. P levels were reduced by at least 50% in glucose starved cells and double starved cells (relative to controls) (**Fig 5.8D**). In contrast, QLR supplementation into double starvation media increased P levels by 4-fold (relative double starvation or glucose starvation levels). Interestingly, P levels in QLR-supplemented double starved cells were mildly higher than in control cells. These data also suggest that P is produced by inter-conversion in QLR-supplemented cells.

Taken together, these data suggest that QLR-addback generates substantial amounts of E which is then readily interconverted to several other (but not all) amino acids. Overall, these findings suggest that amino acid metabolism is stimulated when QLR is supplemented into starvation media. This major QLR-addback dependent

metabolic reprogramming occurs independently of glucose levels. Therefore, our data indicate that cells facing QLR-addback (which is associated with mitochondrial hyperfusion) may be more active in urea cycle and amino acid metabolism pathways. Speculatively, mitochondrial fusion may be helping to support these altered metabolic activities.

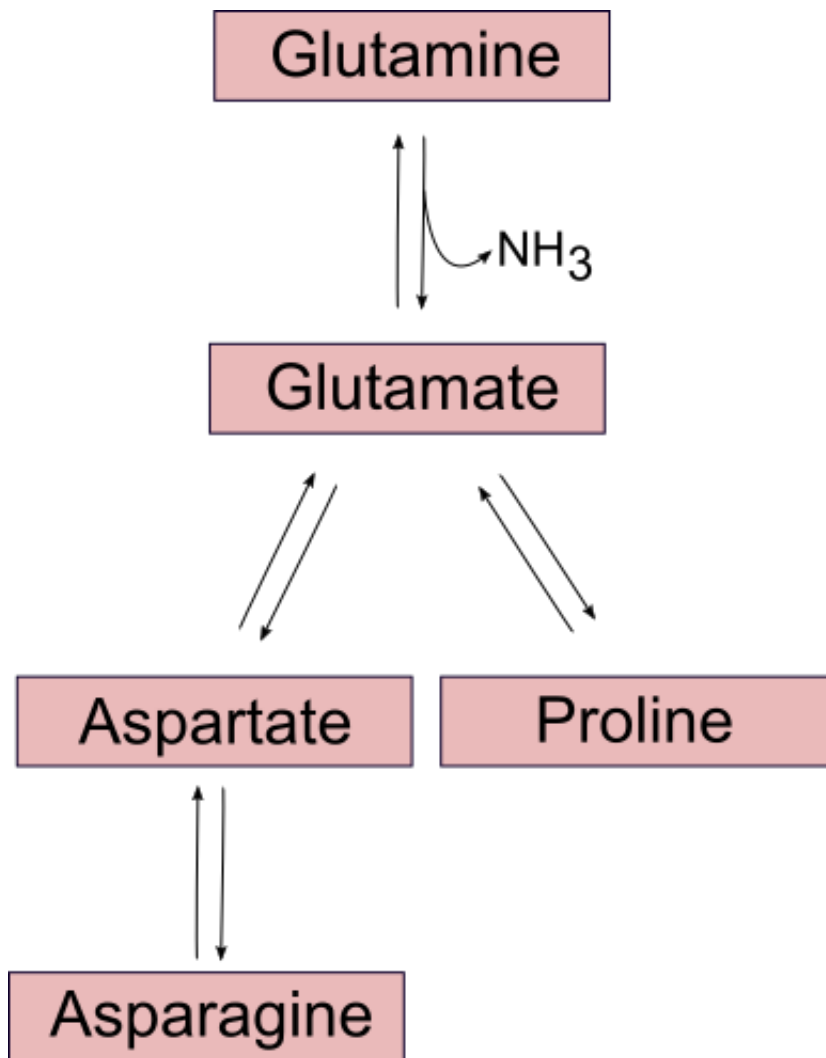


**Figure 5.7: Glutamate metabolism.** The carbon and nitrogen backbones of glutamine is distributed into glutamate during glutamine catabolism and ammonia is generated as a bi-product. Glutamate serves as the precursor for the *de novo* synthesis of nonessential amino acids such as proline, aspartate and asparagine.

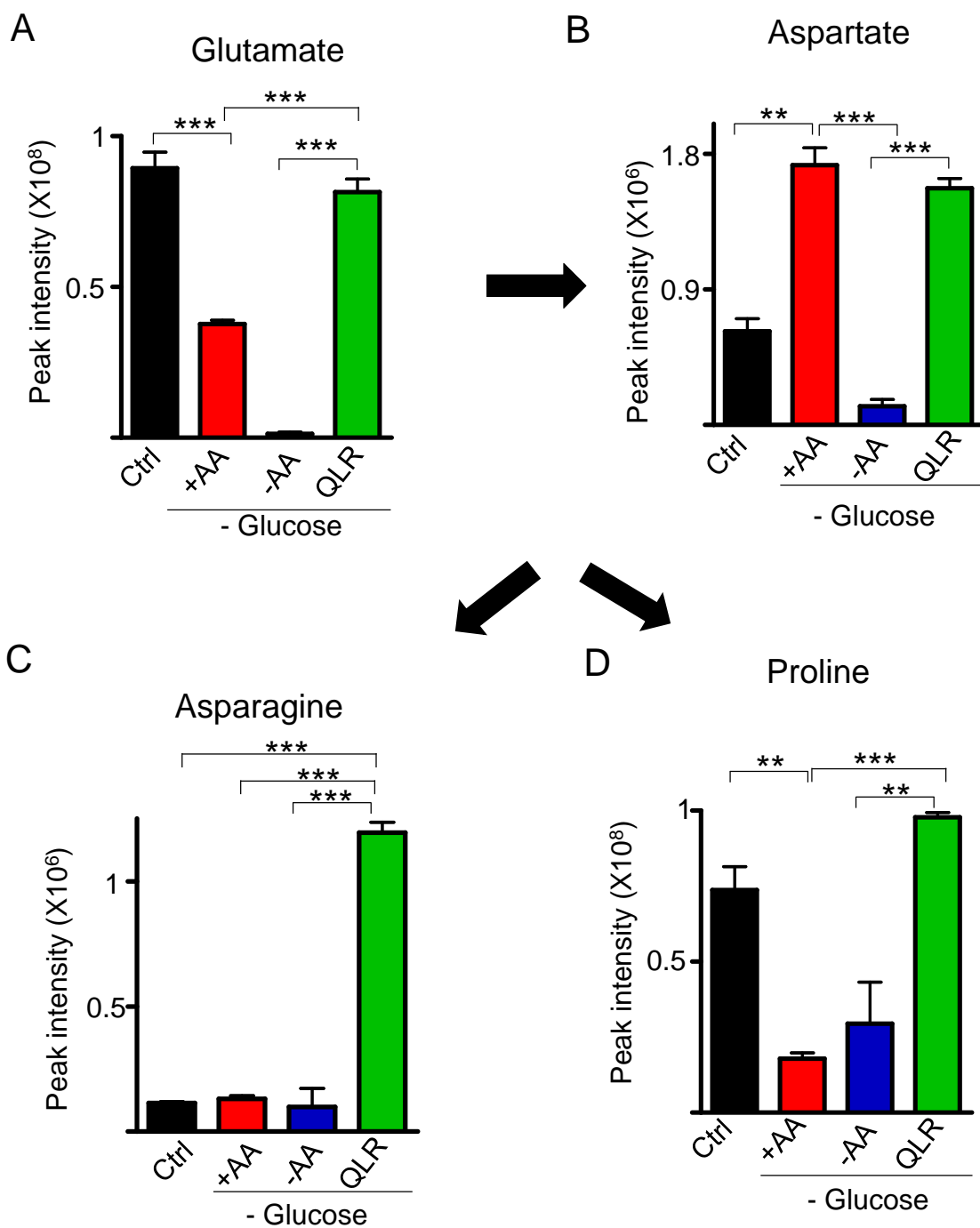


**Figure 5.8: The supplementation of QLR maximizes glutamate metabolism.** 4T1 cells were maintained in full media (Ctrl), starved of glucose alone (+AA, -glucose), starved of all amino acids and glucose (-AA, - glucose) or starved of amino acid and glucose but supplemented with QLR (QLR, - glucose) for 4h. Starvation media conditions also contained 10% dialysed FBS. Bar graphs show the mean peak intensity of (A) Glutamate (B) Aspartate (C) Asparagine (D) Proline. N=3 independent biological replicates. \* represents  $p < 0.05$ , \*\* ( $p < 0.01$ ), \*\*\* ( $p < 0.001$ ).

### 5.2.1.3 QLR-addback restores REDOX balance to reduce oxidative stress.

We found above that E catabolism is enhanced in QLR-supplemented double starved cells. E catabolism also generates metabolic substrates such as alpha-ketoglutarate that enters the Krebs cycle where NADH is produced. NADH is synthesised from multiple pathways: (1) NADH are produced during glycolysis and pyruvate conversion to acetyl-CoA; (2) Fatty acid catabolism to acetyl-CoA synthesises NADH; (3) mitochondria produce NADH via the Krebs cycle (**Fig 5.9A**).

Studies have shown that  $\text{NAD}^+/\text{NADH}$  maintains REDOX balance and it is critical for the maintenance of mitochondrial homeostasis (Stein and Imai, 2012). Since mitochondrial fusion has been associated with the reduction in oxidative stress (Lee et al., 2014), we studied the effects of QLR-addback on REDOX balance. As follows, we analysed levels of  $\text{NAD}^+$  and NADH in our metabolomics data set.

It was observed that the oxidised form  $\text{NAD}^+$  increased by 4-fold upon glucose starvation regardless of the availability of amino acids (**Fig 5.9B**). There were no significant changes in  $\text{NAD}^+$  between double starvation and QLR-supplemented conditions. In contrast, the reduced form NADH was totally depleted upon glucose starvation alone or double starvation relative to control cells (**Fig 5.9C**). NADH levels in cells treated with QLR-supplemented double starvation media reduced by 80% relative to control cells. To note: QLR-addback significantly increased NADH by 2-fold relative to glucose starved or double starved cells. These data suggest that glycolysis is the main pathway for NADH synthesis. However, QLR-supplemented double starved cells (that have hyperfused mitochondria) show some additional synthesis of NADH from glycolysis-independent sources.

In addition to  $\text{NAD}^+$  and NADH, the GSH/GSSG REDOX pair is also critical for the maintenance of cellular metabolism (Carroll et al., 2016b). GSH scavenges reactive oxygen species leading to the release of water and the formation of its oxidized form GSSG. GSSG is recycled to reform GSH via the donation of reducing power from NADPH (**Fig 5.10A**). Due to GSH buffering capacity of oxidative stress, the ratio of GSH/GSSG is often used as a biomarker to assess the REDOX status intracellularly (lower ratios indicate more oxidative stress) (Kemp et al., 2008, Zitka et al., 2012, Chen et al., 2016b). To further investigate whether QLR-addback reduced oxidative stress, we analysed GSH/GSSG in our metabolomics data.

It was observed that (oxidised) NADP<sup>+</sup> levels did not significantly change following glucose starvation, double starvation nor QLR-addback into double starvation media (**Fig 5.10B**). In contrast, relative to controls, GSH levels reduced by 40% upon glucose starvation alone (**Fig 5.10C**). GSH levels did not show any significant changes upon double starvation relative to control. Also, QLR-supplementation did not lead to any significant changes in GSH levels relative to glucose starved or double starved cells.

Interestingly, oxidized GSSG reduced by 25% after glucose depletion alone relative to control cells (**Fig 5.10D**). Similarly, GSSG reduced by 40% in double starved cells (relative to control) while QLR-supplemented double starved cells showed the lowest levels (60% compared to controls). In fact, GSSG levels upon QLR-addback was reduced by 30% relative to double starved cells. Interestingly, the GSH/GSSG ratio in cells starved of glucose alone was similar to that in control cells (**Fig 5.10E**). In contrast, the GSH/GSSG ratio increased in double starved cells. Moreover, QLR-supplementation further increased the GSH/GSSG ratio. These changes suggest that oxidative stress is lowered upon amino acid starvation, and QLR-addback further reduces levels of oxidative stress.

Taken together, these findings suggest that decreased amino acid availability and (surprisingly) QLR-addback both lead to lower levels of reactive oxygen species and oxidative stress. Therefore, QLR-addback-dependent mitochondrial hyperfusion speculatively might be part of the mechanism that protects cells from oxidative stress.

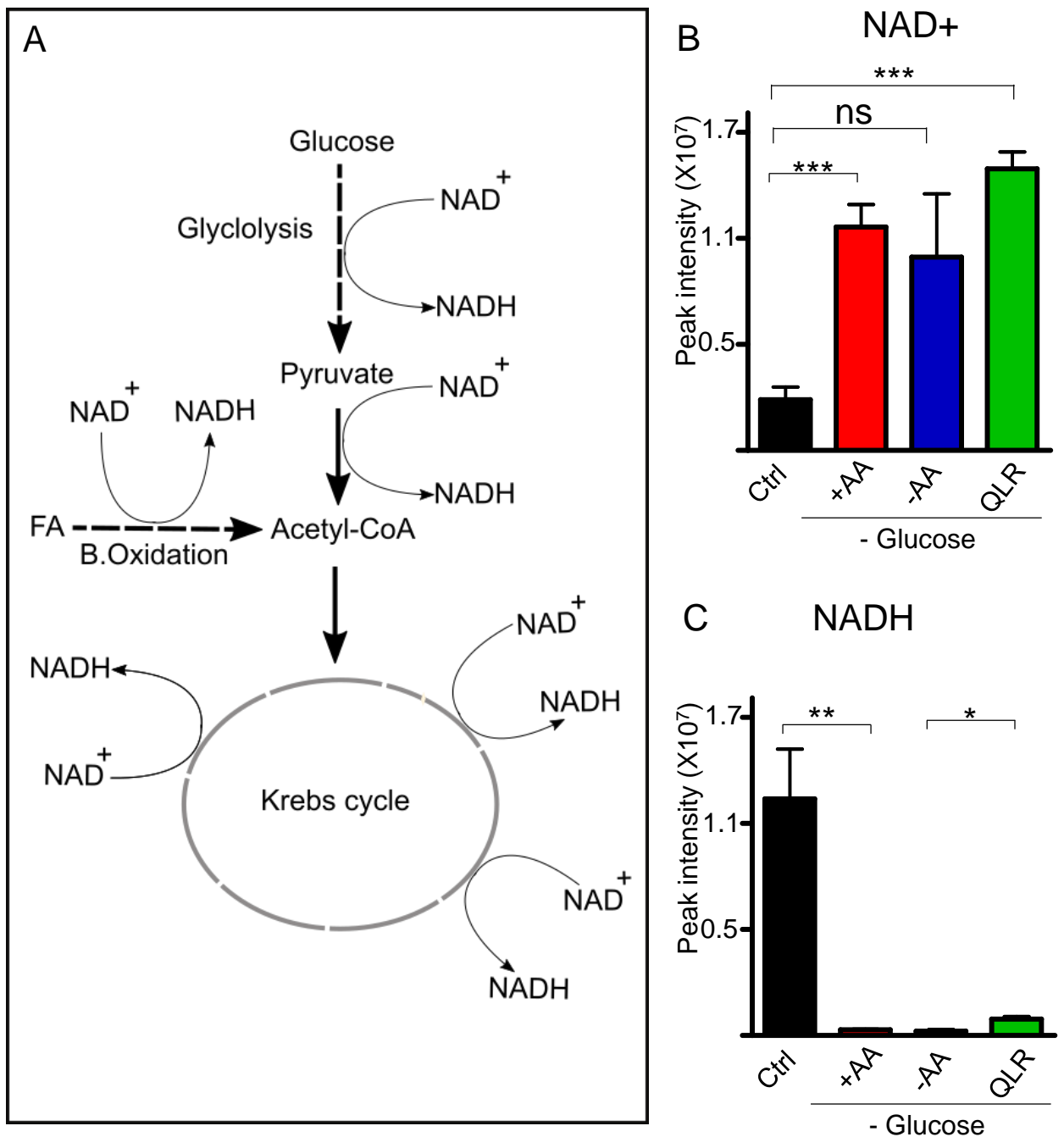
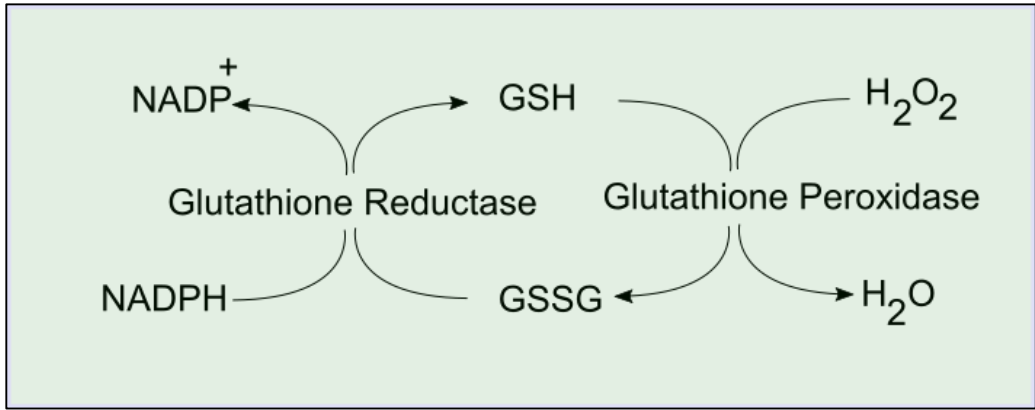
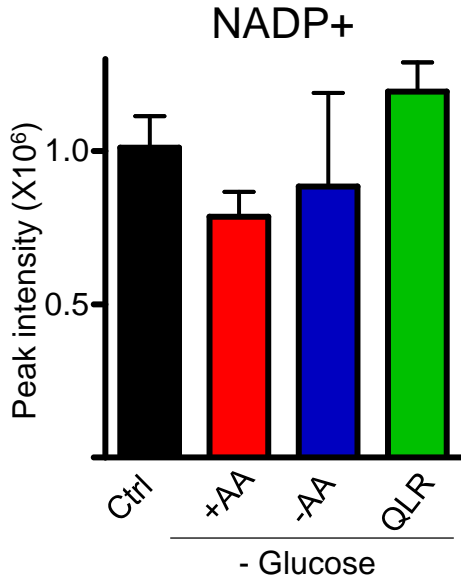


**Figure 5.9: The effect of QLR supplementation on NADH synthesis.** A) Sketch showing sources of NADH from glycolysis, Beta-oxidation and the Krebs cycle pathways. 4T1 cells were maintained in full media (Ctrl), starved of glucose alone (+AA, -glucose), starved of all amino acid and glucose (-AA, -glucose) or starved of amino acid and glucose but supplemented with QLR (QLR, -glucose) for 4h. Starvation media conditions also contained 10% dialysed FBS. Bar graphs show the mean peak intensity of (B) NAD<sup>+</sup> (C) NADH. N=3 independent biological replicates \* represents  $p < 0.05$ , \*\* ( $p < 0.01$ ), \*\*\* ( $p < 0.001$ ).

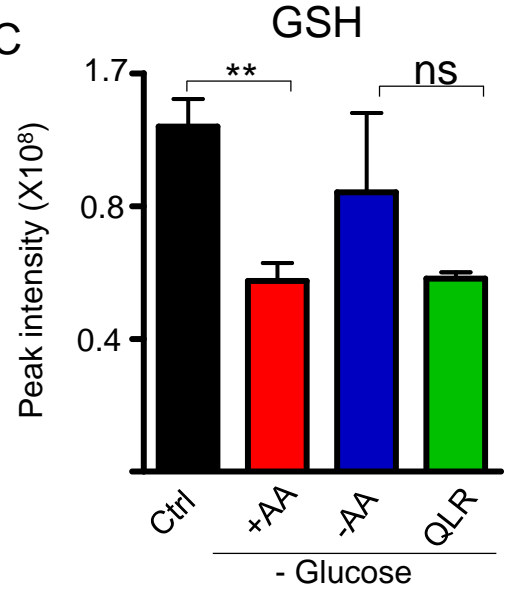
A



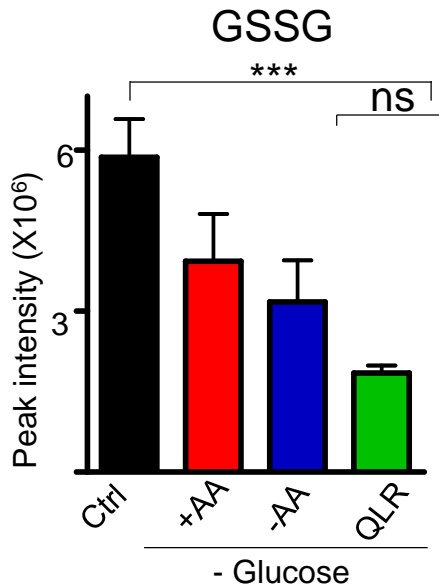
B



C



D



E

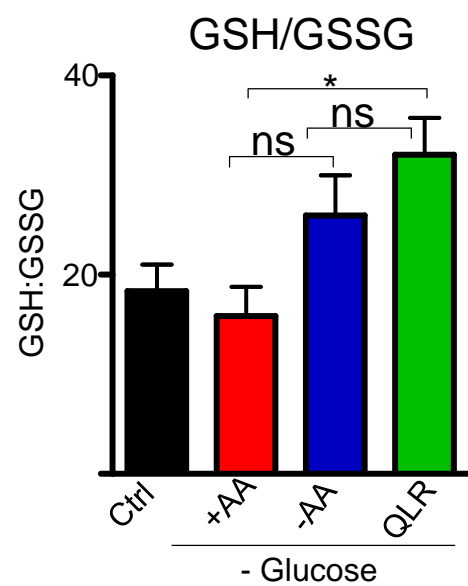


**Figure 5.10: QLR supplementation reduces ROS production.** A) Schematic representation of Glutathione (GSH) and Glutathione-disulfide (GSSG) role in ROS homeostasis. 4T1 cells were maintained in full media (Ctrl), starved of glucose alone (+AA, -glucose), starved of all amino acids and glucose (-AA, - glucose) or starved of amino acid and glucose but supplemented with QLR (QLR, - glucose) for 4h. Starvation media conditions also contained 10% dialysed FBS. Bar graphs show the mean peak intensity of (B) NADP<sup>+</sup> (C) GSH (D) GSSG (E) ratio of GSH/GSSG. N=3 independent biological replicates \* represents p < 0.05, \*\* (p < 0.01), \*\*\* (p < 0.001).

#### 5.2.1.4 Cellular energetics is enhanced by QLR-addback

Studies have shown that mitochondrial fusion can help optimise cellular bioenergetic capacity (Westermann, 2012). It has been suggested that mitochondrial fusion might promote the transfer of bioenergetic metabolites between mitochondrial compartments and mitochondria may hyperfuse as an adaptation to enhanced OXPHOS (Mishra et al., 2014, Westermann, 2012). We found above that NADH is increased upon QLR supplementation into starvation media. Electrons from NADH flow through the E.T.C, and protons accumulate in the intermembrane space which flows back into the matrix through the ATPase complex for ATP synthesis from ADP (**Fig 5.11**).

Since NADH serves as the electron carrier for the eventual synthesis of ATP via the E.T.C, we hypothesised that QLR-addback may enhance ATP levels. We next analysed the effects of QLR-supplementation on levels of metabolites (ADP, ATP, creatine and phosphocreatine) that reflect cellular energy charge levels. It was observed that glucose starvation alone led to a 5-fold increase in ADP levels relative to controls (**Fig 5.12A**). However, double (glucose and amino acid) starvation led to a mild reduction in ADP levels relative to cells starved of glucose alone. In contrast, QLR-supplementation into double starvation media increased ADP levels (e.g. relative to double starvation).

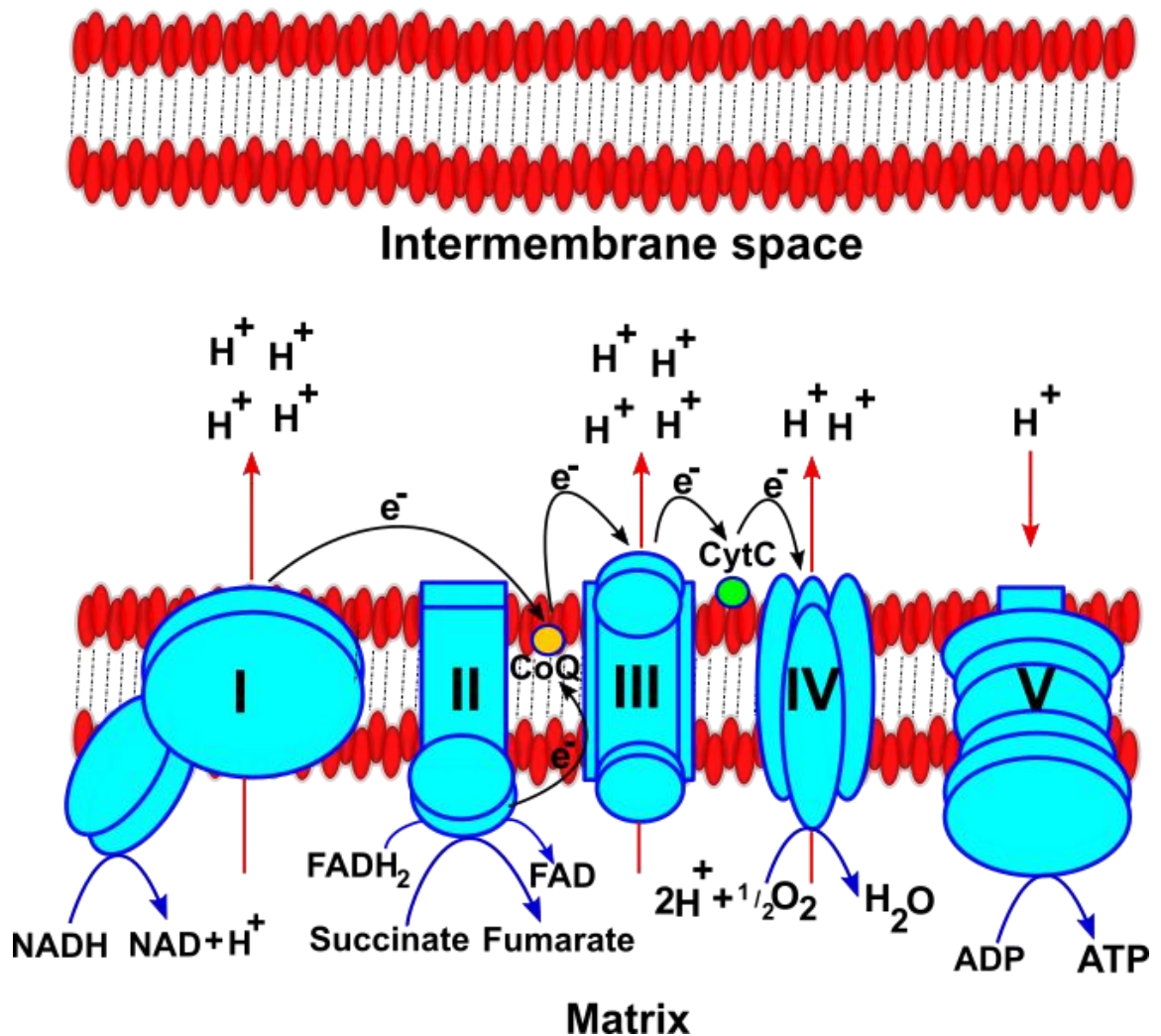
On the other hand, glucose starvation alone led to a 60% reduction in ATP levels (despite having high ADP levels, indicating lower energy charge: ATP/ADP) (**Fig 5.12B**). Interestingly, the levels of ATP were similarly low in double starved cells. Surprisingly, QLR-addback into double starvation media rescued ATP to similar levels as control cells. ATP levels in QLR-supplemented cells was 3-fold higher than the double starvation. This finding suggests non-glycolytic ATP production driven by QLR metabolism.

Moreover, the level of creatine (substrate for synthesis of phosphocreatine, another high energy storage molecule), increased by at least 2-fold in glucose-starved cells and double starved cells relative to control (**Fig 5.12C**). In contrast, QLR supplementation media led to a significant reduction in creatine levels (relative to glucose starved cells). In contrast, it was observed that glucose starvation alone and double starvation both led to 80% reduction in phosphocreatine relative to control (**Fig 5.12D**). Interestingly, supplementation of QLR led to a 4-fold increase in phosphocreatine levels relative to cells starved of glucose or double starved cells.

This further suggests that QLR-supplementation stimulated the synthesis of phosphocreatine and increased the cell energy charge.

Findings in this section suggest that glycolysis-independent energy generation is stimulated by QLR-supplementation. These data suggest that there might potentially be a role of QLR-dependent mitochondrial hyperfusion and mitochondrial-dependent bioenergetics. In addition, our findings indicated that QLR-addback increased the levels of metabolites in the urea cycle, levels of inter-converted amino acids, and lower levels of oxidative stress metabolites. We speculate that these metabolic changes may depend on the mitochondrial hyperfusion that is associated with QLR-addback.

# Electron Transport chain



**Complex I: NADH Reductase**  
**Complex II: Succinate Dehydrogenase**  
**Complex III: Cytochrome Reductase**  
**Complex IV: Cytochrome Oxidase**  
**Complex V: ATP synthase**

**Figure 5.11: The electron transport chain showing the shuttling of electrons.** The electron transport chain comprises of five protein complexes (I – V). NADH and  $FADH_2$  are transported through complex I and II respectively leading to the generation of protons that are pumped into the intermembrane space. Coenzyme Q (CoQ) and cytochrome C (CytC) shuttles electrons into complex III and IV respectively. The proton gradient generated across membrane allows protons to flow through ATP synthase where ATP is formed from ADP.

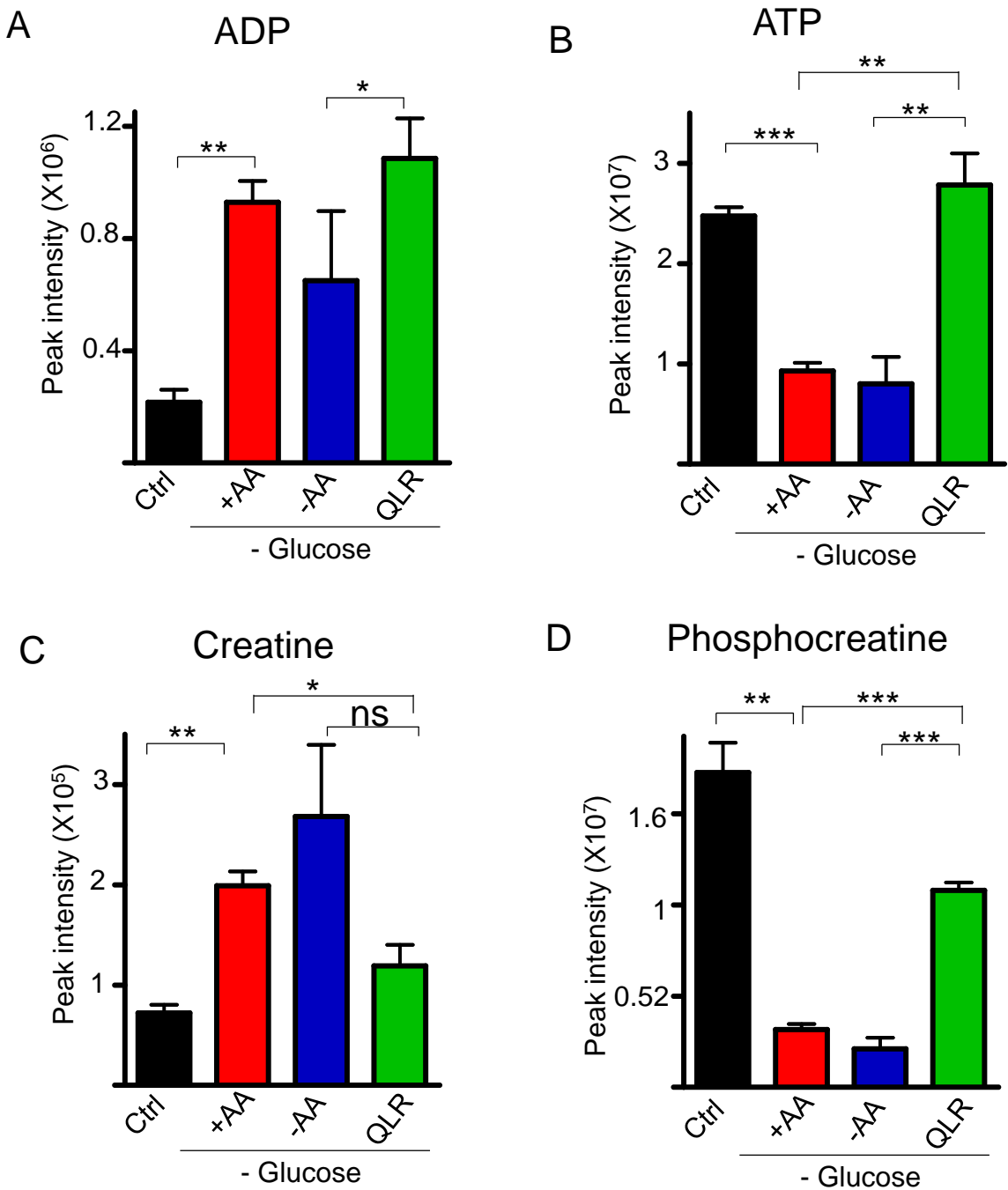


**Figure 5.12: QLR supplementation maximises cellular energy production.** 4T1 cells were maintained in full media (Ctrl), starved of glucose alone (+AA, -glucose), starved of all amino acids and glucose (-AA, - glucose) or starved of amino acid and glucose but supplemented with QLR (QLR, - glucose) for 4h. Starvation media conditions also contained 10% dialysed FBS. Bar graphs show the mean peak intensity of (A) ADP (B) ATP (C) Creatine (D) Phosphocreatine. N=3 independent biological replicates. \* represents  $p < 0.05$ , \*\* ( $p < 0.01$ ), \*\*\* ( $p < 0.001$ ).

### 5.2.1.5 The effects of QLR-addback on nucleotide metabolic pathways.

It was found earlier by Pathway analysis (Fig 5.2) that nucleotide sugar metabolites were significantly over-represented as altered upon QLR supplementation into double starvation media. Interestingly, other recent evidence has revealed that there is a connection between mitochondrial fusion and nucleotide metabolism (Miret-Casals et al., 2017). These authors reported that depletion of the cellular pyrimidine pool increased Mfn1/Mfn2-dependent mitochondrial fusion. Similarly, studies have shown that the signalling cyclic nucleotide cAMP is increased during amino acid starvation (Gomes et al., 2011a). In light of this and our observed Pathway analysis association between nucleotide metabolism and QLR-supplementation, we further analysed details here. We focused on nucleotides (GTP, GDP, AMP and cAMP) that have been previously linked to mitochondrial dynamics. Studies have shown that GTP is an important energy molecule/protein functional co-factor that facilitates membrane fusion and fission via the action of GTP binding mitochondrial regulatory proteins and GTP hydrolysis to GDP (Yan et al., 2018, Kalia et al., 2018). We observed that glucose starvation alone led to 70% reduction in GTP levels relative to controls (**Fig 5.13A**). In contrast, upon double nutrient starvation, GTP levels increased by 3-fold relative to glucose starved cells. Interestingly, QLR-supplementation into double starvation media led to a further increase in GTP levels (e.g. 5-fold increase as compared to glucose starved cells). This suggests that amino acid-dependent mitochondrial hyperfusion may help sustain GTP levels during nutrient stress. On the other hand, it was observed that glucose starvation alone led to 80% reduction in GDP levels relative to control cells (**Fig 5.13B**). Upon double glucose and amino acid starvation, the levels of GDP increased (but not significant) relative to glucose starved cells. In contrast, QLR supplementation into double starvation medium restored GDP to the same level as control cells. In fact, QLR addback led to at least 6-fold increase in GDP levels relative to glucose starved. This suggests that amino acid starvation promotes GTP/GDP interconversion during nutrient stress.

During glucose starvation, AMP has been shown to bind allosterically to the regulatory  $\gamma$ -subunit of AMPK which promotes AMPK activation by facilitating LKB1-dependent phosphorylation of AMPK at Thr172 (Oakhill et al., 2011). Upon activation, AMPK mediates phosphorylation of downstream substrates such as Mff. During E.T.C. collapse, AMPK has been shown to phosphorylate Mff which lead to the recruitment of Drp1 to induce mitochondrial fragmentation (Toyama et al., 2016). Surprisingly, we

observed that AMP levels decreased by 70% in cells starved of glucose alone, or under double starvation, relative to control cells (**Fig 5.13C**). Similarly, AMP levels were reduced by 65% in QLR-supplemented starved cells relative to controls. There were no significant changes in AMP levels between cells treated with the three starvation or addback conditions. These findings suggest unexpectedly that AMP levels are reduced when glucose is withdrawn and glycolysis is halted. However, under these starvation conditions, lack of AMP accumulation suggests that AMPK would not be activated.

cAMP functions as a second messenger to activate PKA. It has been suggested that during amino acid starvation, cAMP levels increases, leading to the downstream activation of PKA which then phosphorylates Drp1 at S637 to promote mitochondrial fusion (Gomes et al., 2011a). Surprisingly, we observed that glucose starvation alone or double starvation led to 60% reduction in cAMP levels relative to controls (**Fig 5.13D**). Interestingly, in contrast to the reported model, starvation of amino acids (in glucose-depleted cells) did not alter cAMP levels when compared to glucose starved cells (containing full amino acids). Surprisingly, QLR supplementation into double starvation media led to a 3-fold increase in cAMP levels relative to cells under glucose starvation or double starvation. This suggests that cAMP synthesis is rescued in cells treated with QLR-supplementation. The data also suggest that full amino acid starvation-induced mitochondrial fusion does not occur as a result of increased cAMP.

Taken together, the findings in this subsection suggests that QLR-addback dependent mitochondrial hyperfusion correlates with increased levels of multiple metabolites linked to nucleotide biogenesis (especially those required for activation of mitochondrial fusion). More broadly, this metabolite profile experiment (**As summarised in table 5.2**) suggests that QLR-addback into double starvation media increases the rate of the urea cycle and E catabolism to enhance NADH production for the sustenance of cellular energetics during nutrients stress.

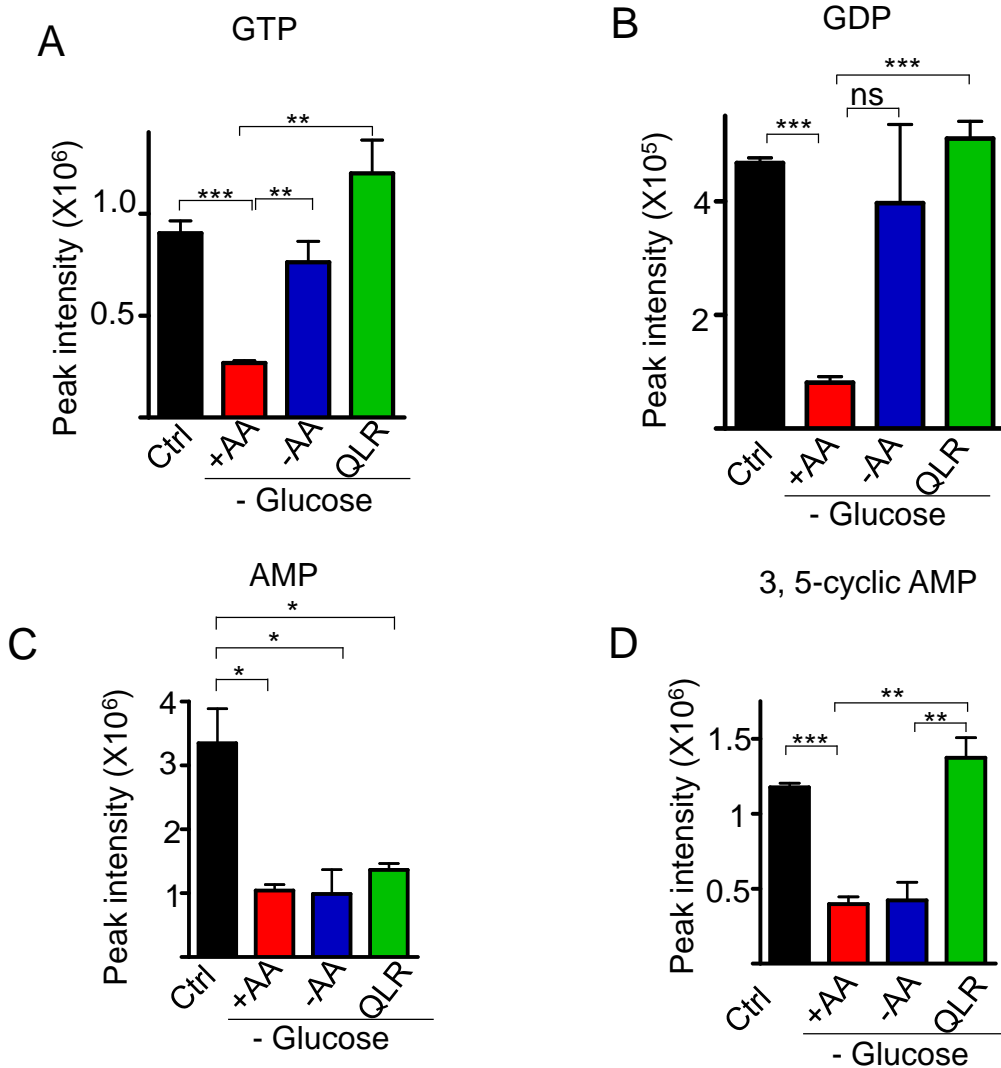


**Figure 5.13: The effect of the supplementation of QLR on nucleotide metabolism.** 4T1 cells were maintained in full media (Ctrl), starved of glucose alone (+AA, -glucose), starved of all amino acids and glucose (-AA, - glucose) or starved of amino acid and glucose but supplemented with QLR (QLR, - glucose, -AA) for 4h. Starvation media conditions also contained 10% dialysed FBS. Bar graphs show the mean peak intensity of (A) GTP (B) GDP (C) AMP (D) 3,5-cyclic AMP. N=3 biological replicates. \* represents  $p < 0.05$ , \*\* ( $p < 0.01$ ), \*\*\* ( $p < 0.001$ ), ns (not significant).

**Table 5.2: Summary of key significant metabolic changes after QLR addback in no glucose media**

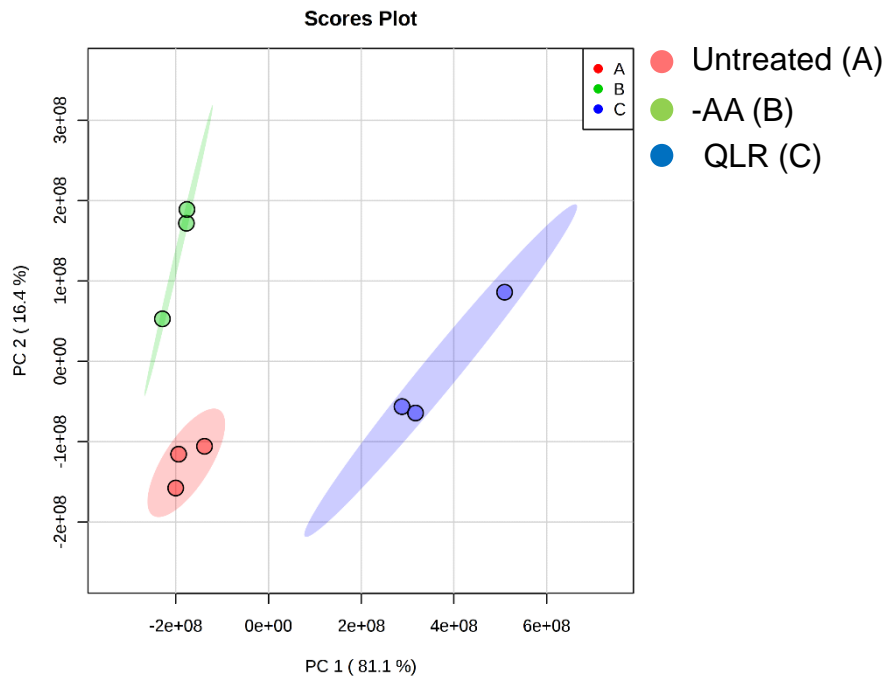
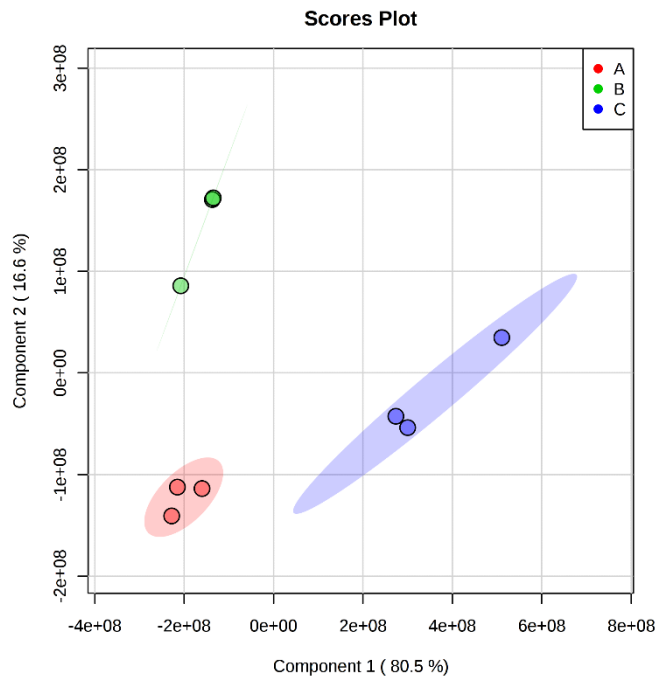
The effect of amino acid starvation on metabolites (After -AA relative to AA). The effect of QLR addback into amino acid starvation media on metabolites relative to full amino acid starvation (After QLR addback relative -AA). N.A indicate metabolite is not significantly altered.

<b>Summary of key significant metabolic changes between groups</b>		
<b>No glucose media</b>		
<b>Metabolites</b>	<b>After -AA relative to AA</b>	<b>After QLR addback relative -AA</b>
Acetyl-CoA	Reduced	Increased
ADP	N.A	Increased
Arginine	Reduced	Increased
Argininosuccinate	Reduced	Increased
Asparagine	N.A	Increased
Aspartate	Reduced	Increased
ATP	N.A	Increased
CAMP	N.A	Increased
Glutamate	Reduced	Increased
GTP	Increased	N.A
NADH	N.A	Increased
Ornithine	N.A	Increased
Phosphocreatine	N.A	Increased
Proline	N.A	Increased
Ribose-5-phosphate	Increased	Reduced

## 5.2.2 The metabolic profile of cells treated to amino acid addback in the presence of glucose

We observed above that QLR addback could reprogram reactions in the urea cycle, E catabolism and cellular energetics. This addback condition was performed into glucose and amino acid starvation medium and this experimental design was to minimise generation of metabolites from glycolysis. We had already confirmed in Chapter 3 that stimulation of mitochondrial hyperfusion by QLR-addback could occur independently of glucose levels. As we identified QLR-dependent metabolic changes in the context of double (glucose and amino acid) starvation media, we aimed to further confirm if similar patterns of reprogramming could be observed in starvation media containing glucose. Therefore, a similar metabolomics experiment was repeated using cells treated with EBSS (as our more commonly used amino acid starvation media containing glucose). 4T1 cells were maintained in full nutrient control media or starved of all amino acids (EBSS) or incubated in EBSS supplemented with QLR. After 4-hours, cellular extracted metabolites were analysed on LC/MS/MS.

Firstly, the metabolomic data were confirmed for data quality and robustness. Multivariate analysis demonstrated that there was close clustering of biological replicates within each treatment group and clear separation between the three treatment groups, as indicated by the PCA (**Fig 5.14A**) and PLS-DA scored plots (**Fig 5.14B**). Interestingly, similarly to the metabolomics experiments performed in glucose-free starvation, ORA and Pathway enrichment analysis indicated that metabolic pathways involving multiple amino acids (R, P, H, E and D were among the top twenty most enriched pathways upon QLR-supplementation into EBSS (relative to EBSS starvation) (**Fig 5.15A, B**). ORA also identified alterations of the urea cycle, ammonia recycling, and electron transport chain. Bioinformatic analysis confirmed that alterations of the urea cycle and amino acid metabolism were generally associated with low FDR ranging from 0.008 to 0.05 (**Table 5.3**).

**A****B**

**Figure 5.14: Metabolomics LC-MS/MS analysis of 4T1 cells starved of amino acid (-AA) with or without QLR supplementation.** A) Principal-Component Analysis (PCA) score plot showing the separation between treatment groups. B) Partial Least Squares- Discriminant Analysis (PLS-DA) showing the supervised classification of the treatment groups. Starvation media conditions also contained 10% dialysed FBS.

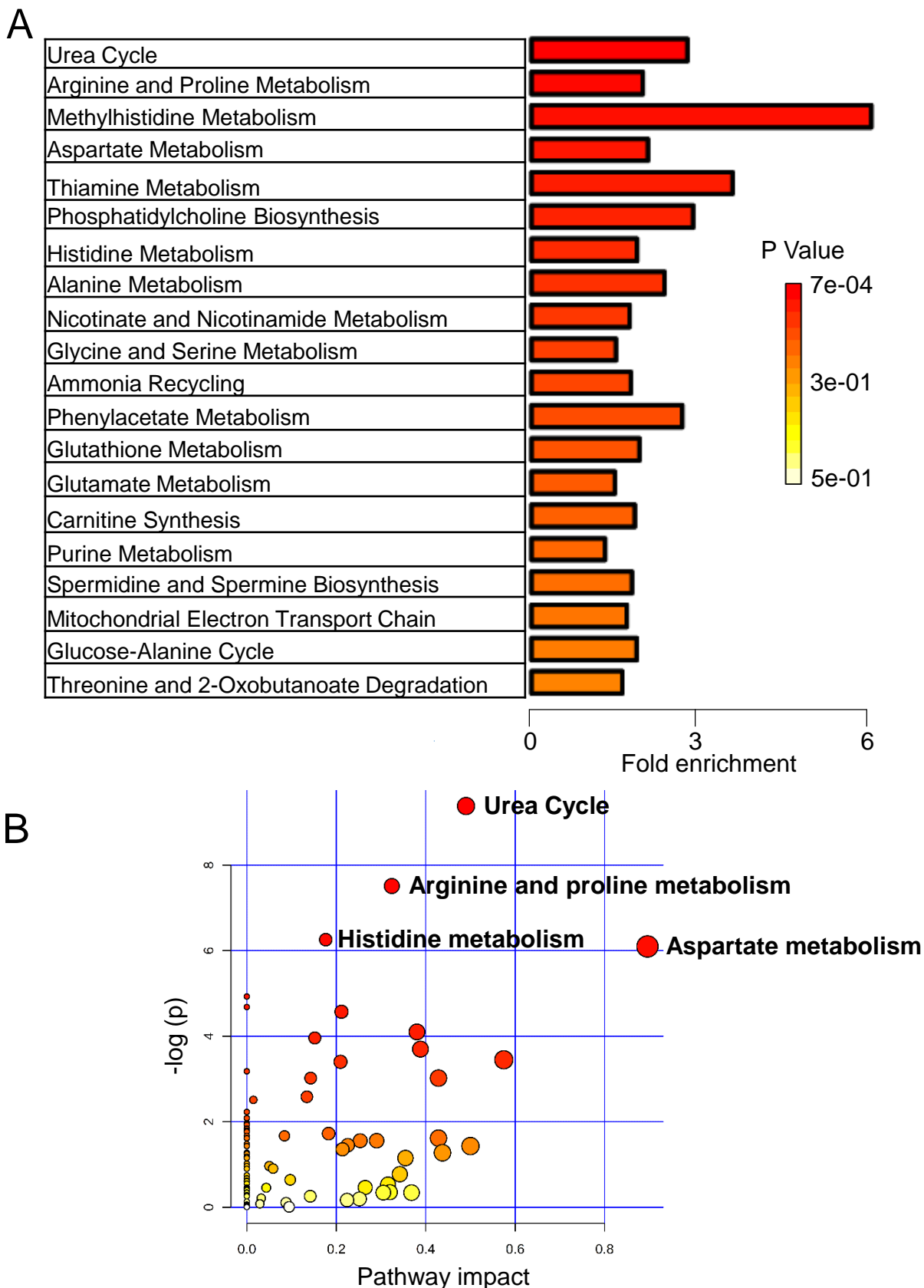


**Table 5.3: Detailed results of pathway analysis of relevant pathways after amino acid starvation with or without QLR supplementation.** Total: total number of metabolites in the pathway; the hits indicate the matched number from the analysed data; Raw p signifies the original P value calculated from the enrichment analysis; FDR is the adjusted p value using the false discovery rate; the impact represents the pathway impact value calculated from the topology analysis.

Pathway	Total	Hits	Raw p	FDR	Impact
Urea Cycle	25	10	8.43E-05	0.008345	0.49012
Arginine and Proline Metabolism	47	13	0.000547	0.027079	0.32424
Histidine Metabolism	35	10	0.001918	0.055599	0.17641
Aspartate Metabolism	30	9	0.002246	0.055599	0.89583
Alanine Metabolism	13	5	0.007243	0.1195	0
Thiamine Metabolism	9	4	0.00926	0.12803	0
Phosphatidylcholine Biosynthesis	14	5	0.010346	0.12803	0.21171
Ammonia Recycling	27	7	0.016577	0.18235	0.38031
Nicotinate and Nicotinamide Metabolism	34	8	0.019088	0.18897	0.15203
Carnitine Synthesis	17	5	0.024793	0.22314	0.38824
Glutamate Metabolism	44	9	0.031799	0.25391	0.57458
Purine Metabolism	66	12	0.033342	0.25391	0.20944
Phenylacetate Metabolism	8	3	0.041612	0.29426	0
Threonine and 2-Oxobutanoate Degradation	14	4	0.048837	0.30218	0.14286
Spermidine and Spermine Biosynthesis	14	4	0.048837	0.30218	0.42857
Mitochondrial Electron Transport Chain	16	4	0.075536	0.43988	0.13433
Glycine and Serine Metabolism	52	9	0.08119	0.44654	0.014647

### 5.2.2.1 QLR-addback restores amino acid catabolism in EBSS conditions

The urea cycle, R and P metabolism were the most significantly altered pathways after QLR addback as shown above. Due to the roles of these pathways in amino acid metabolism, we filtered through metabolites in the Excel macro library and highlighted metabolites involved in amino acid metabolism. The fold changes of these metabolites were uploaded into Heatmapper to generate heatmap to observe amino acid-dependent metabolic profile after amino acid starvation and QLR addback.

Similar to the profile in the double starvation experiment, heatmap clustering showed that many groups of metabolites associated with amino acid pathways were depleted upon amino acid starvation in EBSS (**Fig 5.16**). Surprisingly, some metabolites also increased upon amino acid starvation in EBSS. It was also observed that QLR supplementation into EBSS restored (or elevated) levels of some metabolites. This profile confirms QLR addback re-enters and re-fuels many amino acid catabolic pathways.

We analysed further metabolites of the urea cycle since this was a highly affected pathway upon addback (similar to the double starvation experiment). It was observed that amino acid starvation led to a 75% reduction in ornithine levels relative to untreated cells while QLR-addback significantly increased ornithine by 2-fold (**Fig 5.17A**). Similarly, citrulline levels diminished by 85% following amino acid starvation relative to untreated cells. In addition, further slight reduction was observed when QLR was added back into EBSS (**Fig 5.17B**). Similar to the observations in double starvation, incubation in EBSS led to a total depletion in arginosuccinate levels relative to untreated cells (**Fig 5.17C**). Also consistent, QLR-addback into EBSS led to a 5-fold increase in argininosuccinate relative to untreated cells. This suggests that the urea cycle is enhanced leading to argininosuccinate accumulation upon QLR-supplementation.

It was observed earlier (**Fig 5.8**) that QLR addback into double (glucose and amino acid) starved cells have enhanced amino acid E interconversion to D and N. To clarify whether consistent trends occurred in EBSS starvation media, metabolites from E catabolism were analysed. Amino acid starvation led to at least 90% reduction in E and D levels relative to untreated cells. Upon QLR addback into EBSS, levels of E and D were restored to similar levels as untreated cells (**Fig 5.18A, B**). Consistent with observations in double starved cells, amino acid starvation did not alter N levels

but QLR addback into EBSS led to 3-fold increase in N (**Fig 5.18C**). These findings indicated that E catabolism to non-essential amino acids is maximised in QLR supplemented-amino acid starved as observed earlier in our double starvation experiment.

Amino acid E derived from Q and R metabolism can be further converted to alpha-ketoglutarate via the Krebs cycle (**Fig 5.19**). Similarly, citrate is also synthesised from acetyl-CoA which is produced from L. Biochemical studies have also shown that argininosuccinate in the urea cycle can also be converted to fumarate which is metabolised in the Krebs cycle (Barmore and Stone, 2019). Since QLR all feed into the Krebs cycle, we analysed the metabolites of this pathway.

Initially, it was observed that most of the Krebs cycle metabolites could not be detected in the double starvation metabolomics dataset. In contrast, in this EBSS starvation experiment, three metabolites of the Krebs cycle could be detected (**Fig 5.20**). Interestingly, it was observed that there were no significant changes in citrate upon amino acid starvation or QLR supplementation (although a mild increase under starvation was observed) (**Fig 5.20A**). This suggests that there may be a constant supply of acetyl-CoA via pyruvate from glucose catabolism.

It was observed that amino acid starvation led to 80% reduction in fumarate levels (despite having the same levels of citrate) (**Fig 5.20B**). In contrast, QLR-addback into EBSS increased fumarate levels relative to untreated cells. In fact, QLR addback led to a 14-fold increase in fumarate levels relative to cells starved in EBSS. Similar trends were observed with malate levels (**Fig 5.20C**).

Collectively, these data further suggest that the urea cycle, amino acid catabolism and the Krebs cycle are maximised (or at least replenished) in cells treated with QLR-supplementation. In addition, these QLR-addback dependent increases still occurred in the context of sufficient levels of glucose and glycolysis, suggesting that these are primarily reflections of amino acid metabolic pathways.

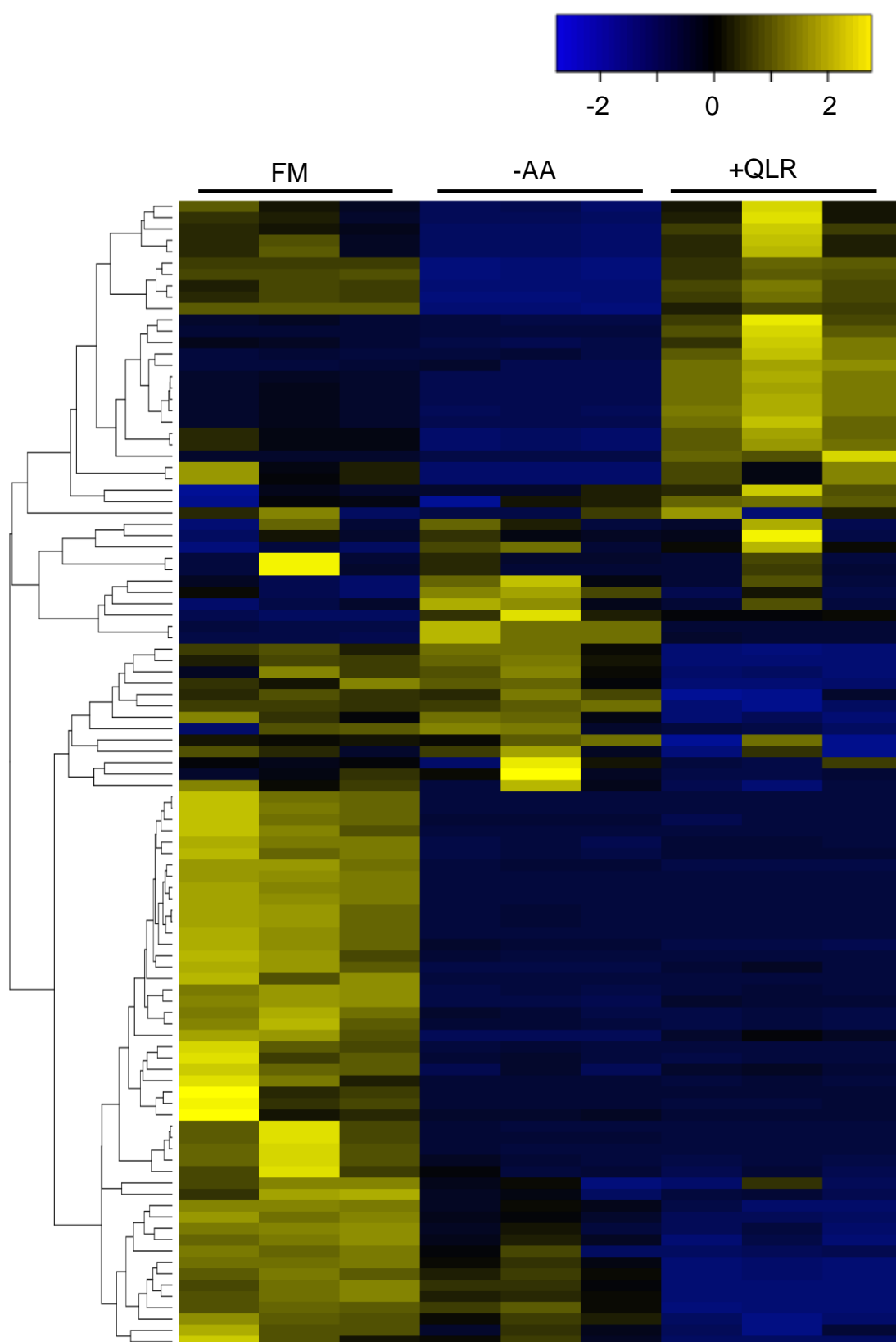


**Figure 5.16 : Heat map showing the profile of metabolites involved in amino acid metabolism after amino acid starvation with or without QLR supplementation.** 4T1 cells were treated with full media (UN), starved of either all amino acids (-AA) or starved of amino acid but supplemented with (QLR) for 4h. Each treatment group has three independent biological replicates. Starvation media conditions also contained 10% dialysed FBS. Metabolites involved amino acid metabolism were highlighted on the excel macro library and all the highlighted metabolites were processed into heat map.

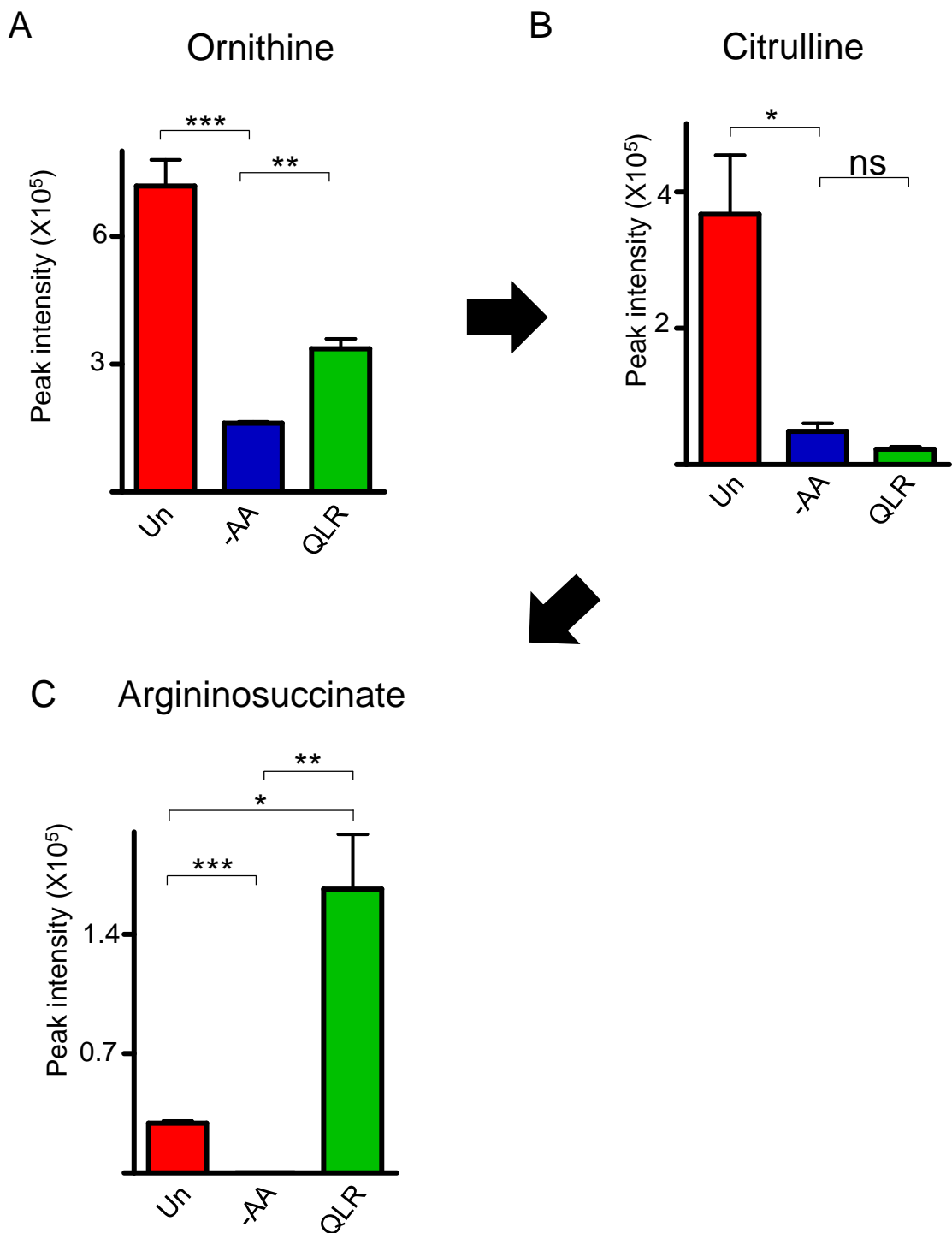


**Figure 5.17: The supplementation of Glutamine (Q), Leucine (L) and Arginine (R) drives Argininosuccinate flux in 4T1 cells.** 4T1 cells were treated with full media (UN), starved of either all amino acids (-AA) or starved of amino acid but supplemented with (QLR) for 4h. Starvation media conditions also contained 10% dialysed FBS. Bar graphs show the mean peak intensity of (A) Ornithine (B) Citrulline and (C) Argininosuccinate. N=3 independent biological replicate. Black arrow show the synthesis direction. \* represents  $p < 0.05$ , \*\* ( $p < 0.01$ ), \*\*\* ( $p < 0.001$ ).

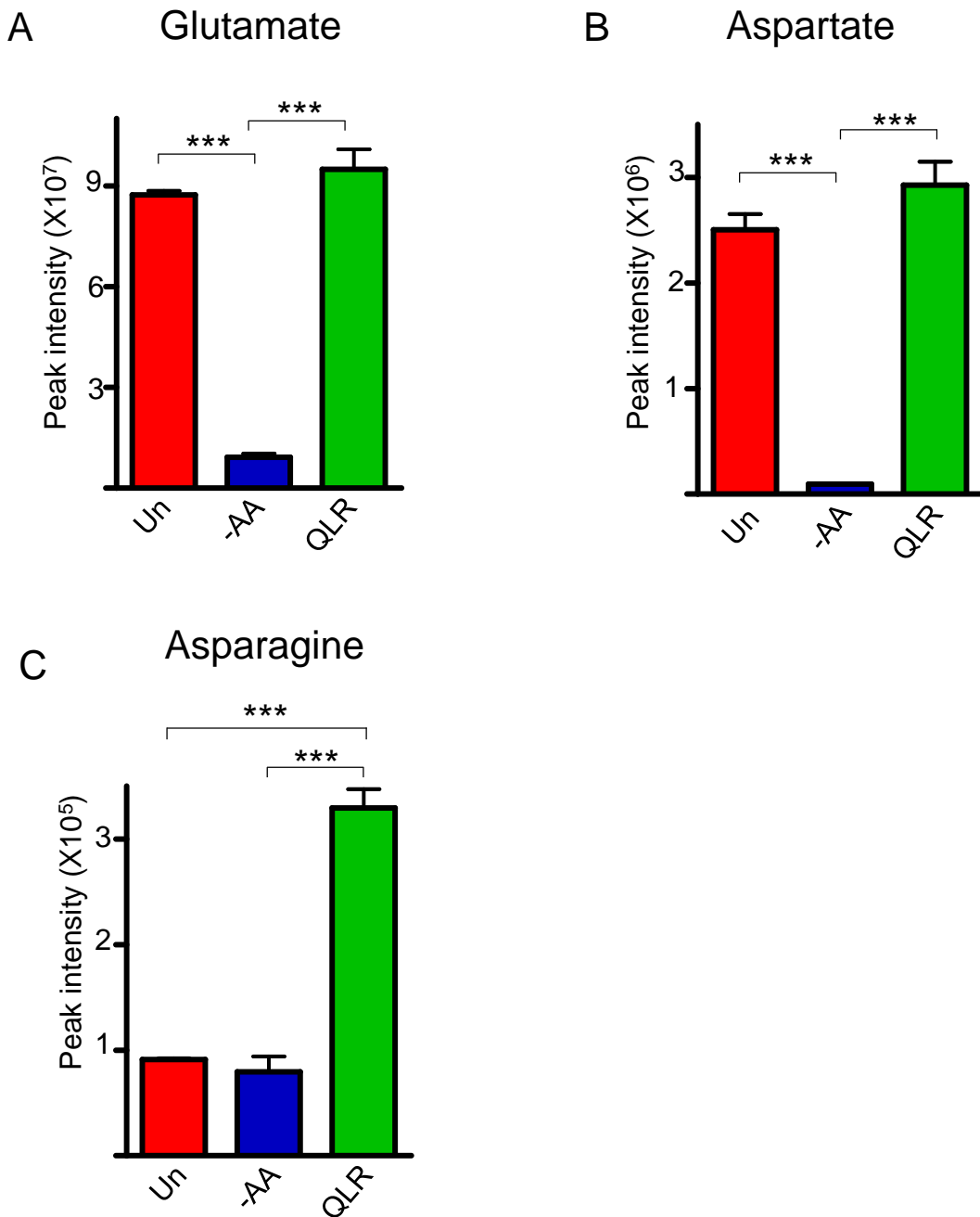


**Figure 5.18: The supplementation of Glutamine (Q), Leucine (L) and Arginine (R) drives Asparagine synthesis in 4T1 cells.** 4T1 cells were treated with full media (UN), starved of either all amino acids (-AA) or starved of amino acid but supplemented with (QLR) for 4h. Starvation media conditions also contained 10% dialysed FBS. Bar graphs show the mean peak intensity of (A) Glutamate and (B) Aspartate (C) Asparagine. N=3 independent biological replicate. Black arrow show the synthesis direction. \* represents  $p < 0.05$ , \*\* ( $p < 0.01$ ), \*\*\* ( $p < 0.001$ ).

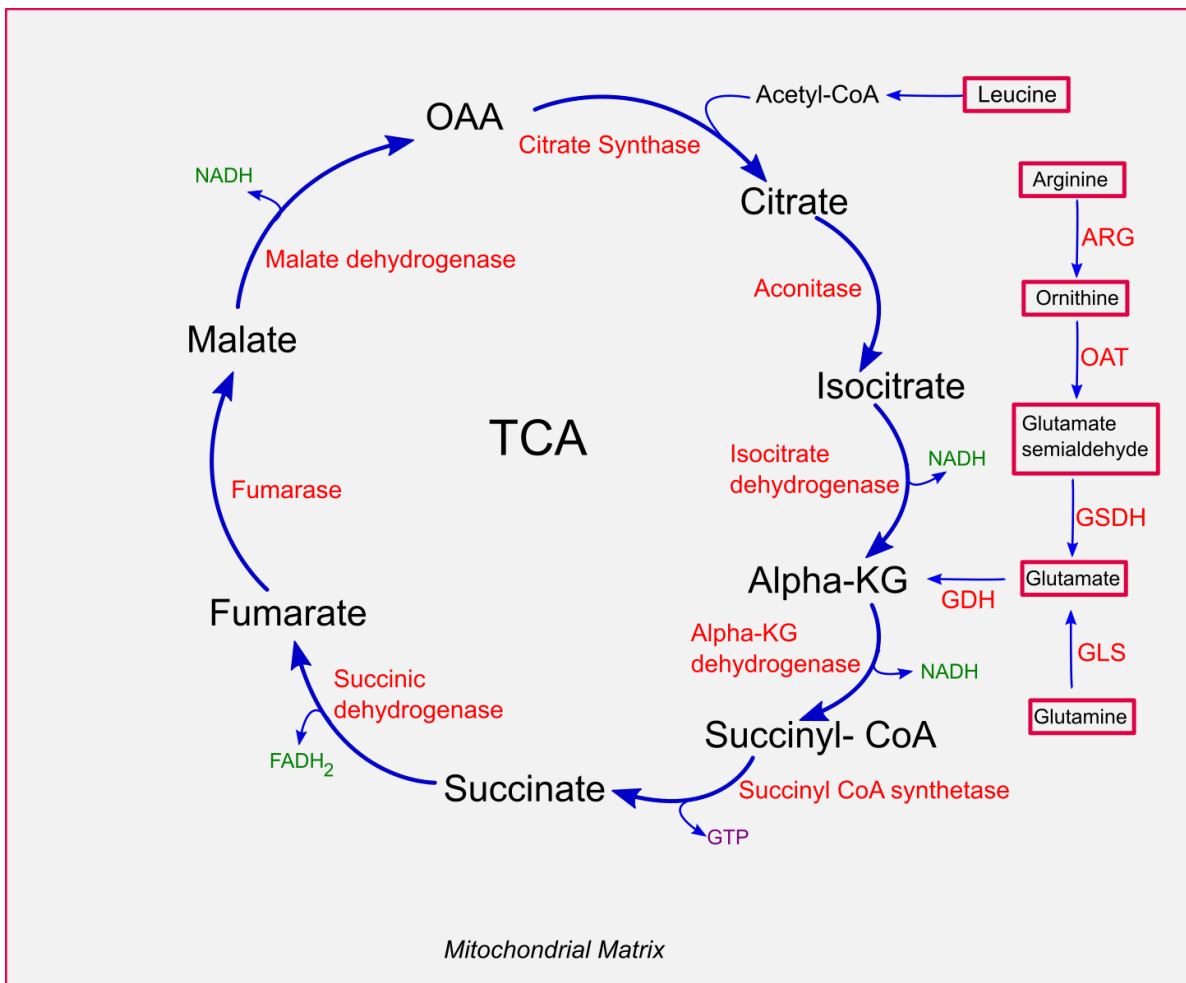


**Figure 5.19: QLR metabolism in Tricarboxylic Acid (TCA) cycle (also referred to as Krebs cycle).** This shows the recycling of metabolites of TCA cycle and their enzymes (in red). Leucine enters the TCA cycle by conversion to acetyl-CoA which undergoes condensation with oxaloacetate (OAA) to form citrate as the first reaction process catalysed by citrate synthase. Citrate is converted to isocitrate by Aconitase and isocitrate is converted to alpha-ketoglutarate and NADH by oxidative decarboxylation catalysed by isocitrate dehydrogenase. Arginine enters the Krebs cycle in a multi-step reaction involving arginine conversion to ornithine (Catalysed by arginase (ARG)), ornithine to glutamate semialdehyde (Catalysed by ornithine- $\delta$ -aminotransferase (OAT)), then glutamate semialdehyde to glutamate (Catalysed by glutamate semialdehyde dehydrogenase (GSDH)). Similarly, glutamine is converted to glutamate by Glutaminase (GLS). Glutamate formed from arginine or glutamine is converted to alpha-ketoglutarate by deamination which enters the Krebs cycle. In the cycle, alpha-ketoglutarate is further converted to succinyl-CoA and NADH in a process catalysed by alpha-ketoglutarate dehydrogenase. Succinyl-CoA generates succinate and GTP. Subsequently, succinate is oxidized to fumarate and FADH<sub>2</sub> by succinate dehydrogenase. The next step of fumarate hydration to malate is catalysed by fumarase also referred to as fumarate hydratase (Fh). The 'last' reaction of the cycle recycles oxaloacetate from malate in a process catalysed by malate dehydrogenase which releases NADH.

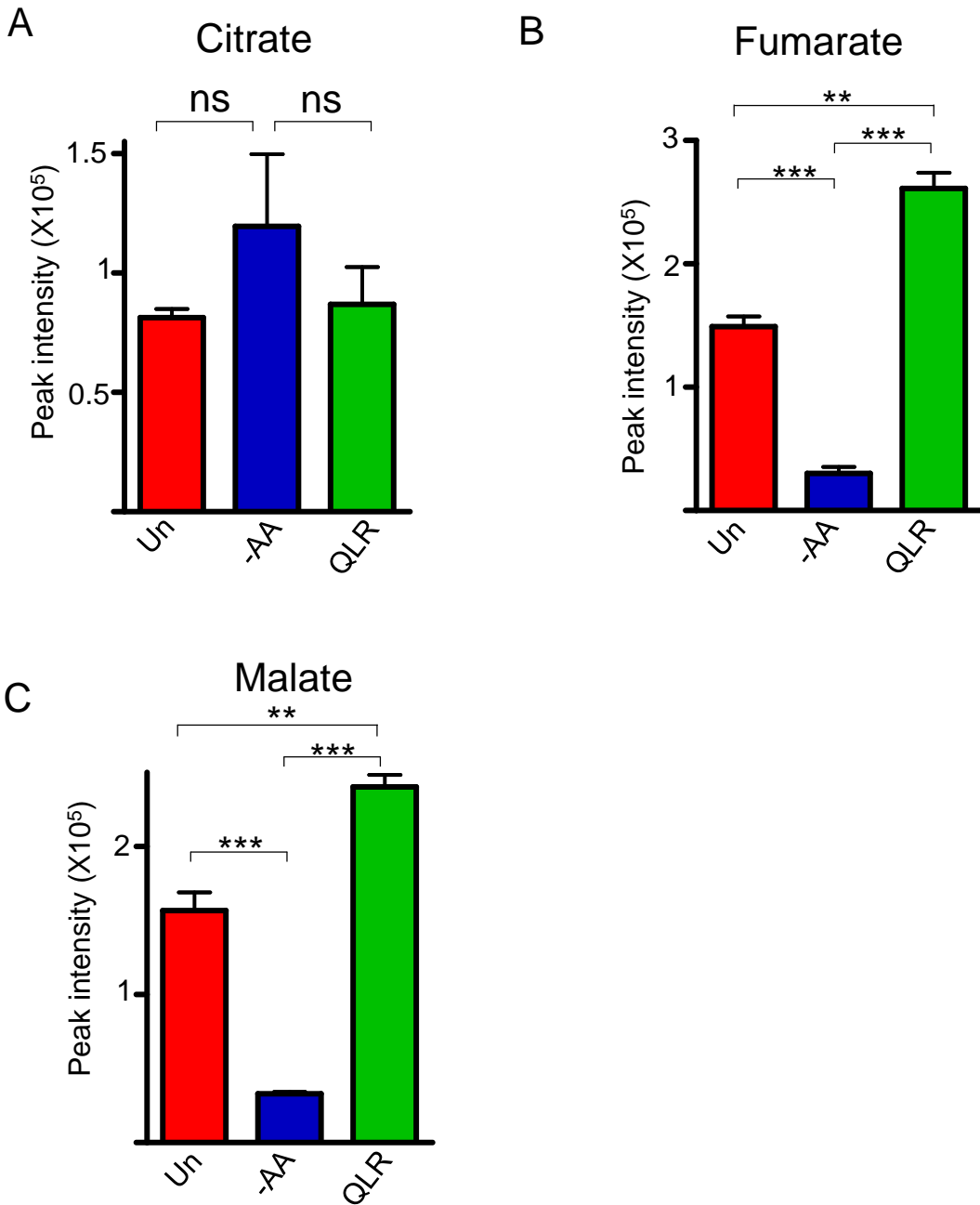


**Figure 5.20: The supplementation of Glutamine (Q), Leucine (L) and Arginine (R) increased TCA cycle metabolites in 4T1 cells.** 4T1 cells were maintained in full media (UN), starved of either all amino acid (-AA) or starved of amino acid but supplemented with (QLR) for 4h. Starvation media conditions also contained 10% dialysed FBS Bar graphs show the mean peak intensity of (A) Citrate (B) Fumarate and (C) Malate. N=3 independent biological replicate. p < 0.05, \*\* (p < 0.01), \*\*\* (p < 0.001).

### 5.2.2.2 QLR-addback into EBSS increased cellular energy

We further clarified whether QLR-addback dependent increases in NADH and cellular energy (observed earlier in the double starvation experiment) were also present under EBSS starvation contexts. The Krebs cycle is one of the major sources of NADH which is synthesized at three reactions. As established earlier in Fig 5.9, other sources such as glycolysis can account for over 90% of NADH levels in 4T1 cells. Interestingly, in EBSS starvation media (which contains glucose), QLR addback led to a 25% increase in NAD<sup>+</sup> and NADH levels but not significant (**Fig 5.21A, B**). Although this change in NADH was not significant, the 25% increase observed upon QLR-addback appears to support our earlier conclusion that NADH is generated upon QLR-addback as a result of metabolic recycling in the Krebs cycle.

As observed previously, ADP and ATP levels were reduced upon amino acid starvation but supplementation of QLR back into EBSS restored both ADP and ATP levels (**Fig 5.22A, B**). In fact, QLR-addback led to mild increases in ADP and ATP relative to untreated cells. Therefore, ATP (and ADP) synthesis appear to be promoted by QLR-supplementation (during which mitochondria are hyperfused).

On the other hand, amino acid starvation led to a 30% reduction of creatine levels relative to untreated cells. Upon QLR supplementation into EBSS, there was an even greater (70%) reduction relative to untreated cells (**Fig 5.22C**). This trend mirrors changes in creatine levels in the double starvation experiment. Creatine was effectively converted into high energy phosphocreatine upon amino acid starvation (despite having a lower creatine level) (**Fig 5.22D**). However, phosphocreatine level was higher in QLR-supplemented cells. This suggests that QLR-supplementation is able to re-feed metabolic pathways that ultimately lead to storage of cell energy equivalents in ATP and phosphocreatine.

Together, QLR addback into EBSS increases the rate of the urea cycle, E catabolism and the Krebs cycle to enhance NADH production and of cellular energetics. These effects occurred even in the presence of glucose and therefore appear to reflect downstream steps following metabolism of supplemented QLR and are overall consistent with observations from the double nutrient (glucose and amino acid) starvation metabolomics experiment.

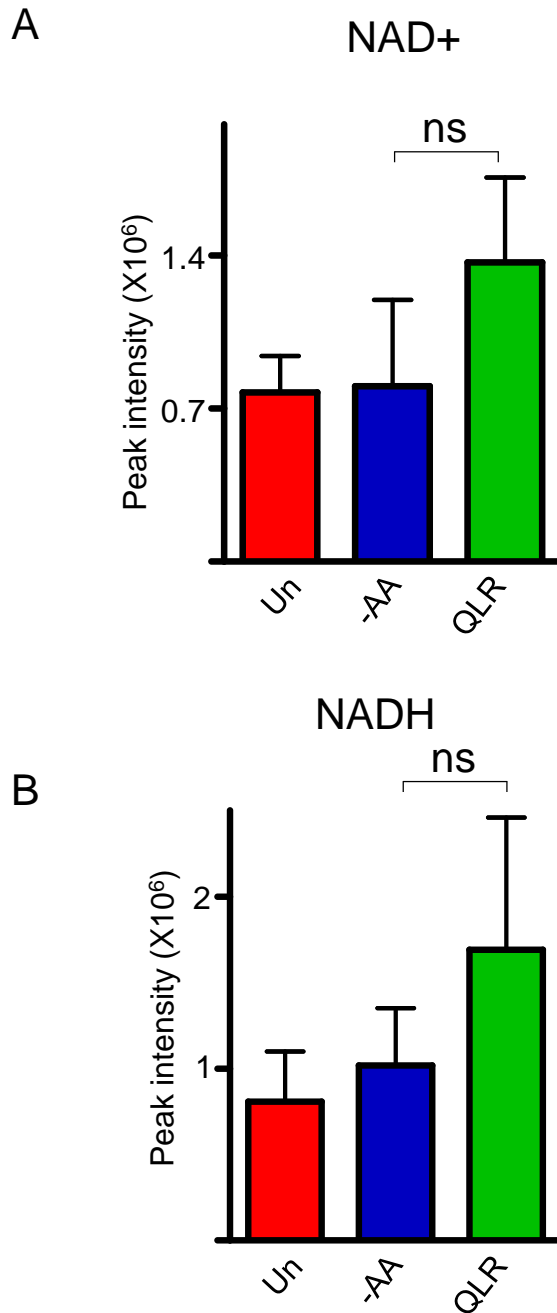


**Figure 5.21: QLR supplementation increased NADH synthesis.** 4T1 cells were maintained in full media (UN), starved of either all amino acids (-AA) or starved of amino acid but supplemented with (QLR) for 4h. Starvation media conditions also contained 10% dialysed FBS. Bar graphs show the mean peak intensity of (A) NAD<sup>+</sup> (B) NADH. N=3 independent biological replicate

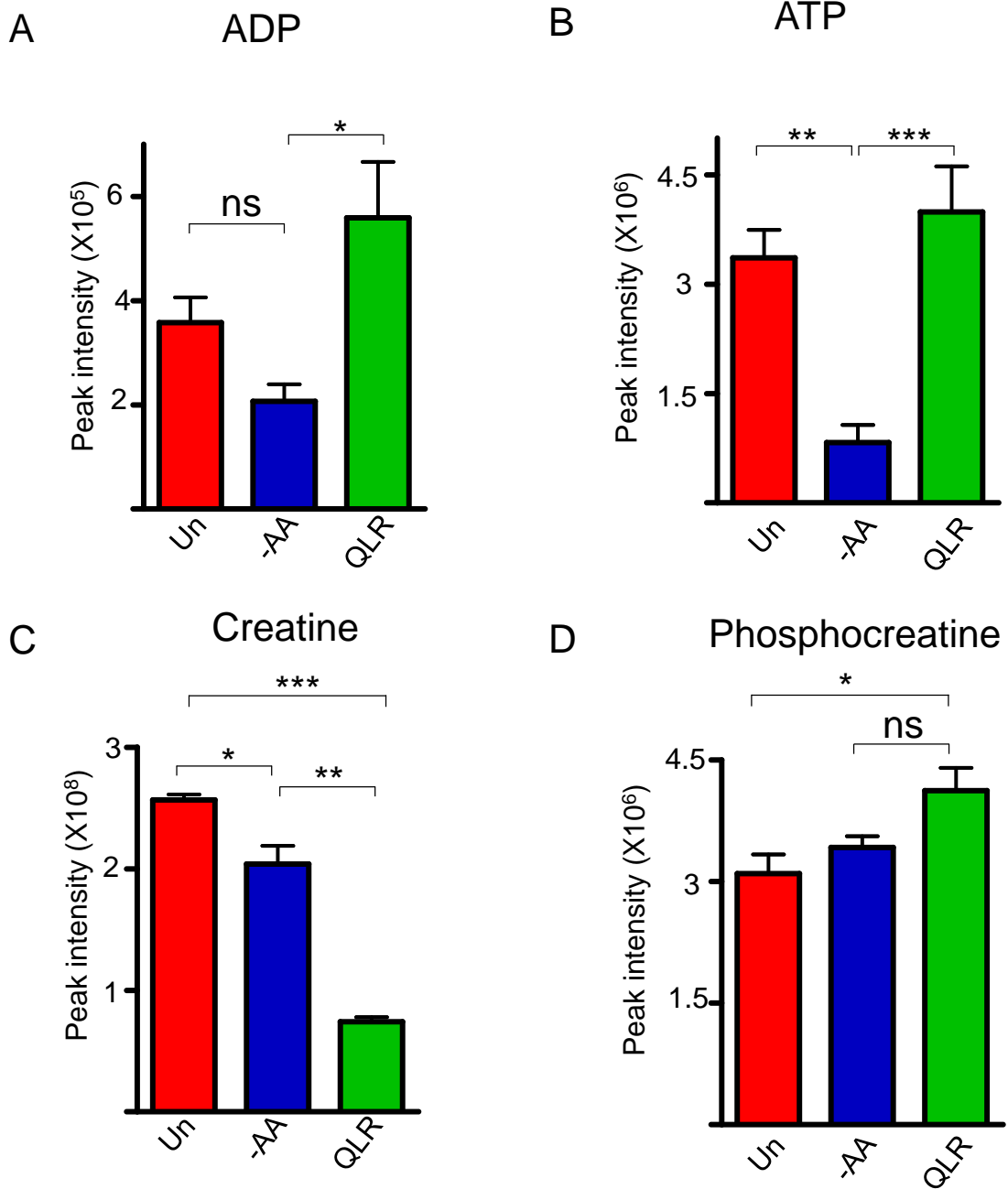


**Figure 5.22: QLR supplementation into amino acid-starved cells restore cellular energy.** 4T1 cells were treated with full media (UN), starved of either all amino acids (-AA) or starved of amino acid but supplemented with (QLR) for 4h. Starvation media conditions also contained 10% dialysed FBS. Bar graphs show the mean peak intensity of (A) ADP (B) ATP (C) Creatine (D) Phosphocreatine. N=3 independent biological replicate \* represents  $p < 0.05$ , \*\* ( $p < 0.01$ ), \*\*\* ( $p < 0.001$ ).

### 5.2.2.3 Effects of QLR-addback into EBSS on nucleotide and lipid metabolism

We observed a nutrient-dependent change in metabolites involved in nucleotide metabolism and mitochondrial dynamics in double starvation conditions. We thus further clarified whether QLR-dependent increases in GTP and AMP (observed earlier in double starvation) were also present under EBSS starvation contexts.

GTP levels did not significantly change upon amino acid starvation in EBSS relative to controls with full nutrient (**Fig 5.23A**). However, supplementation of QLR into EBSS led to a 2-fold increase in GTP levels relative to cells starved in EBSS, therefore further suggesting that QLR-addback stimulates GTP synthesis. Similarly, QLR supplementation led to a 3-fold increase in AMP levels relative to cells in EBSS (**Fig 5.23B**). These findings suggest that while QLR-addback increased GTP and AMP under both EBSS and double (glucose and amino acid, **Fig 5.13**) dPBS starvation media, their levels upon amino acid starvation are affected by glucose availability.

Recently, it was reported that lipid metabolism is altered during serine starvation which promotes mitochondrial fragmentation (Gao et al., 2018). It was shown that serine starvation led to a decrease in ceramide levels accompanied by reduced glutamine catabolism to alpha-ketoglutarate in mitochondria. Since these authors suggested that changes in lipid metabolism can alter mitochondrial metabolism and mitochondrial dynamics, we wanted to understand whether QLR addback-dependent mitochondrial hyperfusion was associated with changes in lipid metabolism.

We highlighted metabolites involved in lipid metabolism and identified taurine and phosphodimethylethanolamine as two of the most significantly altered lipid metabolites after QLR-addback into amino acid starvation media. Studies indeed have shown that taurine is required for proper mitochondrial function. For example, taurine was reported to function as an antioxidant, therefore protects mitochondria against oxidative stress (Yang et al., 2013c, Jong et al., 2017). It was observed that amino acid starvation in EBSS led to a 20% reduction in taurine levels relative to controls (**Fig 5.24A**). However, QLR-addback led to a further 50% reduction in taurine levels relative to cells incubated in EBSS. This suggests that QLR amino acid re-feeding (and its associated hyperfused mitochondria) leads to depletion or inhibits synthesis of taurine.

Phosphodimethylethanolamine is an intermediate of glycerophospholipid metabolism which is used for the biosynthesis of cardiolipin (Schlame, 2008). However, the

association of glycerophospholipid metabolism and nutrient-dependent mitochondrial hyperfusion is uncharacterised. Building on this, it was observed that amino acid starvation led to a 25% reduction in phosphodimethylethanolamine levels relative to untreated cells (**Fig 5.24B**). Interestingly, QLR-addback into amino acid starvation media further reduced the levels of phosphodimethylethanolamine by at least 70%. These findings highlight that QLR-addback can drive the depletion of specific lipids.

Studies have shown that during amino acid starvation, fatty acids are distributed between compartments of fused mitochondria (Rambold et al., 2015). This suggests that lipid trafficking within mitochondria may play a role in regulating mitochondrial fusion. To clarify the link between lipid metabolism and QLR-dependent mitochondrial hyperfusion, we studied the potential role of Translocator protein 18kDA (TSPO). More specifically, we used TSPO-deficient human retinal pigment epithelium cells (ARPE19) that were shown to have dysfunctional mitochondrial lipid cholesterol trafficking (Biswas et al., 2017). TSPO has been shown to localise to the outer mitochondrial membrane where it shuttles cholesterol from the outer mitochondrial membrane to the inner membrane (Biswas et al., 2017, Lacapere and Papadopoulos, 2003). Metabolomic studies have also shown that the loss of TSPO leads to further dysfunctional lipid metabolism, leading to intracellular lipid accumulation and ROS production (Alamri et al., 2019).

To investigate whether mitochondrial hyperfusion involved lipid metabolism, wildtype ARPE19 and CRISPR-targeted TSPO deficient cells (Biswas et al., 2017) were starved in EBSS or in EBSS with supplemented QLR. Starvation of wildtype ARPE19 cells in EBSS and the further supplementation of QLR both led to mitochondrial fusion (as we observed in other cell types) (**Fig 5.25A**). Similar mitochondrial fusion responses could be observed in TSPO-CRISPR ARPE cells. Upon quantification, we found that starvation in EBSS led to a significant increase in mitochondrial length and QLR-addback led to further hyperfusion (**Fig 5.25B**). However, QLR-addback led to a further increase in mitochondrial length (up to 2-fold longer relative to cells starved of all amino acids, in both TSPO wildtype and TSPO KO cells). However, the level of mitochondrial hyperfusion was significantly lower in QLR-addback treated TSPO KO cells relative to QLR-addback treated wildtype cells. This indicated that TSPO KO cells (deficient in lipid trafficking) can still respond to QLR-addback by stimulating mitochondrial hyperfusion, albeit to a lesser extent. Therefore, these results suggest that QLR-addback dependent mitochondrial hyperfusion is not occurring as a result of reduced mitochondrial lipid trafficking or changes in lipid metabolism.

Collectively, these data suggest that QLR-addback into amino acid starvation media can robustly reprogram multiple pathways in cellular lipid metabolism. However, inhibition of a mitochondrial lipid transporter could only partially inhibit amino acid-dependent hyperfusion. Therefore, altered generation of lipid metabolites may be playing some regulatory role during QLR-dependent mitochondrial hyperfusion. In addition, similar metabolomics changes in the urea cycle, E metabolism and bioenergetics could be observed after QLR-addback into EBSS amino acid starvation media (containing glucose), consistent with our earlier observations in double starvation contexts.

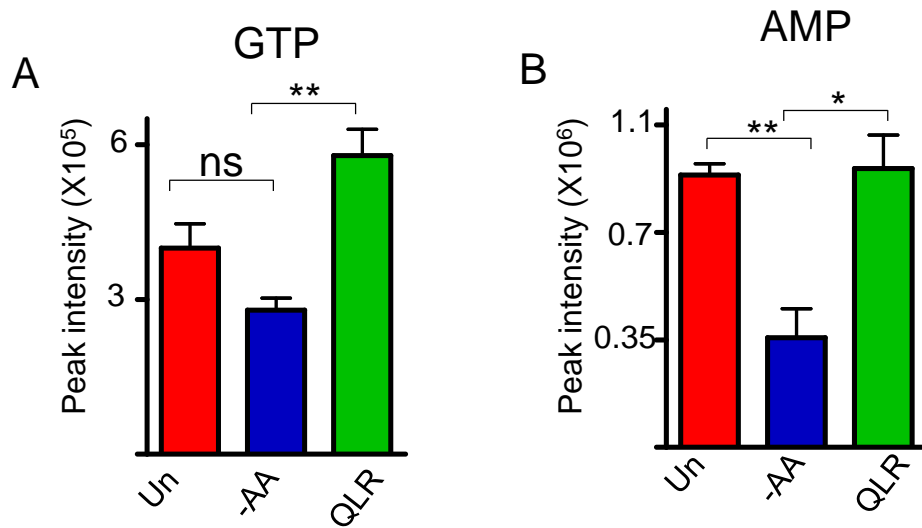


**Figure 5.23: QLR supplementation into amino acid-starved cells alter nucleotide metabolism.** 4T1 cells were treated with full media (UN), starved of either all amino acids (-AA) or starved of amino acid but supplemented with (QLR) for 4h. Starvation media conditions also contained 10% dialysed FBS. Bar graphs show the mean peak intensity of (A) GTP (B) AMP. N= 3 independent biological replicates. \* represents  $p < 0.05$ , \*\* ( $p < 0.01$ ), \*\*\* ( $p < 0.001$ ).

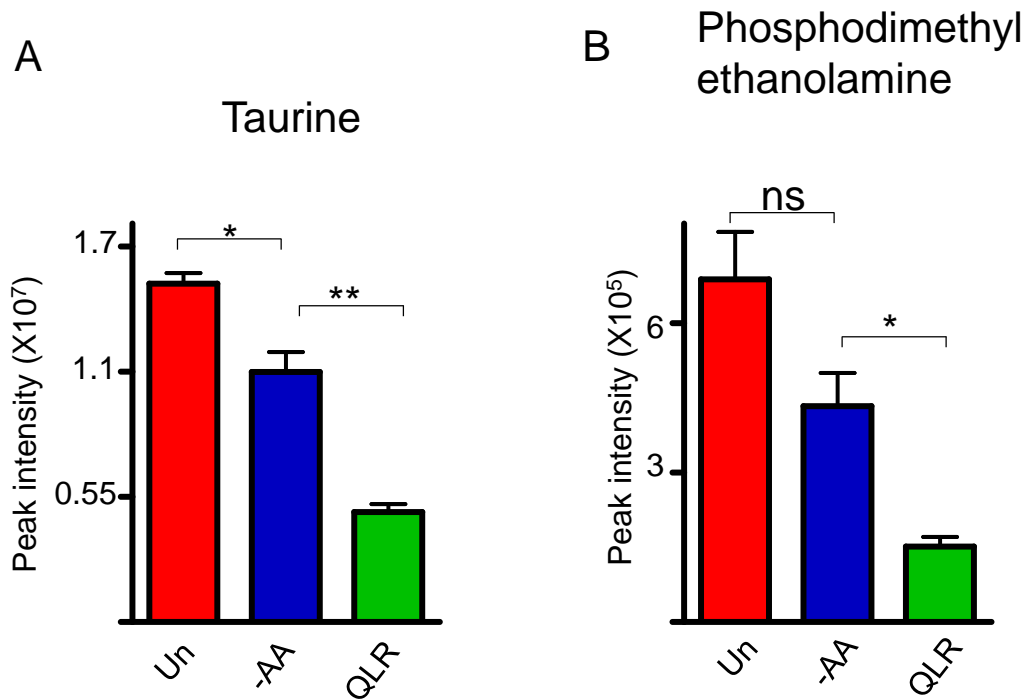


**Figure 5.24: QLR supplementation into amino acid-starved cells alter lipid metabolism.** 4T1 cells were treated with full media (UN), starved of either all amino acids (-AA) or starved of amino acid but supplemented with (QLR) for 4h. Starvation media conditions also contained 10% dialysed FBS. Bar graphs show the mean peak intensity of (A) Taurine (B) Phosphodimethyl ethanolamine. N=3 independent biological replicates. \* represents  $p < 0.05$ , \*\* ( $p < 0.01$ ), \*\*\* ( $p < 0.001$ ), ns (non significant).

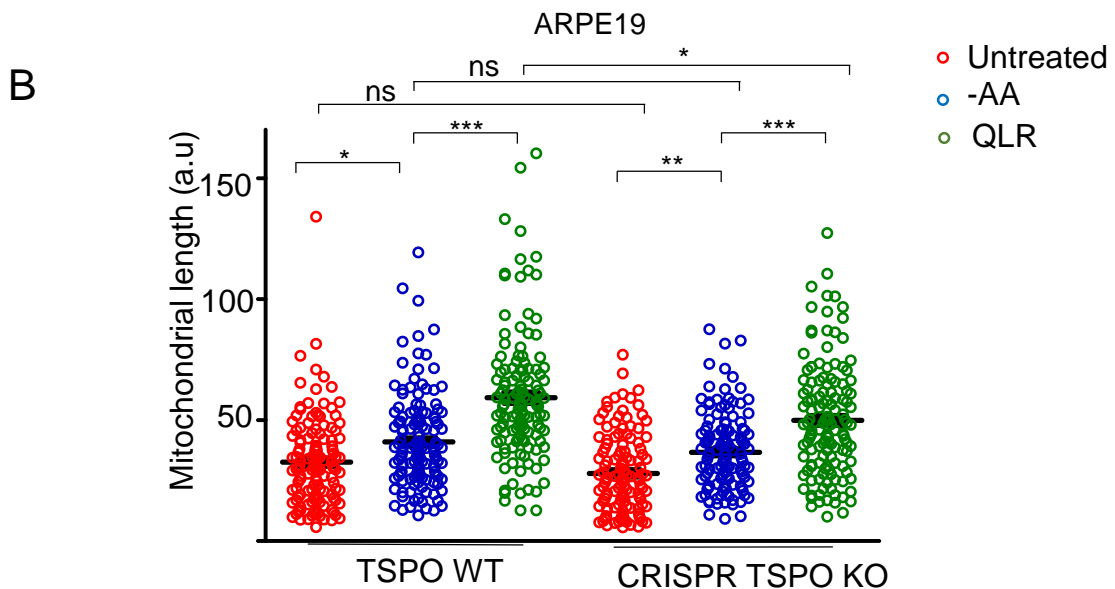
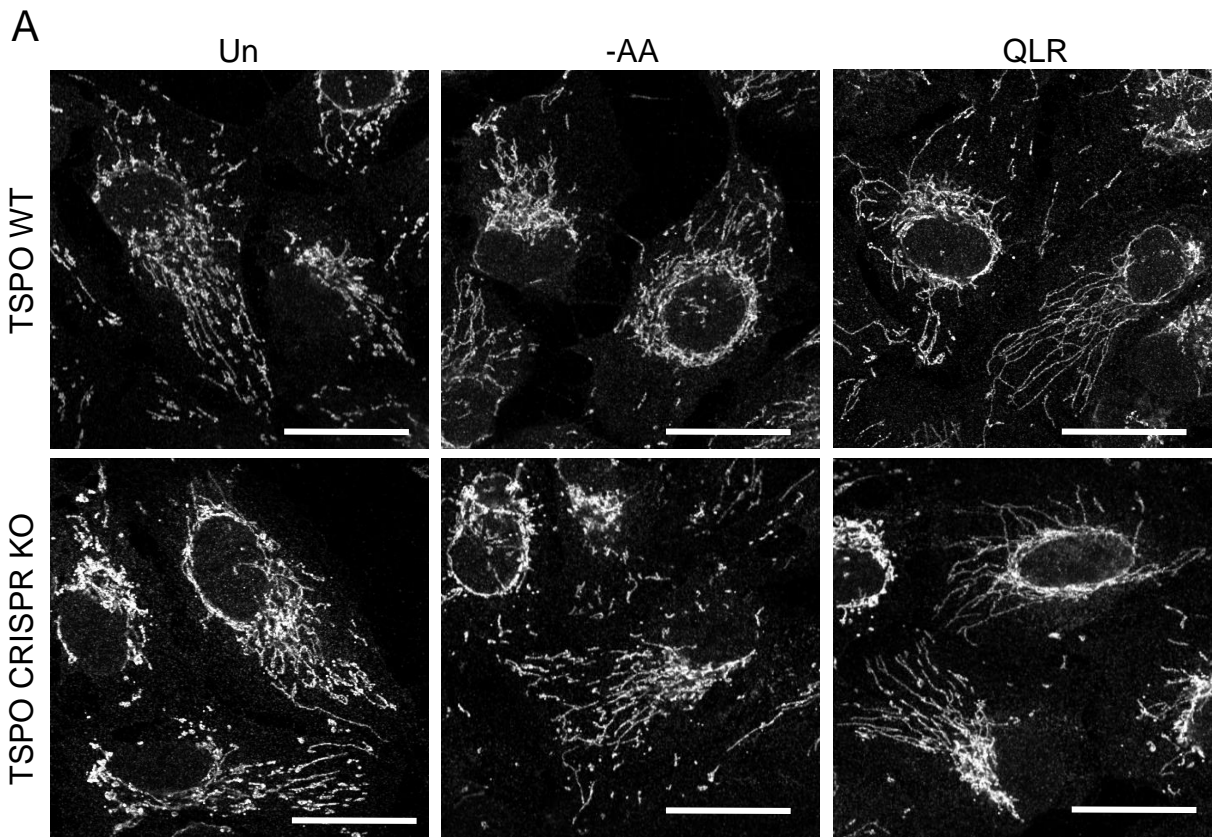


**Figure 5.25: Q, L, R-induced hyperfusion is independent of TSPO-mediated lipid transport.**

(A) Representative images of WT and ARPE19 CRISPR TSPO cells in full media (Un), starved of either all amino acids (-AA) or starved of amino acid but supplemented with (QLR) for 4h in EBSS. Starvation media conditions also contained 10% dialysed FBS. Mitochondrial membrane is stained with antibody against TOM20. (B) Beeswarm plot showing similar mitochondrial hyperfusion in WT and CRISPR TSPO cells. Each dot represents the mean length of 10 mitochondria within a cell. Each treatment shows between 120-150 cells quantified from three independent experiments. \* represents  $p < 0.05$ , \*\* ( $p < 0.01$ ), \*\*\* ( $p < 0.001$ ), ns (non significant) analysed with one way ANOVA, Bonferroni post test. Scale:  $25\mu\text{m}$

#### 5.2.2.4 Distinct cellular metabolism profiles following QLR or single amino acid addback

Studies have shown that intermediates of the Krebs cycle can be replenished from Q via anaplerotic reactions (Owen et al., 2002). Since it was shown earlier that addback of Q alone into amino acid starvation media stimulated lower levels of mitochondrial hyperfusion relative to QLR addback (Refer to Fig 3.4), LC/MS/MS metabolomics were performed to compare metabolic changes between these 2 addback conditions. It was observed that similar metabolic pattern was observed for QLR addback versus Q addback alone (**As summarised in Table 5.4**). However, Q-addback treated cells have some distinct metabolic patterns relative to QLR-addback treated cells. It was observed that 4-guanidinobutanal, 4-aminobutanoate and spermidine were significantly different between QLR- and Q-treated cells (**Fig 5.26**). Therefore, levels of these metabolites were further assessed. Studies have demonstrated that R serves as precursor for guanidino compounds such as 4-guanidinobutanal and 4-aminobutanoate. Both these metabolites have been shown to be elevated in patients with arginase deficiency and high plasma R levels (Burrage et al., 2019). It was observed that amino acid starvation led to depletion of 4-guanidinobutanal while QLR-addback restored levels (**Fig 5.26A**). In contrast, Q addback did not restore levels of 4-guanidinobutanal (which fits expectations since R is lacking). Surprisingly, levels of 4-aminobutanoate were sustained in amino acid starved, QLR-addback and Q-addback treated cells (**Fig 5.26B**). The levels of 4-aminobutanoate in QLR-addback treated cells were significantly lower relative to cells starved of all amino acid. Similarly, levels of 4-aminobutanoate in Q-addback treated cells were also significantly lower relative to QLR-treated cells. However, R is not the only precursor contributing to 4-aminobutanoate, since this could be maintained from other sources when R is lacking.

On the other hand, studies have shown that spermidine is synthesised in the polyamine pathway by R conversion to ornithine which is further converted to putrescine, spermidine and spermine (Pegg, 2009). Studies have shown that spermidine can have pro-apoptotic functions when its concentration is raised to promote release of cytochrome c, cleaved-caspase 3, BAX and inhibition of Bcl-2 (Mandal et al., 2015, Chen et al., 2018). Interestingly, it was observed that amino acid starvation did not alter the levels of spermidine relative to untreated cells (**Fig 5.26C**). In contrast, QLR-addback increased spermidine levels by 2-fold relative to cells starved of all amino acid. Surprisingly, the addback of Q alone further increased

spermidine levels by ~2-fold relative to QLR-addback treated cells. Therefore, QLR- vs. Q-addback can lead to distinct metabolic profiles that include distinct changes in the pro-apoptotic metabolite spermidine.

Taken together, these data further confirmed, via an independent experiment, QLR-dependent metabolic changes observed in earlier EBSS contexts (including increased E metabolism, reduced oxidative stress and increased cellular energetics). However, we found that these changes did not correlate with patterns of mitochondrial hyperfusion, since cells facing Q-addback alone had similar metabolic pathways as QLR-addback alone. We had shown earlier that mitochondrial hyperfusion is associated with QLR-addback (but not Q-addback). However, cells facing Q-addback did show a distinct pattern in a small number of metabolites.

**Table 5.4: Summary of key significant metabolic changes after QLR and Q addback in EBSS**

The effect of amino acid starvation on metabolites (After -AA relative to AA). The effect of QLR addback into amino acid starvation media on metabolites relative to full amino acid starvation (After QLR addback relative -AA). The effect of Q addback on metabolites relative to QLR (Q addback relative to QLR). N.A indicate metabolite is not significantly altered. N.I indicate metabolite was not identified. Note, summary is pool from two independent metabolomics experiment (i.e QLR metabolomics and separate QLR Vs Q experiment)

<b>Summary of key significant metabolic changes between groups</b>			
<b>EBSS media</b>			
<b>Metabolites</b>	<b>After -AA relative to AA</b>	<b>After QLR addback relative -AA</b>	<b>Q addback relative to QLR</b>
Arginine	Reduced	Increased	Reduced
Argininosuccinate	N.A	Increased	N.I
Asparagine	N.A	Increased	N.I
Aspartate	Reduced	Increased	N.A
ATP	Reduced	Increased	N.A
Citruline	Reduced	N.S	N.A
Fumarate	Reduced	Increased	N.I
Glutamate	Reduced	Increased	N.A
GSH	N.A	Reduced	N.A
GSSG	N.A	Reduced	N.A
Malate	Reduced	Increased	N.I
Ornithine	Reduced	Increased	N.A

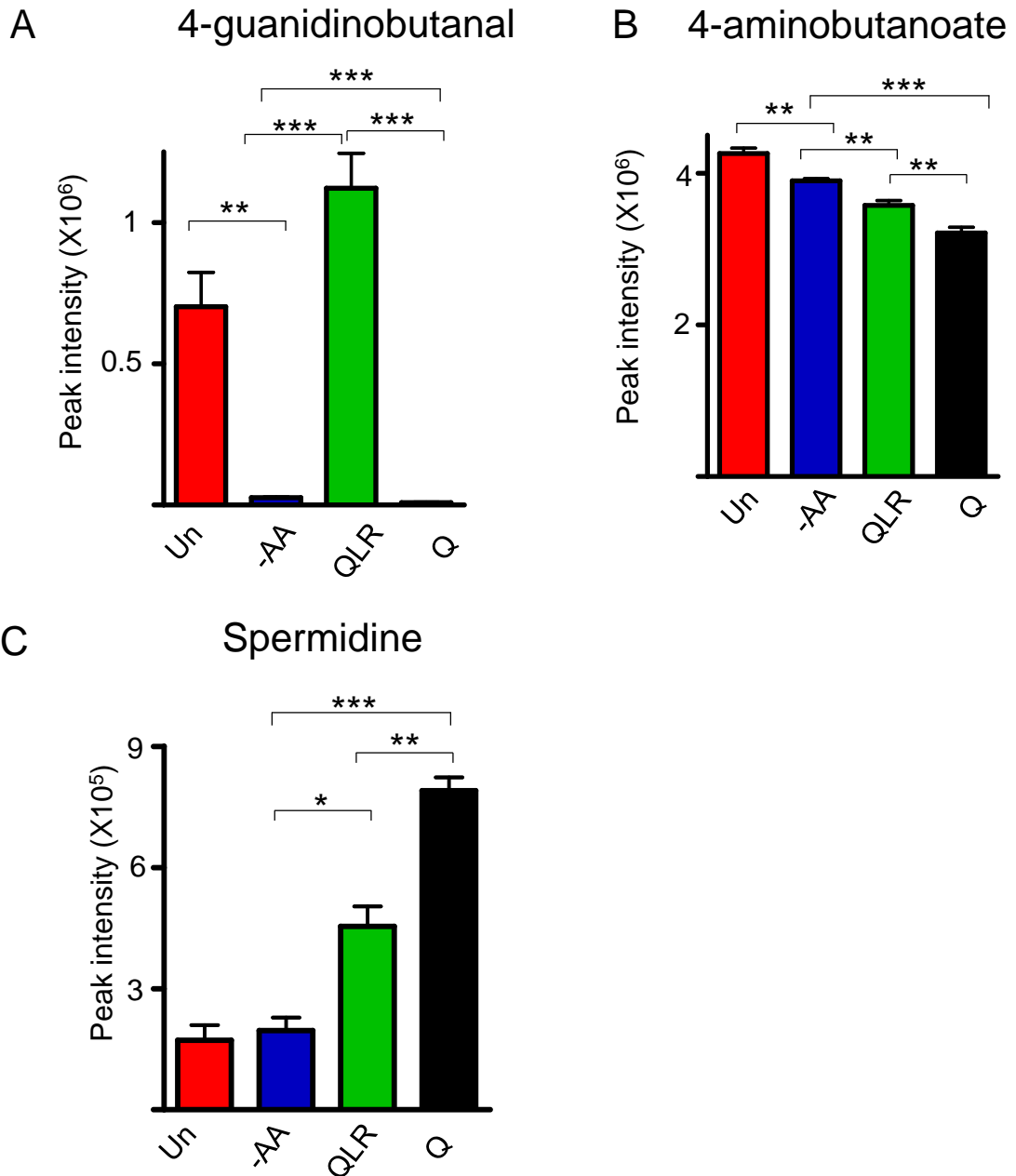


**Figure 5.26: Metabolic variations between QLR and Q-addback.** 4T1 cells were treated with full media (UN), starved of either all amino acids (-AA), or starved of amino acid but supplemented with (QLR) or with Q alone for 4h. Starvation media conditions also contained 10% dialysed FBS. Bar graphs show the mean peak intensity of (A) 4-guanidinobutanal (B) 4-aminobutanoate (C) Spermidine N=4 independent biological replicates. \* represents  $p < 0.05$ , \*\* ( $p < 0.01$ ), \*\*\* ( $p < 0.001$ ).

### **5.2.3 The Krebs cycle is required for QLR-dependent mitochondrial hyperfusion**

Studies have shown that metabolites generated from Q-dependent anaplerotic reactions can play roles to modulate amino acid sensing pathways (Duran et al., 2012, Son et al., 2019). For example, it has been shown that the supplementation of alpha-ketoglutarate blocks amino acid starvation-induced autophagy (Baracco et al., 2019). Since we showed earlier that addback of Q, L and R amino acids stimulate mitochondrial hyperfusion (Refer to Fig 3.4), we hypothesise that mitochondria sense QLR-dependent metabolites generated in synergy during QLR-supplementation into amino acid starvation media.

The carbon backbone derived from metabolism of Q, L and R all feed directly into the Krebs cycle at different points (Refer to Fig 5.19). In addition, R is an intermediate in the urea cycle. We next wanted to determine whether the Krebs cycle (and by extension the urea cycle) was required for QLR-addback dependent mitochondrial hyperfusion. Therefore, we investigated mitochondrial hyperfusion in a cell model lacking fumarate hydratase (Fh, also referred to as fumarase) (Zheng et al., 2015).

Fumarate hydratase 1 (Fh1) gene codes for Fh, which is an enzyme that catalyzes the reversible hydration of fumarate to form malate in the Krebs cycle. Fh has been shown to localize within mitochondria and cytosol/nucleus where it has dual functions (Adam et al., 2013, Yogev et al., 2010). In the cytosol, Fh functions during the DNA damage response by translocating to the nucleus and catalysing reverse conversion of malate to fumarate for DNA repair. In contrast, mitochondrial-localised Fh participates in the Krebs cycle by canonically converting fumarate to malate.

The deficiency of Fh has been shown to underlie pathogenesis of hereditary leiomyomatosis and renal cell cancer (HLRCC) and kidney cancer (Tomlinson et al., 2002). Cells lacking Fh function have aberrant metabolism characterised by reduced mitochondrial respiration, dysfunctional Krebs cycle and dysregulated urea cycle / R metabolism (Frezza et al., 2011, Yang et al., 2010, Zheng et al., 2013, Tyrakis et al., 2017, Adam et al., 2013, Raimundo et al., 2008). For example, it was initially reported that Fh deficient cells were unable to convert fumarate to malate thereby truncating the Krebs cycle and leading to the accumulation of oncometabolites that promote tumorigenesis (Yang et al., 2010, Raimundo et al., 2008, Tyrakis et al., 2017). Similarly, it has been shown that while normal cells synthesize argininosuccinate from D and citrulline via the urea cycle (Refer to fig 5.5), in contrast, Fh deficient cells

reversely produce argininosuccinate from fumarate and R (Zheng et al., 2013). In addition, E levels have also been shown to be depleted in Fh deficient cells (Adam et al., 2013). These studies show that Fh deficient cells have dysregulated urea cycle, E catabolism and Krebs cycle. Therefore, this is a useful system to test effects on QLR-dependent mitochondrial hyperfusion.

We utilised immortalized kidney cells from mice homozygous for a conditionally targeted Fh1 allele which contains LoxP sites flanking exons 3 and 4 (Fh1 fl/fl) (Frezza et al., 2011). We could compare Fh1 fl/fl cells as control (wildtype Fh1) with two different deletion clones (Fh -/- clone1 and Fh -/- clone19) that were isolated from Fh1 fl/fl cells infected with recombinant adenovirus expressing Cre recombinase (Frezza et al., 2011). Therefore, Fh1 fl/fl, Fh1 -/- clone1 and Fh1 -/- clone19 cells were starved of either all amino acids (EBSS) or starved of amino acid but supplemented with QLR for 4h. Cells were fixed and mitochondrial fusion was quantified.

Initial observation of mitochondrial structure in (fl/fl) wildtype, clone1 and clone19 cells indicate that mitochondria were small and fragmented in all untreated cell types (**Fig 5.27A**). However, clone19 cells often had rounded and swollen mitochondria, albeit less observed in untreated clone1 cells. Interestingly, amino acid starvation led to mitochondrial fusion in wildtype, clone1 and clone19 cells. QLR-addback (into EBSS) led to strong mitochondrial hyperfusion in wildtype cells. Surprisingly, both clone1 and clone19 cells did not undergo any observable QLR-dependent mitochondrial fusion.

Upon quantification, in wildtype Fh1 fl/fl cells, amino acid starvation increased mitochondrial length by 3-fold relative to untreated cells (**Fig 5.27B**). Also in Fh1 fl/fl cells, QLR-addback into amino acid starvation media further increased mitochondrial length relative to cells starved of all amino acid. With Fh1 deficiency, amino acid starvation still led to 3-fold increase in mitochondrial length in both clone1 and clone19 cells. However, QLR-addback mitochondrial hyperfusion length was totally blocked in both clone1 and clone19 cells.

We confirmed that wildtype Fh1 fl/fl expressed normal levels of Fh while both Fh1 -/- clone1 and clone19 did not express any protein (**Fig 5.27C**). These findings suggest that a functional Krebs cycle is required for QLR-addback dependent mitochondrial hyperfusion, possibly due to urea cycle or amino acid E metabolism. However, the Krebs cycle was not required for amino acid starvation-induced mitochondrial fusion. These results further suggest that amino acid starvation vs. QLR-dependent mitochondrial fusion involve different mechanisms.

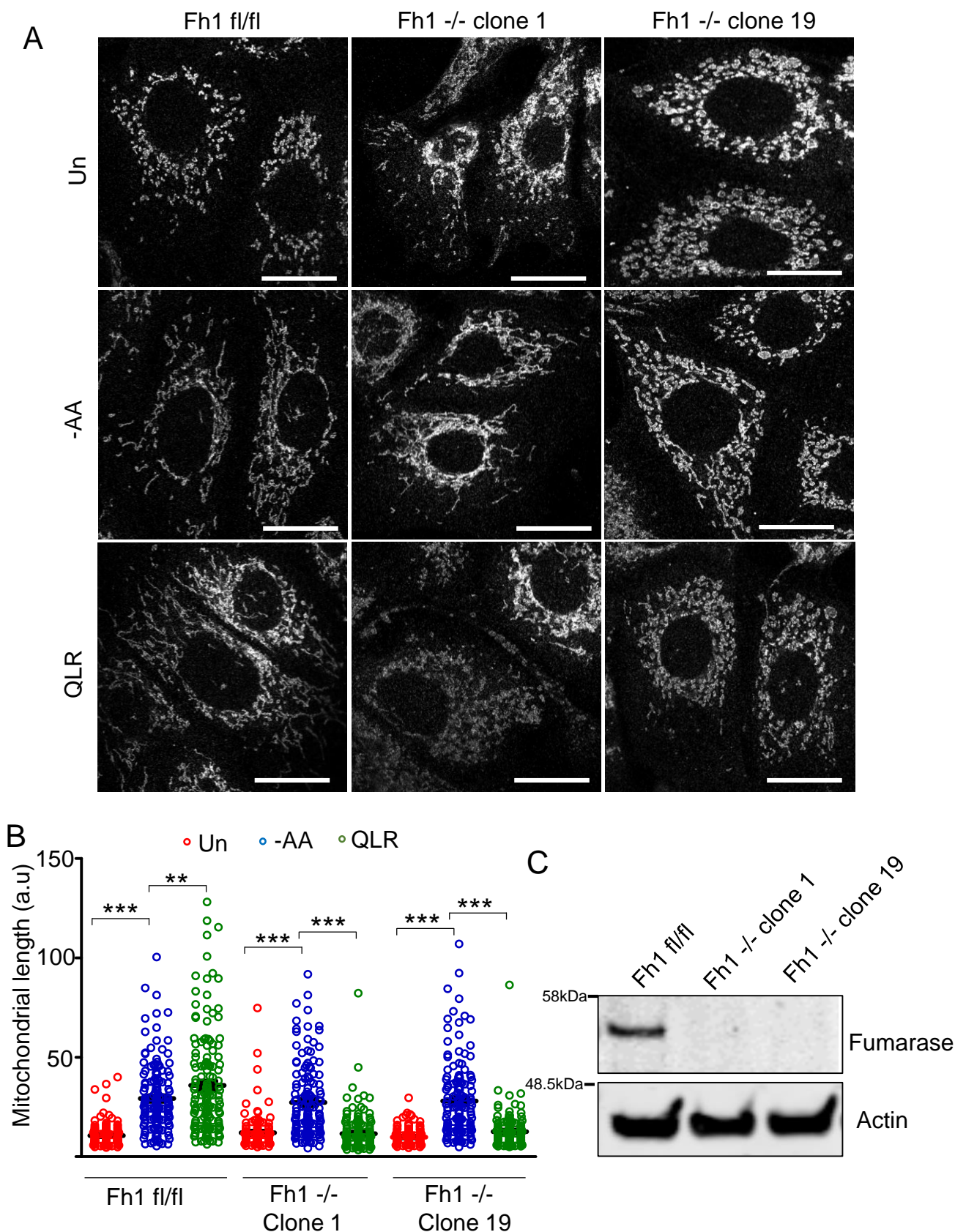


**Figure 5.27: Q, L, R-induced hyperfusion requires an efficient Krebs cycle.** (A) Representative images of Fumarate hydratase-1 (Fh1) control cells (Fh1 fl/fl) and Fh KO cells (Fh1<sup>-/-</sup> clone1) (Fh<sup>-/-</sup> clone19) maintained in full media (Un), starved of either all amino acids (-AA) or starved of amino acid but supplemented with (QLR) for 4h. Starvation media conditions also contained 10% dialysed FBS. Mitochondrial membrane is stained with antibody against TOM20. B) Each dot represents the mean length of 10 mitochondria within a cell. Each treatment shows between 120-150 cells quantified from three independent experiments. C) Western blot showing the absence of fumarase enzyme. \*\* p, 0.01, \*\*\* indicate P < 0.001 analysed with one way ANOVA, Bonferroni post test. Scale:25µm

Multiple studies have shown that cellular metabolism is dramatically reprogrammed in Fh deficient cells (Yang et al., 2013b, Zheng et al., 2013). This metabolic reprogramming is characterised by aberrant depletion and accumulation of distinct metabolites such as fumarate and argininosuccinate. To determine how metabolic changes in Fh1 deficient cells might reveal clues about hyperfusion, we performed metabolomics of wildtype Fh1 fl/fl and clone1 deleted cells after amino acid starvation vs QLR supplementation.

PCA scores plot showed that there is a close clustering within replicates of each treatment groups in both cell types (**Fig 5.28A**). Clear separation between treatment groups was also observed. Similarly, PLS-DA analysis also demonstrated tight clustering and good separation within and between each treatment groups (**Fig 5.28B**). These findings indicate that this metabolomic data set is overall of robust quality and that there were distinct metabolic changes between each treatment groups in both cell types.

ORA indicated that metabolites of the urea cycle, nucleotide sugar metabolism, D metabolism, ammonia recycling and the E.T.C. were among the top 20 pathways altered (when comparing wildtype vs. clone1 cells under the QLR-addback condition) (**Fig 5.29A**). Pathway analysis also identified the urea cycle as the most significantly altered pathway between wildtype vs. Fh1 deleted cells (under the QLR-addback condition) (**Fig 5.29B**). **Table 5.5** shows that the urea cycle has an FDR of 0.000194. These findings suggest that defective QLR-dependent mitochondrial hyperfusion in Fh1-deficient cells are associated with changes in amino acid metabolism pathways.

To investigate further the metabolic changes in amino acid metabolism, heatmap clustermap analysis was performed (for all metabolites involved in amino acid metabolism). The heatmap showed that many amino acid metabolites were differentially altered following amino acid starvation and QLR-addback in both wildtype and Fh deficient cells (**Fig 5.30**). Interestingly, the heatmap illustrated that a group of QLR-addback dependent metabolites were depleted in Fh deficient cells (highlighted in red dashed box). The red dashed boxes highlight metabolic clusters that have reduced levels in Fh1 KO cells relative to corresponding wildtype. Groups of metabolites could also be seen to accumulate in Fh deficient cells (highlighted in green dashed boxes). The green dashed boxes highlight metabolic clusters that have increased levels in Fh1 KO cells relative to corresponding wildtype. This indicated that QLR-dependent amino acid metabolism is dysregulated upon Fh loss of function.

Studies have reported that R and ornithine levels were similar in Fh deficient cells (under full nutrient condition) relative to wildtype (although argininosuccinate was increased with Fh-loss) (Adam et al., 2013). Our LC/MS/MS analysis indicated that metabolites of the urea cycle were significantly altered in the Fh1 experiment, which generally agrees with our other metabolomics data. As follows, it was investigated in detail how urea cycle metabolites are altered in Fh-deficient cells. R levels were similar in both wildtype and Fh deficient cells in the control (untreated) nutrient condition (**Fig 5.31A**). It was observed that amino acid starvation led to the total depletion of R in both wild type and Fh deficient cells. QLR-addback into amino acid starvation media overall restored R levels in wildtype cells. However, QLR-addback led to significantly higher R accumulation in Fh deficient cells (3-fold higher). This finding suggests that R metabolism to downstream intermediates (following QLR-addback) is inefficient without Fh function and flux via the Krebs cycle.

Consistent with the previously reported metabolic profile in Fh deficiency (Adam et al., 2013), it was also observed that ornithine levels were similar in both untreated wildtype and Fh deficient cells (**Fig 5.31B**). Interestingly, amino acid starvation or QLR-addback did not significantly alter ornithine levels in both wildtype and Fh deficient cells. This finding suggests that ornithine levels are not strongly affected by the varying nutrient conditions or status of Fh function. Surprisingly, this lack of effect in ornithine differed from our earlier data sets (Fig 5.17 and 5.27).

Studies have shown that argininosuccinate is a metabolic biomarker for Fh deficiency, produced via conversion of R and fumarate by argininosuccinate lyase (ASL) (Zheng et al., 2013). In wildtype cells, starvation of all amino acids led to total depletion of argininosuccinate (relative to untreated) while QLR-addback restored the levels (**Fig 5.31C**). A similar amino acid-dependent argininosuccinate profile was observed in Fh-deficient cells, although higher levels of accumulation were observed. In line with the previously reported profile in Fh deficient cells, argininosuccinate in untreated and QLR-addback Fh deficient cells were 74-fold and 71-fold higher relative to wildtype. This finding indicates that argininosuccinate (and potentially other intermediates) of the urea cycle accumulate upon Fh deficiency.

Taken together, the similar ornithine levels in both wildtype and Fh deficient cells (Fig 5.36B) does not support the forward conversion of ornithine to argininosuccinate. Therefore, this suggests that R back conversion to argininosuccinate is over-activated in Fh deficient cells. Overall, these findings suggest that QLR-addback dependent

mitochondrial hyperfusion might be blocked in Fh deficient cells due to dysregulation of the urea cycle, perhaps involving argininosuccinate conversion.

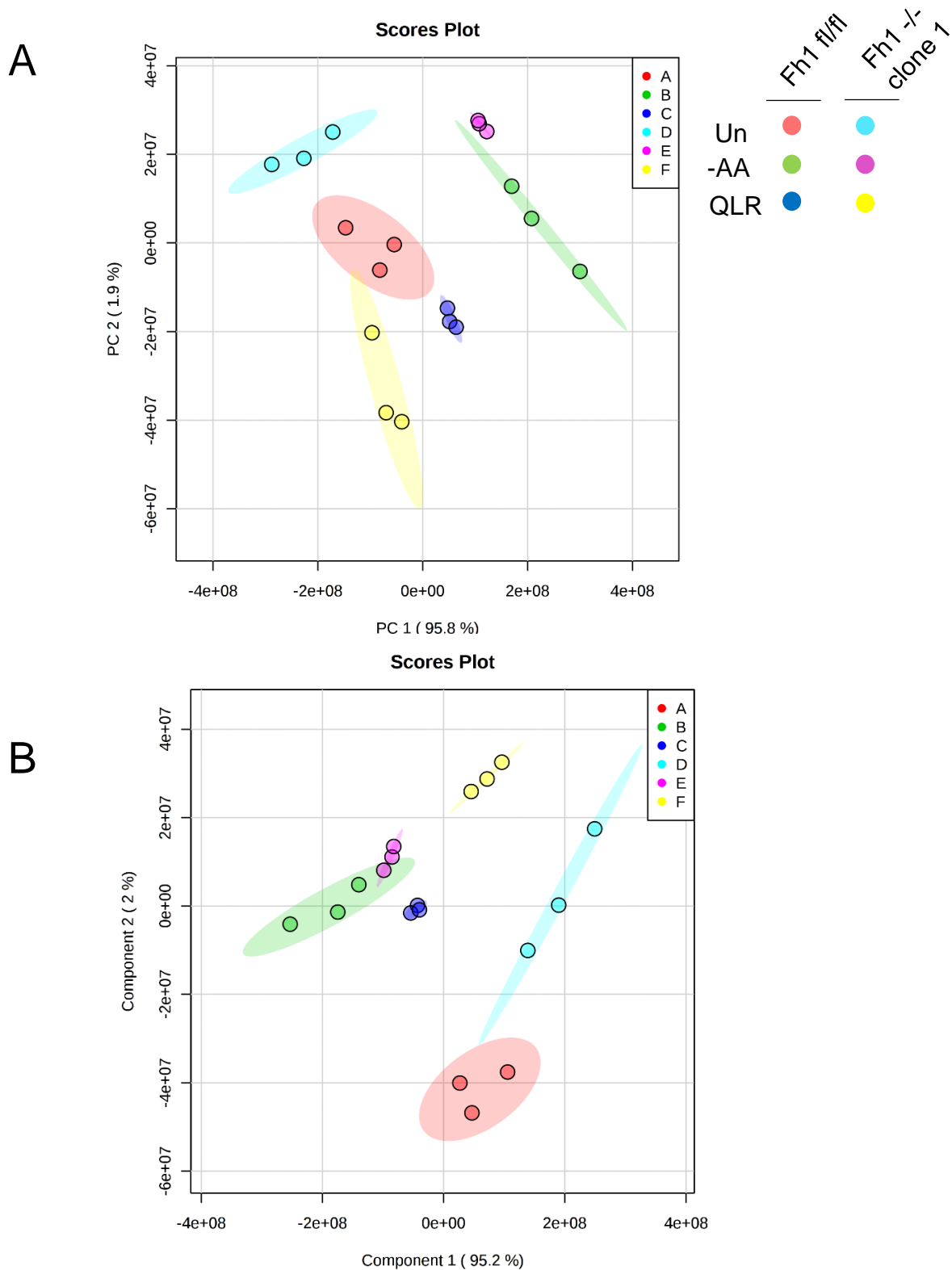
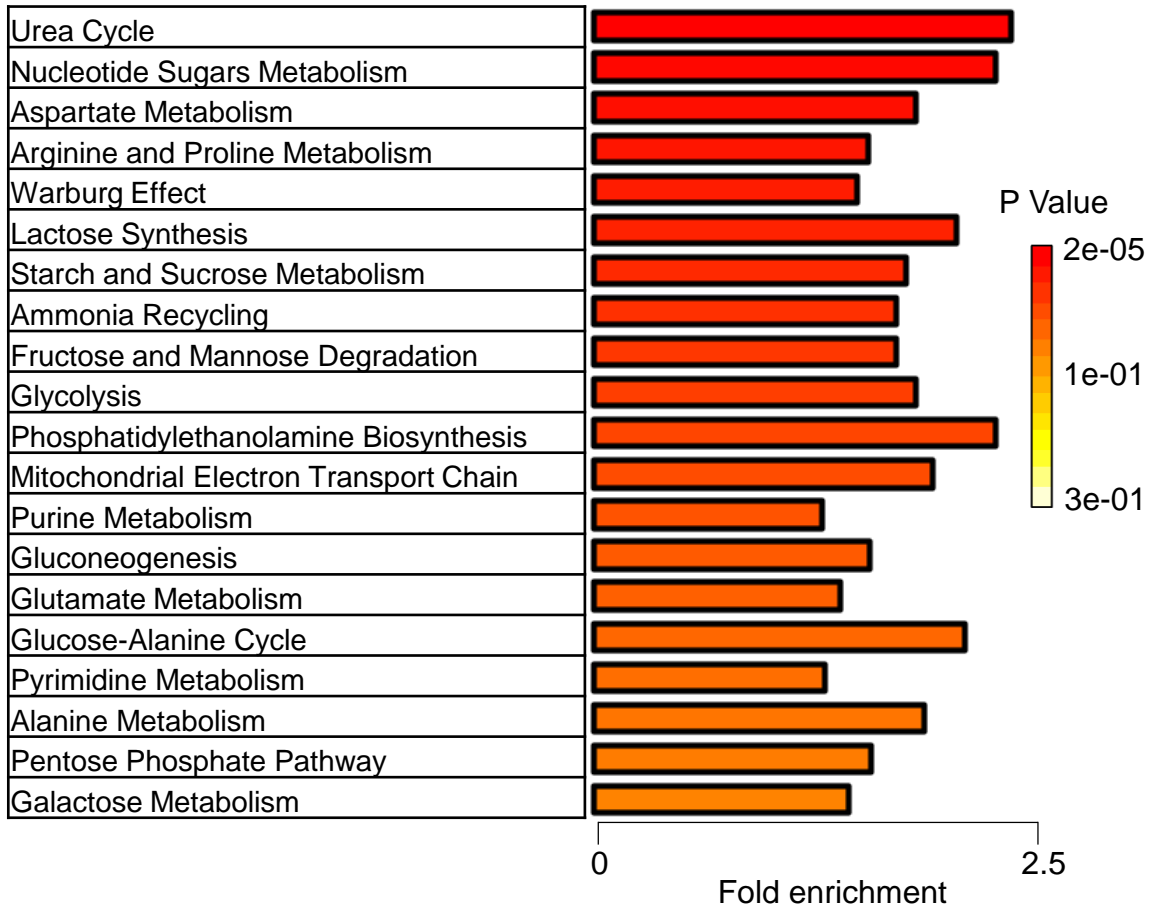


**Figure 5.28: Metabolomics LC-MS/MS analysis of Fumarate hydratase deficient cells.** Fumarate hydratase-1 (Fh1) control cells (Fh1 fl/fl) and Fh1 KO cells (Fh1<sup>-/-</sup> clone1) were maintained in full media (Un), starved of either all amino acids (-AA) or starved of amino acid but supplemented with (QLR) for 4h. Starvation media conditions also contained 10% dialysed FBS. A) Principal-Component Analysis (PCA) score plot showing the separation between treatment groups. B) Partial Least Squares-Discriminant Analysis (PLS-DA) showing the supervised classification of the treatment groups. N=3 independent biological replicate

A



B

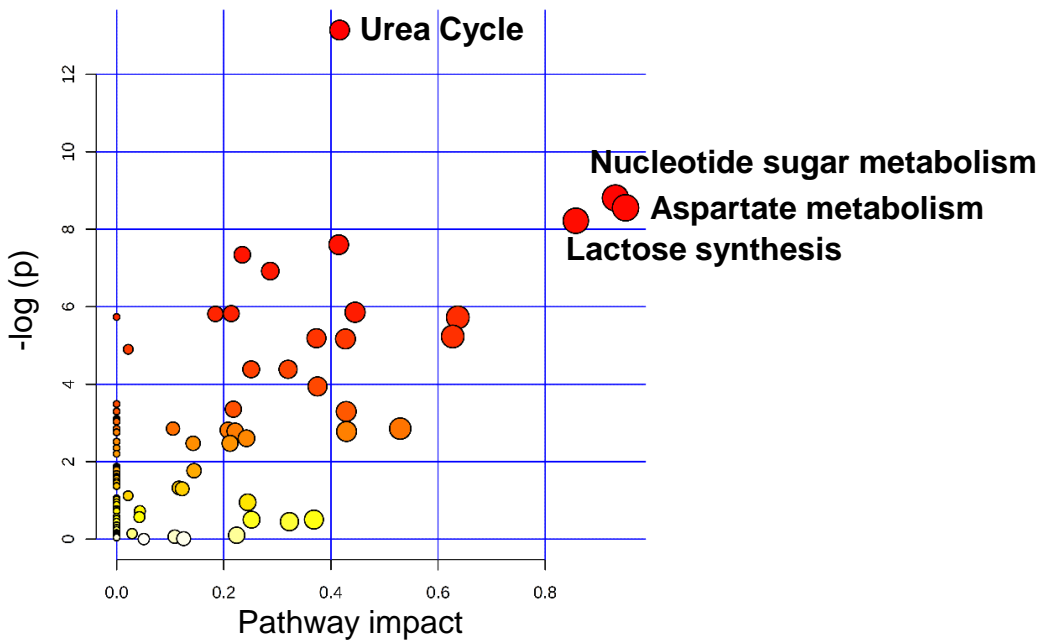


**Figure 5.29: Pathway analysis of metabolites with significant changes after QLR supplementation into amino acid-starved Fh1 fl/fl relative to amino acid-starved Fh1<sup>-/-</sup> (clone1) cells.** (A) Over-representation analysis (ORA) showing the top 20 enriched pathways based on significantly ( $p < 0.05$ ) altered metabolites between wildtype and clone1 cells under the QLR-addback condition. Ranked according to significant p values (Top  $\rightarrow$  Down, Darkest shade most significant) (B) Pathway analysis indicating the most relevant pathways. The darker the shade the greater the significance and the larger the circle, the more the metabolites involved in the pathway. Starvation media conditions also contained 10% dialysed FBS.

**Table 5.5: Detailed results of pathway analysis of relevant pathways after QLR supplementation into amino acid-starved Fh1 fl/fl cells relative to Fh1-/- clone1 cells.** Total: total number of metabolites in the pathway; the hits indicate the matched number from the analysed data; Raw p signifies the original P value calculated from the enrichment analysis; FDR is the adjusted p value using the false discovery rate; the impact represents the pathway impact value calculated from the topology analysis.

Pathway	Total	Hits	Raw p	FDR	Impact
Urea Cycle	25	15	1.96E-06	0.000194	0.41628
Nucleotide Sugars Metabolism	17	10	0.000149	0.006359	0.93103
Aspartate Metabolism	30	14	0.000193	0.006359	0.95
Lactose Synthesis	15	9	0.000269	0.006666	0.85714
Arginine and Proline Metabolism	47	18	0.0005	0.009896	0.41456
Starch and Sucrose Metabolism	26	12	0.000649	0.010702	0.23466
Ammonia Recycling	27	12	0.000988	0.013977	0.28684
Purine Metabolism	66	21	0.002859	0.026918	0.44513
Mitochondrial Electron Transport Chain	16	8	0.002961	0.026918	0.21393
Fructose and Mannose Degradation	30	12	0.002985	0.026918	0.18449
Alanine Metabolism	13	7	0.003231	0.026918	0
Glycolysis	23	10	0.003263	0.026918	0.63688
Pyrimidine Metabolism	52	17	0.005349	0.037586	0.62739
Gluconeogenesis	32	12	0.00559	0.037586	0.37299
Glutamate Metabolism	44	15	0.005695	0.037586	0.42714
Galactose Metabolism	33	12	0.007442	0.046044	0.021739
Pentose Phosphate Pathway	27	10	0.012477	0.065009	0.25122
Citric Acid Cycle	27	10	0.012477	0.065009	0.32009
Glucose-Alanine Cycle	10	5	0.019407	0.096063	0.375
Cardiolipin Biosynthesis	11	5	0.03056	0.14407	0
Riboflavin Metabolism	15	6	0.034934	0.15287	0.21795
Phenylacetate Metabolism	8	4	0.03706	0.15287	0
Malate-Aspartate Shuttle	8	4	0.03706	0.15287	0.42857
Phosphatidylethanolamine Biosynthesis	12	5	0.045035	0.16992	0
Glycerolipid Metabolism	24	8	0.04678	0.16992	0
Ethanol Degradation	16	6	0.047889	0.16992	0
Phytanic Acid Peroxisomal Oxidation	20	7	0.04806	0.16992	0

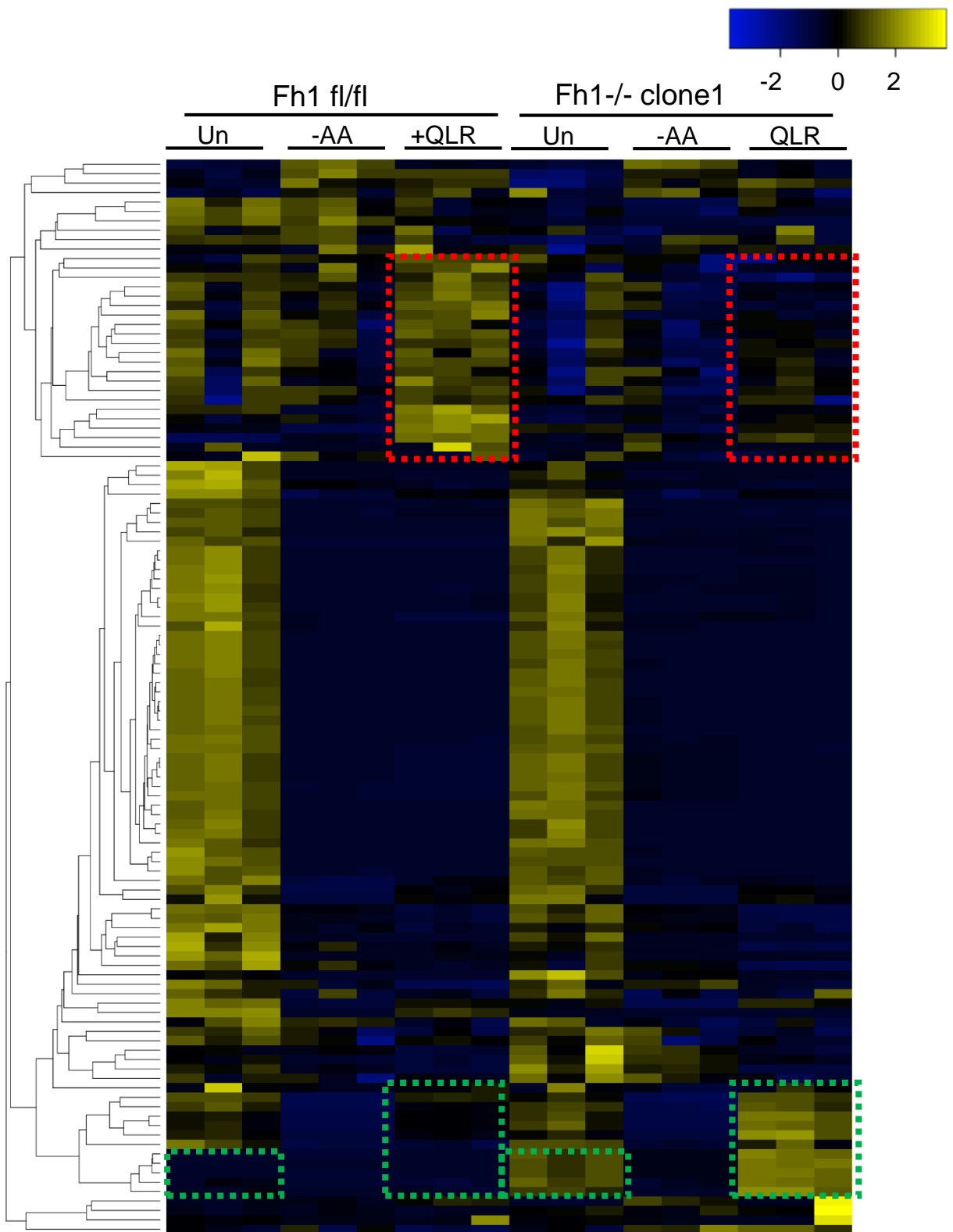


**Figure 5.30: Heat map showing the profile of metabolites involved in amino acid metabolism in Fh deficient cells.** Fumarate hydratase-1 (Fh1) control cells (Fh1 fl/fl) and Fh1 KO cells (Fh1-/- clone1) were maintained in full media (Un), starved of either all amino acids (-AA) or starved of amino acid but supplemented with (QLR) for 4h. Starvation media conditions also contained 10% dialysed FBS. Each treatment group has three independent biological replicates. All metabolites involved amino acid metabolism were highlighted on the excel macro library and processed into heatmap. Red dashed boxes highlight metabolic clusters that have reduced levels in Fh1 KO cells relative to corresponding wildtype. Green dashed boxes highlight metabolic clusters that have increased levels in Fh1 KO cells relative to corresponding wildtype.

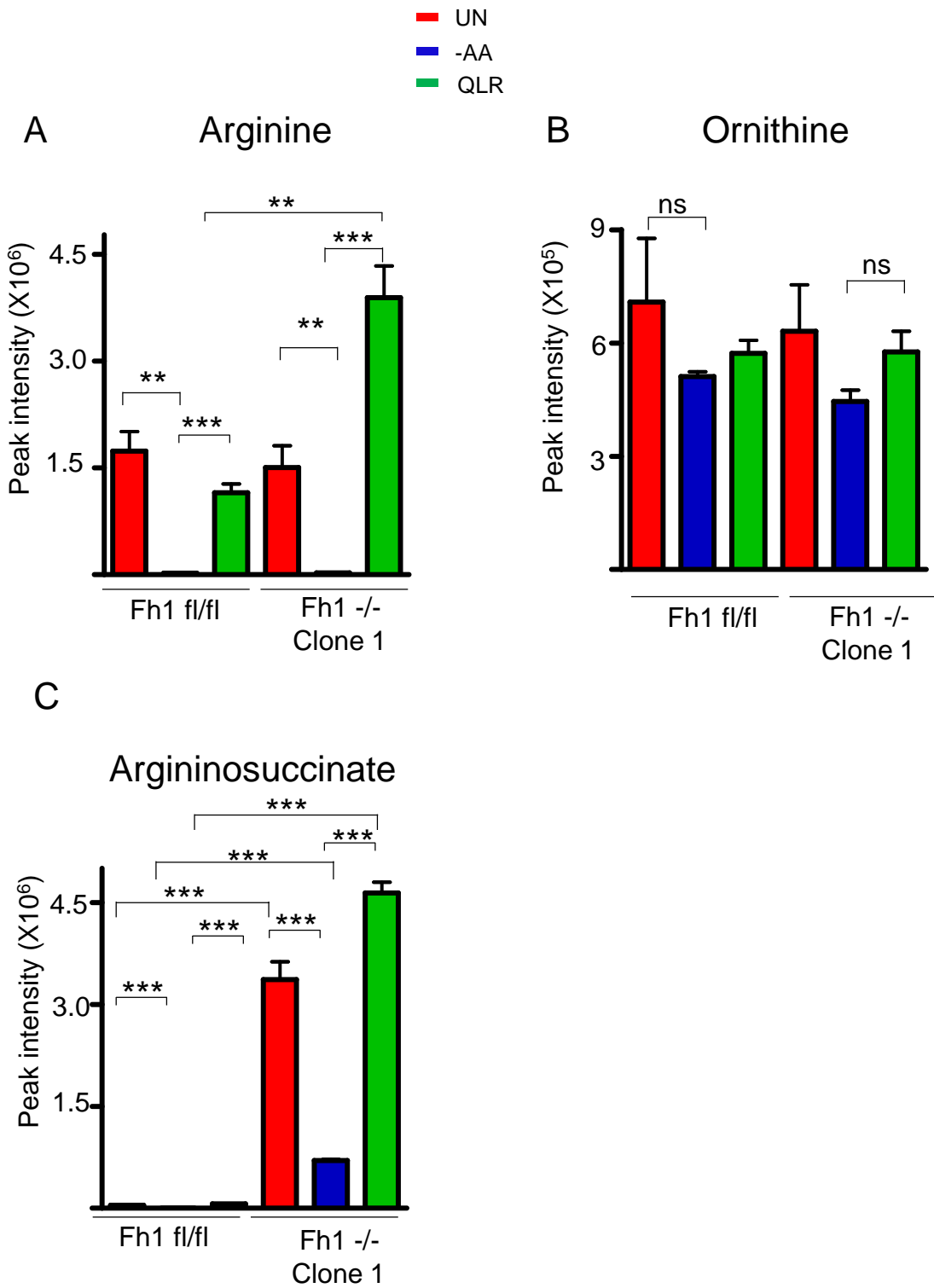


**Figure 5.31: Argininosuccinate flux is maximised in fumarate hydratase KO cells.** Fumarate hydratase (Fh1) control (Fh1 fl/fl) and Fh1 KO (Fh1-/- clone1) cells were maintained in full media (Un), starved of either all amino acids (-AA) or starved of amino acid but supplemented with (QLR) for 4h. Starvation media conditions also contained 10% dialysed FBS. Bar graphs show the mean peak intensity of (A) Arginine (B) Ornithine and (C) Argininosuccinate. N=3 independent biological replicate. \* represents  $p < 0.05$ , \*\* ( $p < 0.01$ ), \*\*\* ( $p < 0.001$ ).

Studies have highlighted that Fh deficiency leads to suppression of E biogenesis which is characterised by reduced E and D levels (Adam et al., 2013). Accordingly, the effect of Fh deficiency on E metabolism in our dataset was explored. As expected, amino acid starvation led to total Q depletion while QLR-addback restored levels in both Fh wildtype and Fh deficient cells (**Fig 5.32A**). Interestingly, Q levels were significantly higher by 2-fold in QLR-supplemented Fh deficient cells (relative to wildtype cells). This accumulation of Q further suggests that glutaminolysis is decreased when the Krebs cycle is blocked by Fh deficiency.

Consistent with our previous observation (Fig 5.18), amino acid starvation led to at least 70% depletion of E in wildtype and Fh-deficient cells. QLR-addback into amino acid starvation media significantly increased E levels by at least 3-fold (relative to amino acid-starved cells) in both wildtype and Fh-deficient cells. In line with previous profiling of Fh-deficient cells (Adam et al., 2013), it was observed that E levels in both untreated and full amino acid starved Fh deficient cells was 40% lower relative to wildtype controls (**Fig 5.32B**). In contrast, E levels in both wildtype and Fh deficient cells following QLR-supplementation were similar. Therefore, this confirms that conversion Q to E by GLS (in QLR-addback) is not altered in Fh-deficient cells.

We observed that amino acid starvation led to a 90% reduction in D levels in both wildtype and Fh deficient cells, as expected (**Fig 5.32C**). A clear QLR-dependent increase in D levels was observed in wildtype cells. In line with the previously reported profile of Fh-deficient cells (Adam et al., 2013), the levels of D were reduced by 80% in Fh deficient cells (vs. wildtype), both in full nutrient or addback conditions. This suggests that conversion of Q/E to D by glutamate-oxaloacetate transaminase (GOT) is blocked in Fh-deficient cells due to the lack of Krebs cycle derived oxaloacetate.

Interestingly, levels of amino acid N also showed a distinct dysregulated pattern in Fh deficient cells. It was observed that amino acid starvation led to at least 70% reduction in N levels in both wildtype and Fh deficient cells relative to their corresponding untreated cells, as expected (**Fig 5.32D**). Consistent with our previous observation (Fig 5.18C), in wildtype cells, QLR-addback led to 3-fold increase in N levels relative to untreated cells. QLR-addback also increased N levels by 17-fold relative to amino acid starved Fh wildtype cells.

Surprisingly, N levels increased mildly in both untreated and amino acid starved Fh deficient cells relative to their corresponding wildtypes. In contrast, N levels reduced by 50% in QLR-supplemented Fh deficient cells relative to wildtype cells. This finding suggests that Fh deficiency does not lower basal N levels but inhibits QLR-dependent

generation of N. Therefore, the generation of N by asparagine-synthetase from D is inhibited in Fh deficient cells since there is loss of the Krebs cycle and a depletion of oxaloacetate (and hence D).

Since it was observed in (Fig 5.37C) that E catabolism is reduced in Fh deficient cells, we analysed whether E conversion to P is also dysregulated. E is converted to pyrroline-5-carboxylate (P5C) (catalysed by P5C synthase) and P5C undergoes reduction to generate P (catalysed by P5C reductase) (Spinelli and Haigis, 2018). Amino acid starvation led to the reduction in P while QLR-addback restored levels in wildtype cells (**Fig 5.32E**). In contrast, E conversion to P was inhibited in Fh deficient cells. Levels of P were reduced by 50% in both untreated and QLR-addback conditions in Fh deficient cells relative to wildtype. In Fh deficient cells, P levels did not significantly increase after QLR addback relative to full starvation. These findings indicate that Fh deficient cells are unable to carry out E conversion to generate P.

Taken together, these observations indicate that Fh deficiency (and blockage of the Krebs cycle) have clear effects on specific amino acid metabolic pathways. Rates of glutaminolysis are reduced. Generation of amino acids D and P are particularly affected with distinct effects as compared, for example, with N. Therefore, the blockage of QLR-dependent mitochondrial hyperfusion in Fh deficient cells is associated with poor efficiency in several amino acid catabolic or interconversion pathways. These data suggest that QLR-dependent mitochondrial hyperfusion may be caused by sensing of downstream Krebs cycle associated metabolites, as opposed to direct sensing of Q, L or R. This model is consistent with our earlier data suggesting that QLR-dependent mitochondrial hyperfusion does not occur via MTORC1 amino acid sensing mechanisms.

The metabolic profile in Fh deficient cells has also been shown to include dramatic reprogramming of the Krebs cycle such as a reduction in citrate, alpha-ketoglutarate and malate levels, and by the accumulation of fumarate and succinate (Frezza et al., 2011, Adam et al., 2013, Zheng et al., 2013). To confirm whether a similar signature is observed, we studied metabolites of the Krebs cycle in Fh deficient cells after QLR-supplementation. In wildtype cells, amino acid starvation led to 30% reduction in citrate levels relative to untreated cells (**Fig 5.33A**). Also, in wildtype cells, QLR supplementation led to further 50% reduction in citrate (relative full starvation). A similar citrate profile was observed in Fh deficient cells. However, the level of citrate in each treatment group was reduced by at least 70% relative to their corresponding treatments in the wildtype cells. These findings agree with the model that Fh

deficiency leads to overall citrate depletion. QLR-addback possibly may be depleting citrate as the Krebs cycle is likely abnormally halted, as further suggested below by other metabolites.

It was observed that amino acid starvation led to a 75% reduction in alpha-ketoglutarate levels relative to untreated cells in both wildtype and Fh deficient cells (**Fig 5.33B**). QLR supplementation only led to mild increases in alpha-ketoglutarate levels (relative to full starvation) and this pattern was generally similar in both wildtype and Fh deficient cells. In line with the expected alpha-ketoglutarate profile of Fh deficient cells, the levels of alpha-ketoglutarate were reduced by at least 50% in all treatments of Fh deficient cells relative to wildtype. This finding suggests that Fh deficiency suppresses basal levels of alpha-ketoglutarate. Also, QLR-addback does not lead to alpha-ketoglutarate accumulation.

Interestingly, it was observed that succinate levels were reduced by 50% upon amino acid starvation, without any further QLR-addback dependent change, in wildtype cells (**Fig 5.33C**). In line with the reported metabolic profile of succinate in Fh deficient cells (Frezza et al., 2011, Adam et al., 2013), succinate levels increased by 3-fold under control conditions upon Fh loss. In contrast, in Fh deficient cells, QLR-addback into amino acid starvation led to a 3-fold increase in succinate levels relative to full starvation. In the starvation or QLR supplementation condition, there was at least 2-fold increase in succinate in Fh deficient cells relative to the corresponding wildtype. This finding indicates that Fh deficiency blocks the Krebs cycle such that there is accumulation of succinate when amino acids are available.

Consistent with our previous data (Refer to Fig 5.20), in Fh wildtype cells, amino acid starvation led to 90% reduction in fumarate levels relative to untreated cells. QLR-addback to wildtype cells increased fumarate levels by 7-fold (relative to amino acid starved cells) (**Fig 5.33D**). Surprisingly, the QLR-addback dependent increase in fumarate was inhibited in Fh deficient cells. Also, in contrast to previous report that fumarate levels increase in Fh deficient cells (Sciacovelli et al., 2016), levels of fumarate were generally reduced by at least 90% relative to wildtype. These findings suggest that succinate to fumarate conversion (carried out by the succinate dehydrogenase complex in the inner mitochondrial membrane) is also defective in the Fh deficient cells that we are investigating.

Fh converts fumarate to malate. Studies have accordingly shown that upon Fh depletion, malate levels were reduced (Frezza et al., 2011, Adam et al., 2013). Consistent with this, malate levels were reduced by at least 60% in our dataset under

all treatment groups in Fh deficient cells relative to corresponding wildtype (**Fig 5.33E**). Furthermore, in line with our data from 4T1 cells (Fig 5.20), amino acid starvation led to 70% reduction in malate levels in both wildtype and Fh deficient cells. However, while QLR-addback increased malate level by 3-fold relative to amino acid starved wildtype cells, there was no QLR-dependent increase of malate in Fh deficient cells. These findings suggest that Fh-deficient cells are unable to process QLR-supplemented amino acids to generate malate. However, Fh deficient cells in full nutrient media were still able to generate basal levels of malate from reversible conversion of oxaloacetate (formed from pyruvate via pyruvate carboxylase).

Together, these findings confirm that QLR-addback (to amino acid-free conditions) leads to dramatic metabolic re-feeding/re-programming of the Krebs cycle, urea cycle, and amino acid interconversion pathways. Several, but not all, metabolic changes were blocked (or altered) when Krebs cycle enzyme Fh is deleted. There was accumulation of urea cycle intermediates. Several amino acids were no longer produced through conversion of Q. Therefore, we have defined several metabolite changes that correlate with the blocked QLR-dependent mitochondrial hyperfusion observed in Fh deficient cells.

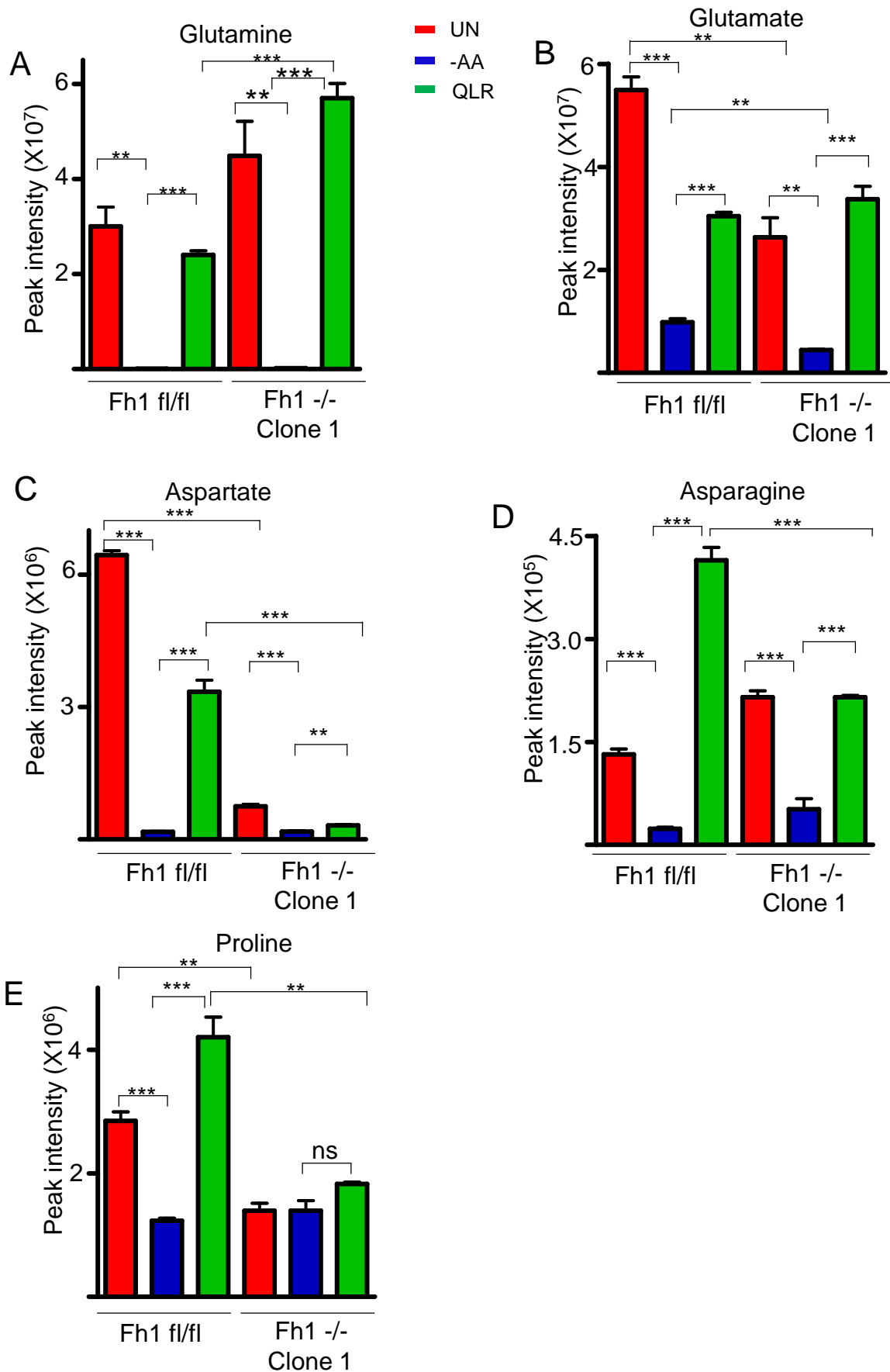


**Figure 5.32: QLR-induced glutamate metabolism flux is inhibited in fumarate hydratase KO cells.** Fumarate hydratase (Fh1) control (Fh1 fl/fl) and Fh KO (Fh1-/- clone1) cells were maintained in full media (Un), starved of either all amino acids (-AA) or starved of amino acid but supplemented with (QLR) for 4h. Starvation media conditions also contained 10% dialysed FBS. Bar graphs show the mean peak intensity of (A) Glutamine (B) Glutamate (C) Aspartate (D) Asparagine (E) Proline. N=3 independent biological replicate. \* represents  $p < 0.05$ , \*\* ( $p < 0.01$ ), \*\*\* ( $p < 0.001$ ).

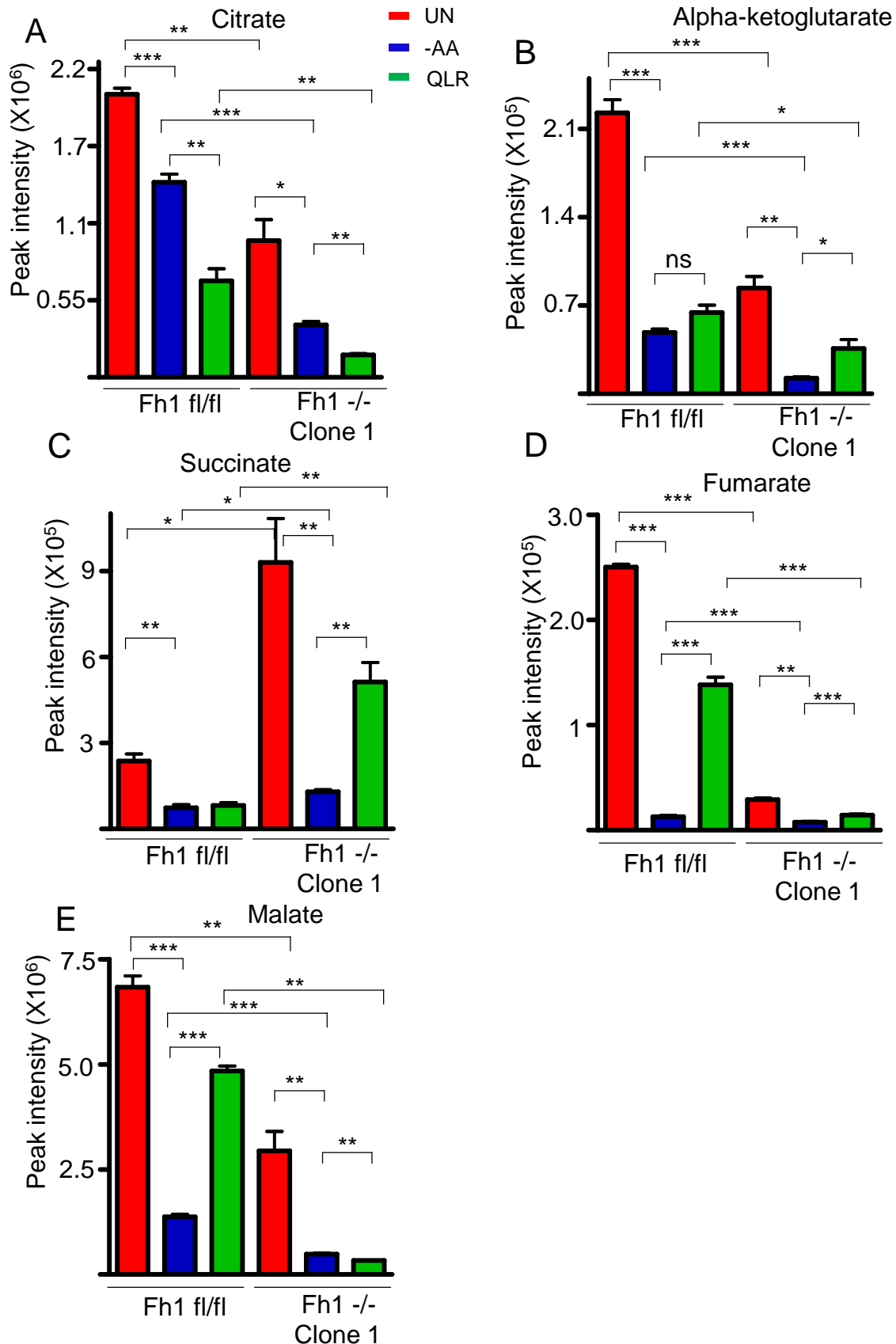


**Figure 5.33. Effect of Fumarate Hydratase-1 (Fh1) KO on metabolites of the Krebs cycle during amino acid starvation with or without the supplementation of QLR.** Fumarate hydratase (Fh1) control (Fh1 fl/fl) and Fh1 KO (Fh1 -/- clone1) cells were maintained in full media (Un), starved of either all amino acids (-AA) or starved of amino acid but supplemented with (QLR) for 4h. Starvation media conditions also contained 10% dialysed FBS. Bar graphs show the mean peak intensity of (A) Citrate (B) Alpha-ketoglutarate (C) Succinate (D) Fumarate (E) Malate. N=3 independent biological replicate. \* represents  $p < 0.05$ , \*\* ( $p < 0.01$ ), \*\*\* ( $p < 0.001$ ).

### 5.2.3.1 Cellular energy is diminished in Fumarase deficient cells

Studies have suggested that dysregulation of the Krebs cycle due to Fh deficiency severely reduces bioenergetic capacity (Tyrakis et al., 2017, Frezza et al., 2011). Since we observed that QLR-dependent re-fuelling of the Krebs cycle is blocked in Fh-deficient cells, it was investigated whether cellular bioenergetics is also blocked.

NAD<sup>+</sup> levels were reduced by at least 40% in all treatments of Fh deficient cells relative to their corresponding wildtype (**Fig 5.34A**). Similar to our previous observation in EBSS media (Refer to Fig 2.1), amino acid starvation alone or QLR-addback did not significantly alter NADH levels relative to untreated cells (in both wildtype and Fh deficient cells) (**Fig 5.34B**). Surprisingly, levels of NADH were overall greatly increased by at least 4-fold in Fh deficient cells relative to wildtype. This suggests that Fh deficiency increases the production of NADH from other pathways such as glycolysis independently of the Krebs cycle. Also, NADH may not be effectively utilised in the E.T.C. of Fh deficient cells, hence promoting NADH buildup.

NADH serves as the electron donor molecule for ATP generation in the E.T.C. Therefore, we next assessed whether ATP levels were altered in the Fh deficiency dataset. It was observed that amino acid starvation led to a 25% reduction in ADP levels while QLR-addback restored the levels in wildtype cells (**Fig 5.35A**). Therefore, amino acid depletion tends to lower levels of nucleotides. Amino acid dependent-changes in ADP levels were not significant in Fh deficient cells, suggesting that the link between amino acids and nucleotides requires the Krebs cycle. Interestingly, ADP levels were overall generally similar in both wildtype and Fh deficient cells. Therefore, this suggests that the contribution of Fh to nucleotides like ADP may be only partial.

Furthermore, a similar metabolic profile was observed for ATP in wildtype cells. In wildtype cells, amino acid starvation led to a 25% reduction in ATP levels relative to untreated cells. QLR-addback restored ATP levels (**Fig 5.35B**). Similarly, in Fh deficient cells, amino acid starvation led to a mild decrease in ATP levels. However, QLR-addback did not significantly restore the levels. Interestingly, levels of ATP in amino acid starved or QLR addback Fh deficient cells were significantly lower relative to their corresponding wildtype. This finding indicates that Fh deficient cells accumulate sufficient levels of ATP but at a significantly reduced rate relative to wildtype cells.

Taken together, these findings indicate that QLR-dependent generation of ATP is inhibited in Fh deficient cells. The findings highlighted that enhanced NADH levels in Fh deficient cells did not correlate with levels of ATP. Therefore, NADH usage in the E.T.C. appears less efficient in Fh deficient cells. Overall, we speculate that NADH processing into the E.T.C. for the synthesis of ATP might be required for QLR-induced mitochondrial hyperfusion. In addition, key metabolic changes in Fh KO cells are summarised in **table 5.6**.

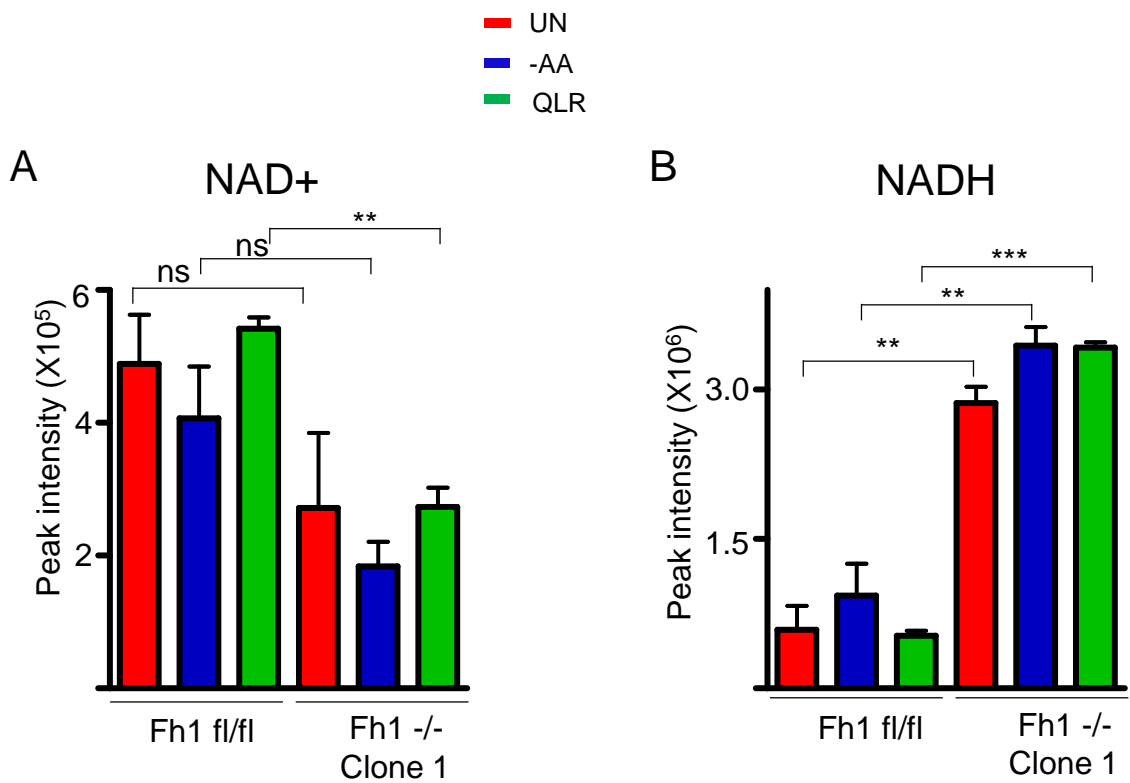


**Figure 5.34. NADH levels are increased in Fumarate hydratase-1 (Fh1) KO.** Fumarate hydratase (Fh1) control (Fh1 fl/fl) and Fh1 KOs (Fh1<sup>-/-</sup> clone1) cells were maintained in full media (Un), starved of either all amino acids (-AA) or starved of amino acid but supplemented with (QLR) for 4h. Starvation media conditions also contained 10% dialysed FBS. Bar graphs show the mean peak intensity of (A) NAD<sup>+</sup> (B) NADH. N=3 independent biological replicate. \* represents p < 0.05, \*\* (p < 0.01), \*\*\* (p < 0.001).

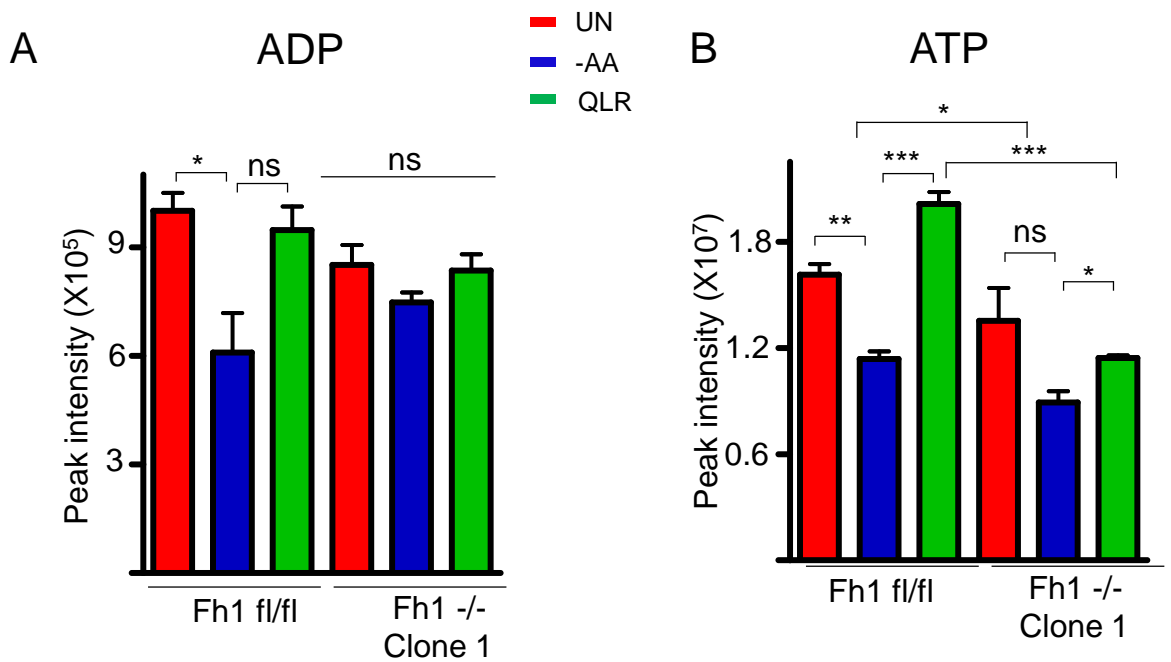


**Figure 5.35. Cellular energy is reduced in Fumarate hydratase-1 (Fh1) KO.** Fumarate hydratase (Fh1) control (Fh1 fl/fl) and Fh1 KOs (Fh1-/- clone1) cells were maintained in full media (Un), starved of either all amino acids (-AA) or starved of amino acid but supplemented with (QLR) for 4h. Starvation media conditions also contained 10% dialysed FBS. Bar graphs show the mean peak intensity of (A) ADP (B) ATP. N=3 independent biological replicate. \* represents  $p < 0.05$ , \*\* ( $p < 0.01$ ), \*\*\* ( $p < 0.001$ ).

**Table 5.6: Summary of key significant metabolic changes after QLR adback in Fh KO**

The effect of QLR adback on metabolites in wildtype relative to full amino acid starvation (QLR adback relative -AA (WT)). The effect of QLR adback on metabolites in Fh KO relative to full amino acid starvation (QLR adback relative -AA (WT)). The effect of Fh KO on QLR adback-changes, i.e metabolic levels in QLR Fh KO relative to QLR in wildtype (Effect of Fh KO on QLR-metabolism). N.A indicate metabolite is not significantly altered.

### Summary of key significant metabolic changes after QLR in Fh KO

Metabolites	QLR adback relative - AA (WT)	QLR adback relative - AA (Fh KO)	Effect of Fh KO on QLR-metabolism
Alpha ketoglutarate	N.A	Increased	Reduced
Arginine	Increased	Increased	Increased
Argininosuccinate	Increased	Increased	Increased
Asparagine	Increased	Increased	Reduced
Aspartate	Increased	N.A	Reduced
ATP	Increased	Increased	Reduced
Citrate	Reduced	Reduced	Reduced
Fumarate	Increased	Increased	Reduced
Glutamate	Increased	Increased	N.A
Malate	Increased	Reduced	Reduced
NADH	N.A	N.A	Increased
Succinate	N.A	Increased	Increased

Studies have shown that loss of Fh is sufficient to cause E.T.C defects leading to the depletion of mitochondrial-generated ATP (Tyrakis et al., 2017). Since we found that ATP levels were reduced in QLR-supplemented Fh deficient cells, it was next tested whether this inhibition is due to poor NADH shuttling into the E.T.C.

The compound rotenone blocks complex-I of the E.T.C leading the inhibition of NADH consumption (Palmer et al., 1968). To investigate the roles of the E.T.C. mitochondrial fusion, 4T1-SU9 GFP cells were starved of either all amino acids or supplemented with QLR for 4h. Rotenone (1 $\mu$ M) was added to the starvation media to block the complex-1 of the E.T.C. It was observed that rotenone did not alter mitochondrial dynamics in 4T1 cells maintained in full media (**Fig 5.36A**). Surprisingly, rotenone did not block mitochondrial fusion in 4T1-SU9 GFP cells starved of all amino acids. In contrast, QLR- dependent mitochondrial hyperfusion was blocked by rotenone. Upon quantification, rotenone alone indeed did not alter mitochondrial length (**Fig 5.36B**). Similarly, while amino acid starvation led to mitochondrial fusion, rotenone did not significantly block this response. In contrast, relative to QLR supplemented conditions, rotenone addition to QLR-addback reduced the extent of mitochondrial hyperfusion in at least 25% of the cells. This finding suggests that NADH usage by the E.T.C. is required for QLR-addback induced mitochondrial hyperfusion.

Overall, our data indicate that QLR addback enhanced the urea cycle, E metabolism and the Krebs cycle, thereby increasing the rate of the E.T.C and ATP levels. Supplementation of Q alone only restores E metabolism and ATP levels but did not lead to mitochondrial hyperfusion. Genetic targeting of Fh, a Krebs cycle enzyme, blocks QLR-dependent mitochondrial hyperfusion. Lastly, inhibition of the E.T.C suppresses QLR-dependent mitochondrial hyperfusion. Therefore, our data support a model in which combined metabolic reprogramming is required for QLR-dependent mitochondrial hyperfusion.

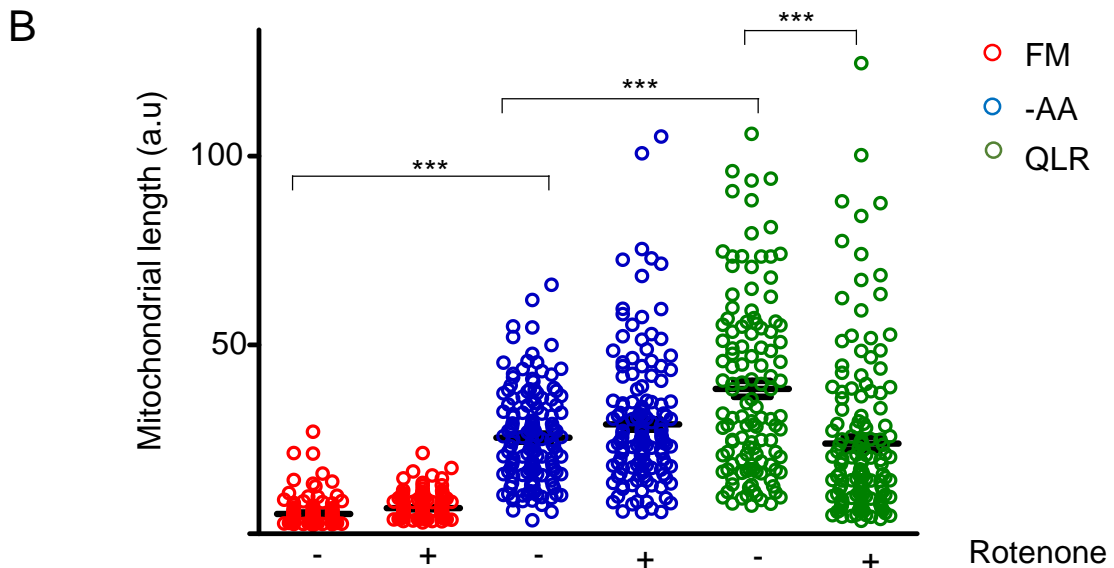
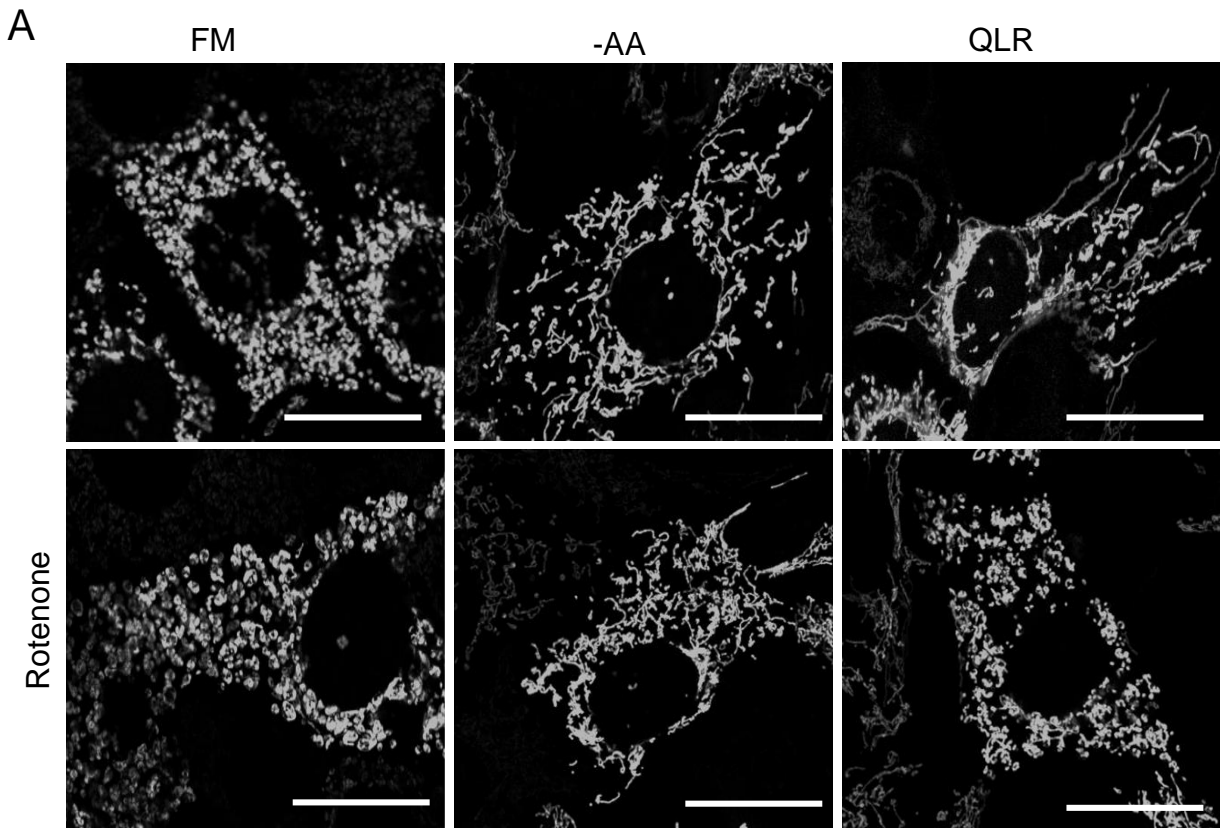


**Figure 5.36: Q, L, R-induced hyperfusion requires the electron transfer process in complex I of the E.T.C.** (A) Representative images of 4T1-SU9 GFP cells maintained in full media (FM), starved of either all amino acids (-AA) or starved of amino acid but supplemented with (QLR), +/- Rotenone (1 $\mu$ M) for 4h. Starvation media conditions also contained 10% dialysed FBS. (B) Each dot represents the mean length of 10 mitochondria within a cell. Each treatment shows between 120-150 cells quantified from three independent experiments. \*\*\* indicate  $P < 0.001$  analysed with one way ANOVA, Bonferroni post test. Scale: 25 $\mu$ m

## 5.2.4 The role of mitochondrial fusion in QLR-addback dependent metabolic re-programming

A number of studies have suggested a model in which mitochondria respond to metabolic changes by altering their shape and size, thereby modulating function (Mishra and Chan, 2016). For example, it has been suggested that increased mitochondrial fusion supports the ability to maintain sufficient ATP levels (Gomes et al., 2011a). It was observed above (in our experiments) that QLR-supplemented amino acid starved cells have increased ATP levels. It was also observed that metabolites of the urea cycle, E metabolism and Krebs cycle are increased in QLR-supplemented cells. These metabolic changes due to QLR addback speculatively may cause mitochondrial hyperfusion. However, given the proposed link between mitochondrial form upstream of function, we also wondered if the metabolic changes also required mitochondrial hyperfusion, in a reciprocal inter-dependent relationship.

To ascertain whether metabolic re-programming from QLR required mitochondrial hyperfusion, we studied the metabolic fingerprint in fusion-deficient Mfn1 KO cells. Wildtype MEF and Mfn1 KO cells were maintained in full nutrients media or starved of either all amino acids or supplemented with QLR. After 4-hours, metabolites were extracted for LC/MS/MS.

PCA demonstrated that there was closer association in overall metabolite patterns between amino acid starvation and QLR-addback conditions in both wildtype and Mfn1 KO cells (**Fig 5.37A**). Similar close relationships were observed in PLS-DA although replicates within each treatment appeared better clustered using this analysis method (**Fig 5.37B**). PLS-DA also highlighted clear shifts in metabolites due to QLR-addback (in both cell types). Mfn1 KO had the strongest effect (vs wildtype) in the control full nutrient condition. These findings indicate that there may be a combination of complex effects in the metabolite patterns due to roles of Mfn1-dependent fusion and extracellular nutrients.

ORA analysis highlighted metabolites involved in nucleotide sugar metabolism, pyrimidine metabolism and lactose synthesis to be the most significantly altered when comparing between wildtype vs. Mfn1 KO cells (QLR-addback condition) (**Fig 5.38A**). Metabolites of glutathione metabolism, D/E metabolism, and urea cycle were also significantly altered. Similarly, pathway analysis also indicated that nucleotide sugar metabolism, pyrimidine metabolism, lactose synthesis and starch metabolism were altered in Mfn1 KO cells relative wildtype cells (in the QLR-supplemented condition)

**(Fig 5.38B)**. However, the FDR rates of all these highlighted metabolic changes were 1, therefore indicating lower confidence relative to earlier metabolomics experiments **(Table 5.7)**. This higher FDR is consistent with the close clustering observed in PCA and PLS-DA. Putting this into consideration, we focused analyses on the same set of QLR-dependent metabolites from the urea cycle, amino acid metabolism, Krebs cycle and bioenergetics.

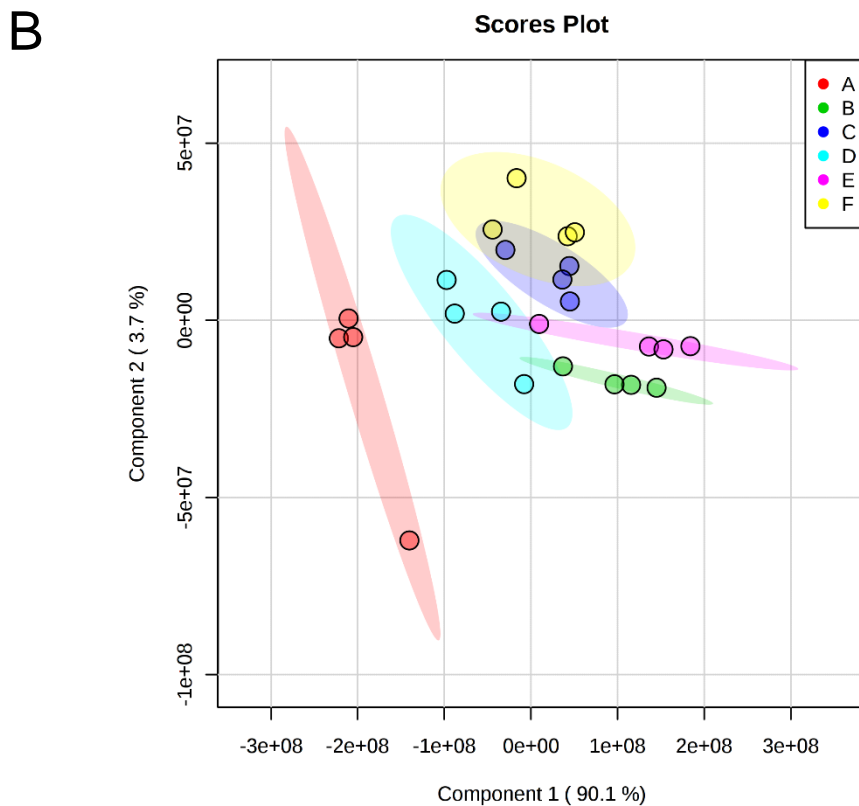
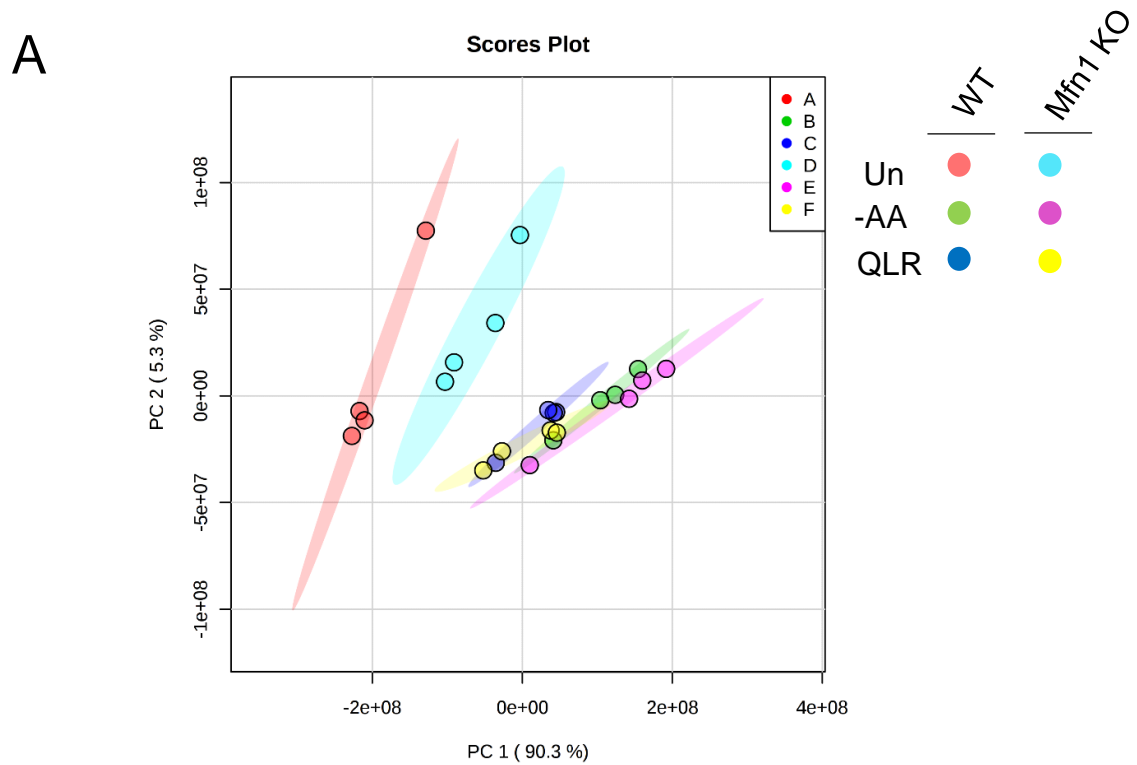
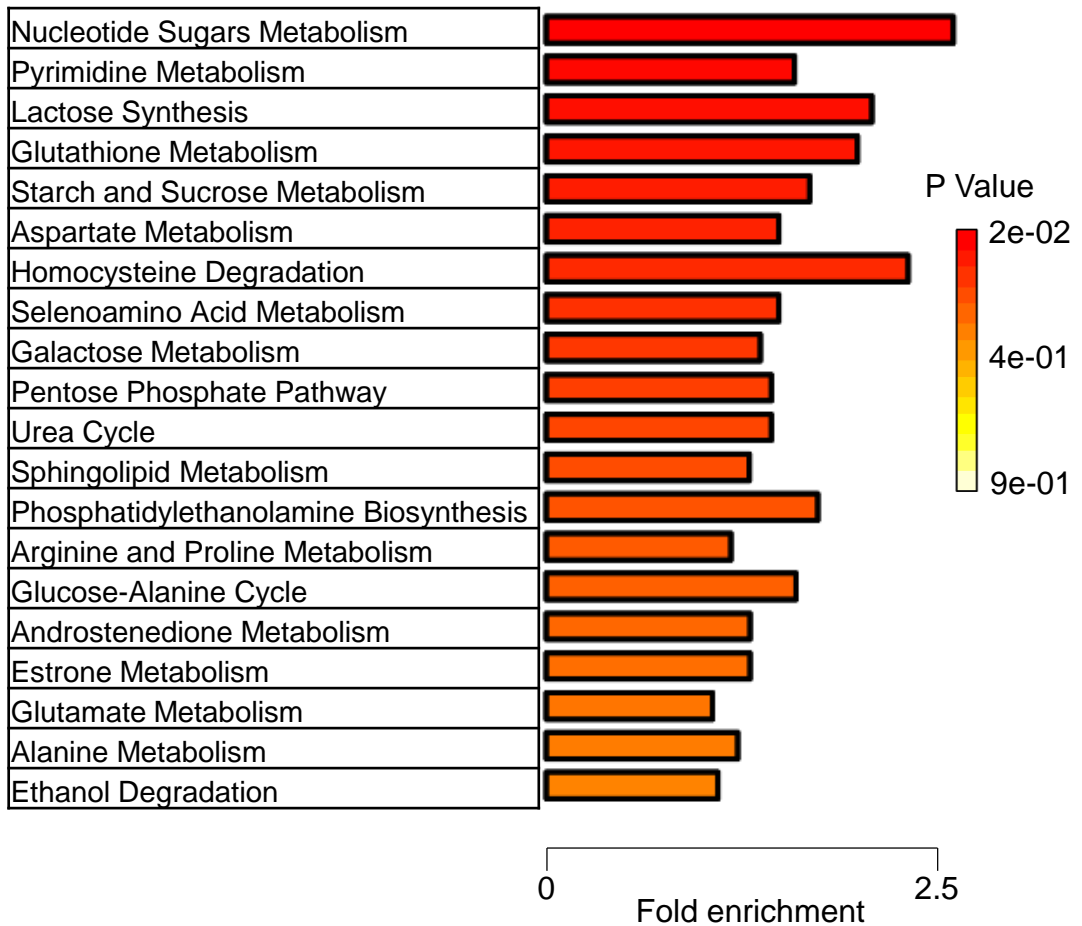


**Figure 5.37: Metabolomics LC-MS/MS analysis of mitofusin-1 deficient cells.** Wild type MEF and Mfn1 KO MEF were maintained in full media (Un), starved of either all amino acids (-AA) or starved of amino acid but supplemented with QLR for 4h. Starvation media conditions also contained 10% dialysed FBS. A) Principal-Component Analysis (PCA) score plot showing the separation between treatment groups. B) Partial Least Squares- Discriminant Analysis (PLS-DA) showing the supervised classification of the treatment groups. N=4 independent biological replicate.

A



B

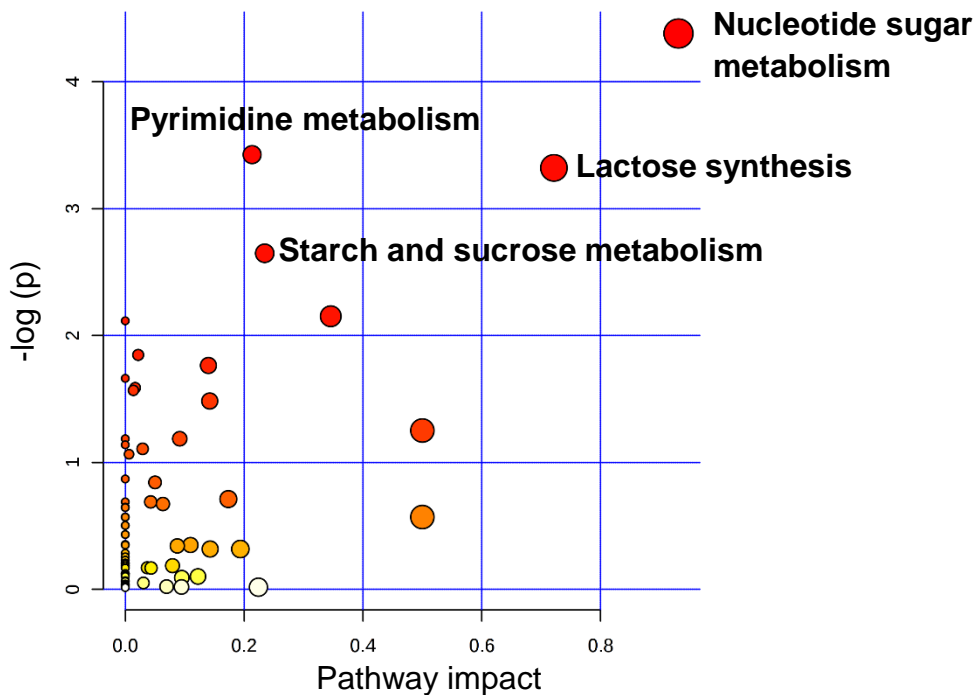


**Figure 5.38: Pathway analysis of metabolites with significant changes after QLR supplementation into amino acid-starved WT MEF relative to Mfn1 KO MEF.** Wild type MEF and Mfn1 KO MEF were maintained in full media (Un), starved of either all amino acids (-AA) or starved of amino acid but supplemented with QLR for 4h. Starvation media conditions also contained 10% dialysed FBS. (A) Over-representation analysis (ORA) showing the top 20 enriched pathways based on significantly ( $p < 0.05$ ) altered metabolites. Ranked according to significant p values (Top  $\rightarrow$  Down, Darkest shade most significant) (B) Pathway analysis indicating the most relevant pathways. The darker the shade the greater the significance. The larger the circle, the more the metabolites involved in the pathway.

**Table 5.7: Detailed results of the pathway analysis of relevant pathways after QLR supplementation into amino acid-starved WT MEF relative to Mfn1 KO MEF.** Total: total number of metabolites in the pathway; the hits indicate the matched number from the analysed data; Raw p signifies the original P value calculated from the enrichment analysis; FDR is the adjusted p value using the false discovery rate; the impact represents the pathway impact value calculated from the topology analysis.

Pathway	Total	Hits	Raw p	FDR	Impact
Nucleotide Sugars Metabolism	17	5	0.012516	1	0.93103
Pyrimidine Metabolism	52	9	0.032511	1	0.21348
Lactose Synthesis	15	4	0.036095	1	0.72143
Starch and Sucrose Metabolism	26	5	0.070738	1	0.23466
Aspartate Metabolism	30	5	0.11621	1	0.34583
Homocysteine Degradation	7	2	0.12044	1	0
Galactose Metabolism	33	5	0.15758	1	0.021739
Urea Cycle	25	4	0.17125	1	0.13996
Selenoamino Acid Metabolism	26	4	0.18952	1	0
Sphingolipid Metabolism	36	5	0.20414	1	0.016636
Pentose Phosphate Pathway	27	4	0.2084	1	0.013685
Arginine and Proline Metabolism	47	6	0.22661	1	0.14217
Phosphatidylethanolamine Biosynthesis	12	2	0.28589	1	0.5
Estrone Metabolism	22	3	0.30506	1	0
Glutathione Metabolism	22	3	0.30506	1	0.091683
Alanine Metabolism	13	2	0.31987	1	0
Androstenedione Metabolism	23	3	0.33029	1	0.02924
Glutamate Metabolism	44	5	0.34463	1	0.00636
Ethanol Degradation	16	2	0.4188	1	0
Ammonia Recycling	27	3	0.43024	1	0.050121

To investigate how metabolites involved in amino acid metabolism are altered in fusion deficient Mfn1 KO cells, a heatmap was generated for metabolites involved amino acid metabolism that show  $p < 0.2$  (based on T-test) between wildtype vs. Mfn1 KO (QLR-addback cells). Heatmap and cluster analyses demonstrated that many metabolites were depleted during amino acid starvation in both wildtype and Mfn1 KO cells (**Fig 5.39**). It also showed that some metabolites in amino acid starved wildtype cells were inhibited in Mfn1 KO cells (highlighted in yellow dotted box). Interestingly, the heatmap also demonstrated that a group of metabolites in QLR addback wildtype cells were dependent on Mfn1 expression (highlighted in red dotted box). Also, another group of metabolites accumulated only during QLR-addback in both wildtype and Mfn1 KO cells (highlighted in green dotted box).

Data mining of metabolites in the urea cycle indicated that R levels did not significantly change in Mfn1 KO cells relative to wildtype cells in all treatments (**Fig 5.40A**). In contrast, ornithine levels in untreated Mfn1 KO cells were significantly higher relative to wildtype cells (**Fig 5.40B**). However, differences in ornithine were less apparent following amino acid starvation or QLR-addback. Similarly, citrulline levels were similar in Mfn1 KO vs wildtype in the basal condition (**Fig 5.40C**).

Although argininosuccinate is just downstream of citrulline in the urea cycle, this metabolite showed a different trend. QLR-addback led to strong increase of argininosuccinate levels in wildtype cells (**Fig 5.40D**). QLR-dependent argininosuccinate accumulation was increased further in Mfn1 KO cells. Taken together, fusion deficient cells appear to show similar levels of urea cycle metabolites as wildtype (although ornithine in basal state and argininosuccinate metabolites in QLR addback for Mfn1 KO were higher). Therefore, fusion may have affected flux in these pathways. However, changes in urea cycle metabolites following QLR-addback even occurred in Mfn1 KO and therefore are not strictly dependent on functional mitochondrial fusion.

In contrast, it was observed that Q and E levels overall were not different when comparing Mfn1 KO cells relative to wildtype (**Fig 5.41A/B**). Moreover, there was clear accumulation of Q and E following QLR-addback, and this accumulation was Mfn1-independent. This finding indicates that mitochondrial fusion is not required for Q deamination to form E.

Similarly, D levels were also maintained in Mfn1 KO cells at similar levels as in wildtype cells in all starvation conditions (**Fig 5.41C**). Strikingly, it was observed that QLR-addback led to a massive increase in N levels, in both wildtype and Mfn1 KO

cells (**Fig 5.41D**). However, the extent of N generation following QLR-addback was significantly lower in Mfn1 KO cells relative to wildtype. Similar trends were observed for P (**Fig 5.41E**). P levels increased after QLR addback in both wildtype and Mfn1 KO cells but the level was lower in QLR-addback Mfn1 KO cells. Altogether, these findings suggest that mitochondrial fusion is not required for initial stages of Q metabolism and conversion to D after QLR-addback. However, the efficiency for synthesis of N and P during QLR addback was reduced in fusion-deficient cells. Therefore, mitochondrial fusion appears to modulate the rates of certain mitochondrially localised amino acid metabolism pathways.

Consistent with this notion, we detected changes in the levels of certain metabolites of the Krebs cycle in Mfn1 KO cells. It was observed that citrate levels were significantly reduced in amino acid starved and QLR supplemented amino acid starved Mfn1 KO cells relative to their corresponding wildtype (**Fig 5.42A**). In fact, there was a mild QLR-addback dependent reduction of citrate in wildtype cells, which was not observed in Mfn1 KO cells.

In contrast, there were no significant differences in the levels of alpha-ketoglutarate between wildtype and Mfn1 KO cells (when comparing each nutrient condition) (**Fig 5.42B**). Similar to data from wildtype Fh1 fl/fl kidney cells, QLR-addback did not lead to any clear accumulation of alpha-ketoglutarate. It was also observed that succinate levels were generally depleted following amino acid starvation (and were not rescued by QLR-addback, similar to trends in Fh1 fl/fl cells) (**Fig 5.42C**). Succinate levels were similar between wildtype and Mfn1 KO (in the three treatment groups).

QLR supplementation (into amino acid starvation media) led to a clear increase in fumarate (**Fig 5.42D**). This accumulation was generally present in both wildtype and Mfn KO1 cells. However, the QLR-dependent build-up fumarate was significantly higher in Mfn1 KO cells vs wildtype. There was also a QLR-dependent rescue of malate levels in both wildtype and Mfn1 KO cells. The level of malate in Mfn1 KO cells was similar to wildtype in all treatment groups (although significantly lower for QLR addback) (**Fig 5.42E**). These findings suggest that mitochondrial fusion does not greatly alter levels of Krebs cycle metabolites (except for some very weak changes in some QLR-responses).

Lastly, we analysed how NADH levels and ATP levels were maintained in Mfn1 KO cells. It was observed that NAD<sup>+</sup> levels in wildtype cells were reduced following starvation and were not replenished with QLR-addback (similar to Fh1 fl/fl cells). Overall, NAD<sup>+</sup> levels were generally similar in Mfn1 KO vs the wildtype. However, the

only difference that was significant could be found in the amino acid starved condition **(Fig 5.43A)**.

Interestingly, amino acid starvation appeared to deplete NADH, while QLR-addback had a rescue effect, in wildtype cells **(Fig 5.43B)**. However, these NADH nutrient-dependent changes did not show significance due to high variability. In contrast, NADH levels did not show any discernable QLR-dependent trend in Mfn1 KO cells. Therefore, these preliminary data suggest that Mfn1-dependent fusion may help maintain NADH levels following QLR-addback.

Interestingly, it was observed that levels of ADP and ATP were generally well maintained in fusion deficient cells **(Fig 5.44)**. In fact, QLR-addback increased ATP levels in both wildtype and Mfn1 KO cells to very similar extents **(Fig 5.44B)**. Therefore, this suggests that QLR-addback dependent increase in cellular ATP levels does not require mitochondrial fusion.

Overall, this data set further confirms several QLR-addback responsive metabolites from the urea cycle, amino acid metabolism and Krebs cycle in wildtype MEF cells. These findings, combined with datasets from 4T1 breast cancer and Fh1 fl/fl mouse epithelial kidney cells, better highlight the most robust generalizable metabolic changes that follow QLR-addback. The Mfn1 KO experiment here also highlights that mitochondria-dependent metabolic pathways such as the urea cycle, amino acid conversion and Krebs cycle can be modulated by levels of mitochondrial fusion **(As summarised in table 5.8)**. Several metabolites in each of these pathways were altered (although modestly in most cases) in fusion-deficient cells. In our working model, this suggests that QLR-dependent metabolite changes may play more of a causative role promoting mitochondrial hyperfusion, rather than being a downstream result of mitochondrial hyperfusion.

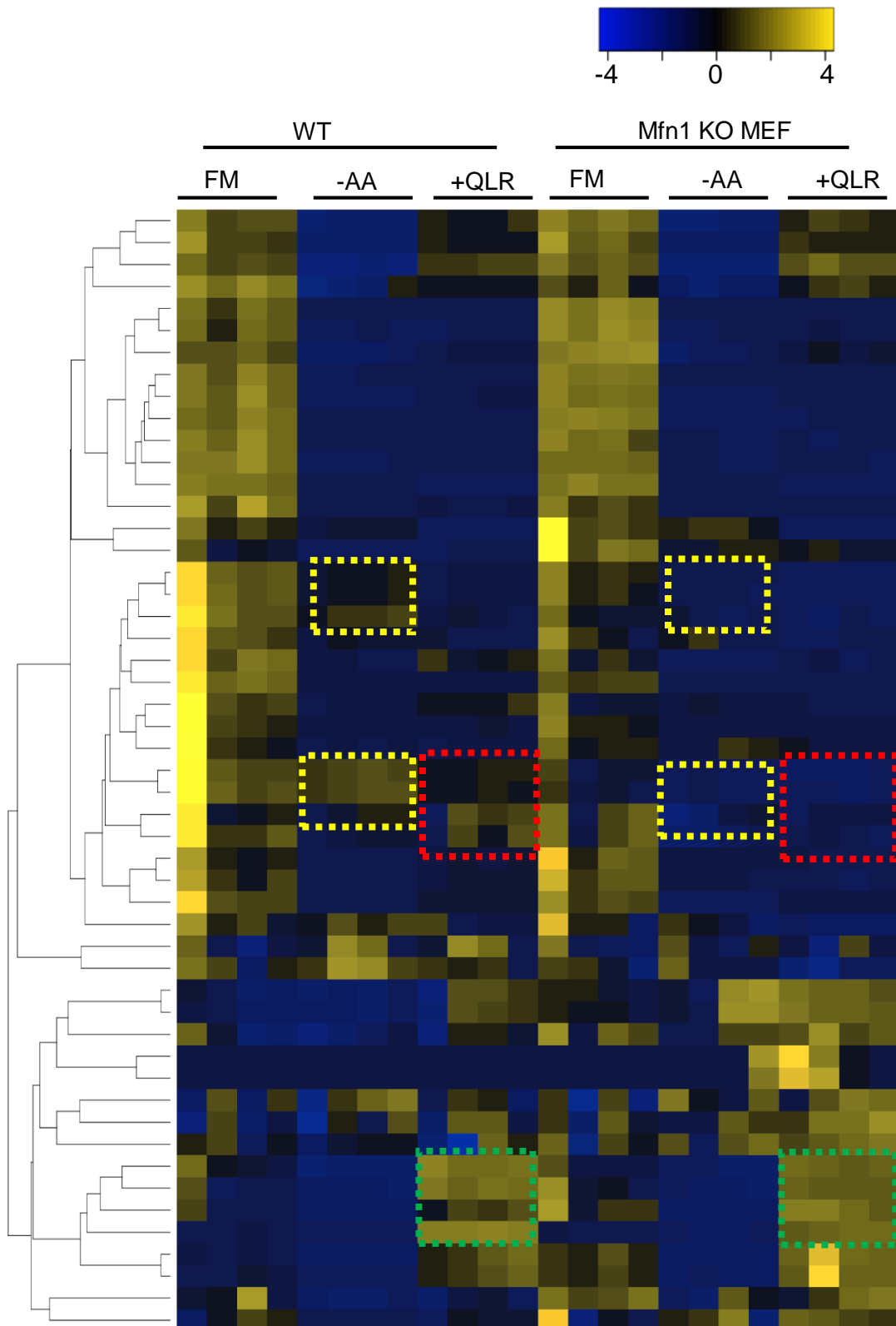


**Figure 5.39: Heat map showing the profile of metabolites involved in amino acid metabolism after Mfn1 KO.** Wild type MEF and Mfn1 KO MEF were maintained in full media (Un), starved of either all amino acids (-AA) or starved of amino acid but supplemented with QLR for 4h. Starvation media conditions also contained 10% dialysed FBS. Each treatment group has four independent biological replicates. Metabolites involved amino acid metabolism were highlighted on the excel macro library and those whose p-value is less than 0.2 based on t.test analysis between QLR-addback wildtype and QLR-addback Mfn1 KO were processed into heatmap

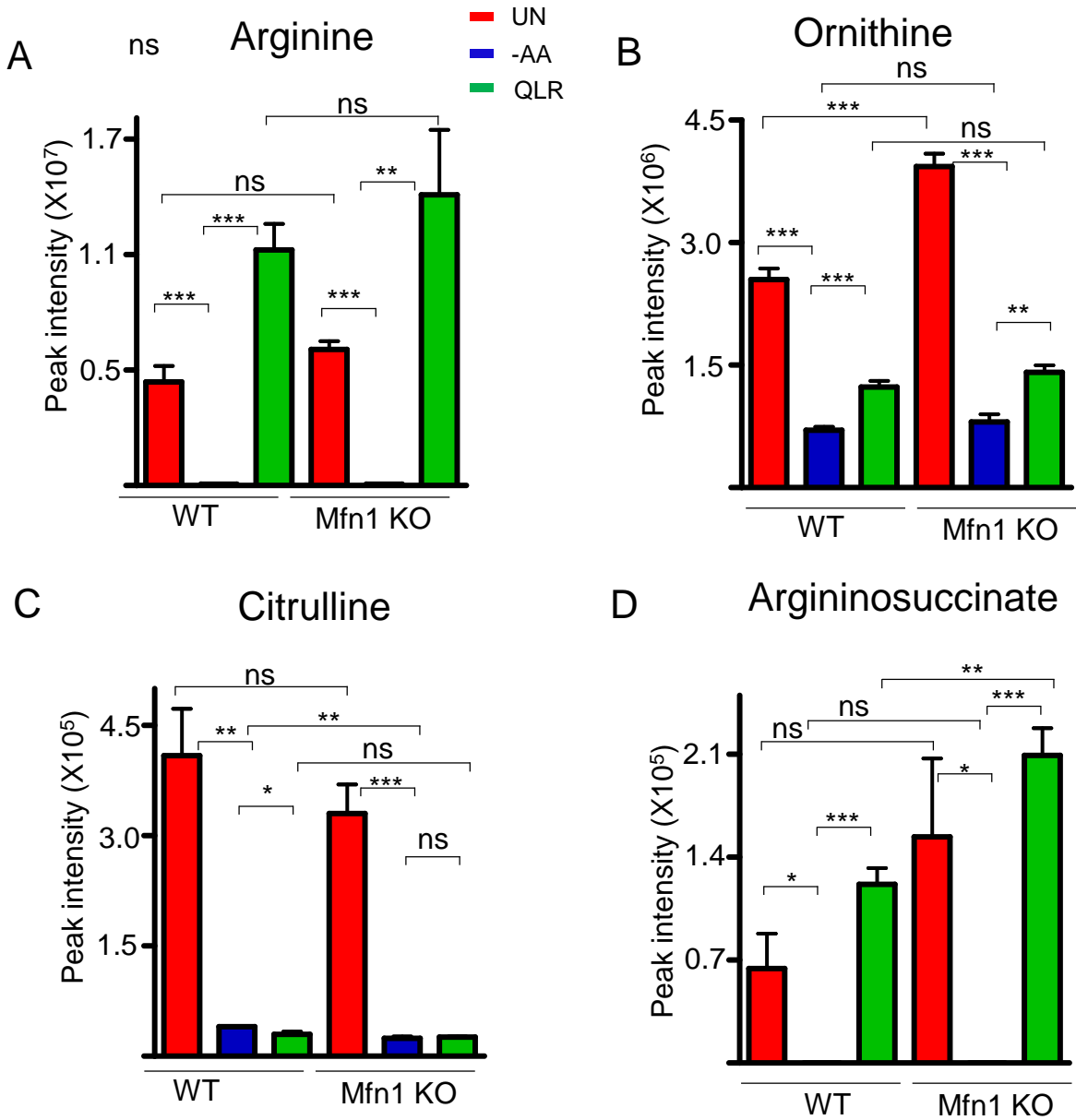


**Figure 5.40: Argininosuccinate levels is increased in Mfn1 KO MEF.** Wild type MEF and Mfn1 KO MEF were maintained in full media (Un), starved of either all amino acids (-AA) or starved of amino acid but supplemented with QLR for 4h. Starvation media conditions also contained 10% dialysed FBS. Bar graphs show the mean peak intensity of (A) Arginine (B) Ornithine (C) Citrulline (D) Argininosuccinate. N=4 independent biological replicate. \* represents \*\* (p < 0.01), \*\*\* (p < 0.001), ns (non significant).

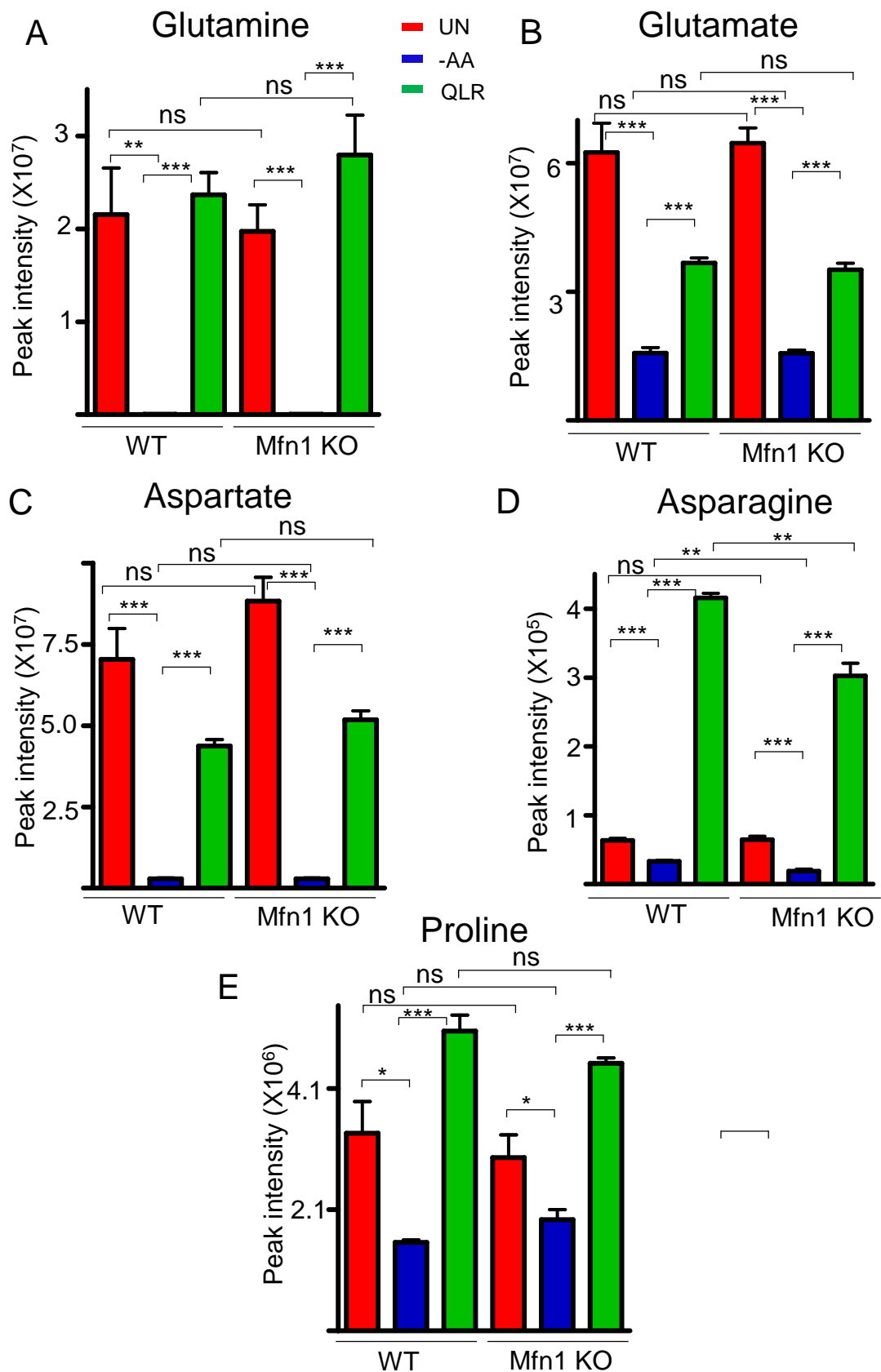


**Figure 5.41: Effect of Mfn1 KO on glutamate metabolism after amino acid starvation with or without QLR supplementation.** Wild type MEF and Mfn1 KO MEF were maintained in full media (Un), starved of either all amino acids (-AA) or starved of amino acid but supplemented with QLR for 4h. Starvation media conditions also contained 10% dialysed FBS. Bar graphs show the mean peak intensity of (A) Glutamine (B) Glutamate (C) Aspartate (D) Asparagine (E) Proline. N=4 independent biological replicate. \*\* (p < 0.01), ns (non significant).

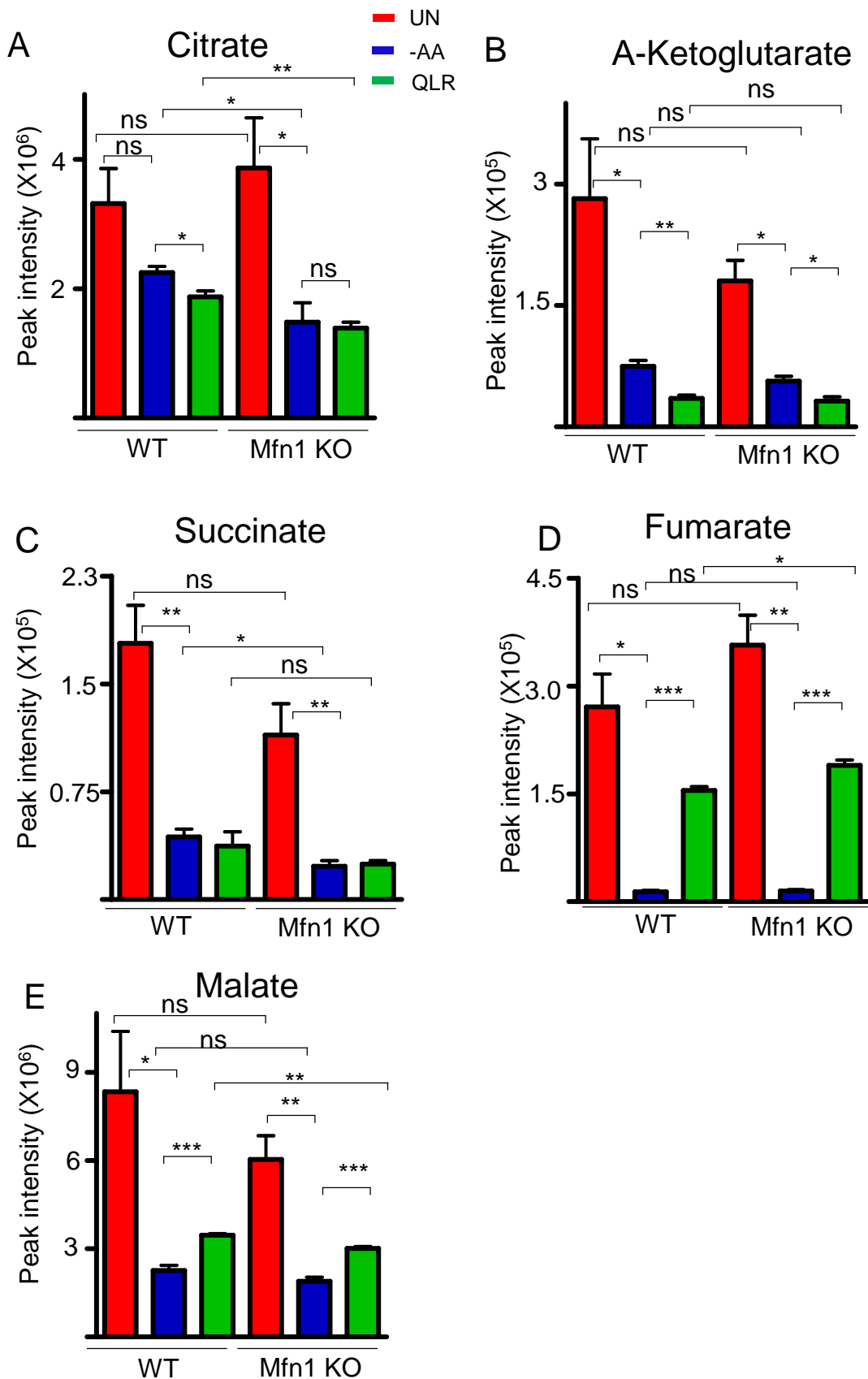


**Figure 5.42: Effect of Mfn1 KO on metabolites of the Krebs cycle during amino acid starvation with or without QLR supplementation.** Wild type MEF and Mfn1 KO MEF were maintained in full media (Un), starved of either all amino acids (-AA) or starved of amino acid but supplemented with QLR for 4h. Starvation media conditions also contained 10% dialysed FBS. Bar graphs show the mean peak intensity of (A) Citrate (B) Alpha-ketoglutarate (C) Succinate (D) Fumarate (E) Malate. N=4 independent biological replicate. N=4 independent biological replicate. \* represents  $p < 0.05$ , \*\* ( $p < 0.01$ ), \*\*\* ( $p < 0.001$ ).

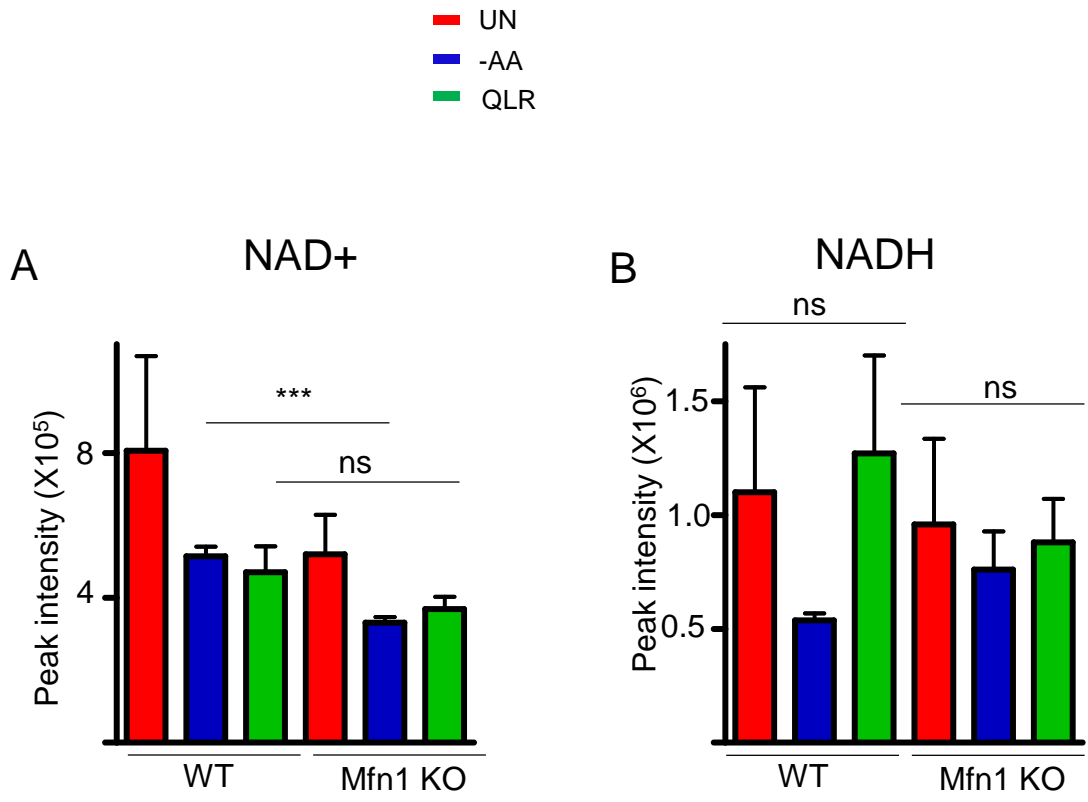


**Figure 5.43: Effect of Mfn1 KO on NADH level.** Wild type MEF and Mfn1 KO MEF were maintained in full media (Un), starved of either all amino acids (-AA) or starved of amino acid but supplemented with QLR for 4h. Starvation media conditions also contained 10% dialysed FBS. Bar graphs show the mean peak intensity of (A) NAD+ (B) NADH (C) GSSG. N=4 independent biological replicate. \* represents  $p < 0.05$ , \*\* ( $p < 0.01$ ), \*\*\* ( $p < 0.001$ ).

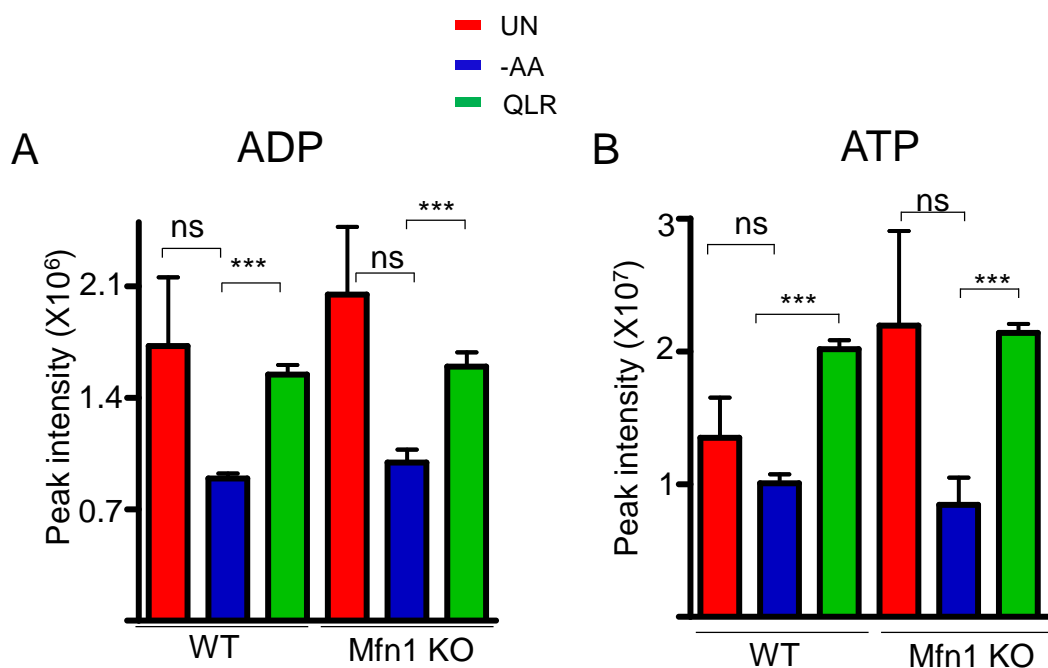


**Figure 5.44: Effect of Mfn1 KO on ATP levels during amino acid starvation with or without QLR supplementation.** Wild type MEF and Mfn1 KO MEF were maintained in full media (Un), starved of either all amino acids (-AA) or starved of amino acid but supplemented with QLR for 4h. Starvation media conditions also contained 10% dialysed FBS. Bar graphs show the mean peak intensity of (A) ADP (B) ATP. N=4 independent biological replicate. \* represents  $p < 0.05$ , \*\* ( $p < 0.01$ ), \*\*\* ( $p < 0.001$ ).

**Table 5.8: Summary of key significant metabolic changes after QLR addback in Mfn1 KO**

The effect of QLR addback on metabolites in wildtype relative to full amino acid starvation (QLR addback relative -AA (WT)). The effect of QLR addback on metabolites in Mfn1 KO relative to full amino acid starvation (QLR addback relative -AA (WT)). The effect of Mfn1 KO on QLR addback-changes, i.e. metabolic levels in QLR Mfn1 KO relative to QLR in wildtype (Effect of Mfn1 KO on QLR-metabolism). N.A indicate metabolite is not significantly altered.

---

**Summary of key significant metabolic changes after QLR in Mfn1 KO**

<b>Metabolites</b>	<b>QLR addback relative – AA (WT)</b>	<b>QLR addback relative - AA (Mfn1 KO)</b>	<b>Effect of Mfn1 KO on QLR-metabolism</b>
Argininosuccinate	Increased	Increased	Increased
Asparagine	Increased	Increased	Reduced
Citrate	Reduced	N.S	Reduced
Fumarate	Increased	Increased	Increased
Malate	Increased	Increased	Reduced

## **5.3 Discussion**

### **5.31 Metabolomics as a high-resolution robust tool for studying cellular metabolism**

A range of studies have focused on understanding how cellular metabolism is inter-related with mitochondrial degradation, mitochondrial damage and mitochondrial remodelling (Schrepfer and Scorrano, 2016, Mishra and Chan, 2016, Galluzzi et al., 2014). This interest is due to the emerging better molecular understanding of mitochondria in the pathogenesis metabolic disorders (Maddocks et al., 2017, Maddocks et al., 2013, Buck et al., 2016, Tezze et al., 2017, Bach et al., 2003). By doing comparative genomic, proteomic, transcriptomic and metabolic analyses, potential key targets and mitochondrial pathways in normal health and in a diseased state are now being defined (Kuhl et al., 2017, Maldonado et al., 2019).

Metabolomics is a powerful approach that collects unbiased relatively large datasets to explore and highlight key metabolic biomarkers that can identify the most affected biochemical pathways under any given experimentally controlled condition. In this chapter, we aimed to use untargeted metabolomics to gain further insight into the amino acid-dependent mitochondrial hyperfusion response that we characterised in the earlier chapters of this thesis. More specifically, we aimed to: 1) identify the key metabolites in the central amino acid, carbohydrate and energy metabolic pathways that are perturbed during nutrient starvation stress and QLR supplementation; 2) explore if metabolite changes potentially may play a causal role in promoting hyperfusion; or 3) alternatively, if hyperfusion may play a reciprocal role in the regulation of metabolic pathway flux.

### **5.32 Nucleotide metabolism is altered during amino acid-dependent mitochondrial hyperfusion.**

Studies have suggested that there is a relationship between nucleotide metabolism and mitochondrial function, however, the molecular mechanism is not clear (Miret-Casals et al., 2017). For example, genes regulating nucleotide metabolism are upregulated in *Drosophila* model of Parkinson disease and it has been suggested that this pathway may be a mechanism to reduce mitochondrial dysfunction (Tufi et al., 2014). This agrees with these author's observations that enhancing nucleotide metabolism with pharmacological approaches ameliorate Parkinson-related

mitochondrial dysfunction. Therefore, these studies place mitochondrial function in close relationship with cellular nucleotide metabolism.

We show here that metabolites involved in both purine and pyrimidine metabolism are altered after QLR-supplementation into amino acid starvation condition. This agrees with an earlier report that *de novo* synthesis of purine derivatives decreases during amino acid starvation (Boss, 1984). However, the changes we have observed here in nucleotide metabolism are highly dependent on glucose and Q since they are the major sources of carbon and nitrogen.

GTP is a purine nucleotide triphosphate that plays multiple important roles in energy regulation and cellular signalling. GTP hydrolysis is needed to drive both structural and kinetic changes of Mfn1 and Opa1 (Ishihara et al., 2004, Sekiguchi et al., 2001). We showed here that QLR addback into amino acid starvation media promotes GTP synthesis. This suggests that mitochondrial hyperfusion may be a response to the high levels of GTP generated during QLR-addback. This highlights a potential novel pathway involving the nucleotide metabolite (GTP) as a signalling molecule that can regulate mitochondrial fusion when present in the cell at increased levels.

Interestingly, it is shown here that cAMP, a well characterised cyclic nucleotide second messenger, did not increase in response to full amino acid starvation conditions. These results contradict the current model linking increased cAMP during amino acid starvation to mitochondrial fusion. Using an exchanged protein directly activated by cAMP (EPAC)-based fluorescence resonance energy transfer (FRET) probe, it was shown that cAMP increase upon amino acid starvation in MEF (Gomes et al., 2011a). However, the massive depletion in ATP levels that we observed during amino acid starvation does not seem to correlate with cAMP increases since ATP is required for cAMP generation. While it is possible that cAMP increases over time upon starvation, biochemically, cAMP levels would be expected to drop upon amino acid starvation relative to cells with full nutrients. Interestingly, our metabolomics finding here correlates with our previous results in earlier chapters that PKA-inhibitor H89 does not block amino acid starvation-induced mitochondrial fusion. Hence, the process appears to involve a PKA/cAMP-independent mechanism.

On the other hand, we also showed here that QLR supplementation increased cAMP levels. Interestingly, this agrees with our observation that QLR-dependent mitochondrial hyperfusion is PKA-dependent. These findings, therefore, indicate that

changes in cAMP are not involved during amino acid-starvation-dependent mitochondrial fusion, but rather are involved during addback-dependent hyperfusion.

### **5.33 Amino acid metabolism is altered during nutrient deprivation**

Multiple pathways are coordinated during metabolism of extracellular derived amino acids such as the Krebs cycle, phosphocreatine pathway, glutathione metabolism, glutamate catabolism, ammonia generation and the urea cycle. These pathways have their own defined functional importance in metabolism but are highly inter-linked via the exchange of intermediates. This highlights the overall complexity in trying to understand and dissect definitive singular metabolic changes in a dynamically inter-connected metabolic network.

Our different analyses consistently revealed (not surprisingly) that the amino acid related metabolic profile robustly re-programmed following QLR supplementation. Although the effect of full amino acid starvation on cellular metabolism has been previously studied, the parallel effects on mitochondrial fusion were not considered (Johnson et al., 2014, Shen et al., 2016, Steinhauser et al., 2018). Clearly, we show here that metabolites of the Krebs cycle and the urea cycle are altered in multiple cell types under the addback condition that is tightly associated with mitochondrial hyperfusion.

#### **5.3.3.1 The urea cycle and the Krebs cycle are regulated by amino acid-dependent mitochondrial hyperfusion**

One round of the urea cycle is completed at the expense of one mole each of carbamoyl phosphate, D (aspartate), and ATP. Each round produces one mole of urea and one mole of fumarate. Fumarate can also be reversibly converted to argininosuccinate, linking the urea cycle with consumption of this Krebs cycle intermediate. However, the urea cycle has a unique essential function in converting toxic ammonium equivalents to excrete metabolic waste as urea. Importantly, reactions of the urea cycle are located across the mitochondria and cytoplasm. Carbamoyl phosphate is combined with ornithine to form citrulline, which is then transported into the cytoplasm. Once in the cytoplasm, citrulline is converted to argininosuccinate then to R, and finally to ornithine, which is transported back into the mitochondria to join with more carbamoyl phosphate.

Overall, in our different LC/MS/MS experiments, the urea cycle was often identified as the most significantly altered pathway, for example with the QLR and Q addback datasets. The urea cycle was also robustly altered when comparing wildtype and Fh deficient cells. This agrees with previous findings on urea cycle function in Fh deficient cells (Zheng et al., 2013). Fh deficient cells are, therefore, unable to catabolise QLR to feed into the urea cycle. This is generally in line with expectations. Without Fh function, the Krebs cycle is halted and carbon atoms from QLR metabolism cannot be incorporated. Fumarate levels unexpectedly dropped in Fh KO cells (as opposed to accumulation). It appears Fh deficiency might drive fumarate towards argininosuccinate (further detailed below). The blockage of QLR carbon backbone metabolism might explain why Fh KO cells do not show hyperfusion in the QLR-addback condition. This suggests that hyperfusion requires active metabolism of Q, L and R and does not take place via direct sensing per se of native amino acids.

Our data also showed that Mfn1 KO cells are generally competent in maintaining the urea cycle. However, there were minor but significant accumulation of several urea cycle intermediates when mitochondrial fusion was blocked. This suggests that normal fusion activity can help maintain efficient flux of the substrates or perhaps the levels or activities of urea cycle enzymes. For a causal mechanism of the urea cycle in controlling fusion, roles for intermediate in mitochondrial dynamics has not yet been described. No literature has been reported to directly link both pathways.

Notwithstanding, the role of R in maintaining mitochondrial homeostasis suggests that this intermediate via the urea cycle might potentially regulate mitochondrial fusion. For example, studies have shown that R starvation leads to perturbations in mitochondrial function (Qiu et al., 2014, Cheng et al., 2018). Cheng et al (2018) reported that R starvation downregulates OXPHOS related genes which led to the reduction in OCR and ATP generation. This study also suggested that R starvation disrupts NADH shuttling into mitochondria and also impairs the balance between NAD<sup>+</sup> and NADH. These R starvation-induced changes in mitochondrial metabolism are all consistent with increased mitochondrial fragmentation. Therefore, our findings here suggest a model where QLR availability enhances R recycling in the urea cycle, therefore promoting NADH shuttling, OXPHOS and ATP. In response, mitochondria might sense these metabolic changes during QLR-addback to induce hyperfusion to better support homeostasis.

Although it is not shown here, R could mechanistically feed into cellular energetics via its further conversion to alpha-ketoglutarate to aid the synthesis of NADH via the

Krebs cycle. Another potential mechanism is through the urea cycle where excess cytosolic R is hydrolysed to form urea and cytosolic ornithine. Ornithine transported back into the mitochondria can be converted after several steps to eventually form argininosuccinate and then to cytosolic fumarate (Adam et al., 2013). The portion of cytosolic fumarate that gets re-imported back into mitochondria can subsequently re-enter the Krebs cycle, therefore, promoting the metabolic cycling for NADH production. While previous studies have suggested that both mechanisms are involved in the enhancement of cellular energetics, the additional presence of L and Q will provide more substrates for Krebs cycle intermediates. Metabolic tracer studies will be needed to identify the main metabolic shuttling patterns of R, Q and L in our system. So far, our data support a model where the metabolic effects of QLR are greater than Q-alone, suggesting certain degrees of inter-dependency.

Other reported tracer studies have shown that argininosuccinate production in Fh KO cells was from both R and fumarate (Adam et al., 2013). The accumulation of fumarate in Fh-deficient cells has been shown to promote succination and inhibition of Fe-S clusters in complex-1 of the E.T.C leading to reduced mitochondrial respiration (Tyraakis et al., 2017). Thus, E.T.C dysfunction in Fh deficient cells may explain in part why there was no hyperfusion in response to QLR-addback. Interestingly, rotenone E.T.C. inhibition blocked QLR-dependent mitochondrial hyperfusion. Moreover, rotenone and Fh deficiency both inhibited QLR-addback induced mitochondrial hyperfusion but not full amino acid starvation-induced mitochondrial hyperfusion. Therefore, hyperfusion in response to QLR-addback appears to more strongly require NADH shuttling and the E.T.C. Our current working model is that QLR-dependent mitochondrial hyperfusion involves enhanced amino acid metabolism, elevated NADH synthesis and shuttling into E.T.C.

### **5.3.3.2 Truncation of the Krebs cycle and urea cycle lead to mitochondrial dysfunction**

The role of fumarase on cellular metabolism have been well studied (Adam et al., 2013, Cipolat et al., 2006, Frezza et al., 2011, Tyraakis et al., 2017, Zheng et al., 2015, Zheng et al., 2013, Pollard et al., 2007, Johnson et al., 2018b, Yogev et al., 2010). Yet, it is surprising that there are only few reports on Fh roles in mitochondrial dynamics, since this was one of the most evident abnormalities we observed in our studies. It was observed here that Fh deficient cells have dysfunctional mitochondria characterized by dense and swollen matrix. Similar findings have noted that mitochondria of Fh deficient cells were “oedematous” but the underlying cause was

not defined (O'Flaherty et al., 2010, Yang et al., 2010). Interestingly, it was observed here that amino acid starvation ameliorated this swollen phenotype by inducing basal mitochondrial fusion. However, QLR addback promoted mitochondrial swelling. Therefore, this suggests that the inability to efficiently process amino acids through the Krebs cycle may lead to metabolites that promote abnormal swelling. It is possible that truncation and build-up of Krebs cycle metabolites alter mitochondrial infrastructure hence promoting downstream mitochondrial dysfunction. Our findings, therefore, might suggest that promoting mitochondrial fusion in Fh deficient cells (e.g. via full starvation) may ameliorate mitochondrial dysfunction. Hence, forced mitochondrial fusion might be a therapeutic strategy in diseases where Fh is deregulated.

### **5.3.3.3 Wider effects of Fh deficiency on cellular metabolism**

Studies have shown that the genetic loss of Fh has a drastic effect on both the cytoplasmic and mitochondrial metabolic network, affecting the urea cycle, R metabolism, Krebs cycle and E.T.C (Tyrakis et al., 2017, Adam et al., 2013). Our metabolomics studies in Fh cells are generally in agreement with previous profiling data (Adam et al., 2013, Zheng et al., 2013). For example, we could detect accumulation of argininosuccinate, while R and ornithine levels were maintained. There were multiple defects in E catabolism and Krebs cycle in our study (characterised by depleted E, D, malate, citrate and alpha-ketoglutarate levels, but with elevated succinate) (Adam et al., 2013).

Interestingly, previous studies found fumarate elevated in Fh deficient cells (Frezza et al., 2011, Pollard et al., 2007, Pollard et al., 2005). As mentioned above, we observed a reduction in fumarate levels in Fh KO cells. However, while increased levels of fumarate have been reported as a biomarker of Fh-deficient cells (Pollard et al., 2005), other studies have suggested fumarate reduction in Fh deficient contexts. In line with our findings, levels of fumarate were found to be dependent on the stage of tumour development and when the loss of Fh occurs (Yogev et al., 2010, Jiang et al., 2015, Raimundo et al., 2008, Leshets et al., 2018). This suggests that fumarate accumulation might only occur at the early stage of tumorigenesis, which could mean that upon continuous cell culture, accumulated fumarate is transformed to other intermediates such as argininosuccinate.

There are other noted differences between our observations on Krebs cycle metabolites vs. other reported studies. In line with our observation, (Adam et al., 2013) reported that E and alpha-ketoglutarate levels were diminished in Fh deficient cells.

In contrast, E and alpha-ketoglutarate were shown by others to be increased in Fh deficient human-derived cell lines (Goncalves et al., 2018). Despite these difference, these studies all highlight that the Krebs cycle and the urea cycle are dysregulated in Fh deficient cells.

#### **5.3.3.4 N (Asparagine) is a potential metabolic regulator of cell fate and mitochondrial dynamics**

Studies have shown that mitochondria from amino acid starved cells were more competent in amino acid catabolism (Johnson et al., 2014). We observed a massive increase in N synthesis in the presence of QLR addback. Interestingly, this great increase was blocked in Fh deficient cells. Therefore, a functional Krebs cycle was required to derive N from excess Q, L and R.

The Krebs cycle begins with the combination of oxaloacetate and acetyl-CoA to form citrate (catalysed by citrate synthase). It has been reported that inhibition of citrate synthase suppressed the Krebs cycle but led to an activation of N synthesis (Zhang et al., 2014b). These authors showed that it occurs via amination of oxaloacetate to form D, which undergoes another transamination reaction to form N, and that this was a response to Q starvation-induced apoptosis. Interestingly, N was shown to directly reduce apoptosis, thus serving as a metabolic regulator of cell fate. In addition, N was suggested to be a metabolic biomarker of an enhanced Krebs cycle. Taken together, the findings suggest that the QLR-dependent increase of N might reflect that the Krebs cycle is maximised. This may explain why the QLR-dependent N increase is blocked in Fh-KO cells that are unable to process the Krebs cycle. This is in line with a model where QLR from the addback enters Krebs cycle metabolism and thereby increases generation of anaplerotic intermediates.

Studies have also suggested a correlation between the levels of N and mitochondrial fusion. It was shown that Atg5 KO in KRAS-driven tumour cells led to autophagy inhibition and a further accumulation of fragmented and dysfunctional mitochondria (Lin et al., 2018). In addition, metabolic rewiring occurred in Atg5 KO KRAS-driven tumour cells, characterised by reduced N levels despite having increased asparagine synthetase enzyme activity. Interestingly, while Atg5 KO in KRAS-driven tumour cells reduced cell survival and cell migration, N supplementation (or inhibition of mitochondrial fission adaptor protein, Mff) rescued these phenotypes. These effects suggest that enhanced N levels may have the same effects as increasing mitochondrial fusion. Relevant to our studies, increased N levels may directly help

promote mitochondrial hyperfusion. It will be interesting to test whether supplementing cells with N can stimulate mitochondrial hyperfusion. Our data support a model wherein QLR-addback during amino acid starvation fuels the Krebs cycle and cellular metabolism, to generate downstream metabolites which promote mitochondrial hyperfusion.

### **5.34 Mitochondrial hyperfusion prevents stress-induced oxidative stress**

Studies have highlighted a close relationship between mitochondrial shape, function and ROS (Willems et al., 2015, Chen et al., 2003b). This understanding is based on observations that the mediators of mitochondrial dynamics can be directly regulated by molecules that reflect the REDOX status of the cell. For example, mitofusins have a REDOX sensitive cysteine residue located at the mitochondrial intermembrane space (IMS) which promotes Mfn oligomerization hence mitochondrial fusion (Shutt et al., 2012, Mattie et al., 2017). Reciprocally, mitochondrial fusion has been shown to reduce mitochondrial ROS during glucose starvation (Lee et al., 2014). Similarly, high glucose concentration was shown to stimulate mitochondrial fragmentation leading to an increase in mitochondrial ROS (Yu et al., 2006). Interestingly, high glucose-induced ROS accumulation was blocked in cells where Drp1 was inhibited or where fusion mediators were overexpressed. These studies all support a model in which mitochondrial hyperfusion serves to reduce ROS levels during nutrient stress.

In line with this model, it was observed here that QLR-addback led to a reduction in the ratio of GSH / GSSG, a biomarker for oxidative stress (Zitka et al., 2012). It has been shown that the higher the ratio, the lower the oxidative damage in the cell. Therefore, our data fit into the model that hyperfused mitochondria promotes ROS scavenging, leading to a lower oxidative status. However, in contrast to Lee et al (2014), where it was shown that glucose starvation-induced fusion lowered oxidative stress, the GSH / GSSG ratio in our data in glucose starved cells indicated no change in the REDOX state. This is likely due to the low basal level of fusion occurring in glucose starved 4T1 cells. In fact, GSH/GSSG correlated with levels of mitochondrial hyperfusion, with QLR addback and Q addback showing greater GSH/GSSG ratios relative to cells in full starvation. Therefore, one key role amino acid-dependent mitochondrial hyperfusion may be to protect cells from oxidative stress.

Furthermore, we observed a QLR-dependent reduction in taurine levels. Taurine is a lipid metabolite that contains a sulfonic acid group that has been implicated in the

maintenance of ROS. For example, taurine is characterised as a conditional non-protein amino acid which scavenges free radicals such as NO, O<sub>2</sub><sup>-</sup>, ONOO but not H<sub>2</sub>O<sub>2</sub> (Higuchi et al., 2012). Interestingly, supplementation of taurine is currently a purported popular approach used for the reduction of oxidative stress and lipid peroxidation. Taurine supplementation has been shown to reduce apoptosis, ROS and mitigates the loss of membrane potential in iron-overloading induced stress (Zhang et al., 2014c). Similarly, it has been suggested that high levels of taurine is a compensatory mechanism to mitigate ROS production during oxidative stress (Takano et al., 2016). These findings indicate that low taurine levels can reflect as a biomarker for reduced oxidative stress. Consistent with this model, we observed that QLR-addback into amino acid starvation media led to a reduction in taurine levels. This finding agrees with data on GSG/GSSG ratios, consistent with the model that mitochondrial hyperfusion overall lowers levels of oxidative stress.

### **5.35 Cellular energetics do not require mitochondrial hyperfusion**

Many studies have linked mitochondrial hyperfusion to the rate of cellular bioenergetics. For example, (Gomes et al., 2011a) reported that mitochondrial fusion under amino acid starvation sustains ATP production to promote cell survival. Similarly, it has been shown that fragmented mitochondria generate lower ATP levels even when nutrients are in excess (Jheng et al., 2012). Interestingly, fusion mediators such as Mfn2 and Opa1 have been shown to also directly regulate cellular energetics independent of their fusion roles (Bach et al., 2003, Patten et al., 2014, Pich et al., 2005). This all suggests that cellular energetics and mitochondrial fusion may have both inter-dependent and independent mechanisms, although details are still unclear.

In contrast with this model, it was found here that fusion deficient Mfn1 KO cells were overall competent in maintaining normal ATP levels. Similarly, addback of Q alone enhanced ATP levels to similar extents as QLR-addback, despite lower levels of associated mitochondrial hyperfusion. In line with our findings, Lee et al., 2014 reported that Mfn1 KO cells maintained energy production to similar levels as wildtype cells during glucose-starvation induced mitochondrial fusion. Although it was observed that Mfn1 KO cells were less efficient in maintaining the levels of metabolic intermediates needed for synthesizing mitochondrial-dependent cellular energy, our findings here suggest that mitochondrial fusion is not strictly required for the maintenance of cellular energetics. We need to add that our starvation experiments

with Mfn1 KO cells was performed in glucose-sufficient contexts (EBSS). Therefore, a background level of ATP generation was also taking place via glycolysis.

It remains possible that there is a wider relationship between fusion and ATP generated through the E.T.C, as studies have shown that ATPase activity is increased upon fusion (Gomes et al., 2011a). Interestingly, QLR-addback greatly enhanced ATP levels in double glucose and amino acid starvation contexts, hence focussing ATP generation through the E.T.C, and not glycolysis. Therefore, it would be interesting to further assess the relationship of mitochondrial-generated ATP and fusion when cells are forced to depend on mitochondrial energy via galactose supplementation or glucose starvation. (MacVicar and Lane, 2014) reported that cells forced to respire via OXPHOS have increased mitochondrial length as a result of reduced Drp1-mitochondrial localization. This agrees with our observed increase in NADH synthesis after QLR addback to double glucose and amino acid starvation (since NADH feeds OXPHOS-dependent ATP generation). While it is clear that QLR-dependent increase of ATP observed in the double starvation condition is sourced from mitochondria, it is still not clear where the QLR-dependent ATP seen in EBSS starvation experiments is derived.

### **5.36 Conclusion**

We characterised here the unique metabolic signatures in cells during amino acid starvation and addback. The addback condition can also be thought of as limited starvation of 17 of the 20 amino acids in normal full nutrient media. Our data, together with the other chapters, suggest that mitochondria respond to amino acid availability by sensing metabolic intermediates of downstream catabolism. This metabolic sensing control of mitochondrial dynamics may form a direct response to control metabolic rates and ROS scavenging. In our model, QLR addback increases anaplerotic reactions which promote downstream mitochondrial hyperfusion. QLR addback replenishes metabolites of the Krebs cycle, urea cycle and amino acid inter-conversion. In line with this, our findings suggest efficient flux of the urea cycle, Krebs cycle and E metabolism, in addition to NADH shuttling into the E.T.C, are critical for QLR-dependent mitochondrial hyperfusion. We thereby propose a model where mitochondrial hyperfusion occurs in response to increased metabolic rates. Overall, the data in this chapter indicate that there is signal from amino acid availability and downstream metabolites resulting in mitochondrial hyperfusion.

## **Chapter 6**

### **General Discussion**

## 6.0 General Discussion

The aim of this project was to study the inter-relationship between mitochondrial dynamics and nutrient availability/starvation. This interest stemmed from several initial reports indicating the elongation of mitochondria during starvation to avoid mitophagy. As we characterised mitochondrial fusion in response to differing amino acid availability conditions, we focused on kinases that have been previously shown to regulate mitochondrial dynamics. Lastly, we were particularly interested in understanding how mitochondrial hyperfusion may play a role in maintaining metabolic homeostasis during nutrient stress. Below, we review the key findings of this project and integration into current models of nutrient-dependent mitochondrial dynamics.

Altogether, our findings indicated that mitochondria mainly undergo fusion in response to changes in amino acid levels rather than other types of nutrient starvation such as glucose or serum. We identified an unexpected distinct role of Q, L and R in the stimulation of mitochondrial hyperfusion. We then focused on understanding how and why this previously-unreported QLR-dependent mitochondrial remodelling was occurring.

To our surprise, results indicate that this unique amino acid sensing occurs independently of MTORC1, in contrast to a model which suggested that MTORC1 inhibition promotes mitochondrial fusion during amino acid starvation. Rather, we found here that amino acid-dependent mitochondrial hyperfusion requires the functions of the Ulk1 complex. In contrast to other studies demonstrating AMPK and PKA as regulators of mitochondrial dynamics (Toyama et al., 2016, Cereghetti et al., 2008), we found that amino acid-dependent mitochondrial hyperfusion does not involve AMPK or PKA-dependent phosphorylation of Drp1 at S637. Furthermore, we found that QLR-dependent mitochondrial hyperfusion requires the formation of intermediates of the urea and Krebs cycle. The biological significance of QLR-addback induced mitochondrial hyperfusion may be to enhance ROS-scavenging, hence reducing oxidative stress that may arise from increased amino acid metabolism.

Findings in this thesis suggest that mitochondria have unique amino acid and metabolic sensing mechanisms that link cellular metabolism to mitochondrial remodelling.

## **6.1 Amino acid-dependent mitochondrial hyperfusion is an amino acid-sensing response, not an MTORC1-inhibition response**

Mitochondrial fusion during amino acid starvation has been shown by studies (Rambold et al., 2011, Gomes et al., 2011a). However, there are no detailed mechanisms linking amino acid availability to the control of mitochondrial dynamics. One established mechanism suggests that mitochondrial fusion during amino acid starvation occurs upon the inhibition of MTORC1 (Gomes et al., 2011a). However, details on how MTORC1 inhibition promotes mitochondrial fusion were never elucidated.

Initially, it appeared reasonable that MTORC1 inhibition was linked to mitochondrial fusion during amino acid starvation due to the known roles of MTORC1 for amino acid sensing and suppression of autophagy (Hosokawa et al., 2009a, Kim and Guan, 2019). In this model, mitochondrial fusion served to protect mitochondria from degradation during autophagy to maintain energy production and promote survival (Gomes et al., 2011a).

Curiously, we reasoned that since MTORC1 senses regulatory amino acids Q, L and R, their supplementation into amino acid starvation conditions would reactivate MTORC1 and inhibit mitochondrial fusion. Indeed, we confirmed that QLR-addback reactivated MTORC1 as shown by the downstream phosphorylation of MTORC1 targets. In fact, we showed that QLR-addback sufficiently blocked autophagy as shown by the inhibition of p62 and LC3B positive autophagosome formation, consistent with the literature including other work from our laboratory (Nwadike et al., 2018, Saxton et al., 2016a, Chantranupong et al., 2016, Wolfson et al., 2016, Jewell et al., 2015).

Paradoxically, QLR-addback into amino acid starvation media led to extensive and dramatic mitochondrial hyperfusion (rather than inhibiting fusion). Interestingly, the level of hyperfusion observed in QLR-addback treated cells was similar to stress-induced mitochondrial hyperfusion (Tondera et al., 2009, Lebeau et al., 2018). Also, QLR-dependent hyperfusion occurred in line with the canonical fusion pathways requiring Mfn1 and Opa1 function (Cipolat et al., 2004). In addition, full amino acid starvation stimulated mitochondrial fusion in Fh deficient cells that have a dysregulated Krebs cycle, but hyperfusion was blocked when QLR was added back. Rotenone treatment also inhibited QLR-addback induced mitochondrial hyperfusion

but not amino acid starvation-induced fusion. Therefore, we found that QLR-addback induced hyperfusion is unique from amino acid starvation-induced fusion.

To further investigate the role of MTORC1 in QLR-addback induced hyperfusion, we inhibited MTORC1. Firstly, we targeted MTOR activity with Torin1, a well-established ATP-competitive inhibitor (Thoreen et al., 2009). Secondly, we removed growth factors that promote MTORC1 lysosomal localization and activation (Sancak et al., 2007, Yang et al., 2017). Indeed, both Torin1 and serum depletion blocked MTORC1 activity when QLR were added back. However, QLR addback still promoted mitochondrial hyperfusion when MTORC1 was inhibited. Interestingly, in contrast to the previous model, MTOR inhibition via Torin1 or serum depletion did not increase further mitochondrial fusion during amino acid starvation or stimulate fusion when used alone. Therefore, we concluded that amino acid-dependent mitochondrial hyperfusion is a unique response occurring independently of MTORC1.

## **6.2 Mitochondria have an intrinsic amino acid sensing mechanism that requires glutaminase**

Surprisingly, our results indicated that MTORC1 was not the main mechanism driving amino acid-dependent mitochondrial hyperfusion. Rather, amino acid availability seemed to be sensed via other means. In line with this notion, studies have shown that MTORC1 sensing of L or Q is dependent on amino acid metabolism, for example, the synthesis of E by glutaminase (GLS) (Duran et al., 2012, Tan et al., 2017, Son et al., 2019). This suggests that mitochondrial-dependent metabolism occurs upstream of MTORC1 translocation to the lysosome and activation during amino acid-sensing (Duran et al., 2012, Sancak et al., 2008). Therefore, we considered whether mitochondria may have their own unique amino acid sensing mechanism.

Indeed, a recent study further reported that GLS senses Q availability to promote mitochondrial fusion (Cai et al., 2018). Similarly to Rambold et al. (2011), Cai et al. (2018) observed that glutamine starvation led to mitochondrial fusion in MEF. Cai et al. (2018) could show that GLS deficiency blocked mitochondrial fusion in Q starved cells. Intriguingly, the re-expression of mutant GLS isoforms (that are unable to catalyze Q conversion to E) into Q-starved GLS-deficient cells rescued mitochondrial hyperfusion. Therefore, this suggests that GLS can promote mitochondrial hyperfusion independent of its enzymatic activity. In support of this notion, it was also shown that the inhibition of GLS activity with inhibitors (such as BPTES, DON or 968) alone is not sufficient to stimulate mitochondrial fusion. Instead, it was observed that

GLS-dependent stimulation of mitochondrial fusion by Q starvation required the ability of GLS to oligomerise into tetramers. Therefore, GLS-dependent mitochondrial fusion may occur via structural changes rather than catalytic function. Overall, GLS perhaps might sense Q starvation by undergoing structural re-arrangement to stimulate mitochondrial fusion although further mechanistic details are not yet known.

On the other hand, in line with our data from Fh deficient cells, Cai et al. (2018) showed that E or alpha-ketoglutarate supplementation blocked Q-starvation induced mitochondrial fusion. These findings therefore support a model where enzymes involved in amino acid metabolism can also function as mitochondrial sensors to signal amino acid availability to control mitochondrial hyperfusion.

Interestingly, studies have shown that mitochondrial glutaminases exist mostly as inactive dimers but their ability to form tetramers is dependent on allosteric binding of inorganic phosphates (Cassago et al., 2012, Godfrey et al., 1977, Morehouse and Curthoys, 1981). It has been suggested that GLS may be a possible substrate of yet to be identified kinases (Han et al., 2018). It is also shown that GLS activity is regulated by the binding of E to the active site (Li et al., 2016b). Although the regulators of GLS structural changes have yet to be identified, it is possible that GLS ability to oligomerise and transmit metabolic signals is also dependent on the metabolic processing of Q, L and R.

### **6.3 Ulk1/2 signalling, not PKA signalling regulate amino acid-dependent mitochondrial hyperfusion.**

Overall, we also showed here that Ulk1, AMPK and PKA regulate mitochondrial dynamics. Indeed, due to the particular interest of our lab in Ulk1 signalling, it was exciting to identify a novel role of Ulk1 signalling in the regulation of mitochondrial dynamics. Previous studies have already linked AMPK and PKA to the regulation of mitochondrial dynamics (Toyama et al., 2016, Cereghetti et al., 2008, Gomes et al., 2011a).

The current model suggests a pro fission role for AMPK, due to the observation that AMPK phosphorylates Mff to promote mitochondrial fragmentation during mitochondrial damage (Toyama et al., 2016). In contrast, we observed a pro-fusion role for AMPK, due to the observation that AMPK  $\alpha 1/\alpha 2$  DKO MEF have more fragmented mitochondria relative to wildtype cells. However, AMPK DKO cells were still able to stimulate QLR-dependent mitochondrial hyperfusion. Therefore, QLR-

sensing does not require AMPK signalling, although AMPK may play other roles in mitochondrial dynamics.

On the other hand, the current PKA model suggests that increased cAMP leads to activation of PKA and phosphorylation of Drp1 at S637 to drive mitochondrial fusion (Gomes et al., 2011a). Interestingly, our data confirm that the cAMP-PKA mechanism functions for mitochondrial fusion. Our findings also agree with the observation that PKA-phosphorylation of Drp1-S637 inhibits fission in OXPHOS-active RPE1 cells, thus serving as a mechanism to evade CCCP-induced mitochondrial degradation (MacVicar and Lane, 2014). Similar to our studies, MacVicar and Lane (2014) also showed that Frsk activates PKA-dependent phosphorylation of Drp1 S637, which could be inhibited by the PKA inhibitor, H89. However, to our surprise, the cAMP-PKA-Drp1 signalling pathway does not fully account for amino acid-dependent mitochondrial hyperfusion.

Therefore, we concluded that while AMPK and PKA are regulators of mitochondrial dynamics, they are not involved in the regulation of amino acid addback-dependent mitochondrial hyperfusion. Ulk1 signalling may play a stronger role for amino acid-dependent mitochondrial hyperfusion.

### **6.3.1 Amino acid-dependent mitochondrial hyperfusion does not require the cAMP-PKA-Drp1 signalling pathway**

We were intrigued by our observations that amino acid-dependent mitochondrial hyperfusion was independent of the cAMP-PKA-Drp1 mechanism, since this has been reported in multiple studies (Gomes et al., 2011a, Li et al., 2017). However, more recent findings (Cai et al., 2018) support a nutrient-dependent mitochondrial fusion model that can function independently of the cAMP-PKA-Drp1 pathway. Therefore, multiple mechanisms appear to be involved.

Firstly, during amino acid starvation, cAMP levels did not robustly change in our experiments. These observations were consistent with the Cai et al. (2018) study where it was shown that Q starvation promoted mitochondrial hyperfusion but cAMP levels did not increase. Interestingly, cAMP levels have been previously shown to reduce following amino acid starvation in Morhenn et al. (1974). It was reported that V and W starvation led to the reduction of cAMP levels in both 3T3 and SV3T3 cells. Therefore, our findings and multiple others show that cAMP levels do not always correlate with mitochondrial fusion during amino acid starvation.

The canonical cAMP-PKA mechanism highlights that PKA is activated when cAMP levels increase (Gomes et al., 2011a). In this model, cAMP generated from adenylyl cyclase binds to the regulatory units of PKA, promoting PKA catalytic units to detach from the PKA tetramer complex. However, our data indicate that cAMP levels are not altered upon amino acid starvation but PKA becomes activated. This suggests that PKA activation observed here during amino acid starvation is occurring via cAMP-independent mechanisms (Niu et al., 2001, Dulin et al., 2001, Kohr et al., 2010, Zhong et al., 1997).

Frsk activates adenylyl cyclase leading to the increase in cAMP levels and downstream activation of PKA (Litvin et al., 2003). In support, Frsk activated PKA as shown by the phosphorylation of Creb and Drp1. However, Frsk did not stimulate mitochondrial hyperfusion (via PKA-dependent phosphorylation of Drp1 at S637) as strongly as QLR-dependent mitochondrial hyperfusion. This agrees with Cai et al. (2018) which found that Frsk did not lead to extensive mitochondrial hyperfusion despite inducing high levels of cAMP. These results indicate that PKA-dependent phosphorylation is not absolutely required for amino acid dependent-mitochondrial hyperfusion. Indeed, we found that PKA activity is not required for amino acid-dependent mitochondrial hyperfusion since H89 did not inhibit the response. We also observed that Drp1-S637 phosphorylation was not increased by either amino acid starvation or QLR-addback.

Therefore, our results present an alternative model for mitochondrial hyperfusion independent of cAMP-PKA-Drp1-S637 phosphorylation. In our model, mitochondria appear to sense amino acid availability more through changes in downstream amino acid metabolism.

### **6.3.2 Ulk1/2 signalling regulates cellular metabolism**

Our data here strongly indicate that Ulk1/2 signalling regulates amino acid-dependent mitochondrial hyperfusion. Speculatively, some enzymes required for amino acid metabolism might be substrates of Ulk1. If this was the case, upon Ulk1 inhibition, amino acid metabolism could be altered, therefore abrogating mitochondrial amino acid sensing. It would be interesting to further study cellular metabolism in Ulk1/2 KO models.

Interestingly, a recent study has shown that Ulk1/2 directly regulate glycolytic enzymes during amino acid and growth factor starvation (Li et al., 2016a). In Li et al. (2016a), Ulk1/2 was shown to phosphorylate hexokinase (HK1, at Ser124 and

Ser364), Enolase 1 (ENO1, at Ser115 and Ser282), fructose-1, 6-biphosphatase-1 (FBP1, at Ser63 and Ser88) and phosphofructose kinase 1 (PFK1, at Ser74 and Ser762). These Ulk1 phosphorylation events increased the catalytic activity of HK1 (but reduced the activities of ENO1, FBP1, and PFK1) during amino acid and serum starvation. These modifications promoted utilization of glucose-6-phosphate in the pentose phosphate pathway for the synthesis of NADPH and REDOX homeostasis. Therefore, this study is consistent with the possibility of Ulk1-dependent regulation of amino acid metabolism (e.g. speculatively by targeting GLS or other enzymes required for amino acid metabolism).

Interestingly, it has been shown that inhibition of GLS2 stimulates autophagy by activating AMPK and Ulk1 (Lee et al., 2014). This further supports crosstalk mechanisms between amino acid metabolism and Ulk1. The possible regulation of amino acid metabolic enzymes by Ulk1 remains an exciting potential area for exploration. Interestingly, another independent study reported that cells with Ulk1 silencing have reduced  $\beta$ -oxidation, oxygen consumption and ATP synthesis which all led to increased mitochondrial-generated ROS (Ro et al., 2013). We also consistently showed that hyperfused mitochondria have reduced oxidative state as shown by higher GSH/GSSG. Interestingly, Ulk1 phosphorylation of glycolytic enzymes was shown to also promote the synthesis of ROS-scavenging metabolites (Li et al., 2016). This further supports a model where Ulk1/2 deficient cells facing QLR-addback may exacerbate metabolic deficiencies hence leading to mitochondrial fragmentation.

Our data showed that mitochondrial amino acid sensing occurred normally in autophagy-deficient Atg5 KO cells which suggested that the mitochondrial-specific Ulk1 role was independent of autophagy. Indeed, Ulk1 phosphorylation of glycolytic enzymes occurred independently of autophagy but was dependent on Atg13 and FIP200 (Li et al., 2016). This resembles our trends with amino acid-dependent mitochondrial hyperfusion, which also required Atg13 and FIP200. Our data clearly establishes that the Ulk1-complex regulates amino acid-dependent mitochondrial hyperfusion, speculatively via Ulk1 regulation of cellular metabolism.

## **6.4 Mitochondria hyperfuse to meet metabolic demand during amino acid starvation-dependent stress**

Multiple studies have demonstrated that both mitochondrial fission and fusion are critical for the maintenance of cellular homeostasis. For example, fission is critical for the quality control of mitochondria by segregating damaged mitochondrial regions for degradation (Twig et al., 2008). Similarly, mitochondria must be divided equally to daughter cells during cellular division and fission is required for embryonic development and apoptosis (Ishihara et al., 2009, Mitra et al., 2009).

On the other hand, mitochondrial fusion is required for embryonic development, dilution of mutated DNA and energy generation (Chen et al., 2003, Chen et al., 2010). Mitochondrial hyperfusion has been reported to increase longevity in *C.elegans*, thereby promoting healthy ageing (Chaudhari and Kipreos, 2017). Mitochondrial hyperfusion sustains the rate and efficiency of OXPHOS by promoting oxygen consumption and E.T.C. capacities (Rossignol et al., 2004, Mishra et al., 2014, Cogliati et al., 2013). During conditions of enhanced OXPHOS, mitochondrial fusion also prevents damage-induced mitochondrial degradation to maintain high metabolic rates (MacVicar and Lane, 2014). Another suggested role for hyperfusion is restriction of mitochondrial degradation (Gomes et al., 2011a, Rambold et al., 2011). Lastly, mitochondrial fusion reduces mitochondrial-dependent ROS generation (Lee et al., 2014). We show here that mitochondrial hyperfusion promotes metabolic homeostasis by potentially aligning mitochondrial shape to mitochondrial function.

According to our data, nutrient (amino acid) addback conditions that drive hyperfused mitochondria also lead to formation of more metabolic intermediates representing energy production pathways. Cells undergoing QLR-dependent mitochondrial hyperfusion had greater levels Krebs cycle intermediates. Loss of fusion in Mfn1 KO reduced the levels of some of these metabolites. Cells generally maintained levels of cellular ATP regardless of mitochondrial fusion (as long as glucose and amino acid are available). However, our data suggest that cells with mitochondrial hyperfusion have more mitochondrial-dependent ATP generation, likely via OXPHOS. This is in line with previous studies in which ATPase activity was increased in cells undergoing fusion (Gomes et al., 2011a). Overall, our data suggest that mitochondrial hyperfusion is a specific response to changes in metabolic demand that help enhance mitochondrial function.

Decline or inefficient mitochondrial function is associated with increased generation of ROS. Our data showed that cells undergoing mitochondrial hyperfusion have reduced oxidative stress as shown by reduced taurine levels and increased GSH/GSSG ratio. This correlates with previous studies suggesting that mitochondrial hyperfusion prevents the build-up of ROS (Lee et al., 2014). Based on this, we conclude that during amino acid starvation, mitochondria are unable to maximally meet metabolic demands. In response, mitochondria adapt to help sustain function and cell homeostasis via fusion and helping to reduce ROS. On the other hand, the presence of Q, L and R during addback provides replenishment of certain intermediates (including those from glutaminolysis) to promote mitochondrial metabolic function and further ROS-scavenging activity.

We propose a summary model (**Fig 6.1**) whereby mitochondria sense the availability of Q, L and R through metabolic pathways. As a regulatory mechanism, the Ulk1 complex speculatively regulates enzymes to control rates of cellular metabolism during nutrient stress. Mitochondrial hyperfusion occurs in response to amino acid-dependent metabolism via a putative signal linking amino acid metabolism, mitochondrial dynamics and mitochondrial function. As such, mitochondria hyperfuse to match mitochondrial shape to their functional state. Functionally, mitochondrial hyperfuse to meet metabolic demands such as maintaining levels of Krebs cycle metabolites and reducing ROS during amino acid starvation-dependent stress.

We show that the signal linking amino acid availability to mitochondrial hyperfusion is independent of MTORC1 and the canonical cAMP-PKA-Drp1 pathway (**Fig 6.2**). While AMPK is required for the maintenance of mitochondrial dynamics, Ulk1 plays stronger roles for mitochondrial hyperfusion. Amino acid starvation led to depletion of metabolites in the urea cycle, Krebs cycle, cellular ATP and ROS maintenance. In contrast, QLR addback replenished the urea cycle, Krebs cycle, and cellular ATP but led to a reduction in ROS levels. Our evidence indicates that these metabolic changes are associated with amino acid-dependent mitochondrial hyperfusion and we speculate that a subset may be causal.

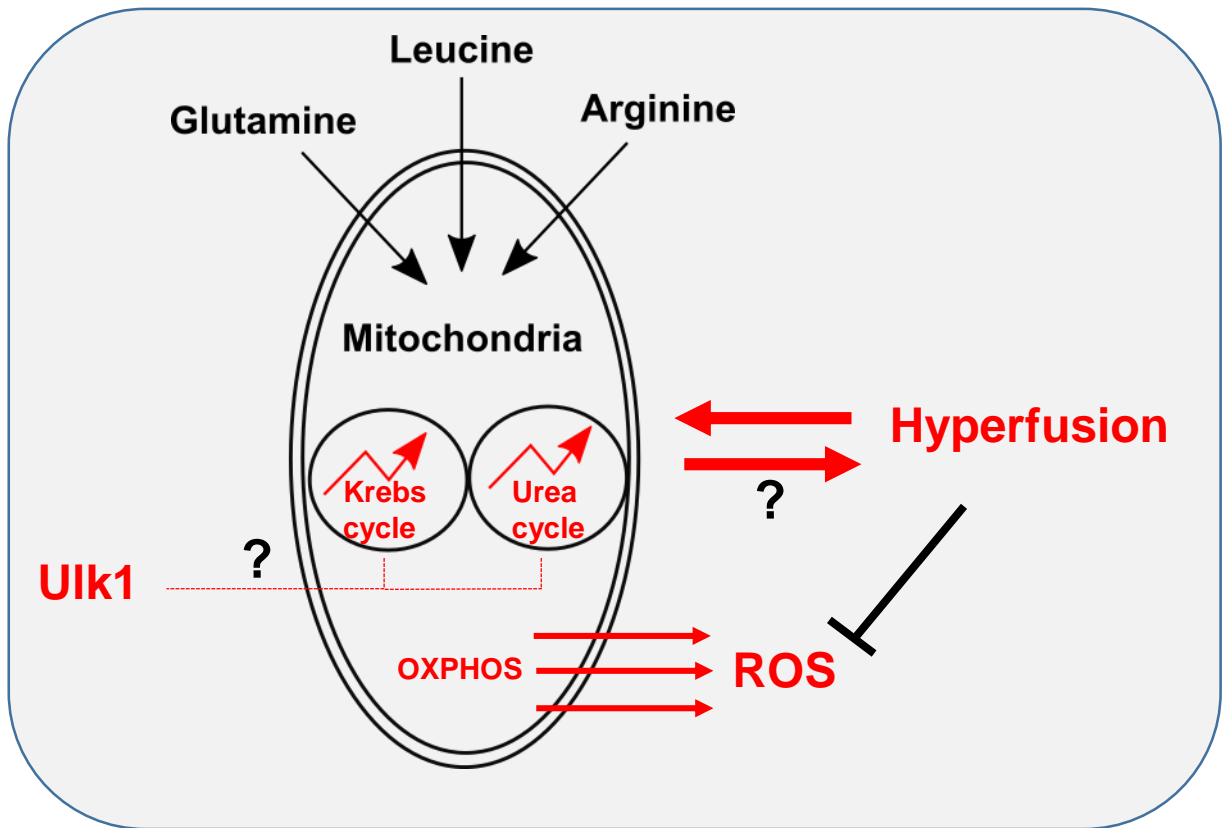


**Figure 6.1: Proposed model for QLR-addback induced mitochondrial hyperfusion.**

We propose a model whereby mitochondria sense the availability of glutamine, leucine and arginine through metabolic pathways they feed and the enzymes that catalyse their metabolic catabolism. As a cellular regulatory check, the Ulk1 complex regulates these enzymes and metabolic pathways to control cellular metabolism during nutrient stress. Mitochondrial hyperfusion occurs in response to amino acid-dependent metabolism and there is a signal linking amino acid metabolism, mitochondrial dynamics and mitochondrial function. Functionally, mitochondrial hyperfuse to meet metabolic demands such as maintaining levels of Krebs cycle metabolites and reducing ROS during amino acid starvation-dependent stress.

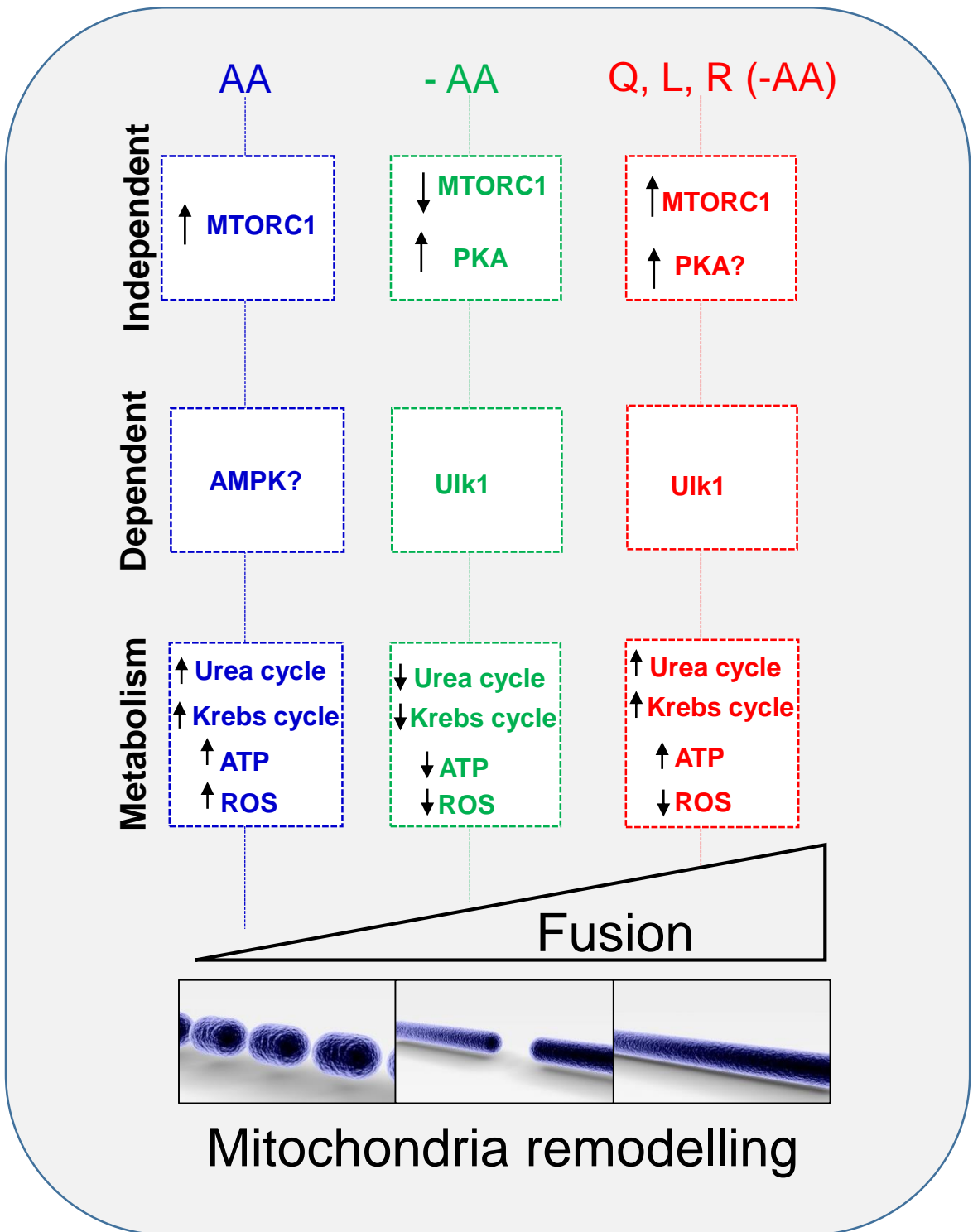


**Figure 6.2: Summary model of amino acid-dependent mitochondrial dynamics.** Our model indicates that mitochondria sense regulatory amino acids Q, L and R independently of MTORC1, PKA and AMPK but dependent on the Ulk1 complex. The supplementation of QLR increased distinct metabolites that represents an increase in the urea cycle, the Krebs cycle, ATP levels and a decrease in ROS.

## 6.5 Future work

In the course of this study, we have highlighted interesting areas to be explored. Further studies should measure oxygen consumption rate in QLR-addback cells relative to amino acid starved cells to assess the extent of rescue in OXPHOS. Studies should further explore the signalling pathways that connect mitochondrial amino acid sensing to mitochondrial dynamics. We showed here that AMPK and PKA, two likely mechanisms are largely not involved. Further studies should focus on Ulk1-dependent amino acid-dependent metabolism, and how enzymes involved in metabolism could affect mitochondrial dynamics (Cai et al., 2018). Studies could use metabolomics to study amino acid flux in Ulk1/2 KO cells. To specifically identify changes in mitochondrial-dependent metabolites, a rapid technique that quantifies metabolites after mitochondria isolation should be utilised (Chen et al., 2016b). Also, the effects of pharmacological targeting of Ulk1 on cellular metabolism should be studied with metabolomics. We should also study whether there is Ulk1-dependent regulation of GLS or other enzymes required for amino acid metabolism. For example, mass spectrometry phosphorylation proteomic analysis of GLS upon amino acid starvation and QLR-addback (in normal vs Ulk1 inhibited conditions) may give insight into whether Ulk1 binds and phosphorylate GLS.

On the other hand, studies have clearly shown that AMPK, MTORC1 and Ulk1 crosstalk for autophagy regulation (Kim et al., 2011b, Chan, 2009, Nwadike et al., 2018). While we showed that MTORC1 has limited roles in the regulation of mitochondrial dynamics, other studies have shown that long term inhibition of MTORC1 promotes mitochondrial hyperfusion (Morita et al., 2017). It is not yet clear how MTORC1, AMPK and Ulk signalling might converge to regulate mitochondrial dynamics so future studies should explore if this coordinated signalling pathway regulates mitochondrial dynamics at the basal state. Using molecular sensors, recent evidence suggests that AMPK signalling is compartmentalized with unique mitochondrial-AMPK pools similar to PKA-mitochondrial domains (Miyamoto et al., 2015). Roles of these mitochondrial AMPK pools on mitochondrial function have not been reported yet.

Due to the off-target limitations of PKA inhibitors (Limbutara et al., 2019), future studies should clarify the role of PKA in the regulation of mitochondrial dynamics (e.g. in cells where the PKA-catalytic units have been deleted (Isobe et al., 2017) or where cAMP generation has been blocked due to adenylyl cyclase KO (Soto-Velasquez et

al., 2018)). Further studies could investigate amino acid starvation or QLR-supplementation in these genetic PKA functional deficient cell models.

PKA and MTORC1 can be inter-dependent. It was reported recently that insulin and serum-dependent activation of MTORC1 required the AKAP1-PKA mitochondrial axis (Rinaldi et al., 2017). A recent study also showed that PKA can inhibit MTORC1 via phosphorylation of Raptor at S791 in multiple cell types (Jewell et al., 2019). In further contrast, another study reported that PKA activates MTORC1 via phosphorylation of Raptor at S791 (Liu et al., 2016b). PKA may regulate MTORC1 via yet another mechanism because mutation of phospho-Raptor S791 did not fully block MTORC1 inhibition (Jewell et al., 2019). Therefore, the regulatory inter-relationship between MTORC1 and PKA may have multiple or context specific mechanisms that need to be clarified further, especially in terms of mitochondrial regulation.

Surprisingly, there were some data in our studies that raise questions relative to findings of Jewell et al. (2019). We consistently showed here that amino acid starvation strongly led to the phosphorylation of CREB. In contrast, amino acid starvation did not lead to the phosphorylation of CREB in Jewell et al. (2019). Also, we also clearly showed that Frsk did not alter MTORC1 activity via the MTORC1-dependent phosphorylation of S6. In contrast, Frsk led to the inhibition of MTORC1 via reduced phosphorylation of S6K in Jewell et al. (2019). Another important discrepancy from these authors is that H89 blocked PKA leading to the reactivation of MTORC1 in their cell systems. This contradicts with our findings showing that H89 blocked both PKA and MTORC1/S6K. HEK293A were used in Jewell et al. (2019) while MEF, U2OS and 4T1 cells were used in our studies so cell-dependent responses may be involved. Further careful examination of this issue may shed light on potential tissue-specific or cancer-specific aspects of PKA-MTORC1 crosstalk, which would have important implications.

## References

- Abraham, R. T. 2015. Cell biology. Making sense of amino acid sensing. *Science*, 347, 128-9.
- Abu-Remaileh, M., Wyant, G. A., Kim, C., Laqtom, N. N., Abbasi, M., Chan, S. H., Freinkman, E. & Sabatini, D. M. 2017. Lysosomal metabolomics reveals V-ATPase- and mTOR-dependent regulation of amino acid efflux from lysosomes. *Science (New York, N.Y.)*, 358, 807-813.
- Acin-Perez, R., Gatti, Domenico L., Bai, Y. & Manfredi, G. 2011a. Protein Phosphorylation and Prevention of Cytochrome Oxidase Inhibition by ATP: Coupled Mechanisms of Energy Metabolism Regulation. *Cell Metabolism*, 13, 712-719.
- Acin-Perez, R., Russwurm, M., Gunnewig, K., Gertz, M., Zoidl, G., Ramos, L., Buck, J., Levin, L. R., Rassow, J., Manfredi, G. & Steegborn, C. 2011b. A phosphodiesterase 2A isoform localized to mitochondria regulates respiration. *J Biol Chem*, 286, 30423-32.
- Acin-Perez, R., Salazar, E., Kamenetsky, M., Buck, J., Levin, L. R. & Manfredi, G. 2009. Cyclic AMP produced inside mitochondria regulates oxidative phosphorylation. *Cell Metab*, 9, 265-76.
- Adam, J., Yang, M., Bauerschmidt, C., Kitagawa, M., O'Flaherty, L., Maheswaran, P., Ozkan, G., Sahgal, N., Baban, D., Kato, K., Saito, K., Iino, K., Igarashi, K., Stratford, M., Pugh, C., Tennant, D. A., Ludwig, C., Davies, B., Ratcliffe, P. J., El-Bahrawy, M., Ashrafian, H., Soga, T. & Pollard, P. J. 2013. A role for cytosolic fumarate hydratase in urea cycle metabolism and renal neoplasia. *Cell Rep*, 3, 1440-8.
- Affaitati, A., Cardone, L., de Cristofaro, T., Carlucci, A., Ginsberg, M. D., Varrone, S., Gottesman, M. E., Avvedimento, E. V. & Feliciello, A. 2003. Essential role of A-kinase anchor protein 121 for cAMP signaling to mitochondria. *J Biol Chem*, 278, 4286-94.
- Ahlberg, J., Marzella, L. & Glaumann, H. 1982. Uptake and degradation of proteins by isolated rat liver lysosomes. Suggestion of a microautophagic pathway of proteolysis. *Lab Invest*, 47, 523-32.
- Akabane, S., Uno, M., Tani, N., Shimazaki, S., Ebara, N., Kato, H., Kosako, H. & Oka, T. 2016. PKA Regulates PINK1 Stability and Parkin Recruitment to Damaged Mitochondria through Phosphorylation of MIC60. *Mol Cell*, 62, 371-84.
- Akepati, V. R., Muller, E. C., Otto, A., Strauss, H. M., Portwich, M. & Alexander, C. 2008. Characterization of OPA1 isoforms isolated from mouse tissues. *J Neurochem*, 106, 372-83.
- Alamri, A., Biswas, L., Watson, D. G. & Shu, X. 2019. Deletion of TSPO Resulted in Change of Metabolomic Profile in Retinal Pigment Epithelial Cells. *International journal of molecular sciences*, 20, 1387.
- Alemu, E. A., Lamark, T., Torgersen, K. M., Birgisdottir, A. B., Larsen, K. B., Jain, A., Olsvik, H., Overvatn, A., Kirkin, V. & Johansen, T. 2012. ATG8 family proteins act as scaffolds for assembly of the ULK complex: sequence requirements for LC3-interacting region (LIR) motifs. *J Biol Chem*, 287, 39275-90.
- Alers, S., Loffler, A. S., Paasch, F., Dieterle, A. M., Keppeler, H., Lauber, K., Campbell, D. G., Fehrenbacher, B., Schaller, M., Wesselborg, S. & Stork, B. 2011. Atg13 and FIP200 act independently of Ulk1 and Ulk2 in autophagy induction. *Autophagy*, 7, 1423-33.
- Alexander, C., Votruba, M., Pesch, U. E., Thiselton, D. L., Mayer, S., Moore, A., Rodriguez, M., Kellner, U., Leo-Kottler, B., Auburger, G., Bhattacharya, S. S. & Wissinger, B. 2000. OPA1, encoding a dynamin-related GTPase, is mutated in autosomal dominant optic atrophy linked to chromosome 3q28. *Nat Genet*, 26, 211-5.
- Allen, G. F., Toth, R., James, J. & Ganley, I. G. 2013. Loss of iron triggers PINK1/Parkin-independent mitophagy. *EMBO Rep*, 14, 1127-35.
- Alonezi, S., Tusiimire, J., Wallace, J., Dufton, M. J., Parkinson, J. A., Young, L. C., Clements, C. J., Park, J. K., Jeon, J. W., Ferro, V. A. & Watson, D. G. 2017. Metabolomic Profiling of the Synergistic Effects of Melittin in Combination with Cisplatin on Ovarian Cancer Cells. *Metabolites*, 7.
- Amati-Bonneau, P., Valentino, M. L., Reynier, P., Gallardo, M. E., Bornstein, B., Boissiere, A., Campos, Y., Rivera, H., de la Aleja, J. G., Carroccia, R., Iommarini, L., Labauge, P., Figarella-Branger, D., Marcocelles, P., Furby, A., Beauvais, K., Letournel, F.,

- Liguori, R., La Morgia, C., Montagna, P., Liguori, M., Zanna, C., Rugolo, M., Cossarizza, A., Wissinger, B., VERNY, C., Schwarzenbacher, R., Martin, M. A., Arenas, J., Ayuso, C., Garesse, R., Lenaers, G., Bonneau, D. & Carelli, V. 2008. OPA1 mutations induce mitochondrial DNA instability and optic atrophy 'plus' phenotypes. *Brain*, 131, 338-51.
- Amchenkova, A. A., Bakeeva, L. E., Chentsov, Y. S., Skulachev, V. P. & Zorov, D. B. 1988. Coupling membranes as energy-transmitting cables. I. Filamentous mitochondria in fibroblasts and mitochondrial clusters in cardiomyocytes. *J Cell Biol*, 107, 481-95.
- Anand, R., Wai, T., Baker, M. J., Kladt, N., Schauss, A. C., Rugarli, E. & Langer, T. 2014. The i-AAA protease YME1L and OMA1 cleave OPA1 to balance mitochondrial fusion and fission. *J Cell Biol*, 204, 919-29.
- Anderson, G. R., Wardell, S. E., Cakir, M., Yip, C., Ahn, Y. R., Ali, M., Yllanes, A. P., Chao, C. A., McDonnell, D. P. & Wood, K. C. 2018. Dysregulation of mitochondrial dynamics proteins are a targetable feature of human tumors. *Nat Commun*, 9, 1677.
- Anderson, S., Bankier, A. T., Barrell, B. G., de Bruijn, M. H., Coulson, A. R., Drouin, J., Eperon, I. C., Nierlich, D. P., Roe, B. A., Sanger, F., Schreier, P. H., Smith, A. J., Staden, R. & Young, I. G. 1981. Sequence and organization of the human mitochondrial genome. *Nature*, 290, 457-65.
- Antoniades, H. N. & Owen, A. J. 1982. Growth factors and regulation of cell growth. *Annu Rev Med*, 33, 445-63.
- Anwar, T., Liu, X., Suntio, T., Marjamaki, A., Biazik, J., Chan, E. Y. W., Varjosalo, M. & Eskelinen, E. L. 2019. ER-Targeted Beclin 1 Supports Autophagosome Biogenesis in the Absence of ULK1 and ULK2 Kinases. *Cells*, 8.
- Arasaki, K., Mikami, Y., Shames, S. R., Inoue, H., Wakana, Y. & Tagaya, M. 2017. Legionella effector Lpg1137 shuts down ER-mitochondria communication through cleavage of syntaxin 17. *Nat Commun*, 8, 15406.
- Arasaki, K., Nagashima, H., Kurosawa, Y., Kimura, H., Nishida, N., Dohmae, N., Yamamoto, A., Yanagi, S., Wakana, Y., Inoue, H. & Tagaya, M. 2018. MAP1B-LC1 prevents autophagosome formation by linking syntaxin 17 to microtubules. *EMBO Rep*, 19.
- Arasaki, K., Shimizu, H., Mogari, H., Nishida, N., Hirota, N., Furuno, A., Kudo, Y., Baba, M., Baba, N., Cheng, J., Fujimoto, T., Ishihara, N., Ortiz-Sandoval, C., Barlow, L. D., Raturi, A., Dohmae, N., Wakana, Y., Inoue, H., Tani, K., Dacks, J. B., Simmen, T. & Tagaya, M. 2015. A role for the ancient SNARE syntaxin 17 in regulating mitochondrial division. *Dev Cell*, 32, 304-17.
- Arstila, A. U. & Trump, B. F. 1968. Studies on cellular autophagocytosis. The formation of autophagic vacuoles in the liver after glucagon administration. *Am J Pathol*, 53, 687-733.
- Awad, J. A., Johnson, R. A., Jakobs, K. H. & Schultz, G. 1983. Interactions of forskolin and adenylate cyclase. Effects on substrate kinetics and protection against inactivation by heat and N-ethylmaleimide. *J Biol Chem*, 258, 2960-5.
- Axe, E. L., Walker, S. A., Manifava, M., Chandra, P., Roderick, H. L., Habermann, A., Griffiths, G. & Ktistakis, N. T. 2008. Autophagosome formation from membrane compartments enriched in phosphatidylinositol 3-phosphate and dynamically connected to the endoplasmic reticulum. *J Cell Biol*, 182, 685-701.
- Aylett, C. H., Sauer, E., Imseng, S., Boehringer, D., Hall, M. N., Ban, N. & Maier, T. 2016. Architecture of human mTOR complex 1. *Science*, 351, 48-52.
- Babicki, S., Arndt, D., Marcu, A., Liang, Y., Grant, J. R., Maciejewski, A. & Wishart, D. S. 2016. Heatmapper: web-enabled heat mapping for all. *Nucleic Acids Res*, 44, W147-53.
- Bach, D., Pich, S., Soriano, F. X., Vega, N., Baumgartner, B., Oriola, J., Dagaard, J. R., Lloberas, J., Camps, M., Zierath, J. R., Rabasa-Lhoret, R., Wallberg-Henriksson, H., Laville, M., Palacin, M., Vidal, H., Rivera, F., Brand, M. & Zorzano, A. 2003. Mitofusin-2 determines mitochondrial network architecture and mitochondrial metabolism. A novel regulatory mechanism altered in obesity. *J Biol Chem*, 278, 17190-7.
- Baker, M. J., Lampe, P. A., Stojanovski, D., Korwitz, A., Anand, R., Tatsuta, T. & Langer, T. 2014. Stress-induced OMA1 activation and autocatalytic turnover regulate OPA1-dependent mitochondrial dynamics. *Embo j*, 33, 578-93.

- Ban, T., Ishihara, T., Kohno, H., Saita, S., Ichimura, A., Maenaka, K., Oka, T., Mihara, K. & Ishihara, N. 2017. Molecular basis of selective mitochondrial fusion by heterotypic action between OPA1 and cardiolipin. *Nat Cell Biol*, 19, 856-863.
- Bar-Peled, L., Chantranupong, L., Cherniack, A. D., Chen, W. W., Ottina, K. A., Grabiner, B. C., Spear, E. D., Carter, S. L., Meyerson, M. & Sabatini, D. M. 2013. A Tumor suppressor complex with GAP activity for the Rag GTPases that signal amino acid sufficiency to mTORC1. *Science*, 340, 1100-6.
- Bar-Peled, L., Schweitzer, L. D., Zoncu, R. & Sabatini, D. M. 2012. Ragulator is a GEF for the rag GTPases that signal amino acid levels to mTORC1. *Cell*, 150, 1196-208.
- Baracco, E. E., Castoldi, F., Durand, S., Enot, D. P., Tadic, J., Kainz, K., Madeo, F., Chery, A., Izzo, V., Maiuri, M. C., Pietrocola, F. & Kroemer, G. 2019. alpha-Ketoglutarate inhibits autophagy. *Aging (Albany NY)*, 11, 3418-3431.
- Barmore, W. & Stone, W. L. 2019. Physiology, urea cycle. *StatPearls [Internet]*. StatPearls Publishing.
- Barr, F. A. 2013. Review series: Rab GTPases and membrane identity: causal or inconsequential? *J Cell Biol*, 202, 191-9.
- Basu, B., Dean, E., Puglisi, M., Greystoke, A., Ong, M., Burke, W., Cavallin, M., Bigley, G., Womack, C., Harrington, E. A., Green, S., Oelmann, E., de Bono, J. S., Ranson, M. & Banerji, U. 2015. First-in-Human Pharmacokinetic and Pharmacodynamic Study of the Dual m-TORC 1/2 Inhibitor AZD2014. *Clin Cancer Res*, 21, 3412-9.
- Baur, J. A., Pearson, K. J., Price, N. L., Jamieson, H. A., Lerin, C., Kalra, A., Prabhu, V. V., Allard, J. S., Lopez-Lluch, G., Lewis, K., Pistell, P. J., Poosala, S., Becker, K. G., Boss, O., Gwinn, D., Wang, M., Ramaswamy, S., Fishbein, K. W., Spencer, R. G., Lakatta, E. G., Le Couteur, D., Shaw, R. J., Navas, P., Puigserver, P., Ingram, D. K., de Cabo, R. & Sinclair, D. A. 2006. Resveratrol improves health and survival of mice on a high-calorie diet. *Nature*, 444, 337-42.
- Beetz, C., Schüle, R., Deconinck, T., Tran-Viet, K.-N., Zhu, H., Kremer, B. P. H., Frints, S. G. M., van Zelst-Stams, W. A. G., Byrne, P., Otto, S., Nygren, A. O. H., Baets, J., Smets, K., Ceulemans, B., Dan, B., Nagan, N., Kassubek, J., Klimpe, S., Klopstock, T., Stolze, H., Smeets, H. J. M., Schrander-Stumpel, C. T. R. M., Hutchinson, M., van de Warrenburg, B. P., Braastad, C., Deufel, T., Pericak-Vance, M., Schöls, L., de Jonghe, P. & Züchner, S. 2008. REEP1 mutation spectrum and genotype/phenotype correlation in hereditary spastic paraplegia type 31. *Brain : a journal of neurology*, 131, 1078-1086.
- Bejarano, E., Murray, J. W., Wang, X., Pampliega, O., Yin, D., Patel, B., Yuste, A., Wolkoff, A. W. & Cuervo, A. M. 2018. Defective recruitment of motor proteins to autophagic compartments contributes to autophagic failure in aging. *Aging Cell*, 17, e12777.
- Belenguer, P. & Pellegrini, L. 2013. The dynamin GTPase OPA1: more than mitochondria? *Biochim Biophys Acta*, 1833, 176-83.
- Bellot, G., Garcia-Medina, R., Gounon, P., Chiche, J., Roux, D., Pouyssegur, J. & Mazure, N. M. 2009. Hypoxia-Induced Autophagy Is Mediated through Hypoxia-Inducible Factor Induction of BNIP3 and BNIP3L via Their BH3 Domains. *Molecular and Cellular Biology*, 29, 2570.
- Bendell, J. C., Kelley, R. K., Shih, K. C., Grabowsky, J. A., Bergsland, E., Jones, S., Martin, T., Infante, J. R., Mischel, P. S., Matsutani, T., Xu, S., Wong, L., Liu, Y., Wu, X., Mortensen, D. S., Chopra, R., Hege, K. & Munster, P. N. 2015. A phase I dose-escalation study to assess safety, tolerability, pharmacokinetics, and preliminary efficacy of the dual mTORC1/mTORC2 kinase inhibitor CC-223 in patients with advanced solid tumors or multiple myeloma. *Cancer*, 121, 3481-90.
- Benjamini, Y. & Hochberg, Y. 1995. Controlling the False Discovery Rate: A Practical and Powerful Approach to Multiple Testing. *Journal of the Royal Statistical Society. Series B (Methodological)*, 57, 289-300.
- Bento, C. F., Renna, M., Ghislat, G., Puri, C., Ashkenazi, A., Vicinanza, M., Menzies, F. M. & Rubinsztein, D. C. 2016. Mammalian Autophagy: How Does It Work? *Annu Rev Biochem*, 85, 685-713.
- Berg, J., Tymoczko, J. & Stryer, L. 2002a. Ammonium ion is converted into urea in most terrestrial vertebrates. *Biochemistry. Freeman WH and Company, New York*, 959-965.

- Berg, J., Tymoczko, J. & Stryer, L. 2002b. The pentose phosphate pathway generates NADPH and synthesizes five-carbon sugars. *Biochemistry, 5th ed.*; WH Freeman: New York, NY, USA.
- Betts, M. J. & Robert, R. B. 2003. Amino Acid Properties and Consequences of Substitutions. *Bioinformatics for Geneticists*.
- Bhutia, Y. D. & Ganapathy, V. 2016. Glutamine transporters in mammalian cells and their functions in physiology and cancer. *Biochimica et Biophysica Acta (BBA) - Molecular Cell Research*, 1863, 2531-2539.
- Birgisdottir, A. B., Lamark, T. & Johansen, T. 2013. The LIR motif - crucial for selective autophagy. *J Cell Sci*, 126, 3237-47.
- Biswas, L., Zhou, X., Dhillon, B., Graham, A. & Shu, X. 2017. Retinal pigment epithelium cholesterol efflux mediated by the 18 kDa translocator protein, TSPO, a potential target for treating age-related macular degeneration. *Hum Mol Genet*, 26, 4327-4339.
- Bitterman, J. L., Ramos-Espiritu, L., Diaz, A., Levin, L. R. & Buck, J. 2013. Pharmacological distinction between soluble and transmembrane adenylyl cyclases. *J Pharmacol Exp Ther*, 347, 589-98.
- Bjorkoy, G., Lamark, T., Brech, A., Outzen, H., Perander, M., Overvatn, A., Stenmark, H. & Johansen, T. 2005. p62/SQSTM1 forms protein aggregates degraded by autophagy and has a protective effect on huntingtin-induced cell death. *J Cell Biol*, 171, 603-14.
- Boland, M. L., Chourasia, A. H. & Macleod, K. F. 2013. Mitochondrial dysfunction in cancer. *Front Oncol*, 3, 292.
- Bordt, E. A., Clerc, P., Roelofs, B. A., Saladino, A. J., Tretter, L., Adam-Vizi, V., Cherok, E., Khalil, A., Yadava, N., Ge, S. X., Francis, T. C., Kennedy, N. W., Picton, L. K., Kumar, T., Uppuluri, S., Miller, A. M., Itoh, K., Karbowski, M., Sesaki, H., Hill, R. B. & Polster, B. M. 2017. The Putative Drp1 Inhibitor mdivi-1 Is a Reversible Mitochondrial Complex I Inhibitor that Modulates Reactive Oxygen Species. *Developmental Cell*, 40, 583-594.e6.
- Boss, G. R. 1984. Decreased phosphoribosylpyrophosphate as the basis for decreased purine synthesis during amino acid starvation of human lymphoblasts. *J Biol Chem*, 259, 2936-41.
- Bowen, B. P. & Northen, T. R. 2010. Dealing with the unknown: metabolomics and metabolite atlases. *J Am Soc Mass Spectrom*, 21, 1471-6.
- Broer, A., Wagner, C. A., Lang, F. & Broer, S. 2000. The heterodimeric amino acid transporter 4F2hc/y+LAT2 mediates arginine efflux in exchange with glutamine. *Biochem J*, 349 Pt 3, 787-95.
- Brown, E. J., Albers, M. W., Shin, T. B., Ichikawa, K., Keith, C. T., Lane, W. S. & Schreiber, S. L. 1994. A mammalian protein targeted by G1-arresting rapamycin-receptor complex. *Nature*, 369, 756-8.
- Brunet, A., Bonni, A., Zigmond, M. J., Lin, M. Z., Juo, P., Hu, L. S., Anderson, M. J., Arden, K. C., Blenis, J. & Greenberg, M. E. 1999. Akt promotes cell survival by phosphorylating and inhibiting a Forkhead transcription factor. *Cell*, 96, 857-68.
- Buck, J., Sinclair, M. L., Schapal, L., Cann, M. J. & Levin, L. R. 1999. Cytosolic adenylyl cyclase defines a unique signaling molecule in mammals. *Proc Natl Acad Sci U S A*, 96, 79-84.
- Buck, M. D., O'Sullivan, D., Klein Geltink, R. I., Curtis, J. D., Chang, C. H., Sanin, D. E., Qiu, J., Kretz, O., Braas, D., van der Windt, G. J., Chen, Q., Huang, S. C., O'Neill, C. M., Edelson, B. T., Pearce, E. J., Sesaki, H., Huber, T. B., Rambold, A. S. & Pearce, E. L. 2016. Mitochondrial Dynamics Controls T Cell Fate through Metabolic Programming. *Cell*, 166, 63-76.
- Budanov, A. V. & Karin, M. 2008. p53 target genes sestrin1 and sestrin2 connect genotoxic stress and mTOR signaling. *Cell*, 134, 451-60.
- Budovskaya, Y. V., Stephan, J. S., Reggiori, F., Klionsky, D. J. & Herman, P. K. 2004. The Ras/cAMP-dependent protein kinase signaling pathway regulates an early step of the autophagy process in *Saccharomyces cerevisiae*. *J Biol Chem*, 279, 20663-71.
- Bujak, A. L., Crane, J. D., Lally, J. S., Ford, R. J., Kang, S. J., Rebalka, I. A., Green, A. E., Kemp, B. E., Hawke, T. J., Schertzer, J. D. & Steinberg, G. R. 2015. AMPK activation of muscle autophagy prevents fasting-induced hypoglycemia and myopathy during aging. *Cell Metab*, 21, 883-90.

- Burdyga, A., Surdo, N. C., Monterisi, S., Di Benedetto, G., Grisan, F., Penna, E., Pellegrini, L., Bortolozzi, M., Swietach, P., Pozzan, T. & Lefkimmatis, K. 2018. Phosphatases control PKA-dependent functional microdomains at the outer mitochondrial membrane. *Proc Natl Acad Sci U S A*, 115, E6497-e6506.
- Burrage, L. C., Thistlethwaite, L., Stroup, B. M., Sun, Q., Miller, M. J., Nagamani, S. C. S., Craigen, W., Scaglia, F., Sutton, V. R., Graham, B., Kennedy, A. D., Milosavljevic, A., Lee, B. H. & Elsea, S. H. 2019. Untargeted metabolomic profiling reveals multiple pathway perturbations and new clinical biomarkers in urea cycle disorders. *Genet Med*, 21, 1977-1986.
- Cai, W. F., Zhang, C., Wu, Y. Q., Zhuang, G., Ye, Z., Zhang, C. S. & Lin, S. C. 2018. Glutaminase GLS1 senses glutamine availability in a non-enzymatic manner triggering mitochondrial fusion. *Cell Res*, 28, 865-867.
- Caino, M. C., Ghosh, J. C., Chae, Y. C., Vaira, V., Rivadeneira, D. B., Favarsani, A., Rampini, P., Kossenkov, A. V., Aird, K. M., Zhang, R., Webster, M. R., Weeraratna, A. T., Bosari, S., Languino, L. R. & Altieri, D. C. 2015. PI3K therapy reprograms mitochondrial trafficking to fuel tumor cell invasion. *Proc Natl Acad Sci U S A*, 112, 8638-43.
- Call, J. A., Wilson, R. J., Laker, R. C., Zhang, M., Kundu, M. & Yan, Z. 2017. Ulk1-mediated autophagy plays an essential role in mitochondrial remodeling and functional regeneration of skeletal muscle. *Am J Physiol Cell Physiol*, 312, C724-c732.
- Cao, Y. L., Meng, S., Chen, Y., Feng, J. X., Gu, D. D., Yu, B., Li, Y. J., Yang, J. Y., Liao, S., Chan, D. C. & Gao, S. 2017. MFN1 structures reveal nucleotide-triggered dimerization critical for mitochondrial fusion. *Nature*, 542, 372-376.
- Carelli, V., Ross-Cisneros, F. N. & Sadun, A. A. 2004. Mitochondrial dysfunction as a cause of optic neuropathies. *Prog Retin Eye Res*, 23, 53-89.
- Carling, D., Aguan, K., Woods, A., Verhoeven, A. J., Beri, R. K., Brennan, C. H., Sidebottom, C., Davison, M. D. & Scott, J. 1994. Mammalian AMP-activated protein kinase is homologous to yeast and plant protein kinases involved in the regulation of carbon metabolism. *J Biol Chem*, 269, 11442-8.
- Carlson, C. A. & Kim, K. H. 1973. Regulation of hepatic acetyl coenzyme A carboxylase by phosphorylation and dephosphorylation. *J Biol Chem*, 248, 378-80.
- Carobbio, S., Frigerio, F., Rubi, B., Vetterli, L., Bloksgaard, M., Gjinovci, A., Pournourmohammadi, S., Herrera, P. L., Reith, W., Mandrup, S. & Maechler, P. 2009. Deletion of glutamate dehydrogenase in beta-cells abolishes part of the insulin secretory response not required for glucose homeostasis. *J Biol Chem*, 284, 921-9.
- Carroll, B., Maetzel, D., Maddocks, O. D., Otten, G., Ratcliff, M., Smith, G. R., Dunlop, E. A., Passos, J. F., Davies, O. R., Jaenisch, R., Tee, A. R., Sarkar, S. & Korolchuk, V. I. 2016a. Control of TSC2-Rheb signaling axis by arginine regulates mTORC1 activity. *Elife*, 5.
- Carroll, D., Howard, D., Zhu, H., Paumi, C. M., Vore, M., Bondada, S., Liang, Y., Wang, C. & St Clair, D. K. 2016b. Simultaneous quantitation of oxidized and reduced glutathione via LC-MS/MS: An insight into the redox state of hematopoietic stem cells. *Free radical biology & medicine*, 97, 85-94.
- Cassago, A., Ferreira, A. P. S., Ferreira, I. M., Fornezari, C., Gomes, E. R. M., Greene, K. S., Pereira, H. M., Garratt, R. C., Dias, S. M. G. & Ambrosio, A. L. B. 2012. Mitochondrial localization and structure-based phosphate activation mechanism of Glutaminase C with implications for cancer metabolism. *Proceedings of the National Academy of Sciences*, 109, 1092-1097.
- Cassidy-Stone, A., Chipuk, J. E., Ingerman, E., Song, C., Yoo, C., Kuwana, T., Kurth, M. J., Shaw, J. T., Hinshaw, J. E., Green, D. R. & Nunnari, J. 2008. Chemical inhibition of the mitochondrial division dynamin reveals its role in Bax/Bak-dependent mitochondrial outer membrane permeabilization. *Dev Cell*, 14, 193-204.
- Cereghetti, G. M., Stangherlin, A., Martins de Brito, O., Chang, C. R., Blackstone, C., Bernardi, P. & Scorrano, L. 2008. Dephosphorylation by calcineurin regulates translocation of Drp1 to mitochondria. *Proc Natl Acad Sci U S A*, 105, 15803-8.
- César-Razquin, A., Snijder, B., Frappier-Brinton, T., Isserlin, R., Gyimesi, G., Bai, X., Reithmeier, Reinhart A., Hepworth, D., Hediger, Matthias A., Edwards, Aled M. & Superti-Furga, G. 2015. A Call for Systematic Research on Solute Carriers. *Cell*, 162, 478-487.

- Cesarini, E., Cerioni, L., Canonico, B., Di Sario, G., Guidarelli, A., Lattanzi, D., Savelli, D., Guescini, M., Nasoni, M. G., Bigini, N., Cuppini, R., Stocchi, V., Ambrogini, P., Papa, S. & Luchetti, F. 2018. Melatonin protects hippocampal HT22 cells from the effects of serum deprivation specifically targeting mitochondria. *PLoS One*, 13, e0203001.
- Chae, S., Kim, S. J., Do Koo, Y., Lee, J. H., Kim, H., Ahn, B. Y., Ha, Y. C., Kim, Y. H., Jang, M. G., Koo, K. H., Choi, S. H., Lim, S., Park, Y. J., Jang, H. C., Hwang, D., Lee, S. W. & Park, K. S. 2018. A mitochondrial proteome profile indicative of type 2 diabetes mellitus in skeletal muscles. *Exp Mol Med*, 50, 129.
- Chagoyen, M. & Pazos, F. 2013. Tools for the functional interpretation of metabolomic experiments. *Brief Bioinform*, 14, 737-44.
- Chakrabarti, R., Ji, W.-K., Stan, R. V., de Juan Sanz, J., Ryan, T. A. & Higgs, H. N. 2018. INF2-mediated actin polymerization at the ER stimulates mitochondrial calcium uptake, inner membrane constriction, and division. *The Journal of Cell Biology*, 217, 251-268.
- Chambers, M. C., Maclean, B., Burke, R., Amodei, D., Ruderman, D. L., Neumann, S., Gatto, L., Fischer, B., Pratt, B., Egertson, J., Hoff, K., Kessner, D., Tasman, N., Shulman, N., Frewen, B., Baker, T. A., Brusniak, M. Y., Paulse, C., Creasy, D., Flashner, L., Kani, K., Moulding, C., Seymour, S. L., Nuwaysir, L. M., Lefebvre, B., Kuhlmann, F., Roark, J., Rainer, P., Detlev, S., Hemenway, T., Huhmer, A., Langridge, J., Connolly, B., Chadick, T., Holly, K., Eckels, J., Deutsch, E. W., Moritz, R. L., Katz, J. E., Agus, D. B., MacCoss, M., Tabb, D. L. & Mallick, P. 2012. A cross-platform toolkit for mass spectrometry and proteomics. *Nat Biotechnol*, 30, 918-20.
- Chan, E. Y. 2009. mTORC1 phosphorylates the ULK1-mAtg13-FIP200 autophagy regulatory complex. *Sci Signal*, 2, pe51.
- Chan, E. Y., Kir, S. & Tooze, S. A. 2007. siRNA screening of the kinome identifies ULK1 as a multidomain modulator of autophagy. *J Biol Chem*, 282, 25464-74.
- Chan, E. Y., Longatti, A., McKnight, N. C. & Tooze, S. A. 2009. Kinase-inactivated ULK proteins inhibit autophagy via their conserved C-terminal domains using an Atg13-independent mechanism. *Mol Cell Biol*, 29, 157-71.
- Chan, E. Y. & Tooze, S. A. 2009. Evolution of Atg1 function and regulation. *Autophagy*, 5, 758-65.
- Chang, C., Su, H., Zhang, D., Wang, Y., Shen, Q., Liu, B., Huang, R., Zhou, T., Peng, C., Wong, Catherine C. L., Shen, H.-M., Lippincott-Schwartz, J. & Liu, W. 2015. AMPK-Dependent Phosphorylation of GAPDH Triggers Sirt1 Activation and Is Necessary for Autophagy upon Glucose Starvation. *Molecular Cell*, 60, 930-940.
- Chang, C. R. & Blackstone, C. 2007. Cyclic AMP-dependent protein kinase phosphorylation of Drp1 regulates its GTPase activity and mitochondrial morphology. *J Biol Chem*, 282, 21583-7.
- Chantranupong, L., Scaria, S. M., Saxton, R. A., Gygi, M. P., Shen, K., Wyant, G. A., Wang, T., Harper, J. W., Gygi, S. P. & Sabatini, D. M. 2016. The CASTOR Proteins Are Arginine Sensors for the mTORC1 Pathway. *Cell*, 165, 153-64.
- Chantranupong, L., Wolfson, R. L., Orozco, J. M., Saxton, R. A., Scaria, S. M., Bar-Peled, L., Spooner, E., Isasa, M., Gygi, S. P. & Sabatini, D. M. 2014. The Sestrins interact with GATOR2 to negatively regulate the amino-acid-sensing pathway upstream of mTORC1. *Cell reports*, 9, 1-8.
- Chappie, J. S., Acharya, S., Leonard, M., Schmid, S. L. & Dyda, F. 2010. G domain dimerization controls dynamin's assembly-stimulated GTPase activity. *Nature*, 465, 435-40.
- Chaudhari, S. N. & Kipreos, E. T. 2017. Increased mitochondrial fusion allows the survival of older animals in diverse *C. elegans* longevity pathways. *Nat Commun*, 8, 182.
- Chaudhry, R. & Varacallo, M. 2018. Biochemistry, Glycolysis. *StatPearls [Internet]*. StatPearls Publishing.
- Cheadle, J. P., Reeve, M. P., Sampson, J. R. & Kwiatkowski, D. J. 2000. Molecular genetic advances in tuberous sclerosis. *Hum Genet*, 107, 97-114.
- Chen, G., Han, Z., Feng, D., Chen, Y., Chen, L., Wu, H., Huang, L., Zhou, C., Cai, X., Fu, C., Duan, L., Wang, X., Liu, L., Liu, X., Shen, Y., Zhu, Y. & Chen, Q. 2014. A regulatory signaling loop comprising the PGAM5 phosphatase and CK2 controls receptor-mediated mitophagy. *Mol Cell*, 54, 362-77.
- Chen, H., Chomyn, A. & Chan, D. C. 2005. Disruption of fusion results in mitochondrial heterogeneity and dysfunction. *J Biol Chem*, 280, 26185-92.

- Chen, H., Detmer, S. A., Ewald, A. J., Griffin, E. E., Fraser, S. E. & Chan, D. C. 2003a. Mitofusins Mfn1 and Mfn2 coordinately regulate mitochondrial fusion and are essential for embryonic development. *J Cell Biol*, 160, 189-200.
- Chen, H., McCaffery, J. M. & Chan, D. C. 2007. Mitochondrial fusion protects against neurodegeneration in the cerebellum. *Cell*, 130, 548-62.
- Chen, M., Chen, Z., Wang, Y., Tan, Z., Zhu, C., Li, Y., Han, Z., Chen, L., Gao, R., Liu, L. & Chen, Q. 2016a. Mitophagy receptor FUNDC1 regulates mitochondrial dynamics and mitophagy. *Autophagy*, 12, 689-702.
- Chen, Q., Lin, R. Y. & Rubin, C. S. 1997. Organelle-specific targeting of protein kinase AII (PKAII). Molecular and in situ characterization of murine A kinase anchor proteins that recruit regulatory subunits of PKAII to the cytoplasmic surface of mitochondria. *J Biol Chem*, 272, 15247-57.
- Chen, Q., Vazquez, E. J., Moghaddas, S., Hoppel, C. L. & Lesnefsky, E. J. 2003b. Production of reactive oxygen species by mitochondria: central role of complex III. *J Biol Chem*, 278, 36027-31.
- Chen, S. D., Yang, J. L., Lin, T. K. & Yang, D. I. 2019a. Emerging Roles of Sestrins in Neurodegenerative Diseases: Counteracting Oxidative Stress and Beyond. *J Clin Med*, 8.
- Chen, W. W., Freinkman, E. & Sabatini, D. M. 2017. Rapid immunopurification of mitochondria for metabolite profiling and absolute quantification of matrix metabolites. *Nature Protocols*, 12, 2215.
- Chen, W. W., Freinkman, E., Wang, T., Birsoy, K. & Sabatini, D. M. 2016b. Absolute Quantification of Matrix Metabolites Reveals the Dynamics of Mitochondrial Metabolism. *Cell*, 166, 1324-1337 e11.
- Chen, Y., Cann, M. J., Litvin, T. N., Iourgenko, V., Sinclair, M. L., Levin, L. R. & Buck, J. 2000. Soluble adenylyl cyclase as an evolutionarily conserved bicarbonate sensor. *Science*, 289, 625-8.
- Chen, Y., Csordas, G., Jowdy, C., Schneider, T. G., Csordas, N., Wang, W., Liu, Y., Kohlhaas, M., Meiser, M., Bergem, S., Nerbonne, J. M., Dorn, G. W., 2nd & Maack, C. 2012. Mitofusin 2-containing mitochondrial-reticular microdomains direct rapid cardiomyocyte bioenergetic responses via interorganelle Ca<sup>2+</sup> crosstalk. *Circ Res*, 111, 863-75.
- Chen, Y. & Dorn, G. W., 2nd 2013. PINK1-phosphorylated mitofusin 2 is a Parkin receptor for culling damaged mitochondria. *Science*, 340, 471-5.
- Chen, Y., Zhuang, H., Chen, X., Shi, Z. & Wang, X. 2018. Spermidine-induced growth inhibition and apoptosis via autophagic activation in cervical cancer. *Oncol Rep*, 39, 2845-2854.
- Chen, Z., Lei, C., Wang, C., Li, N., Srivastava, M., Tang, M., Zhang, H., Choi, J. M., Jung, S. Y., Qin, J. & Chen, J. 2019b. Global phosphoproteomic analysis reveals ARMC10 as an AMPK substrate that regulates mitochondrial dynamics. *Nat Commun*, 10, 104.
- Cheng, C. T., Qi, Y., Wang, Y. C., Chi, K. K., Chung, Y., Ouyang, C., Chen, Y. R., Oh, M. E., Sheng, X., Tang, Y., Liu, Y. R., Lin, H. H., Kuo, C. Y., Schones, D., Vidal, C. M., Chu, J. C., Wang, H. J., Chen, Y. H., Miller, K. M., Chu, P., Yen, Y., Jiang, L., Kung, H. J. & Ann, D. K. 2018. Arginine starvation kills tumor cells through aspartate exhaustion and mitochondrial dysfunction. *Commun Biol*, 1, 178.
- Cheung, P. C., Salt, I. P., Davies, S. P., Hardie, D. G. & Carling, D. 2000. Characterization of AMP-activated protein kinase gamma-subunit isoforms and their role in AMP binding. *Biochem J*, 346 Pt 3, 659-69.
- Chevrollier, A., Guillet, V., Loiseau, D., Gueguen, N., de Crescenzo, M. A., Verny, C., Ferre, M., Dollfus, H., Odent, S., Milea, D., Goizet, C., Amati-Bonneau, P., Procaccio, V., Bonneau, D. & Reynier, P. 2008. Hereditary optic neuropathies share a common mitochondrial coupling defect. *Ann Neurol*, 63, 794-8.
- Chiang, H. L. & Dice, J. F. 1988. Peptide sequences that target proteins for enhanced degradation during serum withdrawal. *J Biol Chem*, 263, 6797-805.
- Chijiwa, T., Mishima, A., Hagiwara, M., Sano, M., Hayashi, K., Inoue, T., Naito, K., Toshioka, T. & Hidaka, H. 1990. Inhibition of forskolin-induced neurite outgrowth and protein phosphorylation by a newly synthesized selective inhibitor of cyclic AMP-dependent protein kinase, N-[2-(p-bromocinnamylamino)ethyl]-5-isoquinolinesulfonamide (H-89), of PC12D pheochromocytoma cells. *J Biol Chem*, 265, 5267-72.

- Cho, B., Cho, H. M., Kim, H. J., Jeong, J., Park, S. K., Hwang, E. M., Park, J. Y., Kim, W. R., Kim, H. & Sun, W. 2014. CDK5-dependent inhibitory phosphorylation of Drp1 during neuronal maturation. *Exp Mol Med*, 46, e105.
- Cho, D. H., Nakamura, T., Fang, J., Cieplak, P., Godzik, A., Gu, Z. & Lipton, S. A. 2009. S-nitrosylation of Drp1 mediates beta-amyloid-related mitochondrial fission and neuronal injury. *Science*, 324, 102-5.
- Chong, J., Soufan, O., Li, C., Caraus, I., Li, S., Bourque, G., Wishart, D. S. & Xia, J. 2018. MetaboAnalyst 4.0: towards more transparent and integrative metabolomics analysis. *Nucleic Acids Research*, 46, W486-W494.
- Chourasia, A. H., Tracy, K., Frankenberger, C., Boland, M. L., Sharifi, M. N., Drake, L. E., Sachleben, J. R., Asara, J. M., Locasale, J. W., Karczmar, G. S. & Macleod, K. F. 2015. Mitophagy defects arising from BNip3 loss promote mammary tumor progression to metastasis. *EMBO Rep*, 16, 1145-63.
- Christensen, H. N. 1990. Role of amino acid transport and countertransport in nutrition and metabolism. *Physiol Rev*, 70, 43-77.
- Chung, J., Kuo, C. J., Crabtree, G. R. & Blenis, J. 1992. Rapamycin-FKBP specifically blocks growth-dependent activation of and signaling by the 70 kd S6 protein kinases. *Cell*, 69, 1227-1236.
- Cipolat, S., Martins de Brito, O., Dal Zilio, B. & Scorrano, L. 2004. OPA1 requires mitofusin 1 to promote mitochondrial fusion. *Proc Natl Acad Sci U S A*, 101, 15927-32.
- Cipolat, S., Rudka, T., Hartmann, D., Costa, V., Serneels, L., Craessaerts, K., Metzger, K., Frezza, C., Annaert, W., D'Adamio, L., Derks, C., Dejaegere, T., Pellegrini, L., D'Hooge, R., Scorrano, L. & De Strooper, B. 2006. Mitochondrial rhomboid PARL regulates cytochrome c release during apoptosis via OPA1-dependent cristae remodeling. *Cell*, 126, 163-75.
- Closs, E. I., Boissel, J. P., Habermeier, A. & Rotmann, A. 2006. Structure and function of cationic amino acid transporters (CATs). *J Membr Biol*, 213, 67-77.
- Cogliati, S., Enriquez, J. A. & Scorrano, L. 2016. Mitochondrial Cristae: Where Beauty Meets Functionality. *Trends Biochem Sci*, 41, 261-73.
- Cogliati, S., Frezza, C., Soriano, M. E., Varanita, T., Quintana-Cabrera, R., Corrado, M., Cipolat, S., Costa, V., Casarin, A., Gomes, L. C., Perales-Clemente, E., Salviati, L., Fernandez-Silva, P., Enriquez, J. A. & Scorrano, L. 2013. Mitochondrial cristae shape determines respiratory chain supercomplexes assembly and respiratory efficiency. *Cell*, 155, 160-71.
- Coloff, J. L., Murphy, J. P., Braun, C. R., Harris, I. S., Shelton, L. M., Kami, K., Gygi, S. P., Selfors, L. M. & Brugge, J. S. 2016. Differential Glutamate Metabolism in Proliferating and Quiescent Mammary Epithelial Cells. *Cell Metab*, 23, 867-80.
- Corbin, J. D., Sugden, P. H., West, L., Flockhart, D. A., Lincoln, T. M. & McCarthy, D. 1978. Studies on the properties and mode of action of the purified regulatory subunit of bovine heart adenosine 3':5'-monophosphate-dependent protein kinase. *J Biol Chem*, 253, 3997-4003.
- Cosson, P., Marchetti, A., Ravazzola, M. & Orci, L. 2012. Mitofusin-2 independent juxtaposition of endoplasmic reticulum and mitochondria: an ultrastructural study. *PLoS One*, 7, e46293.
- Crane, J. D., Devries, M. C., Safdar, A., Hamadeh, M. J. & Tarnopolsky, M. A. 2010. The effect of aging on human skeletal muscle mitochondrial and intramyocellular lipid ultrastructure. *J Gerontol A Biol Sci Med Sci*, 65, 119-28.
- Creek, D. J., Jankevics, A., Burgess, K. E., Breitling, R. & Barrett, M. P. 2012. IDEOM: an Excel interface for analysis of LC-MS-based metabolomics data. *Bioinformatics*, 28, 1048-9.
- Cribbs, J. T. & Strack, S. 2007. Reversible phosphorylation of Drp1 by cyclic AMP-dependent protein kinase and calcineurin regulates mitochondrial fission and cell death. *EMBO Rep*, 8, 939-44.
- Darshi, M., Mendiola, V. L., Mackey, M. R., Murphy, A. N., Koller, A., Perkins, G. A., Ellisman, M. H. & Taylor, S. S. 2011. ChChd3, an inner mitochondrial membrane protein, is essential for maintaining crista integrity and mitochondrial function. *J Biol Chem*, 286, 2918-32.
- Daste, F., Sauvanet, C., Bavdek, A., Baye, J., Pierre, F., Le Borgne, R., David, C., Rojo, M., Fuchs, P. & Taresté, D. 2018. The heptad repeat domain 1 of Mitofusin has

- membrane destabilization function in mitochondrial fusion. *EMBO reports*, 19, e43637.
- Daumke, O. & Roux, A. 2017. Mitochondrial Homeostasis: How Do Dimers of Mitofusins Mediate Mitochondrial Fusion? *Curr Biol*, 27, R353-R356.
- Davies, S. P., Reddy, H., Caivano, M. & Cohen, P. 2000. Specificity and mechanism of action of some commonly used protein kinase inhibitors. *Biochem J*, 351, 95-105.
- de Brito, O. M. & Scorrano, L. 2008. Mitofusin 2 tethers endoplasmic reticulum to mitochondria. *Nature*, 456, 605-610.
- De Duve, C. 1963. The lysosome. *Sci Am*, 208, 64-72.
- Delettre, C., Lenaers, G., Griffoin, J. M., Gigarel, N., Lorenzo, C., Belenguer, P., Pelloquin, L., Grosgeorge, J., Turc-Carel, C., Perret, E., Astarie-Dequeker, C., Lasquelléc, L., Arnaud, B., Ducommun, B., Kaplan, J. & Hamel, C. P. 2000. Nuclear gene OPA1, encoding a mitochondrial dynamin-related protein, is mutated in dominant optic atrophy. *Nat Genet*, 26, 207-10.
- Dell'Acqua, M. L., Faux, M. C., Thorburn, J., Thorburn, A. & Scott, J. D. 1998. Membrane-targeting sequences on AKAP79 bind phosphatidylinositol-4, 5-bisphosphate. *Embo j*, 17, 2246-60.
- Demetriades, C., Doumpas, N. & Teleman, A. A. 2014. Regulation of TORC1 in response to amino acid starvation via lysosomal recruitment of TSC2. *Cell*, 156, 786-99.
- Depaoli, M. R., Karsten, F., Madreiter-Sokolowski, C. T., Klec, C., Gottschalk, B., Bischof, H., Eroglu, E., Waldeck-Weiermair, M., Simmen, T., Graier, W. F. & Malli, R. 2018. Real-Time Imaging of Mitochondrial ATP Dynamics Reveals the Metabolic Setting of Single Cells. *Cell Rep*, 25, 501-512.e3.
- Deter, R. L., Baudhuin, P. & De Duve, C. 1967. Participation of lysosomes in cellular autophagy induced in rat liver by glucagon. *J Cell Biol*, 35, C11-6.
- Detmer, S. A., Vande Velde, C., Cleveland, D. W. & Chan, D. C. 2008. Hindlimb gait defects due to motor axon loss and reduced distal muscles in a transgenic mouse model of Charcot-Marie-Tooth type 2A. *Hum Mol Genet*, 17, 367-75.
- Di Bartolomeo, S., Corazzari, M., Nazio, F., Oliverio, S., Lisi, G., Antonioli, M., Pagliarini, V., Matteoni, S., Fuoco, C., Giunta, L., Amelio, M., Nardacci, R., Romagnoli, A., Piacentini, M., Cecconi, F. & Fimia, G. M. 2010. The dynamic interaction of AMBRA1 with the dynein motor complex regulates mammalian autophagy. *The Journal of Cell Biology*, 191, 155.
- Di Benedetto, G., Gerbino, A. & Lefkimmiatis, K. 2017. Shaping mitochondrial dynamics: The role of cAMP signalling. *Biochem Biophys Res Commun*.
- Di Benedetto, G., Scalzotto, E., Mongillo, M. & Pozzan, T. 2013. Mitochondrial Ca<sup>2+</sup> Uptake Induces Cyclic AMP Generation in the Matrix and Modulates Organelle ATP Levels. *Cell Metabolism*, 17, 965-975.
- Diao, J., Liu, R., Rong, Y., Zhao, M., Zhang, J., Lai, Y., Zhou, Q., Wilz, L. M., Li, J., Vivona, S., Pfuetzner, R. A., Brunger, A. T. & Zhong, Q. 2015. ATG14 promotes membrane tethering and fusion of autophagosomes to endolysosomes. *Nature*, 520, 563-6.
- Dibble, Christian C., Elis, W., Menon, S., Qin, W., Klekota, J., Asara, John M., Finan, Peter M., Kwiatkowski, David J., Murphy, Leon O. & Manning, Brendan D. 2012. TBC1D7 Is a Third Subunit of the TSC1-TSC2 Complex Upstream of mTORC1. *Molecular Cell*, 47, 535-546.
- Dickey, A. S. & Strack, S. 2011. PKA/AKAP1 and PP2A/Bbeta2 regulate neuronal morphogenesis via Drp1 phosphorylation and mitochondrial bioenergetics. *J Neurosci*, 31, 15716-26.
- Din, S., Mason, M., Volkens, M., Johnson, B., Cottage, C. T., Wang, Z., Joyo, A. Y., Quijada, P., Erhardt, P., Magnuson, N. S., Konstandin, M. H. & Sussman, M. A. 2013. Pim-1 preserves mitochondrial morphology by inhibiting dynamin-related protein 1 translocation. *Proc Natl Acad Sci U S A*, 110, 5969-74.
- Ding, W. X., Ni, H. M., Li, M., Liao, Y., Chen, X., Stolz, D. B., Dorn, G. W., 2nd & Yin, X. M. 2010. Nix is critical to two distinct phases of mitophagy, reactive oxygen species-mediated autophagy induction and Parkin-ubiquitin-p62-mediated mitochondrial priming. *J Biol Chem*, 285, 27879-90.
- Disatnik, M. H., Ferreira, J. C., Campos, J. C., Gomes, K. S., Dourado, P. M., Qi, X. & Mochly-Rosen, D. 2013. Acute inhibition of excessive mitochondrial fission after myocardial infarction prevents long-term cardiac dysfunction. *J Am Heart Assoc*, 2, e000461.

- Dodge, K. L., Khouangsathiene, S., Kapiloff, M. S., Mouton, R., Hill, E. V., Houslay, M. D., Langeberg, L. K. & Scott, J. D. 2001. mAKAP assembles a protein kinase A/PDE4 phosphodiesterase cAMP signaling module. *Embo j*, 20, 1921-30.
- Dodgson, S. J., Forster, R. E., 2nd, Storey, B. T. & Mela, L. 1980. Mitochondrial carbonic anhydrase. *Proc Natl Acad Sci U S A*, 77, 5562-6.
- Dooley, H. C., Razi, M., Polson, H. E., Girardin, S. E., Wilson, M. I. & Tooze, S. A. 2014. WIPI2 links LC3 conjugation with PI3P, autophagosome formation, and pathogen clearance by recruiting Atg12-5-16L1. *Mol Cell*, 55, 238-52.
- Drusian, L., Nigro, E. A., Mannella, V., Pagliarini, R., Pema, M., Costa, A. S. H., Benigni, F., Larcher, A., Chiaravalli, M., Gaude, E., Montorsi, F., Capitanio, U., Musco, G., Frezza, C. & Boletta, A. 2018. mTORC1 Upregulation Leads to Accumulation of the Oncometabolite Fumarate in a Mouse Model of Renal Cell Carcinoma. *Cell Rep*, 24, 1093-1104.e6.
- Dubois, F., Vandermoere, F., Gernez, A., Murphy, J., Toth, R., Chen, S., Geraghty, K. M., Morrice, N. A. & MacKintosh, C. 2009. Differential 14-3-3 affinity capture reveals new downstream targets of phosphatidylinositol 3-kinase signaling. *Mol Cell Proteomics*, 8, 2487-99.
- Ducommun, S., Deak, M., Sumpton, D., Ford, R. J., Nunez Galindo, A., Kussmann, M., Viollet, B., Steinberg, G. R., Foretz, M., Dayon, L., Morrice, N. A. & Sakamoto, K. 2015. Motif affinity and mass spectrometry proteomic approach for the discovery of cellular AMPK targets: identification of mitochondrial fission factor as a new AMPK substrate. *Cell Signal*, 27, 978-88.
- Dulin, N. O., Niu, J., Browning, D. D., Ye, R. D. & Voyno-Yasenetskaya, T. 2001. Cyclic AMP-independent activation of protein kinase A by vasoactive peptides. *J Biol Chem*, 276, 20827-30.
- Dumollard, R., Duchen, M. & Carroll, J. 2007. The role of mitochondrial function in the oocyte and embryo. *Curr Top Dev Biol*, 77, 21-49.
- Dunn, W. A., Jr. 1990a. Studies on the mechanisms of autophagy: formation of the autophagic vacuole. *J Cell Biol*, 110, 1923-33.
- Dunn, W. A., Jr. 1990b. Studies on the mechanisms of autophagy: maturation of the autophagic vacuole. *J Cell Biol*, 110, 1935-45.
- Duran, R. V., Oppliger, W., Robitaille, A. M., Heiserich, L., Skendaj, R., Gottlieb, E. & Hall, M. N. 2012. Glutaminolysis activates Rag-mTORC1 signaling. *Mol Cell*, 47, 349-58.
- Duvezin-Caubet, S., Jagasia, R., Wagener, J., Hofmann, S., Trifunovic, A., Hansson, A., Chomyn, A., Bauer, M. F., Attardi, G., Larsson, N. G., Neupert, W. & Reichert, A. S. 2006. Proteolytic processing of OPA1 links mitochondrial dysfunction to alterations in mitochondrial morphology. *J Biol Chem*, 281, 37972-9.
- Duvezin-Caubet, S., Koppen, M., Wagener, J., Zick, M., Israel, L., Bernacchia, A., Jagasia, R., Rugarli, E. I., Imhof, A., Neupert, W., Langer, T. & Reichert, A. S. 2007. OPA1 processing reconstituted in yeast depends on the subunit composition of the m-AAA protease in mitochondria. *Mol Biol Cell*, 18, 3582-90.
- Dyall, S. D., Brown, M. T. & Johnson, P. J. 2004. Ancient invasions: from endosymbionts to organelles. *Science*, 304, 253-7.
- Efeyan, A., Zoncu, R., Chang, S., Gumper, I., Snitkin, H., Wolfson, R. L., Kirak, O., Sabatini, D. D. & Sabatini, D. M. 2013. Regulation of mTORC1 by the Rag GTPases is necessary for neonatal autophagy and survival. *Nature*, 493, 679-83.
- Egan, D. F., Chun, M. G., Vamos, M., Zou, H., Rong, J., Miller, C. J., Lou, H. J., Raveendra-Panickar, D., Yang, C. C., Sheffler, D. J., Teriete, P., Asara, J. M., Turk, B. E., Cosford, N. D. & Shaw, R. J. 2015. Small Molecule Inhibition of the Autophagy Kinase ULK1 and Identification of ULK1 Substrates. *Mol Cell*, 59, 285-97.
- Egan, D. F., Shackelford, D. B., Mihaylova, M. M., Gelino, S., Kohnz, R. A., Mair, W., Vasquez, D. S., Joshi, A., Gwinn, D. M., Taylor, R., Asara, J. M., Fitzpatrick, J., Dillin, A., Viollet, B., Kundu, M., Hansen, M. & Shaw, R. J. 2011. Phosphorylation of ULK1 (hATG1) by AMP-activated protein kinase connects energy sensing to mitophagy. *Science*, 331, 456-61.
- Ehse, S., Raschke, I., Mancuso, G., Bernacchia, A., Geimer, S., Tondera, D., Martinou, J. C., Westermann, B., Rugarli, E. I. & Langer, T. 2009. Regulation of OPA1 processing and mitochondrial fusion by m-AAA protease isoenzymes and OMA1. *J Cell Biol*, 187, 1023-36.

- Eisner, V., Picard, M. & Hajnoczky, G. 2018. Mitochondrial dynamics in adaptive and maladaptive cellular stress responses. *Nat Cell Biol*, 20, 755-765.
- El Fissi, N., Rojo, M., Aouane, A., Karatas, E., Poliacikova, G., David, C., Royet, J. & Rival, T. 2018. Mitofusin gain and loss of function drive pathogenesis in Drosophila models of CMT2A neuropathy. *EMBO Rep*, 19.
- Elbaz-Alon, Y., Rosenfeld-Gur, E., Shinder, V., Futerman, A. H., Geiger, T. & Schuldiner, M. 2014. A dynamic interface between vacuoles and mitochondria in yeast. *Dev Cell*, 30, 95-102.
- Eng, C. P., Sehgal, S. N. & Vezina, C. 1984. Activity of rapamycin (AY-22,989) against transplanted tumors. *J Antibiot (Tokyo)*, 37, 1231-7.
- Enserink, J. M., Christensen, A. E., de Rooij, J., van Triest, M., Schwede, F., Genieser, H. G., Doskeland, S. O., Blank, J. L. & Bos, J. L. 2002. A novel Epac-specific cAMP analogue demonstrates independent regulation of Rap1 and ERK. *Nat Cell Biol*, 4, 901-6.
- Escobar-Henriques, M. & Joaquim, M. 2019. Mitofusins: Disease Gatekeepers and Hubs in Mitochondrial Quality Control by E3 Ligases. *Frontiers in physiology*, 10, 517-517.
- Eura, Y., Ishihara, N., Yokota, S. & Mihara, K. 2003. Two mitofusin proteins, mammalian homologues of FZO, with distinct functions are both required for mitochondrial fusion. *J Biochem*, 134, 333-44.
- Farooqui, J. Z., Lee, H. W., Kim, S. & Paik, W. K. 1983. Studies on compartmentation of S-adenosyl-L-methionine in *Saccharomyces cerevisiae* and isolated rat hepatocytes. *Biochim Biophys Acta*, 757, 342-51.
- Filadi, R., Greotti, E., Turacchio, G., Luini, A., Pozzan, T. & Pizzo, P. 2015. Mitofusin 2 ablation increases endoplasmic reticulum-mitochondria coupling. *Proc Natl Acad Sci U S A*, 112, E2174-81.
- Fimia, G. M., Stoykova, A., Romagnoli, A., Giunta, L., Di Bartolomeo, S., Nardacci, R., Corazzari, M., Fuoco, C., Ucar, A., Schwartz, P., Gruss, P., Piacentini, M., Chowdhury, K. & Cecconi, F. 2007. Ambra1 regulates autophagy and development of the nervous system. *Nature*, 447, 1121-5.
- Flippo, K. H. & Strack, S. 2017. Mitochondrial dynamics in neuronal injury, development and plasticity. *Journal of Cell Science*, 130, 671.
- Franco, A., Kitsis, R. N., Fleischer, J. A., Gavathiotis, E., Kornfeld, O. S., Gong, G., Biris, N., Benz, A., Qvit, N., Donnelly, S. K., Chen, Y., Mennerick, S., Hodgson, L., Mochly-Rosen, D. & Dorn II, G. W. 2016. Correcting mitochondrial fusion by manipulating mitofusin conformations. *Nature*, 540, 74-79.
- Frank, S., Gaume, B., Bergmann-Leitner, E. S., Leitner, W. W., Robert, E. G., Catez, F., Smith, C. L. & Youle, R. J. 2001. The role of dynamin-related protein 1, a mediator of mitochondrial fission, in apoptosis. *Dev Cell*, 1, 515-25.
- Frezza, C., Zheng, L., Folger, O., Rajagopalan, K. N., MacKenzie, E. D., Jerby, L., Micaroni, M., Chaneton, B., Adam, J., Hedley, A., Kalna, G., Tomlinson, I. P., Pollard, P. J., Watson, D. G., Deberardinis, R. J., Shlomi, T., Ruppin, E. & Gottlieb, E. 2011. Haem oxygenase is synthetically lethal with the tumour suppressor fumarate hydratase. *Nature*, 477, 225-8.
- Friedman, J. R., Lackner, L. L., West, M., DiBenedetto, J. R., Nunnari, J. & Voeltz, G. K. 2011. ER Tubules Mark Sites of Mitochondrial Division. *Science*, 334, 358-362.
- Frolkis, A., Knox, C., Lim, E., Jewison, T., Law, V., Hau, D. D., Liu, P., Gautam, B., Ly, S., Guo, A. C., Xia, J., Liang, Y., Shrivastava, S. & Wishart, D. S. 2010. SMPDB: The Small Molecule Pathway Database. *Nucleic Acids Res*, 38, D480-7.
- Gallagher, L., Williamson, L. & Chan, E. 2016. Advances in Autophagy Regulatory Mechanisms. *Cells*, 5, 24.
- Gallagher, L. E., Radhi, O. A., Abdullah, M. O., McCluskey, A. G., Boyd, M. & Chan, E. Y. W. 2017. Lysosomotropism depends on glucose: a chloroquine resistance mechanism. *Cell Death Dis*, 8, e3014.
- Galluzzi, L., Pietrocola, F., Levine, B. & Kroemer, G. 2014. Metabolic control of autophagy. *Cell*, 159, 1263-76.
- Gammage, P. A. & Frezza, C. 2019. Mitochondrial DNA: the overlooked oncogenome? *BMC Biol*, 17, 53.
- Gan, B., Peng, X., Nagy, T., Alcaraz, A., Gu, H. & Guan, J.-L. 2006. Role of FIP200 in cardiac and liver development and its regulation of TNF $\alpha$  and TSC–mTOR signaling pathways. *The Journal of Cell Biology*, 175, 121-133.

- Gandre-Babbe, S. & van der Bliek, A. M. 2008. The novel tail-anchored membrane protein Mff controls mitochondrial and peroxisomal fission in mammalian cells. *Mol Biol Cell*, 19, 2402-12.
- Ganley, I. G., Lam du, H., Wang, J., Ding, X., Chen, S. & Jiang, X. 2009. ULK1.ATG13.FIP200 complex mediates mTOR signaling and is essential for autophagy. *J Biol Chem*, 284, 12297-305.
- Gao, X., Lee, K., Reid, M. A., Sanderson, S. M., Qiu, C., Li, S., Liu, J. & Locasale, J. W. 2018. Serine Availability Influences Mitochondrial Dynamics and Function through Lipid Metabolism. *Cell Reports*, 22, 3507-3520.
- Garami, A., Zwartkruis, F. J., Nobukuni, T., Joaquin, M., Rocco, M., Stocker, H., Kozma, S. C., Hafen, E., Bos, J. L. & Thomas, G. 2003. Insulin activation of Rheb, a mediator of mTOR/S6K/4E-BP signaling, is inhibited by TSC1 and 2. *Mol Cell*, 11, 1457-66.
- Garcia-Bermudez, J., Sanchez-Arago, M., Soldevilla, B., Del Arco, A., Nuevo-Tapióles, C. & Cuezva, J. M. 2015. PKA Phosphorylates the ATPase Inhibitory Factor 1 and Inactivates Its Capacity to Bind and Inhibit the Mitochondrial H(+)-ATP Synthase. *Cell Rep*, 12, 2143-55.
- Garcia, J., Han, D., Sancheti, H., Yap, L. P., Kaplowitz, N. & Cadenas, E. 2010. Regulation of mitochondrial glutathione redox status and protein glutathionylation by respiratory substrates. *J Biol Chem*, 285, 39646-54.
- Gatica, D., Lahiri, V. & Klionsky, D. J. 2018. Cargo recognition and degradation by selective autophagy. *Nat Cell Biol*, 20, 233-242.
- Gegg, M. E., Cooper, J. M., Chau, K. Y., Rojo, M., Schapira, A. H. & Taanman, J. W. 2010. Mitofusin 1 and mitofusin 2 are ubiquitinated in a PINK1/parkin-dependent manner upon induction of mitophagy. *Hum Mol Genet*, 19, 4861-70.
- Geisler, S., Holmstrom, K. M., Skujat, D., Fiesel, F. C., Rothfuss, O. C., Kahle, P. J. & Springer, W. 2010. PINK1/Parkin-mediated mitophagy is dependent on VDAC1 and p62/SQSTM1. *Nat Cell Biol*, 12, 119-31.
- Germain, M., Mathai, J. P., McBride, H. M. & Shore, G. C. 2005. Endoplasmic reticulum BIK initiates DRP1-regulated remodelling of mitochondrial cristae during apoptosis. *Embo j*, 24, 1546-56.
- Godfrey, S., Kuhlenschmidt, T. & Curthoys, P. 1977. Correlation between activation and dimer formation of rat renal phosphate-dependent glutaminase. *J Biol Chem*, 252, 1927-31.
- Gomes, L. C., Di Benedetto, G. & Scorrano, L. 2011a. During autophagy mitochondria elongate, are spared from degradation and sustain cell viability. *Nat Cell Biol*, 13, 589-98.
- Gomes, L. C., Di Benedetto, G. & Scorrano, L. 2011b. Essential amino acids and glutamine regulate induction of mitochondrial elongation during autophagy. *Cell Cycle*, 10, 2635-9.
- Gomes, L. C. & Scorrano, L. 2011. Mitochondrial elongation during autophagy: a stereotypical response to survive in difficult times. *Autophagy*, 7, 1251-3.
- Gómez-Sánchez, R., Rose, J., Guimarães, R., Mari, M., Papinski, D., Rieter, E., Geerts, W. J., Hardenberg, R., Kraft, C., Ungermann, C. & Reggiori, F. 2018. Atg9 establishes Atg2-dependent contact sites between the endoplasmic reticulum and phagophores. *The Journal of Cell Biology*, 217, 2743.
- Goncalves, E., Sciacovelli, M., Costa, A. S. H., Tran, M. G. B., Johnson, T. I., Machado, D., Frezza, C. & Saez-Rodriguez, J. 2018. Post-translational regulation of metabolism in fumarate hydratase deficient cancer cells. *Metab Eng*, 45, 149-157.
- Gong, R., Li, L., Liu, Y., Wang, P., Yang, H., Wang, L., Cheng, J., Guan, K. L. & Xu, Y. 2011. Crystal structure of the Gtr1p-Gtr2p complex reveals new insights into the amino acid-induced TORC1 activation. *Genes Dev*, 25, 1668-73.
- Gonzalez, G. A. & Montminy, M. R. 1989. Cyclic AMP stimulates somatostatin gene transcription by phosphorylation of CREB at serine 133. *Cell*, 59, 675-80.
- Gonzalez Montoro, A., Auffarth, K., Honscher, C., Bohnert, M., Becker, T., Warscheid, B., Reggiori, F., van der Laan, M., Frohlich, F. & Ungermann, C. 2018. Vps39 Interacts with Tom40 to Establish One of Two Functionally Distinct Vacuole-Mitochondria Contact Sites. *Dev Cell*, 45, 621-636.e7.
- Gorman, G. S., Schaefer, A. M., Ng, Y., Gomez, N., Blakely, E. L., Alston, C. L., Feeney, C., Horvath, R., Yu-Wai-Man, P., Chinnery, P. F., Taylor, R. W., Turnbull, D. M. &

- McFarland, R. 2015. Prevalence of nuclear and mitochondrial DNA mutations related to adult mitochondrial disease. *Ann Neurol*, 77, 753-9.
- Grahame Hardie, D., Carling, D. & T.R. Sim, A. 1989. The AMP-activated protein kinase: a multisubstrate regulator of lipid metabolism. *Trends in Biochemical Sciences*, 14, 20-23.
- Green, C. R., Wallace, M., Divakaruni, A. S., Phillips, S. A., Murphy, A. N., Ciaraldi, T. P. & Metallo, C. M. 2016. Branched-chain amino acid catabolism fuels adipocyte differentiation and lipogenesis. *Nat Chem Biol*, 12, 15-21.
- Grimmsrud, P. A., Carson, J. J., Hebert, A. S., Hubler, S. L., Niemi, N. M., Bailey, D. J., Jochem, A., Stapleton, D. S., Keller, M. P., Westphall, M. S., Yandell, B. S., Attie, A. D., Coon, J. J. & Pagliarini, D. J. 2012. A quantitative map of the liver mitochondrial phosphoproteome reveals posttranslational control of ketogenesis. *Cell Metab*, 16, 672-83.
- Grunwald, D. S., Otto, N. M., Park, J. M., Song, D. & Kim, D. H. 2019. GABARAPs and LC3s have opposite roles in regulating ULK1 for autophagy induction. *Autophagy*, 1-15.
- Gu, X., Orozco, J. M., Saxton, R. A., Condon, K. J., Liu, G. Y., Krawczyk, P. A., Scaria, S. M., Harper, J. W., Gygi, S. P. & Sabatini, D. M. 2017. SAMTOR is an S-adenosylmethionine sensor for the mTORC1 pathway. *Science*, 358, 813-818.
- Guo, X., Disatnik, M. H., Monbureau, M., Shamloo, M., Mochly-Rosen, D. & Qi, X. 2013. Inhibition of mitochondrial fragmentation diminishes Huntington's disease-associated neurodegeneration. *J Clin Invest*, 123, 5371-88.
- Gutierrez, M. G., Munafo, D. B., Beron, W. & Colombo, M. I. 2004. Rab7 is required for the normal progression of the autophagic pathway in mammalian cells. *J Cell Sci*, 117, 2687-97.
- Gwinn, D. M., Shackelford, D. B., Egan, D. F., Mihaylova, M. M., Mery, A., Vasquez, D. S., Turk, B. E. & Shaw, R. J. 2008. AMPK phosphorylation of raptor mediates a metabolic checkpoint. *Mol Cell*, 30, 214-26.
- Hailey, D. W., Rambold, A. S., Satpute-Krishnan, P., Mitra, K., Sougrat, R., Kim, P. K. & Lippincott-Schwartz, J. 2010. Mitochondria supply membranes for autophagosome biogenesis during starvation. *Cell*, 141, 656-67.
- Haj Slimane, Z., Bedioun, I., Lechene, P., Varin, A., Lefebvre, F., Mateo, P., Domergue-Dupont, V., Dewenter, M., Richter, W., Conti, M., El-Armouche, A., Zhang, J., Fischmeister, R. & Vandecasteele, G. 2014. Control of cytoplasmic and nuclear protein kinase A by phosphodiesterases and phosphatases in cardiac myocytes. *Cardiovasc Res*, 102, 97-106.
- Hamasaki, M., Furuta, N., Matsuda, A., Nezu, A., Yamamoto, A., Fujita, N., Oomori, H., Noda, T., Haraguchi, T., Hiraoka, Y., Amano, A. & Yoshimori, T. 2013. Autophagosomes form at ER-mitochondria contact sites. *Nature*, 495, 389-93.
- Han, J. M., Jeong, S. J., Park, M. C., Kim, G., Kwon, N. H., Kim, H. K., Ha, S. H., Ryu, S. H. & Kim, S. 2012. Leucyl-tRNA synthetase is an intracellular leucine sensor for the mTORC1-signaling pathway. *Cell*, 149, 410-24.
- Han, T., Zhan, W., Gan, M., Liu, F., Yu, B., Chin, Y. E. & Wang, J. B. 2018. Phosphorylation of glutaminase by PKCepsilon is essential for its enzymatic activity and critically contributes to tumorigenesis. *Cell Res*, 28, 655-669.
- Han, X. J., Lu, Y. F., Li, S. A., Kaitsuka, T., Sato, Y., Tomizawa, K., Nairn, A. C., Takei, K., Matsui, H. & Matsushita, M. 2008. CaM kinase I alpha-induced phosphorylation of Drp1 regulates mitochondrial morphology. *J Cell Biol*, 182, 573-85.
- Hanna, R. A., Quinsay, M. N., Orogo, A. M., Giang, K., Rikka, S. & Gustafsson, A. B. 2012. Microtubule-associated protein 1 light chain 3 (LC3) interacts with Bnip3 protein to selectively remove endoplasmic reticulum and mitochondria via autophagy. *J Biol Chem*, 287, 19094-104.
- Hara, K., Maruki, Y., Long, X., Yoshino, K., Oshiro, N., Hidayat, S., Tokunaga, C., Avruch, J. & Yonezawa, K. 2002. Raptor, a binding partner of target of rapamycin (TOR), mediates TOR action. *Cell*, 110, 177-89.
- Hara, T., Takamura, A., Kishi, C., Iemura, S., Natsume, T., Guan, J. L. & Mizushima, N. 2008. FIP200, a ULK-interacting protein, is required for autophagosome formation in mammalian cells. *J Cell Biol*, 181, 497-510.
- Harada, H., Becknell, B., Wilm, M., Mann, M., Huang, L. J.-s., Taylor, S. S., Scott, J. D. & Korsmeyer, S. J. 1999a. Phosphorylation and Inactivation of BAD by Mitochondria-Anchored Protein Kinase A. *Molecular Cell*, 3, 413-422.

- Harada, H., Becknell, B., Wilm, M., Mann, M., Huang, L. J., Taylor, S. S., Scott, J. D. & Korsmeyer, S. J. 1999b. Phosphorylation and inactivation of BAD by mitochondria-anchored protein kinase A. *Mol Cell*, 3, 413-22.
- Hardie, D. G. 2007. AMP-activated/SNF1 protein kinases: conserved guardians of cellular energy. *Nat Rev Mol Cell Biol*, 8, 774-85.
- Hardie, D. G. & Carling, D. 1997. The AMP-activated protein kinase--fuel gauge of the mammalian cell? *Eur J Biochem*, 246, 259-73.
- Hardie, D. G., Carling, D. & Carlson, M. 1998. The AMP-activated/SNF1 protein kinase subfamily: metabolic sensors of the eukaryotic cell? *Annu Rev Biochem*, 67, 821-55.
- Hardie, D. G., Schaffer, B. E. & Brunet, A. 2016. AMPK: An Energy-Sensing Pathway with Multiple Inputs and Outputs. *Trends in Cell Biology*, 26, 190-201.
- Harding, T. M., Morano, K. A., Scott, S. V. & Klionsky, D. J. 1995. Isolation and characterization of yeast mutants in the cytoplasm to vacuole protein targeting pathway. *J Cell Biol*, 131, 591-602.
- Hawley, S. A., Boudeau, J., Reid, J. L., Mustard, K. J., Udd, L., Makela, T. P., Alessi, D. R. & Hardie, D. G. 2003. Complexes between the LKB1 tumor suppressor, STRAD alpha/beta and MO25 alpha/beta are upstream kinases in the AMP-activated protein kinase cascade. *J Biol*, 2, 28.
- Hawley, S. A., Pan, D. A., Mustard, K. J., Ross, L., Bain, J., Edelman, A. M., Frenguelli, B. G. & Hardie, D. G. 2005. Calmodulin-dependent protein kinase kinase-beta is an alternative upstream kinase for AMP-activated protein kinase. *Cell Metab*, 2, 9-19.
- Hayashi-Nishino, M., Fujita, N., Noda, T., Yamaguchi, A., Yoshimori, T. & Yamamoto, A. 2009. A subdomain of the endoplasmic reticulum forms a cradle for autophagosome formation. *Nat Cell Biol*, 11, 1433-7.
- He, X. D., Gong, W., Zhang, J. N., Nie, J., Yao, C. F., Guo, F. S., Lin, Y., Wu, X. H., Li, F., Li, J., Sun, W. C., Wang, E. D., An, Y. P., Tang, H. R., Yan, G. Q., Yang, P. Y., Wei, Y., Mao, Y. Z., Lin, P. C., Zhao, J. Y., Xu, Y., Xu, W. & Zhao, S. M. 2018. Sensing and Transmitting Intracellular Amino Acid Signals through Reversible Lysine Aminoacylations. *Cell Metab*, 27, 151-166.e6.
- Head, B., Griparic, L., Amiri, M., Gandre-Babbe, S. & van der Bliek, A. M. 2009. Inducible proteolytic inactivation of OPA1 mediated by the OMA1 protease in mammalian cells. *J Cell Biol*, 187, 959-66.
- Heitman, J., Movva, N. R. & Hall, M. N. 1991. Targets for cell cycle arrest by the immunosuppressant rapamycin in yeast. *Science*, 253, 905-9.
- Herzig, S. & Shaw, R. J. 2018. AMPK: guardian of metabolism and mitochondrial homeostasis. *Nature reviews. Molecular cell biology*, 19, 121-135.
- Hess, K. C., Liu, J., Manfredi, G., Mühlischlegel, F. A., Buck, J., Levin, L. R. & Barrientos, A. 2014. A mitochondrial CO<sub>2</sub>-adenylyl cyclase-cAMP signalosome controls yeast normoxic cytochrome c oxidase activity. *The FASEB Journal*, 28, 4369-4380.
- Higuchi, M., Celino, F. T., Shimizu-Yamaguchi, S., Miura, C. & Miura, T. 2012. Taurine plays an important role in the protection of spermatogonia from oxidative stress. *Amino Acids*, 43, 2359-69.
- Hilger, D., Masureel, M. & Kobilka, B. K. 2018. Structure and dynamics of GPCR signaling complexes. *Nat Struct Mol Biol*, 25, 4-12.
- Hinchy, E. C., Gruszczczyk, A. V., Willows, R., Navaratnam, N., Hall, A. R., Bates, G., Bright, T. P., Krieg, T., Carling, D. & Murphy, M. P. 2018. Mitochondria-derived ROS activate AMP-activated protein kinase (AMPK) indirectly. *J Biol Chem*, 293, 17208-17217.
- Ho, T. T., Warr, M. R., Adelman, E. R., Lansinger, O. M., Flach, J., Verovskaya, E. V., Figueroa, M. E. & Passegue, E. 2017. Autophagy maintains the metabolism and function of young and old stem cells. *Nature*.
- Holen, I., Gordon, P. B. & Seglen, P. O. 1993. Inhibition of hepatocytic autophagy by okadaic acid and other protein phosphatase inhibitors. *Eur J Biochem*, 215, 113-22.
- Honscher, C., Mari, M., Auffarth, K., Bohnert, M., Griffith, J., Geerts, W., van der Laan, M., Cabrera, M., Reggiori, F. & Ungermann, C. 2014. Cellular metabolism regulates contact sites between vacuoles and mitochondria. *Dev Cell*, 30, 86-94.
- Horne, D. W., Holloway, R. S. & Wagner, C. 1997. Transport of S-adenosylmethionine in isolated rat liver mitochondria. *Arch Biochem Biophys*, 343, 201-6.
- Hosios, A. M., Hecht, V. C., Danai, L. V., Johnson, M. O., Rathmell, J. C., Steinhauser, M. L., Manalis, S. R. & Vander Heiden, M. G. 2016. Amino Acids Rather than Glucose

- Account for the Majority of Cell Mass in Proliferating Mammalian Cells. *Dev Cell*, 36, 540-9.
- Hosokawa, N., Hara, T., Kaizuka, T., Kishi, C., Takamura, A., Miura, Y., Iemura, S., Natsume, T., Takehana, K., Yamada, N., Guan, J. L., Oshiro, N. & Mizushima, N. 2009a. Nutrient-dependent mTORC1 association with the ULK1-Atg13-FIP200 complex required for autophagy. *Mol Biol Cell*, 20, 1981-91.
- Hosokawa, N., Sasaki, T., Iemura, S., Natsume, T., Hara, T. & Mizushima, N. 2009b. Atg101, a novel mammalian autophagy protein interacting with Atg13. *Autophagy*, 5, 973-9.
- Hurley, R. L., Anderson, K. A., Franzoni, J. M., Kemp, B. E., Means, A. R. & Witters, L. A. 2005. The Ca<sup>2+</sup>/calmodulin-dependent protein kinase kinases are AMP-activated protein kinase kinases. *J Biol Chem*, 280, 29060-6.
- Hyde, R., Taylor, P. M. & Hundal, H. S. 2003. Amino acid transporters: roles in amino acid sensing and signalling in animal cells. *The Biochemical journal*, 373, 1-18.
- Ingerman, E., Perkins, E. M., Marino, M., Mears, J. A., McCaffery, J. M., Hinshaw, J. E. & Nunnari, J. 2005. Dnm1 forms spirals that are structurally tailored to fit mitochondria. *J Cell Biol*, 170, 1021-7.
- Inoki, K., Li, Y., Zhu, T., Wu, J. & Guan, K. L. 2002. TSC2 is phosphorylated and inhibited by Akt and suppresses mTOR signalling. *Nat Cell Biol*, 4, 648-57.
- Inoki, K., Ouyang, H., Zhu, T., Lindvall, C., Wang, Y., Zhang, X., Yang, Q., Bennett, C., Harada, Y., Stankunas, K., Wang, C. Y., He, X., MacDougald, O. A., You, M., Williams, B. O. & Guan, K. L. 2006. TSC2 integrates Wnt and energy signals via a coordinated phosphorylation by AMPK and GSK3 to regulate cell growth. *Cell*, 126, 955-68.
- Inoki, K., Zhu, T. & Guan, K. L. 2003. TSC2 mediates cellular energy response to control cell growth and survival. *Cell*, 115, 577-90.
- Ishihara, N., Eura, Y. & Mihara, K. 2004. Mitofusin 1 and 2 play distinct roles in mitochondrial fusion reactions via GTPase activity. *J Cell Sci*, 117, 6535-46.
- Ishihara, N., Fujita, Y., Oka, T. & Mihara, K. 2006. Regulation of mitochondrial morphology through proteolytic cleavage of OPA1. *Embo j*, 25, 2966-77.
- Ishihara, N., Nomura, M., Jofuku, A., Kato, H., Suzuki, S. O., Masuda, K., Otera, H., Nakanishi, Y., Nonaka, I., Goto, Y., Taguchi, N., Morinaga, H., Maeda, M., Takayanagi, R., Yokota, S. & Mihara, K. 2009. Mitochondrial fission factor Drp1 is essential for embryonic development and synapse formation in mice. *Nat Cell Biol*, 11, 958-66.
- Isobe, K., Jung, H. J., Yang, C. R., Claxton, J., Sandoval, P., Burg, M. B., Raghuram, V. & Knepper, M. A. 2017. Systems-level identification of PKA-dependent signaling in epithelial cells. *Proc Natl Acad Sci U S A*, 114, E8875-e8884.
- Issaq, S. H., Teicher, B. A. & Monks, A. 2014. Bioenergetic properties of human sarcoma cells help define sensitivity to metabolic inhibitors. *Cell cycle (Georgetown, Tex.)*, 13, 1152-1161.
- Itakura, E., Kishi-Itakura, C., Koyama-Honda, I. & Mizushima, N. 2012. Structures containing Atg9A and the ULK1 complex independently target depolarized mitochondria at initial stages of Parkin-mediated mitophagy. *J Cell Sci*, 125, 1488-99.
- Itakura, E., Kishi, C., Inoue, K. & Mizushima, N. 2008. Beclin 1 forms two distinct phosphatidylinositol 3-kinase complexes with mammalian Atg14 and UVRAG. *Mol Biol Cell*, 19, 5360-72.
- Ivosev, G., Burton, L. & Bonner, R. 2008. Dimensionality Reduction and Visualization in Principal Component Analysis. *Analytical Chemistry*, 80, 4933-4944.
- Jahnsen, T., Hedin, L., Kidd, V. J., Beattie, W. G., Lohmann, S. M., Walter, U., Durica, J., Schulz, T. Z., Schiltz, E., Browner, M. & et al. 1986. Molecular cloning, cDNA structure, and regulation of the regulatory subunit of type II cAMP-dependent protein kinase from rat ovarian granulosa cells. *J Biol Chem*, 261, 12352-61.
- James, D. I., Parone, P. A., Mattenberger, Y. & Martinou, J. C. 2003. hFis1, a novel component of the mammalian mitochondrial fission machinery. *J Biol Chem*, 278, 36373-9.
- Jendrach, M., Pohl, S., Voth, M., Kowald, A., Hammerstein, P. & Bereiter-Hahn, J. 2005. Morpho-dynamic changes of mitochondria during ageing of human endothelial cells. *Mech Ageing Dev*, 126, 813-21.

- Jewell, J. L., Fu, V., Hong, A. W., Yu, F. X., Meng, D., Melick, C. H., Wang, H., Lam, W. M., Yuan, H. X., Taylor, S. S. & Guan, K. L. 2019. GPCR signaling inhibits mTORC1 via PKA phosphorylation of Raptor. *Elife*, 8.
- Jewell, J. L., Kim, Y. C., Russell, R. C., Yu, F. X., Park, H. W., Plouffe, S. W., Tagliabracchi, V. S. & Guan, K. L. 2015. Metabolism. Differential regulation of mTORC1 by leucine and glutamine. *Science*, 347, 194-8.
- Jheng, H. F., Tsai, P. J., Guo, S. M., Kuo, L. H., Chang, C. S., Su, I. J., Chang, C. R. & Tsai, Y. S. 2012. Mitochondrial fission contributes to mitochondrial dysfunction and insulin resistance in skeletal muscle. *Mol Cell Biol*, 32, 309-19.
- Jhun, B. S., J, O. U., Adaniya, S. M., Mancini, T. J., Cao, J. L., King, M. E., Landi, A. K., Ma, H., Shin, M., Yang, D., Xu, X., Yoon, Y., Choudhary, G., Clements, R. T., Mende, U. & Sheu, S. S. 2018a. Protein kinase D activation induces mitochondrial fragmentation and dysfunction in cardiomyocytes. *J Physiol*, 596, 827-855.
- Jhun, B. S., O-Uchi, J., Adaniya, S. M., Cypress, M. W. & Yoon, Y. 2018b. Adrenergic Regulation of Drp1-Driven Mitochondrial Fission in Cardiac Physio-Pathology. *Antioxidants (Basel, Switzerland)*, 7, 195.
- Ji, W. K., Chakrabarti, R., Fan, X., Schoenfeld, L., Strack, S. & Higgs, H. N. 2017. Receptor-mediated Drp1 oligomerization on endoplasmic reticulum. *J Cell Biol*, 216, 4123-4139.
- Jia, R. & Bonifacino, J. S. 2019. Lysosome Positioning Influences mTORC2 and AKT Signaling. *Mol Cell*, 75, 26-38.e3.
- Jiang, P., Nishimura, T., Sakamaki, Y., Itakura, E., Hatta, T., Natsume, T. & Mizushima, N. 2014. The HOPS complex mediates autophagosome-lysosome fusion through interaction with syntaxin 17. *Mol Biol Cell*, 25, 1327-37.
- Jiang, Y., Qian, X., Shen, J., Wang, Y., Li, X., Liu, R., Xia, Y., Chen, Q., Peng, G., Lin, S. Y. & Lu, Z. 2015. Local generation of fumarate promotes DNA repair through inhibition of histone H3 demethylation. *Nat Cell Biol*, 17, 1158-68.
- Johnson, M. A., Vidoni, S., Durigon, R., Pearce, S. F., Rorbach, J., He, J., Brea-Calvo, G., Minczuk, M., Reyes, A., Holt, I. J. & Spinazzola, A. 2014. Amino acid starvation has opposite effects on mitochondrial and cytosolic protein synthesis. *PLoS One*, 9, e93597.
- Johnson, M. O., Wolf, M. M., Madden, M. Z., Andrejeva, G., Sugiura, A., Contreras, D. C., Maseda, D., Liberti, M. V., Paz, K., Kishton, R. J., Johnson, M. E., de Cubas, A. A., Wu, P., Li, G., Zhang, Y., Newcomb, D. C., Wells, A. D., Restifo, N. P., Rathmell, W. K., Locasale, J. W., Davila, M. L., Blazar, B. R. & Rathmell, J. C. 2018a. Distinct Regulation of Th17 and Th1 Cell Differentiation by Glutaminase-Dependent Metabolism. *Cell*, 175, 1780-1795.e19.
- Johnson, T. I., Costa, A. S. H., Ferguson, A. N. & Frezza, C. 2018b. Fumarate hydratase loss promotes mitotic entry in the presence of DNA damage after ionising radiation. *Cell Death Dis*, 9, 913.
- Jong, C. J., Ito, T., Prentice, H., Wu, J.-Y. & Schaffer, S. W. 2017. Role of Mitochondria and Endoplasmic Reticulum in Taurine-Deficiency-Mediated Apoptosis. *Nutrients*, 9, 795.
- Joo, J. H., Dorsey, F. C., Joshi, A., Hennessy-Walters, K. M., Rose, K. L., McCastlain, K., Zhang, J., Iyengar, R., Jung, C. H., Suen, D. F., Steeves, M. A., Yang, C. Y., Prater, S. M., Kim, D. H., Thompson, C. B., Youle, R. J., Ney, P. A., Cleveland, J. L. & Kundu, M. 2011. Hsp90-Cdc37 chaperone complex regulates Ulk1- and Atg13-mediated mitophagy. *Mol Cell*, 43, 572-85.
- Joo, J. H., Wang, B., Frankel, E., Ge, L., Xu, L., Iyengar, R., Li-Harms, X., Wright, C., Shaw, T. I., Lindsten, T., Green, D. R., Peng, J., Hendershot, L. M., Kilic, F., Sze, J. Y., Audhya, A. & Kundu, M. 2016. The Noncanonical Role of ULK/ATG1 in ER-to-Golgi Trafficking Is Essential for Cellular Homeostasis. *Mol Cell*, 62, 491-506.
- Jordens, I., Fernandez-Borja, M., Marsman, M., Dusseljee, S., Janssen, L., Calafat, J., Janssen, H., Wubbolts, R. & Neefjes, J. 2001. The Rab7 effector protein RILP controls lysosomal transport by inducing the recruitment of dynein-dynactin motors. *Curr Biol*, 11, 1680-5.
- Joshi, A. U., Saw, N. L., Shamloo, M. & Mochly-Rosen, D. 2017. Drp1/Fis1 interaction mediates mitochondrial dysfunction, bioenergetic failure and cognitive decline in Alzheimer's disease. *Oncotarget*, 9, 6128-6143.

- Judith, D., Jefferies, H. B. J., Boeing, S., Frith, D., Snijders, A. P. & Tooze, S. A. 2019. ATG9A shapes the forming autophagosome through Arfaptin 2 and phosphatidylinositol 4-kinase IIIbeta. *J Cell Biol*, 218, 1634-1652.
- Jung, C. H., Jun, C. B., Ro, S. H., Kim, Y. M., Otto, N. M., Cao, J., Kundu, M. & Kim, D. H. 2009. ULK-Atg13-FIP200 complexes mediate mTOR signaling to the autophagy machinery. *Mol Biol Cell*, 20, 1992-2003.
- Jung, J., Genau, H. M. & Behrends, C. 2015. Amino Acid-Dependent mTORC1 Regulation by the Lysosomal Membrane Protein SLC38A9. *Mol Cell Biol*, 35, 2479-94.
- Jung, J. U., Ravi, S., Lee, D. W., McFadden, K., Kamradt, M. L., Toussaint, L. G. & Sitcheran, R. 2016. NIK/MAP3K14 Regulates Mitochondrial Dynamics and Trafficking to Promote Cell Invasion. *Curr Biol*.
- Kabeya, Y., Mizushima, N., Ueno, T., Yamamoto, A., Kirisako, T., Noda, T., Kominami, E., Ohsumi, Y. & Yoshimori, T. 2000. LC3, a mammalian homologue of yeast Apg8p, is localized in autophagosome membranes after processing. *Embo j*, 19, 5720-8.
- Kahn, B. B., Alquier, T., Carling, D. & Hardie, D. G. 2005. AMP-activated protein kinase: ancient energy gauge provides clues to modern understanding of metabolism. *Cell Metab*, 1, 15-25.
- Kaizuka, T., Hara, T., Oshiro, N., Kikkawa, U., Yonezawa, K., Takehana, K., Iemura, S., Natsume, T. & Mizushima, N. 2010. Tti1 and Tel2 are critical factors in mammalian target of rapamycin complex assembly. *J Biol Chem*, 285, 20109-16.
- Kalender, A., Selvaraj, A., Kim, S. Y., Gulati, P., Brule, S., Viollet, B., Kemp, B. E., Bardeesy, N., Dennis, P., Schlager, J. J., Marette, A., Kozma, S. C. & Thomas, G. 2010. Metformin, independent of AMPK, inhibits mTORC1 in a rag GTPase-dependent manner. *Cell Metab*, 11, 390-401.
- Kalia, R., Wang, R. Y., Yusuf, A., Thomas, P. V., Agard, D. A., Shaw, J. M. & Frost, A. 2018. Structural basis of mitochondrial receptor binding and constriction by DRP1. *Nature*, 558, 401-405.
- Kamada, Y., Yoshino, K., Kondo, C., Kawamata, T., Oshiro, N., Yonezawa, K. & Ohsumi, Y. 2010. Tor directly controls the Atg1 kinase complex to regulate autophagy. *Mol Cell Biol*, 30, 1049-58.
- Kanai, Y., Segawa, H., Miyamoto, K., Uchino, H., Takeda, E. & Endou, H. 1998. Expression cloning and characterization of a transporter for large neutral amino acids activated by the heavy chain of 4F2 antigen (CD98). *J Biol Chem*, 273, 23629-32.
- Kanehisa, M., Sato, Y., Furumichi, M., Morishima, K. & Tanabe, M. 2018. New approach for understanding genome variations in KEGG. *Nucleic Acids Research*, 47, D590-D595.
- Karanasios, E., Stapleton, E., Manifava, M., Kaizuka, T., Mizushima, N., Walker, S. A. & Ktistakis, N. T. 2013. Dynamic association of the ULK1 complex with omegasomes during autophagy induction. *J Cell Sci*, 126, 5224-38.
- Karanasios, E., Walker, S. A., Okkenhaug, H., Manifava, M., Hummel, E., Zimmermann, H., Ahmed, Q., Domart, M. C., Collinson, L. & Ktistakis, N. T. 2016. Autophagy initiation by ULK complex assembly on ER tubulovesicular regions marked by ATG9 vesicles. *Nat Commun*, 7, 12420.
- Kashatus, J. A., Nascimento, A., Myers, L. J., Sher, A., Byrne, F. L., Hoehn, K. L., Counter, C. M. & Kashatus, D. F. 2015. Erk2 phosphorylation of Drp1 promotes mitochondrial fission and MAPK-driven tumor growth. *Mol Cell*, 57, 537-51.
- Katsuragi, Y., Ichimura, Y. & Komatsu, M. 2015. p62/SQSTM1 functions as a signaling hub and an autophagy adaptor. *Febs j*.
- Katz, L. A. 2012. Origin and diversification of eukaryotes. *Annu Rev Microbiol*, 66, 411-27.
- Kawasaki, H., Springett, G. M., Mochizuki, N., Toki, S., Nakaya, M., Matsuda, M., Housman, D. E. & Graybiel, A. M. 1998. A family of cAMP-binding proteins that directly activate Rap1. *Science*, 282, 2275-9.
- Kemp, B. E., Graves, D. J., Benjamini, E. & Krebs, E. G. 1977. Role of multiple basic residues in determining the substrate specificity of cyclic AMP-dependent protein kinase. *J Biol Chem*, 252, 4888-94.
- Kemp, M., Go, Y. M. & Jones, D. P. 2008. Nonequilibrium thermodynamics of thiol/disulfide redox systems: a perspective on redox systems biology. *Free Radic Biol Med*, 44, 921-37.

- Kim, D. H., Sarbassov, D. D., Ali, S. M., King, J. E., Latek, R. R., Erdjument-Bromage, H., Tempst, P. & Sabatini, D. M. 2002. mTOR interacts with raptor to form a nutrient-sensitive complex that signals to the cell growth machinery. *Cell*, 110, 163-75.
- Kim, E., Goraksha-Hicks, P., Li, L., Neufeld, T. P. & Guan, K. L. 2008. Regulation of TORC1 by Rag GTPases in nutrient response. *Nat Cell Biol*, 10, 935-45.
- Kim, H., An, S., Ro, S. H., Teixeira, F., Park, G. J., Kim, C., Cho, C. S., Kim, J. S., Jakob, U., Lee, J. H. & Cho, U. S. 2015. Janus-faced Sestrin2 controls ROS and mTOR signalling through two separate functional domains. *Nat Commun*, 6, 10025.
- Kim, H., Scimia, M. C., Wilkinson, D., Trelles, R. D., Wood, M. R., Bowtell, D., Dillin, A., Mercola, M. & Ronai, Z. A. 2011a. Fine-tuning of Drp1/Fis1 availability by AKAP121/Siah2 regulates mitochondrial adaptation to hypoxia. *Mol Cell*, 44, 532-44.
- Kim, I., Rodriguez-Enriquez, S. & Lemasters, J. J. 2007. Selective degradation of mitochondria by mitophagy. *Arch Biochem Biophys*, 462, 245-53.
- Kim, J. & Guan, K. L. 2019. mTOR as a central hub of nutrient signalling and cell growth. *Nat Cell Biol*, 21, 63-71.
- Kim, J., Kundu, M., Viollet, B. & Guan, K. L. 2011b. AMPK and mTOR regulate autophagy through direct phosphorylation of Ulk1. *Nat Cell Biol*, 13, 132-41.
- Kim, J. H., Seo, D., Kim, S.-J., Choi, D. W., Park, J. S., Ha, J., Choi, J., Lee, J.-H., Jung, S. M., Seo, K.-W., Lee, E.-W., Lee, Y. S., Cheong, H., Choi, C. Y. & Park, S. H. 2018. The deubiquitinating enzyme USP20 stabilizes ULK1 and promotes autophagy initiation. *EMBO reports*, 19, e44378.
- Kimura, S., Noda, T. & Yoshimori, T. 2008. Dynein-dependent movement of autophagosomes mediates efficient encounters with lysosomes. *Cell Struct Funct*, 33, 109-22.
- Kirkin, V., Lamark, T., Sou, Y. S., Bjorkoy, G., Nunn, J. L., Bruun, J. A., Shvets, E., McEwan, D. G., Clausen, T. H., Wild, P., Bilusic, I., Theurillat, J. P., Overvatn, A., Ishii, T., Elazar, Z., Komatsu, M., Dikic, I. & Johansen, T. 2009. A role for NBR1 in autophagosomal degradation of ubiquitinated substrates. *Mol Cell*, 33, 505-16.
- Kirwan, G. M., Johansson, E., Kleemann, R., Verheij, E. R., Wheelock, A. M., Goto, S., Trygg, J. & Wheelock, C. E. 2012. Building multivariate systems biology models. *Anal Chem*, 84, 7064-71.
- Kleinboelting, S., van den Heuvel, J. & Steegborn, C. 2014. Structural analysis of human soluble adenylyl cyclase and crystal structures of its nucleotide complexes-implications for cyclase catalysis and evolution. *Febs j*, 281, 4151-64.
- Klionsky, D. J., Abdelmohsen, K., Abe, A., Abedin, M. J., Abeliovich, H., Acevedo Arozena, A., Adachi, H., Adams, C. M., Adams, P. D., Adeli, K., Adhietty, P. J., Adler, S. G., Agam, G., Agarwal, R., Aghi, M. K., Agnello, M., Agostinis, P., Aguilar, P. V., Aguirre-Ghiso, J., Airolidi, E. M., Ait-Si-Ali, S., Akematsu, T., Akporiaye, E. T., Al-Rubeai, M., Albaiceta, G. M., Albanese, C., Albani, D., Albert, M. L., Aldudo, J., Algul, H., Alirezai, M., Alloza, I., Almasan, A., Almonte-Beceril, M., Alnemri, E. S., Alonso, C., Altan-Bonnet, N., Altieri, D. C., Alvarez, S., Alvarez-Erviti, L., Alves, S., Amadoro, G., Amano, A., Amantini, C., Ambrosio, S., Amelio, I., Amer, A. O., Amessou, M., Amon, A., An, Z., Anania, F. A., Andersen, S. U., Andley, U. P., Andreadi, C. K., Andrieu-Abadie, N., Anel, A., Ann, D. K., Anoopkumar-Dukie, S., Antoniolli, M., Aoki, H., Apostolova, N., Aquila, S., Aquilano, K., Araki, K., Arama, E., Aranda, A., Araya, J., Arcaro, A., Arias, E., Arimoto, H., Ariosa, A. R., Armstrong, J. L., Arnould, T., Arsov, I., Asanuma, K., Askanas, V., Asselin, E., Atarashi, R., Atherton, S. S., Atkin, J. D., Attardi, L. D., Auburger, P., Auburger, G., Aurelian, L., Autelli, R., Avagliano, L., Avantaggiati, M. L., Avrahami, L., Awale, S., Azad, N., Bachetti, T., Backer, J. M., Bae, D. H., Bae, J. S., Bae, O. N., Bae, S. H., Baehrecke, E. H., Baek, S. H., Baghdiguian, S., Bagniewska-Zadworna, A., et al. 2016. Guidelines for the use and interpretation of assays for monitoring autophagy (3rd edition). *Autophagy*, 12, 1-222.
- Klionsky, D. J., Baehrecke, E. H., Brumell, J. H., Chu, C. T., Codogno, P., Cuervo, A. M., Debnath, J., Deretic, V., Elazar, Z., Eskelinen, E. L., Finkbeiner, S., Fueyo-Margareto, J., Gewirtz, D., Jaattela, M., Kroemer, G., Levine, B., Melia, T. J., Mizushima, N., Rubinsztein, D. C., Simonsen, A., Thorburn, A., Thumm, M. & Tooze, S. A. 2011. A comprehensive glossary of autophagy-related molecules and processes (2nd edition). *Autophagy*, 7, 1273-94.

- Klionsky, D. J., Cregg, J. M., Dunn, W. A., Jr., Emr, S. D., Sakai, Y., Sandoval, I. V., Sibirny, A., Subramani, S., Thumm, M., Veenhuis, M. & Ohsumi, Y. 2003. A unified nomenclature for yeast autophagy-related genes. *Dev Cell*, 5, 539-45.
- Kobayashi, S. 2015. Choose Delicately and Reuse Adequately: The Newly Revealed Process of Autophagy. *Biol Pharm Bull*, 38, 1098-103.
- Kohr, M. J., Traynham, C. J., Roof, S. R., Davis, J. P. & Ziolo, M. T. 2010. cAMP-independent activation of protein kinase A by the peroxynitrite generator SIN-1 elicits positive inotropic effects in cardiomyocytes. *J Mol Cell Cardiol*, 48, 645-8.
- Konno, H., Konno, K. & Barber, G. N. 2013. Cyclic dinucleotides trigger ULK1 (ATG1) phosphorylation of STING to prevent sustained innate immune signaling. *Cell*, 155, 688-98.
- Korge, P., Calmettes, G. & Weiss, J. N. 2015. Increased reactive oxygen species production during reductive stress: The roles of mitochondrial glutathione and thioredoxin reductases. *Biochimica et biophysica acta*, 1847, 514-525.
- Korobova, F., Ramabhadran, V. & Higgs, H. N. 2013. An Actin-Dependent Step in Mitochondrial Fission Mediated by the ER-Associated Formin INF2. *Science*, 339, 464-467.
- Korolchuk, V. I., Saiki, S., Lichtenberg, M., Siddiqi, F. H., Roberts, E. A., Imarisio, S., Jahreiss, L., Sarkar, S., Futter, M., Menzies, F. M., O'Kane, C. J., Deretic, V. & Rubinsztein, D. C. 2011. Lysosomal positioning coordinates cellular nutrient responses. *Nat Cell Biol*, 13, 453-60.
- Korwitz, A., Merkwirth, C., Richter-Dennerlein, R., Tröder, S. E., Sprenger, H.-G., Quirós, P. M., López-Otín, C., Rugarli, E. I. & Langer, T. 2016. Loss of OMA1 delays neurodegeneration by preventing stress-induced OPA1 processing in mitochondria. *The Journal of Cell Biology*.
- Kory, N., Wyant, G. A., Prakash, G., Uit de Bos, J., Bottanelli, F., Pacold, M. E., Chan, S. H., Lewis, C. A., Wang, T., Keys, H. R., Guo, Y. E. & Sabatini, D. M. 2018. SFXN1 is a mitochondrial serine transporter required for one-carbon metabolism. *Science*, 362.
- Koshiba, T., Detmer, S. A., Kaiser, J. T., Chen, H., McCaffery, J. M. & Chan, D. C. 2004. Structural basis of mitochondrial tethering by mitofusin complexes. *Science*, 305, 858-62.
- Kovacina, K. S., Park, G. Y., Bae, S. S., Guzzetta, A. W., Schaefer, E., Birnbaum, M. J. & Roth, R. A. 2003. Identification of a proline-rich Akt substrate as a 14-3-3 binding partner. *J Biol Chem*, 278, 10189-94.
- Krebs, H. A. 1982. The discovery of the ornithine cycle of urea synthesis. *Trends in Biochemical Sciences*, 7, 76-78.
- Ktistakis, N. T. 2019. ER platforms mediating autophagosome generation. *Biochim Biophys Acta Mol Cell Biol Lipids*.
- Kuhl, I., Miranda, M., Atanassov, I., Kuznetsova, I., Hinze, Y., Mourier, A., Filipovska, A. & Larsson, N. G. 2017. Transcriptomic and proteomic landscape of mitochondrial dysfunction reveals secondary coenzyme Q deficiency in mammals. *Elife*, 6.
- Kuma, A., Hatano, M., Matsui, M., Yamamoto, A., Nakaya, H., Yoshimori, T., Ohsumi, Y., Tokuhisa, T. & Mizushima, N. 2004. The role of autophagy during the early neonatal starvation period. *Nature*, 432, 1032-6.
- Kundu, M. 2011. ULK1, mammalian target of rapamycin, and mitochondria: linking nutrient availability and autophagy. *Antioxid Redox Signal*, 14, 1953-8.
- Kundu, M., Lindsten, T., Yang, C. Y., Wu, J., Zhao, F., Zhang, J., Selak, M. A., Ney, P. A. & Thompson, C. B. 2008. Ulk1 plays a critical role in the autophagic clearance of mitochondria and ribosomes during reticulocyte maturation. *Blood*, 112, 1493-502.
- Kuroyanagi, H., Yan, J., Seki, N., Yamanouchi, Y., Suzuki, Y., Takano, T., Muramatsu, M. & Shirasawa, T. 1998. Human ULK1, a novel serine/threonine kinase related to UNC-51 kinase of *Caenorhabditis elegans*: cDNA cloning, expression, and chromosomal assignment. *Genomics*, 51, 76-85.
- Lacapere, J. J. & Papadopoulos, V. 2003. Peripheral-type benzodiazepine receptor: structure and function of a cholesterol-binding protein in steroid and bile acid biosynthesis. *Steroids*, 68, 569-85.
- Laderoute, K. R., Amin, K., Calaoagan, J. M., Knapp, M., Le, T., Orduna, J., Foretz, M. & Viollet, B. 2006. 5'-AMP-activated protein kinase (AMPK) is induced by low-oxygen and glucose deprivation conditions found in solid-tumor microenvironments. *Mol Cell Biol*, 26, 5336-47.

- Lamming, D. W., Ye, L., Katajisto, P., Goncalves, M. D., Saitoh, M., Stevens, D. M., Davis, J. G., Salmon, A. B., Richardson, A., Ahima, R. S., Guertin, D. A., Sabatini, D. M. & Baur, J. A. 2012. Rapamycin-induced insulin resistance is mediated by mTORC2 loss and uncoupled from longevity. *Science*, 335, 1638-43.
- Lane, A. N. & Fan, T. W. 2015. Regulation of mammalian nucleotide metabolism and biosynthesis. *Nucleic Acids Res*, 43, 2466-85.
- Laplante, M. & Sabatini, D. M. 2012. mTOR signaling in growth control and disease. *Cell*, 149, 274-93.
- Latorre-Pellicer, A., Moreno-Loshuertos, R., Lechuga-Vieco, A. V., Sánchez-Cabo, F., Torroja, C., Acín-Pérez, R., Calvo, E., Aix, E., González-Guerra, A., Logan, A., Bernad-Miana, M. L., Romanos, E., Cruz, R., Cogliati, S., Sobrino, B., Carracedo, Á., Pérez-Martos, A., Fernández-Silva, P., Ruíz-Cabello, J., Murphy, M. P., Flores, I., Vázquez, J. & Enríquez, J. A. 2016. Mitochondrial and nuclear DNA matching shapes metabolism and healthy ageing. *Nature*, advance online publication.
- Laurenza, A., Sutkowski, E. M. & Seamon, K. B. 1989. Forskolin: a specific stimulator of adenylyl cyclase or a diterpene with multiple sites of action? *Trends Pharmacol Sci*, 10, 442-7.
- Lavie, J., Serrat, R., Bellance, N., Courtand, G., Dupuy, J. W., Tesson, C., Couprie, I., Brice, A., Lacombe, D., Durr, A., Stevanin, G., Darios, F., Rossignol, R., Goizet, C. & Benard, G. 2017. Mitochondrial morphology and cellular distribution are altered in SPG31 patients and are linked to DRP1 hyperphosphorylation. *Hum Mol Genet*, 26, 674-685.
- Lawrence, B. P. & Brown, W. J. 1992. Autophagic vacuoles rapidly fuse with pre-existing lysosomes in cultured hepatocytes. *J Cell Sci*, 102 ( Pt 3), 515-26.
- Lawrence, R. E., Cho, K. F., Rappold, R., Thrun, A., Tofaute, M., Kim, D. J., Moldavski, O., Hurley, J. H. & Zoncu, R. 2018. A nutrient-induced affinity switch controls mTORC1 activation by its Rag GTPase-Ragulator lysosomal scaffold. *Nat Cell Biol*, 20, 1052-1063.
- Lawrence, R. E. & Zoncu, R. 2019. The lysosome as a cellular centre for signalling, metabolism and quality control. *Nature Cell Biology*.
- Lazarou, M., Sliter, D. A., Kane, L. A., Sarraf, S. A., Wang, C., Burman, J. L., Sideris, D. P., Fogel, A. I. & Youle, R. J. 2015. The ubiquitin kinase PINK1 recruits autophagy receptors to induce mitophagy. *Nature*, 524, 309-14.
- Lazarus, M. B., Novotny, C. J. & Shokat, K. M. 2015. Structure of the human autophagy initiating kinase ULK1 in complex with potent inhibitors. *ACS chemical biology*, 10, 257-261.
- Lebeau, J., Saunders, J. M., Moraes, V. W. R., Madhavan, A., Madrazo, N., Anthony, M. C. & Wiseman, R. L. 2018. The PERK Arm of the Unfolded Protein Response Regulates Mitochondrial Morphology during Acute Endoplasmic Reticulum Stress. *Cell Rep*, 22, 2827-2836.
- Leboucher, G. P., Tsai, Y. C., Yang, M., Shaw, K. C., Zhou, M., Veenstra, T. D., Glickman, M. H. & Weissman, A. M. 2012. Stress-induced phosphorylation and proteasomal degradation of mitofusin 2 facilitates mitochondrial fragmentation and apoptosis. *Mol Cell*, 47, 547-57.
- Lee, D. C., Carmichael, D. F., Krebs, E. G. & McKnight, G. S. 1983. Isolation of a cDNA clone for the type I regulatory subunit of bovine cAMP-dependent protein kinase. *Proc Natl Acad Sci U S A*, 80, 3608-12.
- Lee, D. F., Kuo, H. P., Chen, C. T., Hsu, J. M., Chou, C. K., Wei, Y., Sun, H. L., Li, L. Y., Ping, B., Huang, W. C., He, X., Hung, J. Y., Lai, C. C., Ding, Q., Su, J. L., Yang, J. Y., Sahin, A. A., Hortobagyi, G. N., Tsai, F. J., Tsai, C. H. & Hung, M. C. 2007. IKK beta suppression of TSC1 links inflammation and tumor angiogenesis via the mTOR pathway. *Cell*, 130, 440-55.
- Lee, E. J. & Tournier, C. 2011. The requirement of uncoordinated 51-like kinase 1 (ULK1) and ULK2 in the regulation of autophagy. *Autophagy*, 7, 689-95.
- Lee, H.-J., Kremer, D. M., Sajjakulnukit, P., Zhang, L. & Lyssiotis, C. A. 2019. A large-scale analysis of targeted metabolomics data from heterogeneous biological samples provides insights into metabolite dynamics. *Metabolomics*, 15, 103.
- Lee, H., Smith, S. B. & Yoon, Y. 2017. The Short Variant of the Mitochondrial Dynamamin OPA1 Maintains Mitochondrial Energetics and Cristae Structure. *J Biol Chem*.

- Lee, J. E., Westrate, L. M., Wu, H., Page, C. & Voeltz, G. K. 2016. Multiple dynamin family members collaborate to drive mitochondrial division. *Nature*, 540, 139-143.
- Lee, J. Y., Kapur, M., Li, M., Choi, M. C., Choi, S., Kim, H. J., Kim, I., Lee, E., Taylor, J. P. & Yao, T. P. 2014. MFN1 deacetylation activates adaptive mitochondrial fusion and protects metabolically challenged mitochondria. *J Cell Sci*, 127, 4954-63.
- Lee, K. C., Shorr, R., Rodriguez, R., Maturo, C., Boteju, L. W. & Sheldon, A. 2011. Formation and anti-tumor activity of uncommon in vitro and in vivo metabolites of CPI-613, a novel anti-tumor compound that selectively alters tumor energy metabolism. *Drug Metab Lett*, 5, 163-82.
- Lee, M., Kim, J. H., Yoon, I., Lee, C., Fallahi Sichani, M., Kang, J. S., Kang, J., Guo, M., Lee, K. Y., Han, G., Kim, S. & Han, J. M. 2018. Coordination of the leucine-sensing Rag GTPase cycle by leucyl-tRNA synthetase in the mTORC1 signaling pathway. *Proc Natl Acad Sci U S A*, 115, E5279-e5288.
- Lee, S. B., Kim, J. J., Kim, T. W., Kim, B. S., Lee, M. S. & Yoo, Y. D. 2010. Serum deprivation-induced reactive oxygen species production is mediated by Romo1. *Apoptosis*, 15, 204-18.
- Lefkimmatis, K. 2014. cAMP signalling meets mitochondrial compartments. *Biochemical Society Transactions*, 42, 265.
- Lefkimmatis, K., Leronni, D. & Hofer, A. M. 2013. The inner and outer compartments of mitochondria are sites of distinct cAMP/PKA signaling dynamics. *J Cell Biol*, 202, 453-62.
- Lefkimmatis, K. & Zaccolo, M. 2014. cAMP signaling in subcellular compartments. *Pharmacol Ther*, 143, 295-304.
- Lei, H. T., Ma, J., Sanchez Martinez, S. & Gonen, T. 2018. Crystal structure of arginine-bound lysosomal transporter SLC38A9 in the cytosol-open state. *Nat Struct Mol Biol*, 25, 522-527.
- Leshets, M., Silas, Y. B. H., Lehming, N. & Pines, O. 2018. Fumarase: From the TCA Cycle to DNA Damage Response and Tumor Suppression. *Front Mol Biosci*, 5, 68.
- Levine, B. & Klionsky, D. J. 2017. Autophagy wins the 2016 Nobel Prize in Physiology or Medicine: Breakthroughs in baker's yeast fuel advances in biomedical research. *Proceedings of the National Academy of Sciences*, 114, 201.
- Levine, B. & Kroemer, G. 2019. Biological Functions of Autophagy Genes: A Disease Perspective. *Cell*, 176, 11-42.
- Lewis, M. R. & Lewis, W. H. 1914. MITOCHONDRIA IN TISSUE CULTURE. *Science*, 39, 330-3.
- Li, J., Huang, Q., Long, X., Guo, X., Sun, X., Jin, X., Li, Z., Ren, T., Yuan, P., Huang, X., Zhang, H. & Xing, J. 2017. Mitochondrial elongation-mediated glucose metabolism reprogramming is essential for tumour cell survival during energy stress. *Oncogene*.
- Li, L., Kim, E., Yuan, H., Inoki, K., Goraksha-Hicks, P., Schiesher, R. L., Neufeld, T. P. & Guan, K. L. 2010. Regulation of mTORC1 by the Rab and Arf GTPases. *J Biol Chem*, 285, 19705-9.
- Li, T. Y., Sun, Y., Liang, Y., Liu, Q., Shi, Y., Zhang, C. S., Zhang, C., Song, L., Zhang, P., Zhang, X., Li, X., Chen, T., Huang, H. Y., He, X., Wang, Y., Wu, Y. Q., Chen, S., Jiang, M., Chen, C., Xie, C., Yang, J. Y., Lin, Y., Zhao, S., Ye, Z., Lin, S. Y., Chiu, D. T. & Lin, S. C. 2016a. ULK1/2 Constitute a Bifurcate Node Controlling Glucose Metabolic Fluxes in Addition to Autophagy. *Mol Cell*, 62, 359-370.
- Li, Y., Erickson, J. W., Stalneck, C. A., Katt, W. P., Huang, Q., Cerione, R. A. & Ramachandran, S. 2016b. Mechanistic Basis of Glutaminase Activation: A KEY ENZYME THAT PROMOTES GLUTAMINE METABOLISM IN CANCER CELLS. *J Biol Chem*, 291, 20900-20910.
- Liang, X. H., Jackson, S., Seaman, M., Brown, K., Kempkes, B., Hibshoosh, H. & Levine, B. 1999. Induction of autophagy and inhibition of tumorigenesis by beclin 1. *Nature*, 402, 672-6.
- Liesa, M. & Shirihai, O. S. 2013. Mitochondrial dynamics in the regulation of nutrient utilization and energy expenditure. *Cell Metab*, 17, 491-506.
- Limbutara, K., Kelleher, A., Yang, C. R., Raghuram, V. & Knepper, M. A. 2019. Phosphorylation Changes in Response to Kinase Inhibitor H89 in PKA-Null Cells. *Sci Rep*, 9, 2814.
- Lin, H. H., Chung, Y., Cheng, C. T., Ouyang, C., Fu, Y., Kuo, C. Y., Chi, K. K., Sadeghi, M., Chu, P., Kung, H. J., Li, C. F., Limesand, K. H. & Ann, D. K. 2018. Autophagic

- reliance promotes metabolic reprogramming in oncogenic KRAS-driven tumorigenesis. *Autophagy*, 14, 1481-1498.
- Lin, S. C. & Hardie, D. G. 2018. AMPK: Sensing Glucose as well as Cellular Energy Status. *Cell Metab*, 27, 299-313.
- Lin, S. Y., Li, T. Y., Liu, Q., Zhang, C., Li, X., Chen, Y., Zhang, S. M., Lian, G., Liu, Q., Ruan, K., Wang, Z., Zhang, C. S., Chien, K. Y., Wu, J., Li, Q., Han, J. & Lin, S. C. 2012. GSK3-TIP60-ULK1 signaling pathway links growth factor deprivation to autophagy. *Science*, 336, 477-81.
- Litvin, T. N., Kamenetsky, M., Zarifyan, A., Buck, J. & Levin, L. R. 2003. Kinetic properties of "soluble" adenylyl cyclase. Synergism between calcium and bicarbonate. *J Biol Chem*, 278, 15922-6.
- Liu, C. C., Lin, Y. C., Chen, Y. H., Chen, C. M., Pang, L. Y., Chen, H. A., Wu, P. R., Lin, M. Y., Jiang, S. T., Tsai, T. F. & Chen, R. H. 2016a. Cul3-KLHL20 Ubiquitin Ligase Governs the Turnover of ULK1 and VPS34 Complexes to Control Autophagy Termination. *Mol Cell*, 61, 84-97.
- Liu, D., Bordicchia, M., Zhang, C., Fang, H., Wei, W., Li, J. L., Guilherme, A., Guntur, K., Czech, M. P. & Collins, S. 2016b. Activation of mTORC1 is essential for beta-adrenergic stimulation of adipose browning. *J Clin Invest*, 126, 1704-16.
- Liu, L., Feng, D., Chen, G., Chen, M., Zheng, Q., Song, P., Ma, Q., Zhu, C., Wang, R., Qi, W., Huang, L., Xue, P., Li, B., Wang, X., Jin, H., Wang, J., Yang, F., Liu, P., Zhu, Y., Sui, S. & Chen, Q. 2012. Mitochondrial outer-membrane protein FUNDC1 mediates hypoxia-induced mitophagy in mammalian cells. *Nat Cell Biol*, 14, 177-85.
- Liu, R. & Chan, D. C. 2015. The mitochondrial fission receptor Mff selectively recruits oligomerized Drp1. *Molecular biology of the cell*, 26, 4466-4477.
- Liu, T., Yu, R., Jin, S.-B., Han, L., Lendahl, U., Zhao, J. & Nistér, M. 2013. The mitochondrial elongation factors MIEF1 and MIEF2 exert partially distinct functions in mitochondrial dynamics. *Experimental Cell Research*, 319, 2893-2904.
- Lomas, O. & Zaccolo, M. 2014. Phosphodiesterases maintain signaling fidelity via compartmentalization of cyclic nucleotides. *Physiology (Bethesda)*, 29, 141-9.
- Long, X., Lin, Y., Ortiz-Vega, S., Yonezawa, K. & Avruch, J. 2005. Rheb binds and regulates the mTOR kinase. *Curr Biol*, 15, 702-13.
- Losier, T. T., Akuma, M., McKee-Muir, O. C., LeBlond, N. D., Suk, Y., Alsaadi, R. M., Guo, Z., Reshke, R., Sad, S., Campbell-Valois, F. X., Gibbings, D. J., Fullerton, M. D. & Russell, R. C. 2019. AMPK Promotes Xenophagy through Priming of Autophagic Kinases upon Detection of Bacterial Outer Membrane Vesicles. *Cell Rep*, 26, 2150-2165.e5.
- Loson, O. C., Meng, S., Ngo, H., Liu, R., Kaiser, J. T. & Chan, D. C. 2015. Crystal structure and functional analysis of MiD49, a receptor for the mitochondrial fission protein Drp1. *Protein Sci*, 24, 386-94.
- Loson, O. C., Song, Z., Chen, H. & Chan, D. C. 2013. Fis1, Mff, MiD49, and MiD51 mediate Drp1 recruitment in mitochondrial fission. *Mol Biol Cell*, 24, 659-67.
- Lum, J. J., Bauer, D. E., Kong, M., Harris, M. H., Li, C., Lindsten, T. & Thompson, C. B. 2005. Growth factor regulation of autophagy and cell survival in the absence of apoptosis. *Cell*, 120, 237-48.
- Ma, L., Chen, Z., Erdjument-Bromage, H., Tempst, P. & Pandolfi, P. P. 2005. Phosphorylation and functional inactivation of TSC2 by Erk implications for tuberous sclerosis and cancer pathogenesis. *Cell*, 121, 179-93.
- Ma, Y. & Taylor, S. 2002. A 15-Residue Bifunctional Element in d-AKAP1 Is Required for Both Endoplasmic Reticulum and Mitochondrial Targeting. *Journal of Biological Chemistry*, 277, 27328-27336.
- MacVicar, T. D. & Lane, J. D. 2014. Impaired OMA1-dependent cleavage of OPA1 and reduced DRP1 fission activity combine to prevent mitophagy in cells that are dependent on oxidative phosphorylation. *J Cell Sci*, 127, 2313-25.
- Maddocks, O. D., Berkers, C. R., Mason, S. M., Zheng, L., Blyth, K., Gottlieb, E. & Vousden, K. H. 2013. Serine starvation induces stress and p53-dependent metabolic remodelling in cancer cells. *Nature*, 493, 542-6.
- Maddocks, O. D., Labuschagne, C. F., Adams, P. D. & Vousden, K. H. 2016. Serine Metabolism Supports the Methionine Cycle and DNA/RNA Methylation through De Novo ATP Synthesis in Cancer Cells. *Mol Cell*, 61, 210-21.

- Maddocks, O. D. K., Athineos, D., Cheung, E. C., Lee, P., Zhang, T., van den Broek, N. J. F., Mackay, G. M., Labuschagne, C. F., Gay, D., Kruiswijk, F., Blagih, J., Vincent, D. F., Campbell, K. J., Ceteci, F., Sansom, O. J., Blyth, K. & Vousden, K. H. 2017. Modulating the therapeutic response of tumours to dietary serine and glycine starvation. *Nature*, 544, 372-376.
- Maldonado, E. M., Taha, F., Rahman, J. & Rahman, S. 2019. Systems Biology Approaches Toward Understanding Primary Mitochondrial Diseases. *Front Genet*, 10, 19.
- Mammucari, C., Milan, G., Romanello, V., Masiero, E., Rudolf, R., Del Piccolo, P., Burden, S. J., Di Lisi, R., Sandri, C., Zhao, J., Goldberg, A. L., Schiaffino, S. & Sandri, M. 2007. FoxO3 controls autophagy in skeletal muscle in vivo. *Cell Metab*, 6, 458-71.
- Mandal, S., Mandal, A. & Park, M. H. 2015. Depletion of the polyamines spermidine and spermine by overexpression of spermidine/spermine N<sup>1</sup>-acetyltransferase 1 (SAT1) leads to mitochondria-mediated apoptosis in mammalian cells. *The Biochemical journal*, 468, 435-447.
- Manning, B. D., Tee, A. R., Logsdon, M. N., Blenis, J. & Cantley, L. C. 2002. Identification of the tuberous sclerosis complex-2 tumor suppressor gene product tuberin as a target of the phosphoinositide 3-kinase/akt pathway. *Mol Cell*, 10, 151-62.
- Marcinko, K., Bujak, A. L., Lally, J. S., Ford, R. J., Wong, T. H., Smith, B. K., Kemp, B. E., Jenkins, Y., Li, W., Kinsella, T. M., Hitoshi, Y. & Steinberg, G. R. 2015. The AMPK activator R419 improves exercise capacity and skeletal muscle insulin sensitivity in obese mice. *Mol Metab*, 4, 643-51.
- Mari, M., Griffith, J., Rieter, E., Krishnappa, L., Klionsky, D. J. & Reggiori, F. 2010. An Atg9-containing compartment that functions in the early steps of autophagosome biogenesis. *J Cell Biol*, 190, 1005-22.
- Mari, M. & Reggiori, F. 2010. Atg9 reservoirs, a new organelle of the yeast endomembrane system? *Autophagy*, 6, 1221-3.
- Marin, T. L., Gongol, B., Zhang, F., Martin, M., Johnson, D. A., Xiao, H., Wang, Y., Subramaniam, S., Chien, S. & Shyy, J. Y. 2017. AMPK promotes mitochondrial biogenesis and function by phosphorylating the epigenetic factors DNMT1, RBBP7, and HAT1. *Sci Signal*, 10.
- Martel, R. R., Klicius, J. & Galet, S. 1977. Inhibition of the immune response by rapamycin, a new antifungal antibiotic. *Can J Physiol Pharmacol*, 55, 48-51.
- Martinez-Lopez, N., Athonvarangkul, D. & Singh, R. 2015. Autophagy and aging. *Adv Exp Med Biol*, 847, 73-87.
- Martinou, I., Desagher, S., Eskes, R., Antonsson, B., Andre, E., Fakan, S. & Martinou, J. C. 1999. The release of cytochrome c from mitochondria during apoptosis of NGF-deprived sympathetic neurons is a reversible event. *J Cell Biol*, 144, 883-9.
- Matsunaga, K., Saitoh, T., Tabata, K., Omori, H., Satoh, T., Kurotori, N., Maejima, I., Shirahama-Noda, K., Ichimura, T., Isobe, T., Akira, S., Noda, T. & Yoshimori, T. 2009. Two Beclin 1-binding proteins, Atg14L and Rubicon, reciprocally regulate autophagy at different stages. *Nat Cell Biol*, 11, 385-96.
- Matsuura, A., Tsukada, M., Wada, Y. & Ohsumi, Y. 1997. Apg1p, a novel protein kinase required for the autophagic process in *Saccharomyces cerevisiae*. *Gene*, 192, 245-50.
- Mattie, S., Riemer, J., Wideman, J. G. & McBride, H. M. 2017. A new mitofusin topology places the redox-regulated C terminus in the mitochondrial intermembrane space. *J Cell Biol*.
- Matulef, K. & Zagotta, W. N. 2003. Cyclic nucleotide-gated ion channels. *Annu Rev Cell Dev Biol*, 19, 23-44.
- Mavrakakis, M., Lippincott-Schwartz, J., Stratakis, C. A. & Bossis, I. 2006. Depletion of type IA regulatory subunit (RI $\alpha$ ) of protein kinase A (PKA) in mammalian cells and tissues activates mTOR and causes autophagic deficiency. *Hum Mol Genet*, 15, 2962-71.
- McAlpine, F., Williamson, L. E., Tooze, S. A. & Chan, E. Y. 2013. Regulation of nutrient-sensitive autophagy by uncoordinated 51-like kinases 1 and 2. *Autophagy*, 9, 361-73.
- McGlinchey, R. P. & Lee, J. C. 2015. Cysteine cathepsins are essential in lysosomal degradation of alpha-synuclein. *Proc Natl Acad Sci U S A*, 112, 9322-7.

- Mears, J. A., Lackner, L. L., Fang, S., Ingerman, E., Nunnari, J. & Hinshaw, J. E. 2011. Conformational changes in Dnm1 support a contractile mechanism for mitochondrial fission. *Nat Struct Mol Biol*, 18, 20-6.
- Meng, J. & Ferguson, S. M. 2018. GATOR1-dependent recruitment of FLCN-FNIP to lysosomes coordinates Rag GTPase heterodimer nucleotide status in response to amino acids. *J Cell Biol*, 217, 2765-2776.
- Menon, S., Dibble, Christian C., Talbott, G., Hoxhaj, G., Valvezan, Alexander J., Takahashi, H., Cantley, Lewis C. & Manning, Brendan D. 2014. Spatial Control of the TSC Complex Integrates Insulin and Nutrient Regulation of mTORC1 at the Lysosome. *Cell*, 156, 771-785.
- Mercer, C. A., Kaliappan, A. & Dennis, P. B. 2009. A novel, human Atg13 binding protein, Atg101, interacts with ULK1 and is essential for macroautophagy. *Autophagy*, 5, 649-62.
- Mercer, T. J., Gubas, A. & Tooze, S. A. 2018. A molecular perspective of mammalian autophagosome biogenesis. *J Biol Chem*, 293, 5386-5395.
- Merrill, R. A., Dagda, R. K., Dickey, A. S., Cribbs, J. T., Green, S. H., Usachev, Y. M. & Strack, S. 2011. Mechanism of Neuroprotective Mitochondrial Remodeling by PKA/AKAP1. *PLOS Biology*, 9, e1000612.
- Miret-Casals, L., Sebastian, D., Brea, J., Rico-Leo, E. M., Palacin, M., Fernandez-Salguero, P. M., Loza, M. I., Albericio, F. & Zorzano, A. 2017. Identification of New Activators of Mitochondrial Fusion Reveals a Link between Mitochondrial Morphology and Pyrimidine Metabolism. *Cell Chem Biol*.
- Mishra, P., Carelli, V., Manfredi, G. & Chan, D. C. 2014. Proteolytic cleavage of Opa1 stimulates mitochondrial inner membrane fusion and couples fusion to oxidative phosphorylation. *Cell Metab*, 19, 630-41.
- Mishra, P. & Chan, D. C. 2016. Metabolic regulation of mitochondrial dynamics. *J Cell Biol*, 212, 379-87.
- Mishra, P., Varuzhanyan, G., Pham, A. H. & Chan, D. C. 2015. Mitochondrial Dynamics is a Distinguishing Feature of Skeletal Muscle Fiber Types and Regulates Organellar Compartmentalization. *Cell Metab*, 22, 1033-44.
- Misko, A., Jiang, S., Wegorzewska, I., Milbrandt, J. & Baloh, R. H. 2010. Mitofusin 2 is necessary for transport of axonal mitochondria and interacts with the Miro/Milton complex. *The Journal of neuroscience : the official journal of the Society for Neuroscience*, 30, 4232-4240.
- Mitra, K., Wunder, C., Roysam, B., Lin, G. & Lippincott-Schwartz, J. 2009. A hyperfused mitochondrial state achieved at G1-S regulates cyclin E buildup and entry into S phase. *Proc Natl Acad Sci U S A*, 106, 11960-5.
- Miyamoto, T., Rho, E., Sample, V., Akano, H., Magari, M., Ueno, T., Gorshkov, K., Chen, M., Tokumitsu, H., Zhang, J. & Inoue, T. 2015. Compartmentalized AMPK signaling illuminated by genetically encoded molecular sensors and actuators. *Cell Rep*, 11, 657-70.
- Mizushima, N. 2009. Physiological functions of autophagy. *Curr Top Microbiol Immunol*, 335, 71-84.
- Mizushima, N. 2010. The role of the Atg1/ULK1 complex in autophagy regulation. *Curr Opin Cell Biol*, 22, 132-9.
- Mizushima, N. & Komatsu, M. 2011. Autophagy: renovation of cells and tissues. *Cell*, 147, 728-41.
- Mizushima, N., Noda, T. & Ohsumi, Y. 1999. Apg16p is required for the function of the Apg12p-Apg5p conjugate in the yeast autophagy pathway. *Embo j*, 18, 3888-96.
- Molina, A. J., Wikstrom, J. D., Stiles, L., Las, G., Mohamed, H., Elorza, A., Walzer, G., Twig, G., Katz, S., Corkey, B. E. & Shirihai, O. S. 2009. Mitochondrial networking protects beta-cells from nutrient-induced apoptosis. *Diabetes*, 58, 2303-15.
- Momcilovic, M., Hong, S. P. & Carlson, M. 2006. Mammalian TAK1 activates Snf1 protein kinase in yeast and phosphorylates AMP-activated protein kinase in vitro. *J Biol Chem*, 281, 25336-43.
- Monterisi, S. & Zaccolo, M. 2017. Components of the mitochondrial cAMP signalosome. *Biochem Soc Trans*, 45, 269-274.
- Morehouse, R. F. & Curthoys, N. P. 1981. Properties of rat renal phosphate-dependent glutaminase coupled to Sepharose. Evidence that dimerization is essential for activation. *Biochem J*, 193, 709-16.

- Morhenn, V., Kram, R., Hershko, A. & Tomkins, G. M. 1974. Studies on amino acid control of cellular function. *Cell*, 1, 91-94.
- Morita, M., Gravel, S. P., Chenard, V., Sikstrom, K., Zheng, L., Alain, T., Gandin, V., Avizonis, D., Arguello, M., Zakaria, C., McLaughlan, S., Nouet, Y., Pause, A., Pollak, M., Gottlieb, E., Larsson, O., St-Pierre, J., Topisirovic, I. & Sonenberg, N. 2013. mTORC1 controls mitochondrial activity and biogenesis through 4E-BP-dependent translational regulation. *Cell Metab*, 18, 698-711.
- Morita, M., Prudent, J., Basu, K., Goyon, V., Katsumura, S., Hulea, L., Pearl, D., Siddiqui, N., Strack, S., McGuirk, S., St-Pierre, J., Larsson, O., Topisirovic, I., Vali, H., McBride, H. M., Bergeron, J. J. & Sonenberg, N. 2017. mTOR Controls Mitochondrial Dynamics and Cell Survival via MTFP1. *Mol Cell*, 67, 922-935 e5.
- Mortensen, M., Ferguson, D. J., Edelmann, M., Kessler, B., Morten, K. J., Komatsu, M. & Simon, A. K. 2010. Loss of autophagy in erythroid cells leads to defective removal of mitochondria and severe anemia in vivo. *Proc Natl Acad Sci U S A*, 107, 832-7.
- Mortimore, G. E., Lardeux, B. R. & Adams, C. E. 1988. Regulation of microautophagy and basal protein turnover in rat liver. Effects of short-term starvation. *J Biol Chem*, 263, 2506-12.
- Mortimore, G. E. & Poso, A. R. 1986. The lysosomal pathway of intracellular proteolysis in liver: regulation by amino acids. *Adv Enzyme Regul*, 25, 257-76.
- Mortimore, G. E., Poso, A. R. & Lardeux, B. R. 1989. Mechanism and regulation of protein degradation in liver. *Diabetes Metab Rev*, 5, 49-70.
- Mortimore, G. E. & Ward, W. F. 1976. Behavior of the lysosomal system during organ perfusion. An inquiry into the mechanism of hepatic proteolysis. *Front Biol*, 45, 157-84.
- Moruno-Manchon, J. F., Perez-Jimenez, E. & Knecht, E. 2013. Glucose induces autophagy under starvation conditions by a p38 MAPK-dependent pathway. *Biochem J*, 449, 497-506.
- Mourier, A., Motori, E., Brandt, T., Lagouge, M., Atanassov, I., Galinier, A., Rappl, G., Brodesser, S., Hultenby, K., Dieterich, C. & Larsson, N. G. 2015. Mitofusin 2 is required to maintain mitochondrial coenzyme Q levels. *J Cell Biol*, 208, 429-42.
- Mozdy, A. D., McCaffery, J. M. & Shaw, J. M. 2000. Dnm1p GTPase-mediated mitochondrial fission is a multi-step process requiring the novel integral membrane component Fis1p. *J Cell Biol*, 151, 367-80.
- Munday, M. R., Campbell, D. G., Carling, D. & Hardie, D. G. 1988. Identification by amino acid sequencing of three major regulatory phosphorylation sites on rat acetyl-CoA carboxylase. *Eur J Biochem*, 175, 331-8.
- Munoz, J. P., Ivanova, S., Sanchez-Wandelmer, J., Martinez-Cristobal, P., Noguera, E., Sancho, A., Diaz-Ramos, A., Hernandez-Alvarez, M. I., Sebastian, D., Mauvezin, C., Palacin, M. & Zorzano, A. 2013. Mfn2 modulates the UPR and mitochondrial function via repression of PERK. *Embo j*, 32, 2348-61.
- Murakawa, T., Okamoto, K., Omiya, S., Taneike, M., Yamaguchi, O. & Otsu, K. 2019. A Mammalian Mitophagy Receptor, Bcl2-L-13, Recruits the ULK1 Complex to Induce Mitophagy. *Cell Rep*, 26, 338-345.e6.
- Murakawa, T., Yamaguchi, O., Hashimoto, A., Hikoso, S., Takeda, T., Oka, T., Yasui, H., Ueda, H., Akazawa, Y., Nakayama, H., Taneike, M., Misaka, T., Omiya, S., Shah, A. M., Yamamoto, A., Nishida, K., Ohsumi, Y., Okamoto, K., Sakata, Y. & Otsu, K. 2015. Bcl-2-like protein 13 is a mammalian Atg32 homologue that mediates mitophagy and mitochondrial fragmentation. *Nat Commun*, 6, 7527.
- Murakoshi, M., Osamura, Y. & Watanabe, K. 1985. Mitochondrial alterations in aged rat adrenal cortical cells. *Tokai J Exp Clin Med*, 10, 531-6.
- Nakagawa, I., Amano, A., Mizushima, N., Yamamoto, A., Yamaguchi, H., Kamimoto, T., Nara, A., Funao, J., Nakata, M., Tsuda, K., Hamada, S. & Yoshimori, T. 2004. Autophagy defends cells against invading group A Streptococcus. *Science*, 306, 1037-40.
- Naon, D., Zaninello, M., Giacomello, M., Varanita, T., Grespi, F., Lakshminarayanan, S., Serafini, A., Semenzato, M., Herkenne, S., Hernandez-Alvarez, M. I., Zorzano, A., De Stefani, D., Dorn, G. W., 2nd & Scorrano, L. 2016. Critical reappraisal confirms that Mitofusin 2 is an endoplasmic reticulum-mitochondria tether. *Proc Natl Acad Sci U S A*, 113, 11249-11254.

- Narendra, D., Tanaka, A., Suen, D. F. & Youle, R. J. 2008. Parkin is recruited selectively to impaired mitochondria and promotes their autophagy. *J Cell Biol*, 183, 795-803.
- Narendra, D. P., Jin, S. M., Tanaka, A., Suen, D. F., Gautier, C. A., Shen, J., Cookson, M. R. & Youle, R. J. 2010. PINK1 is selectively stabilized on impaired mitochondria to activate Parkin. *PLoS Biol*, 8, e1000298.
- Neinast, M. D., Jang, C., Hui, S., Murashige, D. S., Chu, Q., Morscher, R. J., Li, X., Zhan, L., White, E., Anthony, T. G., Rabinowitz, J. D. & Arany, Z. 2019. Quantitative Analysis of the Whole-Body Metabolic Fate of Branched-Chain Amino Acids. *Cell Metab*, 29, 417-429.e4.
- Neves-Zaph, S. R. 2017. Phosphodiesterase Diversity and Signal Processing Within cAMP Signaling Networks. *Adv Neurobiol*, 17, 3-14.
- Nguyen, T. N., Padman, B. S., Usher, J., Oorschot, V., Ramm, G. & Lazarou, M. 2016. Atg8 family LC3/GABARAP proteins are crucial for autophagosome-lysosome fusion but not autophagosome formation during PINK1/Parkin mitophagy and starvation. *J Cell Biol*.
- Nicklin, P., Bergman, P., Zhang, B., Triantafellow, E., Wang, H., Nyfeler, B., Yang, H., Hild, M., Kung, C., Wilson, C., Myer, V. E., MacKeigan, J. P., Porter, J. A., Wang, Y. K., Cantley, L. C., Finan, P. M. & Murphy, L. O. 2009. Bidirectional transport of amino acids regulates mTOR and autophagy. *Cell*, 136, 521-34.
- Nishimura, T., Tamura, N., Kono, N., Shimanaka, Y., Arai, H., Yamamoto, H. & Mizushima, N. 2017. Autophagosome formation is initiated at phosphatidylinositol synthase-enriched ER subdomains. *Embo j*, 36, 1719-1735.
- Niu, J., Vaiskunaite, R., Suzuki, N., Kozasa, T., Carr, D. W., Dulin, N. & Voyno-Yasenetskaya, T. A. 2001. Interaction of heterotrimeric G13 protein with an A-kinase-anchoring protein 110 (AKAP110) mediates cAMP-independent PKA activation. *Curr Biol*, 11, 1686-90.
- Noda, N. N. & Fujioka, Y. 2015. Atg1 family kinases in autophagy initiation. *Cell Mol Life Sci*, 72, 3083-96.
- Nojima, H., Tokunaga, C., Eguchi, S., Oshiro, N., Hidayat, S., Yoshino, K., Hara, K., Tanaka, N., Avruch, J. & Yonezawa, K. 2003. The mammalian target of rapamycin (mTOR) partner, raptor, binds the mTOR substrates p70 S6 kinase and 4E-BP1 through their TOR signaling (TOS) motif. *J Biol Chem*, 278, 15461-4.
- Novak, I., Kirkin, V., McEwan, D. G., Zhang, J., Wild, P., Rozenknop, A., Rogov, V., Lohr, F., Popovic, D., Occhipinti, A., Reichert, A. S., Terzic, J., Dotsch, V., Ney, P. A. & Dikic, I. 2010. Nix is a selective autophagy receptor for mitochondrial clearance. *EMBO Rep*, 11, 45-51.
- Nwadike, C., Williamson, L. E., Gallagher, L. E., Guan, J. L. & Chan, E. Y. W. 2018. AMPK Inhibits ULK1-Dependent Autophagosome Formation and Lysosomal Acidification via Distinct Mechanisms. *Mol Cell Biol*, 38.
- O'Flaherty, L., Adam, J., Heather, L. C., Zhdanov, A. V., Chung, Y. L., Miranda, M. X., Croft, J., Olpin, S., Clarke, K., Pugh, C. W., Griffiths, J., Papkovsky, D., Ashrafian, H., Ratcliffe, P. J. & Pollard, P. J. 2010. Dysregulation of hypoxia pathways in fumarate hydratase-deficient cells is independent of defective mitochondrial metabolism. *Hum Mol Genet*, 19, 3844-51.
- O'Mealey, G. B., Plafker, K. S., Berry, W. L., Janknecht, R., Chan, J. Y. & Plafker, S. M. 2017. A PGAM5-KEAP1-Nrf2 complex is required for stress-induced mitochondrial retrograde trafficking. *J Cell Sci*, 130, 3467-3480.
- Oakhill, J. S., Chen, Z. P., Scott, J. W., Steel, R., Castelli, L. A., Ling, N., Macaulay, S. L. & Kemp, B. E. 2010. beta-Subunit myristoylation is the gatekeeper for initiating metabolic stress sensing by AMP-activated protein kinase (AMPK). *Proc Natl Acad Sci U S A*, 107, 19237-41.
- Oakhill, J. S., Steel, R., Chen, Z. P., Scott, J. W., Ling, N., Tam, S. & Kemp, B. E. 2011. AMPK is a direct adenylate charge-regulated protein kinase. *Science*, 332, 1433-5.
- Ogura, K., Wicky, C., Magnenat, L., Tobler, H., Mori, I., Muller, F. & Ohshima, Y. 1994. *Caenorhabditis elegans* unc-51 gene required for axonal elongation encodes a novel serine/threonine kinase. *Genes Dev*, 8, 2389-400.
- Okamoto, K., Kondo-Okamoto, N. & Ohsumi, Y. 2009. Mitochondria-anchored receptor Atg32 mediates degradation of mitochondria via selective autophagy. *Dev Cell*, 17, 87-97.

- Okatsu, K., Saisho, K., Shimanuki, M., Nakada, K., Shitara, H., Sou, Y. S., Kimura, M., Sato, S., Hattori, N., Komatsu, M., Tanaka, K. & Matsuda, N. 2010. p62/SQSTM1 cooperates with Parkin for perinuclear clustering of depolarized mitochondria. *Genes Cells*, 15, 887-900.
- Olichon, A., Landes, T., Arnaune-Pelloquin, L., Emorine, L. J., Mils, V., Guichet, A., Delettre, C., Hamel, C., Amati-Bonneau, P., Bonneau, D., Reynier, P., Lenaers, G. & Belenguer, P. 2007. Effects of OPA1 mutations on mitochondrial morphology and apoptosis: relevance to ADOA pathogenesis. *J Cell Physiol*, 211, 423-30.
- Onoue, K., Jofuku, A., Ban-Ishihara, R., Ishihara, T., Maeda, M., Koshiba, T., Itoh, T., Fukuda, M., Otera, H., Oka, T., Takano, H., Mizushima, N., Mihara, K. & Ishihara, N. 2013. Fis1 acts as a mitochondrial recruitment factor for TBC1D15 that is involved in regulation of mitochondrial morphology. *Journal of Cell Science*, 126, 176.
- Orlova, M., Kanter, E., Krakovich, D. & Kuchin, S. 2006. Nitrogen availability and TOR regulate the Snf1 protein kinase in *Saccharomyces cerevisiae*. *Eukaryot Cell*, 5, 1831-7.
- Orsi, A., Razi, M., Dooley, H. C., Robinson, D., Weston, A. E., Collinson, L. M. & Tooze, S. A. 2012. Dynamic and transient interactions of Atg9 with autophagosomes, but not membrane integration, are required for autophagy. *Mol Biol Cell*, 23, 1860-73.
- Osellame, L. D., Singh, A. P., Stroud, D. A., Palmer, C. S., Stojanovski, D., Ramachandran, R. & Ryan, M. T. 2016. Cooperative and independent roles of the Drp1 adaptors Mff, MiD49 and MiD51 in mitochondrial fission. *J Cell Sci*, 129, 2170-81.
- Oshiro, N., Takahashi, R., Yoshino, K., Tanimura, K., Nakashima, A., Eguchi, S., Miyamoto, T., Hara, K., Takehana, K., Avruch, J., Kikkawa, U. & Yonezawa, K. 2007. The proline-rich Akt substrate of 40 kDa (PRAS40) is a physiological substrate of mammalian target of rapamycin complex 1. *J Biol Chem*, 282, 20329-39.
- Otera, H., Miyata, N., Kuge, O. & Mihara, K. 2016. Drp1-dependent mitochondrial fission via MiD49/51 is essential for apoptotic cristae remodeling. *J Cell Biol*, 212, 531-44.
- Otera, H., Wang, C., Cleland, M. M., Setoguchi, K., Yokota, S., Youle, R. J. & Mihara, K. 2010. Mff is an essential factor for mitochondrial recruitment of Drp1 during mitochondrial fission in mammalian cells. *J Cell Biol*, 191, 1141-58.
- Ould Amer, Y. & Hebert-Chatelain, E. 2018. Mitochondrial cAMP-PKA signaling: What do we really know? *Biochim Biophys Acta*.
- Owen, O. E., Kalhan, S. C. & Hanson, R. W. 2002. The key role of anaplerosis and cataplerosis for citric acid cycle function. *J Biol Chem*, 277, 30409-12.
- Pal, R., Palmieri, M., Chaudhury, A., Klisch, T. J., di Ronza, A., Neilson, J. R., Rodney, G. G. & Sardiello, M. 2018. Src regulates amino acid-mediated mTORC1 activation by disrupting GATOR1-Rag GTPase interaction. *Nat Commun*, 9, 4351.
- Palmer, C. S., Elgass, K. D., Parton, R. G., Osellame, L. D., Stojanovski, D. & Ryan, M. T. 2013. Adaptor proteins MiD49 and MiD51 can act independently of Mff and Fis1 in Drp1 recruitment and are specific for mitochondrial fission. *J Biol Chem*, 288, 27584-93.
- Palmer, C. S., Osellame, L. D., Laine, D., Koutsopoulos, O. S., Frazier, A. E. & Ryan, M. T. 2011. MiD49 and MiD51, new components of the mitochondrial fission machinery. *EMBO Rep*, 12, 565-73.
- Palmer, G., Horgan, D. J., Tisdale, H., Singer, T. P. & Beinert, H. 1968. Studies on the respiratory chain-linked reduced nicotinamide adenine dinucleotide dehydrogenase. XIV. Location of the sites of inhibition of rotenone, barbiturates, and piericidin by means of electron paramagnetic resonance spectroscopy. *J Biol Chem*, 243, 844-7.
- Palmieri, F. 2013. The mitochondrial transporter family SLC25: identification, properties and pathophysiology. *Mol Aspects Med*, 34, 465-84.
- Pankiv, S., Alemu, E. A., Brech, A., Bruun, J. A., Lamark, T., Overvatn, A., Bjorkoy, G. & Johansen, T. 2010. FYCO1 is a Rab7 effector that binds to LC3 and PI3P to mediate microtubule plus end-directed vesicle transport. *J Cell Biol*, 188, 253-69.
- Pankiv, S., Clausen, T. H., Lamark, T., Brech, A., Bruun, J. A., Outzen, H., Overvatn, A., Bjorkoy, G. & Johansen, T. 2007. p62/SQSTM1 binds directly to Atg8/LC3 to facilitate degradation of ubiquitinated protein aggregates by autophagy. *J Biol Chem*, 282, 24131-45.
- Papa, S., Sardanelli, A. M., Scacco, S. & Technikova-Dobrova, Z. 1999. cAMP-dependent protein kinase and phosphoproteins in mammalian mitochondria. An extension of the cAMP-mediated intracellular signal transduction. *FEBS Lett*, 444, 245-9.

- Park, J. M., Jung, C. H., Seo, M., Otto, N. M., Grunwald, D., Kim, K. H., Moriarity, B., Kim, Y. M., Starker, C., Nho, R. S., Voytas, D. & Kim, D. H. 2016. The ULK1 complex mediates mTORC1 signaling to the autophagy initiation machinery via binding and phosphorylating ATG14. *Autophagy*, 12, 547-64.
- Park, J. M., Seo, M., Jung, C. H., Grunwald, D., Stone, M., Otto, N. M., Toso, E., Ahn, Y., Kyba, M., Griffin, T. J., Higgins, L. & Kim, D. H. 2018. ULK1 phosphorylates Ser30 of BECN1 in association with ATG14 to stimulate autophagy induction. *Autophagy*, 14, 584-597.
- Park, Y. Y., Nguyen, O. T., Kang, H. & Cho, H. 2014. MARCH5-mediated quality control on acetylated Mfn1 facilitates mitochondrial homeostasis and cell survival. *Cell Death Dis*, 5, e1172.
- Parmigiani, A., Nourbakhsh, A., Ding, B., Wang, W., Kim, Y. C., Akopiants, K., Guan, K.-L., Karin, M. & Budanov, A. V. 2014. Sestrins inhibit mTORC1 kinase activation through the GATOR complex. *Cell reports*, 9, 1281-1291.
- Parone, P. A., Da Cruz, S., Tondera, D., Mattenberger, Y., James, D. I., Maechler, P., Barja, F. & Martinou, J. C. 2008. Preventing mitochondrial fission impairs mitochondrial function and leads to loss of mitochondrial DNA. *PLoS One*, 3, e3257.
- Patten, D. A., Wong, J., Khacho, M., Soubannier, V., Mailloux, R. J., Pilon-Larose, K., MacLaurin, J. G., Park, D. S., McBride, H. M., Trinkle-Mulcahy, L., Harper, M. E., Germain, M. & Slack, R. S. 2014. OPA1-dependent cristae modulation is essential for cellular adaptation to metabolic demand. *Embo j*, 33, 2676-91.
- Pearce, L. R., Huang, X., Boudeau, J., Pawlowski, R., Wullschleger, S., Deak, M., Ibrahim, A. F., Goulay, R., Magnuson, M. A. & Alessi, D. R. 2007. Identification of Protor as a novel Rictor-binding component of mTOR complex-2. *Biochem J*, 405, 513-22.
- Pegg, A. E. 2009. Mammalian polyamine metabolism and function. *IUBMB life*, 61, 880-894.
- Peng, M., Yin, N. & Li, M. O. 2017. SZT2 dictates GATOR control of mTORC1 signalling. *Nature*, 543, 433-437.
- Peralta, S., Garcia, S., Yin, H. Y., Arguello, T., Diaz, F. & Moraes, C. T. 2016. Sustained AMPK activation improves muscle function in a mitochondrial myopathy mouse model by promoting muscle fiber regeneration. *Hum Mol Genet*, 25, 3178-3191.
- Perland, E. & Fredriksson, R. 2017. Classification Systems of Secondary Active Transporters. *Trends in Pharmacological Sciences*, 38, 305-315.
- Pesch, U. E., Leo-Kottler, B., Mayer, S., Jurklics, B., Kellner, U., Apfelstedt-Sylla, E., Zrenner, E., Alexander, C. & Wissinger, B. 2001. OPA1 mutations in patients with autosomal dominant optic atrophy and evidence for semi-dominant inheritance. *Hum Mol Genet*, 10, 1359-68.
- Peterson, T. R., Laplante, M., Thoreen, C. C., Sancak, Y., Kang, S. A., Kuehl, W. M., Gray, N. S. & Sabatini, D. M. 2009. DEPTOR is an mTOR inhibitor frequently overexpressed in multiple myeloma cells and required for their survival. *Cell*, 137, 873-86.
- Petherick, K. J., Conway, O. J., Mpamhanga, C., Osborne, S. A., Kamal, A., Saxty, B. & Ganley, I. G. 2015. Pharmacological inhibition of ULK1 kinase blocks mammalian target of rapamycin (mTOR)-dependent autophagy. *J Biol Chem*, 290, 11376-83.
- Pfeifer, U. & Warmuth-Metz, M. 1983. Inhibition by insulin of cellular autophagy in proximal tubular cells of rat kidney. *Am J Physiol*, 244, E109-14.
- Pich, S., Bach, D., Briones, P., Liesa, M., Camps, M., Testar, X., Palacin, M. & Zorzano, A. 2005. The Charcot-Marie-Tooth type 2A gene product, Mfn2, up-regulates fuel oxidation through expression of OXPHOS system. *Hum Mol Genet*, 14, 1405-15.
- Poillet-Perez, L., Xie, X., Zhan, L., Yang, Y., Sharp, D. W., Hu, Z. S., Su, X., Maganti, A., Jiang, C., Lu, W., Zheng, H., Bosenberg, M. W., Mehnert, J. M., Guo, J. Y., Lattime, E., Rabinowitz, J. D. & White, E. 2018. Autophagy maintains tumour growth through circulating arginine. *Nature*.
- Polke, J. M., Laura, M., Pareyson, D., Taroni, F., Milani, M., Bergamin, G., Gibbons, V. S., Houlden, H., Chamley, S. C., Blake, J., Devile, C., Sandford, R., Sweeney, M. G., Davis, M. B. & Reilly, M. M. 2011. Recessive axonal Charcot-Marie-Tooth disease due to compound heterozygous mitofusin 2 mutations. *Neurology*, 77, 168-73.
- Pollard, P. J., Briere, J. J., Alam, N. A., Barwell, J., Barclay, E., Wortham, N. C., Hunt, T., Mitchell, M., Olpin, S., Moat, S. J., Hargreaves, I. P., Heales, S. J., Chung, Y. L., Griffiths, J. R., Dalgleish, A., McGrath, J. A., Gleeson, M. J., Hodgson, S. V., Poulosom, R., Rustin, P. & Tomlinson, I. P. 2005. Accumulation of Krebs cycle

- intermediates and over-expression of HIF1alpha in tumours which result from germline FH and SDH mutations. *Hum Mol Genet*, 14, 2231-9.
- Pollard, P. J., Spencer-Dene, B., Shukla, D., Howarth, K., Nye, E., El-Bahrawy, M., Deheragoda, M., Joannou, M., McDonald, S., Martin, A., Igarashi, P., Varsani-Brown, S., Rosewell, I., Poulson, R., Maxwell, P., Stamp, G. W. & Tomlinson, I. P. 2007. Targeted inactivation of fh1 causes proliferative renal cyst development and activation of the hypoxia pathway. *Cancer Cell*, 11, 311-9.
- Polson, H. E., de Lartigue, J., Rigden, D. J., Reedijk, M., Urbe, S., Clague, M. J. & Tooze, S. A. 2010. Mammalian Atg18 (WIPI2) localizes to omegasome-anchored phagophores and positively regulates LC3 lipidation. *Autophagy*, 6, 506-22.
- Porcelli, V., Fiermonte, G., Longo, A. & Palmieri, F. 2014. The human gene SLC25A29, of solute carrier family 25, encodes a mitochondrial transporter of basic amino acids. *J Biol Chem*, 289, 13374-84.
- Potter, C. J., Pedraza, L. G. & Xu, T. 2002. Akt regulates growth by directly phosphorylating Tsc2. *Nat Cell Biol*, 4, 658-65.
- Prieto, J., Leon, M., Ponsoda, X., Sendra, R., Bort, R., Ferrer-Lorente, R., Raya, A., Lopez-Garcia, C. & Torres, J. 2016. Early ERK1/2 activation promotes DRP1-dependent mitochondrial fission necessary for cell reprogramming. *Nat Commun*, 7, 11124.
- Puente, C., Hendrickson, R. C. & Jiang, X. 2016. Nutrient-regulated Phosphorylation of ATG13 Inhibits Starvation-induced Autophagy. *J Biol Chem*, 291, 6026-35.
- Pyakurel, A., Savoia, C., Hess, D. & Scorrano, L. 2015. Extracellular regulated kinase phosphorylates mitofusin 1 to control mitochondrial morphology and apoptosis. *Mol Cell*, 58, 244-54.
- Qi, X., Disatnik, M. H., Shen, N., Sobel, R. A. & Mochly-Rosen, D. 2011. Aberrant mitochondrial fission in neurons induced by protein kinase C{delta} under oxidative stress conditions in vivo. *Mol Biol Cell*, 22, 256-65.
- Qi, X., Qvit, N., Su, Y. C. & Mochly-Rosen, D. 2013. A novel Drp1 inhibitor diminishes aberrant mitochondrial fission and neurotoxicity. *J Cell Sci*, 126, 789-802.
- Qi, Y., Yan, L., Yu, C., Guo, X., Zhou, X., Hu, X., Huang, X., Rao, Z., Lou, Z. & Hu, J. 2016. Structures of human mitofusin 1 provide insight into mitochondrial tethering. *J Cell Biol*, 215, 621-629.
- Qian, W., Choi, S., Gibson, G. A., Watkins, S. C., Bakkenist, C. J. & Van Houten, B. 2012. Mitochondrial hyperfusion induced by loss of the fission protein Drp1 causes ATM-dependent G2/M arrest and aneuploidy through DNA replication stress. *J Cell Sci*, 125, 5745-57.
- Qiu, F., Chen, Y.-R., Liu, X., Chu, C.-Y., Shen, L.-J., Xu, J., Gaur, S., Forman, H. J., Zhang, H., Zheng, S., Yen, Y., Huang, J., Kung, H.-J. & Ann, D. K. 2014. Arginine Starvation Impairs Mitochondrial Respiratory Function in ASS1-Deficient Breast Cancer Cells. *Science Signaling*, 7, ra31.
- Rabinovitch, R. C., Samborska, B., Faubert, B., Ma, E. H., Gravel, S.-P., Andrzejewski, S., Raissi, T. C., Pause, A., St.-Pierre, J. & Jones, R. G. 2017. AMPK Maintains Cellular Metabolic Homeostasis through Regulation of Mitochondrial Reactive Oxygen Species. *Cell Reports*, 21, 1-9.
- Radhi, O. A., Davidson, S., Scott, F., Zeng, R. X., Jones, D. H., Tomkinson, N. C. O., Yu, J. & Chan, E. Y. W. 2019. Inhibition of the ULK1 protein complex suppresses Staphylococcus-induced autophagy and cell death. *J Biol Chem*, 294, 14289-14307.
- Raimundo, N., Ahtinen, J., Fumic, K., Baric, I., Remes, A. M., Renkonen, R., Lapatto, R. & Suomalainen, A. 2008. Differential metabolic consequences of fumarate hydratase and respiratory chain defects. *Biochim Biophys Acta*, 1782, 287-94.
- Rakovic, A., Grunewald, A., Kottwitz, J., Bruggemann, N., Pramstaller, P. P., Lohmann, K. & Klein, C. 2011. Mutations in PINK1 and Parkin impair ubiquitination of Mitofusins in human fibroblasts. *PLoS One*, 6, e16746.
- Rambold, A. S., Cohen, S. & Lippincott-Schwartz, J. 2015. Fatty acid trafficking in starved cells: regulation by lipid droplet lipolysis, autophagy, and mitochondrial fusion dynamics. *Dev Cell*, 32, 678-92.
- Rambold, A. S., Kostelecky, B., Elia, N. & Lippincott-Schwartz, J. 2011. Tubular network formation protects mitochondria from autophagosomal degradation during nutrient starvation. *Proc Natl Acad Sci U S A*, 108, 10190-5.

- Ramirez-Peinado, S., Leon-Annicchiarico, C. L., Galindo-Moreno, J., Iurlaro, R., Caro-Maldonado, A., Prehn, J. H., Ryan, K. M. & Munoz-Pinedo, C. 2013. Glucose-starved cells do not engage in prosurvival autophagy. *J Biol Chem*, 288, 30387-98.
- Rana, A., Oliveira, M. P., Khamoui, A. V., Aparicio, R., Rera, M., Rossiter, H. B. & Walker, D. W. 2017. Promoting Drp1-mediated mitochondrial fission in midlife prolongs healthy lifespan of *Drosophila melanogaster*. *Nat Commun*, 8, 448.
- Rasheed, N., Lima, T. B., Mercaldi, G. F., Nascimento, A. F. Z., Silva, A. L. S., Righetto, G. L., Bar-Peled, L., Shen, K., Sabatini, D. M., Gozzo, F. C., Aparicio, R. & Smetana, J. H. C. 2019. C7orf59/LAMTOR4 phosphorylation and structural flexibility modulate Regulator assembly. *FEBS Open Bio*.
- Ravikumar, B., Moreau, K., Jahreiss, L., Puri, C. & Rubinsztein, D. C. 2010. Plasma membrane contributes to the formation of pre-autophagosomal structures. *Nat Cell Biol*, 12, 747-57.
- Rebsamen, M., Pochini, L., Stasyk, T., de Araujo, M. E., Galluccio, M., Kandasamy, R. K., Snijder, B., Fauster, A., Rudashevskaya, E. L., Bruckner, M., Scorzoni, S., Filipek, P. A., Huber, K. V., Bigenzahn, J. W., Heinz, L. X., Kraft, C., Bennett, K. L., Indiveri, C., Huber, L. A. & Superti-Furga, G. 2015. SLC38A9 is a component of the lysosomal amino acid sensing machinery that controls mTORC1. *Nature*, 519, 477-81.
- Rehman, J., Zhang, H. J., Toth, P. T., Zhang, Y., Marsboom, G., Hong, Z., Salgia, R., Husain, A. N., Wietholt, C. & Archer, S. L. 2012. Inhibition of mitochondrial fission prevents cell cycle progression in lung cancer. *FASEB J*, 26, 2175-86.
- Reitzer, L. J., Wice, B. M. & Kennell, D. 1979. Evidence that glutamine, not sugar, is the major energy source for cultured HeLa cells. *J Biol Chem*, 254, 2669-76.
- Richter, V., Palmer, C. S., Osellame, L. D., Singh, A. P., Elgass, K., Stroud, D. A., Sesaki, H., Kvensakul, M. & Ryan, M. T. 2014. Structural and functional analysis of MiD51, a dynamin receptor required for mitochondrial fission. *J Cell Biol*, 204, 477-86.
- Rinaldi, L., Sepe, M., Delle Donne, R., Conte, K., Arcella, A., Borzacchiello, D., Amente, S., De Vita, F., Porpora, M., Garbi, C., Oliva, M. A., Procaccini, C., Faicchia, D., Matarese, G., Zito Marino, F., Rocco, G., Pignatiello, S., Franco, R., Insabato, L., Majello, B. & Feliciello, A. 2017. Mitochondrial AKAP1 supports mTOR pathway and tumor growth. *Cell Death Dis*, 8, e2842.
- Ro, S. H., Jung, C. H., Hahn, W. S., Xu, X., Kim, Y. M., Yun, Y. S., Park, J. M., Kim, K. H., Seo, M., Ha, T. Y., Arriaga, E. A., Bernlohr, D. A. & Kim, D. H. 2013. Distinct functions of Ulk1 and Ulk2 in the regulation of lipid metabolism in adipocytes. *Autophagy*, 9, 2103-14.
- Roberts, David J., Tan-Sah, Valerie P., Ding, Eric Y., Smith, Jeffery M. & Miyamoto, S. 2014. Hexokinase-II Positively Regulates Glucose Starvation-Induced Autophagy through TORC1 Inhibition. *Molecular Cell*, 53, 521-533.
- Rocha, A. G., Franco, A., Krezel, A. M., Rumsey, J. M., Alberti, J. M., Knight, W. C., Biris, N., Zacharioudakis, E., Janetka, J. W., Baloh, R. H., Kitsis, R. N., Mochly-Rosen, D., Townsend, R. R., Gavathiotis, E. & Dorn, G. W., 2nd 2018. MFN2 agonists reverse mitochondrial defects in preclinical models of Charcot-Marie-Tooth disease type 2A. *Science*, 360, 336-341.
- Rodrik-Outmezguine, V. S., Okaniwa, M., Yao, Z., Novotny, C. J., McWhirter, C., Banaji, A., Won, H., Wong, W., Berger, M., de Stanchina, E., Barratt, D. G., Cosulich, S., Klinowska, T., Rosen, N. & Shokat, K. M. 2016. Overcoming mTOR resistance mutations with a new-generation mTOR inhibitor. *Nature*, 534, 272-6.
- Roger, A. J., Munoz-Gomez, S. A. & Kamikawa, R. 2017. The Origin and Diversification of Mitochondria. *Curr Biol*, 27, R1177-r1192.
- Ross, F. A., Jensen, T. E. & Hardie, D. G. 2016. Differential regulation by AMP and ADP of AMPK complexes containing different gamma subunit isoforms. *Biochem J*, 473, 189-99.
- Rossignol, R., Gilkerson, R., Aggeler, R., Yamagata, K., Remington, S. J. & Capaldi, R. A. 2004. Energy substrate modulates mitochondrial structure and oxidative capacity in cancer cells. *Cancer Res*, 64, 985-93.
- Roux, P. P., Ballif, B. A., Anjum, R., Gygi, S. P. & Blenis, J. 2004. Tumor-promoting phorbol esters and activated Ras inactivate the tuberous sclerosis tumor suppressor complex via p90 ribosomal S6 kinase. *Proceedings of the National Academy of Sciences of the United States of America*, 101, 13489-13494.

- Rueden, C. T., Schindelin, J., Hiner, M. C., DeZonia, B. E., Walter, A. E., Arena, E. T. & Eliceiri, K. W. 2017. ImageJ2: ImageJ for the next generation of scientific image data. *BMC Bioinformatics*, 18, 529.
- Russell, R. C., Tian, Y., Yuan, H., Park, H. W., Chang, Y. Y., Kim, J., Kim, H., Neufeld, T. P., Dillin, A. & Guan, K. L. 2013. ULK1 induces autophagy by phosphorylating Beclin-1 and activating VPS34 lipid kinase. *Nat Cell Biol*, 15, 741-50.
- Sabatini, D. M., Erdjument-Bromage, H., Lui, M., Tempst, P. & Snyder, S. H. 1994. RAFT1: a mammalian protein that binds to FKBP12 in a rapamycin-dependent fashion and is homologous to yeast TORs. *Cell*, 78, 35-43.
- Sabers, C. J., Martin, M. M., Brunn, G. J., Williams, J. M., Dumont, F. J., Wiederrecht, G. & Abraham, R. T. 1995. Isolation of a protein target of the FKBP12-rapamycin complex in mammalian cells. *J Biol Chem*, 270, 815-22.
- Sabouny, R., Fraunberger, E., Geoffrion, M., Ng, A. C., Baird, S. D., Screatton, R. A., Milne, R., McBride, H. M. & Shutt, T. E. 2017. The Keap1-Nrf2 Stress Response Pathway Promotes Mitochondrial Hyperfusion Through Degradation of the Mitochondrial Fission Protein Drp1. *Antioxid Redox Signal*, 27, 1447-1459.
- Saccone, C., Gissi, C., Lanave, C., Larizza, A., Pesole, G. & Reyes, A. 2000. Evolution of the mitochondrial genetic system: an overview. *Gene*, 261, 153-9.
- Sadasivan, S., Waghray, A., Larner, S. F., Dunn, W. A., Jr., Hayes, R. L. & Wang, K. K. 2006. Amino acid starvation induced autophagic cell death in PC-12 cells: evidence for activation of caspase-3 but not calpain-1. *Apoptosis*, 11, 1573-82.
- Sancak, Y., Bar-Peled, L., Zoncu, R., Markhard, A. L., Nada, S. & Sabatini, D. M. 2010. Ragulator-Rag complex targets mTORC1 to the lysosomal surface and is necessary for its activation by amino acids. *Cell*, 141, 290-303.
- Sancak, Y., Peterson, T. R., Shaul, Y. D., Lindquist, R. A., Thoreen, C. C., Bar-Peled, L. & Sabatini, D. M. 2008. The Rag GTPases bind raptor and mediate amino acid signaling to mTORC1. *Science*, 320, 1496-501.
- Sancak, Y., Thoreen, C. C., Peterson, T. R., Lindquist, R. A., Kang, S. A., Spooner, E., Carr, S. A. & Sabatini, D. M. 2007. PRAS40 is an insulin-regulated inhibitor of the mTORC1 protein kinase. *Mol Cell*, 25, 903-15.
- Sanchez-Sanchez, L., Escobar, M. L., Sandoval-Ramirez, J., Lopez-Munoz, H., Fernandez-Herrera, M. A., Hernandez-Vazquez, J. M., Hilaro-Martinez, C. & Zenteno, E. 2015. Apoptotic and autophagic cell death induced by glucolaxogenin in cervical cancer cells. *Apoptosis*, 20, 1623-35.
- Sanders, M. J., Grondin, P. O., Hegarty, B. D., Snowden, M. A. & Carling, D. 2007. Investigating the mechanism for AMP activation of the AMP-activated protein kinase cascade. *Biochem J*, 403, 139-48.
- Sandilands, E., Serrels, B., McEwan, D. G., Morton, J. P., Macagno, J. P., McLeod, K., Stevens, C., Brunton, V. G., Langdon, W. Y., Vidal, M., Sansom, O. J., Dikic, I., Wilkinson, S. & Frame, M. C. 2011. Autophagic targeting of Src promotes cancer cell survival following reduced FAK signalling. *Nat Cell Biol*, 14, 51-60.
- Sandoval, H., Thiagarajan, P., Dasgupta, S. K., Schumacher, A., Prchal, J. T., Chen, M. & Wang, J. 2008. Essential role for Nix in autophagic maturation of erythroid cells. *Nature*, 454, 232-5.
- Santamaria, D., Barriere, C., Cerqueira, A., Hunt, S., Tardy, C., Newton, K., Caceres, J. F., Dubus, P., Malumbres, M. & Barbacid, M. 2007. Cdk1 is sufficient to drive the mammalian cell cycle. *Nature*, 448, 811-5.
- Santel, A. & Fuller, M. T. 2001. Control of mitochondrial morphology by a human mitofusin. *J Cell Sci*, 114, 867-74.
- Sarbassov, D. D., Ali, S. M., Kim, D. H., Guertin, D. A., Latek, R. R., Erdjument-Bromage, H., Tempst, P. & Sabatini, D. M. 2004. Rictor, a novel binding partner of mTOR, defines a rapamycin-insensitive and raptor-independent pathway that regulates the cytoskeleton. *Curr Biol*, 14, 1296-302.
- Sarbassov, D. D., Ali, S. M., Sengupta, S., Sheen, J. H., Hsu, P. P., Bagley, A. F., Markhard, A. L. & Sabatini, D. M. 2006. Prolonged rapamycin treatment inhibits mTORC2 assembly and Akt/PKB. *Mol Cell*, 22, 159-68.
- Sato, M. & Sato, K. 2011. Degradation of paternal mitochondria by fertilization-triggered autophagy in *C. elegans* embryos. *Science*, 334, 1141-4.

- Saxton, R. A., Chantranupong, L., Knockenhauer, K. E., Schwartz, T. U. & Sabatini, D. M. 2016a. Mechanism of arginine sensing by CASTOR1 upstream of mTORC1. *Nature*, 536, 229-33.
- Saxton, R. A., Knockenhauer, K. E., Wolfson, R. L., Chantranupong, L., Pacold, M. E., Wang, T., Schwartz, T. U. & Sabatini, D. M. 2016b. Structural basis for leucine sensing by the Sestrin2-mTORC1 pathway. *Science*, 351, 53-8.
- Saxton, R. A. & Sabatini, D. M. 2017. mTOR Signaling in Growth, Metabolism, and Disease. *Cell*, 168, 960-976.
- Scalise, M., Galluccio, M., Pochini, L., Cosco, J., Trotta, M., Rebsamen, M., Superti-Furga, G. & Indiveri, C. 2019. Insights into the transport side of the human SLC38A9 transceptor. *Biochim Biophys Acta Biomembr*, 1861, 1558-1567.
- Scalise, M., Pochini, L., Galluccio, M., Console, L. & Indiveri, C. 2017. Glutamine Transport and Mitochondrial Metabolism in Cancer Cell Growth. *Frontiers in oncology*, 7, 306-306.
- Schieber, M. & Chandel, N. S. 2014. ROS function in redox signaling and oxidative stress. *Curr Biol*, 24, R453-62.
- Schimpf, S., Schaich, S. & Wissinger, B. 2006. Activation of cryptic splice sites is a frequent splicing defect mechanism caused by mutations in exon and intron sequences of the OPA1 gene. *Hum Genet*, 118, 767-71.
- Schlame, M. 2008. Cardiolipin synthesis for the assembly of bacterial and mitochondrial membranes. *J Lipid Res*, 49, 1607-20.
- Schneeberger, M., Dietrich, M. O., Sebastian, D., Imbernon, M., Castano, C., Garcia, A., Esteban, Y., Gonzalez-Franquesa, A., Rodriguez, I. C., Bortolozzi, A., Garcia-Roves, P. M., Gomis, R., Nogueiras, R., Horvath, T. L., Zorzano, A. & Claret, M. 2013. Mitofusin 2 in POMC neurons connects ER stress with leptin resistance and energy imbalance. *Cell*, 155, 172-87.
- Schrepfer, E. & Scorrano, L. 2016. Mitofusins, from Mitochondria to Metabolism. *Mol Cell*, 61, 683-94.
- Schwartz, W. 2007. L. Margulis, Symbiosis in Cell Evolution. Life and its Environment on the Early Earth. XXII + 479 S., 104 Abb., 59 Tab. San Francisco 1981. W. H. Freeman and Co. £ 16.40 (Board), £ 9.20 (Paper). *Zeitschrift für allgemeine Mikrobiologie*, 22, 427-427.
- Schworer, C. M., Shiffer, K. A. & Mortimore, G. E. 1981. Quantitative relationship between autophagy and proteolysis during graded amino acid deprivation in perfused rat liver. *J Biol Chem*, 256, 7652-8.
- Sciacovelli, M., Goncalves, E., Johnson, T. I., Zecchini, V. R., da Costa, A. S., Gaude, E., Drubbel, A. V., Theobald, S. J., Abbo, S. R., Tran, M. G., Rajeeve, V., Cardaci, S., Foster, S., Yun, H., Cutillas, P., Warren, A., Gnanapragasam, V., Gottlieb, E., Franze, K., Huntly, B., Maher, E. R., Maxwell, P. H., Saez-Rodriguez, J. & Frezza, C. 2016. Fumarate is an epigenetic modifier that elicits epithelial-to-mesenchymal transition. *Nature*, 537, 544-547.
- Scorrano, L., Ashiya, M., Buttle, K., Weiler, S., Oakes, S. A., Mannella, C. A. & Korsmeyer, S. J. 2002. A distinct pathway remodels mitochondrial cristae and mobilizes cytochrome c during apoptosis. *Dev Cell*, 2, 55-67.
- Scott, J. D., Glaccum, M. B., Zoller, M. J., Uhler, M. D., Helfman, D. M., McKnight, G. S. & Krebs, E. G. 1987. The molecular cloning of a type II regulatory subunit of the cAMP-dependent protein kinase from rat skeletal muscle and mouse brain. *Proc Natl Acad Sci U S A*, 84, 5192-6.
- Sebastian, D., Hernandez-Alvarez, M. I., Segales, J., Soriano, E., Munoz, J. P., Sala, D., Waget, A., Liesa, M., Paz, J. C., Gopalacharyulu, P., Oresic, M., Pich, S., Burcelin, R., Palacin, M. & Zorzano, A. 2012. Mitofusin 2 (Mfn2) links mitochondrial and endoplasmic reticulum function with insulin signaling and is essential for normal glucose homeostasis. *Proc Natl Acad Sci U S A*, 109, 5523-8.
- Seglen, P. O. & Gordon, P. B. 1982. 3-Methyladenine: specific inhibitor of autophagic/lysosomal protein degradation in isolated rat hepatocytes. *Proc Natl Acad Sci U S A*, 79, 1889-92.
- Seglen, P. O., Gordon, P. B. & Poli, A. 1980. Amino acid inhibition of the autophagic/lysosomal pathway of protein degradation in isolated rat hepatocytes. *Biochim Biophys Acta*, 630, 103-18.

- Sehgal, S. N. 2003. Sirolimus: its discovery, biological properties, and mechanism of action. *Transplant Proc*, 35, 7s-14s.
- Sekiguchi, T., Hirose, E., Nakashima, N., Ii, M. & Nishimoto, T. 2001. Novel G proteins, Rag C and Rag D, interact with GTP-binding proteins, Rag A and Rag B. *J Biol Chem*, 276, 7246-57.
- Sengupta, A., Molkenkin, J. D. & Yutzey, K. E. 2009. FoxO transcription factors promote autophagy in cardiomyocytes. *J Biol Chem*, 284, 28319-31.
- Serasinghe, M. N., Wieder, S. Y., Renault, T. T., Elkholi, R., Ascioffa, J. J., Yao, J. L., Jabado, O., Hoehn, K., Kageyama, Y., Sesaki, H. & Chipuk, J. E. 2015. Mitochondrial division is requisite to RAS-induced transformation and targeted by oncogenic MAPK pathway inhibitors. *Mol Cell*, 57, 521-36.
- Shang, L., Chen, S., Du, F., Li, S., Zhao, L. & Wang, X. 2011. Nutrient starvation elicits an acute autophagic response mediated by Ulk1 dephosphorylation and its subsequent dissociation from AMPK. *Proc Natl Acad Sci U S A*, 108, 4788-93.
- Shen, K., Choe, A. & Sabatini, D. M. 2017. Intersubunit Crosstalk in the Rag GTPase Heterodimer Enables mTORC1 to Respond Rapidly to Amino Acid Availability. *Mol Cell*, 68, 821.
- Shen, K., Huang, R. K., Brignole, E. J., Condon, K. J., Valenstein, M. L., Chantranupong, L., Bomaliyamu, A., Choe, A., Hong, C., Yu, Z. & Sabatini, D. M. 2018. Architecture of the human GATOR1 and GATOR1-Rag GTPases complexes. *Nature*, 556, 64-69.
- Shen, K. & Sabatini, D. M. 2018. Regulator and SLC38A9 activate the Rag GTPases through noncanonical GEF mechanisms. *Proc Natl Acad Sci U S A*, 115, 9545-9550.
- Shen, K., Valenstein, M. L., Gu, X. & Sabatini, D. M. 2019. Arg-78 of Npr12 catalyzes GATOR1-stimulated GTP hydrolysis by the Rag GTPases. *J Biol Chem*, 294, 2970-2975.
- Shen, Q., Yamano, K., Head, B. P., Kawajiri, S., Cheung, J. T., Wang, C., Cho, J. H., Hattori, N., Youle, R. J. & van der Bliek, A. M. 2014. Mutations in Fis1 disrupt orderly disposal of defective mitochondria. *Mol Biol Cell*, 25, 145-59.
- Shen, S., Weng, R., Li, L., Xu, X., Bai, Y. & Liu, H. 2016. Metabolomic Analysis of Mouse Embryonic Fibroblast Cells in Response to Autophagy Induced by Acute Starvation. *Sci Rep*, 6, 34075.
- Shibutani, S. T., Saitoh, T., Nowag, H., Munz, C. & Yoshimori, T. 2015. Autophagy and autophagy-related proteins in the immune system. *Nat Immunol*, 16, 1014-24.
- Shimobayashi, M. & Hall, M. N. 2016. Multiple amino acid sensing inputs to mTORC1. *Cell Res*, 26, 7-20.
- Shin, S. H., Lee, E. J., Chun, J., Hyun, S. & Kang, S. S. 2015. ULK2 Ser 1027 Phosphorylation by PKA Regulates Its Nuclear Localization Occurring through Karyopherin Beta 2 Recognition of a PY-NLS Motif. *PLoS One*, 10, e0127784.
- Shutt, T., Geoffrion, M., Milne, R. & McBride, H. M. 2012. The intracellular redox state is a core determinant of mitochondrial fusion. *EMBO Rep*, 13, 909-15.
- Simpson, J. C., Wellenreuther, R., Poustka, A., Pepperkok, R. & Wiemann, S. 2000. Systematic subcellular localization of novel proteins identified by large-scale cDNA sequencing. *EMBO Rep*, 1, 287-92.
- Smirnova, E., Griparic, L., Shurland, D. L. & van der Bliek, A. M. 2001. Dynamin-related protein Drp1 is required for mitochondrial division in mammalian cells. *Mol Biol Cell*, 12, 2245-56.
- Solowska, J. M. & Baas, P. W. 2015. Hereditary spastic paraplegia SPG4: what is known and not known about the disease. *Brain : a journal of neurology*, 138, 2471-2484.
- Son, S. M., Park, S. J., Lee, H., Siddiqi, F., Lee, J. E., Menzies, F. M. & Rubinsztein, D. C. 2019. Leucine Signals to mTORC1 via Its Metabolite Acetyl-Coenzyme A. *Cell metabolism*, 29, 192-201.e7.
- Song, M., Mihara, K., Chen, Y., Scorrano, L. & Dorn, G. W., 2nd 2015. Mitochondrial fission and fusion factors reciprocally orchestrate mitophagic culling in mouse hearts and cultured fibroblasts. *Cell Metab*, 21, 273-85.
- Song, Z., Chen, H., Fiket, M., Alexander, C. & Chan, D. C. 2007. OPA1 processing controls mitochondrial fusion and is regulated by mRNA splicing, membrane potential, and Yme1L. *J Cell Biol*, 178, 749-55.
- Sood, A., Jeyaraju, D. V., Prudent, J., Caron, A., Lemieux, P., McBride, H. M., Laplante, M., Toth, K. & Pellegrini, L. 2014. A Mitofusin-2-dependent inactivating cleavage of

- Opa1 links changes in mitochondria cristae and ER contacts in the postprandial liver. *Proc Natl Acad Sci U S A*, 111, 16017-22.
- Soto-Velasquez, M., Hayes, M. P., Alpsy, A., Dykhuizen, E. C. & Watts, V. J. 2018. A Novel CRISPR/Cas9-Based Cellular Model to Explore Adenylyl Cyclase and cAMP Signaling. *Mol Pharmacol*, 94, 963-972.
- Spinelli, J. B. & Haigis, M. C. 2018. The multifaceted contributions of mitochondria to cellular metabolism. *Nat Cell Biol*, 20, 745-754.
- Spinelli, J. B., Yoon, H., Ringel, A. E., Jeanfavre, S., Clish, C. B. & Haigis, M. C. 2017. Metabolic recycling of ammonia via glutamate dehydrogenase supports breast cancer biomass. *Science*, 358, 941-946.
- Sprenger, H.-G., Wani, G., Hesseling, A., König, T., Patron, M., MacVicar, T., Ahola, S., Wai, T., Barth, E., Rugarli, E. I., Bergami, M. & Langer, T. 2019. Loss of the mitochondrial i-AAA protease YME1L leads to ocular dysfunction and spinal axonopathy. *EMBO molecular medicine*, 11, e9288.
- Srivastava, S. 2017. The Mitochondrial Basis of Aging and Age-Related Disorders. *Genes (Basel)*, 8.
- Steebhorn, C., Litvin, T. N., Levin, L. R., Buck, J. & Wu, H. 2005. Bicarbonate activation of adenylyl cyclase via promotion of catalytic active site closure and metal recruitment. *Nat Struct Mol Biol*, 12, 32-7.
- Stefano, G. B. & Kream, R. M. 2015. Cancer: Mitochondrial Origins. *Med Sci Monit*, 21, 3736-9.
- Stein, L. R. & Imai, S. 2012. The dynamic regulation of NAD metabolism in mitochondria. *Trends Endocrinol Metab*, 23, 420-8.
- Steinhauser, M. L., Olenchock, B. A., O'Keefe, J., Lun, M., Pierce, K. A., Lee, H., Pantano, L., Klibanski, A., Shulman, G. I., Clish, C. B. & Fazeli, P. K. 2018. The circulating metabolome of human starvation. *JCI Insight*, 3.
- Stephan, J. S., Yeh, Y. Y., Ramachandran, V., Deminoff, S. J. & Herman, P. K. 2009. The Tor and PKA signaling pathways independently target the Atg1/Atg13 protein kinase complex to control autophagy. *Proc Natl Acad Sci U S A*, 106, 17049-54.
- Strack, S., Wilson, T. J. & Cribbs, J. T. 2013. Cyclin-dependent kinases regulate splice-specific targeting of dynamin-related protein 1 to microtubules. *J Cell Biol*, 201, 1037-51.
- Strappazon, F., Nazio, F., Corrado, M., Cianfanelli, V., Romagnoli, A., Fimia, G. M., Campello, S., Nardacci, R., Piacentini, M., Campanella, M. & Cecconi, F. 2015. AMBRA1 is able to induce mitophagy via LC3 binding, regardless of PARKIN and p62/SQSTM1. *Cell Death Differ*, 22, 517.
- Strappazon, F., Vietri-Rudan, M., Campello, S., Nazio, F., Florenzano, F., Fimia, G. M., Piacentini, M., Levine, B. & Cecconi, F. 2011. Mitochondrial BCL-2 inhibits AMBRA1-induced autophagy. *Embo j*, 30, 1195-208.
- Sugawara, K., Suzuki, N. N., Fujioka, Y., Mizushima, N., Ohsumi, Y. & Inagaki, F. 2004. The crystal structure of microtubule-associated protein light chain 3, a mammalian homologue of *Saccharomyces cerevisiae* Atg8. *Genes Cells*, 9, 611-8.
- Sugiura, A., Nagashima, S., Tokuyama, T., Amo, T., Matsuki, Y., Ishido, S., Kudo, Y., McBride, H. M., Fukuda, T., Matsushita, N., Inatome, R. & Yanagi, S. 2013. MITOL regulates endoplasmic reticulum-mitochondria contacts via Mitofusin2. *Mol Cell*, 51, 20-34.
- Sugo, M., Kimura, H., Arasaki, K., Amemiya, T., Hirota, N., Dohmae, N., Imai, Y., Inoshita, T., Shiba-Fukushima, K., Hattori, N., Cheng, J., Fujimoto, T., Wakana, Y., Inoue, H. & Tagaya, M. 2018. Syntaxin 17 regulates the localization and function of PGAM5 in mitochondrial division and mitophagy. *Embo j*, 37.
- Sun, Q., Fan, W., Chen, K., Ding, X., Chen, S. & Zhong, Q. 2008. Identification of Barkor as a mammalian autophagy-specific factor for Beclin 1 and class III phosphatidylinositol 3-kinase. *Proc Natl Acad Sci U S A*, 105, 19211-6.
- Suzuki, K., Kubota, Y., Sekito, T. & Ohsumi, Y. 2007. Hierarchy of Atg proteins in pre-autophagosomal structure organization. *Genes Cells*, 12, 209-18.
- Szablewski, L. 2011. Glucose homeostasis-mechanism and defects. *Diabetes-Damages and Treatments*, 2.
- Taguchi, N., Ishihara, N., Jofuku, A., Oka, T. & Mihara, K. 2007. Mitotic phosphorylation of dynamin-related GTPase Drp1 participates in mitochondrial fission. *J Biol Chem*, 282, 11521-9.

- Takahashi, Y., Coppola, D., Matsushita, N., Cualing, H. D., Sun, M., Sato, Y., Liang, C., Jung, J. U., Cheng, J. Q., Mule, J. J., Pledger, W. J. & Wang, H. G. 2007. Bif-1 interacts with Beclin 1 through UVRAG and regulates autophagy and tumorigenesis. *Nat Cell Biol*, 9, 1142-51.
- Takahashi, Y., Meyerkord, C. L. & Wang, H. G. 2009. Bif-1/endophilin B1: a candidate for crescent driving force in autophagy. *Cell Death Differ*, 16, 947-55.
- Takano, S., Fujibayashi, K., Fujioka, N., Ueno, E., Wakasa, M., Kawai, Y. & Kajinami, K. 2016. Circulating Glutamate and Taurine Levels Are Associated with the Generation of Reactive Oxygen Species in Paroxysmal Atrial Fibrillation. *Dis Markers*, 2016, 7650976.
- Takehige, K., Baba, M., Tsuboi, S., Noda, T. & Ohsumi, Y. 1992. Autophagy in yeast demonstrated with proteinase-deficient mutants and conditions for its induction. *J Cell Biol*, 119, 301-11.
- Tan, H. W. S., Sim, A. Y. L. & Long, Y. C. 2017. Glutamine metabolism regulates autophagy-dependent mTORC1 reactivation during amino acid starvation. *Nat Commun*, 8, 338.
- Tardito, S., Oudin, A., Ahmed, S. U., Fack, F., Keunen, O., Zheng, L., Miletic, H., Sakariassen, P. O., Weinstock, A., Wagner, A., Lindsay, S. L., Hock, A. K., Barnett, S. C., Ruppin, E., Morkve, S. H., Lund-Johansen, M., Chalmers, A. J., Bjerkvig, R., Niclou, S. P. & Gottlieb, E. 2015. Glutamine synthetase activity fuels nucleotide biosynthesis and supports growth of glutamine-restricted glioblastoma. *Nat Cell Biol*, 17, 1556-68.
- Tasken, K. A., Collas, P., Kemmner, W. A., Witczak, O., Conti, M. & Tasken, K. 2001. Phosphodiesterase 4D and protein kinase a type II constitute a signaling unit in the centrosomal area. *J Biol Chem*, 276, 21999-2002.
- Taylor, P. M. 2014. Role of amino acid transporters in amino acid sensing. *Am J Clin Nutr*, 99, 223s-230s.
- Tezze, C., Romanello, V., Desbats, M. A., Fadini, G. P., Albiero, M., Favaro, G., Ciciliot, S., Soriano, M. E., Morbidoni, V., Cerqua, C., Loeffler, S., Kern, H., Franceschi, C., Salvioli, S., Conte, M., Blaauw, B., Zampieri, S., Salviati, L., Scorrano, L. & Sandri, M. 2017. Age-Associated Loss of OPA1 in Muscle Impacts Muscle Mass, Metabolic Homeostasis, Systemic Inflammation, and Epithelial Senescence. *Cell Metab*, 25, 1374-1389.e6.
- Thomas, J. D., Zhang, Y. J., Wei, Y. H., Cho, J. H., Morris, L. E., Wang, H. Y. & Zheng, X. F. 2014. Rab1A is an mTORC1 activator and a colorectal oncogene. *Cancer Cell*, 26, 754-69.
- Thoreen, C. C., Kang, S. A., Chang, J. W., Liu, Q., Zhang, J., Gao, Y., Reichling, L. J., Sim, T., Sabatini, D. M. & Gray, N. S. 2009. An ATP-competitive mammalian target of rapamycin inhibitor reveals rapamycin-resistant functions of mTORC1. *J Biol Chem*, 284, 8023-32.
- Thoreen, C. C. & Sabatini, D. M. 2009. Rapamycin inhibits mTORC1, but not completely. *Autophagy*, 5, 725-6.
- Thornton, C., Snowden, M. A. & Carling, D. 1998. Identification of a novel AMP-activated protein kinase beta subunit isoform that is highly expressed in skeletal muscle. *J Biol Chem*, 273, 12443-50.
- Thumm, M., Egner, R., Koch, B., Schlumpberger, M., Straub, M., Veenhuis, M. & Wolf, D. H. 1994. Isolation of autophagocytosis mutants of *Saccharomyces cerevisiae*. *FEBS Lett*, 349, 275-80.
- Tian, L., Neuber-Hess, M., Mewburn, J., Dasgupta, A., Dunham-Snary, K., Wu, D., Chen, K. H., Hong, Z., Sharp, W. W., Kutty, S. & Archer, S. L. 2017. Ischemia-induced Drp1 and Fis1-mediated mitochondrial fission and right ventricular dysfunction in pulmonary hypertension. *J Mol Med (Berl)*, 95, 381-393.
- Tian, W., Li, W., Chen, Y., Yan, Z., Huang, X., Zhuang, H., Zhong, W., Chen, Y., Wu, W., Lin, C., Chen, H., Hou, X., Zhang, L., Sui, S., Zhao, B., Hu, Z., Li, L. & Feng, D. 2015. Phosphorylation of ULK1 by AMPK regulates translocation of ULK1 to mitochondria and mitophagy. *FEBS Lett*, 589, 1847-54.
- Tilokani, L., Nagashima, S., Paupe, V. & Prudent, J. 2018. Mitochondrial dynamics: overview of molecular mechanisms. *Essays in biochemistry*, 62, 341-360.
- Todkar, K., Ilamathi, H. S. & Germain, M. 2017. Mitochondria and Lysosomes: Discovering Bonds. *Frontiers in cell and developmental biology*, 5, 106-106.

- Tomlinson, I. P., Alam, N. A., Rowan, A. J., Barclay, E., Jaeger, E. E., Kelsell, D., Leigh, I., Gorman, P., Lamlum, H., Rahman, S., Roylance, R. R., Olpin, S., Bevan, S., Barker, K., Hearle, N., Houlston, R. S., Kiuru, M., Lehtonen, R., Karhu, A., Vilkki, S., Laiho, P., Eklund, C., Vierimaa, O., Aittomaki, K., Hietala, M., Sistonen, P., Paetau, A., Salovaara, R., Herva, R., Launonen, V. & Aaltonen, L. A. 2002. Germline mutations in FH predispose to dominantly inherited uterine fibroids, skin leiomyomata and papillary renal cell cancer. *Nat Genet*, 30, 406-10.
- Tomoda, T., Bhatt, R. S., Kuroyanagi, H., Shirasawa, T. & Hatten, M. E. 1999. A mouse serine/threonine kinase homologous to *C. elegans* UNC51 functions in parallel fiber formation of cerebellar granule neurons. *Neuron*, 24, 833-46.
- Tondera, D., Czauderna, F., Paulick, K., Schwarzer, R., Kaufmann, J. & Santel, A. 2005. The mitochondrial protein MTP18 contributes to mitochondrial fission in mammalian cells. *J Cell Sci*, 118, 3049-59.
- Tondera, D., Grandemange, S., Jourdain, A., Karbowski, M., Mattenberger, Y., Herzig, S., Da Cruz, S., Clerc, P., Raschke, I., Merkwirth, C., Ehses, S., Krause, F., Chan, D. C., Alexander, C., Bauer, C., Youle, R., Langer, T. & Martinou, J. C. 2009. SLP-2 is required for stress-induced mitochondrial hyperfusion. *Embo j*, 28, 1589-600.
- Tondera, D., Santel, A., Schwarzer, R., Dames, S., Giese, K., Klippel, A. & Kaufmann, J. 2004. Knockdown of MTP18, a novel phosphatidylinositol 3-kinase-dependent protein, affects mitochondrial morphology and induces apoptosis. *J Biol Chem*, 279, 31544-55.
- Tooze, S. A. & Yoshimori, T. 2010. The origin of the autophagosomal membrane. *Nat Cell Biol*, 12, 831-5.
- Torres-Quesada, O., Mayrhofer, J. E. & Stefan, E. 2017. The many faces of compartmentalized PKA signalosomes. *Cell Signal*, 37, 1-11.
- Toyama, E. Q., Herzig, S., Courchet, J., Lewis, T. L., Jr., Loson, O. C., Hellberg, K., Young, N. P., Chen, H., Polleux, F., Chan, D. C. & Shaw, R. J. 2016. Metabolism. AMP-activated protein kinase mediates mitochondrial fission in response to energy stress. *Science*, 351, 275-81.
- Truscott, K. N., Lowth, B. R., Strack, P. R. & Dougan, D. A. 2010. Diverse functions of mitochondrial AAA+ proteins: protein activation, disaggregation, and degradation. *Biochem Cell Biol*, 88, 97-108.
- Tsuboyama, K., Koyama-Honda, I., Sakamaki, Y., Koike, M., Morishita, H. & Mizushima, N. 2016. The ATG conjugation systems are important for degradation of the inner autophagosomal membrane. *Science*, 354, 1036-1041.
- Tsukada, M. & Ohsumi, Y. 1993. Isolation and characterization of autophagy-defective mutants of *Saccharomyces cerevisiae*. *FEBS Lett*, 333, 169-74.
- Tsun, Z. Y., Bar-Peled, L., Chantranupong, L., Zoncu, R., Wang, T., Kim, C., Spooner, E. & Sabatini, D. M. 2013. The folliculin tumor suppressor is a GAP for the RagC/D GTPases that signal amino acid levels to mTORC1. *Mol Cell*, 52, 495-505.
- Tufi, R., Gandhi, S., de Castro, I. P., Lehmann, S., Angelova, P. R., Dinsdale, D., Deas, E., Plun-Favreau, H., Nicotera, P., Abramov, A. Y., Willis, A. E., Mallucci, G. R., Loh, S. H. & Martins, L. M. 2014. Enhancing nucleotide metabolism protects against mitochondrial dysfunction and neurodegeneration in a PINK1 model of Parkinson's disease. *Nat Cell Biol*, 16, 157-66.
- Tumbarello, D. A., Waxse, B. J., Arden, S. D., Bright, N. A., Kendrick-Jones, J. & Buss, F. 2012. Autophagy receptors link myosin VI to autophagosomes to mediate Tom1-dependent autophagosome maturation and fusion with the lysosome. *Nat Cell Biol*, 14, 1024-35.
- Twig, G., Elorza, A., Molina, A. J., Mohamed, H., Wikstrom, J. D., Walzer, G., Stiles, L., Haigh, S. E., Katz, S., Las, G., Alroy, J., Wu, M., Py, B. F., Yuan, J., Deeney, J. T., Corkey, B. E. & Shirihai, O. S. 2008. Fission and selective fusion govern mitochondrial segregation and elimination by autophagy. *Embo j*, 27, 433-46.
- Tyrakis, P. A., Yurkovich, M. E., Sciacovelli, M., Papachristou, E. K., Bridges, H. R., Gaude, E., Schreiner, A., D'Santos, C., Hirst, J., Hernandez-Fernaund, J., Springett, R., Griffiths, J. R. & Frezza, C. 2017. Fumarate Hydratase Loss Causes Combined Respiratory Chain Defects. *Cell Rep*, 21, 1036-1047.
- Um, J. H. & Yun, J. 2017. Emerging role of mitophagy in human diseases and physiology. *BMB Rep*, 50, 299-307.

- Vadlamudi, R. K., Joung, I., Strominger, J. L. & Shin, J. 1996. p62, a phosphotyrosine-independent ligand of the SH2 domain of p56lck, belongs to a new class of ubiquitin-binding proteins. *J Biol Chem*, 271, 20235-7.
- Valsecchi, F., Ramos-Espiritu, L. S., Buck, J., Levin, L. R. & Manfredi, G. 2013. cAMP and mitochondria. *Physiology (Bethesda)*, 28, 199-209.
- Valverde, D. P., Yu, S., Boggavarapu, V., Kumar, N., Lees, J. A., Walz, T., Reinisch, K. M. & Melia, T. J. 2019. ATG2 transports lipids to promote autophagosome biogenesis. *The Journal of Cell Biology*, 218, 1787.
- van Venrooij, W. J., Henshaw, E. C. & Hirsch, C. A. 1972. Effects of deprivation of glucose or individual amino acids on polyribosome distribution and rate of protein synthesis in cultured mammalian cells. *Biochim Biophys Acta*, 259, 127-37.
- Vander Haar, E., Lee, S. I., Bandhakavi, S., Griffin, T. J. & Kim, D. H. 2007. Insulin signalling to mTOR mediated by the Akt/PKB substrate PRAS40. *Nat Cell Biol*, 9, 316-23.
- Velikkakath, A. K. G., Nishimura, T., Oita, E., Ishihara, N. & Mizushima, N. 2012. Mammalian Atg2 proteins are essential for autophagosome formation and important for regulation of size and distribution of lipid droplets. *Molecular biology of the cell*, 23, 896-909.
- Vera-Ramirez, L., Vodnala, S. K., Nini, R., Hunter, K. W. & Green, J. E. 2018. Autophagy promotes the survival of dormant breast cancer cells and metastatic tumour recurrence. *Nat Commun*, 9, 1944.
- Vezina, C., Kudelski, A. & Sehgal, S. N. 1975. Rapamycin (AY-22,989), a new antifungal antibiotic. I. Taxonomy of the producing streptomycete and isolation of the active principle. *J Antibiot (Tokyo)*, 28, 721-6.
- Villar, V. H., Nguyen, T. L., Delcroix, V., Terés, S., Bouche-careilh, M., Salin, B., Bodineau, C., Vacher, P., Priault, M., Soubeyran, P. & Durán, R. V. 2017. mTORC1 inhibition in cancer cells protects from glutaminolysis-mediated apoptosis during nutrient limitation. *Nature communications*, 8, 14124-14124.
- Wai, T., Garcia-Prieto, J., Baker, M. J., Merkwirth, C., Benit, P., Rustin, P., Ruperez, F. J., Barbas, C., Ibanez, B. & Langer, T. 2015. Imbalanced OPA1 processing and mitochondrial fragmentation cause heart failure in mice. *Science*, 350, aad0116.
- Wai, T. & Langer, T. 2016. Mitochondrial Dynamics and Metabolic Regulation. *Trends Endocrinol Metab*, 27, 105-17.
- Walsh, D. A., Perkins, J. P. & Krebs, E. G. 1968. An adenosine 3',5'-monophosphate-dependant protein kinase from rabbit skeletal muscle. *J Biol Chem*, 243, 3763-5.
- Wang, B., Iyengar, R., Li-Harms, X., Joo, J. H., Wright, C., Lavado, A., Horner, L., Yang, M., Guan, J.-L., Frase, S., Green, D. R., Cao, X. & Kundu, M. 2018. The autophagy-inducing kinases, ULK1 and ULK2, regulate axon guidance in the developing mouse forebrain via a noncanonical pathway. *Autophagy*, 14, 796-811.
- Wang, D., Wang, J., Bonamy, G. M. C., Meeusen, S., Bruschi, R. G., Turk, C., Yang, P. & Schultz, P. G. 2012a. A Small Molecule Promotes Mitochondrial Fusion in Mammalian Cells. *Angewandte Chemie International Edition*, 51, 9302-9305.
- Wang, L., Harris, T. E. & Lawrence, J. C., Jr. 2008. Regulation of proline-rich Akt substrate of 40 kDa (PRAS40) function by mammalian target of rapamycin complex 1 (mTORC1)-mediated phosphorylation. *J Biol Chem*, 283, 15619-27.
- Wang, L., Harris, T. E., Roth, R. A. & Lawrence, J. C., Jr. 2007. PRAS40 regulates mTORC1 kinase activity by functioning as a direct inhibitor of substrate binding. *J Biol Chem*, 282, 20036-44.
- Wang, L., Zhu, L., Wu, K., Chen, Y., Lee, D. Y., Gucek, M. & Sack, M. N. 2019a. Mitochondrial GCN5L1 regulates glutaminolysis, mTORC1 activity and murine liver regeneration. *Hepatology*.
- Wang, Q. & Holst, J. 2015. L-type amino acid transport and cancer: targeting the mTORC1 pathway to inhibit neoplasia. *Am J Cancer Res*, 5, 1281-94.
- Wang, S., Tsun, Z. Y., Wolfson, R. L., Shen, K., Wyant, G. A., Plovanich, M. E., Yuan, E. D., Jones, T. D., Chantranupong, L., Comb, W., Wang, T., Bar-Peled, L., Zoncu, R., Straub, C., Kim, C., Park, J., Sabatini, B. L. & Sabatini, D. M. 2015. Metabolism. Lysosomal amino acid transporter SLC38A9 signals arginine sufficiency to mTORC1. *Science*, 347, 188-94.
- Wang, W., Wang, Y., Long, J., Wang, J., Haudek, S. B., Overbeek, P., Chang, B. H., Schumacker, P. T. & Danesh, F. R. 2012b. Mitochondrial fission triggered by

- hyperglycemia is mediated by ROCK1 activation in podocytes and endothelial cells. *Cell Metab*, 15, 186-200.
- Wang, X. & Proud, C. G. 2009. Nutrient control of TORC1, a cell-cycle regulator. *Trends Cell Biol*, 19, 260-7.
- Wang, Y., Bai, C., Ruan, Y., Liu, M., Chu, Q., Qiu, L., Yang, C. & Li, B. 2019b. Coordinative metabolism of glutamine carbon and nitrogen in proliferating cancer cells under hypoxia. *Nature Communications*, 10, 201.
- Wang, Z., Jiang, H., Chen, S., Du, F. & Wang, X. 2012c. The mitochondrial phosphatase PGAM5 functions at the convergence point of multiple necrotic death pathways. *Cell*, 148, 228-43.
- Watson, D. G., Tonelli, F., Alossaimi, M., Williamson, L., Chan, E., Gorshkova, I., Berdyshev, E., Bittman, R., Pyne, N. J. & Pyne, S. 2013. The roles of sphingosine kinases 1 and 2 in regulating the Warburg effect in prostate cancer cells. *Cell Signal*, 25, 1011-7.
- Webster, B. R., Scott, I., Traba, J., Han, K. & Sack, M. N. 2014. Regulation of autophagy and mitophagy by nutrient availability and acetylation. *Biochimica et biophysica acta*, 1841, 525-534.
- Weckmann, K., Diefenthaler, P., Baeken, M. W., Yusifli, K., Turck, C. W., Asara, J. M., Behl, C. & Hajieva, P. 2018. Metabolomics profiling reveals differential adaptation of major energy metabolism pathways associated with autophagy upon oxygen and glucose reduction. *Sci Rep*, 8, 2337.
- Weerasekara, V. K., Panek, D. J., Broadbent, D. G., Mortenson, J. B., Mathis, A. D., Logan, G. N., Prince, J. T., Thomson, D. M., Thompson, J. W. & Andersen, J. L. 2014. Metabolic-stress-induced rearrangement of the 14-3-3zeta interactome promotes autophagy via a ULK1- and AMPK-regulated 14-3-3zeta interaction with phosphorylated Atg9. *Mol Cell Biol*, 34, 4379-88.
- Weidberg, H., Shvets, E., Shpilka, T., Shimron, F., Shinder, V. & Elazar, Z. 2010. LC3 and GATE-16/GABARAP subfamilies are both essential yet act differently in autophagosome biogenesis. *Embo j*, 29, 1792-802.
- Weir, H. J., Yao, P., Huynh, F. K., Escoubas, C. C., Goncalves, R. L., Burkewitz, K., Laboy, R., Hirschey, M. D. & Mair, W. B. 2017. Dietary Restriction and AMPK Increase Lifespan via Mitochondrial Network and Peroxisome Remodeling. *Cell Metabolism*, 26, 884-896.e5.
- Westermann, B. 2010. Mitochondrial fusion and fission in cell life and death. *Nat Rev Mol Cell Biol*, 11, 872-84.
- Westermann, B. 2012. Bioenergetic role of mitochondrial fusion and fission. *Biochim Biophys Acta*, 1817, 1833-8.
- Wijdeven, R. H., Janssen, H., Nahidiazar, L., Janssen, L., Jalink, K., Berlin, I. & Neefjes, J. 2016. Cholesterol and ORP1L-mediated ER contact sites control autophagosome transport and fusion with the endocytic pathway. *Nat Commun*, 7, 11808.
- Wikstrom, J. D., Mahdavian, K., Liesa, M., Sereda, S. B., Si, Y., Las, G., Twigg, G., Petrovic, N., Zingaretti, C., Graham, A., Cinti, S., Corkey, B. E., Cannon, B., Nedergaard, J. & Shrihail, O. S. 2014. Hormone-induced mitochondrial fission is utilized by brown adipocytes as an amplification pathway for energy expenditure. *Embo j*, 33, 418-36.
- Willems, P. H., Rossignol, R., Dieteren, C. E., Murphy, M. P. & Koopman, W. J. 2015. Redox Homeostasis and Mitochondrial Dynamics. *Cell Metab*, 22, 207-18.
- Wise, D. R. & Thompson, C. B. 2010. Glutamine addiction: a new therapeutic target in cancer. *Trends in Biochemical Sciences*, 35, 427-433.
- Wold, M. S., Lim, J., Lachance, V., Deng, Z. & Yue, Z. 2016. ULK1-mediated phosphorylation of ATG14 promotes autophagy and is impaired in Huntington's disease models. *Mol Neurodegener*, 11, 76.
- Wolfson, R. L., Chantranupong, L., Saxton, R. A., Shen, K., Scaria, S. M., Cantor, J. R. & Sabatini, D. M. 2016. Sestrin2 is a leucine sensor for the mTORC1 pathway. *Science*, 351, 43-8.
- Wolfson, R. L., Chantranupong, L., Wyant, G. A., Gu, X., Orozco, J. M., Shen, K., Condon, K. J., Petri, S., Kedir, J., Scaria, S. M., Abu-Remaileh, M., Frankel, W. N. & Sabatini, D. M. 2017. KICSTOR recruits GATOR1 to the lysosome and is necessary for nutrients to regulate mTORC1. *Nature*, 543, 438-442.
- Wong, P. M., Feng, Y., Wang, J., Shi, R. & Jiang, X. 2015. Regulation of autophagy by coordinated action of mTORC1 and protein phosphatase 2A. *Nat Commun*, 6, 8048.

- Wong, Y. C., Ysselstein, D. & Krainc, D. 2018. Mitochondria-lysosome contacts regulate mitochondrial fission via RAB7 GTP hydrolysis. *Nature*, 554, 382-386.
- Woods, A., Dickerson, K., Heath, R., Hong, S. P., Momcilovic, M., Johnstone, S. R., Carlson, M. & Carling, D. 2005. Ca<sup>2+</sup>/calmodulin-dependent protein kinase kinase-beta acts upstream of AMP-activated protein kinase in mammalian cells. *Cell Metab*, 2, 21-33.
- Woods, A., Johnstone, S. R., Dickerson, K., Leiper, F. C., Fryer, L. G., Neumann, D., Schlattner, U., Wallimann, T., Carlson, M. & Carling, D. 2003. LKB1 is the upstream kinase in the AMP-activated protein kinase cascade. *Curr Biol*, 13, 2004-8.
- Wu, H., Wei, H., Sehgal, S. A., Liu, L. & Chen, Q. 2016a. Mitophagy receptors sense stress signals and couple mitochondrial dynamic machinery for mitochondrial quality control. *Free Radic Biol Med*.
- Wu, S., Zhou, F., Zhang, Z. & Xing, D. 2011. Mitochondrial oxidative stress causes mitochondrial fragmentation via differential modulation of mitochondrial fission-fusion proteins. *Febs j*, 278, 941-54.
- Wu, W., Lin, C., Wu, K., Jiang, L., Wang, X., Li, W., Zhuang, H., Zhang, X., Chen, H., Li, S., Yang, Y., Lu, Y., Wang, J., Zhu, R., Zhang, L., Sui, S., Tan, N., Zhao, B., Zhang, J., Li, L. & Feng, D. 2016b. FUNDC1 regulates mitochondrial dynamics at the ER-mitochondrial contact site under hypoxic conditions. *Embo j*, 35, 1368-84.
- Wu, W., Tian, W., Hu, Z., Chen, G., Huang, L., Li, W., Zhang, X., Xue, P., Zhou, C., Liu, L., Zhu, Y., Zhang, X., Li, L., Zhang, L., Sui, S., Zhao, B. & Feng, D. 2014. ULK1 translocates to mitochondria and phosphorylates FUNDC1 to regulate mitophagy. *EMBO Rep*, 15, 566-75.
- Wyant, G. A., Abu-Remaileh, M., Wolfson, R. L., Chen, W. W., Freinkman, E., Danai, L. V., Vander Heiden, M. G. & Sabatini, D. M. 2017. mTORC1 Activator SLC38A9 Is Required to Efflux Essential Amino Acids from Lysosomes and Use Protein as a Nutrient. *Cell*, 171, 642-654.e12.
- Xia, J. & Wishart, D. S. 2010. MetPA: a web-based metabolomics tool for pathway analysis and visualization. *Bioinformatics*, 26, 2342-4.
- Xia, J. & Wishart, D. S. 2011. Metabolomic data processing, analysis, and interpretation using MetaboAnalyst. *Curr Protoc Bioinformatics*, Chapter 14, Unit 14.10.
- Xiao, B., Heath, R., Saiu, P., Leiper, F. C., Leone, P., Jing, C., Walker, P. A., Haire, L., Eccleston, J. F., Davis, C. T., Martin, S. R., Carling, D. & Gamblin, S. J. 2007. Structural basis for AMP binding to mammalian AMP-activated protein kinase. *Nature*, 449, 496-500.
- Xiao, B., Sanders, M. J., Underwood, E., Heath, R., Mayer, F. V., Carmena, D., Jing, C., Walker, P. A., Eccleston, J. F., Haire, L. F., Saiu, P., Howell, S. A., Aasland, R., Martin, S. R., Carling, D. & Gamblin, S. J. 2011. Structure of mammalian AMPK and its regulation by ADP. *Nature*, 472, 230-3.
- Xie, J., Ponuwei, G. A., Moore, C. E., Willars, G. B., Tee, A. R. & Herbert, T. P. 2011. cAMP inhibits mammalian target of rapamycin complex-1 and -2 (mTORC1 and 2) by promoting complex dissociation and inhibiting mTOR kinase activity. *Cellular signalling*, 23, 1927-1935.
- Xie, Z. & Klionsky, D. J. 2007. Autophagosome formation: core machinery and adaptations. *Nat Cell Biol*, 9, 1102-9.
- Xu, Y., Shen, J. & Ran, Z. 2019. Emerging views of mitophagy in immunity and autoimmune diseases. *Autophagy*, 1-15.
- Yamamoto, A., Tagawa, Y., Yoshimori, T., Moriyama, Y., Masaki, R. & Tashiro, Y. 1998. Bafilomycin A1 prevents maturation of autophagic vacuoles by inhibiting fusion between autophagosomes and lysosomes in rat hepatoma cell line, H-4-II-E cells. *Cell Struct Funct*, 23, 33-42.
- Yamano, K., Fogel, A. I., Wang, C., van der Bliek, A. M. & Youle, R. J. 2014. Mitochondrial Rab GAPs govern autophagosome biogenesis during mitophagy. *Elife*, 3, e01612.
- Yamashita, S. I., Jin, X., Furukawa, K., Hamasaki, M., Nezu, A., Otera, H., Saigusa, T., Yoshimori, T., Sakai, Y., Mihara, K. & Kanki, T. 2016. Mitochondrial division occurs concurrently with autophagosome formation but independently of Drp1 during mitophagy. *J Cell Biol*, 215, 649-665.
- Yan, L., Qi, Y., Huang, X., Yu, C., Lan, L., Guo, X., Rao, Z., Hu, J. & Lou, Z. 2018. Structural basis for GTP hydrolysis and conformational change of MFN1 in mediating membrane fusion. *Nat Struct Mol Biol*, 25, 233-243.

- Yang, H., Jiang, X., Li, B., Yang, H. J., Miller, M., Yang, A., Dhar, A. & Pavletich, N. P. 2017. Mechanisms of mTORC1 activation by RHEB and inhibition by PRAS40. *Nature*, 552, 368-373.
- Yang, H., Rudge, D. G., Koos, J. D., Vaidialingam, B., Yang, H. J. & Pavletich, N. P. 2013a. mTOR kinase structure, mechanism and regulation. *Nature*, 497, 217-23.
- Yang, Q., Inoki, K., Ikenoue, T. & Guan, K. L. 2006. Identification of Sin1 as an essential TORC2 component required for complex formation and kinase activity. *Genes Dev*, 20, 2820-32.
- Yang, Y., Lane, A. N., Ricketts, C. J., Sourbier, C., Wei, M. H., Shuch, B., Pike, L., Wu, M., Rouault, T. A., Boros, L. G., Fan, T. W. & Linehan, W. M. 2013b. Metabolic reprogramming for producing energy and reducing power in fumarate hydratase null cells from hereditary leiomyomatosis renal cell carcinoma. *PLoS One*, 8, e72179.
- Yang, Y., Valera, V. A., Padilla-Nash, H. M., Sourbier, C., Vocke, C. D., Vira, M. A., Abu-Asab, M. S., Bratslavsky, G., Tsokos, M., Merino, M. J., Pinto, P. A., Srinivasan, R., Ried, T., Neckers, L. & Linehan, W. M. 2010. UOK 262 cell line, fumarate hydratase deficient (FH-/FH-) hereditary leiomyomatosis renal cell carcinoma: in vitro and in vivo model of an aberrant energy metabolic pathway in human cancer. *Cancer Genet Cytogenet*, 196, 45-55.
- Yang, Y., Zhang, Y., Liu, X., Zuo, J., Wang, K., Liu, W. & Ge, J. 2013c. Exogenous taurine attenuates mitochondrial oxidative stress and endoplasmic reticulum stress in rat cardiomyocytes. *Acta Biochim Biophys Sin (Shanghai)*, 45, 359-67.
- Yang, Z. & Klionsky, D. J. 2009. An overview of the molecular mechanism of autophagy. *Curr Top Microbiol Immunol*, 335, 1-32.
- Yao, C.-H., Wang, R., Wang, Y., Kung, C.-P., Weber, J. D. & Patti, G. J. 2019. Mitochondrial fusion supports increased oxidative phosphorylation during cell proliferation. *eLife*, 8, e41351.
- Ye, J., Coulouris, G., Zaretskaya, I., Cutcutache, I., Rozen, S. & Madden, T. L. 2012. Primer-BLAST: a tool to design target-specific primers for polymerase chain reaction. *BMC bioinformatics*, 13, 134-134.
- Yeh, Y. Y., Wrasman, K. & Herman, P. K. 2010. Autophosphorylation within the Atg1 activation loop is required for both kinase activity and the induction of autophagy in *Saccharomyces cerevisiae*. *Genetics*, 185, 871-82.
- Yogev, O., Yogev, O., Singer, E., Shaulian, E., Goldberg, M., Fox, T. D. & Pines, O. 2010. Fumarase: a mitochondrial metabolic enzyme and a cytosolic/nuclear component of the DNA damage response. *PLoS Biol*, 8, e1000328.
- Yoshii, S. R., Kishi, C., Ishihara, N. & Mizushima, N. 2011. Parkin mediates proteasome-dependent protein degradation and rupture of the outer mitochondrial membrane. *J Biol Chem*, 286, 19630-40.
- Yoshii, S. R. & Mizushima, N. 2017. Monitoring and Measuring Autophagy. *Int J Mol Sci*, 18.
- Yoshimi, N., Futamura, T., Kakumoto, K., Salehi, A. M., Sellgren, C. M., Holmen-Larsson, J., Jakobsson, J., Palsson, E., Landen, M. & Hashimoto, K. 2016. Blood metabolomics analysis identifies abnormalities in the citric acid cycle, urea cycle, and amino acid metabolism in bipolar disorder. *BBA Clin*, 5, 151-8.
- Yoshimori, T., Yamamoto, A., Moriyama, Y., Futai, M. & Tashiro, Y. 1991. Bafilomycin A1, a specific inhibitor of vacuolar-type H(+)-ATPase, inhibits acidification and protein degradation in lysosomes of cultured cells. *J Biol Chem*, 266, 17707-12.
- Youle, R. J. 2019. Mitochondria—Striking a balance between host and endosymbiont. *Science*, 365, eaaw9855.
- Yu-Wai-Man, P. & Chinnery, P. F. 2013. Dominant optic atrophy: novel OPA1 mutations and revised prevalence estimates. *Ophthalmology*, 120, 1712-1712.e1.
- Yu-Wai-Man, P., Griffiths, P. G. & Chinnery, P. F. 2011. Mitochondrial optic neuropathies - disease mechanisms and therapeutic strategies. *Prog Retin Eye Res*, 30, 81-114.
- Yu, T., Robotham, J. L. & Yoon, Y. 2006. Increased production of reactive oxygen species in hyperglycemic conditions requires dynamic change of mitochondrial morphology. *Proc Natl Acad Sci U S A*, 103, 2653-8.
- Zachari, M., Gudmundsson, S. R., Li, Z., Manifava, M., Shah, R., Smith, M., Stronge, J., Karanasiou, E., Piunti, C., Kishi-Itakura, C., Vihinen, H., Jokitalo, E., Guan, J.-L., Buss, F., Smith, A. M., Walker, S. A., Eskelinen, E.-L. & Ktistakis, N. T. 2019. Selective Autophagy of Mitochondria on a Ubiquitin-Endoplasmic-Reticulum Platform. *Developmental Cell*.

- Zaja, I., Bai, X., Liu, Y., Kikuchi, C., Dosenovic, S., Yan, Y., Canfield, S. G. & Bosnjak, Z. J. 2014. Cdk1, PKCdelta and calcineurin-mediated Drp1 pathway contributes to mitochondrial fission-induced cardiomyocyte death. *Biochem Biophys Res Commun*, 453, 710-21.
- Zanna, C., Ghelli, A., Porcelli, A. M., Karbowski, M., Youle, R. J., Schimpf, S., Wissinger, B., Pinti, M., Cossarizza, A., Vidoni, S., Valentino, M. L., Rugolo, M. & Carelli, V. 2008. OPA1 mutations associated with dominant optic atrophy impair oxidative phosphorylation and mitochondrial fusion. *Brain*, 131, 352-67.
- Zetterqvist, Ö., Ragnarsson, U., Humble, E., Berglund, L. & Engström, L. 1976. The minimum substrate of cyclic AMP-stimulated protein kinase, as studied by synthetic peptides representing the phosphorylatable site of pyruvate kinase (type L) of rat liver. *Biochemical and Biophysical Research Communications*, 70, 696-703.
- Zhang, C. S., Hawley, S. A., Zong, Y., Li, M., Wang, Z., Gray, A., Ma, T., Cui, J., Feng, J. W., Zhu, M., Wu, Y. Q., Li, T. Y., Ye, Z., Lin, S. Y., Yin, H., Piao, H. L., Hardie, D. G. & Lin, S. C. 2017a. Fructose-1,6-bisphosphate and aldolase mediate glucose sensing by AMPK. *Nature*, 548, 112-116.
- Zhang, C. S., Jiang, B., Li, M., Zhu, M., Peng, Y., Zhang, Y. L., Wu, Y. Q., Li, T. Y., Liang, Y., Lu, Z., Lian, G., Liu, Q., Guo, H., Yin, Z., Ye, Z., Han, J., Wu, J. W., Yin, H., Lin, S. Y. & Lin, S. C. 2014a. The lysosomal v-ATPase-Ragulator complex is a common activator for AMPK and mTORC1, acting as a switch between catabolism and anabolism. *Cell Metab*, 20, 526-40.
- Zhang, F., Qi, Y., Zhou, K., Zhang, G., Linask, K. & Xu, H. 2015. The cAMP phosphodiesterase Prune localizes to the mitochondrial matrix and promotes mtDNA replication by stabilizing TFAM. *EMBO reports*, 16, 520.
- Zhang, H., Liu, B., Li, T., Zhu, Y., Luo, G., Jiang, Y., Tang, F., Jian, Z. & Xiao, Y. 2018. AMPK activation serves a critical role in mitochondria quality control via modulating mitophagy in the heart under chronic hypoxia. *International journal of molecular medicine*, 41, 69-76.
- Zhang, J., Fan, J., Venneti, S., Cross, J. R., Takagi, T., Bhinder, B., Djballah, H., Kanai, M., Cheng, E. H., Judkins, A. R., Pawel, B., Baggs, J., Cherry, S., Rabinowitz, J. D. & Thompson, C. B. 2014b. Asparagine plays a critical role in regulating cellular adaptation to glutamine depletion. *Mol Cell*, 56, 205-218.
- Zhang, P., McGrath, B. C., Reinert, J., Olsen, D. S., Lei, L., Gill, S., Wek, S. A., Vattam, K. M., Wek, R. C., Kimball, S. R., Jefferson, L. S. & Cavener, D. R. 2002. The GCN2 eIF2alpha kinase is required for adaptation to amino acid deprivation in mice. *Mol Cell Biol*, 22, 6681-8.
- Zhang, W., Wang, X., Li, P., Xiao, H., Zhang, W., Wang, H. & Tang, B. 2017b. Illuminating Superoxide Anion and pH Enhancements in Apoptosis of Breast Cancer Cells Induced by Mitochondrial Hyperfusion Using a New Two-Photon Fluorescence Probe. *Anal Chem*, 89, 6840-6845.
- Zhang, Y. L., Guo, H., Zhang, C. S., Lin, S. Y., Yin, Z., Peng, Y., Luo, H., Shi, Y., Lian, G., Zhang, C., Li, M., Ye, Z., Ye, J., Han, J., Li, P., Wu, J. W. & Lin, S. C. 2013. AMP as a low-energy charge signal autonomously initiates assembly of AXIN-AMPK-LKB1 complex for AMPK activation. *Cell Metab*, 18, 546-55.
- Zhang, Z., Liu, D., Yi, B., Liao, Z., Tang, L., Yin, D. & He, M. 2014c. Taurine supplementation reduces oxidative stress and protects the liver in an iron-overload murine model. *Mol Med Rep*, 10, 2255-62.
- Zhang, Z., Liu, L., Wu, S. & Xing, D. 2016. Drp1, Mff, Fis1, and MiD51 are coordinated to mediate mitochondrial fission during UV irradiation-induced apoptosis. *Faseb j*, 30, 466-76.
- Zhao, J., Liu, T., Jin, S., Wang, X., Qu, M., Uhlen, P., Tomilin, N., Shupliakov, O., Lendahl, U. & Nister, M. 2011. Human MIEF1 recruits Drp1 to mitochondrial outer membranes and promotes mitochondrial fusion rather than fission. *Embo j*, 30, 2762-78.
- Zheng, L., Cardaci, S., Jerby, L., MacKenzie, E. D., Sciacovelli, M., Johnson, T. I., Gaude, E., King, A., Leach, J. D., Edrada-Ebel, R., Hedley, A., Morrice, N. A., Kalna, G., Blyth, K., Ruppin, E., Frezza, C. & Gottlieb, E. 2015. Fumarate induces redox-dependent senescence by modifying glutathione metabolism. *Nat Commun*, 6, 6001.
- Zheng, L., MacKenzie, E. D., Karim, S. A., Hedley, A., Blyth, K., Kalna, G., Watson, D. G., Szlosarek, P., Frezza, C. & Gottlieb, E. 2013. Reversed argininosuccinate lyase activity in fumarate hydratase-deficient cancer cells. *Cancer Metab*, 1, 12.

- Zhong, H., SuYang, H., Erdjument-Bromage, H., Tempst, P. & Ghosh, S. 1997. The transcriptional activity of NF-kappaB is regulated by the IkappaB-associated PKAc subunit through a cyclic AMP-independent mechanism. *Cell*, 89, 413-24.
- Zhong, Y., Wang, Q. J., Li, X., Yan, Y., Backer, J. M., Chait, B. T., Heintz, N. & Yue, Z. 2009. Distinct regulation of autophagic activity by Atg14L and Rubicon associated with Beclin 1-phosphatidylinositol-3-kinase complex. *Nat Cell Biol*, 11, 468-76.
- Zhou, C., Ma, K., Gao, R., Mu, C., Chen, L., Liu, Q., Luo, Q., Feng, D., Zhu, Y. & Chen, Q. 2017. Regulation of mATG9 trafficking by Src- and ULK1-mediated phosphorylation in basal and starvation-induced autophagy. *Cell Res*, 27, 184-201.
- Zipin, J. H., Chen, Y., Nahirney, P., Kamenetsky, M., Wuttke, M. S., Fischman, D. A., Levin, L. R. & Buck, J. 2003. Compartmentalization of bicarbonate-sensitive adenylyl cyclase in distinct signaling microdomains. *Faseb j*, 17, 82-4.
- Zitka, O., Skalickova, S., Gumulec, J., Masarik, M., Adam, V., Hubalek, J., Trnkova, L., Kruseova, J., Eckschlager, T. & Kizek, R. 2012. Redox status expressed as GSH:GSSG ratio as a marker for oxidative stress in paediatric tumour patients. *Oncol Lett*, 4, 1247-1253.
- Zoncu, R., Bar-Peled, L., Efeyan, A., Wang, S., Sancak, Y. & Sabatini, D. M. 2011. mTORC1 senses lysosomal amino acids through an inside-out mechanism that requires the vacuolar H(+)-ATPase. *Science*, 334, 678-83.
- Zuchner, S., De Jonghe, P., Jordanova, A., Claeys, K. G., Guergueltcheva, V., Cherninkova, S., Hamilton, S. R., Van Stavern, G., Krajewski, K. M., Stajich, J., Tournev, I., Verhoeven, K., Langerhorst, C. T., de Visser, M., Baas, F., Bird, T., Timmerman, V., Shy, M. & Vance, J. M. 2006. Axonal neuropathy with optic atrophy is caused by mutations in mitofusin 2. *Ann Neurol*, 59, 276-81.
- Zuchner, S., Mersyanova, I. V., Muglia, M., Bissar-Tadmouri, N., Rochelle, J., Dadali, E. L., Zappia, M., Nelis, E., Patitucci, A., Senderek, J., Parman, Y., Evgrafov, O., Jonghe, P. D., Takahashi, Y., Tsuji, S., Pericak-Vance, M. A., Quattrone, A., Battaloglu, E., Polyakov, A. V., Timmerman, V., Schroder, J. M. & Vance, J. M. 2004. Mutations in the mitochondrial GTPase mitofusin 2 cause Charcot-Marie-Tooth neuropathy type 2A. *Nat Genet*, 36, 449-51.
- Züchner, S., Wang, G., Tran-Viet, K.-N., Nance, M. A., Gaskell, P. C., Vance, J. M., Ashley-Koch, A. E. & Pericak-Vance, M. A. 2006. Mutations in the novel mitochondrial protein REEP1 cause hereditary spastic paraplegia type 31. *American journal of human genetics*, 79, 365-369.